СИБИРСКИЙ ЖУРНАЛ НАУКИ И ТЕХНОЛОГИЙ

Том 19, № 1

Красноярск 2018

СИБИРСКИЙ ЖУРНАЛ НАУКИ И ТЕХНОЛОГИЙ

Том 19, № 1

SIBERIAN JOURNAL OF SCIENCE AND TECHNOLOGY

Vol. 19, No 1

К СВЕДЕНИЮ ЧИТАТЕЛЕЙ

«Сибирский журнал науки и технологий» является научным, производственно-практическим рецензируемым изданием. Свидетельство о регистрации средства массовой информации ПИ № ФС 77-70577 от 03.08.2017 г. выдано Федеральной службой по надзору в сфере связи, информационных технологий и массовых коммуникаций (Роскомнадзор).

ISSN 2587-6066.

Подписной индекс в каталоге «Пресса России» – 39263.

Зарегистрирован в Российском индексе научного цитирования (РИНЦ).

Включен в базу данных Ulrich's Periodicals Directory американского издательства Bowker.

Входит в перечень журналов ВАК по следующим группам научных специальностей:

01.04.00 – физика;
05.02.00 – машиностроение и машиноведение;
05.07.00 – авиационная и ракетно-космическая техника;
05.13.00 – информатика, вычислительная техника и управление;
08.00.00 – экономические науки.

Выпускается с 2000 года. До 2002 года журнал носил название «Вестник Сибирской аэрокосмической академии имени академика М. Ф. Решетнева» («Вестник САА»), до мая 2017 года – «Вестник Сибирского государственного аэрокосмического университета имени академика М. Ф. Решетнева».

Каждый выпуск журнала включает четыре раздела:

1 раздел. Математика, механика, информатика.
2 раздел. Авиационная и ракетно-космическая техника.
3 раздел. Технологические процессы и материалы.
4 раздел. Экономика.

Статьи публикуются бесплатно после обязательного рецензирования и при оформлении их в соответствии с требованиями редакции (www.vestnik.sibsau.ru). Журнал выходит 4 раза в год.

Электронная версия журнала представлена на сайте Научной электронной библиотеки (http://www.elibrary.ru) и сайте журнала (www.vestnik.sibsau.ru)

При перепечатке или цитировании материалов из журнала «Сибирский журнал науки и технологий» ссылка обязательна.

Учредитель и издатель

ФГБОУ ВО «Сибирский государственный университет науки и технологий имени академика М. Ф. Решетнева» (СибГУ им. М. Ф. Решетнева)

АДРЕС РЕДАКЦИИ, УЧРЕДИТЕЛЯ И ИЗДАТЕЛЯ:
Сибирский государственный университет науки и технологий имени академика М. Ф. Решетнева,
Российская Федерация, 660037, Красноярск,
проспект имени газеты «Красноярский рабочий», 31,
П-416. Тел./ факс (391)291-90-19
E-mail: vestnik@sibsau.ru

Редактор: О. А. Плехова
Редактор английского текста С. Г. Эфа
Оригинал-макет и верстка О. В. Булатниковой
Подписано в печать 26.03.2018. Формат 70×108/16.
Бумага офсетная. Печать плоская. Усл. печ. л. 22,4.
Уч.-изд. л. 28,0. Тираж 1000 экз. Заказ 31. С 120/18.
Редакционно-издательский отдел СибГУ им. М.Ф. Решетнева.
Отпечатано в редакционно-издательском центре
СибГУ им. М.Ф. Решетнева.
Российская Федерация, 660037, г. Красноярск,
просп. им. газ. «Красноярский рабочий», 31.
Дата выхода в свет: 27.04.2018. Свободная цена

INFORMATION FOR AUTHORS AND SUBSCRIBERS

Siberian Journal of Science and Technology is a research, production and practical peer-reviewed journal. Included by the Higher Attestation Commission of the Russian Federation in the Index of Leading Russian Peer-Reviewed Journals and Periodicals, in which significant scientific dissertation results should be published when applying for a Dr.Sc. degree.

The journal is the official periodical of Reshetnev Siberian State University of Science and Technology.

Certificate of Registration as a Mass Media Resource. Certificate: PI No. FC 77-50577, dated 03 August 2017, given by Federal Supervision Agency for Information Technology, Communications and Mass Media.

The Journal is included in the following subscription catalogue 39263 – Pressa Rossii.

The journal is registered in the Russian Science Citation Index (RSCI). The journal is indexed in the database of Ulrich's Periodicals Directory.

The journal was first published in 2000. Prior to 2002 it had the title *Vestnik Sibirskoi aerokosmicheskoi akademii imeni academika M. F. Reshetneva (Vestnik SAA)*, prior to may 2017 it had the title *Vestnik Sibirskogo gosudarstvennogo aerokosmicheskogo universiteta imeni akademika M. F. Reshetneva (Vestnik SibGAU)*.

The Journal is recommended for publishing the main results of research when applying for Cand. Sc. degree and Dr. Sc. degree upon the following specialties:

01.04.00 – physics;
05.02.00 – machine engineering and science of mechanics;
05.07.00 – aviation and spacecraft engineering;
05.13.00 – management, computer technology and informatics;
08.00.00 – economics. Each issue consists of four parts.

Each issue consists of four parts:

Part 1. Mathematics, Mechanics, Computer Science.
Part 2. Aviation and Spacecraft Engineering.
Part 3. Technological Processes and Material Science.
Part 4. Economics Aerospace Industry.

Papers prepared in accordance with the editorial guidelines (www.vestnik.sibsau.ru) are published free of charge after being peer reviewed.

The journal is published four times a year.

An online version can been viewed at http://www.elibrary.ru

Siberian Journal of Science and Technology should be cited when reprinting or citing materials from the journal.

CONTACTS. Website: www.vestnik.sibsau.ru
Address: Reshetnev Siberian State University of Science and Technology.
31, Krasnoyarsky Rabochy Av., Krasnoyarsk,
660037, Russian Federation.
Tel./fax (391)291-90-19; e-mail: vestnik@sibsau.ru

Editor O. A. Plekhova, *Editor* (*English Language*) S. G. Efa
Layout original O. V. Bulatnikova
Signed (for printing): 26.03.2018. Format 70×108/16.
Offset Paper. Print flat. 22,4. Published sheets 28,0.
1000 copies. Order 31. C 120/18.
Printing and Publication Department
Reshetnev University.
Printed in the Department of copying and duplicating equipment Reshetnev University.
31, Krasnoyarsky Rabochy Av., Krasnoyarsk,
660037, Russian Federation.
Date of publication: 27.04.2018. Free price

СОДЕРЖАНИЕ

CONTENTS

Раздел
Part
1

МАТЕМАТИКА, МЕХАНИКА, ИНФОРМАТИКА

MATHEMATICS, MECHANICS, COMPUTER SCIENCE

UDC 629.13.01

Siberian Journal of Science and Technology. 2018, Vol. 19, No. 1, P. 8–16

VERIFICATION OF FINITE-ELEMENT MODEL SPACECRAFT VIA TEST RESULTS

D. F. Balyakov

Reshetnev Siberian State University of Science and Technology
31, Krasnoyarsky Rabochy Av., Krasnoyarsk, 660037, Russian Federation
E-mail: d-bolyakov@iss-reshetnev.ru

The question of ensuring strength, durability and survivability of a spacecraft construction with mathematical modeling complexes is a modern trend in satellites design. This approach is based on the shortening of the prelaunch preparation stage. In particular, this is due to the reduction in the number of vibration tests of a spacecraft (SC). In the present work, using the example of vibration tests of "Express-1000K" service system module, we consider the verification technique for the mathematical model of communication satellites, output by a pair of payloads. The choice of this research object was caused by the conceptual scheme for modern space vehicles constructing, based on the modular principle. The service system module is the basic supporting structure of the spacecraft, able to integrate with any payload (information support, scientific research, geodesy and remote sensing, navigation) and is a universal tool in a satellite construction. In tests with harmonic vibration, the first longitudinal and transverse tone of the spacecraft oscillations are well identified, which can be fairly easily predicted applying the finite-element model. Proceeding from this, the accuracy of forecasts depends, to a greater extent, on the complexity of the modeled construction and the modeling procedure being used. The study provides a finite-element modeling technique for spacecraft output by a pair of payloads; the dynamic characteristics of the object of investigation by calculation and experimental methods are obtained. The identification procedure was carried out using the 'modal consent' method. The verification technique considered in the study makes it possible to carry out effective adjustment of the finite-element model. The finite-element model obtained by verification results allows to effectively evaluate the behavior of a spacecraft already at the design stage, which enables to shorten the time of vibration tests. The main results of this research were applied in verification of mathematical models of modern spacecraft developed by JSC "ISS". The importance of applying verification methods of the mathematical model of the product at the preliminary (design) stage of spacecraft creation was noted.

Keywords: verification, spacecraft, finite element model, test, identification, dynamics characteristics.

Сибирский журнал науки и технологий. 2018. Т. 19, № 1. С. 8–16

ВЕРИФИКАЦИЯ КОНЕЧНО-ЭЛЕМЕНТНОЙ МОДЕЛИ КОСМИЧЕСКОГО АППАРАТА РЕЗУЛЬТАТАМИ ИСПЫТАНИЙ

Д. Ф. Баляков

Сибирский государственный университет науки и технологий имени академика М. Ф. Решетнева
Российская Федерация, 660037, г. Красноярск, просп. им. газ. «Красноярский рабочий», 31
E-mail: d-bolyakov@iss-reshetnev.ru

Вопрос обеспечения прочности, ресурса и живучести конструкции космического аппарата с помощью комплексов математического моделирования – современная тенденция проектирования спутников. Данный подход основан на сокращении сроков подготовки изделия к запуску. В частности, это происходит за счет уменьшения объема проведения вибрационных испытаний космического аппарата (КА). На примере вибрационных испытаний платформы модуля служебных систем «Экспресс-1000К» рассматривается методика проведения верификации математической модели спутников связи, выводимых парной полезной нагрузкой. Выбор данного объекта исследования обусловлен принципиальной схемой построения современных космических аппаратов, основанных на модульном принципе. Модуль служебных систем является основной несущей конструкцией космического аппарата, способной интегрироваться с любой полезной нагрузкой (информационное обеспечение, научные исследования, геодезия и дистанционное зондирование, навигация), и является универсальным инструментом при построении спутника. При испытаниях гармонической вибрацией хорошо идентифицируются первые продольные и поперечные тона колебаний космического аппарата, которые достаточно легко прогнозируются с использованием конечно-элементной модели. Исходя из этого, точность результатов прогнозов зависит в большей степени от сложности моделируемой конструкции и используемой процедуры моделирования. Приводится методика конечно-элементного моделирования космических аппаратов, выводимых парной полезной нагрузкой, получены динамические характеристики объекта исследования расчетным и экспериментальным методами. Проведена процедура идентификации по методу «модального согласия».

Рассмотренная методика верификации позволяет производить оперативную корректировку конечно-элементной модели космических аппаратов. Конечно-элементная модель, полученная по результатам верификации, позволяет эффективно проводить оценку поведения КА уже на этапе проектирования, что дает возможность сократить время проведения вибрационных испытаний космических аппаратов. Основные результаты данного исследования применены при верификации математических моделей современных космических аппаратов, разрабатываемых в АО «ИСС». Отмечена важность применения методов верификации математической модели изделия на предварительном (проектном) этапе создания космического аппарата.

Ключевые слова: верификация, космический аппарат, конечно-элементная модель, испытания, вибрация, идентификация, динамические параметры.

Introduction. Recently, the interest of scientists and engineers is focused on research in the field of identification and verification design of mathematical models. For example, in [1] verification of the finite-element model of the spacecraft developed by space-rocket enterprise “Energy” is done based on the results of modal tests; in the study [2] verification of mathematical models designed for the analysis of acoustic impact on the antenna system of the spacecraft are carried out.

A distinctive feature of the proposed in the present work method of verification is to conduct a preliminary modal analysis (analysis of frequencies and forms) in order to clarify the installation positions of measuring sensors.

To ensure the most accurate and detailed descriptions of elastic characteristics of a satellite design and to obtain predictions of loading a computational model, built using the finite element method, is mainly used. The spacecraft design is split into different elements, interconnected in a finite number of grid points. When designing a spacecraft, special attention is paid to the development of its mathematical model, adequately describing its mechanical properties, which is possible in combination with the experiment and methods of identification of the spacecraft design parameters. In this article the verification method of finite element models of spacecraft output by a pair of payloads manufactured by the JSC “ISS” are discussed. Descriptions of the calculation method and the calculation mathematical model are suggested. The main results of the numerical simulation test design done with combined payloads harmonic vibration on the basis of the design platform “Express-1000K”, as well as the data of natural experiments are given.

Aims and objectives. The aim of this study is to test the verification method of the finite element model (hereafter FEM) of the platform “Express-1000K” under results of harmonic vibration tests.

Choice of suitable methods, levels and stages of verification shall depend on the product characteristics and relevant categories under claim. Two of the most common verification methods are tests and analysis.

Tests are considered a preferable method of verification due to their efficiency. Application of analysis is required in the absence of possibility to simulate flight conditions on the Ground or in case of economic inexpediency of full range of flight conditions. The scheme of studies and steps to verify the FEM of the spacecraft, providing a better insight into dynamic behavior are presented in fig. 1.

Using FEM spacecraft, based on the results of modal analysis it is possible to determine optimum locations of accelerometers when performing vibration tests on an external mechanical impact, caused by launch vehicles capacities.

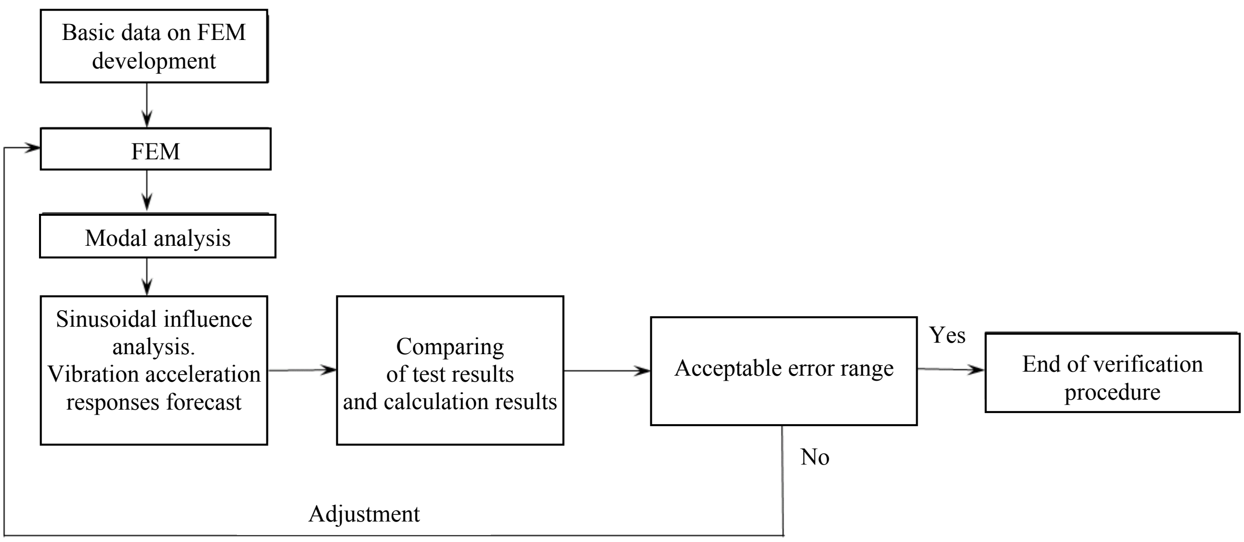

Fig. 1. FEM verification steps

Рис. 1. Последовательность этапов верификации КЭМ КА

Based on the results of SC modal analysis, the installation locations of accelerometers in the most critical points have been selected:

− “accurate” equipment installation areas;

− the attachment of antennas, opening and closing mechanisms;

− equipment installation areas, with natural frequency below 100–150 Hz (solar panels);

− on the basic structure of the spacecraft to control the design capacities in terms of construction strength (adapter, power pipe, release device);

− in places with the maximum displacement (antennas edges, the solar batteries edges).

Numerical simulation. When testing harmonic vibration first longitudinal and transverse tone oscillations of the satellite are identified well, which is fairly easily predicted using FEM SC [3]. Accordingly, the accuracy of the predictions depends more on the complexity of the simulated construction design and applied simulation procedures [4; 5].

In the calculation scheme a real object is replaced by a discrete model that represents a set of nodes and relevant finite elements with appropriate properties. FEM SC has been created in the format of the software module FEMAP [5] and consists of 212517 nodes and 221445 elements.

Proceeding to the simulating procedure, it is necessary to stipulate the following assumptions and limitations:

1. As a global coordinate system to create FEM SC selected is the reference coordinate system PPV (in accordance with the original data), origin of which is located on the junction of the release device and adapter (plane 1*c*), where:

– the *X*-axis is directed along the longitudinal axis of the spacecraft toward the booster stage;

– the *Y*-axis is directed along the first plane (I) stabilization of the spacecraft;

– the *Z*-axis is directed along the fourth surface (IV) of spacecraft stabilization (fig. 2).

2. Thermostated cell panels and panels of the design (SC) are simulated by multilayer elements with the corresponding thicknesses of supporting layers and honeycomb core. Basic structure of the body (BSB), cone-shaped spacecraft adapter are simulated by beam elements. Rods and frames of the solar battery pannels (SB) are simulated with truss elements. For modeling equipment shells, SC antenna reflector elements of plate type are used. Honeycombs are simulated by three-layer plates [6; 7]. Devices, antenna, flanges, bases, supports, fittings are simulated flat elements. Mechanical antennas are simulated by beam elements. The mass of the design is set using the density of materials [8]. Mass of cables, connecting elements, balancing weights is considered as a uniformly distributed mass of the SC design.

3. The equation of the system under consideration motion can be represented as:

$$[M]\{q''\} + [K]\{q'\} + [C]\{q\} = \{F\}, \qquad (1)$$

where {u} – vector of nodal relocation for all system; $\{q''\}$, $\{q'\}$ – vectors of accelerations and speeds of points of system; [With], [To], [M] – “global” stiffness matrixes, damping and masses for all system; {F} – a vector of nodal forces for all system. The matrix of damping [K] can be received formally, similarly to stiffness matrixes and masses, having entered some constant for internal friction and adding appropriate matrixes of elements, however generally it is not the same. Damping matrix task is approximation of dispersion energy. In practice the matrix [K] is set by a constant, built by setting of damping values on different own modes or approximated through matrixes [M] and [C]; or the damping model, which most accurately describes real behavior of construction, is applied.

The General Assembly of the FEM SC is shown in fig. 3.

The research of a model quality begins with finding the Modal Assurance Criterion, MAC. MAC-values are defined as a difference between test results and results of the finite-element analysis in case of harmonic vibration load simulation. Experimental and finite-element modes cannot (even theoretically) be absolutely orthogonal between themselves for that simple reason that it is impossible to do measurement in all points of a subject to tests.

$$\mathrm{MAC}_{ij} = \frac{\left(\{\varphi_{i\text{э}}\}\{\varphi_{j\text{р}}\}\right)^2}{\left(\{\varphi_{i\text{э}}\}\{\varphi_{j\text{э}}\}\right)\left(\{\varphi_{i\text{р}}\}\{\varphi_{j\text{р}}\}\right)}, \qquad (2)$$

where $\{\varphi_{i\text{э}}\}\{\varphi_{j\text{р}}\}$ – analyzed couple of matrix vectors – experimental and estimated respectively.

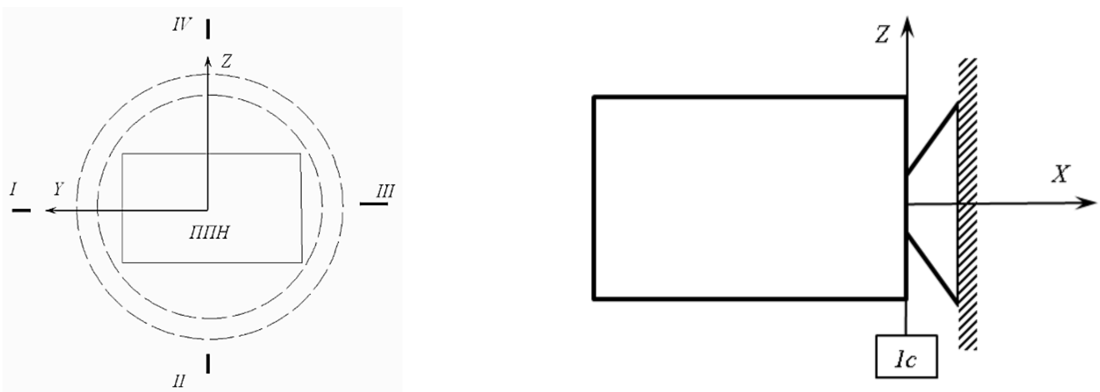

Fig. 2. Coordinate system and stabilization axis location

Рис. 2. Система координат и расположение осей стабилизации

Instead of this MAC-values show the extent of similarity between an experiment and finite – element calculation. Usually the first step in case of dynamic analysis is determination of natural frequencies and forms of oscillations of the design regardless of damping [9].

Frequencies and forms of oscillations characterize the main dynamic properties of the design and show what will be response of the considered construction to dynamic excitation. One of the reasons for natural frequencies and forms of oscillations calculations is the need to assess the dynamic influence between the researched construction and support. Further dynamic tests are usually based on the analysis of natural frequencies. Results of the modal analysis of FEM SC are provided in tab. 1.

FEM SC calculation of acceleration responses under sinusoidal vibration influence is carried out. Levels of sinusoidal vibration in SC adapter joint with booster stage were accepted according to tab. 2.

The amplitude-frequency characteristic (AFC) of acceleration responses of monitor sensors installation on basic construction of the body in X, Y, Z directions respectively under sinusoidal influence is given in fig. 4.

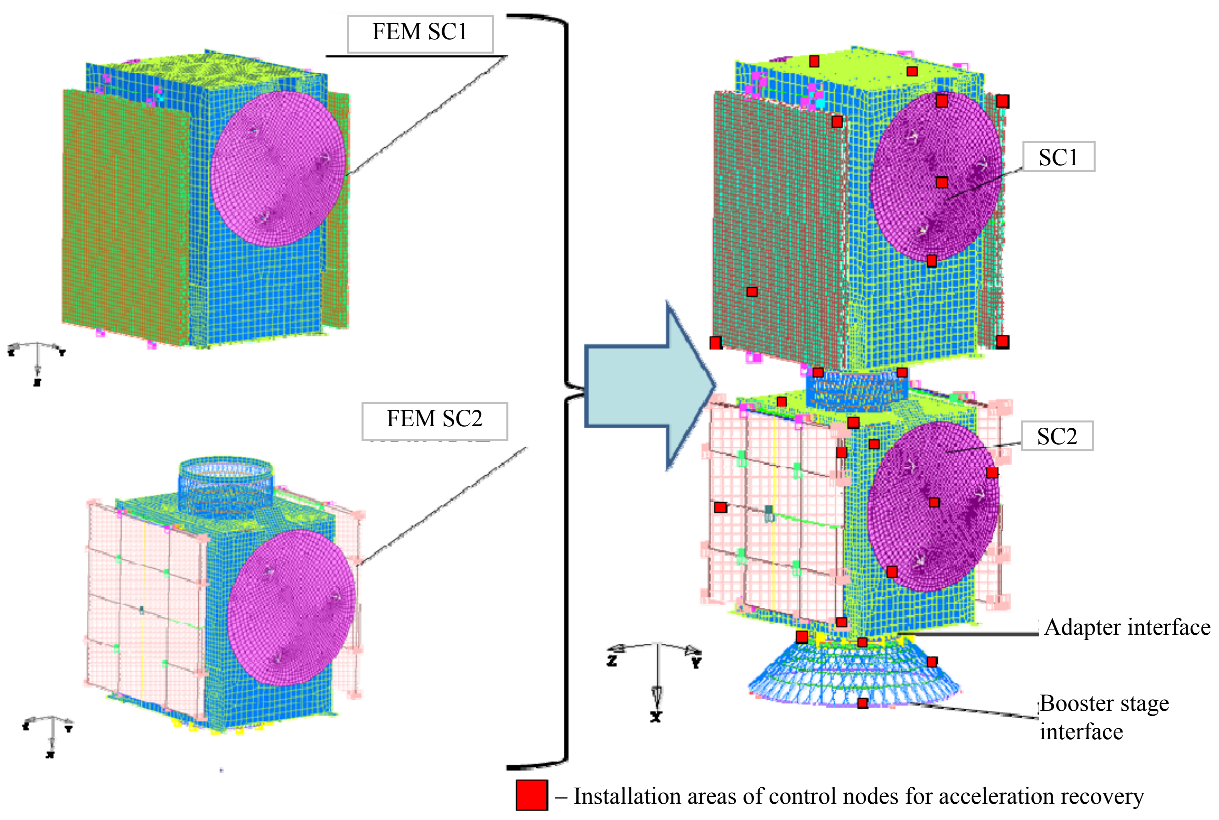

Fig. 3. Final finite element SC model

Рис. 3. Общая сборка КЭМ КА

Table 1

FEM SC modal analysis results

Tone no.	Frequency, Hz	Effective mass, %						Description of satellite oscillation form
		Mx	*My*	*Mz*	*Ix*	*Iy*	*Iz*	
1	5.08	–	2.7	**59.0**	–	**92.0**	4,3	1st SC oscillation tone *Z* direction
2	5.13	–	**59.7**	2.83	–	4.3	**92,4**	1st SC oscillation tone *Y* direction
5	9.36	–	–	–	52.3	–	–	SC rotation around longitudinal axis
7	12.15	–	–	–	14.2	–	–	SC rotation around *X* axis
11	14.07	–	–	**7.7**	–	1.2	–	SC roll oscillation
61	29.98	24.1	–	–	–	–	–	1st SC oscillation tone *X* direction

End of table 1

Tone no.	Frequency, Hz	Effective mass, %						Description of satellite oscillation form
		Mx	*My*	*Mz*	*Ix*	*Iy*	*Iz*	
74	33.68	–	–	–	1.23	–	–	SC rotation around longitudinal axis
81	34.66	8.5	–	–	–	–	–	SB panels
82	43.68	16.9	–	–	–	–	–	SC longitudinal oscillations
121	100.00	1.8	–	–	–	–	–	–
Total effective masses, %		94.9	95.6	94.9	97.2	99.8	99.8	

Table 2

Levels of sinusoidal vibration

Frequency range, Hz	Vibration level, g	
	Evaluating	
	Longitudinal direction (X_{SC})	Transversal direction (Y_{SC}, Z_{SC})
5–10	1.82	0.39
10–20	1.82	0.52
20–100	0.78	0.78

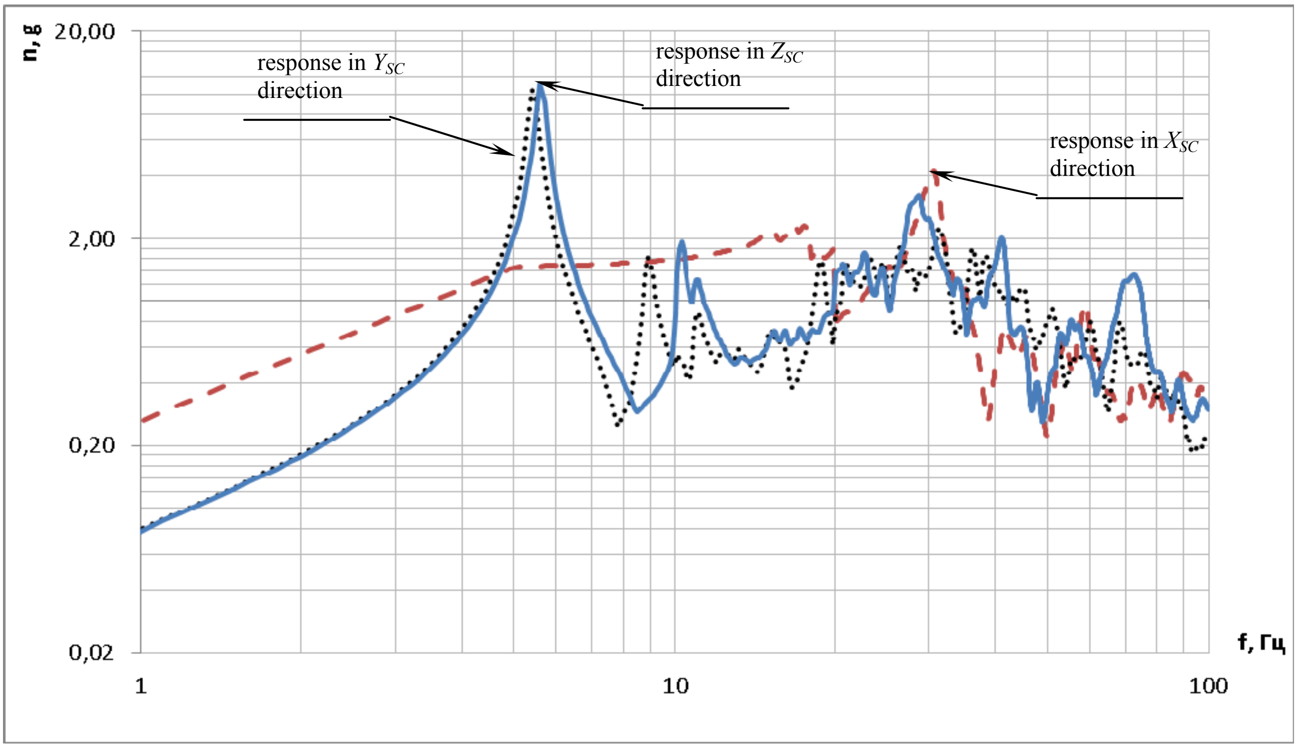

Fig. 4. AFC of acceleration responses on basic construction of the body in *X*, *Y*, *Z* directions respectively

Рис. 4. АЧХ откликов виброускорений силовой конструкции корпуса по осям *X*, *Y*, *Z* соответственно

Tests on the impact of harmonic vibration. Test programs are essential part of the general verification process which purpose is to ensure the product compliance with all requirements to design, characteristics and quality.

For verification process quality improvement tests, which conform to certain requirements, are delivered:

– qualification tests are carried out at the qualification levels, with maximum duration;

– the proto-flight model shall pass the test program with qualification levels, but with the reduced duration.

In case of release section capacity influence (vibration and acoustic) the proto-flight SC model is delivered in a start status, with:

– pyromeans disconnected from means of blasting;

– removable equipment from antennas dismantled, except mirror cubes with protective covers and seats for instrumental full-spheres installation on irradiators, reflectors and opening mechanisms;

Before tests the mass and position of center of masses of SC shall be defined.

Test objective is to confirm storageability of output characteristics of SC after mechanical loadings impacts with qualification levels.

Test tasks are:

– application to SC of vibration loads (sinusoidal vibration in three directions) with qualification levels;

– responses of SC elements measurement in installation areas of accelerometers, in the course of mechanical vibration loads applications;

– determination of transmission ratios of vibration acceleration to fastening assemblies of components.

Vibration tests are carried out in the range from 20 Hz to 100 Hz inclusively.

Test results are shown in fig. 5.

Verification of finite element model. It is considered that in case of MAC-values of 0.8–0.9 experiment and calculation describe one situation. MAC-values above 0.9 are reached in case of well correlated modes. The graphic result of MAC calculation for the considered FEM is provided in fig. 6.

In the estimated MAC model values do not exceed 0.69. These results testify the mismatch of the experiment and calculation. Adjustment of estimated FEM is required. Comparing of calculated and experimental data is provided in tab. 3.

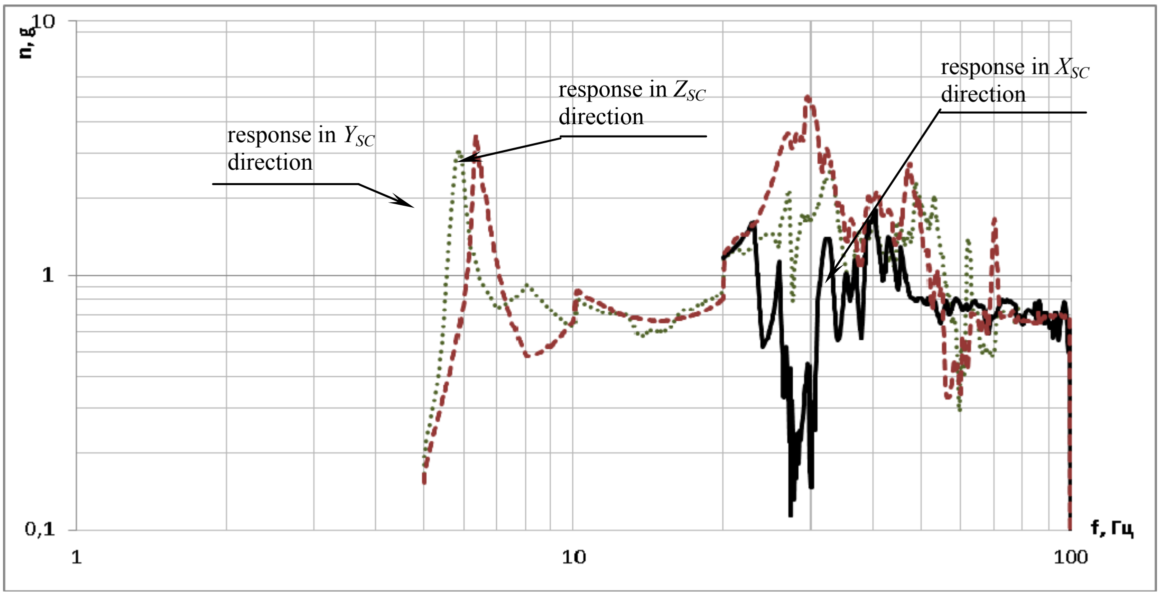

Fig. 5. AFC of acceleration responses on SC basic construction based on vibration test

Рис. 5. АЧХ откликов виброускорений по результатам гармонических вибрационных испытаний конструкции корпуса КА

Theoretical frequency Hz	Experimental frequency Hz		
29,98	**0,69**	**0,28**	**0,27**
5,13	**0,10**	**0,59**	**0,43**
5,08	**0,09**	**0,31**	**0,60**
	34,12	**5,53**	**5,0**

Fig. 6. MAC-identification of FEM and results of harmonic vibration tests of SC

Рис. 6. MAC-идентификация собственных частот колебаний КЭМ
и результатов гармонических вибрационных испытаний конструкции КА

If test results considerably (more than by 10 %) differ from FEM analysis results, then change of some model parameters (damping, distribution of masses, etc.), i. e. FEM adjustment is carried out. Adjustment is understood as specification of a number of FEM parameters (geometrical sections of beam elements, thickness of plates, elastic modules, rigidness and damping in local connections, etc.) by results of comparing with the experimental data.

Adjustments can be done in two ways:

– "manual" adjustment of some model parameters;

– change of model parameters on the basis of optimization task solution under selected criteria (level of oscillation forms mismatch, frequency responses, etc.).

The first way is simpler, however, results of adjustment process are generally defined by the engineer intuitively. The second approach allows to receive the formalized procedure of simultaneous change of selected model parameters in compliance with criteria. In case of all construction it is convenient to carry out adjustment of FEM based on test results of sinusoidal influences of engineering model. The finite-element model specified at this stage is further used for a flight product model.

The main stages of FEM adjustment procedure are as follows: at the end of processing procedures of engineering model test results and analysis, the experimental and analytical modal characteristics of FEM and those of the real product [10–15] are received. Modal characteristics are understood as frequencies and oscillation forms. It is necessary to note that adjustment is, as a rule, done based on sinusoidal influence test results. At the same time, forms of oscillations correspond to the accelerometers forms in installation areas. Comparing stage implies the assessment of differences between the experiment and the analysis in the form of specifically developed criteria. Further the step by step problem of minimization is solved: in case of failure to achieve the minimum, the step of model parameters adjustment is defined; and the procedure of calculation with the specified parameters is repeated. After that the calculation findings are compared with the experiment again. Iterations continue until the minimum with the specified error is achieved. Comparing test results and the modified FEM are provided in tab. 4.

Under the results MAC for the FEM is calculated. The graphic result of calculation is provided in fig. 7.

As can be seen from fig. 4 and according to calculation with formula (2), the MAC value is 0.95. This result says that estimated and experimental modes correlate well between themselves, and therefore, describe one situation.

Table 3

Comparing of calculated and experimental data

Title	Test results		Calculation results	Δ, %
	Frequency values	With error		
f_x, Hz	34.12	35.83	29.98	12.13
		32.49		
f_y, Hz	5.00	5.25	5.08	1.5
		4.76		
f_z, Hz	5.53	5.08	5.13	7.23
		5.23		

Table 4

Comparing test results of "Express 100K" platform and modified FEM

Title	Test results		Calculation results	Δ, %
	Frequency value	With error		
f_x, Гц	34.12	35.83	32.09	5.92
		32.49		
f_y, Гц	5.00	5.25	5.02	0.40
		4.76		
f_z, Гц	5.53	5.08	5.41	2.16
		5.23		

Theoretical frequency Hz	Experimental frequency Hz		
32,09	0,95	0,51	0,48
5,41	0,21	0,91	0,34
5,02	0,11	0,57	0,89
	34,12	5,53	5,0

Fig. 7. MAC-identification of adjusted FEM and test results

Рис. 7. МАС-идентификация собственных частот колебаний откорректированной КЭМ

Conclusion. Thus, the given verification technique allows to make effective adjustment of spacecrafts FEM. The model received under verification results enables effective assessment of SC behaviour already at the design stage. It allows to halve the time on vibration tests and to accelerate preparation of a product for launch, confirming durability and resourcefulness with mathematical calculations.

References

1. Bezmozgii I. M., Sofinskii A. N., Chernyagin A. G. [Modeling vibration of spacecraft techniques]. *Kosmicheskaya technika i technologii.* 2014, No. 3 (6), P. 71–80 (In Russ.).

2. Solovieva T. I., Shatrov A. K. [Complex analyses of spacecraft dynamics]. *Vestnik SibGAU*. 2007, No. 2 (15), P. 201–206 (In Russ.).

3. Balyakov D. F. [Analyses of joint stiffness and natural frequencies of vibration system]. *Engineering and automation problems*. 2017, Vol. 2, No. 2, P. 75–82 (In Russ.).

4. Senashov S. I. Balyakov. D. F. [Spacecraft displacement simulation]. *Izvestiya VUZov. Aviacionnaya tehnika*. 2017, Vol. 59, No. 1, P. 55–60 (In Russ.).

5. Balyakov D. F., Egorov D. V., Shirokova N. N. [Verification and spacecraft design]. *Sbornik trudov X Vserossiiskoi konferencii studentov, aspirantov i molodyh ychenyh "Aktyalnye problem aviacii i kosmonavtiki"* [Proc. X conf. of student, postgraduate student and scientist "Actual problems of aviation and cosmonautics"]. Krasnoyarsk, 2014, P. 496–497.

6. Shimkovich D. G. *FEMAP & NASTRAN Injenernii analiz metodom konechnyh elementov* [FEMAP & NASTRAN Engineering analyses with finite element method]. Moscow, DMK Publ., 2008, 701 p.

7. Ilienko U. E., Kylakova K. P., Zuev N. N. [Oscillation and dynamics loads of launch vehicles and spacecraft]. *Technika vozdushnogo flota*. 1999, Vol. 5, No. 5, P. 24–34 (In Russ.).

8. Ruchkov S. P. *Modelirovanie konstrykcii v srede Femap with NX Nastran* [Costruction modelling in Femap with NX Nastran]. Moscow, DMK Publ., 2013, 784 p.

9. Bate N., Vilson E. *Chislennye metody analiza i metod konechnyh elementov* [Numerical method and finite-element method]. Moscow, Stroizdat Publ., 1982, 448 p.

10. Perelmuter F. V., Slivker V. I. *Raschetnye modeli sooruzheniy i vozmozhnost' ikh analiza* [Models of construction and analyses]. Moscow, DMK Publ., 2011, 709 p.

11. Rudakov K. N. *USG Femap 9.3. Geometricheskoe i konechnoelementnoe modelirovanie* [USG Femap 9.3. Geometrics and finite-element modeling]. Kiev, DMK Publ., 2009, 180 p.

12. Filin A. P. *Prikladnaya mehanika tverdogo deformiruemogo tela* [Mechanics of rigid body]. Moscow, Nauka Publ., 1981, 480 p.

13. Balyakov D. F. [Damping models of mechanic oscillation]. *Reshetnevskie chteniya Materialy XX Mezdynarodnoi konferencii* [Proc. XX Int. conf. "Reshetnevskie chteniya"]. Krasnoyarsk, 2016, P. 116–118 (In Russ.).

14. Senashov S. I. Balyakov D. F. [Identification of displacement] *Materialy VII Mezhdynarodnoi konferencii po matematicheskomy modelirovaniu* [Proc. VII Int. Conf. Of mathematics modeling]. Yakutsk, 2017, P. 152 (In Russ.).

15. Streng G. *Lineinaya algebra i ee primenenie* [Linear algebra]. Moscow, Mir Publ., 1980, 454 p.

Библиографические ссылки

1. Безмозгий И. М., Софинский А. Н., Чернягин А. Г. Моделирование задач вибропрочности конструкций ракетно-космической техники // Космическая техника и технологии. 2014. № 3(6). С. 71–80.

2. Соловьева Т. И., Шатров А. К. Комплексный подход к анализу динамического поведения спутников // Вестник СибГАУ, 2007. Вып. 2(15). С. 201–206.

3. Баляков Д. Ф. Влияние жесткости стыка на собственные частоты колебаний системы // Проблемы машиностроения и автоматизации. 2017. № 2. С. 75–82.

4. Сенашов С. И., Баляков Д. Ф. Моделирование перемещений конструкции космического аппарата // Известия вузов. Авиационная техника. 2017. № 1. С. 55–60.

5. Баляков Д. Ф., Егоров Д. В., Широкова Н. Н. Верификация как неотъемлемая часть проектирования космического аппарата. Сб. тр. X Всероссийской конференции студентов, аспирантов и молодых ученых «Актуальные проблемы авиации и космонавтики». Сиб. гос. аэрокосмич. ун-т. Красноярск. 2014. С. 496–497.

6. Шимкович Д. Г. FEMAP & NASTRAN, Инженерный анализ методом конечных элементов. М. : ДМК Пресс, 2008. 701 с.

7. Расчеты упругих колебаний и динамических нагрузок ракет-носителей космических аппаратов / Ю. Е. Ильенко, К. П. Кулакова, Н. Н. Зуев // Техника воздушного флота. 1999. № 5. С. 24–34.

8. Рычков С. П. Моделирование конструкций в среде Femap with NX Nastran. М. : ДМК Пресс, 2013. 784 с.: ил.

9. Бате Н., Вилсон Е. Численные методы анализа и метод конечных элементов. М. : Стройиздат, 1982. 448 с.

10. Перельмутер А. В., Сливкер В. И. Расчетные модели сооружений и возможность их анализа. М. : СКАД СОФТ, Ассоциация строительных вузов, ДМК Пресс, 2011. 709 с.

11. Рудаков К. Н. USG Femap 9.3. Геометрическое и конечно-элементное моделирование конструкций. Киев, ДМК Пресс, 2009. 180 с.

12. Филин А. П. Прикладная механика твердого деформируемого тела. М. : Наука, 1981. 480 с.

13. Баляков Д. Ф. Модели демпфирования механических колебаний / Д. Ф. Баляков // Решетневские чтения: материалы XX Междунар. конф. Красноярск, 10–14 ноября 2016 г. Красноярск, 2016. Вып. 20. Т. 2. С. 116–118.

14. Сенашов С. И. Особенности идентификации паразитных перемещений / С. И. Сенашов, Д. Ф. Баляков // Материалы VII Междунар. конф. по математическому моделированию. Якутск, 04–08 июля 2017 г. Якутск, 2017. Вып. 2, Т. 1. С. 152.

15. Стренг Г. Линейная алгебра и ее применения. М. : Мир, 1980. 454 с.

UDC 537.32

Siberian Journal of Science and Technology. 2018, Vol. 19, No. 1, P. 17–21

CALCULATION OF CHARACTERISTICS OF THERMOELECTRIC COOLING SYSTEM OF HEAT-LOADED ELEMENTS OF RADIO ELECTRONIC EQUIPMENT

E. N. Vasil'ev

Krasnoyarsk Science Centre SB RAS, Institute of Computational Modelling SB RAS
50/44, Akademgorodok, Krasnoyarsk, 660036, Russian Federation
E-mail: ven@icm.krasn.ru

Modern technologies make it possible to construct electronic devices that combine small sizes and high energy consumption, which requires the optimization of thermal modes. A promising direction to improve cooling intensity of the heat-loaded element (HLE) and precision of temperature control is applying thermoelectric modules (TEMs), which endow the heat release system with a cooling function, i. e., allow to reach temperatures of the HLE below ambient temperature. In the present paper, the processes of heat transfer in thermoelectric system of cooling and temperature control (TESCTC) are comprehensively considered. The temperature field in the capacity of heat-distributing plate (HDP), and influence of the heat flux inhomogeneity on the HLE temperature increase have been defined. The results of operating modes calculations, taking into account the heat-power release of HLE, performance of TEM, parameters of HDP and cooler, and magnitude of thermal resistance of thermal contacts have been presented. The calculation method allows to determine the temperature of HLE and to optimize TESCTC modes to achieve maximum cooling efficiency and lower energy consumption. It has been found that the optimal power supply current of TEM, corresponding to the modes with the maximum efficiency of cooling, depends on the thermal resistance of the heat sink system and the power of the heat load.

Keywords: thermoelectric module, heat mode, heat-loaded element, cooling system, thermal resistance.

Сибирский журнал науки и технологий. 2018. Т. 19, № 1. С. 17–21

РАСЧЕТ ХАРАКТЕРИСТИК ТЕРМОЭЛЕКТРИЧЕСКОЙ СИСТЕМЫ ОХЛАЖДЕНИЯ ТЕПЛОНАГРУЖЕННЫХ ЭЛЕМЕНТОВ РАДИОЭЛЕКТРОННОЙ АППАРАТУРЫ

Е. Н. Васильев

Красноярский научный центр СО РАН, Институт вычислительного моделирования СО РАН
Российская Федерация, 660036, г. Красноярск, Академгородок, 50/44
E-mail: ven@icm.krasn.ru

Современные технологии позволяют производить радиоэлектронные устройства, сочетающие малые размеры и высокое энергопотребление, что обостряет проблему обеспечения оптимальных тепловых режимов. Перспективным направлением для повышения интенсивности охлаждения теплонагруженного элемента (ТНЭ) и точности терморегулирования является применение термоэлектрических модулей (ТЭМ), которые наделяют теплоотводящую систему функцией охлаждения, т. е. дают возможность достигать температуры ТНЭ ниже значения внешней среды. Комплексно рассмотрены процессы теплообмена в термоэлектрической системе охлаждения и терморегулирования (ТЭСОТ). Определено температурное поле в объеме теплораспределяющей пластины (ТРП) и влияние неоднородности теплового потока на увеличение температуры ТНЭ. Представлены результаты расчета режимов работы с учетом мощности тепловыделения ТНЭ, рабочих характеристик ТЭМ, параметров ТРП и кулера, величины термических сопротивлений тепловых контактов. Расчетная методика позволяет определять температуру ТНЭ и проводить оптимизацию режимов ТЭСОТ с целью достижения максимальной эффективности охлаждения и снижения энергозатрат. Установлено, что оптимальная сила тока питания ТЭМ, соответствующая режимам с максимальной эффективностью охлаждения, зависит от термического сопротивления системы теплоотвода и мощности тепловой нагрузки.

Ключевые слова: термоэлектрический модуль, тепловой режим, теплонагруженный элемент, система охлаждения, термическое сопротивление.

Introduction. The resource, operational stability and operating characteristics of the heat-loaded elements (HLE) of radio-electronic equipment significantly depend on their temperature condition, so in case of increase in working temperatures from 20 to 60 °C equipment failure rates increase more than twice [1]. The perspective direction for cooling and temperature control of HLE is the use of thermoelectric modules (TEMs). Thermoelectric system of cooling and temperature control (TESCTC) possess a list of advantages in comparison with other cooling systems, namely: possibility of smooth temperature control in rather broad range by changing of value and direction of supply current TEM; minor thermal inertness; high reliability; absence of moving parts; compactness and small weight; quietness of operation. TESCTC are effectively used for cooling of both miniature objects and large volume refrigerators [2–6].

Construction and characteristics of the cooling system. HLE *1* is considered to be a TESCTC widespread type applied to cooling, construction with heat distributing plate (HDP) *2*, TEM *3* and a cooler *4* (fig. 1). HDP is necessary for alignment of thermal power distribution arriving from HLE on TEM surface. At the same time TEM performs the function of a thermal pump transferring heat from the cold side to the hot. The cooler removes the total thermal power produced by both HLE and TEM to the external environment. These elements of the system have thermal contacts on the boundaries. On the areas of contact surface A the cooler removes heat to the external environment having temperature T_0. The boundary of B corresponds to the contact surface of the cooler with the hot side of HLE which temperature is described by average value of T_2. The cold side of HLE (B surface) has average temperature of T_1. HLE seat (D surface) is characterized by average value of temperature T_e. In case of HLE suspension from the considered construction, the normal heat-eliminating system, which is widely applied to HLE cooling, for example, in the computer equipment, is widely used.

Typical options of temperature distributions which can be implemented in TESCTC are given in fig. 2. Ambient temperature T_0 is the original value directly influencing HLE seat temperature. For the normal heat-eliminating system temperature value T_e of HLE seat certainly exceeds T_0 value, increase in temperature is assured due to the temperature fluctuations caused by thermal resistance of HLE and cooler (line *4*). The negative temperature drop made by HLE allows to reduce temperature T_e, which in this case can either exceed value of T_0 (line *2*), or be lower than this value (line *1*). Under certain conditions influence of own heat release of HLE can on the contrary lead to its additional heating (line *3*), not cooling. When analyzing efficiency of HLE cooling, basic operating characteristics of HLE are used; they can be calculated [7] or received from the vendor. In the present research the influence of HDP thermal resistance, cooler and thermal contacts on characteristics of thermoelectric cooling and HLE temperature are studied. HLE temperature is determined by the ambient temperature and the sum of temperature drops of all construction elements. During calculations temperature drops were calculated gradually at first in configuration "TEM-cooler", then in HDP in terms of thermal influence of HLE and TEM. The analysis of TESCTC characteristics is carried out on the example of serial TEM of NPO "Kristall".

Temperature calculation of the heat-loaded element. Values and temperature drop ratio depend on operating characteristics and parameters of all TESCTC construction elements and their cross impact [8–11]. In TESCTC in case of heat exchange of TEM with an external environment from its hot side, it is necessary to remove the total thermal power developed by HLE and TEM, which is, as a rule, considerably higher than HLE power due to rather low refrigerating coefficient of TEM. It causes the corresponding growth of temperature drop on thermal contacts and the cooler, which, as a result, leads to lowering of cooling efficiency. The difference of temperatures ΔT_0 between the cold side of TEM and the environment is determined from expression [11]

$$\Delta T_0 = T_1 - T_0 = R_s(Q+W) - \Delta T_{\text{TEM}} = \\ = R_s Q + R_s U(I,Q)I - \Delta T_{\text{TEM}}(I,Q),$$

here T_1, T_0 – temperature values of the hot side TEM and environment; R_s – total thermal resistance of the cooler and its thermal contact with TEM; Q, W – heat release capacities of HLE and natural energy consumption of TEM; $\Delta T_{\text{TEM}} = T_2 - T_1$ – temperature drop between the cold and hot sides of TEM; U, I – power and current intensity of power supply of TEM. Operating characteristics of TEM from the manufacturer $Q(\Delta T_{\text{TEM}})$ and $U(\Delta T_{\text{TEM}})$ are basic data for dependences determination $U(I, Q)$ and $\Delta T_{\text{TEM}}(I, Q)$ and further calculation ΔT. The method of dependences calculation is presented in [10; 11].

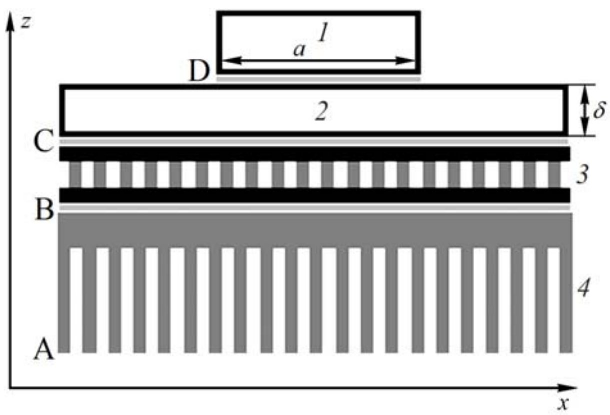

Fig. 1. Thermoelectric cooling system

Рис. 1. Схема термоэлектрической системы охлаждения

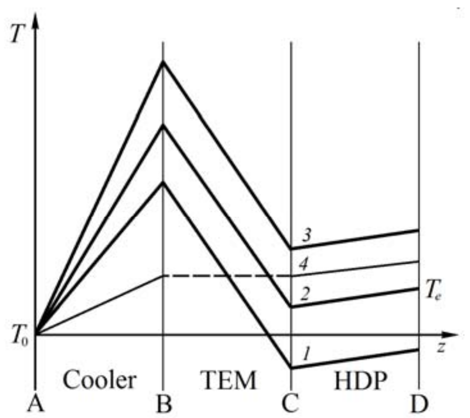

Fig. 2 Temperature distribution in the cooling system

Рис. 2. Распределение температуры в системе охлаждения

Dependences of the cold side temperature drops of TEM and the environment on the power consumption under Q = 40 W and R_s = 0.1, 0.3 and 0.5 K/W are presented in fig. 3 for TEM "S–127–14–11" (solid lines) and "S–199–14–11" (broken lines), having maximum refrigerating values 79.3 and 124.2 W. Negative values ΔT_0 correspond to the modes, in which cold side temperatures of TEM are lower than ambient temperature. Temperature drop values ΔT_0 considerably depend on R_s, variation interval of values ΔT_0 for the fixed W within the range of R_s = 0–0.5 K/W averages at about 55–60 °C. For the given dependencies presence of least values is typical. This least values correlate with the best values of energy consumption W, under which the maximum cooling of HLE can be achieved. When increasing R_s from 0.1 to 0.5 K/W these values W fall from 103 W to 38 W for TEM "S–127–14–11" and from 120 W to 37 W for TEM "S–199–14–11".

For temperature drop losses in HDP measurement mathematical model based on numerical solution of the three-dimensional equation of heat conduction is used with regard to the load characteristic of TEM:

$$c_v \rho \frac{\partial T}{\partial t} = \lambda \left(\frac{\partial^2 T}{\partial x^2} + \frac{\partial^2 T}{\partial y^2} + \frac{\partial^2 T}{\partial z^2} \right),$$

where c, ρ, λ – specific heat capacity, density and heat conduction coefficient of material; T – temperature; t – time; x, y, z – spatial coordinates. Values c, ρ and λ in all estimated area had constant values corresponding to copper. HDP sizes were equal in cross x and y directions were equal to TEM 40×40 мм^2 overall dimensions, in z direction its thickness δ varied. The HLE seat was set in the center of HDP's upper surface in the form of a square with side a. On the upper and lower boundaries of HDP inhomogenuity of heat fluxes, caused by influence of HLE and TEM was considered. To solve this equation the method of total approximation with splitting of the task into spatial coordinates [12] was applied.

Based on calculations distributions of temperature HDP with different values of its thickness δ and HLE size a were obtained. The integral parameter characterizing heat-transmitting ability of HDP is the thermal resistance of R. Quantitative thermal resistance is calculated as the relation of average temperatures of HLE seat difference and the bottom surface of HDP to the transferred thermal power, where time value R depends both on heat conduction of HDP material and HLE and HLE sizes. Dependences R on thickness of copper HDP are shown in fig. 4 for different values a, curves *1*, *2*, *3*, *4* and *5* correspond to values 22.5, 17.5, 12.5, 7.5 and 2.5 of mm. Based on values of thermal resistance R and power of heat release of HLE, Q value of temperature drop on HDP is defined by the expression $\Delta T_{\text{HDP}} = RQ$. The figure shows that the range of best values δ makes approximately from 3 mm where a = 22.5 mm up to 5 mm where a = 2.5 mm. Optimization of HDP parameters allows to minimize temperature drop and as a result to reduce HLE temperature. Besides, calculations proved that inhomogenuity of the temperature field of TEM cold side leads to essential increase in thermal resistance of HDP compared to the case of isothermal heat-eliminating surface [13; 14]. This increase R is explained by the increase in average length of heat transmission in HDP capacity, caused by lower values of temperature on TEM edges. Lowering thermal resistance value and losses of HDP temperature drop can be assured by applying materials with higher coefficient of heat conduction or hyper heat-conducting plates (plane thermal pipes) in which high effective heat conduction is reached due to phase transformations of the heat carrier in case of movement in the porous environment [15; 16].

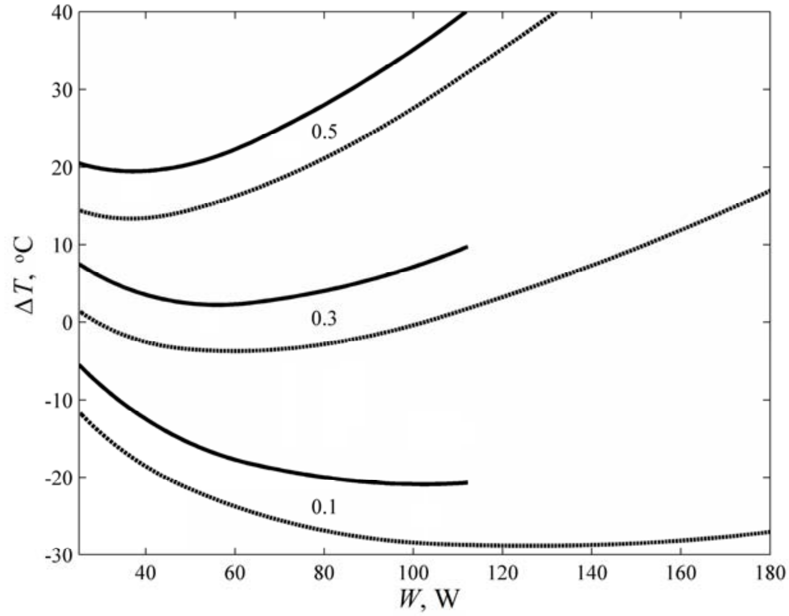

Fig. 3. Dependences of the TEM cold side temperature drops and the environment on the power consumption under Q = 40 W and various values of R_s

Рис. 3. Зависимости разности температур холодной стороны ТЭМ и окружающей среды от потребляемой мощности при Q = 40 W и различных значениях R_s

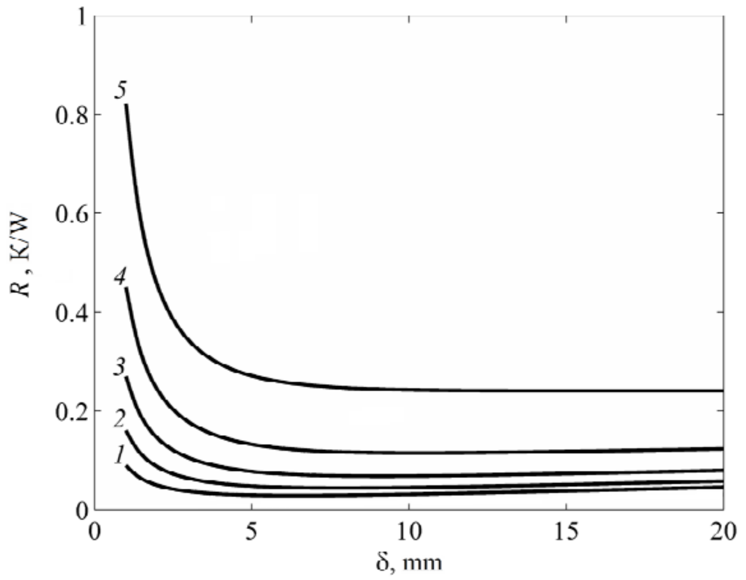

Fig. 4. Dependencies $R(\delta)$ for the cooper HDP, curves *1*, *2*, *3*, *4* and *5* correspond to a = 22.5, 17.5, 12.5, 7.5 and 2.5 mm

Рис. 4. Зависимости $R(\delta)$ для медной ТРП, кривые *1*, *2*, *3*, *4* и *5* соответствуют a = 22.5, 17.5, 12.5, 7.5 и 2.5 мм

Thus, the considered two-step algorithm allows to calculate HLE temperature. At the first stage temperature of the TEM cold side is determined by calculation of total temperature drop in the "cooler – TEM" system with regard to the HLE thermal power, operating characteristics of TEM, cooler thermal resistance and thermal contacts, ambient temperature. Then temperature drop in HDP is calculated and based on HDP temperature distribution on the upper boundary of HDP with regard to the thermal resistance of heat contact on its seat, foundation temperature is determined. Final expression for average temperature of HLE seat calculation has the following appearance

$$T_e = T_0 + \Delta T_0 + RQ.$$

Under the known internal thermal resistance of HLE (information of the vendor) its influence is considered the same way, herewith the temperature of the semiconductor crystal, located in the HLE case, will be defined.

Conclusion. In the present paper heat exchanging processes in TESCTC are considered; the algorithm allowing to carry out calculation of HLE temperature and TESCTC modes optimization to increase cooling efficiency of HLE and lowering of TEM energy consumption are provided. It is stated that the value of effective power consumption of TEM corresponding to the modes with maximum cooling efficiency depends on the thermal resistance of the cooler and power of HLE heat release.

Acknowledgments. This study was supported by the Russian Foundation for Basic Research, administration of the Krasnoyarsk Territory, and Krasnoyarsk Territory foundation supporting scientific research activity (project No. 16-41-242104).

Благодарности. Исследование выполнено при финансовой поддержке Российского фонда фундаментальных исследований, Правительства Красноярского края, Красноярского краевого фонда поддержки научной и научно-технической деятельности в рамках научного проекта № 16-41-242104.

References

1. Nenashev A. P. *Konstruirovanie radioelektronnykh sredstv* [Designing of radio-electronic means]. Moscow, Vysshaya Shkola Publ., 1990, 432 p. (In Russ.).

2. Chang Y. W., Chang C. C., Ke M. T., Chen S. L. Thermoelectric air-cooling module for electronic devices. *Applied Thermal Engineering*. 2009, Vol. 29, No. 13, P. 2731–2737.

3. Huang H. S., Weng Y. C., Chang C. C., Chen S. L., Ke M. T. Thermoelectric water-cooling device applied to electronic equipment *International Communications in Heat and Mass Transfer*. 2010, Vol. 37, No. 2, P. 140–146.

4. Zhu L., Tan H., Yu J. Analysis on optimal heat exchanger size of thermoelectric cooler for electronic cooling applications. *Energy conversion and management*. 2013, Vol. 76, P. 685–690.

5. Gladushchenko V. N., Derevyanko V. A., Vasil'ev E. N. et al. [Thermoelectricity in engineering problems of the modern technology of cooling]. *Elektronnye i elektromekhanicheskie sistemy i ustroistva* [Electronic and electromechanical systems and devices]. Tomsk, AO NPC Polus Publ., 2016, P. 177–183 (In Russ.).

6. Derevyanko V. A., Gladushchenko V. N., Vasil'ev E. N. et al. *Termoelektricheskiy blok okhlazhdeniya* [Thermoelectric cooling module]. Patent RF, no. 2511922, 2014.

7. Vasil'ev E. N. [Mathematical Model for the Calculation of the Characteristics of the Cooling Thermoelectric Modules]. *Journal of Siberian Federal University. Engineering & Technologies.* 2015, Vol. 8, No. 8, P. 1017–1023 (In Russ.).

8. Vasil'ev E. N., Derevyanko V. A. [Calculation of thermoelectric modules efficiency for radio electronic components cooling]. *Materialy XX Mezhdunar. nauch. konf. "Reshetnevskie chteniya*" [Materials XVII Intern. Scientific. Conf "Reshetnev reading"]. Krasnoyarsk, 2013, P. 211–213 (In Russ.).

9. Vasil'ev E. N., Derevyanko V. A. [Analysis of thermoelectric modules efficiency in cooling systems]. *Vestnik SibGAU*. 2013, No. 4(50), P. 9–13 (In Russ.).

10. Vasil'ev E. N. Calculation and Optimization of Thermoelectric Cooling Modes of Thermally Loaded Elements. *Technical Physics*. 2017, Vol. 62, No. 1, P. 90–96.

11. Vasil'ev E. N. Optimization of Thermoelectric Cooling Regimes for Heat-Loaded Elements Taking into Account the Thermal Resistance of the Heat-Spreading System. *Technical Physics.* 2017, Vol. 62, No. 9, P. 1300–1306.

12. Samarskii A. A. *Teoriya raznostnykh skhem* [The theory of difference schemes]. Moscow, Nauka Publ., 1989, 616 p. (In Russ.).

13. Glinskii I. A., Zenchenko N. V. Computer simulation of the heat distribution element for high power microwave transistors. *Russian Microelectronics*. 2015, Vol. 44, No. 4, P. 236–240.

14. Semenyuk V. A., Bezverkhov D. B. Modeling and Minimization of Intercascade Thermal Resistance in Multi-Stage Thermoelectric Cooler. Proc. of the XVI Int. Conf. on Thermoelectrics. Dresden, Germany, 1997, IEEE, P. 701–704.

15. Vasil'ev E. N., Derevyanko V. A., Kosenko V. E. et al. [Computational modeling of heat exchange in thermoregulation systems of space vehicle]. *Vychislitel'nye tekhnologii*. 2009, Vol. 14, No. 6, P. 19–28. (In Russ.).

16. Vasil'ev E. N., Nikiforova E. S. [Mathematical model of heat exchange processes in honeycomb panels with heat pipes]. *Vestnik SibGAU*. 2005, No. 3, P. 23–26 (In Russ.).

Библиографические ссылки

1. Ненашев А. П. Конструирование радиоэлектронных средств. М. : Высш. школа, 1990. 432 с.

2. Thermoelectric air-cooling module for Chang electronic devices / Y. W. Chang [et al.] // *Applied Thermal Engineering*. 2009. Vol. 29, No. 13, P. 2731–2737.

3. Thermoelectric water-cooling device applied to electronic equipment / H. S. Huang [et al.] // *International Communications in Heat and Mass Transfer.* 2010. Vol. 37, No. 2. P. 140–146.

4. Zhu L., Tan H., Yu J. Analysis on optimal heat exchanger size of thermoelectric cooler for electronic cooling applications // *Energy conversion and management*. 2013. Vol. 76. P. 685–690.

5. Термоэлектричество в инженерных задачах современной техники охлаждения / В. М. Гладущенко [и др.] // Электронные и электромеханические системы и устройства. Томск : АО «НПЦ «Полюс». 2016. С. 177–183.

6. Пат. 2511922 Российская Федерация, МПК^7 F 25 B 21/02. Термоэлектрический блок охлаждения / Деревянко В. А., Гладущенко В. М., Васильев Е. Н. и др. № 2012142405/06 ; заявл. 04.10.2012 ; опубл. 10.04.2014, Бюл. № 10.

7. Васильев Е. Н. Математическая модель для расчета характеристик термоэлектрических модулей охлаждения // Журнал Сиб. федер. ун-та. Сер. «Техника и технология». 2015. Т. 8. № 8. С. 1017–1023.

8. Васильев Е. Н., Деревянко В. А. Расчет эффективности термоэлектрических модулей для охлаждения радиоэлектронных элементов // Решетневские чтения : материалы XVII Междунар. науч. конф. (12–14 нояб. 2013, г. Красноярск) / под общ. ред. Ю. Ю. Логинова ; Сиб. гос. аэрокосмич. ун-т. Красноярск, 2013. Т. 1. С. 211–213.

9. Васильев Е. Н., Деревянко В. А. Анализ эффективности применения термоэлектрических модулей в системах охлаждения радиоэлементов // Вестник СибГАУ. 2013. № 4(50). С. 9–13.

10. Васильев Е. Н. Расчет и оптимизация режимов термоэлектрического охлаждения теплонагруженных элементов // Журнал технической физики. 2017. Т. 87, № 1. С. 80–86.

11. Васильев Е. Н. Оптимизация режимов термоэлектрического охлаждения теплонагруженных элементов с учетом термического сопротивления теплоотводящей системы // Журнал технической физики. 2017. Т. 87, № 9. С. 1290–1296.

12. Самарский А. А. Теория разностных схем. М. : Наука, 1989. 616 с.

13. Глинский И. А., Зенченко Н. В. Расчет теплораспределяющего элемента конструкции для мощных СВЧ-транзисторов // Микроэлектроника. 2015. Т. 44, № 4. С. 269–274.

14. Semenyuk V. A., Bezverkhov D. B. Modeling and Minimization of Intercascade Thermal Resistance in Multi-Stage Thermoelectric Cooler // Proc. of the XVI Inter. Conf. on Thermoelectrics. Dresden, Germany, 1997, IEEE. P. 701–704.

15. Вычислительное моделирование процессов теплообмена в системах терморегулирования космических аппаратов / Е. Н. Васильев [и др.] // Вычислительные технологии. 2009. Т. 14, № 6. С. 19–28.

16. Васильев Е. Н., Никифорова Е. С. Математическое моделирование теплового режима гипертеплопроводного радиатора мощного радиоэлемента // Вестник СибГАУ. 2005. Вып. 3. С. 23–26.

UDC 621.397.6

Siberian Journal of Science and Technology. 2018, Vol. 19, No. 1, P. 22–26

CAMERA-TO-TOUCHSCREEN DESIGN

R. W. Likhonina*, L. Kohout, J. Kadlec

The Czech Academy of Sciences, Institute of Information Theory and Automation
Pod Vodárenskou věží 4, CZ-182 08, Prague 8, Czech Republic
*E-mail: likhonina@utia.cas.cz

The present paper describes an FPGA design of a camera-to-touchscreen demonstrator that has been prepared using Xilinx Vivado 2015.2 and SDK 2015.2 tools. The demonstrator consists of MicroZed 7020 Carrier Board, Avnet 7-inch Zed Touch Display and Avnet Toshiba Industrial 1080P60 Camera Module. The camera transmits a full HD video signal at 60 frames per seconds to MicroZed 7020 board, which processes it and sends to the LCD display with active area of 800×480 pixels. As the display has smaller resolution, only a fragment of the whole video frame can be seen at once on the display, whereas the full image is stored in the memory. By touching the screen one can travel along the stored video frame and look through the whole image. The design can be used, for example, as a car rear view mirror monitor benefiting from touchscreen technologies.

Keywords: Zynq, FPGA, touchscreen display, camera, full HD, SDSoC.

Сибирский журнал науки и технологий. 2018. Т. 19, № 1. С. 22–26

ПРОЕКТНОЕ РЕШЕНИЕ ПЕРЕДАЧИ ВИДЕОСИГНАЛА С FULL HD КАМЕРЫ НА WVGA СЕНСОРНЫЙ ДИСПЛЕЙ

Р. Н. Лихонина*, Л. Когоут, И. Кадлец

Академия наук Чешской Республики, Институт теории информации и автоматизации
Чешская Республика, CZ-182 08, Прага 8, Pod Vodárenskou věží, 4
*E-mail: likhonina@utia.cas.cz

Описывается проектное решение передачи сигнала с камеры на сенсорный дисплей. Данное решение разработано на основе ППВМ-технологии с использованием программного обеспечения Xilinx Vivado 2015.2 и SDK 2015.2. Демонстратор, представленный в работе, включает плату-носитель MicroZed 7020, 7-дюймовый сенсорный дисплей от компании Avnet и промышленную камеру Toshiba 1080P60 от компании Avnet. Камера передает full HD видеосигнал со скоростью 60 кадров в секунду на плату MicroZed 7020, которая обрабатывает видеосигнал и посылает его на ЖК-дисплей с активной площадью 800×480 пикселей. Поскольку разрешение дисплея меньше, чем разрешение камеры, на дисплее отображается только фрагмент целего видеокадра, тогда как полное изображение сохраняется в памяти на плате. Просмотреть целое изображение возможно, перемещаясь по сенсорному экрану при помощи касания, просматривая отдельные фрагменты изображения. Данное проектное решение может быть использовано, например, в качестве монитора заднего вида в автомобиле, тем самым извлекается польза из сенсорных технологий.

Ключевые слова: Zynq, ППВМ, сенсорный дисплей, камера, full HD, SDSoC.

Introduction. Touchscreen technology has steadily come into our life. It is hard to imagine that only a few decades ago it was something unattainable. From the first finger-driven touchscreens invented by E. A. Johnson in 1965 and development of resistive and capacitive touchscreens to the latest optical touchscreen technology based on detection of an object's shadow, it did not passed much time [1; 2]. However, the rapid development of touchscreen technologies due to a large interest in this area is obvious. There is a growing number of devices that benefit from it: smartphones, tablets, computer monitors, eBook readers, game devices, GPS navigators etc. The touchscreens are foreseen to be used also in home appliances. The researchers continue working on the touchscreens that will use so called "microfluid" technology, where buttons rise up due to the fluid pressure on the covered layer when the keypad is in use [2].

The present paper aims at describing a field-programmable gate array (FPGA) design, which demonstrates one of the applications the touchscreen technology can be used for.

The design is based on two demonstrators available at Avnet's webpages. The first one, Toshiba TCM3232PB Frame Buffer Design Tutorial, shows the reference design for using Toshiba camera and getting the HDMI output. It describes step-by-step process how to setup the Toshiba camera module and run a simple design that initializes the image sensor and HDMI output interface and implements a frame buffer in the programmable logic (PL) I/Os [3].

The second design is ALI3 Display Reference Design demonstrating the capabilities of touchscreen display and presenting simple interactive GUIs, which can serve as a start point for more complex applications [4].

However, there is no design available at Avnet, which would send a video stream from camera to a display with touchscreen capabilities, so that an end-user could provide some actions with an image he/she sees on the display.

This work is aimed at combining two example designs from Avnet mentioned above in a way that it would be possible to receive a cropped image from Full HD camera on a WVGA display and observe the whole scene by moving the image, thus, benefiting from touchscreen technology.

Briefly speaking the present design illustrates how to get a video signal from a full HD camera (1920×1080 pixels) to WVGA LCD display with an active area of 800×480 pixels. A video frame is transmitted by the camera at 60 fps with pixel clock 148.5 MHz to MicroZed 7020 board. The board processes the signal and sends it to the LCD display working at pixel clock 33.33 MHz. The output signal is in RGB format. The smaller display resolution results in video cropping. Thus, only a fragment of the whole frame is seen on the display, whereas the full image is stored in the memory. By touching the screen one can move the image and look through the whole picture.

The scene of interest can be then zoomed if extending the presented design with two finger interaction and zoom capabilities. The design can be used as a car rearview mirror or for home door entry applications.

Moreover, it is worth to note that the camera-to-touchscreen design benefits from FPGA technology. FPGA is an integrated circuit enabling a designer to configure it after its manufacturing. It is widely used in common embedded applications. To create an FPGA design, Xilinx tools – Vivado 2015.2 for a hardware part and SDK 2015.2 for the software – are required.

Methodology. The camera-to-touchscreen design described in the paper is created using the following HW components:

1. MicroZed Embedded Vision Carrier Card and MicroZed 7020 board with a processing system with two Cortex A9 cores and a 28 nm programmable logic. It includes two DDR3 memory components totaling 1GB of random access memory [3; 4].

2. Avnet Toshiba TCM3232PB full HD color image sensor capable of delivering a video signal at 60 fps. Two technologies are implemented there: High Dynamic Range (HDR) technology and Color Noise Reduction (CNR) technology [3].

3. Avnet 7-inch WVGA TFT-LCD display with an industrial projective capacitive touch sensor. The display has an active area of 800×480 pixels, frame rate of 60 Hz, pixel rate of 33.33 MHz and pixel format 24 bits RGB [4].

The hardware design is prepared in Xilinx Vivado 2015.2. This software is purposed for synthesis and analysis of HDL designs and suitable for system on a chip (SoC) development as well as for high-level synthesis, which enables C, C++ and SystemC programs to be directly targeted into Xilinx devices without manually creating RTL.

Using IP Integrator and a list of available IP cores the hardware design has been created. The IP cores used in the design are shown in fig. 1.

The camera sends frames coded in Bayer matrix, received by TCM receiver at 24 MHz. These frames pass through Color Filter Array Interpolation (CFA) and Color Correction Matrix (CCM) blocks.

CFA aims at reconstructing the missing color components of an image obtained from an RGB or CMY Bayer filtered sensor by means of interpolations using information from neighboring pixels. This process is called CFA demosaicing [5]. In the present design it also converts a video signal to RGB color space.

CCM is used for adjusting white balance, color, brightness or contrast in an image. It multiplies the pixel values with some coefficients, which strengthen or weaken them. Mathematically it is expressed as a 3×3 matrix multiplication. The weights in equation define a color-correction matrix. The example of color-correction matrix for RGB data can be seen below. For more information refer to [6].

$$\begin{bmatrix} R_C \\ G_C \\ B_C \end{bmatrix} = \begin{bmatrix} K_{11} & K_{12} & K_{13} \\ K_{21} & K_{22} & K_{23} \\ K_{31} & K_{32} & K_{33} \end{bmatrix} \begin{bmatrix} R \\ G \\ B \end{bmatrix} + \begin{bmatrix} O_1 \\ O_2 \\ O_3 \end{bmatrix},$$

where R_C, G_C, B_C are corrected colors for RGB input data; K_n are weights; O_n are offsets used for achieving black levels [6].

Video Direct Memory Access (VDMA) writes to and results from DDR3 24-bit RGB frames. This core provides handling three frame buffers with internal lock between them to avoid image tearing. VDMA output is sent to Video Out block to map video data on output timing coming from Video Timing Controller (VTC). ALI3 Controller passes the video signal through physical interface to display with 33 MHz pixel clock. Communication between the blocks runs at clock rate of 150 MHz, while peripheral configurations use 100 MHz clock speed. The Zynq processing system performs the whole video chain initialization. The image processing operations are fulfilled outside the processor. It contributes to fast functioning of the system. To detect touches on display the system uses interrupts. The interrupt routine analyzes it and performs appropriate actions (a video frame shift in certain direction on the display).

The next step after finishing the design is to validate it. The validation process helps to find the errors in the design that could prevent the hardware from working properly. The most frequent errors can appear in connections between blocks or in parameter settings for individual blocks.

If validation is successful, then so called HDL (Hardware Description Language) wrapper can be generated. It is basically a top-level description of the system. The synthesis process in its turn will generate all source files for the IP blocks as well as any relevant constraints files.

After design implementation, i. e. placing and routing the netlist onto the FPGA device resources, and generation of a bitstream file with configuration data for implementation in the PL, the building of the hardware image is complete and the hardware platform can be exported to SDK (Software Development Kit) environment, where different software applications can be created.

As a basis for software development of camera-to-touchscreen application the previously mentioned designs from Avnet are used [3; 4].

Results. The complete camera-to-touchscreen demo kit can be seen in fig. 2 [7]. Its components are the same as it was described in previous chapters.

The resultant software is programmed in such a way, that it enables to transfer a full HD image from TCM receiver to touchscreen LCD display with resolution 800×480 pixels at frame rate 60 fps. By touching the screen we can see the whole picture part by part. After interrupt occurs, the processor knows that a touch event has taken place and evaluates the concurrent touch events in a way, that it saves X and Y coordinates of two concurrent events, and makes subtraction: $X = X2 - X1$, resp. $Y = Y2 - Y1$. If there is 0 for some axis, then there will be no movement in this direction. If X is a non-zero variable, the image will move for 40 pixels left or right depending on a variable sign. The same is valid for Y, but the shift is down/up. The directions of movement are similar one has in his touchscreen mobile phone [7]. The number of pixels for moving in each direction has been taken optionally after testing image incremental movement. The chosen number is optimal for demonstrating the capabilities of the design, but it can be changed if necessary. The example of the camera-to-touchscreen demo functioning is shown in fig. 3.

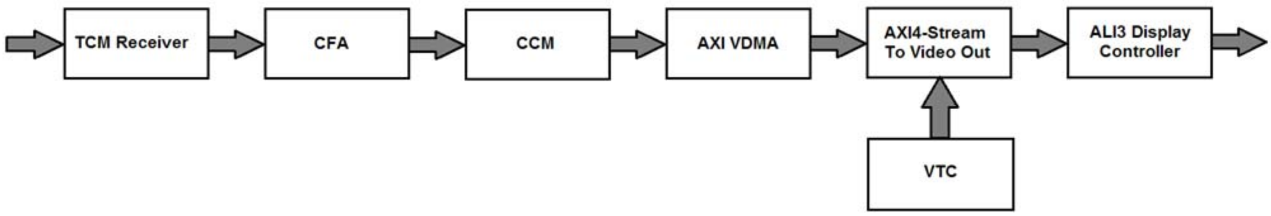

Fig. 1. Hardware block diagram

Рис. 1. Диаграмма аппаратного блока

Fig. 2. Complete camera-to-touchscreen demo kit

Рис. 2. Демонстрационный вариант Full HD камеры

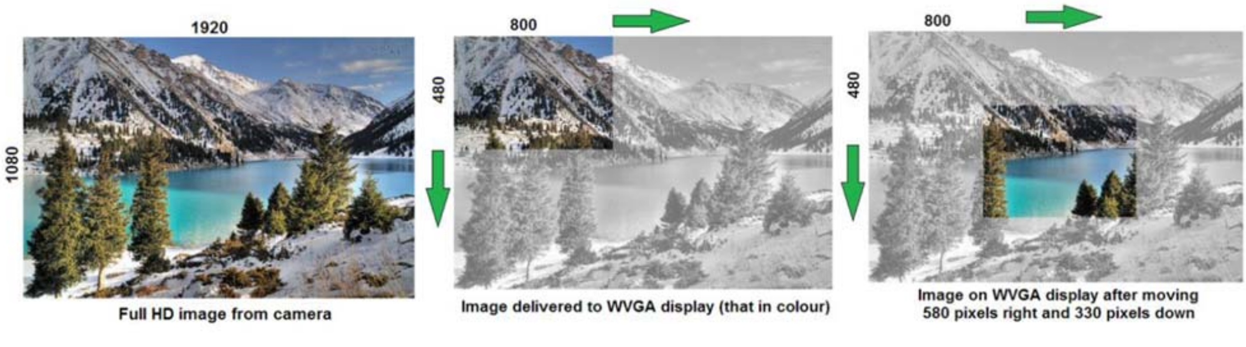

Fig. 3. Example of SW application

Рис. 3. Пример применения программного обеспечения

Discussion. The present design demonstrates a camera-to-touchscreen technology, which can be used for different applications.

It can be complemented with more sophisticated designs such as face detection, vehicle recognition, edge detection, optical flow designs and many others. For these purposes the SDSoC (Software-Defined System On Chip) environment is a good tool to use.

The SDSoC is a system compiler, which targets a base platform and is capable to compile C/C++ functions into programmable logic. The system compiler works one level above the Vivado HLS compiler. After analyzing a program and determining the data flow between software and hardware functions, it generates an application specific SoC including a complete boot image with firmware, operating system, and application executable. Compilation itself is performed by the Xilinx HLS compiler. HLS compiles the transformed C/C++ to the HDL code. The HDL code and the corresponding cores are automatically packed into the IP-XACT format and serve as input for Vivado IP integrator. The Xilinx SDSoC environment also automatically generates compatible data-mover IP-cores and the interface IP-cores for the programmable logic part of the ZYNQ device. This can result in automated generation of new SoC system with new HW accelerators, which replace the original SW based system. It can reduce the energy per pixel in case of video processing algorithms [8].

It is also worth to note that the SDSoC system includes OpenCV libraries, which comprise different mathematical functions such as Gaussian, Median, Bilateral, Canny edge detection, SVM, LK Optical Flow and etc. [9]

Moreover, there is still a space for improvements and optimization for the presented design. One of the directions for improvement is to solve the problem of a false touch event registration, which was not fully managed in the present demonstrator. Though the design functions satisfactory for demonstration purposes, in future it would be desirable to get rid of these errors by making more precise calibration and, perhaps, by implementing some additional filtering.

Besides, the display supports two finger touches and gesture recognition. It means that there is a possibility to use the image scaling in a way we are used to making it in our mobile phones. This function could be a useful extension of the presented demonstrator bringing further benefits for some applications including, e. g., home entry systems or car in-cabin systems.

There are also other possibilities, which can be profitable for some applications. For example, it is possible to connect one more block, on Screen Display block, in the hardware design, that enables alpha blending and composition of external video inputs. It supports several layers, so the user can configure multiple input video sources. Each video source layer can be displayed at different cropped sizes, positions, and transparency [10].

Conclusion. The present paper describes camera-to-touchscreen-display design, which allows getting a full HD image from camera module and sends it to 800×480 display, so that on display there is only a part of the whole image, but the full image is stored in memory. We can see the whole image part by part by touching display and so moving the image right/left or/and up/down. The mathematical models are a part of system generation process and are hidden in the separate blocks of the design. The design can be also complemented with complex mathematical functions for edge detection, optical flow or image recognition applications using the SDSoC environment, which compiles C/C++ functions for the target platform.

The present design is based on two original designs for the camera and for the display from Avnet, Inc. However, the Avnet's designs do not allow getting the image from camera to display and move along it as it was described in the present article.

In this paper the principle of design was presented in more details. Besides, this paper summarizes the strengths and drawbacks of the design, and names some other possibilities and space for improvements as, for example, to get rid out of false detection of touch events, to add an image scaling or even to use On Screen Display and benefit from several layers for multiple input video sources, to use complex algorithms for edge detection and image recognition capabilities and etc.

Such kind of displays can be used as a car rear viewer with more functionality or, for example, in home entry systems. The application field of such displays can be quite broad and is not limited by above mentioned examples. There is a space for engineers' imagination.

Acknowledgements. This work has been supported from project ALMARVI, project number ARTEMIS JU 621439, MSMT 7H14004.

Благодарности. Работа выполнена при поддержке грантов: проект ALMARVI, проект ARTEMIS JU 621439, MSMT 7H14004.

References

1. Types of Touch Screen Technologies. Baanto. Available at http://baanto.com/types-of-touch-screen-technologies (accessed 05.03.2017).

2. Ion F. The past, present, and future of touch: From touch displays to the Surface: A brief history of touchscreen technology. ARSTechnica. 2013, P. 1–3. Available at http://arstechnica.com/gadgets/2013/04/from-touch-displays-to-thesurface-a-brief-history-of-touchscreen-technology/1/ (accessed 05.03.2017).

3. Toshiba Industrial 1080P60 Camera Module: Getting Started Guide. Avnet Electronics, 2015, Version 1.2, P. 4–12. Available at https://zedboard.org/content/getting-started-guide-3 - 2 (accessed 10.03.2017).

4. MicroZed Embedded Vision Carrier (EMBV): ALI3 Display Reference Design and Tutorial. Avnet Electronics. 2015, Version 2014.4, P. 1–4. Available at http://zedboard.org/product/microzed-embedded-vision-kits (accessed 10.03.2017).

5. Color Filter Array Interpolation v7.0. LogiCORE IP Product Guide. Xilinx. 2015, PG002, P. 4–7. Available at http://www.xilinx.com/support/documentation/ipdocumentation/vcfa/v70/pg002vcfa.pdf (accessed 11.03.2017).

6. Color Correction Matrix v6.0. LogiCORE IP Product Guide. Xilinx. 2015, PG001, P. 4–6. Available at http://www.xilinx.com/support/documentation/ipdocumentation/vccm/v60/pg001vccm.pdf (accessed 11.03.2017).

7. Likhonina R., Kohout L., Kadlec J. Camera to Touchscreen Demonstration for MicroZed 7020 carrier board, Avnet 7-inch Zed Touch Display and Avnet Toshiba Industrial 1080P60 Camera Module. Czech Acad Sci, Inst Inform Th & Autom, 2016, P. 3–9.

8. Kadlec J., Pohl Z., Steven van der Vlugt, Jääskeläinen P., Koskinen L. Algorithms, Design Methods, and Many-Core Execution Platform for Low-Power Massive Data-Rate Video and Image Processing. Almarvi, 2016, P. 45–46.

9. SDSoC Environment User Guide. Xilinx. 2017, UG1027 (v2017.2), P. 6–9. Available at https://www.xilinx.com/cgi-bin/docs/rdoc?v=2017.2;d=ug1027-sdsoc-user-guide.pdf (accessed 15.08.2017).

10. Video On-Screen Display v6.0. LogiCORE IP Product Guide. Xilinx. 2015, PG010, P. 4–7. Available at http://www.xilinx.com/support/documentation/ipdocumentation/vosd/v60/pg010vosd.pdf (accessed 15.03.2017).

UDC 539.3

Siberian Journal of Science and Technology. 2018, Vol. 19, No. 1, P. 27–36

MULTIGRID FINITE ELEMENTS IN THE CALCULATIONS OF MULTILAYER CYLINDRICAL SHELLS

A. D. Matveev[1*], A. N. Grishanov[2]

[1]Institute of Computational Modeling
50/44, Akademgorodok, Krasnoyarsk, 660036, Russian Federation
[2]Novosibirsk State Technical University
20, Karl Marx Av., Novosibirsk, 630073, Russian Federation
[*]E-mail: mtv241@mail.ru

An effective numerical method for calculating linearly elastic multilayer cylindrical shells under static loading implemented on the basis of Finite Element Method (FEM) procedures using the multilayer curved Lagrangian multigrid finite elements (MFE) of the shell type was proposed. Such shells are widely used in rocket-space and aircraft engineering. MFE are developed in local Cartesian coordinate systems based on small (basic) shell partitions that take into account their heterogeneous structure, irregular shape, combined loading and fixing. The stress strained state (SSS) in the MFE was described by the equations of the three-dimensional elasticity problem without using the additional kinematical and static hypotheses, which allow one to use MFE for the shells of various thicknesses to be calculated. The procedure of constructing the Langrage polynomials in local curvilinear coordinate systems used to develop the shell MFE is presented. The displacements in the MFE were approximated by the power and Lagrange polynomials of different orders. When constructing a n-grid finite element (FE), $n \geq 2$, n-nested grids were used. The fine grid was generated by the basic partition of the MFE; the other (coarse) grids were used to reduce its dimension. According to the method, the nodes of the coarse MFE grids are located on the common boundaries of the different modular layers of the shell. The proposed law of the expansion in the number of discrete models using MFE with a constant thickness, multiple of the shell thickness, provides a uniform and rapid convergence of approximate solutions, allowing one to frame solutions with a small error. Multigrid discrete models have $10^3 \ldots 10^6$ times less unknown MFE than the basic ones. The implementation of the MFE for multigrid models requires $10^4 \ldots 10^7$ times less computer storage space than for the reference models, which allows one using the proposed method to calculate some large shells. An example of calculating a multilayer cylindrical local loading shell of irregular shape was given. In the calculation, three-grid shell – type FE, developed on the basis of the reference models having from 2 million to 3.7 billion of the nodal MFE unknowns were used. To study the approximate solution convergence and error, a well-known numerical method was used.

Keywords: elasticity, cylindrical shells, composites, multigrid finite elements of shell type, Lagrange polynomials, small error.

Сибирский журнал науки и технологий. 2018. Т. 19, № 1. С. 27–36

МНОГОСЕТОЧНЫЕ КОНЕЧНЫЕ ЭЛЕМЕНТЫ В РАСЧЕТАХ МНОГОСЛОЙНЫХ ЦИЛИНДРИЧЕСКИХ ОБОЛОЧЕК

А. Д. Матвеев[1*], А. Н. Гришанов[2]

[1]Институт вычислительного моделирования СО РАН
Российская Федерация, 660036, г. Красноярск, Академгородок, 50/44
[2]Новосибирский государственный технический университет
Российская Федерация, 630073, г. Новосибирск, просп. К. Маркса, 20
[*]E-mail: mtv241@mail.ru

Предложен эффективный численный метод расчета линейно-упругих многослойных цилиндрических оболочек при статическом нагружении с применением многослойных криволинейных лагранжевых многосеточных конечных элементов (МнКЭ) оболочечного типа. Такие оболочки широко используются в ракетно-космической и авиационной технике. МнКЭ проектируются в локальных декартовых системах координат на основе мелких (базовых) разбиений оболочек, которые учитывают их неоднородную структуру, сложную форму, сложное нагружение и закрепление. Напряженное деформированное состояние в МнКЭ описывается уравнениями трехмерной задачи теории упругости без использования дополнительных кинематических и статических гипотез, что позволяет применять МнКЭ для расчета многослойных оболочек различной толщины. Показана процедура построения в локальных криволинейных системах координат полиномов Лагранжа, которые применяются при проектировании оболочечных МнКЭ. Перемещения в МнКЭ аппроксимируются степенными *и лагранжевыми полиномами различных порядков. При построении n -сеточного конечного элемента (КЭ), n ≥ 2, используют n вложенных сеток. Мелкая сетка порождена базовым разбиением МнКЭ, остальные n – 1 (крупные) сетки применяются для понижения его размерности. В предлагаемом методе узлы крупных сеток МнКЭ расположены на общих границах разномодульных слоев оболочки. Закон измельчения дискретных моделей, в которых используются МнКЭ с постоянной толщиной, кратной толщине оболочки, порождает равномерную и быструю сходимость приближенных решений, что дает возможность строить решения с малой погрешностью. Многосеточные дискретные модели имеют в 10^3–10^6 раз меньше узловых неизвестных, чем базовые. Реализация метода конечных элементов (МКЭ) для многосеточных моделей требует в 10^4–10^7 раз меньше объема памяти ЭВМ, чем для базовых, что позволяет использовать предложенный метод для расчета оболочек больших размеров. В приведенном расчете многослойной цилиндрической оболочки сложной формы, имеющей локальное нагружение, используются оболочечные трехсеточные КЭ, построенные на базовых моделях, которые имеют от 2 миллионов до 3,7 миллиарда неизвестных МКЭ. Для анализа сходимости приближенных решений используется известный численный метод.*

Ключевые слова: упругость, цилиндрические оболочки, композиты, многосеточные конечные элементы оболочечного типа, полиномы Лагранжа, малая погрешность.

Introduction. Finite Element Method (FEM) [1; 2] is widely used in the study of stress strained state (SSS) of elastic shells [3–6]. In the calculation of shells, constructing the curvilinear finite elements (FE) causes various difficulties [3], in particular, related to the fulfillment of conformality conditions, which is necessary for the convergence of finite element solutions [7]. These difficulties are largely due to the fact that to reduce the order of equations in the theory of shells, hypotheses are introduced, that impose certain restrictions on the fields of displacement, strain and stress [8–14], which generates irreducible errors in solutions and limits the applications of these theories. For example, in the work [15; 16] three-dimensional finite elements are considered with a given distribution of displacements through the thickness, given the compression of the shell. In the work [17] the review of the basic options of use of FEM for calculation of composite plates and covers in two-dimensional statement is presented. The attempts to calculate composite cylindrical shells with application of FE in the formulation of the three-dimensional problem of elasticity theory with account of their structure leads to systems of linear algebraic equations (SLAE) of the finite element method of high order (more 10^6). Application for such discrete shell models of calculation of ANSYS, NASTRAN etc. [3] is difficult. In addition, the solution obtained for the systems of high-order FEM equations contains a computational error, which is difficult to determine the exact value.

In this regard, there is a need to develop such variants of FEM, in which the composite cylindrical shell is considered in a three-dimensional formulation, but which lead to SLAE of a low order in compliance with the permissible level of SSS error values. In the works [18–20] calculations of composite cylindrical panels and shells with the help of multigrid finite element (MFE) are carried out, that was constructed using power polynomials.

In this paper, we propose an efficient numerical method of calculating linearly elastic multilayer cylindrical shells using a multilayer curvilinear Lagrangian MFE. Constructing n net finite element (FE), $n \geq 2$, n of enclosed grid is used. Small grids are made by basic splitting of MFE, the other $n-1$ (larger) grids are used to reduce its dimension. The aim of this work is to develop Lagrangian curved multilayer shell-type MFE. A procedure for constructing Lagrange polynomials of different orders in local curvilinear coordinates is proposed. In constructing approximate solutions a multi-layer Lagrangian, MFE shell with a constant thickness, a multiple of the thickness of the shell is used. The order of the Lagrange polynomial in thickness is taken by a multiple to the number of shell layers. Calculations show that the arrangement of nodes of large MFE grids on the common boundaries of different-modular shell layers provides homogenous and fast convergence of sequences of finite-element solutions, which allows to construct approximate solutions with low error. The proposed MFE are effective in calculating the SSS of multilayer cylindrical shells of different thicknesses, especially in the calculation of thin shells having a complex shape, the complex nature of the fixations and loads. Multilayer shells are widely used in rocket-space and aviation technology.

The advantages are as follows. Multilayer Lagrangian shell MFE:

– take into account the heterogeneous structure of the shells;

– describe the three-dimensional stress state in multilayer shells;

– form multigrid discrete shell models, the dimension of which is much smaller than the dimensions of the base models;

– generate the numerical solution with fast convergence to accurate, which allows us to construct solutions with a small error.

Calculations show that application of the FEM for multigrid discrete models requires 10^3–10^7 time less computer memory than the base models need. The implementation of the proposed method on single-processor computers requires a small amount of time. To analyze the convergence of approximate solutions constructed for the initial problem, we use the well-known numerical method [2]. The implementation of this method is performed by constructing a sequence of approximate solutions for a similar test problem using MFE, which are used in solving the original problem. An example of calculating a 4-layer shell of complex shape using 4-layer Lagrangian shell three-grid FE is given. The results of the calculations show the high efficiency of the application of the proposed three-grid FE.

1. Homogeneous curvilinear single-grid FE. The procedure for constructing curvilinear homogeneous single-grid FE, which form a basic discrete model of the shell, is briefly considered as the example of FE V_e of the 1st order, located in the local Cartesian coordinate system $O_1x_1y_1z_1$ (fig. 1). For FE V_e designations are given: $h_x^e \times h_y^e \times h_z^e$ – characteristic sizes, $z_1O_1y_1$ – a symmetry plane, cd – an axis of a shell, R_1^e (R_2^e) – radius of curvature of the bottom (top) surface, h_z^e – thickness, h_y^e – length, $h_x^e = \alpha_e R_1^e$, α_e – an opening angle. The shape of the FE V_e is a straight prism with height h_y^e. Deformation of FE V_e is described by the equations of the three-dimensional problem of the theory of elasticity [1], shown in coordinate system $O_1x_1y_1z_1$. Using a first order polynomial (in the coordinate system $O_1x_1y_1z_1$), for FE V_e we define the stiffness matrix $\left[K_e^1\right]$ and the nodal force vector $\mathbf{P}_e^1$ with formulas [1; 2]

$$[K_e^1] = \int_{V_e} [B_e]^T [D_e][B_e] dV,$$
$$\mathbf{P}_e^1 = \int_{V_e} [N_e]^T \mathbf{F}_e dV + \int_{S_e} [N_e]^T \mathbf{q}_e dS, \tag{1}$$

where $[B_e]$, $[D_e]$ are the matrix of differentiation and modules of elasticity of the FE V_e; $\mathbf{F}_e$, $\mathbf{q}_e$ are the volume and surface forces vectors FE V_e; $[N_e]$ is the matrix of shape functions; V_e, S_e are the area and the surface of the FE V_e.

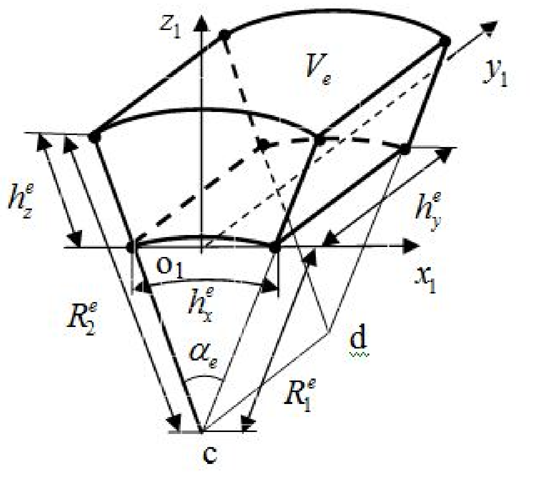

Fig. 1. Single-grid FE V_e

Рис. 1. Односеточный КЭ V_e

Note that the continuity of displacements is violated on the curvilinear boundaries of the FE V_e (fig. 1). However, as it's known [21], the implementation of continuous displacements at the boundaries of curvilinear FE is not a necessary condition for convergence of numerical solutions to the exact one. Calculations show that when the characteristic sizes of curved homogeneous FE V_e decrease, the numerical solutions converge to the exact ones. Procedures for the construction of homogeneous curvilinear single-grid FE of 2nd and 3rd order, which are geometrically similar to the form of FE V_e (fig. 1), are analogous to the procedure in § 1.

2. Multilayer curvilinear Lagrangian two-grid FE

The procedure of constructing multilayer curvilinear two-grid FE (TGFE) with the use of Lagrange polynomials is considered with the example of a three-layer TGFE V_a of the 3rd order with its thickness equal to h that is used in the calculation of 3-layer shells with the thickness h. In the calculation of m-layer shell m-layer Lagrangian TGFE of m-order in thickness are used. TGFE is located in a local Cartesian coordinate system $O_2x_2y_2z_2$ (fig. 2), its dimensions are $h_x^a \times h_y^a \times h$, h – thickness, h_y^a – length. Suppose that the bonds between the components of the inhomogeneous structure of TGFE are ideal. Basic partitioning of R_a TGFE, which consists of a homogeneous curvilinear FE V_e of the 1st order (fig. 1), takes into account in TGFE inhomogeneous structure, a complex type of loading and fastening, and generates a small curvilinear grid h_a, $e = 1, \ldots, M$, M is the total number of FE V_e. On the grid h_a we define the large curvilinear grid $H_a \subset h_a$, TGFE, the nodes of this grid are marked with dots, 64 nodes in fig. 2. Note that the nodes of the large grid H_a lie on the common boundaries of different-modular layers TGFE (fig. 2), in general they have different thickness. Suppose the axis O_1y_1 (fig. 1) is parallel to the axis O_2y_2 (fig. 2). Thus we can use a formula of relation between the nodal displacement vectors $\boldsymbol{\delta}_e^1$ $\boldsymbol{\delta}_e$, FE V_e, which correspond to the local Cartesian coordinate systems $O_1x_1y_1z_1$ and $O_2x_2y_2z_2$

$$\boldsymbol{\delta}_e^1 = [T_e]\boldsymbol{\delta}_e, \tag{2}$$

where $[T_e]$ is a square matrix of rotations [2], $e = 1, \ldots, M$.

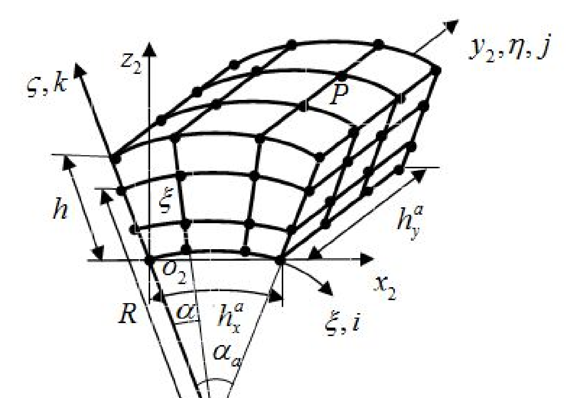

Fig. 2. Three-Layer TGFE V_a

Рис. 2. Трехслойный ДвКЭ V_a

We consider the construction of Lagrange polynomials in the local curvilinear coordinate system $O_2\xi\eta\varsigma$ on a large grid H_a (fig. 2). Suppose that the node $P(i,j,k)$ of grid H_a (dimensions $n_1 \times n_2 \times n_3$) has coordinates ξ_i, η_j, ζ_k, in fig. 2 $i = j = 3$, $k = 4$. Note that $y_2 = \eta$ for small opening angles α_a, TGFE we can see that $x_2 \approx \xi$, $z_2 \approx \zeta$. We have

$$x_2 = \xi, \quad y_2 = \eta, \quad z_2 = \zeta. \tag{3}$$

The base function N_{ijk} for a node $P(i,j,k)$ in the Cartesian coordinate system $O_2x_2y_2z_2$ using Lagrange polynomials $L_i(x_2)$, $L_j(y_2)$, $L_k(z_2)$ [2] is written in the form of

$$N_{ijk}(x_2,y_2,z_2) = L_i(x_2)L_j(y_2)L_k(z_2),$$
$$L_i(x_2) = \prod_{n=1,n\neq i}^{n_1} \frac{x_2 - x_{2,n}}{x_{2,i} - x_{2,n}}, \quad L_j(y_2) = \prod_{n=1,n\neq j}^{n_2} \frac{y_2 - y_{2,n}}{y_{2,j} - y_{2,n}}, \tag{4}$$
$$L_k(z_2) = \prod_{n=1,n\neq k}^{n_3} \frac{z_2 - z_{2,n}}{z_{2,k} - z_{2,n}},$$

where $x_{2,i}$, $y_{2,j}$, $z_{2,k}$ are the coordinates of the node $P(i,j,k)$ in the coordinate system $O_2x_2y_2z_2$.

For a point with a coordinate ξ lying on the cylindrical surface of the radius R, we have $\xi = \alpha R$, α is the angle for the coordinate ξ, fig. 3. Considering (3) the ratio of the form $\xi = \alpha R$, $\xi_i = \alpha_i R$ in (4), we obtain $N_{ijk}(\alpha,\eta,\zeta) = L_i(\alpha)L_j(\eta)L_k(\zeta)$, where $L_i(\alpha)$, $L_j(\eta)$, $L_k(\zeta)$ are the Lagrange polynomials, having the form

$$L_i(\alpha) = \prod_{n=1,n\neq i}^{n_1} \frac{\alpha - \alpha_n}{\alpha_i - \alpha_n}, \quad L_j(\eta) = \prod_{n=1,n\neq j}^{n_2} \frac{\eta - \eta_n}{\eta_j - \eta_n},$$
$$L_k(\zeta) = \prod_{n=1,n\neq k}^{n_3} \frac{\zeta - \zeta_n}{\zeta_k - \zeta_n}. \tag{5}$$

It is convenient to use Lagrange polynomials (5) in calculations. Displacement functions u_a, v_a, w_a TGFE, constructed on the grid H_a using Lagrange polynomials (5), are presented in the form of

$$u_a = \sum_{\beta=1}^{n_0} N_\beta q_\beta^u, \quad v_a = \sum_{\beta=1}^{n_0} N_\beta q_\beta^v, \quad w_a = \sum_{\beta=1}^{n_0} N_\beta q_\beta^w, \tag{6}$$

where q_β^u, q_β^v, q_β^w, N_β are displacements and shape function of the β node of grid H_a, $n_0 = n_1n_2n_3$, in the present case $n_0 = 64$ (fig. 2).

Using (1), (2), the stiffness matrix $[K_e]$ and the nodal forces vector P_e of FE V_e in the coordinate system $O_2x_2y_2z_2$, we present $[K_e] = [T_e]^T[K_e^1][T_e]$, $\mathbf{P}_e = [T_e]^T \mathbf{P}_e^1$ [1]. The functional of the full potential energy Π_a of the basic partition of the R_a TGFE V_a can be written in the form of

$$\Pi_a = \sum_{e=1}^{M} \left(\frac{1}{2} \boldsymbol{\delta}_e^T [K_e]\, \boldsymbol{\delta}_e - \boldsymbol{\delta}_e^T \mathbf{P}_e \right). \tag{7}$$

Using small partitions R_a, the functional (7) has a high dimension and generates a multinodal FE with a large number of nodal unknowns, which is not effective for practice. To reduce the dimension of the functional (7), we use the following procedure. Using (6), the vector of nodal displacements $\boldsymbol{\delta}_e$ FE V_e is shown through the vector of nodal displacements $\boldsymbol{\delta}_a$ of large grid H_a TGFE V_a

$$\boldsymbol{\delta}_e = [A_e^a]\boldsymbol{\delta}_a, \tag{8}$$

where $[A_e^a]$ is a rectangular matrix $e = 1,...,M$.

Substituting (8) in (7) and following the principle of the minimum of total potential energy for TGFE V_a, $\partial\Pi_a(\boldsymbol{\delta}_a)/\partial\boldsymbol{\delta}_a = 0$ we obtain a ratio $[K_a]\boldsymbol{\delta}_a = \mathbf{F}_a$ corresponding to the equilibrium state of TGFE V_a, where

$$[K_a] = \sum_{e=1}^{M} [A_e^a]^T [K_e][A_e^a], \quad \mathbf{F}_a = \sum_{e=1}^{M} [A_e^a]^T \mathbf{P}_e. \tag{9}$$

The matrix $[K_a]$ is called the stiffness matrix, $\mathbf{F}_a$ is nodal forces vector of TGFE V_a. Note that the functions u_a, v_a, w_a are used only to reduce the dimension of the functional (7), the large grid H_a determines the dimension of the TGFE V_a, which is less than the dimension of the base partition R_a.

Note 1. By virtue of (8) the dimension of the vector $\boldsymbol{\delta}_a$ (i. e. the dimension of the TGFE V_a) does not depend on the M which is the total number of FE V_e constituting the TGFE V_a. Consequently, it is possible to use arbitrarily small base partitions R_a, which allows to take into account the heterogeneous and micro-homogeneous structure of the TGFE V_a.

Note 2. In formula (9), matrices $[K_e]$, $\mathbf{P}_e$, $[A_e^a]$ are constructed taking into account the curvilinear form of the base FE V_e (see formula (1)), which represent the region TGFE V_a geometrically accurately. Consequently, the matrices $[K_a]$, $\mathbf{F}_a$ are also determined taking into account the curvilinear form of the TGFE V_a.

Note 3. The determination of the stresses in TGFE V_a can be shown as follows. Let the vector $\boldsymbol{\delta}_a$ be found. With the help of the formulas (8), (2) we find vectors $\boldsymbol{\delta}_e$, $\boldsymbol{\delta}_e^1$ nodal displacements of FE V_e ($e = 1, ..., M$) respectively, in coordinate systems $O_2x_2y_2z_2$ and $O_1x_1y_1z_1$. Using vector $\boldsymbol{\delta}_e^1$ we count the tension in the FE V_e with algorithms of the finite element method [1; 2].

Note 4. Lagrange polynomials are used in Lagrangian TGFE polynomials, determined by formulas (5), which have the order of the polynomial multiple of the number of layers in the thickness of the shell on the coordinate z (i. e. ζ). The calculations show that the location of the nodes of the large grid H_a TGFE at the boundaries of heterogeneous layers provides a homogenous and rapid convergence of sequences of approximate solutions.

The procedures of constructing composite Lagrangian TGFE of *n*-order, geometrically similar to TGFE V_a (fig. 2), with the application of Lagrange polynomials of n -order, are similar to the procedure of § 2.

Calculations show that by increasing the dimensions of the basic partitions of TGFE (i. e., by increasing the number *M*), the time spent on the construction of matrices $[K_a]$ и $\mathbf{F}_a$ and formulas (9) significantly increase. In this case, it is advisable to apply 3-grid finite elements, for the construction of which less time is required and which generate the discrete shell model of lower dimension than TGFE.

3. Multilayer curvilinear Lagrangian three-grid FE.

The procedure of constructing curvilinear three-grid FE (ThGFE) with the use of Lagrange polynomials is considered by the example of a six-layer ThGFE V_b of the 6-th order with its thickness h_z^b, that is used in the calculation of 6-layer shells with thickness h, where $h = h_z^b$. In the calculation of *m*-layer shell *m*-layer Lagrangian ThGFE of *m*-order thickness are used. ThGFE V_b with the size $h_x^b \times h_y^b \times h_z^b$ is located in the local Cartesian coordinate system $O_3x_3y_3z_3$ (fig. 3).

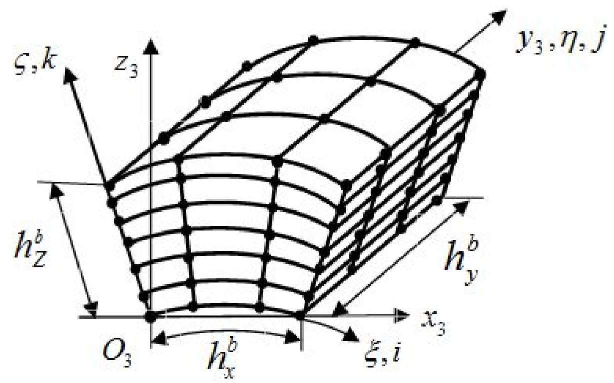

Fig. 3. Six-Layer, ThGFE V_b

Рис. 3. Шестислойный ТрКЭ V_b

The area of ThGFE consists of N curved 6-ply TGFE V_a^n with thickness *h*, $n = 1, \ldots, N$ that geometrically accurately represent the area of ThGFE. TGFE V_a^n make the partition R_b. The large grids H_a TGFE form a small grid h_b ThGFE. On the grid h_b we define large grid of $H_b \subset h_b$ ThGFE. The nodes of the large grid H_b marked with points (112 nodes) lie on the common boundaries of different-modular layers of ThGFE (fig. 3).

Suppose that the axis O_2y_2 of ThGFE (fig. 2) is parallel to the axis O_3y_3 (fig. 3). Suppose that $\boldsymbol{\delta}_n^a$, $\mathbf{q}_n^a$ are the vectors of nodal displacements, $[K_a^n]$, $[M_n^a]$ are the stiffness matrices and $\mathbf{F}_n^a, \mathbf{P}_n^a$ are the vectors of nodal forces TGFE V_n^a responsible for the coordinate systems $O_2x_2y_2z_2$ and $O_3x_3y_3z_3$, $n = 1, \ldots, N$ respectively. According to the FEM [1] we define the following formula: $\boldsymbol{\delta}_n^a = [T_n^a]\,\mathbf{q}_n^a$, where $[T_n^a]$ is the rotations matrix [2], $[M_n^a] = [T_n^a]^T [K_n^a][T_n^a]$, $\mathbf{P}_n^a = [T_n^a]^T \mathbf{F}_n^a$. Taking into account these relations, the total potential energy of the Π_b ThGFE V_b, i. e. the partition of R_b, is presented in the form of

$$\Pi_b = \sum_{n=1}^{N} \left(\frac{1}{2} \left(\mathbf{q}_n^a\right)^T \left[M_n^a \right] \mathbf{q}_n^a - \left(\mathbf{q}_n^a\right)^T \mathbf{P}_n^a \right). \qquad (10)$$

Functions of the displacements u_p, v_p, w_p ThGFE V_b on the large grid H_b, using Lagrange polynomials are presented in the form of

$$u_p = \sum_{\beta=1}^{n_0} N_\beta q_\beta^u, \quad v_p = \sum_{\beta=1}^{n_0} N_\beta q_\beta^v, \quad w_p = \sum_{\beta=1}^{n_0} N_\beta q_\beta^w, \qquad (11)$$

where q_β^u, q_β^v, q_β^w, N_β are displacements and shape function of the β node of grid H_b, $n_0 = n_1 n_2 n_3$, in this case $n_0 = 112$ (fig. 3).

To reduce the dimension of the functional (10) we use functions (11). Let's denote: $\boldsymbol{\delta}_b$ is the vector of nodal displacements of a large grid H_b. Expressing the nodal displacements of vector $\mathbf{q}_n^a$ TGFE V_n^a through the nodal displacement of vector $\boldsymbol{\delta}_b$ of the grid H_b ThGFE V_b, we can see the equality

$$\mathbf{q}_n^a = \left[A_n^b \right] \boldsymbol{\delta}_b, \qquad (12)$$

where $[A_n^b]$ is a rectangular matrix, $n = 1, \ldots, N$.

Using (12) in (10) and minimizing functional Π_b in displacement of $\boldsymbol{\delta}_b$, we obtain the ratio for the ThGFE V_b $[K_b]\boldsymbol{\delta}_b = \mathbf{F}_b$ that corresponds to its equilibrium state, where

$$[K_b] = \sum_{n=1}^{N} [A_n^b]^T [M_n^a][A_n^b], \quad \mathbf{F}_b = \sum_{n=1}^{N} [A_n^b]^T \mathbf{P}_n^a. \qquad (13)$$

The matrix $[K_b]$ will be called the stiffness matrix, $\mathbf{F}_b$ is the vector of nodal forces ThGFE V_b. Note that the large grid H_b determines the dimension of the ThGFE V_b, which is less than the partition dimension R_b consisting of the TGFE V_n^a.

Note 5. By virtue of (12) the dimension of the vector $\boldsymbol{\delta}_b$ (i. e. the dimension of the ThGFE V_b) does not depend on the total number of TGFE V_n^a components of ThGFE. This means that the splitting of a ThGFE V_b into a TGFE V_n^a and, consequently, into single-grid FE V_e (see § 2) can be arbitrarily small, which allows to describe with arbitrarily small error the three-dimensional stress state in the ThGFE taking into account its inhomogeneous structure.

Note 6. Note that the number of layers of TGFE may be less than the number of layers of the shell. For example, constructing six-layered ThGFE you can use a three-layered TGFE (fig. 2) or two-layered TGFE. As calculations show, this leads to a decrease in time costs with a minor change in the error of the solution.

In the formula (13), matrices $[M_n^a]$, $\mathbf{P}_n^a$, $[A_n^b]$ are constructed taking into account the curvilinear form of TGFE V_n^a (see § 2), which geometrically represent the area accurately, ThGFE V_b. Consequently, the matrices $[K_b]$, $\mathbf{F}_b$ are also determined taking into account the curvilinear form of the ThGFE V_b.

The procedure of determining stresses in the ThGFE V_b is similar to the procedure for determining stresses in the TGFE.

Using ThGFE, according to the procedure similar to § 3, we construct four-grid FE, and the k grid of FE, $k \geq 4$. Note that the k grid generate a discrete FE shell model of lower dimension than the $k-1$ FE grid. The described method can be used to calculate multilayer shells with layers of different thicknesses.

Small enough partitions of composite shells are presented as homogeneous MFE, which are designed according to the procedures similar to § 1–3.

4. The results of numerical experiments. Consider the problem of deformation of a four-layered elastic cylindrical shell V_0 of a complex shape with length $2L$. The shell, clamped from two ends, is located in the Cartesian coordinate system $Oxyz$. When $y = 0$; $2L$, displacement $u = v = w = 0$. The radius of the shell on the median surface $R = 2.0$ m, the thickness of the shell $h = 0.03$ m, length $2L = 12.0$ m, i. e V_0 is a thin shell with large geometric dimensions. The left symmetrical part of the shell is shown in fig. 4. Point A lies at the intersection of the planes Oyz and $y = L$ on the top surface of the shell. Shell layers are isotropic homogeneous bodies. The upper and lower layers have $h/12$ thickness, the inner 2 layers have $5h/12$. The Young's modules of 4 layers (starting from the bottom) are equal to: 10, 3, 5, 20 GPA, respectively. Poisson's ratio is 0.3. There is a uniformly distributed tensile radial load $q = 0.05$ MPa (fig. 4) on the outer surface of the shell $3L/4 \leq y \leq L$ with the opening angle $\alpha = \pi/2$, which is symmetrical to the planes Oyz and $y = L$. In the area of the shell clamps there are cutouts symmetrical to the plane Oyz, the opening angle of each cut is equal to the $\pi/2$ length is $L/4$ (fig. 4). As the shape, loading and fastening of the shell are symmetrical to the planes Oyz and $y = L$, we use 1/4 of the shell in the calculations.

The basic discrete model R_n^0 of the shell consists of a curved homogeneous single grid FE of the 1st order V_e^n, geometrically similar to FE V_e (fig. 1). The model grid R_n^0 has a dimension of $m_n^1 \times m_n^2 \times m_n^3$, where

$$m_n^1 = 324n + 1,\ \ m_n^2 = 324n + 1,$$
$$m_n^3 = 12n + 1,\ \ n = 1,\ ...,10, \tag{14}$$

m_n^1 is the dimension of the circular coordinate; m_n^2 – the axis Oy, m_n^3 – axis Oz. Characteristic sizes h_{xn}^e, h_{yn}^e, h_{zn}^e FE V_e^n are defined by the following formulas

$$h_{xn}^e = h_{x1}^e / n,\ \ h_{yn}^e = h_{y1}^e / n,$$
$$h_{zn}^e = h_{z1}^e / n,\ \ n = 1,\ ...,10, \tag{15}$$

where h_{x1}^e, h_{y1}^e, h_{z1}^e are characteristic dimensions of FE V_e^1 of the 1st order corresponding to the discrete model R_1^0, where $h_{x1}^e = \alpha_1 R_e$, $h_{y1}^e = L/324$, $h_{z1}^e = h/12$, $\alpha_1 = \pi/324$, R_e is the radius of the lower cylindrical surface FE V_e^1.

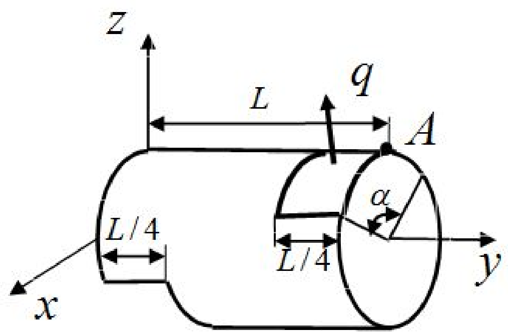

Fig. 4. Left symmetric part of the shell V_0

Рис. 4. Левая симметричная часть оболочки V_0

On base models R_n^0, $n = 1,\ ...,10$ we construct multigrid discrete models R_n of shell V_0 consisting of Lagrangian shell ThGFE with sizes $81h_{xn}^e \times 81h_{yn}^e \times h$ where $h = 12nh_{zn}^e$. For all basic discrete models, ThGFE have a fixed size coordinate z which is equal to the thickness of the shell h. ThGFE are constructed on the procedure shown in § 3 and consist of Lagrangian TGFE with dimensions $9h_{xn}^e \times 9h_{yn}^e \times h$, according to the procedure shown in § 2.

The ThGFE uses Lagrange polynomials defined by the formulas (5), which have the third order of the polynomial by coordinates *x*, *y*, and the forth order by coordinate z, which corresponds to the number of layers in the thickness of the shell. As shown by numerical calculations, if the nodes of large grids H_a and H_b of two-grid and three-grid FE lie on the common boundaries of multimodulus layers, discrete models R_n provide even and fast convergence of a sequence of finite element solutions.

The results of the calculations for discrete models R_n are given in tab. 1, where we see: w_n, σ_n are maximum radial displacement and equivalent stress for the model R_n, $n = 6, ..., 10$. We can find the stress σ_n with the 4th strength theory. As you know, using the maximum equivalent stress the factors of safety of structures are determined. We find the values $\delta_{\sigma,n}(\%)$, $\delta_{w,n}(\%)$ with the formulas

$$\delta_{\sigma,n}(\%) = 100\ \% \cdot |\,\sigma_n - \sigma_{n-1}\,| / \sigma_n ,$$

$$\delta_{w,n}(\%) = 100\ \% \cdot |\,w_n - w_{n-1}\,| / w_n ,\quad n = 2, ..., 10 .$$

The nature of changes in values $\delta_{w,n}(\%)$, $\delta_{\sigma,n}(\%)$ (tab. 1) shows rapid convergence of the equivalent stresses σ_n and displacements w_n. Since the values for the model R_{10} are small, $\delta_{w,10} = 0.00116179$, $\delta_{\sigma,10} = 0.00719947$ it can be considered from the point of view of engineering practice that the displacement of $w_{10} = 30.289362$ mm and $\sigma_{10} = 31.371908$ MPa are made with low error, i. e., w_{10}, σ_{10} are little different from the exact (see § 5).

The dimension of the underlying discrete model R_{10}^0 is 3722110998 (more than 3.7 billion), the width of the tape of the system equations (SE) FEM is 1176610 (over 1.1 million). Multigrid model R_{10} has 203090 nodal unknowns, the width of the tape SE FEM is equal to 5445. Application of the FEM for the multigrid model R_{10} requires 3960366 (approximately 3.96 million) less times than the amount of computer memory of the base model R_{10}^0.

5. The study of the convergence of approximate solutions. To study the convergence of approximate solutions constructed using the new MFE, we use the following numerical method, the brief essence of which is shown below. With the kind of new MFE that are used in the solution of the original problem (see § 4), the similar (test) problem with known exact solution u_0 is solved. Suppose that $\|u_0 - u_h\| \to 0$ when $h \to 0$, where u_h is the solution of the test problem, constructed with the help of a family of new MFE, h is the characteristic size of MFE. Then we consider that the solutions constructed with the help of a family of new MFE and for the initial problem converge in the limit ($h \to 0$) to the exact one.

We consider the deformation of a 4-layer cylindrical shell V_1 as a test problem, which is located in the Cartesian coordinate system $Oxyz$, to have the same geometric dimensions, fastening conditions and elastic modules as the shell V_0 in § 4. However, the shell V_1 has no cutouts. When $3L/4 \le y \le 5L/4$ the radial tensile uniform load of $p = 0.1$ MPa acts on the outer surface of the shell V_1, i. e. axisymmetric three-dimensional stress state is realized in the shell V_1 [1].

As you know [1], the sequence of approximate solutions of the axisymmetric problem, constructed by MFE with the use of standard FE, which are homogeneous rings with a rectangular cross-section, in the limit (when $h_m \to 0$ h_m is the characteristic size of the standard FE) converge to the exact solution. Calculations are carried out for discrete models Q_n, $n = 1, ..., 14$, shell V_1. The results of calculations are given in tab. 2 for models Q_n where, $n = 7, ..., 14$, w_n^0, σ_n^0 are the deflection and equivalent voltage at the point A (fig. 4), dimensions of models Q_n are given in the plane Oyz. The parameters of $\delta_{w,n}^0(\%)$, $\delta_{\sigma,n}^0(\%)$ are determined by the formulas

$$\begin{aligned} \delta_{w,n}^0(\%) &= 100\ \% \cdot |\,w_n^0 - w_{n-1}^0\,| / w_n^0 , \\ \delta_{\sigma,n}^0(\%) &= 100\ \% \cdot |\,\sigma_n^0 - \sigma_{n-1}^0\,| / \sigma_n^0 ,\ \ n = 2, ..., 14. \end{aligned} \tag{16}$$

Table 1

Displacements w_n and equivalent stresses σ_n for models R_n

R_n	R_6	R_7	R_8	R_9	R_{10}
w_n	30.032632	30.136577	30.205840	30.254172	30.289362
$\delta_{w,n}(\%)$	0.550568	0.344913	0.229303	0.159753	**0.116179**
σ_n	30.074687	30.544130	30.881125	31.146047	31.371908
$\delta_{\sigma,n}(\%)$	2.374768	1.536934	1.091265	0.850580	**0.719947**

Table 2

Displacements w_n^0 and equivalent stresses σ_n^0 for models Q_n

N	Dimensions of models	$w_n^0 \cdot 10^3$, м	$\delta_{w,n}^0(\%)$	σ_n^0, MPa	$\delta_{\sigma,n}^0(\%)$
7	2269×43	2.24419205	0.0001359	21.9642981	0.0006719
8	2593×49	2.24419400	0.0000868	21.9641839	0.0005199
9	2917×55	2.24419529	0.0000574	21.9640928	0.0004147
10	3241×61	2.24419632	0.0000458	21.9640199	0.0003319
11	3565×67	2.24419706	0.0000329	21,.9639594	0.0002754
12	3889×73	2.24419754	0.0000213	21.9639074	0.0002367

End of table 2

N	Dimensions of models	$w_n^0 \cdot 10^3$, м	$\delta_{w,n}^0(\%)$	σ_n^0, MPa	$\delta_{\sigma,n}^0(\%)$
13	4213×79	2.24419797	0.0000147	21.9638637	0.0001989
14	4537×85	**2.24419832**	0.0000155	**21.9638261**	0.0001711

Table 3

Displacements w_n^p and stresses σ_n^p for models R_n

n	$w_n^p \cdot 10^3$, м	$\delta_{w,n}^p(\%)$	σ_n^p, MPa	$\delta_{\sigma,n}^p(\%)$
7	2.24416383	0.0001038	21.9641016	0.0060703
8	2.24416590	0.0000922	21.9649716	0.0039608
9	2.24416869	0.0001243	21.9655875	0.0028039
10	2.24417150	0.0002810	21.9660517	0.0021132
11	2.24417898	0.0003333	21.9664194	0.0016739
12	2.24418121	0.0000993	21.9667143	0.0013424
13	2.24418263	0.0000632	21.9669569	0.0011043
14	**2.24418427**	0.0000730	**21.9671598**	0.0009236

The nature of the values change of $\delta_{w,n}^0(\%)$, $\delta_{\sigma,n}^0(\%)$ shows the rapid convergence of stresses σ_n^0 and displacements w_n^0 to the exact solution w_0, σ_0 of the axisymmetric problem [1]. As the sizes, $\delta_{w,14}^0 = 0.000000155$ $\delta_{\sigma,14}^0 = 0.000001711$ are sufficiently small, the displacement of $w_{14}^0 = 2.24419832 \cdot 10^{-3}$ m and the equivalent stress $\sigma_{14}^0 = \ = 21.9638261$ MPa can be considered as the exact solution, i. e. we believe $w_0 = w_{14}^0$, $\sigma_0 = \sigma_{14}^0$.

We consider the solution of this axisymmetric MFE problem with the use of FE, which were used in solving the problem in § 4. We construct approximate solutions of the axisymmetric problem using the laws of grinding (14), (15) of basic partitions. The results of calculations are given in the tab. 3, where, w_n^p, σ_n^p is the deflection and equivalent stress at the point A for a multigrid discrete model R_n, $n = 7, ..., 14$. The parameters $\delta_{w,n}^p(\%)$, $\delta_{\sigma,n}^p(\%)$ are determined by formulas similar to formulas (16). The nature of the change in values $\delta_{w,n}^p(\%)$, $\delta_{\sigma,n}^p(\%)$ demonstrates the rapid convergence of stresses σ_n^p and displacements w_n^p to the limit values w_0^p, σ_0^p. The errors for displacement w_{14}^p and stress σ_{14}^p $\delta_w(\%) = 100\ \% \cdot | w_{14}^0 - w_{14}^p | / w_{14}^0$, $\delta_\sigma(\%) = 100\ \% \times$ $\times | \sigma_{14}^0 - \sigma_{14}^p | / \sigma_{14}^0$, respectively, are equal to 0.00062828 % 0.0151749 %. In tab. 2, 3 values w_{14}^0, σ_{14}^0, w_{14}^p, σ_{14}^p, are marked in bold. From the point of view of engineering practice, because of the smallness of the values $\delta_w(\%)$, $\delta_\sigma(\%)$, we can assume that $w_0^p = w_0$, $\sigma_0^p = \sigma_0$. Then we can conclude that the proposed ThGFE generate solutions σ_n^p, w_n^p that in the limit (at $n \to \infty$) tend (from the point of view of engineering practice) to the exact solution of the axisymmetric problem.

The shell V_0 considered in § 4 differs from the shell V_1 considered in § 5 by the presence of cutouts and the method of applying the load, with full coincidence of the dimensions, boundary conditions and physical characteristics of the shells. In addition, when constructing sequences of approximate solutions for the initial and test problems, the same family of proposed ThGFE is used. Therefore, it can be assumed that the proposed shell ThGFE, which provide uniform convergence of approximate solutions for the test problem (for the shell V_1), generate solutions w_n, σ_n that in the limit (at $n \to \infty$) will converge (from the point of view of engineering practice) to the exact values of displacement and equivalent stress for the original problem (for the shell V_0), see § 4.

Conclusion. In this work we propose a numerical method of calculation of multilayered linear elastic cylindrical thin and medium-thickness shells with the use of curvilinear Lagrangian shell type MFE. Application of the MFE for multigrid discrete shell models requires much less computer memory than the base models, which allows to construct solutions with a small error and can explore SSS of shells of large geometric dimensions. The above calculations show the high efficiency of the proposed curvilinear Lagrangian shell MFE in the analysis of three-dimensional SSS multilayer shells.

References

1. Zenkevich O. *Metod konechnykh elementov v tekhnike* [The finite element method in engineering science]. Moscow, Mir Publ., 1975, 541 p.

2. Norri D., Zh. de Friz. *Vvedenie v metod konechnykh elementov* [An Introduction to Finite Element Analysis]. Moscow, Mir Publ., 1981, 304 p.

3. Golovanov A. I., Tyuleneva O. I., Shigabutdinov A. F. *Metod konechnykh elementov v statike i dinamike tonkostennykh konstruktsiy* [Finite Element Method in statics

and dynamics of thin-wall constructions]. Moscow, Fizmatlit Publ., 2006, 392 p.

4. Klochkov Yu. V., Nikolayev A. P., Shubovich A. A. *Analiz napryazhenno-deformirovan- nogo sostoyaniya obolochek vrashcheniya v geometricheski nelineynoy postanovke pri razlichnykh variantakh interpolyatsii peremeshcheniy* [Analysis of stress-strain state of rotation shells in geometrically non-linear setting with various variants of movement interpolation]. Volgograd, Volgogradsky GAU Publ., 2013, 152 p.

5. Kiselev A. P. [Calculation of thin shells for strength to resist three-dimensional setting, without simplifying hypotheses]. *Izv. vuzov, ser. Stroitel'stvo.* 2008, No. 1, P. 18–23 (In Russ.).

6. Kiselev A. P., Gureeva N. A., Kiseleva R. Z. [Calculating multilayer rotation shells and plates using volume finite elements]. *Izv. vuzov, ser. Stroitel'stvo.* 2010, No. 1, P. 106–112 (In Russ.).

7. Bate K., Wilson E. *Chislennye metody analiza i metod konechnykh elementov* [Numerical methods in finite element analysis]. Moscow, Stroyizdat Publ., 1982, 448 p.

8. Bolotin V. V., Novichkov Yu. N. *Mekhanika mnogosloynykh konstruktsiy* [Mechanics of multilayer structures]. Moscow, Mashinostroenie Publ., 1980, 375 p.

9. Golushko S. K., Nemirovskiy Yu. V. *Pryamye i obratnye zadachi mekhaniki uprugikh kompozitnykh plastin i obolochek vrashcheniya* [Direct and inverse problems of mechanics of elastic composite plates and shells of revolution]. Moscow, Fizmatlit Publ., 2008, 432 p.

10. Ahmed A., Kapuria S. A four-node facet shell element for laminated shells based on the third order zigzag theory. *Composite Structures.* 2016, Vol. 158, P. 112–127.

11. Carrera E., Pagani A. Valvano S. Shell elements with through-the-thickness variable kinematics for the analysis of laminated composite and sandwich structure. *Composites Part B: Engineering.* 2017, Vol. 111, P. 294–314.

12. Yasin M. Y., Kapuria S. An efficient layerwise finite element for shallow composite and sandwich shells. *Composite Structures.* 2013, Vol. 98, P. 202–214.

13. Cinefra M., Carrera E. Shell finite elements with different through-the-thickness kinematics for the linear analysis of cylindrical multilayered structures. *Int. J. Num. Meth. Eng.* 2013, Vol. 93, No. 2, P. 160–182.

14. Rah K., Van Paepegem W., Habraken A. M., Degrieck J. A partial hybrid stress solid-shell element for the analysis of laminated composites. *Comp. Meth. Appl. Mech. Eng.* 2011, Vol. 200, No. 49–52, P. 3526–3539.

15. Kara N., Kumbasar N. Three-dimensional finite element for thick shells of general shape. *Int. J. for Physical and Engineering Sciences*. 2001, Vol. 52, P. 1–7.

16. Sze K. Y. Three-dimensional continuum finite element models for plate / shell analysis. *Prog. Struct. Eng. Mater.* 2002, Vol. 4, P. 400–407.

17. Caliri M. F., Ferreira A. J. M., Tita V. A review on plate and shell theories for laminated and sandwich structures highlighting the Finite Element Method. *Composite Structures.* 2016, Vol. 156, P. 63–77.

18. Matveev A. D., Grishanov A. N. [Multi-grid modeling of three-dimensional composite cylindric panels and shells]. *Materialy X mezhdunarodnoi konferentsii "Setochnye metody dlya kraevykh zadach I prilozheniya" – Materials of Xth International conference "Grid methods for boundary tasks and applications".* Kazan, 2014, P. 459–467 (In Russ.).

19. Matveev A. D., Grishanov A. N. [Two-grid modeling of cylindric shells and panels with variable thickness]. *Vestnik KrasGAU.* 2014, No. 4, P. 90–96 (In Russ.).

20. Matveev A. D., Grishanov A. N. [Multigrid curvilinear elements in three-dimensional analysis of cylindrical composite panels with cavities and holes]. *Uchenye zapiski Kazanskogo universiteta. 2014, Tom 156, Seriya: Fiziko-matematicheskie nauki.* 2014, Vol. 156, Book 4, P. 47–59 (In Russ.).

21. Kabanov V. V., Zheleznov L. P. [To the calculation of a cylindrical shell by the finite element method]. *Prikladnaya mekhanika*. 1985, Vol. 21, No. 9, P. 35–40 (In Russ.).

Библиографические ссылки

1. Зенкевич О. Метод конечных элементов в технике. М. : Мир, 1975. 544 с.

2. Норри Д., Де Фриз Ж. Введение в метод конечных элементов. М. : Мир, 1981. 304 с.

3. Голованов А. И., Тюленева О. И., Шигабутдинов А. Ф. Метод конечных элементов в статике и динамике тонкостенных конструкций. М. : Физматлит, 2006. 392 с.

4. Клочков Ю. В., Николаев А. П., Шубович А. А. Анализ напряженно-деформированного состояния оболочек вращения в геометрически нелинейной постановке при различных вариантах интерполяции перемещений. Волгоград : Волгоградский ГАУ, 2013. 152 с.

5. Киселев А. П. Расчет тонких оболочек на прочность в трехмерной постановке без упрощающих гипотез // Изв. вузов. Строительство. 2008. № 1. С. 18–23.

6. Киселев А. П., Гуреева Н. А., Киселева Р. З. Расчет многослойных оболочек вращения и пластин с использованием объемных конечных элементов // Изв. вузов. Строительство. 2010. № 1. С. 106–112.

7. Бате К., Вилсон Е. Численные методы анализа и метод конечных элементов. М. : Стройиздат, 1982. 448 с.

8. Болотин В. В., Новичков Ю. Н. Механика многослойных конструкций. М. : Машиностроение, 1980. 375 с.

9. Голушко С. К., Немировский Ю. В. Прямые и обратные задачи механики упругих композитных пластин и оболочек вращения. М. : Физматлит, 2008. 432 с.

10. Ahmed A., Kapuria S. A four-node facet shell element for laminated shells based on the third order zigzag theory // Composite Structures. 2016. Vol. 158. P. 112–127.

11. Carrera E., Pagani A. Valvano S. Shell elements with through-the-thickness variable kinematics for the analysis of laminated composite and sandwich structure // Composites. Part B: Engineering. 2017. Vol. 111. P. 294–314.

12. Yasin M. Y., Kapuria S. An efficient layerwise finite element for shallow composite and sandwich shells // Composite Structures. 2013. Vol. 98. P. 202–214.

13. Cinefra M., Carrera E. Shell finite elements with different through-the-thickness kinematics for the linear analysis of cylindrical multilayered structures // Int. J. Num. Meth. Eng. 2013. Vol. 93, No. 2. P. 160–182.

14. A partial hybrid stress solid-shell element for the analysis of laminated composites / K. Rah [et al.] // Comp. Meth. Appl. Mech. Eng. 2011. Vol. 200, No. 49–52. P. 3526–3539.

15. Kara N., Kumbasar N. Three-dimensional finite element for thick shells of general shape // Int. J. for Physical and Engineering Sciences. 2001. Vol. 52. P. 1–7.

16. Sze K. Y. Three-dimensional continuum finite element models for plate / shell analysis // Prog. Struct. Eng. Mater. 2002. Vol. 4. P. 400–407.

17. Caliri M. F., Ferreira A. J. M., Tita V. A review on plate and shell theories for laminated and sandwich structures highlighting the Finite Element Method // Composite Structures. 2016. Vol. 156. P. 63–77.

18. Матвеев А. Д., Гришанов А. Н. Многосеточное моделирование трехмерных композитных цилиндрических панелей и оболочек // Сеточные методы для краевых задач и приложения : материалы X Междунар. конф. Казань, 2014. С. 459–467.

19. Матвеев А. Д., Гришанов А. Н. Двухсеточное моделирование цилиндрических оболочек и панелей переменной толщины // Вестник КрасГАУ. 2014. № 4. С. 90–96.

20. Матвеев А. Д., Гришанов А. Н. Многосеточные криволинейные элементы в трехмерном анализе цилиндрических композитных панелей с полостями и отверстиями // Ученые записки Казанского ун-та. Сер. «Физ.-матем. науки». 2014. Т. 156, кн. 4. С. 47–59.

21. Кабанов В. В., Железнов Л. П. К расчету цилиндрической оболочки методом конечных элементов // Прикладная механика. 1985. Т. XXI, № 9. С. 35–40.

UDC 519.711.3

Siberian Journal of Science and Technology. 2018, Vol. 19, No. 1, P. 37–43

ABOUT NON-PARAMETRIC IDENTIFICATION OF *T*-PROCESSES

A. V. Medvedev[1], D. I. Yareshchenko[2*]

[1]Reshetnev Siberian State University of Science and Technology
31, Krasnoyarsky Rabochy Av., Krasnoyarsk, 660037, Russian Federation
[2]Siberian Federal University
26/1, Academician Kirensky St., Krasnoyarsk, 660074, Russian Federation
[*]E-mail: YareshenkoDI@yandex.ru

This paper is devoted to the construction of a new class of models under incomplete information. We are talking about multidimensional inertia-free objects for the case when the components of the output vector are stochastically dependent, and the character of this dependence is unknown a priori. The study of a multidimensional object inevitably leads to a system of implicit dependencies of the output variables of the object from the input variables, but in this case this dependence extends to some components of the output vector. The key issue in this situation is the definition of the nature of this dependence for which the presence of a priori information is necessary to some extent. Taking into account that the main purpose of the model of such objects is the prediction of output variables with known input, it is necessary to solve a system of nonlinear implicit equations whose form is unknown at the initial stage of the identification problem, but only that one or another output component depends on other variables which determine the state of the object.

Thus, a rather nontrivial situation arises for the solution of a system of implicit nonlinear equations under conditions when there are no usual equations. Consequently, the model of the object (and this is a main identification task) cannot be constructed in the same way as is accepted in the existing theory of identification as a result of a lack of a priori information. If it was possible to parametrize the system of nonlinear equations, then at a known input it would be necessary to solve this system, since in this case it is known, once the parameterization step is overcome. The main content of this article is the solution of the identification problem, in the presence of T-processes, and while the parametrization stage can not be overcome without additional a priori information about the process under investigation.

In this connection, the scheme for solving a system of non-linear equations (which are unknown) can be represented in the form of some successive algorithmic chain. First, a vector of discrepancies is formed on the basis of the available training sample including observations of all components of the input and output variables. And after that, the evaluation of the output of the object with known values of the input variables is based on the Nadaraya-Watson estimates. Thus, for given values of the input variables of the T-process, we can carry out a procedure of estimating the forecast of the output variables.

Numerous computational experiments on the study of the proposed T-models have shown their rather high efficiency. The article presents the results of computational experiments illustrating the effectiveness of the proposed technology of forecasting the values of output variables on the known input.

Keywords: discrete-continuous process, identification, T-models, T-processes.

Сибирский журнал науки и технологий. 2018. Т. 19, № 1. С. 37–43

О НЕПАРАМЕТРИЧЕСКОЙ ИДЕНТИФИКАЦИИ *Т*-ПРОЦЕССОВ

А. В. Медведев[1], Д. И. Ярещенко[2*]

[1]Сибирский государственный университет науки и технологий имени академика М. Ф. Решетнева
Российская Федерация, 660037, просп. им. газ. «Красноярский рабочий», 31
[2]Сибирский федеральный университет
Российская Федерация, 660074, г. Красноярск, ул. Академика Киренского, 26, корп. 1
[*]E-mail: YareshenkoDI@yandex.ru

Рассмотрено построение нового класса моделей в условиях неполной информации. Речь идет о многомерных безынерционных объектах для случая, когда компоненты вектора выходов стохастически зависимы, причем характер этой зависимости априори неизвестен. Исследование многомерного объекта неизбежно приводит к системе неявных зависимостей выходных переменных объекта от входных, но в данном случае подобная зависимость распространяется и на некоторые компоненты вектора выходов. Ключевым вопросом в данной ситуации является определение характера этой зависимости, для чего и необходимо наличие в той или иной степени априорной информации. Учитывая, что основным назначением модели подобного рода объектов *является прогноз выходных переменных при известных входных, необходимо решать систему нелинейных неявных уравнений, вид которых на начальной стадии постановки задачи идентификации неизвестен, а известно лишь, что та или иная компонента выхода зависит от других переменных, определяющих состояние объекта.*

Таким образом, возникает довольно нетривиальная ситуация решения системы неявных нелинейных уравнений в условиях, когда собственно самих уравнений в обычном смысле нет. Следовательно, модель объекта (а эта основная задача идентификации) не может быть построена так, как это принято в существующей теории идентификации в результате недостатка априорной информации. Если бы можно было параметризовать систему нелинейных уравнений, то при известном входе следовало бы решить эту систему, поскольку она в данном случае известна, раз этап параметризации преодолен. Основным содержанием настоящей статьи является решение задачи идентификации при наличии Т-процессов и при том, что этап параметризации не может быть преодолен без дополнительной априорной информации об исследуемом процессе.

В этой связи схема решения системы нелинейных уравнений (которые неизвестны) может быть представлена в виде некоторой последовательной алгоритмической цепочки. Сначала на основании имеющейся обучающей выборки, включающей наблюдения всех компонент входных и выходных переменных, формируется вектор невязок. А уже после этого оценка выхода объекта при известных значениях входных переменных строится на основании оценок Надарая–Ватсона. Таким образом, при заданных значениях входных переменных Т-процесса мы можем осуществить процедуру оценивания прогноза выходных переменных.

Многочисленные вычислительные эксперименты по исследованию предлагаемых Т-моделей показали достаточно высокую их эффективность. Приводятся результаты вычислительных экспериментов, иллюстрирующих эффективность предлагаемой технологии прогноза значений выходных переменных по известным входным.

Ключевые слова: дискретно-непрерывный процесс, идентификация, Т-модели, Т-процессы.

Introduction. In numerous multidimensional real processes output variables are available to measure not only at different time periods but also after a long time. This leads to the fact that dynamic processes have to be considered as non-inertial with delay. For example, while grinding the products time constant is 5–10 minutes, and control of output variable, for example fineness of grinding, is measured once in two hours. In this case investigated process can be presented as non-inertial with delay. If output variables of the object are somehow stochastically dependent, then we call such processes *T*-processes. Similar processes require special view on the problem of identification different from existing ones. The main thing is that identification of such processes should be carried out differently from the existing theory of identification. We should pay special attention to the fact that the term "process" is considered below not as processes of probabilistic nature, such as stationary, Gaussian, Markov, martingales, etc. [1]. Below we will focus on *T*-processes actually occurring or developing over time. In particular technological process, industrial, economic, the process of person's recovery (disease) and many others.

Identification of multidimensional stochastical processes is a topical issue for many technological industrial processes of discrete-continuous nature [2]. The main feature of these processes is that vector of output variables $x = (x_1, x_2, \ldots, x_n)$, consisting of n component is such that the components of this vector are stochastically dependant unknown in advance way. We denote vector of input component – $u = (u_1, u_2, \ldots, u_m)$. This formulation of the problem leads to the fact that the mathematical description of the object is represented as some analogue of the implicit functions of the form $F_j(u, x) = 0$, $j = \overline{1, n}$. The main feature of this task of modeling is that class of dependency $F(\cdot)$ is unknown. Parametric class of vector functions $F_j(u, x, \alpha)$, $j = \overline{1, n}$, where α is a vector of parameters, does not allow to use methods of parametric identification [3; 4] because class of functions accurate to parameters cannot be defined in advance and well known methods of identifications are not suitable in this case [3; 4]. In this way the task of identification can be seen as solving of non-linear equations:

$$F_j(u, x) = 0, \quad j = \overline{1, n} \tag{1}$$

relatively component vector $x = (x_1, x_2, \ldots, x_n)$ at known values of u. In this case it is expediently to use methods of nonparametric statistics [5; 6].

***T*-processes.** Nowadays the role of identification of non-inertial systems with delay is increasing [7; 8]. This is explained by the fact that measurement of some of the most important output variables of dynamic objects is carried out through long periods of time, that exceeds a constant of time of the object [9; 10].

The main feature of identification of multidimensional object is that investigating process is defined with the help of the system of implicit stochastic equations:

$$F_j\left(u(t-\tau),\ x(t),\ \xi(t)\right) = 0, \quad j = \overline{1, n}, \tag{2}$$

where $F_j(\cdot)$ is unknown, τ is delay in different channels of multidimensional system. Further τ is omitted for simplicity.

In general investigated multidimensional system implementing *T*-processes can be presented in fig. 1.

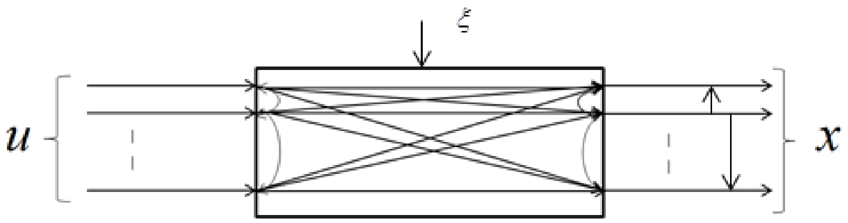

Fig. 1. Multidimensional objects

Рис. 1. Многомерный объект

In fig. 1 the following designations are accepted: $u = (u_1, ..., u_m)$ – m-dimensional vector of input variables, $x = (x_1, ..., x_n)$ – n-dimensional vector of output variables. Through various channels of investigated process dependence of j component of vector **u** can be presented as dependence on components of vector **u:** $x^{<j>} = f_j\left(u^{<j>}\right)$, $j = \overline{1,n}$.

Every j channel depends on several components of vector **u**, for example $u^{<5>} = (u_1, u_3, u_6)$, where $u^{<5>}$ is a compound vector. When building models of real technological and industrial processes (complexes) often vectors **x** and **u** are used as compound vectors. Compound vector is a vector composed from several components of the vector, for example $u^{<j>} = (x_2, x_5, x_7, x_8)$ or another set of components. In this case, the system of equations will be $\hat{F}_j\left(u^{<j>}, x^{<j>}\right) = 0,\ \ j = \overline{1,n}$.

***T*-models.** The processes, which have output variables that have unknown stochastic relationships, were called T-processes, and their models were called T-models. Analyzing the above information it is easy to see, that description of the process in fig. 1 can be accepted as a system of implicit functions:

$$F_j\left(u^{<j>}, x^{<j>}\right) = 0,\ \ j = \overline{1,n}, \tag{3}$$

where $u^{<j>}, x^{<j>}$ are compound vectors. The main feature of modeling of such a process under nonparametric uncertainty is the fact that functions (3) $F_j\left(u^{<j>}, x^{<j>}\right) = 0,\ \ j = \overline{1,n}$ are unknown. Obviously the system of models can be presented as following:

$$\hat{F}_j\left(u^{<j>}, x^{<j>}, \vec{x}_s, \vec{u}_s\right) = 0,\ \ j = \overline{1,n}, \tag{4}$$

where $\vec{x}_s, \vec{u}_s$ are temporary vectors (data received by s time moment), in particular $\vec{x}_s = (x_1, ..., x_s) = (x_{11}, x_{12}, ..., x_{1s}, ..., x_{21}, x_{22}, ..., x_{2s}, ..., x_{n1}, x_{n2}, ..., x_{ns})$, but even in this case $\hat{F}_j(\cdot),\ \ j = \overline{1,n}$ are unknown. In the theory of identification such problems are not solved and are not set. Usually parametric structure is chosen (3), unfortunately it is difficult to fulfill because of lack of apriori information. Long time is required to define parametric structure, that is the model is represented as:

$$F_j\left(u^{<j>}, x^{<j>}, \alpha\right) = 0,\ \ j = \overline{1,n}, \tag{5}$$

where α is a vector of parameters. Then follows the evaluation of parameters according to the elements of training sample $u_i, x_i,\ \ i = \overline{1,s}$ and solution of the system of nonlinear interrelated relations (5). Success in building a model will depend on qualitative parametrization of the system (5).

Further we will consider the problem of building T-models under nonparametric uncertainty, when the system (5) is unknown up to the parameters.

Let the input of the object receive the input variables values, which, of course, are measured. Availability of training sample $x_i, u_i,\ \ i = \overline{1,s}$ is necessary. In this case evaluation of vector components of output variables x at known values of u, as noted above, leads to the need to solve the system of equations (4). If dependence of output component from vector components of input variables is unknown, then it is natural to use the methods of nonparametric evaluation [5; 11].

At a given value of the vector of input variables $u = u'$, it is necessary to solve the system (4) with respect to the vector of output variables x. General scheme of solution of such a system:

1. First a discrepancy is calculated by the formula:

$$\varepsilon_{ij} = F_j\left(u^{<j>}, x^{<j>}(i), \vec{x}_s, \vec{u}_s\right),\ \ j = \overline{1,n}, \tag{6}$$

where we take $F\left(u^{<j>}, x^{<j>}(i), \vec{x}_s, \vec{u}_s\right)$ as nonparametric evaluation of regression of Nadaraya–Watson [10]:

$$\varepsilon_j(i) = F_{\varepsilon j}\left(u^{<j>}, x_j(i)\right) = = x_j(i) - \frac{\sum_{i=1}^{s} x_j[i] \prod_{k=1}^{<n>} \Phi\left(\frac{u'_k - u_k[i]}{c_{su_k}}\right)}{\sum_{i=1}^{s} \prod_{k=1}^{<n>} \Phi\left(\frac{u'_k - u_k[i]}{c_{su_k}}\right)}, \tag{7}$$

where $j = \overline{1,n},\ ,< m >$ is dimension of a compound vector u_k, $< m > \le m$, further this designation is also used for other variables. Bell-shaped functions $\Phi\left(\frac{u'_k - u_k[i]}{c_{su_k}}\right)$ and parameter of fuzziness c_{su_k} satisfy several conditions of convergence and have the following features:

$$\Phi(\cdot) < \infty;\ c_s^{-1} \int_{\Omega(u)} \Phi\left(c_s^{-1}(u-u_i)\right) du = 1;$$

$$\lim_{s\to\infty} c_s^{-1}\Phi\left(c_s^{-1}(u-u_i)\right) = \delta(u-u_i),\ \lim_{s\to\infty} c_s = 0,$$

$$\lim_{s\to\infty} sc_s = \infty .$$

2. Next step is conditional expected value:

$$x_j = M\left\{x \mid u^{<j>}, \varepsilon = 0\right\},\ j = \overline{1,n}. \quad (8)$$

We take nonparametric evaluation of regression of Nadaraya–Watson as an estimate (8) [10]:

$$\hat{x}_j = \frac{\sum_{i=1}^{s} x_j[i] \cdot \prod_{k_1=1}^{<n>} \Phi\left(\frac{u_{k_1} - u_{k_1}[i]}{c_{su}}\right) \prod_{k_2=1}^{<m>} \Phi\left(\frac{\varepsilon_{k_2}[i]}{c_{s\varepsilon}}\right)}{\sum_{i=1}^{s} \prod_{k_1=1}^{<n>} \Phi\left(\frac{u_{k_1} - u_{k_1}[i]}{c_{su}}\right) \prod_{k_2=1}^{<m>} \Phi\left(\frac{\varepsilon_{k_2}[i]}{c_{s\varepsilon}}\right)},\ j = \overline{1,n}, \quad (9)$$

where bell-shaped functions $\Phi(\cdot)$ are taken as triangular core:

$$\Phi\left(\frac{u_{k_1} - u_{k_1}[i]}{c_{su}}\right) = \begin{cases} 1 - \frac{\left|u_{k_1} - u_{k_1}[i]\right|}{c_{su}}, & \frac{\left|u_{k_1} - u_{k_1}[i]\right|}{c_{su}} < 1, \\ 0, & \frac{\left|u_{k_1} - u_{k_1}[i]\right|}{c_{su}} \geq 1. \end{cases}$$

$$\Phi\left(\frac{\varepsilon_{k_2}[i]}{c_{s\varepsilon}}\right) = \begin{cases} 1 - \frac{\left|\varepsilon_{k_2}[i]\right|}{c_{s\varepsilon}}, & \frac{\left|\varepsilon_{k_2}[i]\right|}{c_{s\varepsilon}} < 1, \\ 0, & \frac{\left|\varepsilon_{k_2}[i]\right|}{c_{s\varepsilon}} \geq 1. \end{cases}$$

Carrying out this procedure we obtain the value of output variables x under input influences on the object $u = u'$, this is the main purpose of a required model, which further can be used in different management systems [8], including organizational one [12].

Computational experiment. For computational experiment a simple object with five input variables $u = (u_1, u_2, u_3, u_4, u_5)$ taking random values in the interval $u \in [0,\ 3]$ and with three output variables $x = (x_1, x_2, x_3)$ where $x_1 \in [-2;\ 11]$, $x_2 \in [-1;\ 8]$, $x_3 \in [-1;\ 8]$ was chosen. We will develop a sample of input and output variables based on a system of equations:

$$\begin{cases} x_1 - 2u_1 + 1.5\sqrt{u_2} - u_5^2 - 0.3x_3 = 0; \\ x_2 - 1.5u_4 - 0.3\sqrt{u_5} - 0.6 - 0.3x_1 = 0; \\ x_3 - 2u_2 + 0.9\sqrt{u_3} - 4u_5 - 6.6 + 0.5x_1 - 0.6x_2 = 0. \end{cases} \quad (10)$$

As a result we get a sample of measurements $\vec{u}_s, \vec{x}_s$ where $\vec{u}_s, \vec{x}_s$ are temporary vectors. It should be noted that the process described by the system (10) is only necessary to obtain training samples, there is no other information about the process under investigation. Dealing with a real object, a training sample is formed as a result of measurements which are carried out with available control measures. In the case of stochastic dependence between output variables, the process is naturally described, for example, by the following system of equations:

$$\begin{cases} \hat{F}_{x1}(x_1, x_3, u_1, u_2, u_5) = 0; \\ \hat{F}_{x2}(x_1, x_2, u_4, u_5) = 0; \\ \hat{F}_{x3}(x_1, x_2, x_3, u_2, u_3, u_5) = 0. \end{cases} \quad (11)$$

The system of equations (11) is a dependence, unlike the system (10), known from the available a priori information.

Having got a sample of observation, we can proceed to a studied problem, which is finding the forecast values of output variables **x** at known input **u**. First, discrepancies are calculated (7) using the technique described earlier. We introduce discrepancies as a system:

$$\begin{cases} \varepsilon_1(i) = \hat{F}_1\left(x_1^i, x_3^i, u_1^l, u_2^l, u_5^l\right); \\ \varepsilon_2(i) = \hat{F}_2\left(x_1^i, x_2^i, u_4^l, u_5^l\right); \\ \varepsilon_3(i) = \hat{F}_3\left(x_1^i, x_2^i, x_3^i, u_2^l, u_3^l, u_5^l\right). \end{cases} \quad (12)$$

where $\varepsilon_j, j = \overline{1,3}$ are discrepancies, whose corresponding components of an output vector cannot can't be derived from the parametric equations.

The forecast for the system (11) is carried out according to the formula (9) for each output component of the object.

First, we present the results of a computational experiment without interference. In this case, values of input variables of the newly generated input variables (not included in the training sample) go to the input of the object. A configurable parameter will be a parameter of fuzziness c_s, which in this case, we take equal 0.4 (the value was determined as a result of numerous experiments to reduce the quadratic error between model and object output [13; 14]) the parameter of fuzziness will be taken the same when calculating in the formulas (7) and (9), sample size is $s = 500$. Let's give graphs for object outputs by components x_1, x_2 and x_3.

In fig. 2, 3 and 4 the output values of the variables are marked with a "point", and the output value of the model are marked with a "cross". The figures demonstrate the comparison of the true values of the test sample of the output vector components and their forecasted values obtained by using the algorithm (6)–(9).

We will conduct the results of another computational experiment, in this case, interference ξ is imposed on values of the vector **x** components of the object output. The conditions of the experiment: sample size is $s = 500$, interference acting on the output vector components of an object is $\xi = 5\ \%$, parameter of fuzziness is $c_s = 0.4$ (fig. 5–7).

The conducted computational experiments confirmed the effectiveness of the proposed *T*-models, which are presented not as generally accepted in the theory of model identification, but as some method of forecasting the output variables of the object at the known input $u = u'$. It should be noted that in this case we do not have a model in the sense generally accepted in the theory of identification [15].

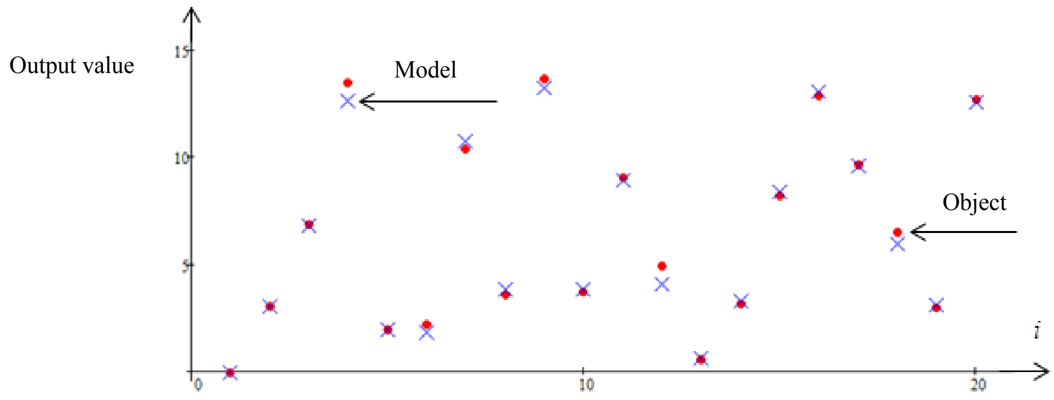

Fig. 2. Forecast of the output variable x_1 with no interference. Error $\delta = 0.71$

Рис. 2. Прогноз выходной переменной x_1 при отсутствии помех. Ошибка $\delta = 0,71$

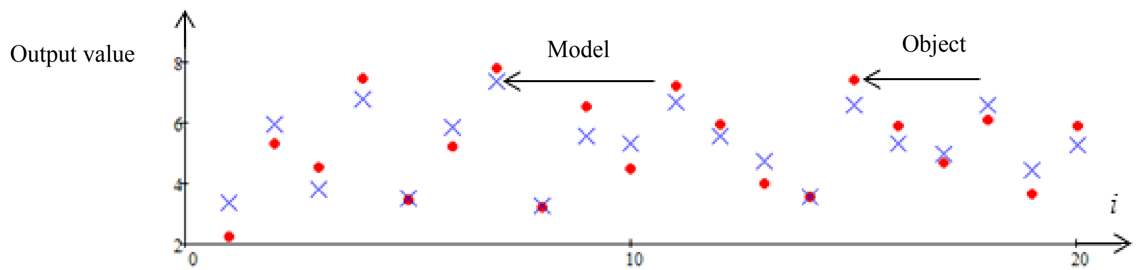

Fig. 3. Forecast of the output variable x_2 with no interference. Error $\delta = 0.71$

Рис. 3. Прогноз выходной переменной x_2 при отсутствии помех. Ошибка $\delta = 0,71$

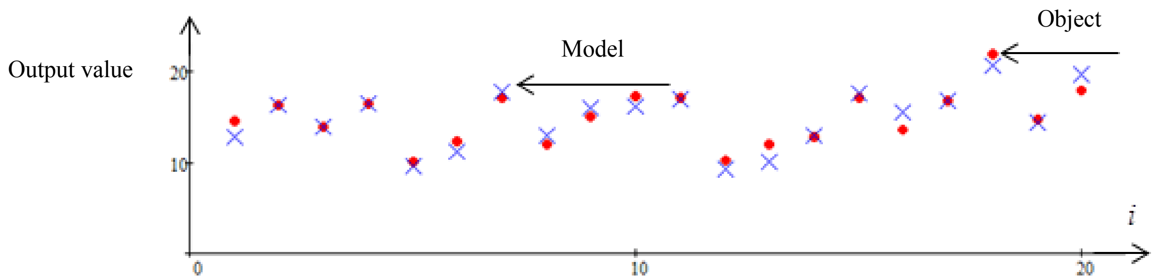

Fig. 4. Forecast of the output variable x_3 with no interference. Error $\delta = 0.71$

Рис. 4. Прогноз выходной переменной x_3 при отсутствии помех. Ошибка $\delta = 0,71$

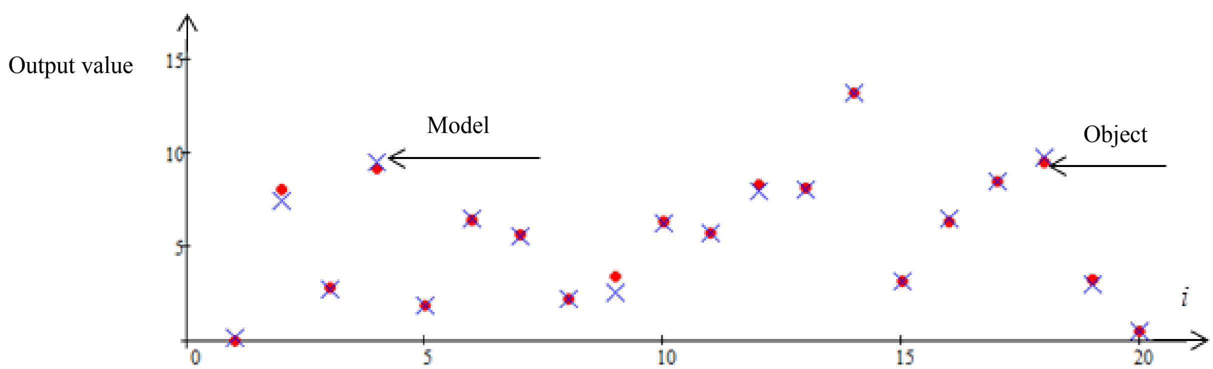

Fig. 5. Forecast of the output variable x_1 with interference 5 %. Error $\delta = 0.77$

Рис. 5. Прогноз выходной переменной x_1 с помехой 5 %. Ошибка $\delta = 0,77$

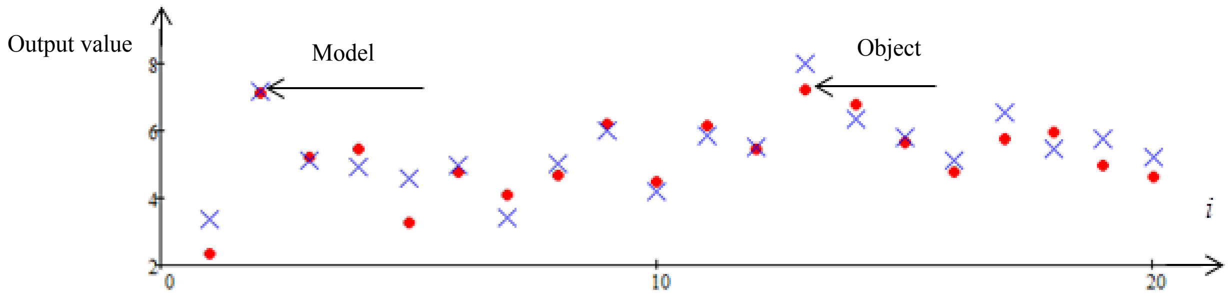

Fig. 6. Forecast of the output variable x_2 with interference 5 %. Error $\delta = 0.77$

Рис. 6. Прогноз выходной переменной x_2 с помехой 5 %. Ошибка $\delta = 0{,}77$

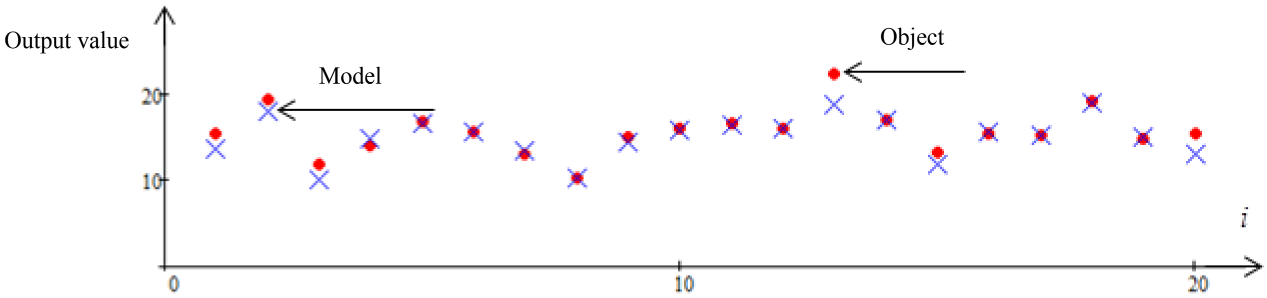

Fig. 7. Forecast of the output variable x_3 with interference 5 %. Error $\delta = 0.77$

Рис. 7. Прогноз выходной переменной x_3 с помехой 5 %. Ошибка $\delta = 0{,}77$

Conclusion. The problem of identification of non-inertial multidimensional objects with delay in unknown stochastic relations of the output vector components is considered. Here a number of features arise, which mean that the identification problem is considered under conditions of nonparametric uncertainty and, as a consequence, cannot be represented up to a set of parameters. On the basis of available a priori hypotheses the system of equations describing the process with the help of compound vectors **x** and **u** is formulated. Nevertheless functions $F(\cdot)$ remain unknown. The article describes the method of calculating the output variables of the object at the known input, which allows them to be used in computer systems for various purposes. Above some particular results of computational studies are given.

The conducted computational experiments showed a sufficiently high efficiency of *T*-modeling. At the same time, not only the issues related to the introduction of interference of different levels, different sizes of training samples, but also objects of different dimensions were studied.

References

1. Dub Dzh. L. *Veroyatnostnye processy* [Probabilistic process]. Moscow, Iz-vo inostrannoy literatury Publ., 1956, 605 p.

2. Medvedev A. V. *Osnovy teorii adaptivnyh sistem: monografiya* [Fundamentals of adaptive systems theory]. Krasnoyarsk, SibGAU Publ., 2015, 526 p.

3. Ehjkhoff P. *Osnovy identifikacii sistem upravleniya* [Basics of identification of control systems]. Moscow, Mir Publ., 1975, 7 p.

4. Cypkin Ya. Z. *Osnovy informacionnoj teorii identifikacii* [Fundamentals of information theory of identification]. Moscow, Nauka Publ., 1984, 320 p.

5. Nadaraya E. A. *Neparametricheskoe ocenivanie plotnosti veroyatnostey i krivoy regressii* [Nonparametric estimation of probability density and regression curve]. Tbilisi, Tbilisskiy universitet Publ., 1983, 194 p.

6. Vasil'ev V. A., Dobrovidov A. V., Koshkin G. M. *Neparametricheskoe ocenivanie funkcionalov ot raspredeleniy stacionarnyh posledovatel'nostey* [Nonparametric estimation of functionals of stationary sequences distributions]. Moscow, Nauka Publ., 2004, 508 p.

7. Sovetov B. Ya., Yakovlev S. A. *Modelirovanie system* [Modeling of systems]. Moscow, Vysshaya shkola Publ., 2001, 343 p.

8. Cypkin Y. Z. *Adaptaciya i obuchenie v avtomaticheskih sistemah* [Adaptation and training in automatic systems]. Moscow, Nauka Publ., 1968, 400 p.

9. Medvedev A. V. [The theory of non-parametric systems]. *Vestnik SibGAU*. 2010, No. 4 (30), P. 4–9 (In Russ.).

10. Fel'dbaum A. A. *Osnovy teorii optimal'nyh avtomaticheskih system* [Fundamentals of the theory of optimal automatic systems]. Moscow, Fizmatgiz Publ., 1963.

11. Medvedev A. V. *Neparametricheskie sistemy adaptacii* [Nonparametric adaptation systems]. Novosibirsk, Nauka Publ., 1983.

12. Medvedev A. V., Yareshchenko D. I. [About modeling of process of acquisition of knowledge by

students at University]. *Vysshee obrazovanie segodnya.* 2017, No. 1, P. 7–10 (In Russ.).

13. Linnik Y. V. *Metod naimen'shih kvadratov i osnovy teorii obrabotki nablyudeniy* [The method of least squares and the foundations of the theory of processing observations]. Moscow, Fizmatlit Publ., 1958, 336 p.

14. Amosov N. M. *Modelirovanie slozhnyh system* [Modeling of complex systems]. Kiev, Naukova dumka Publ., 1968, 81 p.

15. Antomonov Y. G., Harlamov V. I. *Kibernetika i zhizn'* [Cybernetics and life]. Moscow, Sov. Rossiya Publ., 1968, 327 p.

Библиографические ссылки

1. Дуб Дж. Л. Вероятностные процессы. М. : Изд-во иностранной литературы, 1956. 605 с.

2. Медведев А. В. Основы теории адаптивных систем : монография /Сиб. гос. аэрокосмич. ун-т. Красноярск, 2015. 526 с.

3. Эйкхофф П. Основы идентификации систем управления / пер. с англ. В. А. Лотоцкого, А. С. Манделя. М. : Мир, 1975. 7 с.

4. Цыпкин Я. З. Основы информационной теории идентификации. М. : Наука. Главная редакция физико-математической литературы, 1984. 320 с.

5. Надарая Э. А. Непараметрическое оценивание плотности вероятностей и кривой регрессии. Тбилиси : Изд-во Тбил. ун-та, 1983. 194 с.

6. Васильев В. А., Добровидов А. В., Кошкин Г. М. Непараметрическое оценивание функционалов от распределений стационарных последовательностей / отв. ред. Н. А. Кузнецов. М. : Наука, 2004. 508 с.

7. Советов Б. Я., Яковлев С. А. Моделирование систем : учебник для вузов. М. : Высш. шк., 2001. 343 с.

8. Цыпкин Я. З. Адаптация и обучение в автоматических системах. М. : Наука, 1968. 400 с.

9. Медведев А. В. Теория непараметрических систем. Управление 1 // Вестник СибГАУ. 2010. № 4 (30). С. 4–9.

10. Фельдбаум А. А. Основы теории оптимальных автоматических систем. М. : Физматгиз, 1963.

11. Медведев А. В. Непараметрические системы адаптации. Новосибирск : Наука, 1983.

12. Медведев А. В., Ярещенко Д. И. О моделировании процесса приобретения знаний студентами в университете // Высшее образование сегодня. 2017. Вып. 1. С. 7–10.

13. Линник Ю. В. Метод наименьших квадратов и основы теории обработки наблюдений. М. : Физматлит, 1958. 336 с.

14. Амосов Н. М. Моделирование сложных систем. Киев : Наукова думка, 1968. 81 с.

15. Антомонов Ю. Г., Харламов В. И. Кибернетика и жизнь. М. : Сов. Россия, 1968. 327 с.

UDC 621.372.8.01

Siberian Journal of Science and Technology. 2018, Vol. 19, No. 1, P. 44–48

MODAL FILTER SIMULATION WITH LOSSES

R. R. Khazhibekov*, A. M. Zabolotsky, T. R. Gazizov

Tomsk State University of Control Systems and Radioelectronics
40, Lenina Av., Tomsk, 634050, Russian Federation
*E-mail: r300994@mail.ru

Protection of spacecraft on-board equipment against electromagnetic interferences is an actual problem. Much attention is paid to the susceptibility to the excitation of powerful ultra short impulses (nanosecond and subnanosecond impulses). The use of known protection devices to solve this problem is hampered by a number of conflicting requirements. For example, low mass, high reliability, long life. In addition, ultrashort pulses are able to penetrate into various radio-electronic equipment by passing the instrument shields. Protection potential using the devices based on modal filtering is well known. To simulate these devices, rigorous electro-dynamic approach is applied, which requires high computational costs. Approximate quasi-static approach allows to significantly reduce computational costs. The quasi-static simulation was used in this paper, loss record in conductors was realized by means of exact calculation of the matrix of per-unit-length resistances through a change in the matrix of the per-unit-length coefficients of electromagnetic induction when scaling the cross section of conductors. The effect of losses on the shape and amplitude of the pulses at the output of the modal filter is shown. A comparison of simulation results with electrodynamic and quasi-static approaches taking into account losses is presented. Good consistency is obtained. Quasi-static simulation with losses took much less time than the electrodynamic simulation. Analysis of the results suggests that software-based approaches can be used for modal filter simulation.

Keywords: microstrip line, linear delay, wave impedance, modal filtering, quasi-static simulation, protection device.

Сибирский журнал науки и технологий. 2018. Т. 19, № 1. С. 44–48

МОДЕЛИРОВАНИЕ МОДАЛЬНОГО ФИЛЬТРА С УЧЕТОМ ПОТЕРЬ

Р. Р. Хажибеков*, А. М. Заболоцкий, Т. Р. Газизов

Томский государственный университет систем управления и радиоэлектроники
Российская Федерация, 634050, г. Томск, просп. Ленина, 40
*E-mail: r300994@mail.ru

Защита бортовой аппаратуры космического аппарата от электромагнитных помех является актуальной проблемой. Большое внимание уделяется восприимчивости к воздействию мощных сверхкоротких импульсов (импульсов наносекундного и субнаносекундного диапазонов). Использование известных устройств защиты для решения данной задачи затруднено рядом противоречивых требований, например, малой массы, высокой надежности, длительного срока активного существования. Кроме того, сверхкороткие импульсы способны проникать в различную радиоэлектронную аппаратуру, минуя экраны приборов. Известна возможность защиты с помощью устройств, основанных на использовании модальной фильтрации. Для моделирования таких устройств применяют строгий электродинамический подход, который требует больших вычислительных затрат. Приближенный квазистатический подход позволяет значительно уменьшить вычислительные затраты. Использован учет потерь в проводниках при квазистатическом моделировании, реализованный с помощью точного вычисления матрицы погонных сопротивлений через изменение матрицы погонных коэффициентов электромагнитной индукции при масштабировании поперечного сечения проводников. Показано влияние потерь на форму и амплитуду импульсов на выходе модального фильтра. Представлено сравнение результатов моделирования электродинамическим и квазистатическим подходами с учетом потерь. Получена хорошая согласованность. Квазистатическое моделирование заняло значительно меньше времени, чем электродинамическое. Анализ результатов показал, что программно-реализованные подходы можно использовать для моделирования модального фильтра.

Ключевые слова: микрополосковая линия, погонная задержка, волновое сопротивление, модальная фильтрация, квазистатическое моделирование, устройство защиты.

Introduction. As long-term practice of start and maintenance of the spacecrafts (SC) showed, reliability of the elements, devices of airborne computers and control modules functioning is one of the key factors defining success of the mission in general. Reliability assurance in special conditions of harmful space factors impact is connected with specific difficulties. One of such factors is interfering super short impulse (ISI). Its dangers are extensively researched [1–5]. However, the increase in SC effective performance period (up to 15 years) leads to considerable degradation of the used materials' properties and also makes it problematic to predict the new materials' properties mutation in the future SCs. This will inevitably create conditions for harmful effects of ISI, causing improvements of protection against it. The use of the known protection devices is complicated by a number of contradictory requirements, for example, protection of a bigger number of circuits, law mass of the safety device, ability to function effectively for 15 years in space. Therefore creation of new elements and protection devices of airborne computers and control modules from SIS proves to be relevant. Protection against short impulses based on modal filtering [6–11] is suggested. The physical principle of such protection is based on the effect of splitting of interfering impulse in the segment of line into modes, each of which extends with the time delay. In case of unhomogeneous dielectric filling in the cross-section of the connected line segment, the difference of these time delays can exceed duration of interfering impulse, so that one impulse given between the active and reference conductors at the beginning of the segment will split into two impulses at the end of the segment.

Often for the analysis of strip structures quasi static simulation is used. For exact simulation of such structures it is necessary to consider losses both in conductors, and in dielectrics. Meanwhile, accurate loss record is especially important in certain cases. Thus, in modal filters (MF) output amplitude depends on losses.

The purpose of this paper is to compare results of quasi static and electro-dynamic simulations of MF taking into account loss record.

Calculation of resistance per-unit-length matrix. The algorithm of Calculation of resistance per unit length matrix of N-wire transmission line in which (N + 1) reference conductor, in quasi static simulation environment TALGAT [12] looks as follows [13]:

1. Input of conductor parameters: ρ – conductor specific resistance, μ – magnetic conductivity.
2. Input of frequency.
3. Input of the initial geometrical parameters.
4. Calculation of value of conductor boundaries extension ∂n (value 0.1 from the lowest parameter is used by default).
5. Calculation of the conductor's surface resistance using formula

$$R_s = \sqrt{\pi f \mu \rho}. \quad (1)$$

6. Geometrical modeling of cross-section structure under initial parameters.
7. Calculation of per-unit-length initial matrix coefficients of electromagnetic induction **L1**.
8. Extension of all boundaries of cross-section of the reference conductor on Δn.
9. Calculation of inductance matrix **L2** for the changed structure.
10. Calculation of $\Delta\mathbf{L}_{j,k} = \mathbf{L2}_{j,k} - \mathbf{L1}_{j,k}$.
11. Calculation of non-diagonal matrix elements $\mathbf{R}_{jj}$ using formula:

$$\mathbf{R}_{j,k}\Big|_{j\neq k} = \frac{R_s}{\mu_0}\left(\frac{-\Delta\mathbf{L}_{j,k}}{\Delta n}\right), \text{ Om/m.} \quad (2)$$

12. Extension of all boundaries of the cross-section of the 1st from N conductors.
13. Calculation of $\mathbf{L2}_{jj}$.
14. Calculation of $\Delta\mathbf{L}_{jj} = \mathbf{L1}_{jj} - \mathbf{L2}_{jj}$.
15. Calculation of diagonal components of the matrix $\mathbf{R}_{jj}$ using formula:

$$\mathbf{R}_{jj} = \frac{R_s}{\mu_0}\left(\frac{-\Delta\mathbf{L}_{jj}}{\Delta n}\right), \text{ Om/m.} \quad (3)$$

16. Serial repetition of points 12–15 for each of the remained conductors, successively expanding boundaries of this conductor.

The calculation algorithm of matrix **R** has been implemented. In cases where it is required to calculate **L** matrix, functions of the TALGAT system are used. In the algorithm extension of conductor boundaries by value Δn is applied. It is realized programmatically. The user value Δn is set for this purpose, or default value Δn equal to 0.1 from the lowest parameter of structure is used. For calculation of default value of boundary with the lowest length whose value is equated to value of the lowest parameter is found.

In order to expend the conductor i, where $i = 1, 2, \ldots, N$, N – number of conductors multi-wire transmission line, applying scaling against the centre of the conductor, which transforms conductor coordinates $p_{1,i}$; $p_{2,i}$; …; $p_{M,i}$, where M – the number of conductor angles i, into coordinates $p_{1,i}'$; $p_{2,i}'$; …; $p_{N,i}'$ so to obtain the conductor, increased by Δn from all sides. For this purpose scaling coefficients are calculated:

$$f_i^x = \frac{l_i^x + 2\Delta n}{l_i^x}; \; f_i^y = \frac{l_i^y + 2\Delta n}{l_i^y}, \quad (4)$$

where l_i^x, l_i^y – the width and thickness of conductor i. Further conductor center coordinates are calculated $p_{c,i}$ and transformation matrix is built:

$$\begin{matrix} f_i^x & 0 & 0 \\ 0 & f_i^y & 0, \\ p_{c,i}^x(1-f_i^x) & p_{c,i}^y(1-f_i^y) & 1 \end{matrix} \quad (5)$$

where $p_{c,i}^x$ and $p_{c,i}^y$ – components x and y coordinate $p_{c,i}$. Transformation matrix can be applied in the following way:

$$p_{j,i}^{x\,\prime} = f_i^x p_{j,i}^x + p_{c,i}^x\left(1-f_i^x\right);$$
$$p_{j,i}^{y\,\prime} = f_i^y p_{j,i}^y + p_{c,i}^y\left(1-f_i^y\right), \quad (6)$$

where $j = 1, 2, \ldots, M$. For the conductor boundaries extension transformation matrix should be applied (2) to every conductor angle. Extension of the infinite earth is done via displacement of all structure boundaries towards the line of the infinite earth on Δn.

Simulation. The approaches described above are software realised and built-in in the TALGAT system. However, the use of this program for quasi-static simulation of real strip structures and comparing the received results with the results of electro-dynamic simulation was not shown earlier. For simulation MF structure, researched in [14], will be used.

Quasi-static simulation is executed in TALGAT system, electro-dynamic – in CST MWS [15]. The cross-section and the diagram of MF switch are provided in fig. 1, where width and thickness of conductors w = 500 micron and t = 85 micron; conductor spacing – s = 200, distance between edge of the conductor and dielectric edge d = 1000 micron, substrate thickness h = 400 micron, FR-4 substrate material, line length l = 2.5. MF contains three copper conductors: A – the active, O – reference and p – passive. The impulse oscillator is connected to the active conductor with the following parameters: amplitude – 10 V and duration of peak t_d = 100 picoseconds, duration of the front and recession of t_r = t_f = 100 picoseconds. Resistance values are R_1 = R_2 = R_3 = R_4 = = 100 Ohms. Results of simulation taking into account losses and dispersion are provided in fig. 2.

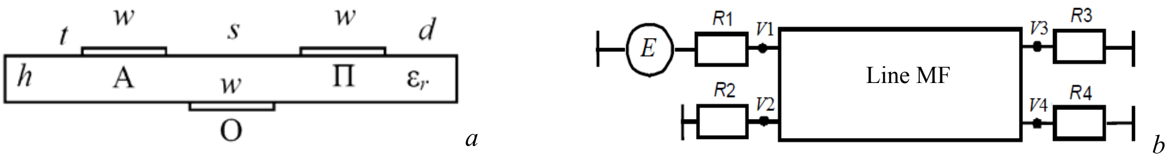

Fig. 1. MF cross-section (a) and connection scheme (b)

Рис. 1. Поперечное сечение (a) и схема включения (b) МФ

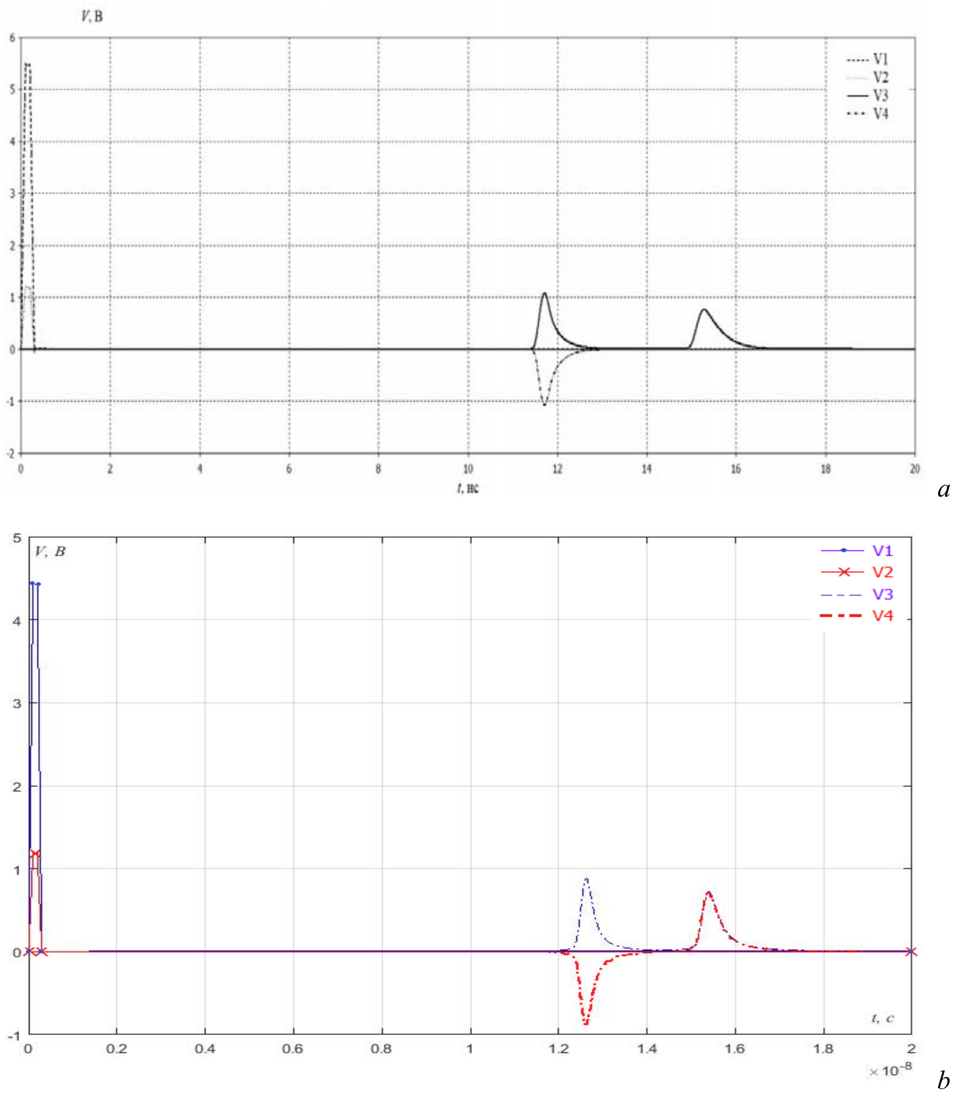

Fig. 2. Voltage waveforms obtained in CST MWS (a) and TALGAT (b)

Рис. 2. Формы напряжения, полученные в CST MWS (a) и TALGAT ($б$)

Table

Comparative results of amplitudes and impulses time delays

Parameter	CST	TALGAT	(CST – TALGAT)/(CST + TALGAT), %
Amplitude of 1st impulse *V*3, B	1.1	0.88	11
Amplitude of 2nd impulse *V*3, B	0.73	0.71	1.4
Amplitude of 1st impulse *V*4, B	–1.1	–0.88	11
Amplitude of 2nd impulse *V*3, B	0.73	0.71	1.4
Time delay of 1st impulse in nodes *V*3 and *V*4, ps	11.6	12.2	2.5
Time delay of 2nd impulse in nodes *V*3 и *V*4, ps	14.9	15	0.3

The results proved that with reference to losses in conductors and dielectrics, wavefront time and impulse drop on the MF output increase. Thus the voltage amplitude of output impulses (*V*3) is much less than a half of amplitude of an input impulse (*V*1). Impulse amplitude of the even mode appeared to be less than impulse amplitude of the odd mode. This results from the fact that currents of the even mode extend mostly in dielectric, while currents of the odd mode – in the air. Fig. 2 shows that voltage waveforms, calculated in TALGAT and CST MWS, coincide. Values of amplitudes and time delays of impulses are given in the table.

Conclusion. Simulation results showed that the maximum deviation under impulses delays makes 2.5 % under amplitudes – 11 %. It proves consistency of results received by means of the approaches described in the present paper. Besides. calculation time in TALGAT was about 1 h, in CST MWS – about 50 h. Therefore. the software realized approaches can be used for MF simulation**.**

Acknowledgments. This work was carried out as a result of the project 8.9562.2017/8.9 of the Ministry of Education and Science of the Russian Federation.

Благодарности. Работа выполнена за счет проекта 8.9562.2017/8.9 Минобрнауки Российской Федерации.

References

1. Mora N., Vega F., Lugrin G., Rachidi F., Rubinstein M. Study and classification of potential IEMI sources. *System and assessment notes.* 2014. Note 41.

2. Gazizov A. T., Zabolotsky A. M., Gazizov T. R. UWB pulse decomposition in simple printed structures. *IEEE Transactions on Electromagnetic Compatibility*. 2016, Vol. 58, No. 4, P. 1136–1142.

3. Orlov P., Gazizov T., Zabolotsky A. Short pulse propagation along microstrip meander delay lines with design constraints: comparative analysis of the quasi-static and electromagnetic approaches. *Applied computational electro-magnetics society journal*. 2016, Vol. 31, No. 3, P. 238–243.

4. Gazizov R. R., Gazizov T. T. [A study of the localization of peak signal values in a printed circuit board of an autonomous navigation system]. *Infokommunikatsionnye tekhnologii*. 2017, Vol. 15, No. 2, P. 170–178 (In Russ.).

5. Surovtsev R. S., Nosov A. V., Zabolotsky A. M., Gazizov T. R. Possibility of protection against UWB pulses based on a turn of a meander microstrip line. *IEEE Transactions on Electromagnetic Compatibility*. 2017, Vol. 59, No. 6, P. 1864–1871.

6. Zabolotsky A. M., Gazizov A. T. Simulation of ultrawide band pulse propagation in asymmetrical modal filter for power network protection. *International Journal of Circuits. Systems and Signal Processing*. 2015, Vol. 9, P. 68–74.

7. Gazizov A. T. [Comparison of measurement results and simulation of the temporal response of the modal filter to the excitation of an ultrashort pulse]. *Doklady TUSUR.* 2015, No. 4(38), P. 149–152 (In Russ.).

8. Zabolotsky A. M. [Using mirror symmetry to improve modal filtering]. *Doklady TUSUR.* 2015, No. 2(36), P. 41–44 (In Russ.).

9. Belousov A. O. [Multi-wire microstrip line as a modal filter for protection against ultrashort pulses]. *Doklady TUSUR.* 2015, No. 3(37), P. 124–128 (In Russ.).

10. Orlov P. Y., Gazizov T. R., Zabolotsky A. M. The impact of coupled conductors in a dielectric material above an ideally conducting plane on the difference of board delay per unit length of even and odd modes. *International Journal of Advanced And Applied Sciences*. 2017, Vol. 4, No. 2, P. 68–71.

11. Dmitrienko I. V. [Analysis of the frequency response of the modal filter to suppress the emitted emissions of the on-board apparatus of the spacecraft]. *Doklady TUSUR.* 2015, No. 4(38), P. 157–160 (In Russ.).

12. Kuksenko S. P., Zabolotsky A. M., Melkoserov A. O., Gazizov T. R. [New features of the TALGAT electromagnetic compatibility simulation system]. *Doklady TUSUR.* 2015, No. 2, P. 45–50 (In Russ.).

13. Mussabaev R. R. [Algorithm for calculating the impedance matrix of a multi-wire transmission line]. *Materialy Mezhdunarodnoy nauchno-tekhnicheskoy konferentsii studentov. aspirantov i molodykh uchenykh "Nauchnaya sessiya TUSUR–2017", posvyashchennoy 55-letiyu TUSURa* [Materials of the International scientific and technical conference of students. graduate students and young scientists "Scientific session of TUSUR-2017". dedicated to the 55th anniversary of TUSUR]. Tomsk, 2017, P. 68–71 (In Russ.).

14. Zabolotsky A. M., Gazizov T. R., Kalimulin I. F. *Novye resheniya dlya obespecheniya elektromagnitnoy sovmestimosti bortovoy radioelektronnoy apparatury kosmicheskogo apparata* [New solutions for ensuring electromagnetic compatibility of on-board radio-electronic apparatus of the spacecraft]. Tomsk, TUSUR Publ., 2016, 288 p.

15. CST STUDIO SUITE [Advertisement]. *IEEE Antennas and Propagation Magazine*. 2013, Vol. 55, Iss. 4, P. c2–c2.

Библиографические ссылки

1. Study and classification of potential IEMI sources / N. Mora [et al.] // System and assessment notes 2014. Note 41.

2. Gazizov A. T., Zabolotsky A. M., Gazizov T. R. UWB pulse decomposition in simple printed structures // IEEE Transactions on Electromagnetic Compatibility. 2016. Vol. 58, No. 4. P. 1136–1142.

3. Orlov P., Gazizov T., Zabolotsky A. Short pulse propagation along microstrip meander delay lines with design constraints: comparative analysis of the quasi-static and electromagnetic approaches // Applied computational electromagnetics society journal. 2016. Vol. 31. no. 3. P. 238–243.

4. Газизов Р. Р., Газизов Т. Т. Исследование локализации пиковых значений сигнала в печатной плате системы автономной навигации // Инфокоммуникационные технологии. 2017. Т. 15. № 2. С. 170–178.

5. Surovtsev R. S., Nosov A. V., Zabolotsky A. M., Gazizov T. R. Possibility of protection against UWB pulses based on a turn of a meander microstrip line // IEEE Transactions on Electromagnetic Compatibility. 2017. Vol. 59. no. 6. P. 1864–1871.

6. Zabolotsky A. M., Gazizov A. T. Simulation of ultrawide band pulse propagation in asymmetrical modal filter for power network protection // International Journal of Circuits. Systems and Signal Processing. 2015. Vol. 9. P. 68–74.

7. Газизов А. Т. Сравнение результатов измерения и моделирования временного отклика модального фильтра на воздействие сверхкороткого импульса // Доклады ТУСУР. 2015. № 4(38). С. 149–152.

8. Заболоцкий А. М. Использование зеркальной симметрии для совершенствования модальной фильтрации // Доклады ТУСУР. 2015. № 2(36). С. 41–44.

9. Белоусов А. О. Многопроводная микрополосковая линия как модальный фильтр для защиты от сверхкоротких импульсов // Доклады ТУСУР. 2015. № 3(37). С. 124–128.

10. Orlov P. Y., Gazizov T. R., Zabolotsky A. M. The impact of coupled conductors in a dielectric material above an ideally conducting plane on the difference of board delay per unit length of even and odd modes // International Journal of Advanced And Applied Sciences. 2017. Vol. 4. no. 2. P. 68–71.

11. Дмитренко И. В. Анализ частотного отклика модального фильтра для подавления излучаемых эмиссий бортовой аппаратуры космического аппарата // Доклады ТУСУР. 2015. № 4(38). С. 157–160.

12. Новые возможности системы моделирования электромагнитной совместимости TALGAT / С. П. Куксенко [и др.] // Доклады ТУСУР. 2015. № 2(36). С. 45–50.

13. Мусабаев Р. Р. Алгоритм вычисления матрицы погонных сопротивлений многопроводной линии передачи // Научная сессия ТУСУР–2017 : материалы Междунар. науч.-технич. конф. студентов, аспирантов и молодых ученых, посвященной 55-летию ТУСУРа. 2017. Ч. 3. С. 68–71.

14. Заболоцкий А. М., Газизов Т. Р. Калимулин И. Ф. Новые решения для обеспечения электромагнитной совместимости бортовой радиоэлектронной аппаратуры космического аппарата. Томск : Изд-во Томск. гос. ун-та систем управления и радиоэлектроники, 2016. 288 с.

15. CST STUDIO SUITE [Advertisement] // IEEE Antennas and Propagation Magazine. 2013. Vol. 55,. iss. 4. P. c2–c2.

Раздел
Part
2

Авиационная и ракетно-космическая техника

Aviation and spacecraft engineering

UDC 621.45 (075.8)

Siberian Journal of Science and Technology. 2018, Vol. 19, No. 1, P. 50–58

THE INFLUENCE OF THE COMBINED PROPULSION SYSTEM PARAMETERS ON THE INTEGRAL DOSE OF RADIATION WHEN PUTTING A SPACECRAFT INTO A GEOSTATIONARY ORBIT

V. I. Birukov[1], V. P. Nazarov[2*], A. V. Kurguzov[1]

[1]Moscow Aviation Institute (National Research University)
4, Volokolamskoe highway, A-80, ГСП-3, Moscow, 125993, Russian Federation
[2]Reshetnev Siberian State University of Science and Technology
31, Krasnoyarsky Rabochy Av., Krasnoyarsk, 660037, Russian Federation
[*]E-mail: nazarov@sibsau.ru

At present to transfer a spacecraft from a low earth to geostationary orbits propulsion systems of two types are most widely used: chemical and electric. Each type has its advantages and disadvantages. The application of any one of them does not always satisfy conflicting requirements. A possible solution may be the use of a combined propulsion system consisting of a chemical and electric propulsion system. This combination allows the spacecraft to be launched faster than using only electric motors, and it is more efficient in terms of the payload mass than using only a chemical propulsion system. Electric propulsion engines (plasma or ionic) need energy sources. Usually, solar batteries are used for these purposes. The idea of using such a combined propulsion system, consisting of a solar electric propulsion system and the Fregat upper stage, was considered within the "Dvina TM" research project. The use of such a propulsion system requires, even at the design stage, to determine the parameters of the various types of engines that make up its structure. For a reasonable choice it is necessary to have information about the influence of the various propulsion system parameters on the final characteristics of the maneuver.

When putting a spacecraft into orbit, it is necessary for the spacecraft to overcome Van Allen belts while the elements of its design are subjected to intensive action of charged particles, which can significantly limit the period of active existence. Using a combined propulsion system, it is possible to shorten the time of being in a field of high radiation level significantly.

The aim of the study was to synthesize a method for estimating the effect of the combined propulsion system parameters on the integral dose of radiation accumulated during the maneuver, when putting a spacecraft into a geostationary orbit. Different variations of the combined propulsion system application (thrust variations) allow to optimize the maneuver of the spacecraft and to reduce the integral dose of radiation.

As a result of the work, a method was proposed to evaluate the influence of the parameters of the combined propulsion system taking into account the passage of the Earth radiation belts, the program was implemented, calculations were made and the results were analyzed.

Keywords: combined propulsion system, electric propulsion system, the Earth's radiation belt.

Сибирский журнал науки и технологий. 2018. Т. 19, № 1. С. 50–58

ВЛИЯНИЕ ЭНЕРГЕТИЧЕСКИХ ХАРАКТЕРИСТИК КОМБИНИРОВАННОЙ ДВИГАТЕЛЬНОЙ УСТАНОВКИ НА ИНТЕГРАЛЬНУЮ ДОЗУ РАДИАЦИИ ПРИ ВЫВОДЕ КОСМИЧЕСКОГО АППАРАТА НА ГЕОСТАЦИОНАРНУЮ ОРБИТУ

В. И. Бирюков[1], В. П. Назаров[2*], А. В. Кургузов[1]

[1]Московский авиационный институт (национальный исследовательский университет)
Российская Федерация, 125993, г. Москва, А-80, ГСП-3, Волоколамское шоссе, 4
[2]Сибирский государственный университет науки и технологий имени академика М. Ф. Решетнева
Российская Федерация, 660037, г. Красноярск, просп. им. газ. «Красноярский рабочий», 31
[*]E-mail: nazarov@sibsau.ru

В настоящее время для перевода космических аппаратов с низкой околоземной орбиты на геостационарную наиболее широко используются двигательные установки двух типов – химические и электроракетные. Каждый тип имеет свои преимущества и недостатки. Применение какого-то одного из них не всегда удовлетворяет противоречивым требованиям к эффективности маневра вывода. Возможным решением может быть использование комбинированной двигательной установки, состоящей из жидкостного ракетного и электроракетного двигателей. Такая комбинация позволяет выводить космический аппарат быстрее и эффективнее с точки зрения большей массы полезной нагрузки и затрат по сравнению с наличием только *одного типа: электроракетного либо жидкостного ракетного двигателя. Электроракетные двигатели (плазменные или ионные) нуждаются в источниках энергии. Обычно для этих целей применяются солнечные батареи. Идея применения подобной комбинированной двигательной установки, состоящей из солнечной электроракетной установки и разгонного блока «Фрегат», рассматривалась в рамках НИР «Двина ТМ». Применение комбинированной двигательной установки такого вида совмещения требует еще на этапе проектирования определения рациональных энергетических характеристик различных типов двигателей. Для обоснованного выбора необходима информация о влиянии отдельных параметров двигательной установки на итоговые характеристики маневра.*

При выводе космическому аппарату приходится преодолевать радиационные пояса Земли, при этом элементы его конструкции подвергаются интенсивному воздействию заряженных частиц, что может значительно ограничить срок активного существования. Используя комбинированную двигательную установку, можно значительно сократить время нахождения космического аппарата в области с высоким уровнем радиации.

Рассмотрены различные сценарии вывода КА с низкой околоземной на расчетную геостационарную орбиту и оценки полученных при этом аппаратурой суммарных доз радиации. Различные варианты применения комбинированной двигательной установки (варьирования тягой) позволяют оптимизировать маневр КА и снизить интегральную дозу радиации.

В результате был предложен метод оценки влияния энергетических характеристик комбинированной двигательной установки с учетом прохождения радиационных поясов Земли, создана программа, проведены расчеты и выполнен анализ полученных результатов.

Ключевые слова: комбинированная двигательная установка, электроракетный двигатель, радиационный пояс Земли.

Introduction. The use of an electric propulsion system (EPS) for the transfer of a spacecraft (SC) from low earth orbit (LEO) to a geostationary orbit (GSO) makes it possible to increase the payload mass (P) delivered to the final transfer orbit in comparison with traditional chemical propulsion systems (CPS), due to more effective use of the working object mass [1; 2]. The reverse side of the EPS application is a long time of performing the orbital lift maneuver (the typical time of transition from LEO to GSO is 200 days), which leads to a general increase in the time required for putting into orbit, in particular, to an increase in time the SC spends in zones with an elevated level of radiation, the so-called Van Allen belts [3–5].

Fig. 1 shows the dependence of the radiation build-up on the thickness of the aluminum shield for a 200-day flight using EPS and the annual location of the SC on GSO. It can be seen that with a protection thickness of 4 mm, the SC radiation build-up of when putting into the GSO reaches 100 KRad, which is a critical level for electronic products manufactured by the most common technology for the production of KMOP electronic circuits [6–9]. For comparison, for a year of the SC location on a GSO with a similar protection, the radiation build-up is only 10 KRad.

Despite the advantages of using EPS from the point of view of P mass, EPS has initial drawbacks and it is necessary to find solutions that allow to overcome them. One of the possible solutions is the use of a combined propulsion system (CPS), which involves a combination of LPRE and EPS in an integrated system and the application of a particular engine to perform a certain phase of maneuver optimally.

For this purpose, it is necessary to determine the rational power characteristics of propulsion systems even at the design stage. To provide rationale for the choice of CPS design parameters, in this work, a study of the influence of various trajectory division variants of the entire trajectory into sections with the inclusion of various propulsion systems (PS) included in CPS was made.

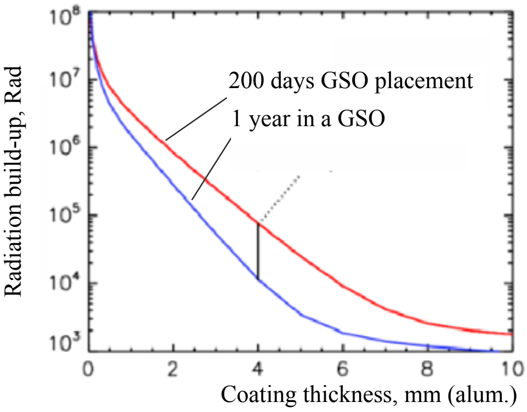

Fig. 1. Dependence of radiation build-up on the protective coating thickness

Рис. 1. Зависимость накопленной дозы радиации от толщины защитного покрытия

Existing software for assessing the effects of radiation on a satellite such as SHIELDOS, SPENVIS, STK SEET, allows to determine the final dose, accumulated by a spacecraft in a certain orbit, but some software is not entirely suitable for evaluating active maneuvers performed using engines of large and small thrust on a certain cyclogram, and the other is inaccessible [10]. Therefore, to carry out the research, it was required, based on existing ionizing radiation (IR) models, to write software adapted to perform the specific research tasks. A significant duration of the low-thrust engine flight requires for the performance of differential equations numerical integration used for various mathematical description phases of the general maneuver, substantial computing powers [11]. This solution required simplification of the existing models, optimization of the algorithms and computational methods, as well as the use of computers with high computational capabilities.

In the process of the research, a technique was developed to assess the spacecraft radiation build-up integral dose, a computer model was created and modeling was performed for a coplanar transition from LEO to GSO.

Formulation of the problem. The spacecraft equipped with EPS is located on LEO (200 km above the Earth). The spacecraft performs a coplanar maneuver of the transition to GSO in two phases. For creating thrust impulses in the first phase, the Fregat upper stage is used to carry out the transfer of the spacecraft from the initial orbit to the intermediate satellite orbit. Another block of several stationary plasma engines (type SPE 140) is used to transfer spacecraft from an intermediate orbit to an inclined geosynchronous orbit of the satellite and to carry out corrections, and then for subsequent transfer to a highly elliptical satellite orbit. Simultaneously, the electric propulsion system (EPS) creates moments of forces around the three axes to control the position of the apparatus relative to the center of mass and to unload the reaction wheel.

It is required to estimate the contribution of each phase to the total dose of SC devices radiation build-up.

Model. In works [1; 2] it was shown that the optimal maneuver of coplanar flight from the LEO to GSO using a pair of large and small thrust engines consists of 2 phases (fig. 2):

1. Gomanov flight with the use of high thrust engines.
2. Orbit raising of a spacecraft to the target highly elliptical orbit along the spiral trajectory by low-thrust engines.

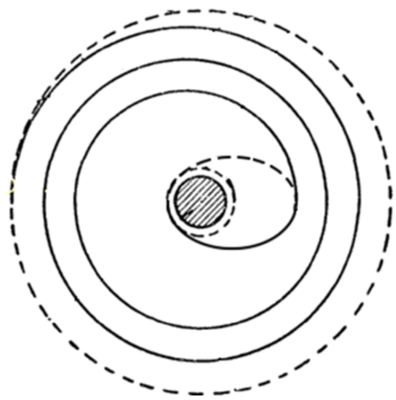

Fig. 2. The trajectory of the flight from LEO to GSO of the satellite using CPS

Рис. 2. Траектория перелета с НОО на ГСО ИСЗ с использованием КДУ

Knowing the initial mass of the spacecraft, the parameters of the propulsion system used in the CPS (thrust, specific impulse), the parameters of the initial and final orbits, one can enter a parameter $k \in (0–1)$, determining the position of the intermediate circular orbit to which the spacecraft is driven using the high-thrust engine in the Gomanov transition.

$$R_2 = R_1 + k\left(R_3 - R_1\right),$$

where R_1 is the radius of LEO; R_3 is the radius of GSO. R_2 can be found analytically with high accuracy. By varying *k* parameter, one can determine the position of the intermediate orbit for each k value and construct a flight cyclogram using analytical dependencies to perform a Gomanov flight in the first phase of the maneuver and analytical dependencies for performing a long flight along a spiral trajectory using a low thruster in the second phase of the maneuver.

Depending on the parameters of the spacecraft, the initial and final orbits and *k* parameter, the spacecraft will move along different trajectories, passing through regions of space with different levels of ionizing radiation from outer space (IROS). Ionizing radiation includes the following types of radiation:

– Radiation from the Earth's natural radiation belts (ENRB) (protons, electrons, α-particles, nuclei);

– Solar cosmic rays (SCR) (protons, electrons, α-particles);

– Solar wind (protons, electrons, α-particles);

– Galactic cosmic rays (GCR) (protons, electrons, α-particles, nuclei);

– Particles in the outer magnetosphere (protons, electrons, α-particles), albedo particles (protons, neutrons), NDO radiation from unclosed drift shells (protons, electrons), precipitating particles during magnetic disturbances (protons, electrons), etc.

The main danger in the spacecraft flight is the emission of ENRB, consisting of charged particles of different penetrating power, with energy from tens of kiV to hundreds of MeV for protons and tens of MeV for electrons which fluxes can reach a large value [12–15].

Galactic cosmic radiation is characterized by small fluxes (up to 5 particles × cm^{-2} × c^{-1}) and high particle energies (up to 1020 eV).

Primary cosmic rays of galactic origin can be attributed to the sources of ENRB particles (high-energy protons arising from the decay of albedo neutrons formed by GCR particles upon interaction with atmospheric nuclei).

SCRs are formed during chromospheric flares on the Sun. Large fluxes of high-energy SCR particles can represent a radiation hazard for semiconductor ERI that are a part of spacecraft instrument units. The total dose of radiation obtained by the spacecraft throughout the maneuver can be received by integrating the individual doses obtained when the space vehicle is located at a specific point in space, the level of ionization radiation (IR) in which is known. To determine the level of IR, the model of IR distribution AR-8 was used [10].

To investigate the effect of phase distribution for the CPS engines on the integral dose received by the spacecraft during the maneuver, a mathematical model was constructed to solve the following main tasks: flight planning, iterative modeling, radiation assessment.

The numerical calculation algorithm for the model is shown in fig. 3 and consists of a series of sequential operations:

1. The parameters of the spacecraft and the parameters of the CPS engines are set.
2. The initial and final orbits are assigned, the distribution of the trajectory maneuver between phases 1 and 2.

3. The initial state vector (position, speed, acceleration) is set.

4. The scheduler performs calculations for the given parameters and builds a cyclogram of switching on the engines.

5. The solver performs the cyclogram step by step, determining the coordinates of the spacecraft at the next step, calculates and summarizes the value of the particle flux at a given point in space.

6. The output unit generates a flight path and an output data set corresponding to a given input data set.

The model of the radiation field. Mass distribution around SC blocks. Calculations of local radiation conditions inside the instrument unit take into account the weakening of the charged particles fluxes by different screening elements. The process of passing particles through matter can be represented by a random sequence of elementary events – their scattering, relaxation, generation, etc., in the intervals between which the particles move freely. The theory is not able to consider the fluctuations in particles energy losses correctly, their angular and energy distribution, and also the theoretical reliable description of the repeated radiation transfer. As a result, a number of approximate calculation methods have been created that are in satisfactory agreement with the experiment [12; 13; 15]. The main characteristics of charged particles deceleration in a substance are the specific losses $S(E)=\dfrac{dE}{dx}$ and particle range $R(E)$ in a substance. The value of $R(E)$ characterizes the braking capacity of the material, it is defined as the average energy lost by the particle per unit of path length. The total range is the path length of a particle with the initial energy E_0, which is braked to a full stop. The relationship of the ranges with energy losses in the material of the structure during braking is described by the expression $R(E)=\int_0^E \dfrac{dE}{S(E)}$. When the particles are decelerated, various loss mechanisms in the material are known. Thus, at low energies, the main role is played by elastic scattering of the particles. For particles with energies $E>1$ МэВ, the mechanisms of braking radiation are activated. Some contribution is made by Cherenkov radiation, transition radiation at medium boundaries, etc. The contribution of each mechanism to the total loss value depends on the particle energy, on the particle type and on the properties of the medium. According to the nature of the charged particles interaction with matter, they are usually divided into heavy (with mass $M >> M_e$) and light ($M \sim M_e$). Several computational models have been developed for determining local radiation conditions behind protective shells of various geometries (for example, hemispheres or half-planes), depending on the material properties and the thickness of the shielding shells. The models are based on the definition of the "range-energy" ratio. Protons and heavier particles lose energy when passing through the protective shell due to the mechanism of ionization of atoms (ionization losses). In this case, the charged particle interacts with the valence electrons of the atom of the shell material. In this case, the energy of the proton E_x passing through a screen of thickness x in the direction of the particle motion with the initial energy E can be determined as:

$$R(E_x)=R(E)-x. \tag{1}$$

This implies the condition for the boundary particles energy completely absorbed by the shielding screen. For particles with energy $E>E_{\text{мин}}$, there is an equality of charged particles flows before and after protection

$$R(E_{\text{мин}})=x. \tag{2}$$

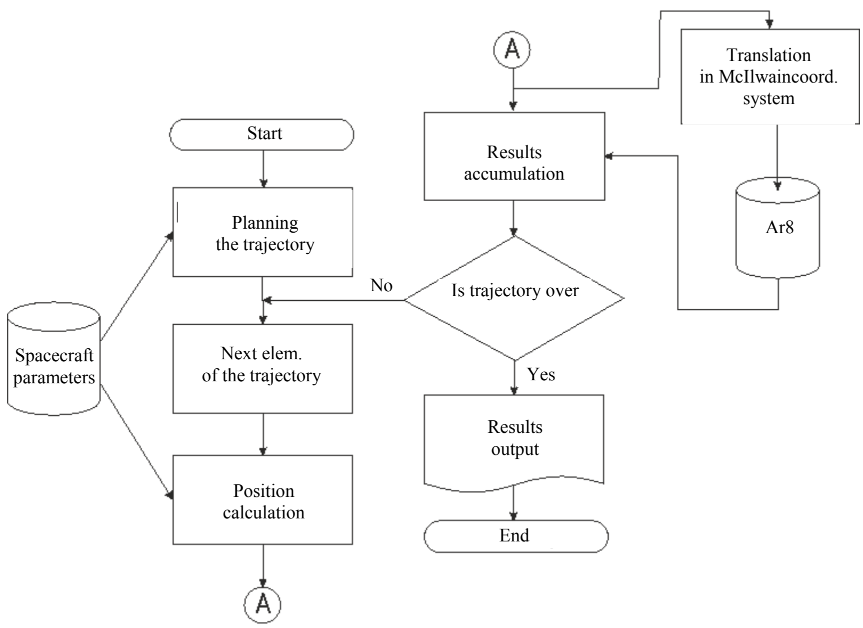

Fig. 3. Block diagram of the simulation algorithm

Рис. 3. Блок-схема алгоритма моделирования

Taking into account the specific losses, the spectrum can be expressed by the dependence

$$\varphi_x(x) = \varphi(E)\frac{S(E)}{S(E_x)_{E=f(E_x)}}. \quad (3)$$

Here $\varphi(E)$ – is the differential spectrum of the particles (protons) before the protection, calculated at the value of the energy E, and $\varphi_x(E_x)$ – is after protection at the point corresponding to the argument E_x. In the arguments of the functions $F(E)$ and $S(E)$ energy values are expressed in terms of E_x.

Often, an empirical relationship is used between range and energy of the form [12; 13]

$$R(E) = \alpha x E^r \quad (4)$$

for initial integral spectra of exponential types:

$$\varphi(>E) = \theta_n\left(\frac{E_н}{E}\right), \quad (5)$$

$$\varphi(>E) = \theta_e \exp\left(-\frac{E}{E_н}\right), \quad (6)$$

$$S(E) = \frac{dE}{dR},$$

further, taking into account the connection between the energy losses and the particle ranges.

For the value of the differential spectra after protection, one can obtain:

$$\varphi_x(E) = n\theta_n E_H^n E^{n-1}\left(1+\frac{x}{R(E)}\right)^{-\frac{n}{r}-1}, \quad (7)$$

$$\varphi_x(E) = \frac{\theta_e}{E_n}\left(1+\frac{x}{R(E)}\right)^{-\frac{n}{r}-1} \exp\left[-\frac{E}{E_H}\left(1+\frac{x}{R(E)}\right)^{\frac{1}{r}}\right]. \quad (8)$$

In both formulas, the subscript x, indicating that this energy value refers to particles that have passed through the defense, is omitted.

To obtain the absorbed dose rate from a stream of charged particles that have passed through a shell of thickness – x, the integral is calculated

$$P_x = \int_{E_1}^{E_2} \varphi_x(E)S(E)dE, \quad (9)$$

where E_1 and E_2 are the boundary energy values for which these energy absorption mechanisms are dominant.

For protons with energies Ep ≥ 10^3 MeV, the contribution to the dose due to ionization is small, therefore we take $E_2 = 10^3$ MeV. The practice of calculating the multiple passage of charged particles through successive shields provides for calculating the function $\varphi_x(E)$ of the differential spectrum, after each successive shell. Taking into account the approximate character of the calculations, in our case a one-time calculation was performed, but with the corresponding summation of the screen thicknesses. There are programs like GEAR 4 [16; 17] and others, which determine local radiation conditions, taking into account the geometry of the absorbing elements. We use assembly of shielding elements from simple sphere objects, cylinders, cones, etc. In our case we use a simplified statement of the problem – a screen in the form of a hemisphere made of aluminum. Fig. 4 shows the dependence of the proton range on its energy when using an aluminum screen. The thicknesses of the cases of the electronic equipment were not taken into account, as the absorption in the cases is carried into the reserve because of the approximate nature of the calculations. The ionization losses were calculated from the formulas (4)–(9) given above with the coefficients according to the data [12; 13]: for the protons α =1.73; r = 3.47 $\cdot 10^{-3}$; for α-particles $\alpha = 1.73$, $r = 3.1\cdot 10^{-4}$.

The radiation build-up received by the SC during the maneuvering time can be determined as the sum of the doses received from the location of the spacecraft in the field with some intensity during the interval

$$D = \int_T P(\vec{r})dt, \quad (10)$$

where D – is the accumulated dose; $P(\vec{r})$ – the intensity of radiation at the space point $\vec{r} = [x\, y\, z]^T$.

Calculation of the local absorbed doses (LAD) inside the SC units under consideration is carried out on the basis of mass distributions along the axes of the instrument blocks coordinates, protective devices and their thicknesses.

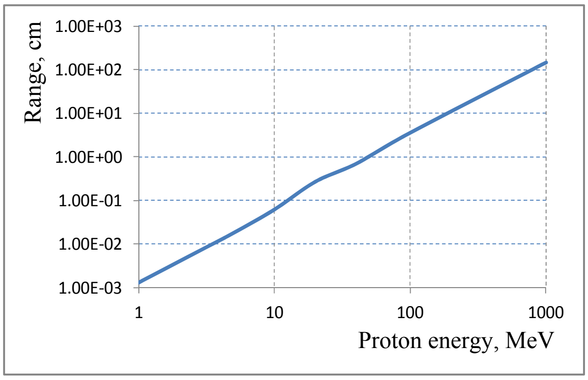

Fig. 4. Dependence of the proton range on its energy (material – aluminum)

Рис. 4. Зависимость пробега протона от его энергии (материал – алюминий)

Local absorbed doses are calculated by the formula:

$$ЛПД = \frac{1}{6} \cdot \sum_{i=1}^{6} D_i, \quad (11)$$

where D_i – is the value of the absorbed dose with a thickness of protection in i direction (there are only 6 of them along the coordinate axes).

The model of the Earth's magnetic field. The Earth's magnetic field is a dipole field whose axis is offset by about 11.4 degrees from the geographical axis. It is known that the intensities of the charged particles fluxes have a high spatial gradient. At low altitudes in the inner zone, a 3 % change in distance creates a 10-fold change in the intensity of the flow. Therefore, it is not possible to use the dipole model to determine the intensity of charged particles flows. It is necessary to use a coordinate system suitable for this task.

The most commonly used is the McIlwain coordinate system in which flows of charged particles having equal intensity are placed on surfaces that can be described in the coordinates L–B. Based on the experimental data collected during the launch of satellites studying the Earth's magnetosphere, a spatial distribution of the intensities was obtained, which formed the basis of the AP 8 and AE 8 models for protons and electrons respectively [16].

The outer radiation belt consists mainly of electrons. A non-large-thickness protective shield protects the spacecraft from their effects effectively. Therefore, in the model only the inner radiation belt, consisting mainly of protons, is considered.

The flight dynamics of the spacecraft is modeled in a geocentric inertial coordinate system. To reduce the computational complexity, it is considered that the starting point of the maneuver coincides with the axis of the inertial GCS. The axis of the magnetic dipole rotates together with the rotation of the Earth. To calculate the IR level at the current point of space, the coordinates of the inertial GCS are transformed into dipole coordinates, after which the IR values are computed in accordance with the AR 8 model [17; 18].

The results of modeling. During modeling, the effect of the parameter k determining the ratio of the total maneuver share per phase realized by the Fregat US to the integral dose of radiation received by the spacecraft during the maneuvering time was studied. The parameter k varied in the range 0–1 in increments of 0.1.

A study of the dependence of the results on the integration step showed that step 1c is sufficient for the convergence of modeling results both in the period of high thrust provided by the Fregat US and during the long spiral transition to the EPS. At the chosen step, the simulation of the longest transition case (full transition to EPS) takes about 20 million steps. Computational complexity, illustrated in the graph (fig. 5), is significant even with the current level of computing facilities and required special measures to obtain results in finite time.

The graphs are given for a spacecraft having the following characteristics:

– initial weight of 3000 kg (CPS consists of LRE and EPS, usually LRE is accepted with low thrust);

– thrust 20 kH;

– specific impulse 3300 m/s.

The EPS has the following characteristics:

– thrust 0,7 H;

– specific impulse of 20,000 m/s.

The initial position of the spacecraft is a circular low Earth orbit with a height of 200 km with zero inclination. The final orbit is GSO.

For the various phase relations, the final characteristics and the transfer trajectory were obtained. An example of the obtained trajectory is shown in fig. 6.

Fig. 7 shows the calculated total radiation doses obtained in the delivery of a spacecraft with a different value of the parameter k. The analysis of the obtained data shows that the use of LRE at the initial stage of positioning phase allows to reduce the total level of the accumulated dose of radiation significantly. However, the use of LRE after passing the Van Allen radiation belts does not have a significant effect on the level of the accumulated radiation dose and its use does not give significant advantages to the dose effects in this sector. With a fully electrical transition, the accumulated dose for 200 days is 100 KRad. If the part of the trajectory with the working LRE is greater than 0.4 from the entire trajectory, the integral value of the accumulated dose varies insignificantly, so, in order to reduce the total dose of accumulated radiation, the use of LRE to perform more than 0.4 of the total transition is not rational.

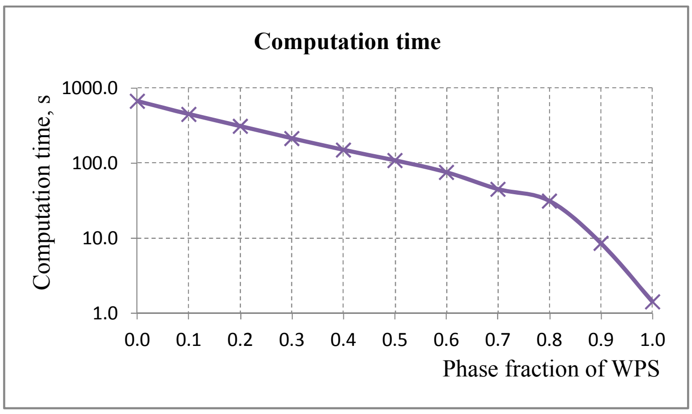

Fig. 5. Required computation time depending on the parameter k

Рис. 5. Требуемое время расчета в зависимости от параметра k

On the other hand, the influence of the working time of LRE as a fraction of the trajectory maneuver phase on the duration of the transition is shown in fig. 8. When using fully electric motors, the duration of the transition is 18 million sec or about 208 days. A balanced ratio between the duration of the transition and the radiation dose received can be selected at the expert level, depending on the mission being implemented and a number of non-formalized factors. The duration of the transition should be considered taking into account the dose effects in the spacecraft design and the choice of the energy characteristics of the engines included in the CPS.

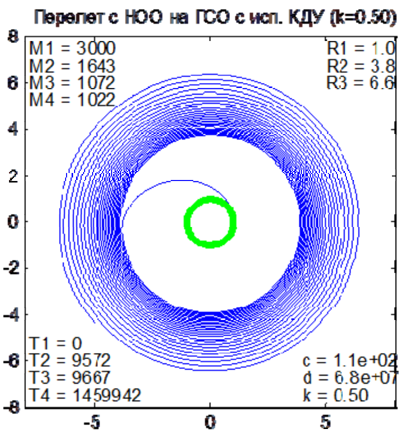

Fig. 6. The example of a trajectory

Рис. 6. Пример траектории

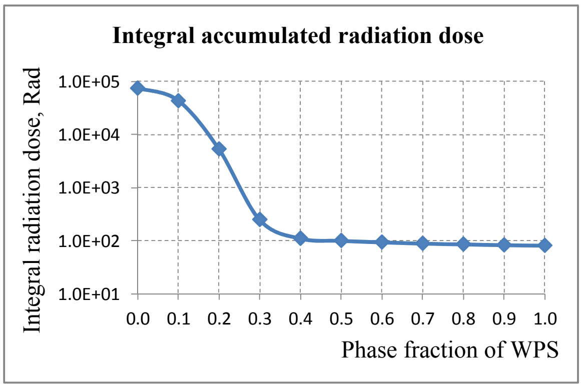

Fig. 7. Diagram of integral accumulated radiation dose depending on the relative duration of the inclusion of CPS LRE

Рис. 7. График интегральной накопленной дозы радиации в зависимости от относительной длительности включения ЖРД КДУ

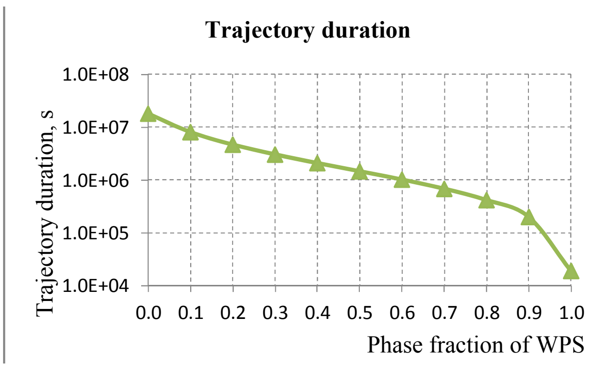

Fig. 8. Duration of trajectory transition depending on the work phase fraction of the LRE

Рис. 8. Длительность траекторного перехода в зависимости от доли фазы работы ЖРД

Conclusion. The use of the CPS, consisting of large and small thrust engines, makes it possible to increase the efficiency of the raising the orbit maneuver from the LEO to the GSO. Efficiency should be understood as a complex indicator, some elements of which can be expressed in numerical form and used in making reasonable decisions at the design stage of CPS for a spacecraft. The calculation performed allows to estimate the influence of the chosen ratio proportion of the maneuver part between different types of engines on the integral dose of radiation received by the spacecraft during the whole maneuver. The rationale for the combination of various propulsion systems in the CPS at the design stage requires an assessment of selection consequences of the CPS parameters for the final characteristics of putting the spacecraft to the target orbit. During the research, a technique was proposed to evaluate the influence of such a choice on the integral dose of radiation received by the spacecraft during the time of transition. The results of the study provide an opportunity for a reasonable decision on the relationship of energy characteristics between the LRE and EPS in the CPS in terms of accumulated radiation dose and the total time of the task. Simulation was carried out for the transition maneuver from LEO on GSO, which is the most widespread and most interesting for optimization. To determine the influence of other factors and different scenarios on the effectiveness of CPS application, further work on modeling and computational research is necessary.

References

1. Gilzin K. A. *Elektricheskie mezhplanetnye korabli* [Electric Interplanetary Ships] Moscow, Nauka Publ., 1970, P. 267.

2. Konstantinov M. S., Kamenkov E., Perelygin B. P. et al. *Mekhanika kosmicheskogo poleta* [The mechanics of space flight: Textbook for technical colleges]. Ed. V. P. Mishina. Moscow, Mashinostroenie Publ., 1989, P. 348.

3. McIlwain C. E. Coordinates for Mapping the Distribution of Magnetically Trapped Particles. *Jour. Geophysical Res.* 1961, No. 66, P. 3681–3691.

4. Runcorn S. K. “The Magnetism of the Earth’s Body” in Handbuch der Physik XLVII “Geophysik I” Springer, 1956, P. 498–533.

5. Van Allen J. A., Ludwig G. H., Ray E. C., McIlwain C. E. Observation of High Intensity Radiation by Satellites 1958 Alpha and Gamma. *Jet Propulsion*. 1958, No. 28, P. 588–592.

6. McIlwain K. E. Coordinates for mapping the distribution of particles trapped by the geomagnetic field. *Operation Starfish. Collection of articles*. Ed. Zhulina I. A. Moscow, Atomizdat Publ., 1964, P. 98–103.

7. Barth J. Applying modeling space radiation environments. 1997 IEEE Nuclear and Space Radiation Effects. Short Course. Applying Computer Simulation Tools to Radiation Effects Problems. Snowmass Conference Center. Snowmass Village, Colorado. 21 July 1997, P. 354–367.

8. The Radiation Design Handbook. European Space Agency. ESTEC, Noordwijk, the Nederland, 1993, 444 p.

9. Fox N., Burch J. L. The Van allen probes mission. Springer, 2013, P. 294.

10. NASA SP-3024 Models of the trapped radiation environment. Vol. I: Inner Zone, National AERONAUTICS AND SPACE ADMINISTRATION, Washington D. C., 1966, P. 178.

11. Lew J. S. “Drift Rate in a Dipole Field”. *Jour. Geophysical Res*. 1961, No. 66, P. 2681–2686.

12. Gegelev I. V., Zubarev A. I., Pudovkin O. L. [Radiation situation on board spacecraft]. *Strategic Missile Forces, TsIPK.* 2001, No. 77, 316 p.

13. Biryukov V. I., Biryukova M. V. [Algorithm for predicting the radiation impact on the microsatellite equipment]. *Vestnik Moskovskogo aviatsionnogo instituta.* 2013, Vol. 20, No. 3, P. 40–49 (In Russ.).

14. Methods for testing and assessing the durability of on-board radio electronic equipment for space vehicles to the effects of electronic and proton emissions of space through dose effects. OST 134-1034-2003.

15. Space Model, t. 2. The impact of the space environment on the materials and equipment of space vehicles. Moscow, MSU SINP, 2007, P. 317.

16. *GOST 25645.211–85. Bezopasnost’ radiatsionnaya ekipazha kosmicheskogo apparata v kosmicheskom polete. Kharakteristiki yadernogo vzaimodeystviya protonov* [State Standard 25645.211–85. Safety of the radiation crew of a spacecraft in space flight. Characteristics of nuclear interaction of protons].

17. Kozlov A. A., Chumakov I. R. [Algorithm for evaluating the structural protection of spacecraft]. *Radiatsionnaya stoykost’ elektronnykh sistem. “Stoykost’-2004”. Nauchno-tekhnicheskiy sbornik.* 2004, Iss. 7, P. 21–22 (In Russ.).

18. *GOST RV 20.57.308–98. Radiatsionnaya stoykost’. Metody rascheta* [State Standard RV 20.57.308–98. Radiation resistance. Methods of calculation].

Библиографические ссылки

1. Гильзин К. А. Электрические межпланетные корабли. 2-е изд. перераб. и доп. М. : Наука, 1970. 267 с.

2. Механика космического полета : учебник для втузов / М. С. Константинов [и др.] ; под ред. В. П. Мишина. М. : Машиностроение, 1989. 348 с.

3. McIlwain C. E. Coordinates for Mapping the Distribution of Magnetically Trapped Particles // Jour. Geophysical Res. 1961, № 66. Pp. 3681–3691.

4. Runcorn S. K. The Magnetism of the Earth’s Body // Geophysik I: Handbuch der Physik XLVII Springer, 1956. Pp. 498–533.

5. Observation of High Intensity Radiation by Satellites 1958 Alpha and Gamma / J. A. Van Allen [et al.] // Jet Propulsion. 1958, № 28. Pp. 588–592.

6. Мак Илуэйн К. Е. Координаты для отображения распределения частиц, захваченных геомагнитным полем // Операция «Морская звезда» : сб. статей / под ред. И. А. Жулина. М. : Атомиздат, 1964. С. 98–103.

7. Barth J. Applying modeling space radiation environments // IEEE Nuclear and Space Radiation Effects. Short Course. Applying Computer Simulation Tools to Radiation Effects Problems / Snowmass Conference Center. Snowmass Village, Colorado, 1997. P. 354–367.

8. The Radiation Design Handbook / European Space Agency. Noordwijk, the Nederland: ESTEC. 1993. 444 p.

9. Fox N., Burch J. L. The Van allen probes mission. Springer, 2013. P. 294.

10. NASA SP-3024. Models of the trapped radiation environment. Vol. I: Inner Zone / National AERONAUTICS AND SPACE ADMINISTRATION. Washington, D.C., 1966. P. 178.

11. Lew J. S. Drift Rate in a Dipole Field // Jour. Geophysical Res. 1961. № 66. Pp. 2681–2686.

12. Гегелев И. В., Зубарев А. И., Пудовкин О. Л. Радиационная обстановка на борту космических аппаратов // РВСН, ЦИПК. 2001. № 77. 316 с.

13. Бирюков В. И., Бирюкова М. В. Алгоритм прогнозирования радиационного воздействия на аппаратуру микроспутника. // Вестник МАИ. 2013. Т. 20, № 3. С. 40–49.

14. Методы испытаний и оценки стойкости бортовой радиоэлектронной аппаратуры космических аппаратов к воздействию электронных и протонных излучений космического пространства по дозовым эффектам: ОСТ 134-1034–2003.

15. Модель космоса. Т. 2. Воздействие космической среды на материалы и оборудование космических аппаратов. М. : МГУ НИИЯФ, 2007. С. 317.

16. Безопасность радиационная экипажа космического аппарата в космическом полете. Характеристики ядерного взаимодействия протонов: ГОСТ 25645.211–85.

17. Козлов А. А., Чумаков А. И. Алгоритм оценки конструкционной защиты космических аппаратов // Стойкость-2004 : науч.-техн. сб. 2004. Вып. 7. С. 21–22.

18. Радиационная стойкость. Методы расчета: ГОСТ РВ 20.57.308–98.

UDC 621.383

Siberian Journal of Science and Technology. 2018, Vol. 19, No. 1, P. 59–65

STUDY OF ANTI-REFLECTIVE COATINGS Ta_2O_5 / SiO_2 FOR IMPROVING THE EFFICIENCY OF MODERN SOLAR CELLS FOR SPACE APPLICATIONS

M. A. Genali[1*], S. K. Sharov[1], A. A. Lebedev[1, 2], N. T. Vagapova[1], B. V. Zhalnin[1]

[1]JSC "Research and Production Enterprise "Kvant"
16, 3rd Mytischinskaya Str., Moscow, 129626, Russian Federation
[2]The National University of Science and Technology "MISiS"
4, Leninsky Av., Moscow, 119049, Russian Federation
[*]E-mail: otdel_17@npp-kvant.ru

Solar cells based on AIIIBV materials in solar arrays are the main energy sources for most modern spacecraft. In spite of the fact that high characteristics have already been achieved, the work for improving solar cells is being continued due to the growth of energy consumption by spacecraft.

One of the directions is decreasing solar radiation reflection by solar cell surface due to the deposition of antireflection coating (ARC). In the article we show the results of the study of ARC (Ta_2O_5 / SiO_2).

We have presented the results of spectral and thickness calculations by special software of ARC on the triple junction (InGaP / InGaAs / Ge) solar cell taking into account cell structure as well.

We have performed the experiment of ARC on the glass-substrate to confirm the manufacturability of the process. ARC deposition has been made by electron-beam evaporation in vacuum. The results of investigation of spectral characteristics of samples obtained by a spectrophotometer confirm the uniformity of covering without relation to the sample position in a machine. Spectral characteristic calculations for glass-substrate coincide with experimental data.

The results of studying spectral characteristics of ARC on a solar cell demonstrate good correspondence with experimental data. The electric characteristics measured by the solar simulator (AM0) before and after the ARC covering on the experimental samples show the increase of short-circuit current up to 122 mA and the rise of efficiency up to 7.5 %. We have demonstrated the results of scanning electron microscopic investigation of ARC on the different positions of solar cells.

Keywords: antireflection coating (ARC), triple junction (TJ) solar cells, current-voltage characteristic, tantalum oxide (V), silicon oxide (IV).

Сибирский журнал науки и технологий. 2018. Т. 19, № 1. С. 59–65

ИССЛЕДОВАНИЕ ПРОСВЕТЛЯЮЩЕГО ПОКРЫТИЯ Ta_2O_5 / SiO_2 СОВРЕМЕННЫХ СОЛНЕЧНЫХ ЭЛЕМЕНТОВ КОСМИЧЕСКОГО НАЗНАЧЕНИЯ

М. А. Генали[1*], С. К. Шаров[1], А. А. Лебедев[1, 2], Н. Т. Вагапова[1], Б. В. Жалнин[1]

[1]АО «Научно-производственное предприятие «Квант»
Российская Федерация, 129626, г. Москва, ул. 3-я Мытищинская, 16
[2]Национальный исследовательский технологический университет «МИСиС»
Российская Федерация, 119049, г. Москва, Ленинский просп., 4
[*]E-mail: otdel_17@npp-kvant.ru

Солнечные элементы (СЭ) на основе материалов AIIIBV в составе солнечных батарей являются основными первичными источниками энергии для большинства современных космических аппаратов (КА). В связи с продолжающимся ростом энергопотребления КА, несмотря на уже достигнутые высокие характеристики, продолжаются работы по совершенствованию СЭ.

Одним из направлений является уменьшение отражения солнечного излучения с фотоактивной поверхности СЭ за счет применения антиотражающего (просветляющего) покрытия (АОП). Приведены результаты исследований АОП на основе слоев оксидов тантала (V) и кремния (IV) (Ta_2O_5 / SiO_2).

Представлены результаты расчета толщин и спектральной характеристики данного покрытия на поверхности трехкаскадного СЭ (InGaP / InGaAs / Ge) с учетом особенностей структуры СЭ, проведенного в специальном программном обеспечении.

Для подтверждения технологичности процесса нанесения АОП проведен эксперимент по нанесению покрытия на стеклянную подложку. Нанесение АОП проводилось методом электронно-лучевого испарения в вакууме. Результаты исследования спектральных характеристик на группе образцов, полученные с помощью спектрофотометра, подтвердили равномерность покрытий вне зависимости от положения образцов в камере *установки. Предварительный расчет спектральной характеристики для АОП на стеклянной подложке показал удовлетворительное совпадение с экспериментальными данными.*

Результаты исследований спектральных характеристик АОП, нанесенного на поверхность СЭ, показали хорошее совпадение с расчетными данными. Измерение электрических характеристик с помощью импульсного имитатора солнечного излучения (АМ0) до и после нанесения АОП на всех экспериментальных образцах СЭ показало прирост тока короткого замыкания в среднем на 122 мА, а КПД – на 7,5 %. Приводятся результаты электронно-микроскопических исследований АОП в различных частях СЭ.

Ключевые слова: просветляющее покрытие, антиотражающее покрытие (АОП), трехкаскадный солнечный элемент, фотоэлектрический преобразователь, вольт-амперная характеристика, оксид тантала (V), оксид кремния (IV).

Introduction. Currently primary energy sources for most spacecraft are solar arrays; their generating part consists of semiconductor devices that perform direct conversion of solar energy into electrical energy. Such devices are called photovoltaic converters or solar cells [1; 2].

Modern triple junction (TJ) solar cells based on AIIIBV semiconducting compounds have high values of output characteristics and resistance to radiation greater than single junction solar cells based on AIIIBV, as well as solar cells based on monocrystalline silicon [3].

However, power requirements to spacecraft are permanently increasing, consequently, requirements to technical characteristics of solar panels are increasing as well, primarily requirements to the efficiency of converting solar radiation flux into electrical energy or efficiency factor.

One of the directions to improve the output characteristics is decreasing the reflection of sunlight from the solar cell surface and thus increasing the penetration of radiation into generating parts of solar cells. The most common reflectivity decreasing method is cell surface antireflection coating (ARC), which represents thin dialectric film with certain reflectivity decreasing characteristics [4].

Single-layer ARC are simple to manufacture and can significantly increase the solar cell conversion efficiency of solar radiation. If some single-layer coating is applied to a semiconductor with a large refractive index, it is possible to achieve near-zero reflection at a certain wavelength, but in this case, changing the wavelength significantly increases the reflection coefficient, and it is a significant drawback [4]. To reduce the reflection over a wider range of wavelengths, we need to use more layers. To obtain low reflection in almost the entire spectral sensitivity region of the solar cell and to maximize their efficiency, one can use two- and three-layer ARC. The further increase in the number of layers theoretically reduces the reflected part of light, but the synthesis of complex coatings (more than 4 layers) is complicated by the difficulty of achieving the required quality in terms of homogeneity and uniformity of application.

When designing ARC, the materials (depending on their refractive indices and required thickness of the layers), are chosen so that the light wave reflected from the front surface of the coating due to interference is extinguished by a wave reflected from the boundary between the dielectric film and the semiconductor material [5]. As a rule, transparent amorphous films of nanometric thickness of the following compositions: ZnS, Ta_2O_5, TiO_2, MgF_2, Al_2O_3 and SiO_2 find use as materials for solar cell ARC [6].

Experimental part. Based on previous studies [7] and analysis of the structures of modern solar cells [8] we planned a comprehensive ARC study based on the materials of tantalum oxide (V) (Ta_2O_5) and silicon (IV) oxide (SiO_2). The study includes the following steps:

– calculation of ARC design by studying the features of the structure of TJ solar cell (InGaP / InGaAs / Ge) obtained by gas phase epitaxy from metalloorganic and hydride compounds;

– pilot-tests of manufacturing methods of ARC on more accessible substrates;

– application of optimized ARC directly to the surface of TJ solar cells (InGaP / InGaAs / Ge), measurement of critical parameters;

– experimental estimation of ARC influence on the solar cell characteristics.

Calculation of ARC based on Ta_2O_5 and SiO_2 materials. For TJ solar cells (InGaP / InGaAs / Ge) obtained by gas phase epitaxy from metalloorganic and hydride compounds, we have carried out a series of ARC calculations based on (Ta_2O_5 / SiO_2), taking into account the features of the solar cell structure. Calculations have been performed in the program OptiLayer Thin Film Software [9].

The maximum sensitivity of TJ solar cells based on AIIIBV is in the range 400–1500 nm, as it is shown in fig. 1 [10]. The long-wave part of the spectrum (from more than 900 nm) is absorbed and transformed by germanium subcell. When the subcells are connected in series, the current contribution of the germanium subcell is not limiting, so the lower stage has a significant current reserve, which allows us to narrow the spectral optimization range to 400–900 nm. Thus, the calculation of the optimization have been carried out taking into account the minimization of reflection in the wavelength range 400–900 nm of the solar radiation spectrum AM0.

It should be noted that there are not sufficient data in the literature to perform the calculations, therefore, we have performed experimental work to obtain dispersion dependencies: each of the layers (Ta_2O_5 and SiO_2) has been deposited on germanium substrates by electron-beam evaporation in vacuum. Dispersion dependences of the deposited layers have been obtained on a spectrometric ellipsometer SENTECH's SENpro in the wavelength range 400–900 nm.

Dispersion dependences of refractive indices Ta_2O_5, SiO_2, InAlP и InGaP [11–14] used in the calculations are shown in fig. 2.

In calculations we have used characteristics of TJ structures (InGaP / InGaAs / Ge): the upper subcell is the layer of composition $In_{0.49}Ga_{0.51}P$ with the thickness ≥ 0.5 μm and above it the wide-gap "window" of the upper subcell is the layer of composition $In_{0.5}Al_{0.5}P$ with the thickness varying from 35 to 100 nm. The thickness of the "window" layer of the upper is comparable to the thicknesses of the ARC layers and the spectral reflection coefficients have large values in comparison with the selected oxides, therefore, the epitaxial layers will have a significant effect on the results of calculations ARC (Ta_2O_5 / SiO_2). It should be noted that we have carried out all the calculations for the light incidence angle 0^o, i. e. along the normal to the surface of a solar cell.

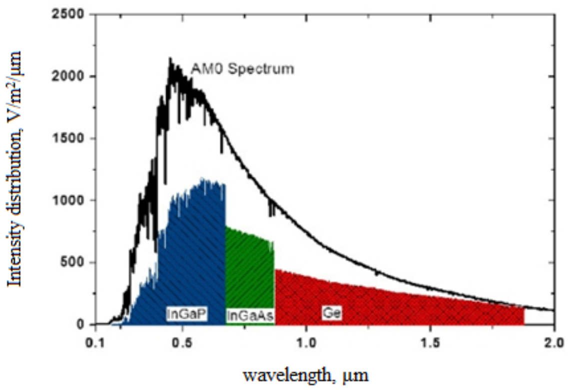

Fig. 1. Spectral distribution of absorption intensity of solar radiation for TJ solar cells

Рис. 1 Спектральное распределение интенсивности поглощения солнечного излучения для трехкаскадных СЭ

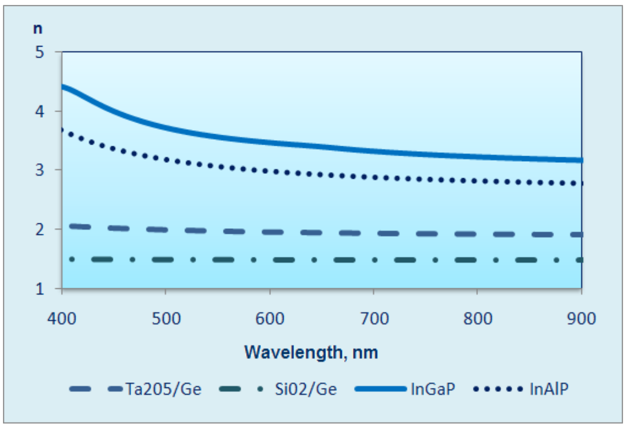

Fig. 2. Dispersion dependences of refractive indices: the dashed line is Ta_2O_5 / Ge; the dot-dashed line is SiO_2 / Ge; the solid line is InGaP, dotted line – InAlP

Рис. 2. Дисперсионные зависимости показателей преломления: пунктирная линия – Ta_2O_5 / Ge; штрих-пунктирная линия – SiO_2 / Ge; сплошная линия – InGaP; точечная линия – InAlP

Fig. 3 shows the calculated spectral characteristic (R (λ)) for ARC consisting of tantalum oxide Ta_2O_5 and silicon oxide SiO_2, taking into account the layer $In_{0.5}Al_{0.5}P$, on the layer $In_{0.49}Ga_{0.51}P$. The calculated thickness of ARC layers is 45 nm for Ta_2O_5 and 60 nm for SiO_2. The root-mean-square deviation of the calculation results from the target values is 3.9 %.

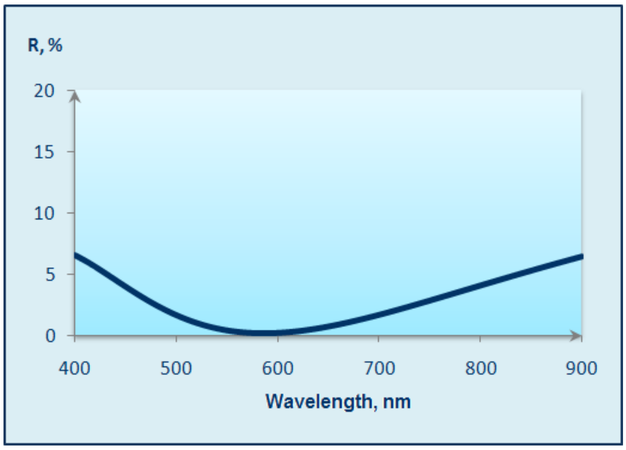

Fig. 3. The calculated spectral characteristic (R (λ)) for ARC (Ta_2O_5 / SiO_2) on the surface of the solar cell

Рис. 3. Рассчитанная спектральная характеристика (R(λ)) для АОП (Ta_2O_5 / SiO_2) на поверхности СЭ

Confirmation of the correspondence between the calculated and experimental values as well as the pilot-tests of manufacturing methods have carried out in another experiment that has included calculation part and physical deposition of ARC layers on the glass substrate.

ARC test (Ta_2O_5 / SiO_2) on a glass substrate. To confirm experimentally the calculated data, we have chosen glass substrates with geometric dimensions corresponding to the overall dimensions of the solar cell and the thickness of approximately 150 μm, the number of substrates is 4 pieces. The deposition of ARC on selected samples has been carried out by the electron beam method of sputtering the target in a high-vacuum industrial equipment, followed by the ARC thermal stabilization process.

The results of measuring the spectral dependence of the reflection obtained with the help of Shimadzu UV-3600 spectrophotometer for all four samples showed good agreement with the calculated dependences. To confirm the uniformity of the coating, as well as the reliability of the results for each sample, we have carried out a series of measurements on different parts of the surface.

The data obtained during the measurement of the spectral characteristics of the layers on a glass substrate, practically coincide with the calculated values in the greater part of the investigated range. It is shown in fig. 4. This fact confirms the reliability of calculations and allows us to expect such a matching of experimental and calculated data for ARC on the surface of a three-stage solar cell.

ARC (Ta_2O_5 / SiO_2) deposition on the TJ solar cell surface. Having carried out a number of necessary growth and build-up processes, we applied ARC (Ta_2O_5 / SiO_2) on the face of the solar cell in a similar way in a high-vacuum equipment with the use of electron-beam sputtering method and subsequent thermal stabilization. The study of the spectral characteristic (R(λ)) of the obtained ARC, similar to the experiment with glass substrates, has been carried out on a spectrophotometer.

The comparison of the experimental and calculated spectral characteristics (R(λ)) for ARC (Ta_2O_5 / SiO_2) on the surface of a TJ solar cell (you can see it in fig. 5) showed good agreement in the spectral range of the upper subcell, and deviations do not exceed 3 %. The variance in the region of more than 720 nm is explained by the presence of a distributed Bragg reflector in the structure of the solar cell between the second and the third subcell, which is not taken into account in the calculations. It should be taken into consideration that nanoscale ARC (Ta_2O_5 / SiO_2) can have composition deviations from stoichiometry in real layers, which can lead to additional measurement errors. Unfortunately, the computational algorithms also do not take into account the contribution of the reflection of the metal contact mesh on the facial area of real samples. Thus, according to estimates [15], the shading for the solar cell of the standard size used in the experiment is 1.82 %.

The dimensions of the contact grid and their contribution to the reflection can be estimated from the image obtained with the scanning electron microscope (SEM) in fig. 6, *a*. This image (fig. 6, *b*) also shows the features of real layers of ARC (Ta_2O_5 / SiO_2) on the solar cell. The studies carried out with the help of SEM confirmed the value of the given layer thicknesses taking into account the measurement inaccuracy on the microscope (fig. 6, *c*, *d*).

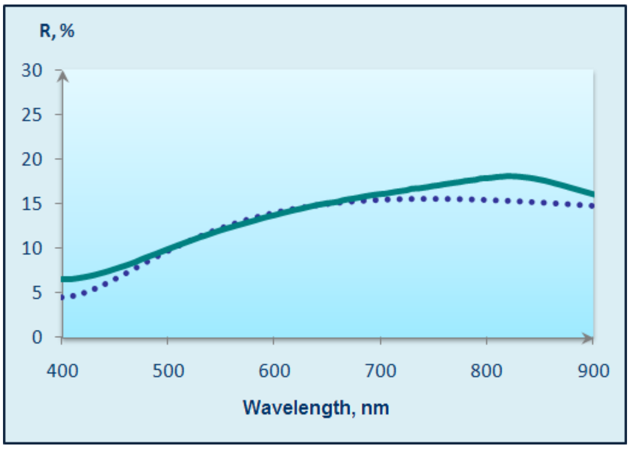

Fig. 4. Comparison of the experimental and calculated spectral characteristics (R(λ)) for (Ta_2O_5 / SiO_2) ARC on a glass substrate: solid line – experimental data, dotted line – calculated data

Рис. 4. Сравнение экспериментальных и расчетных спектральных характеристик (R(λ)) для АОП (Ta_2O_5 / SiO_2) на стеклянной подложке: сплошная линия – экспериментальные данные, точечная линия – расчетные данные

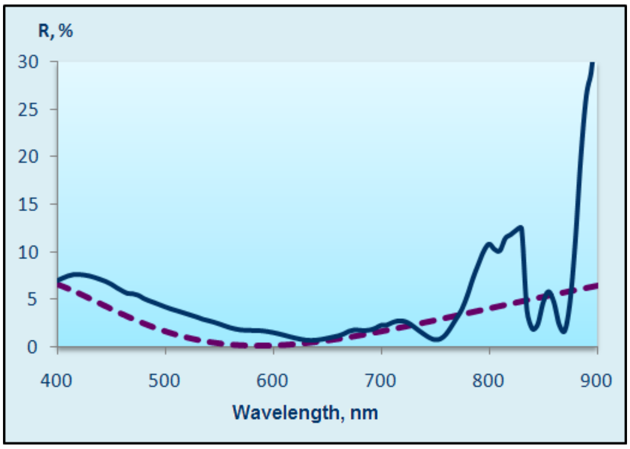

Fig. 5. Comparison of the experimental and calculated spectral characteristics (R(λ)) for ARC (Ta_2O_5 / SiO_2) on the surface of TJ solar cell: solid line – experimental data, dotted line – calculated data

Рис. 5. Сравнение экспериментальных и расчетных спектральных характеристик (R(λ)) для АОП (Ta_2O_5 / SiO_2) на поверхности трехкаскадного СЭ: сплошная линия – экспериментальные данные, пунктирная линия – расчетные данные

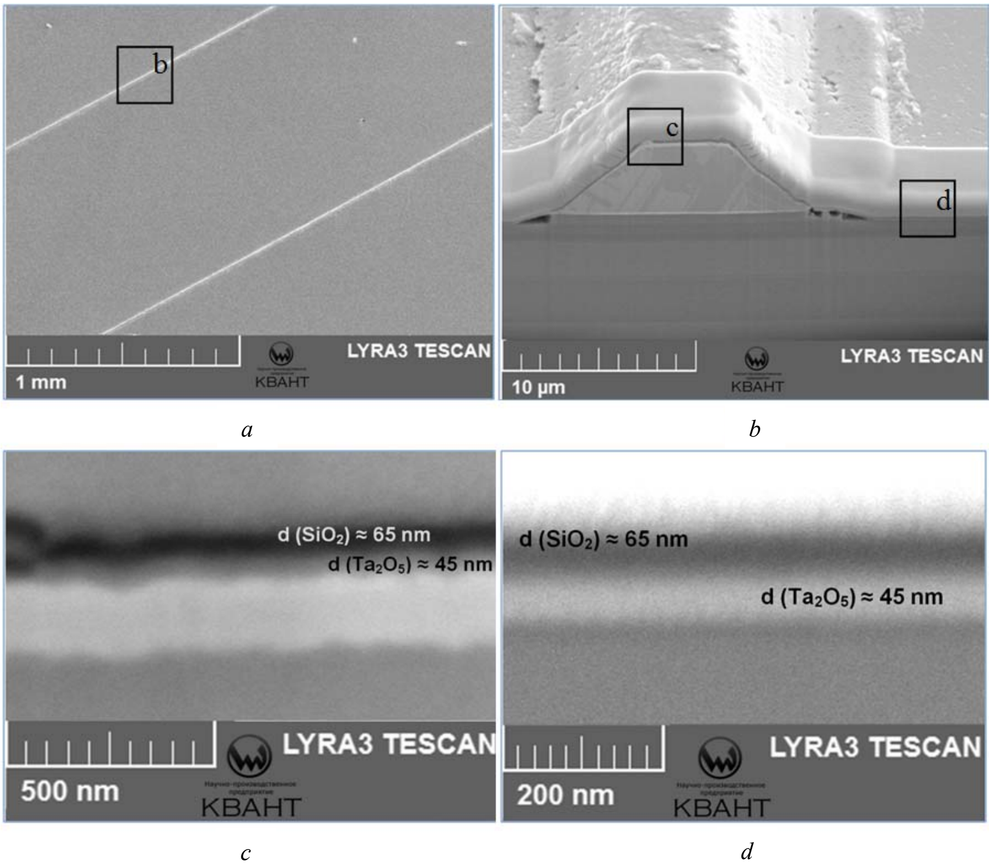

Fig. 6. Results of ARC (Ta_2O_5 / SiO_2) study by SEM

Рис. 6. Результаты исследования АОП (Ta_2O_5 / SiO_2) на СЭМ

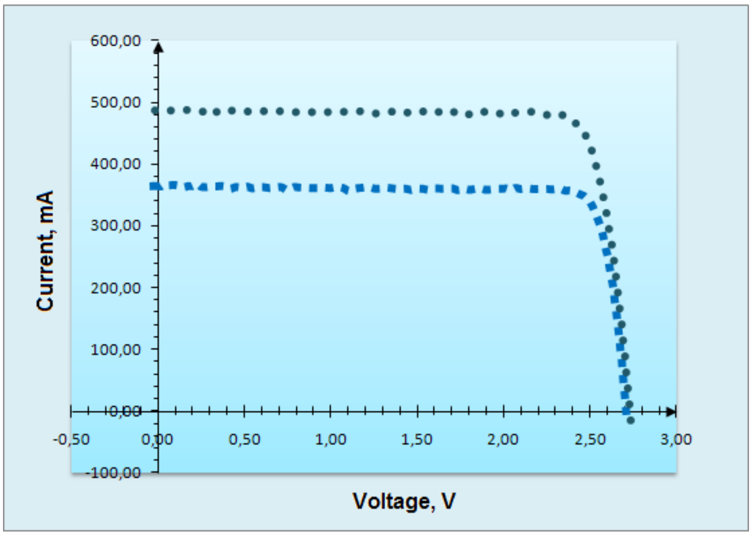

Fig. 7. Volt-ampere characteristic of a solar cell sample: the dotted line is a solar cell sample without ARC, the dashed line is a solar cell sample with ARC (Ta_2O_5 / SiO_2)

Рис. 7. Вольт-амперная характеристика образца СЭ: точечная линия – образец СЭ без АОП, пунктирная линия – образец СЭ с АОП (Ta_2O_5 / SiO_2)

To estimate the effect of ARC (Ta_2O_5 / SiO_2) on the output characteristics of solar cells, we have performed the measurements of the volt-ampere characteristics of solar cells using a pulsed radiation simulator in the AM0 spectrum before and after deposition of ARC on the surface of a TJ solar cell. The results of the experiment are shown in fig. 7. For processing the obtained data, we have used the program for analyzing volt-ampere characteristics of photoelectric converters, which is an element of technology support systems [16; 17].

According to the results of testing a batch of samples, the short-circuit current (I_{sc}) increased on average by 122 mA after applying ARC (Ta_2O_5 / SiO_2) on the solar cell, and the efficiency increased in average by 7.5 %.

Conclusion. We have made calculations of ARC (Ta_2O_5 / SiO_2), taking into account peculiarities of structure of TJ solar cell (InGaP / InGaAs / Ge). The calculations allow suppose that the deposition of this coating is rather promising.

The experiment in deposition of ARC (Ta_2O_5 / SiO_2) on the glass substrate allowed to draw conclusions about its technological effectiveness, as well as the necessity of performing a similar experiment on the surface of a TJ solar cell and to select the necessary modes for carrying out the process. The study of the spectral characterristic R(λ) of the obtained samples has showed the uniformity of coating application in all positions of the samples in a vacuum chamber.

Theoretically calculated and experimentally obtained on the solar cell surface of ARC (Ta_2O_5 / SiO_2) showed an increase in the output characteristics of the solar cells, namely, the I_{sc} increase was approximately 122 mA, and the efficiency increased by about 7.5 %. Electron microscopic study of the experimental samples of solar cells (InGaP / InGaAs / Ge) showed the uniformity of ARC (Ta_2O_5 / SiO_2), and, taking into account the inaccuracy, confirmed the specified thickness parameters of the layer thicknesses.

It should be noted that this coating is optimized for the structure of TJ solar cells (InGaP / InGaAs / Ge) and does not imply additional surface protection. However, for the application of solar cells in space, the front and back surfaces of the device are laminated with special protective glass. The design, which includes directly a solar cell with ARC applied, glue and protective glass is called a stack. The calculation does not take into account the design of the stack, which can have a significant effect on the final result. In the future, a full optical assembly (stack) of a TJ solar cell (InGaP / InGaAs / Ge) with ARC (Ta_2O_5 / SiO_2) should be calculated.

Acknowledgements. The authors are grateful to the staff of the department of the development of advanced transducers and technologies and department of research and production of solar cells at JSC "Research and Production Enterprise "Kvant". We acknowledge the company "TESKAN" Ltd. and personally Lukashova M. V. (specialist, Ph. D.).

The development of support system technology and additioned with IVCAnalysis software module compatible have been carried out in the frames of the program called "UMNIK" (the agreement with the Innovation Promotion Fund № 9106GU2015 of 24.12.15.).

Благодарности. Авторы выражают благодарность сотрудникам отдела разработки перспективных преобразователей и технологий и отдела исследования и изготовления фотопреобразователей АО «НПП «Квант», а также ООО «ТЕСКАН» и лично специалисту, к. ф.-м. н.. М. В. Лукашовой. Разработка системы сопровождения технологии, дополнение ее модулем IVCAnalysis [16; 17] проведена в рамках программы «УМНИК», соглашение с Фондом содействия инновациям № 9106ГУ2015 от 24.12.15 г.).

References

1. Alferov Zh. I., Andreev V. M., Rumyantsev V. D. [Trends and prospects of the development of solar photovoltaics]. *Fizika i tekhnika poluprovodnikov*. 2004, Vol. 38, No. 8, P. 937–948 (In Russ.).

2. Lebedev A. A., Slyshchenko E. V., Vagapova N. T. [Modern state of solar cells for space apllication based on A3B5]. *Tezisy dokladov XX Nauchno-tekhnicheskoy konferentsii molodykh uchenykh i spetsialistov OAO "RKK "Energiya" im. S. P. Koroleva"* [Abstracts of the XX Scientific and Technical Conference of Young Scientists and Specialists of OJSC "RKK "Energia", S.P. Korolev"]. Korolev, 2014, P. 466–467 (in Russ.).

3. Bahrami A., Mohammadnejad S., Soleimaninezhad S. et al. Optimized Single and Double Layer Antireflection Coatings for GaAs Solar Cells. *International journal of renewable energy research*. 2013. Vol. 3, No. 1, P. 79–83.

4. Koltun M. M. *Selektivnyye opticheskiye poverkhnosti preobrazovateley solnechnoy energii* [Selective optical surfaces of solar energy converters]. Moscow, Nauka Publ., 1979, 216 p.

5. Ritter E. [Dielectric film materials for optical applications]. *Fizika tonkikh plonok*. 1975, Vol. 8, P. 7–60 (In Russ.).

6. Saylan S., Milakovich T., Hadi S. A. et al. Multilayer antireflection coating design for GaAs0.69P0.31/Si dual-junction solar cells. *Solar Energy*. 2015, No. 122, P. 76.

7. Zhalnin B. V., Kagan M. B., Semenov V. V. et al. [Development and creation of pilot production of nanostructured cascade solar cells in the A3B5 system]. *Avtonomnaya energetika: tekhnicheskiy progress i ekonomika*. 2009, No. 26 (In Russ.).

8. Slyshchenko Ye. V., Naumova A. A., Vagapova N. T. at al. [Overview of modern photovoltaic space-based converters based on AIIIBV compounds]. *Sbornik tezisov konferentsii "Razrabotka, proizvodstvo, ispytaniya i ekspluatatsiya kosmicheskikh apparatov i sistem", IV Nauchno-tekhnicheskaya konferentsiya molodykh spetsialistov AO "ISS"* [Proceedings of the conference "Development, production, testing and operation of space vehicles and systems", IV Scientific and technical conference of young specialists of JSC "ISS"]. Zheleznogorsk, 2017 (In Russ.).

9. Furman Sh., Tikhonravov A. V. Basics of optics of multilayer systems. Editions Frontiers. Gif-sur Yvette, 1992, P. 242.

10. Forbes D., Hubbard S. Solar-cell-efficiency enhancement using nanostructures. Solar & Alternative Energy, SPIE, 2010. Avalible at: http://spie.org/newsroom/3124-solar-cell-efficiency-enhancement-using-nanostructures?SSO=1 (assessed 25.04.2017).

11. Nanolithogphy Research Labs. Optical Properties of Thin Films for DUV and VUV Microlithograph. Available at: http://www.rit.edu (assessed 27.04.2017).

12. *Ofitsial'niy sait fiziko-tekhnicheskogo instituta imeni A. F. Ioffe Rossiyskoy Akademii Nauk* [The official website of the Physico-Technical Institute named after A. F. Ioffe Russian Academy of Sciences. N, k database on NSM]. Available at: http://www.ioffe.ru (assessed 25.04.2017).

13. Refractive index database. Base of physical parameters of materials. Available at: http://refractiveindex.info (assessed 03.03.17).

14. Levinshtein M., Rumyantsev S., Shur M. Handbook series semiconductor parameters. *Ioffe Institute and Rensselaer Polytechnic Institute*. 1999, Vol. 2.

15. Naumova A. A., Vagapova N. T., Lebedev A. A. [Modeling and calculation of ohmic and optical losses in modern solar cells based on InGaP / InGaAs / Ge]. *Tezisy dokladov XXI Nauchno-tekhnicheskoy konferentsii molodykh uchenykh i spetsialistov OAO "RKK "Energiya" im. S. P. Korolova.* [Abstracts of the XXI Scientific and Technical Conference of Young Scientists and Specialists of JSC "RKK "Energia", S. P. Korolev"]. Korolev, 2017, P. 130–131 (In Russ.).

16. Tsynikin S. A., Lednev A. M., Lebedev A. A. *IVCAnalysis Programma analiza vol't-ampernykh kharakteristik fotoelektricheskikh preobrazovateley i kartografirovaniya dannykh FEP po strukture risunka fotoshablona plastiny* [Program for the analysis of current-voltage characteristics of photoelectric converters and mapping of FEP data on the structure of the pattern of a photomask plate]. Certificate of state registration of the program is RF № 2014662567, 03.12.2014.

17. Lebedev A. A., Lednev A. M., Tsynikin S. A. [Construction of a system for tracking the technology of manufacturing solar cells for space applications based on A3B5 compounds]. *Tezisy dokladov XX Nauchno-tekhnicheskoy konferentsii molodykh uchenykh i spetsialistov OAO "RKK "Energiya" im. S. P. Koroleva"* [Abstracts of the XX Scientific and Technical Conference of Young Scientists and Specialists of OJSC "RKK "Energia", S. P. Korolev"]. Korolev, 2014, P. 466–467 (In Russ.).

Библиографические ссылки

1. Алфёров Ж. И., Андреев В. М., Румянцев В. Д. Тенденции и перспективы развития солнечной фотоэнергетики // Физика и техника полупроводников. 2004. Т. 38, № 8. С. 937–948.

2. Лебедев А. А., Слыщенко Е. В., Вагапова Н. Т. Современное состояние солнечных элементов космического назначения на основе соединений А3В5 // Тезисы докладов XX науч.-техн. конф. молодых ученых и специалистов ОАО «РКК «Энергия» им. С. П. Королёва» (10–14 нояб. 2014, г. Королёв). Королев, 2014. С. 466–467.

3. Optimized Single and Double Layer Antireflection Coatings for GaAs Solar Cells / A. Bahrami [et al.] // International journal of renewable energy research. 2013. Vol. 3, № 1. P. 79–83.

4. Колтун М. М. Селективные оптические поверхности преобразователей солнечной энергии. М. : Наука, 1979. 216 с.

5. Риттер Э. Пленочные диэлектрические материалы для оптических применений // Физика тонких пленок / под ред. Г. Хасса, М. Франкомбра, Р. Гофмана. М. : Мир, 1978. Т. 8. С. 7–60.

6. Multilayer antireflection coating design for GaAs0.69P0.31/Si dual-junction solar cells / S. Saylan [et al.] // Solar Energy. 2015. № 122. С. 76.

7. Разработка и создание опытного производства наноструктурных каскадных ФЭП в системе A_3B_5 / Б. В. Жалнин [и др.] // Автономная энергетика: технический прогресс и экономика. 2009. № 26.

8. Обзор современных фотоэлектрических преобразователей космического назначения на основе соединений AIIIBV / Е. В. Слыщенко [и др.] // Разработка, производство, испытания и эксплуатация космических аппаратов и систем : IV науч.-техн. конф. молодых специалистов АО «ИСС». Железногорск, 2017. 224 с.

9. Furman Sh., Tikhonravov A. V. Basics of optics of multilayer systems. Editions Frontiers. Gif-sur Yvette, 1992. 242 p.

10. Forbes D., Hubbard S. Solar-cell-efficiency enhancement using nanostructures [Электронный ресурс] // Solar & Alternative Energy. SPIE, 2010. URL: http://spie.org/newsroom/3124-solar-cell-efficiency-enhancement-using-nanostructures?SSO=1 (дата обращения: 25.04.2017).

11. Nanolithogphy Research Labs // Optical Properties of Thin Films for DUV and VUV Microlithograph [Электронный ресурс]. URL:http://www.rit.edu (дата обращения: 27.04.2017).

12. Официальный сайт Физико-технического института имени А. Ф. Иоффе Российской академии наук [Электронный ресурс] // n,k database on NSM. URL: http://www.ioffe.ru (дата обращения: 25.04.2017).

13. Refractive index database – база физических параметров материалов [Электронный ресурс]. URL: http://refractiveindex.info/ (дата обращения: 03.03.17).

14. Handbook series semiconductor parameters / под ред. M. Levinshtein, S. Rumyantsev, M. Shur ; Ioffe Institute and Rensselaer Polytechnic Institute,. 1999. Vol. 2.

15. Наумова А. А., Вагапова Н. Т., Лебедев А. А. Построение модели и проведение расчета омических и оптических потерь в современных солнечных элементах на основе гетероструктур InGaP / InGaAs / Ge / Тезисы докладов XXI науч.-техн. конф. молодых ученых и специалистов АО «РКК «Энергия» им. С. П. Королёва» (25 окт.–3 нояб. 2017, г. Королёв. Королев, 2017. С. 130–131.

16. Программа анализа вольт-амперных характеристик фотоэлектрических преобразователей и картографирования данных ФЭП по структуре рисунка фотошаблона пластины : Свид. о гос. регистрации программы для ЭВМ и IVCAnalysis / С. А. Цыникин, А. М. Леднев, А. А. Лебедев № 2014662567 ; регистр. 03.12.14.

17. Лебедев А. А., Леднев А. М., Цыникин С. А. Построение системы сопровождения технологии изготовления солнечных элементов космического назначения на основе соединений А3В5 // Тезисы докладов XX науч.-техн. конф. молодых ученых и специалистов ОАО «РКК «Энергия» им. С. П. Королёва» (10–14 нояб. 2014, г. Королёв). Королев, 2017. С. 466–467.

UDC 629.783

Siberian Journal of Science and Technology. 2018, Vol. 19, No. 1, P. 66–75

DETERMINATION OF THE MINIMAL REFLECTING SURFACE POINTS NUMBER REQUIRED FOR ASSESSMENT OF LARGE-SIZE TRANSFORMABLE ANTENNA PATTERN DEVIATION

G. I. Kalabegashvili*, E. V. Bikeev, M. G. Mathylenko

JSC "Academician M. F. Reshetnev" Information Satellite Systems"
52, Lenin Str., Zheleznogorsk, Krasnoyarsk region, 662972, Russian Federation
*E-mail: Kalabegashvili89@yandex.ru

Construction of communication spacecraft with large-size transformable antennas developed tendencies to increase the operational band frequencies, to reduce specific mass and to increase the overall dimensions of the structures. The improvement of technical performance of communication spacecraft with large-size antennas cannot be achieved without ensuring the required accuracy of antenna pattern and of the antenna gain coefficient at its maximum.

Factors affecting the final quality of large-size structures for space application (of antennas in particular), keep influencing the products through all their service life – from design and production to tests and actual operation. The "direct" elimination of the negative factors affecting the final output is often unprofitable considering the present development of technological support in hi-tech industries. In this respect, control of the ultimate operational characteristics of large-size spacecraft antennas in conditions of real performance, and compensation, if necessary, of deviations from the required values, is optimal with respect to the output/cost ratio. This approach is practical in determining the onboard antenna pattern and compensating its operational distortions in the process of specified spacecraft performance.

There are two methods of measuring the antenna pattern at the orbit. The first method is based on measurements of radio engineering characteristics obtained from ground space vehicles' service stations. This method is sufficiently accurate, but it has several drawbacks. For example, this method increases the number of requirements to ground stations – their number, location and characteristics of the equipment in use. The second method bases on obtaining radio engineering characteristics from the configuration and orientation of antenna reflector. The reflector is imaged as a cloud of checkpoints reflecting the deviations of the construction's configuration and orientation from the specified values.

To obtain the antenna pattern measurements using the second method, an antenna configuration control system (ACCS) must be worked out for measuring the coordinates of the reflector surface points. To perform its specific function, the system should have the following configuration: measuring equipment mounted on the spacecraft casing, and control elements fixed on the construction components. This configuration allows to present the antenna construction components in the form of checkpoint cloud.

In the process of the system development the constructional analysis of the possibility of using the antenna configuration measurements for the its pattern calculation and for further assessment of its deviation from the specified values was made. This article presents the assessment of the required number of monitored checkpoints on the reflector surface. For this purpose, Ku-band of frequencies was chosen as one of the most common frequency bands used by telecommunication spacecraft. Several sets of points were considered, among them the sets belonging both to the deformed reflector profile and to the one without deformation. For each set the antenna pattern calculation was made. Visual representations of the focal beam and the directive antenna gain were compared. The analysis of the obtained data allowed to determine the necessary minimum of checkpoints for antenna pattern calculation with the required accuracy. The obtained data were taken into account in formulating the requirements for the system of orbital control of antenna configuration.

Keywords: large-size transformable antenna, deployable reflector, antenna pattern, orbital adjustment, antenna configuration control system.

Сибирский журнал науки и технологий. 2018. Т. 19, № 1. С. 66–75

ПОИСК МИНИМАЛЬНОГО КОЛИЧЕСТВА ТОЧЕК ОТРАЖАЮЩЕЙ ПОВЕРХНОСТИ РЕФЛЕКТОРА, НЕОБХОДИМОГО ДЛЯ ОЦЕНКИ ОТКЛОНЕНИЯ ДИАГРАММЫ НАПРАВЛЕННОСТИ КРУПНОГАБАРИТНЫХ ТРАНСФОРМИРУЕМЫХ АНТЕНН

Г. И. Калабегашвили*, Е. В. Бикеев, М. Г. Матыленко

АО «Информационные спутниковые системы» имени академика М. Ф. Решетнёва»
Российская Федерация, 662972, г. Железногорск Красноярского края, ул. Ленина, 52
*E-mail: Kalabegashvili89@yandex.ru

В создании связных космических аппаратов с крупногабаритными трансформируемыми антеннами имеются тенденции к увеличению частот рабочего диапазона, снижению удельной массы и возрастанию общих габаритов конструкций. Улучшение технических характеристик связных космических аппаратов с крупногабаритными антеннами невозможно без обеспечения требуемой точности наведения диаграммы направленности, коэффициента усиления в её максимуме.

Факторы, влияющие на конечное качество крупногабаритных конструкций космического назначения, и антенн в частности, присутствуют на всем жизненном цикле данной продукции: от проектирования и изготовления до испытаний и эксплуатации в натурных условиях. При этом прямое устранение причин, негативно влияющих на конечный результат, зачастую является экономически невыгодным при нынешнем развитии технологического обеспечения данных наукоемких производств. В связи с этим контроль конечных эксплуатационных характеристик крупногабаритных антенн космических аппаратов в натурных условиях и, в случае необходимости, парирование их отступлений от требуемых значений являются наиболее оптимальными с точки зрения отношения результат/затраты. Данный подход реализуется при определении диаграммы направленности бортовой антенны и компенсации её искажения в процессе эксплуатации космического аппарата по целевому назначению.

Существуют два способа измерения диаграммы направленности на орбите. Первый способ основан на измерениях радиотехнических характеристик, производимых по наземным станциям обслуживания космических аппаратов. Данный способ, несмотря на приемлемую точность, имеет ряд недостатков. Например, использование данной методики увеличивает количество требований к наземным станциям – их количеству, размещению и характеристикам применяемой аппаратуры. Второй способ основан на определении радиотехнических характеристик, исходя из формы и положения рефлектора антенны. Рефлектор представляют в виде облака измеренных точек, которые отражают отклонения формы и положения конструкции от проектных значений.

Для реализации измерений диаграммы направленности по второму способу необходимо разработать систему контроля геометрии антенны, предназначенную для измерения координат точек поверхности рефлектора. Для выполнения целевых задач системы имеет место следующая схема: измерительная аппаратура, размещенная на корпусе космического аппарата, и контрольные элементы, размещенные на элементах конструкции. Такая конфигурация системы позволяет представлять элементы конструкции антенны в виде облака контрольных точек.

В рамках работ по разработке этой системы проведен проектный анализ возможности применения измерений геометрии антенны для расчета диаграммы направленности и дальнейшей оценки её отклонения от проектных значений. Проведена оценка необходимого количества измеряемых контрольных точек поверхности рефлектора. Для этих целей был выбран Ku-диапазон частот как один из наиболее популярных диапазонов частот, используемых в телекоммуникационных космических аппаратах. Были рассмотрены несколько вариантов наборов точек. Среди них были наборы точек, принадлежащих как недеформированному, так и деформированному профилю рефлектора. По каждому набору был произведен расчет диаграммы направленности антенны. Проведено сравнение визуальных представлений фокального луча и коэффициента направленного действия. В ходе анализа полученных данных было определено минимально необходимое количество контрольных точек для расчета диаграммы направленности с требуемой точностью. Полученные данные были учтены при формировании требований к системе орбитального контроля геометрии антенны.

Ключевые слова: крупногабаритные трансформируемые антенны, развертываемый рефлектор, диаграмма направленности, орбитальная юстировка, система контроля геометрии антенны.

Introduction. Today one of the priority trends in the world satellite construction is producing communication spacecraft (SC) with large-size transformable antennas (LTA) [1; 2]. LTA is a complex technical system on the deployment and on the required configuration of which depend both the quality of the signal provided for subscribers in the required coverage zone, and general accuracy of SC specified performance.

The quality of the signal is determined by the orientation accuracy of antenna pattern (AP) of LTA [3] for the target coverage zone, and by the level of LTA gain in this zone. The necessary radio engineering characteristics (REC) of LTA are determined by its practically applied construction configuration designed with the required accuracy. One of the LTA configuration characteristics that influence its REC is the accuracy of the feed and reflector interposition, greatly dependent on the reflector load-carrying structure – the rod. The next important LTA component (from the point of view of the AP formation) is the reflector [4–6]. The reflector is a rigid framework consisting of a base and spring-type spokes, a form-building structure fastened to the framework, and a net sheet sewn to the form-building structure (fig. 1). To maintain the quality of the signal the form of the net sheet surface of the reflector must be close to the paraboloid of revolution.

Because of the large size of LTA for its rather small weight, the structure rigidity is not sufficient. As a result, during the operation at the orbit the structure is subject to temperature and elastic deformations [7; 8] which, in turn, cause deterioration of the antenna REC and make the signal in the coverage zone weaker.

It is possible to compensate REC deterioration, also with the help of the stated current AP [9].

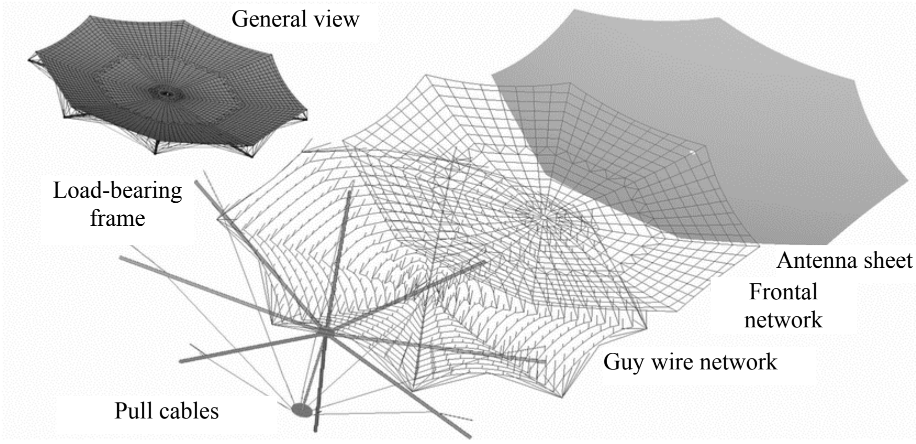

Fig. 1. Reflector design

Рис. 1. Конструкция рефлектора

So the following task can be formulated: to measure the AP and determine the deviations of its axis from the specified values. To assess these AP deviations of SC working at the orbit, two different methods can be used.

The first method is based on the REC measurements made by ground SC service stations. This method is sufficiently accurate, but it has some drawbacks. For example, it can't be applied when the spacecraft is being used for its specified purpose. The requirements for ground stations – their number, location and equipment – also increase when this method is applied.

The second method is based on deriving REC measurements from the configuration and orientation of the antenna reflector. The reflector is imaged as a cloud of monitored checkpoints able to reflect the deviations of the construction's configuration and orientation from the specified values.

To obtain AP measurements using the second method, an antenna configuration control system (ACCS) must be worked out [10–13] for measuring the coordinates of the reflector surface points. The system should have the following components: measuring equipment mounted on the spacecraft casing, and control elements (light reflectors), on the construction elements. This configuration allows to present the LTA construction in the form of a checkpoint cloud.

The initial data required for AP calculation are:

– coordinates of the radio-reflecting surface points or general orientation of the given surface (when radio-reflecting surface deformations are negligible);

– feed directional pattern;

– operation frequency.

Thus ACCS measurements complementing AFS characteristics specified at the stage of its design and production form the initial data sufficient for AP setting.

There is also a problem of the required number of checkpoints. To control the configuration of "rigid" reflectors (reflectors having negligible radio-reflecting surface deformations), it is enough to monitor several checkpoints, the number and location of which is chosen to meet the precision requirements when determining the orientation of such reflectors. However, to control the configuration of elastic large-size reflectors functioning as parts of antennas with UHF operation frequencies, it is necessary to assess the reflecting surface deformations, since the deformation data contribute a lot to REC of the antenna. In these cases the required number of monitored checkpoints can reach several thousand. Besides the factors mentioned, the number of checkpoints determined by ACCS depends on:

– weight and dimensions of control elements;

– structural features of the antenna;

– characteristics of calculation algorithms and on-board computer;

– characteristics of measuring instruments.

This paper shows how the number of checkpoints may influence the precision of REC determination for an antenna with a large-size deformed reflector. A calculation was made to find the AP representing the LTA focal beam electrical axis orientation for different numbers of checkpoints. AP calculations were made both for the theoretically determined reflector profile (without deformation) and for the deformed reflector profile. The lower KU-band frequency was taken for the antenna operational frequency.

Initial data for evaluating the electrical characteristics of antennas. To find the necessary number of points of the reflector surface sufficient for calculating the antenna electrical characteristics with proper accuracy, AP and orientation of the focal beam electrical axis were calculated for the antenna reflector with a 12-meter aperture. The calculations were made for different sets of points: 1488, 1250, 1000, 750, 500, 250, 25.

In the documentation for software sets used to calculate AP, it is advisable to choose the number and orientation of control surfaces that make the distance between two neighboring points not more than $\lambda/(5–6)$ mm, where λ is wave length.

However, it must be taken into account that the reflector surface is a set of flat trapezoidal facets formed by the frontal network checkpoints. It means that the location of points inside the facets can be determined by the points forming each facet. Thus, the influence of points within each facet on the AP can be expressed through the 4 nodal points of the frontal network.

Consequently, the basic data on reflector surface deformations can be derived from coordinates of the frontal network nodal points, and to obtain a reliable AP it is enough to use for calculation the data on points, the distance between which (for the current implementation of the frontal network) does not meet the above-mentioned requirement.

So, for the checkpoints, at their maximum number, the frontal network points with coordinates derived from the reflector finite-element model (FEM) can be taken, in case the model is framed according to the method described in [14].

The deformations were obtained in modelling how the reflector KEM is affected by a model device of reflector configuration finishing adjustment (RCFA). RCFA is a device that allows to adjust the position of the spoke in the plane of the reflector symmetry axis. The main controls are the tie-rod devices which tighten the cords attached to the spokes.

A more detailed description of RCFA model and implementation logic is presented in [15].

The cartogram of distribution of the frontal network checkpoints deviations from the theoretical profile made for the reflector initial design is shown in fig. 2. Deviations are calculated as the shortest distance from frontal network checkpoints to theoretical profile. The SCD of the frontal network checkpoints from the reflector theoretical profile is 0.2 mm.

The deformed configuration was framed artificially by changing the RCFA tie-rods position in FEM. Tie-rod movements are presented in tab. 1.

The cartogram of distribution of the frontal network checkpoints deviations from the theoretical profile for the reflector with deformations is presented in fig. 3. The SCD of the frontal network checkpoints from the reflector theoretical profile is 18.1 mm.

The theoretical paraboloid coordinate system (TPCS) is a coordinate system associated with the SC casing, in which the theoretical location of the reflecting surface points (theoretical profile) of the reflector is described by the canonical equation of paraboloid of revolution.

The reflector coordinate system (RCS) is the coordinate system determined in [9].

The coordinates of different numbers of reflecting surface points were formed by performing the following sequence of actions:

1. The coordinates of a large number (1001000) of the reflecting surface points were formed. The coordinates y and z of these points were calculated from the following parametric equations:

$$\begin{aligned} y &= 3\upsilon\cos(\nu) + 8.3, \\ z &= 3\upsilon\sin(\nu), \end{aligned} \tag{1}$$

where υ – parameter changing from 0.002 to 2 with step of 0.002; ν – parameter changing from 0 to 2π with step of 0.002.

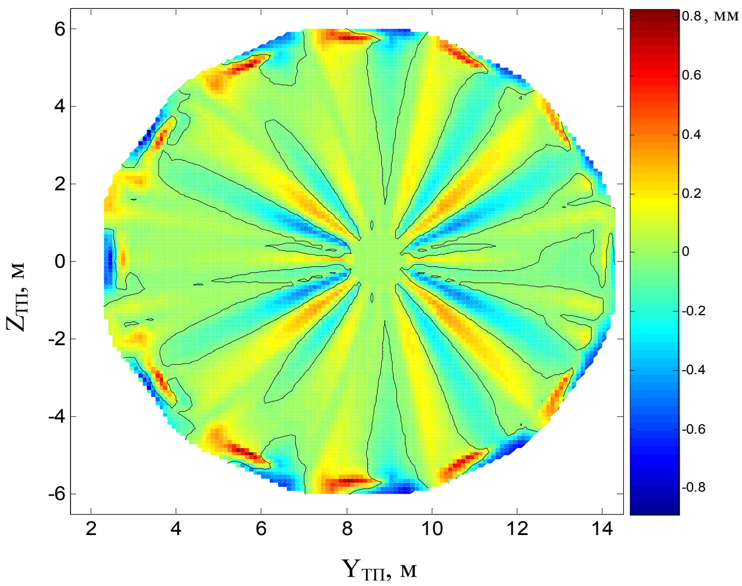

Fig. 2. Distribution of deviations from TP in the initial design

Рис. 2. Распределение отклонений от ТП в проектном состоянии

Table 1

Rod movements, mm

Rod 7	Rod 8	Rod 9	Rod 10	Rod 11	Rod 12	Rod 1	Rod 2	Rod 3	Rod 4	Rod 5	Rod 6
20	0	20	0	20	0	20	0	20	0	20	0

Note: “+” – is the movement in direction of the reflector folding.

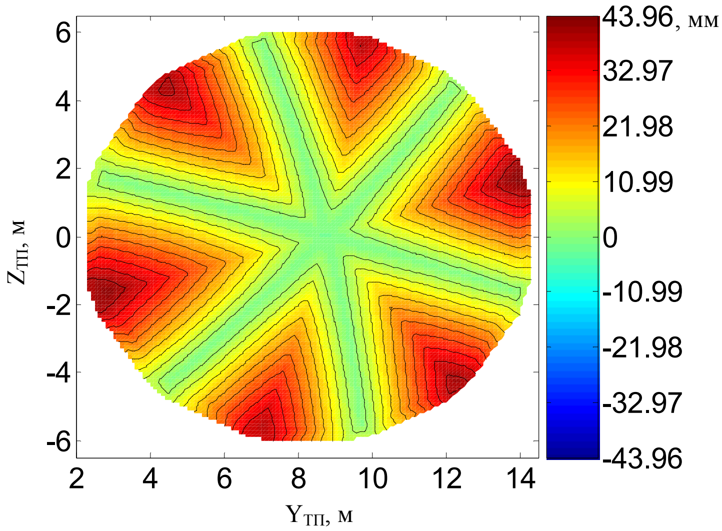

Fig. 3. Distribution of deviations from TP in the deformed state

Рис. 3. Распределение отклонений от ТП в деформированном состоянии

The x coordinates of the deformed and undeformed profile were calculated by interpolating the frontal network checkpoints (1488) of the deformed reflector at the points with y and z coordinates, calculated from the expression (1).

2. The coordinates of the reflecting surface points formed in 1 were recalculated in RCS:

$$\begin{vmatrix} X_{Р} \\ Y_{Р} \\ Z_{Р} \end{vmatrix} = M_{ТП\_Р} \cdot \left(\begin{vmatrix} X_{ТП} \\ Y_{ТП} \\ Z_{ТП} \end{vmatrix} - \begin{vmatrix} X_{Р\_ТП} \\ Y_{Р\_ТП} \\ Z_{Р\_ТП} \end{vmatrix} \right), \quad (2)$$

where $M_{ТП\_Р} = \begin{vmatrix} \cos(\theta) & \sin(\theta) & 0 \\ -\sin(\theta) & \cos(\theta) & 0 \\ 0 & 0 & 1 \end{vmatrix}$ – transition matrix from TPCS to RCS; θ – rotation angle of RCS about the axis of OZ TPCS equal to 26.5651 degr; $X_{ТП}$, $Y_{ТП}$, $Z_{ТП}$ – coordinates of the point in TPCS; $X_{Р}$, $Y_{Р}$, $Z_{Р}$ – coordinates of the point in RCS; $X_{Р\_ТП}$, $Y_{Р\_ТП}$, $Z_{Р\_ТП}$ – coordinates of RCS center location in TPCS equal to [2296.35 mm, 8731.49, mm 0].

3. Coordinates of the required number of reflecting surface points were formed. For the purpose a formation of a network of points uniformly distributed in the *YOZ* RCS plane was carried out: y coordinate of the network points changed from –7 to 7 m; z coordinate of the network points changed from –6 до 6 m; interpoint step relative to both coordinates made h (tab. 2).

The coordinates x of the points of the reflector's deformed and undeformed profiles were determined by interpolation of the points obtained in 2, at the points of the pre-formed network. In the process of interpolation, the network points located outside the radio-reflecting surface were discarded. A network of 250 points of radio-reflecting surface in the *YOZ* plane of RCS after interpolation is shown in fig. 4.

4. The coordinates of the required number of reflecting surface points formed in 3 were recalculated in TPCS

$$\begin{vmatrix} X_{ТП} \\ Y_{ТП} \\ Z_{ТП} \end{vmatrix} = M_{Р\_ТП} \cdot \begin{vmatrix} X_{Р} \\ Y_{Р} \\ Z_{Р} \end{vmatrix} + \begin{vmatrix} X_{Р\_ТП} \\ Y_{Р\_ТП} \\ Z_{Р\_ТП} \end{vmatrix}, \quad (3)$$

where $M_{Р\_ТП} = \begin{vmatrix} \cos(\theta) & -\sin(\theta) & 0 \\ \sin(\theta) & \cos(\theta) & 0 \\ 0 & 0 & 1 \end{vmatrix}$ – transition matrix from RCS to TPCS; θ – rotation angle of RCS about the axis of *OZ* TPCS; $X_{ТП}$, $Y_{ТП}$, $Z_{ТП}$ – coordinates of the point in TPCS; $X_{Р}$, $Y_{Р}$, $Z_{Р}$ – coordinates of the point in RCS; $X_{Р\_ТП}$, $Y_{Р\_ТП}$, $Z_{Р\_ТП}$ – coordinates of RCS center location in TPCS.

A network of 250 points of radio-reflecting surface in *YOZ* plane of TPCS is shown in fig. 5. Dashed lines in fig. 5 show the circle that is the generator of a cylinder, the intersection of which with the paraboloid of revolution forms the radio-reflecting surface.

Antenna REC calculation. That was made for the following numbers of reflector surface points: 1488, 1250, 1000, 750, 500, 250 and 25.

Fig. 6 shows the focal beam pattern at the lower operational band frequency for the antenna reflector theoretical profile at different profile points number.

Fig. 7 shows the focal beam pattern at the lower operational band frequency for the deformed reflector profile of antennas with different profile points number.

Fig. 8 shows the focal beam pattern for the undeformed profile (left) and for the deformed profile (right) at 25 points.

Tab. 3 presents calculations of antenna focal beam DG at the upper KU-band frequency for the deformed reflector profile and for that without deformation.

Analysis of calculation results. Fig. 6 and 8 of the focal beam pattern indicate that with the lower number of reflector's monitored points, the beam pattern is distorted; the effect is present even at 500 checkpoints, and the beam pattern gets completely distorted at 25 checkpoints.

Table 2

Network step *h*, m

Reflecting surface points number	1250	1000	750	500	250
Theoretical profile	0.31775	0.355	0.4098	0.499986	0.7052
Deformed profile	0.317	0.3552	0.40954	0.5	0.7055

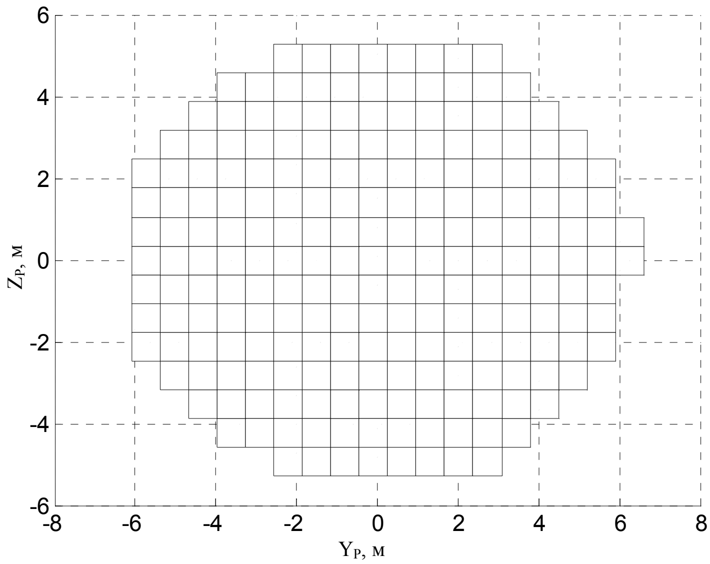

Fig. 4. Network of 250 points in the *YOZ* plane of RCS after interpolation

Рис. 4. Сетка из 250 точек в плоскости *YOZ* СКР после интерполяции

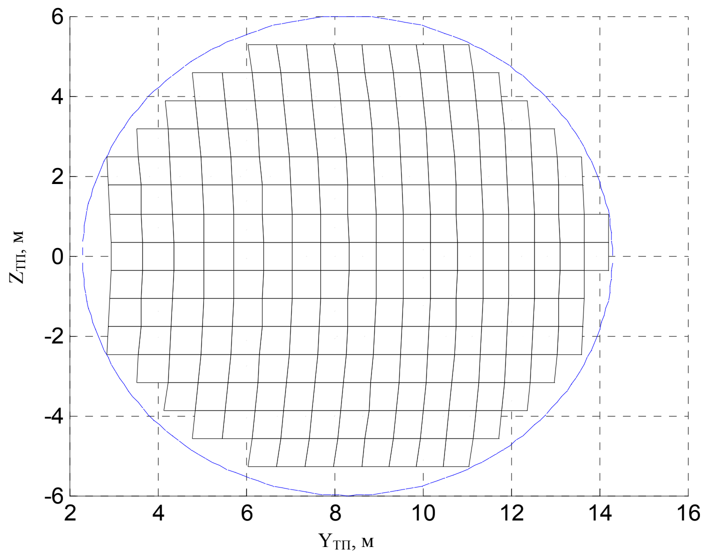

Fig. 5. Network of 250 points in the *YOZ* plane of TPCS

Рис. 5. Сетка из 250 точек в плоскости *YOZ* СКТП

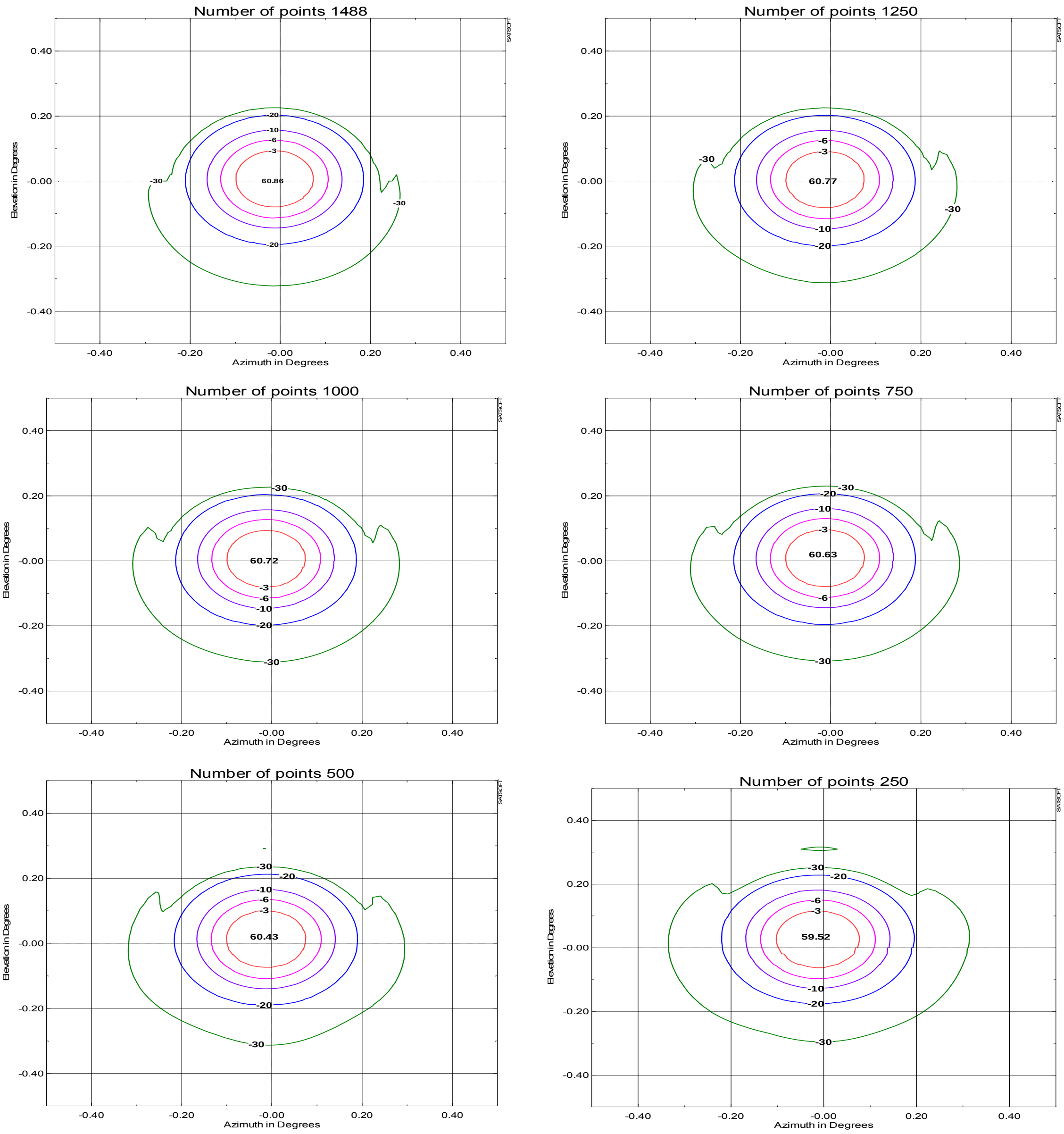

Fig. 6. Focal beam pattern at the lower operational band frequency
with different numbers of the reflector theoretical profile points

Рис. 6. Контур фокального луча на нижней частоте рабочего диапазона
при различном количестве точек теоретического профиля рефлектора

Fig. 7 and 8 showing the focal beam pattern for a deformed reflector indicate that the given reflector deformation causes a deep distortion of the beam. They also confirm that with a decrease in the number of reflector's monitored points the contour of the beam is distorted. For the deformed reflector the beam contour is completely blurred at 25 checkpoints.

The results of directive gain of antenna focal beam calculation presented in tab. 2 confirm the deterioration of focal beam characteristics at the upper operational band frequency with the decrease in the number of reflector's monitored points. The minimum of 250 monitored reflector checkpoints is acceptable; at that the calculated deterioration of the focal beam DG at the upper operational band frequency is 2.21 %. That number of the reflector surface monitored points makes it possible to assess the antenna focal beam electrical characteristics with a permissible error.

Conclusion. The problem of choosing the monitored points number of the reflecting surface considered in this paper is relevant for the problem of design of LTA configuration control system at the orbit. Such system allows to determine the AP when the orientation and form of the LTA components is stated. The proposed approach to determination of the monitored points number, as well as the results of its application for a specific operating antenna are aimed at perspective SC projects and at formulating the technical specification requirements for making SC antenna-feeder systems.

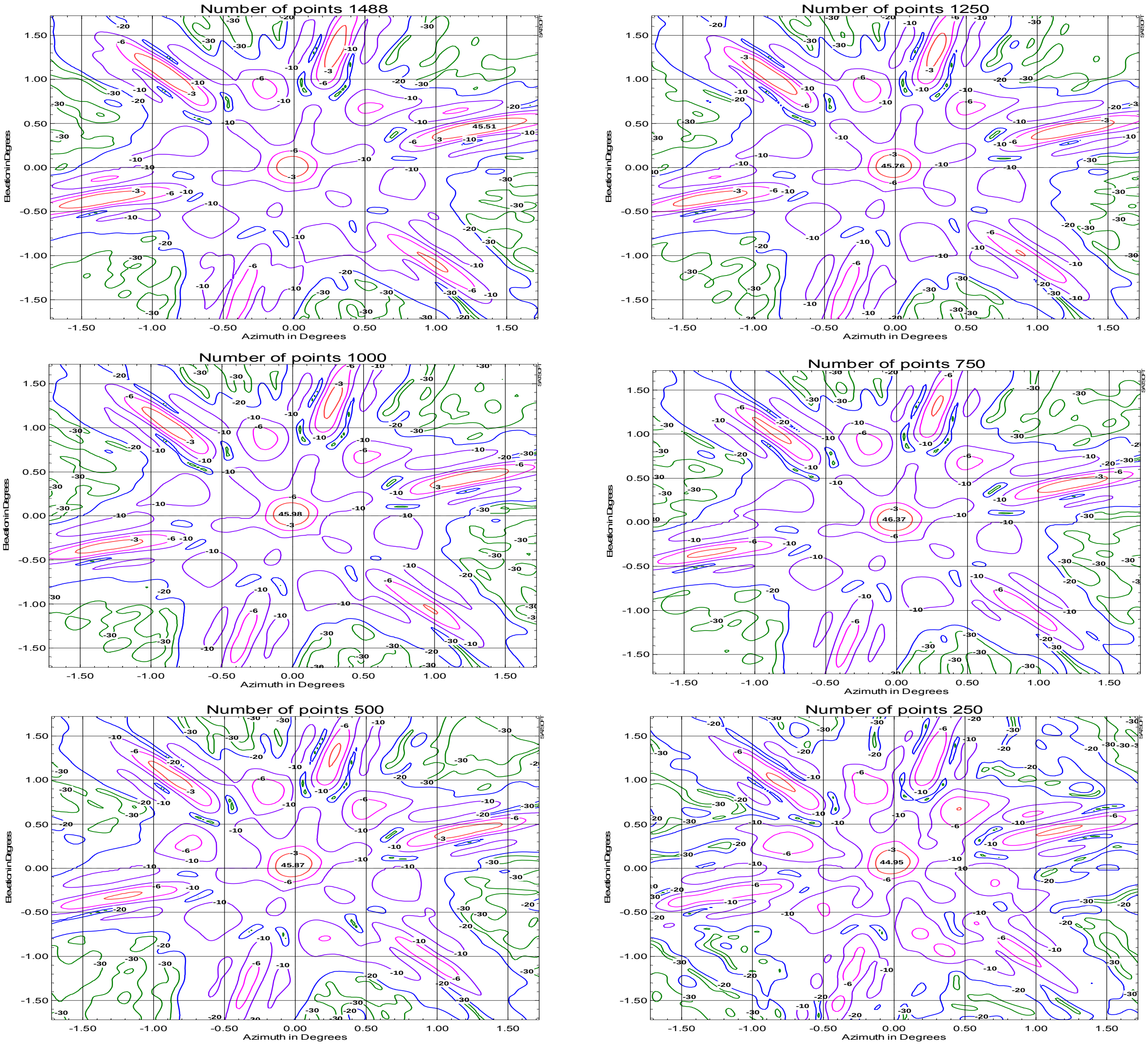

Fig. 7. Focal beam pattern at the lower operational band frequency
with different numbers of the deformed reflector profile points

Рис. 7. Контур фокального луча на нижней частоте рабочего диапазона
при различном количестве точек деформированного профиля рефлектора

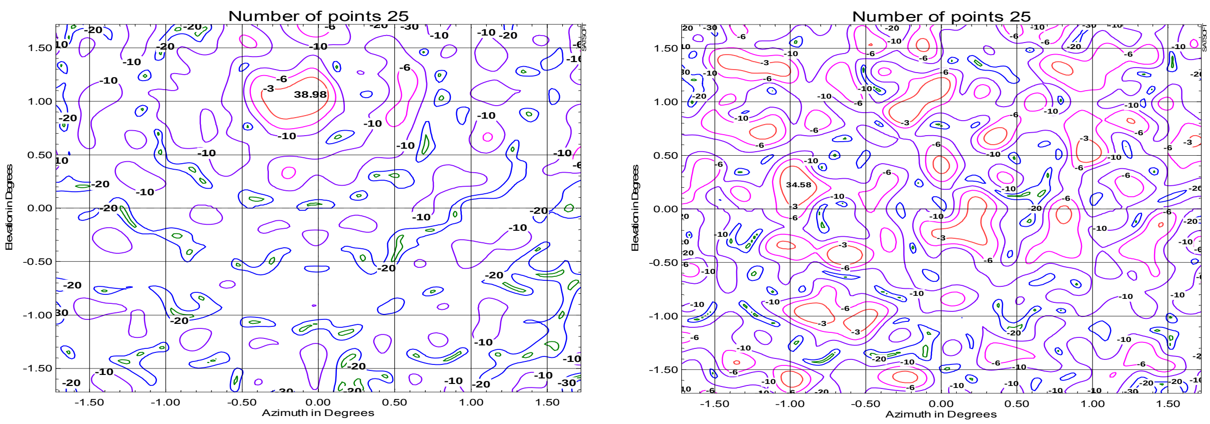

Fig. 8. Focal beam pattern at the lower operational band frequency
with 25 points for both reflector profiles

Рис. 8. Контур фокального луча на нижней частоте рабочего диапазона
при 25 точках для двух профилей рефлектора

Table 3

Directive gain of the antenna focal beam at the upper operational band frequency for different reflector profiles

Number of points	DG, percent	
	Reflector profile without deformation	Deformed reflector profile
1488	100	74.77
1250	99.83	75.15
1000	99.75	75.52
750	99.62	76.17
500	99.26	75.33
250	97.79	73.83
25	64.03	56.80

References

1. Granik M. V., Loman V. I. *Razvertyvaemye zerkal'nye antenny zontichnogo tipa* [Deployable umbrella-type reflector antennas]. Moscow, Radio i svyaz' Publ., 1987, 72 p.

2. Tibert G. Deployable tensegrity structures for space applications. Doctoral thesis Stockholm: Royal Institute of Technology, 2002. Available at: http://www.mech.kth.se/thesis/2002/phd/phd_2002_gunnar_tibert.pdf.

3. Kocherginsky G. N., Erokhin G. A., Kozyrev N. D. *Antenno-fidernye ustroystva.* [Antenna-feeder devices]. Moscow, Radio i svyaz' Publ., 1989, 352 p.

4. Ponomarev S. V. Transformable antenna reflectors of spacecraft. *Vestnik TGU. Ser. Matematika i mekhanika*. 2011, Vol. 4(16), P. 111–119 (In Russ.).

5. Khalimanovich V. I., Velichko A. I., Shipilov G. V., Romanenko V. I. *Zontichnaya antenna kosmicheskogo apparata* [Umbrella-type antenna of spacescraft]. Patent RF, no. 2370864, 2008, 10 p.

6. Testoyedov N. A., Khalimanovich V. I., Velichko A. I., Shipilov G. V., Romanenko A. V. at al. *Razvertyvaemyy transformiruemyy reflektor kosmicheskogo apparata* [Transformable deployable reflector of spacecraft]. Patent RF, no. 2350519, 2007.

7. Banichuk N. V., Karpov N. A., Klimov D. M. at al. *Mekhanika bol'shikh kosmicheskikh konstruktsiy* [Mechanics of large space structures]. Moscow, Factorial Publ., 1977, 302 p.

8. Bey N. A., Zimin V. N. [Transformable large antenna for geostationary spacecraft]. *Antenny*. 2005, Vol. 10, P. 24–27 (In Russ.).

9. Bikeev E. V., Yakimov E. N., Matulenko M. G., Titov G. P. [Method of compensation for the structural deformation of large antennas for spacecraft]. *Vestnik SibGAU*. 2014, No. 3 (17), P. 673–683 (In Russ.).

10. Matulenko M. G., Bikeev E. V., Alekseyenko A. A., Dorofeev M. O.[Control system of large-sized transformable antenna configuration.] *Reshetnevskie chteniya: materialy XVII Mezhdunar. nauch. konf.: v 2 ch.* [Reshetnev's readings: materials XVII Intern. sci. Conf.: in 2 parts]. Part 1, Krasnoyarsk, SibGAU Publ., 2013, P. 194–196 (In Russ.).

11. Rodrigues G., Angevain J-C., Prowald J. S. Active shape control of reconfigurable antenna reflectors. Proceedings of the 2nd International Conference "Advanced Lightweight Structures and Reflector Antennas". 2014.

12. Operational modal analysis via image-based technique of very flexible space structures. M. Sabatini. *Acta Astronautica.* 2013, Vol. 89, P. 139–148.

13. Image-based control of the "PINOCCHIO" experimental free flying platform. M. Sabatini. *Acta Astronautica*. 2014, Vol. 94, No. 1, P. 480–492.

14. Shendalev D. O. [The use of complex finite element modeling software ANSYS in the development of large-scale transformable reflectors]. *Reshetnevskie chteniya: materialy XIX Mezhdunar. nauch. konf.: v 2 ch.* [Reshetnev's readings: materials XIX Intern. sci. Conf.: in 2 parts]. Part 1. Krasnoyarsk, SibGAU Publ., 2015, P. 95–96 (In Russ.).

15. Testoyedov N. A., Khalimanovich V. I., Velichko A. I., Leonov A. V. *Zontichnaya antenna kosmicheskogo apparata* [Umbrella-type antenna of spacecraft]. Patent RF, no. 2423759, 2009.

Библиографические ссылки

1. Гряник М. В., Ломан В. И. Развертываемые зеркальные антенны зонтичного типа. М. : Радио и связь, 1987. 72 с.

2. Tibert G. Deployable tensegrity structures for space applications [Электронный ресурс]. Doctoral thesis Stockholm : Royal Institute of Technology, 2002. URL: http://www.mech.kth.se/thesis/2002/phd/phd_2002_gunnar_tibert.pdf.

3. Кочержевский Г. Н., Ерохин Г. А., Козырев Н. Д. Антенно-фидерные устройства. М. : Радио и связь, 1989. 352 с.

4. Пономарев С. В. Трансформируемые рефлекторы антенн космических аппаратов // Вестник ТГУ. Сер. «Математика и механика». 2011. Вып. 4(16). С. 111–119.

5. Пат. № 2370864 Российская Федерация, H01Q15/16. Зонтичная антенна космического аппарата / Халиманович В. И., Величко А. И., Шипилов Г. В., Романенко А. В. и др. Заявл. 28.08.2008 ; опубл. 20.10.2009.

6. Пат. № 2350519 Российская Федерация, B 64 G 1/22, H 01 Q 15/16. Развертываемый трансформируемый рефлектор космического аппарата / Тестоедов Н. А., Халиманович В. И., Величко А. И., Шипилов Г. В., Романенко А. В. и др. Заявл. 13.06.2007 ; опубл. 27.03.2009.

7. Механика больших космических конструкций / Н. В. Баничук [и др.]. М. : Факториал, 1977. 302 с.

8. Бей Н. А., Зимин В. Н. Трансформируемые антенны больших размеров для геостационарных космических аппаратов // Антенны. 2005. № 10. С. 24–27.

9. Способ компенсации деформаций конструкции крупногабаритной антенны космического аппарата / Е. В. Бикеев, Е. Н. Якимов, М. Г. Матыленко, Г. П. Титов // Вестник СибГАУ. 2014. Т. 17, № 3. С. 673–683.

10. Система контроля геометрии крупногабаритной трансформируемой антенны и ее наведение / М. Г. Матыленко [и др.] // Решетневские чтения : материалы XVII Междунар. науч. конф. В 2 ч. Ч. 1 / под общ. ред. Ю. Ю. Логинова ; Сиб. гос. аэрокосмич. ун-т. Красноярск, 2013. С. 194–196.

11. Rodrigues G., Angevain J-C., Prowald J. S. Active shape control of reconfigurable antenna reflectors // Advanced Lightweight Structures and Reflector Antennas : Proceedings of the 2nd Intern. Conf. 2014.

12. Sabatini M. Operational modal analysis via image based technique of very flexible space structures // Acta Astronautica. 2013. Т. 89. С. 139–148.

13. Sabatini M. Image based control of the “PINOCCHIO” experimental free flying platform // Acta Astronautica. 2014. Т. 94, № 1. С. 480–492.

14. Шендалев Д. О. Применение комплекса конечноэлементного моделирования ANSYS при разработке крупногабаритных трансформируемых рефлекторов // Решетневские чтения : материалы XIX Междунар. науч. конф. В 2 ч. Ч. 1 / Сиб. гос. аэрокосмич. ун-т. Красноярск, 2015. С. 95–96.

15. Пат. № 2423759 Российская Федерация, H 01 Q 15/00. Зонтичная антенна космического аппарата / Тестоедов Н. А., Халиманович В. И., Величко А. И., Леканов А. В. и др. Заявл. 08.03.2007 ; опубл. 10.07.2011.

UDC 629.78.015

Siberian Journal of Science and Technology. 2018, Vol. 19, No. 1, P. 76–81

ANALYSIS OF SPACECRAFT ORBITAL MOTION STABILITY OF GONETS-M NO 37152

I. K. Kolovsky*, D. N. Shmakov, V. N. Podolyakin

JSC "Academician M. F. Reshetnev" Information Satellite Systems"
52, Lenin Str., Zheleznogorsk, Krasnoyarsk region, 662972, Russian Federation
*E-mail: kolovigor@mail.ru

In the present investigation we envisage the spacecraft motion of Gonets-M (Gn-M) orbit group which is located in a circular orbit at a height of 1500 km with an inclination of 82.5 degrees. Its movement is measured based on the current navigation parameters which reveal its orbital motion analysis. Gn-M has a special characteristic feature of rotation with apsidal motion in frozen orbit. Based on this fact, the present study was carried out with the conception of a frozen orbit of Gn-M by investigating eccentricity parameter e and perigee argument w. The comparative analysis is presented as graphs which indicates the variation in the values of eccentricity parameters e and the perigee argument w which is calculated based on the current navigation parameters and the predicted motion of Gn-M. An orbital measurement was carried out by studying three Gn-M of the same orbital plane over a period of one year. The study insight on the complete analysis of specific changing revolution of the nodical period of Gn-M staying at frozen orbit. The amplitude vibrations of an orbital nodical period are calculated and compared with the orbital parameters of Gn-M which are in the same orbital plane. Overall the results obtained in the present investigation are promising enough which can aid in improving the calculation accuracy of orbit correction parameters of Gn-M.

Keywords: spacecraft, orbital parameters, eccentricity, perigee argument, nodical period, ballistics.

Сибирский журнал науки и технологий. 2018. Т. 19, № 1. С. 76–81

АНАЛИЗ СТАБИЛЬНОСТИ ДВИЖЕНИЯ КОСМИЧЕСКОГО АППАРАТА «ГОНЕЦ-М» № 37152 ПО ОРБИТЕ

И. К. Коловский*, Д. Н. Шмаков, В. Н. Подолякин

АО «Информационные спутниковые системы» имени академика М. Ф. Решетнёва»
Российская Федерация, 662972, г. Железногорск Красноярского края, ул. Ленина, 52
*E-mail: kolovigor@mail.ru

Исследуется движение космических аппаратов орбитальной группировки «Гонец-М». Орбитальная группировка «Гонец-М» представляет собой космические аппараты на круговой орбите с высотой 1500 км и наклонением 82,5°. Для анализа движения по орбите используются измерения текущих навигационных параметров космических аппаратов «Гонец-М». Рассмотрены особенности изменения параметров орбиты космических аппаратов «Гонец-М». После анализа орбитального движения была отмечена особенность во вращении линии апсид космического аппарата «Гонец-М» на замороженной орбите. Раскрывается понятие «замороженная орбита». Приведены значения параметров орбиты эксцентриситета e и аргумента перигея w, характеризующие подобные орбиты. Построены сравнительные графики изменения значений параметров орбиты эксцентриситета e и аргумента перигея w, полученных с помощью измерения текущих навигационных параметров, и соответствующих значений, рассчитанных через прогнозирование движения космического аппарата «Гонец-М». Рассмотрено и приведено на одном графике вековое изменение периода обращения в течение года у трех космических аппаратов «Гонец-М» одной орбитальной плоскости. Выявлена особенность изменения величины драконического периода обращения космического аппарата на замороженной орбите. Вычислена величина амплитуды колебания драконического периода обращения. Проводится сравнительный анализ параметров орбиты космических аппаратов «Гонец-М», которые находятся в одной орбитальной плоскости. Полученные результаты могут способствовать повышению точности вычисления параметров коррекции орбиты космического аппарата «Гонец-М».

Ключевые слова: космический аппарат, параметры орбиты, эксцентриситет, аргумент перигея, драконический период обращения, баллистика.

Introduction. The flatness of the Earth leads to the displacement of the satellite orbit perigee [1]. However, after consideration of the orbit group parameters of Gn-M, it was observed that the orbit apsidal line of SC No 37152 vice versa practically retains its position. Despite the fact that the orbital plane inclination of Gn-M is different from the critical value (the critical inclination equal to 63.43 degrees and 116.57 degrees).

It was found out that after the reduction correction Gn-M No 37152 hit the target orbit at a height of 1500 km with an inclination of 82.5 degrees with special laws changes in the orbit parameters – frozen orbit.

The study of the evolution of the orbital parameters *e* and *w* of Gn-M. A frozen orbit is an orbit whose mid elements, particularly the eccentricity *e* and the perigee argument *w*, for a long period of time can take almost constant or within a limited range enclosed values [2–4].

Analysis was studied by measurements of current navigation parameters (MCNP) of SC's No 37152, No 38736, No 38734 which are located in the same orbital plane. Special attention was paid to the following SC orbit parameters: *e*, *w* and the nodical period T_{nd}.

Due to the analysis it turned out that the parameters, obtained after processing MCNP of SC's No 38736, No 38734 behave in the following way: *w* changes in the range from 0 degree to 360 degrees, i. e., it has secular changes, *e* changes in the range from 0.001 to 0.003. The nodical period T_{nd} in addition to the secular component has got a long-period one. On the other hand, orbit parameters *w* and *e* of SC No 37152 change in a completely different way (tab. 1).

It must be noted that SC No 37152 is different in behavior of the considering orbital motion elements according to its own points A1–A5 (tab. 1) in comparison with parameter values at points B1–B5 and C1–C5 of other SC's and in addition to this its secular component of the perigee argument change disappeared.

Therefore, further for the study, we take the values obtained by MCNP, orbit parameters *e* and *w* of SC's No 37152, No 37836 and No 38734 over a period of one year (tab. 1) and compare these values with the predicted values of *e* and *w*. The forecast will be carried out taking into account the influence of the Sun, moon and the resistance of the atmosphere over a period of one year. All the corresponding values will be presented in one graph (fig. 1–3).

Table 1

The MCNP results of SC's No 37152, No 38736, No 38734

SC No 37152					
№	Date	T_{nd}, c	*e*	*w*, °	*i*, °
A1	04.06.16	6955.066	0.0010284	67.778	82.460
A2	06.07.16	6955.067	0.0011624	73.497	82.460
A3	06.11.16	6955.046	0.0009379	73.050	82.459
A4	06.03.17	6955.042	0.0012092	61.417	82.461
A5	07.07.17	6955.019	0.0012199	75.115	82.463
SC No 38736					
№	Date	T_{nd}, *c*	*e*	*w*, °	*i*, °
B1	29.06.16	6955.032	0.0032782	70.250	82.484
B2	22.09.16	6954.957	0.0010319	238.830	82.484
B3	16.11.16	6954.955	0.0028615	107.508	82.487
B4	17.03.17	6954.950	0.0011888	197.741	82.488
B5	17.07.17	6954.914	0.0019047	349.824	82.486
SC No 38734					
№	Date	T_{nd}, *c*	*e*	*w*, °	*i*, °
C1	29.06.16	6954.913	0.0030670	69.888	82.479
C2	21.08.16	6954.883	0.0017654	177.554	82.475
C3	26.11.16	6954.899	0.0028563	91.390	82.482
C4	27.03.17	6954.905	0.0014133	163.996	82.484
C5	05.05.17	6954.892	0.0027339	99.380	82.483

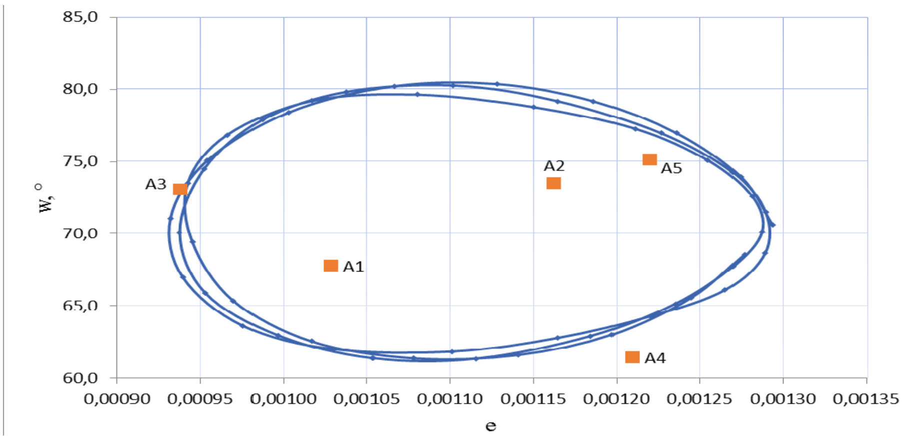

Fig. 1. *e*, *w* orbit parameters change of SC No 37152 over a period of one year

Рис. 1. Изменение параметров *e*, *w* на орбите КА № 37152 на интервале одного года

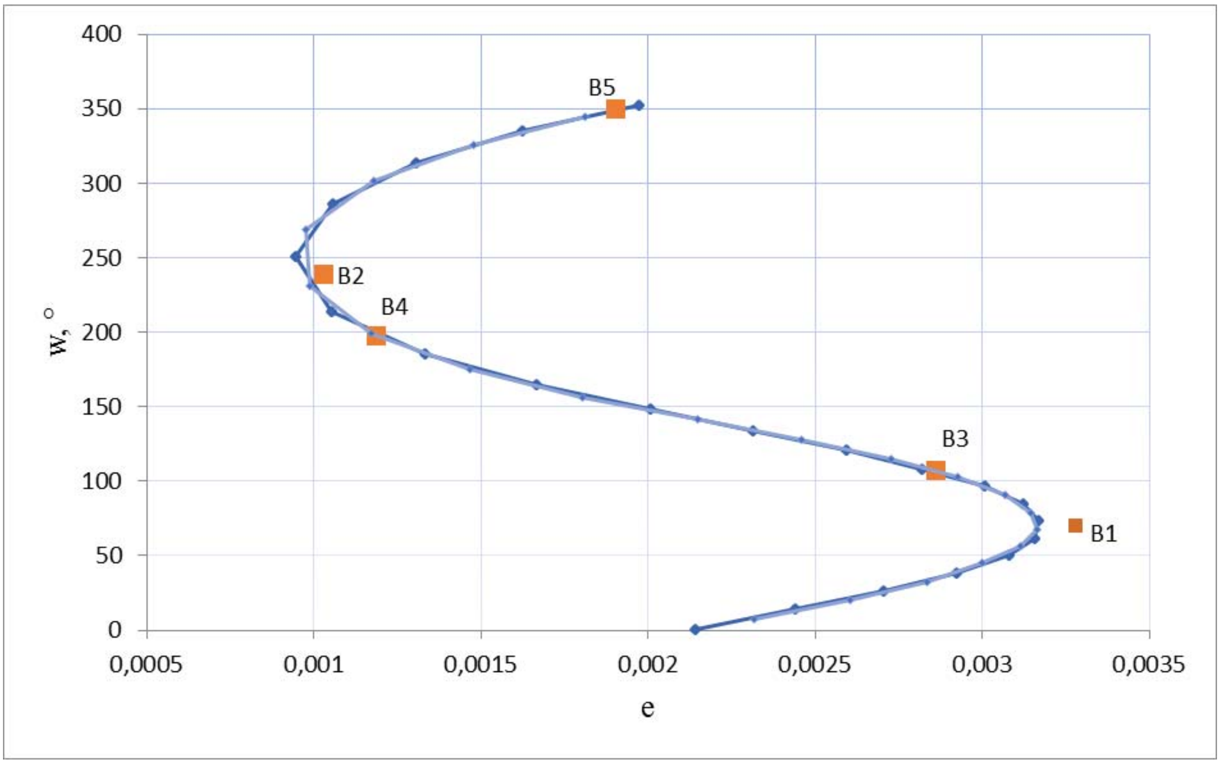

Fig. 2. *e*, *w* orbit parameters change of SC No 38736 over a period of one year

Рис. 2. Изменение параметров *e*, *w* на орбите КА № 38736 на интервале одного года

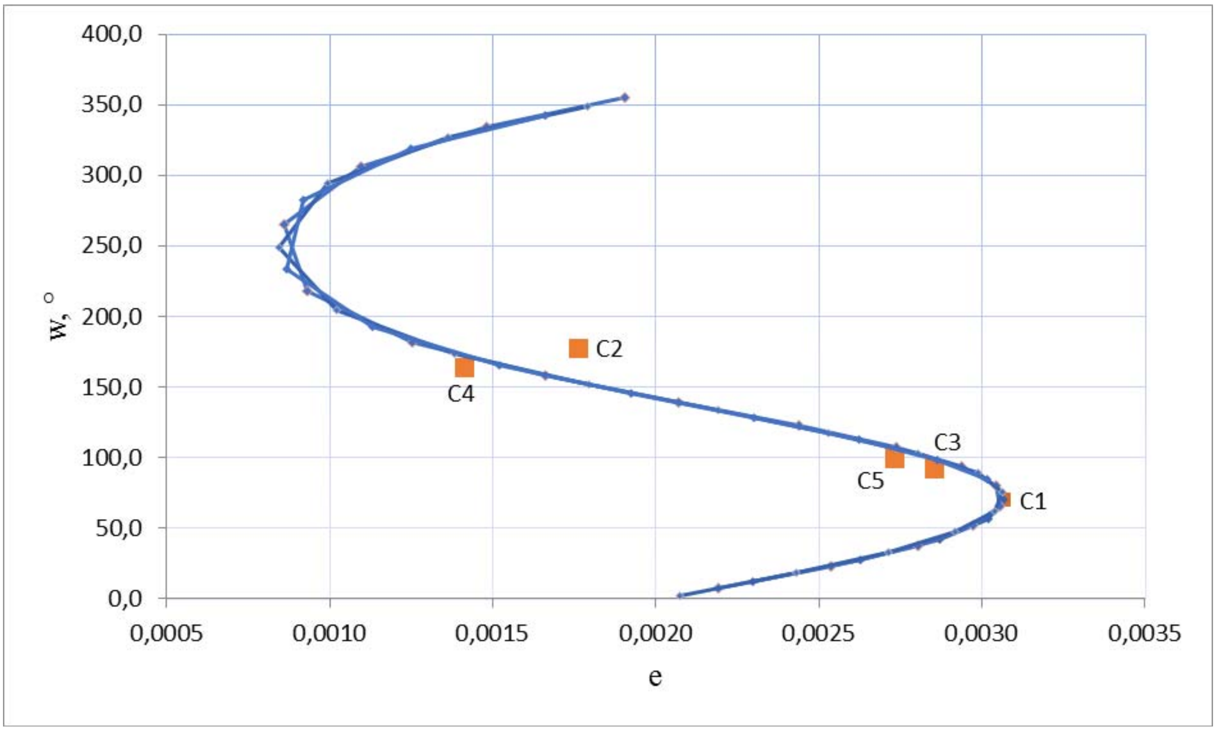

Fig. 3. *e*, *w* orbit parameters change of SC No 38734 over a period of one year

Рис. 3. Изменение параметров *e*, *w* на орбите КА № 38734 на интервале одного года

At the fig. 1, 2 and 3 it can be seen that the values obtained by MCNP are in good agreement with the values calculated by the forecast of SC orbit motion.

Looking at tab. 1 and fig. 1 it can be concluded that in a frozen orbit parameters e and w of SC No 37152 are changing in the following intervals of values

$$0.0009 \le e \le 0.0013;\ 60.0° \le w \le 80.0° \tag{1}$$

The obtained inequalities of e and w changes are assumed as a condition for SC being in a frozen orbit at an orbit height of 1500 km with an inclination of 82.5 degrees.

The orbit period changes of Gn-M. Consideration should be given to the nodical period T_{nd} of Gn-M. The observation of the T_{nd} secular changes according to the NORAD database [5] shows that SC No 37152 has significant decreasing of the amplitude of the long-period component in the nodical period, compared to SC No 38736 and SC No 38734 of the same orbital plane and of the same location in a non-frozen orbit (fig. 4).

It is necessary to pay attention to one more feature of carrying out calculations by T_{nd} using. It is talked about the influence of TGF tesserial harmonics on the average anomaly. These harmonics cause secular perturbation in the average anomaly, what corresponds to the SC secular drift along the trajectory. This secular drift should be taken into account in project calculations where the initial conditions are the use of the sculating orbital elements at some point. If T_{nd} is used as initial conditions, this perturbation should not be taken into account, since it is included as a component of nodical period initial value [6; 7].

The analysis of the secular change in T_{nd} circulation period by all three SCs Gn-M shows that every SC T_{nd} value over a period of one year, starting since 01.06.2016, decreased an average of ~ 0.04 s.

Considering fig. 4 in greater detail, the significant amplitude decreasing of the long-period component can be noted in the nodical period of Gn-M No 37152. The changing nature of treatment period became smooth over time.

The difference in T_{nd} values changes of SC No 37152 and T_{nd} of other orbit group SCs can be explained due to the influence of long-period perturbations [8].

The oscillation amplitude changes of Gn-M sidereal period in orbit. The long-period component is generated by the long-period oscillations of the nodical period, which have an amplitude [9–11]

$$A_{\text{T}} = 3 \cdot C_{2,0} \cdot (R_э/a)^2 \cdot T_{\text{nd}} \cdot (2 - (5 \cdot \sin^2(i))/2) \cdot e, \tag{2}$$

where $C_{2.0} = -1082.627 \cdot 10^{-6}$ – dimensionless constant characterizing the shape of the Earth; $R_э$ = 6378.16 km – the equatorial radius of the Earth [12; 13]; e – the eccentricity of orbit turn; a = 7878.16 km – a large orbit axis; T_{nd} = 6955.0 s – the initial value of Gn-M orbit nodical period [14]; i = 82.5 degrees – the inclination of orbital plane.

On substituting values into expression (2), the following formula is obtained

$$A_T = 6.8 \cdot e. \tag{3}$$

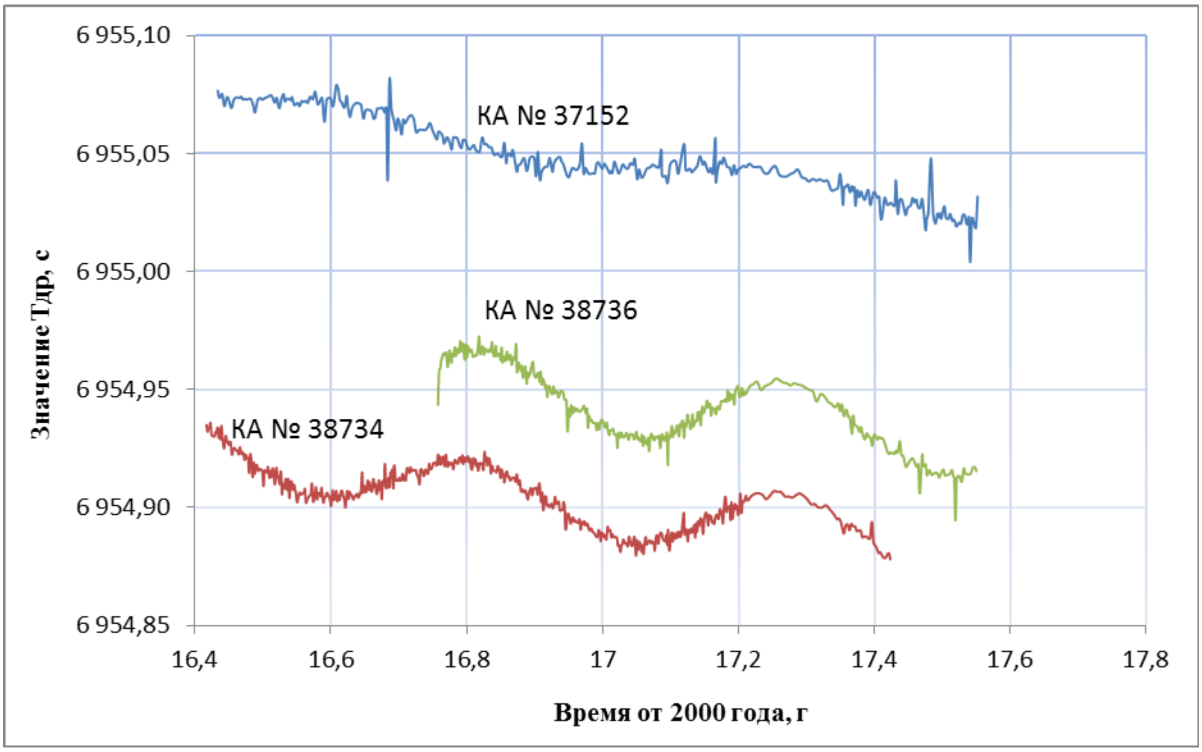

Fig. 4. T_{nd} change of SC No 37152, SC No 38736 and SC No 38734

Рис. 4. Изменение $T_{др}$ КА № 37152, КА № 38736 и КА № 38734

Table 2

A_T, $(T_{nd})_{dk}$ calculations results following MCNP data

SC No 37152					
Date	e	w, °	A_T	$(T_{nd})_{dk}$, c	$1/2\cdot(T_{nd})_{dk}$, c
04.06.16	0.0010284	67.778	0.00699	–0.00265	–0.00133
06.07.16	0.0011624	73.497	0.00790	–0.00225	–0.00113
06.11.16	0.0009379	73.050	0.00638	–0.00186	–0.00093
06.03.17	0.0012092	61.417	0.00822	–0.00394	–0.00197
07.07.17	0.0012199	75.115	0.00830	–0.00214	–0.00107
SC No 38736					
Date	e	w, °	A_T	$(T_{nd})_{dk}$, c	$1/2\cdot(T_{nd})_{dk}$, c
29.06.16	0.0032782	70.250	0.02229	–0.00755	–0.00377
22.09.16	0.0010319	238.830	0.00702	0.00364	0.00182
16.11.16	0.0028615	107.508	0.01946	0.00584	0.00292
17.03.17	0.0011888	197.741	0.00808	0.00770	0.00385
17.07.17	0.0019047	349.824	0.01295	–0.01274	–0.00637
SC No 38734					
Date	e	w, °	A_T	$(T_{nd})_{dk}$, c	$1/2\cdot(T_{nd})_{dk}$, c
29.06.16	0.0030670	69.888	0.02086	–0.00718	–0.00359
21.08.16	0.0017654	177.554	0.01200	0.01199	0.00600
26.11.16	0.0028563	91.390	0.01942	0.00046	0.00023
27.03.17	0.0014133	163.996	0.00961	0.00923	0.00462
05.05.17	0.0027339	99.380	0.01859	0.00301	0.00151

In this case, the long-period oscillations of nodical period $(T_{nd})_{dk}$ at the time of equator passing take the following form [9–11] in the turn

$$(T_{nd})_{dk} = -A_T \cdot \cos(w), \quad (4)$$

where w is the value of the orbit perigee argument in the turn.

Following MCNP data the Gn-M orbits eccentricity is being ranged between 0.001 and 0.004. It follows that the long-period component amplitude of the nodical period A_T is 0.007–0.030 s according to the formula (3).

If Gn-M No 37152 is moving along frozen orbit, its A_T change is different. To check this situation actual values obtained by MCNP, w and e parametres results are taken out of the tab. 1, formulas (3), (4) are used for calculations (tab. 2). In tab. 2 parameter $1/2 \cdot (T_{nd})_{dk}$ means the semirange of T_{nd} long-period oscillations.

It must be noted that the value $(T_{nd})_{dk}$ depends on time. Comparing presented in tab. 2 parameter $1/2\cdot(T_{nd})_{dk}$ with the values of the T_{nd}. behavior by its real observations (see fig. 4) it can be seen that in both cases the semirange of the long-period oscillations of T_{nd} period is about 0.001 s in magnitude. In the tab. 2 t SC No 37152 eccentricity changes from 0.0009 to 0.0013, thus the long-period component amplitude of the nodical period changes in closer limits from 0.007 to 0.009 s.

Conclusion. Presented data point to a potentially promising application area of orbits as a frozen orbit. The detection of the nature changes in the motion of SC Gn-M No 37152 in such an orbit can aid in improving the calculation accuracy of orbit correction parameters, which will be relevant by increasing the number of Gn-M orbit groups, as is proposed in [15], and by a significant reduction of SC retention area at the necessary points of standing, i. e., in connection with the requirements increasing to the structural stability of the orbital group.

References

1. Balk M. B. *Elementy dinamiki kosmicheskogo poleta* [Elements of the dynamics space flight]. Moscow, Nauka Publ., 1965, 340 p.

2. Orbital Mechanics, Third Edition. Edited by Vladimir A. Chobotov. American Institute of Aeronautics and Astronautics Publ., 2002, P. 259–263.

3. Cutting E., Born G. H., Frautnick J. C. Orbit Analysis for SEASAT-A. *Journal of the Astronautical Sciences*. 1978, Vol. XXVI, P. 315–342.

4. Smith J. C. Analysis and Application of Frozen Orbits for the Topex Mission – American Institute of Aeronautics and Astronautics Paper 86-2069-CP, Aug. 1986.

5. The electronic database of North American Aerospace Defense Command (NORAD). Available at: https://www.space-track.org (accessed: 19.06.2017).

6. Duboshin G. N. *Nebesnaya mekhanika. Osnovnye zadachi i metody* [Celestial mechanic. Main tasks and methods]. Moscow, Nauka Publ., 1968, 799 p.

7. Satellite Orbits: Models, Methods and Applications, 1st Edition. Oliver Montenburck, Eberhard Gill. Springer Science & Business Media, 2000, 369 p.

8. Podolyakin V. N., Shmakov D. N., Kolovskiy I. K. [Research of the revolution of the draconic nodal period of the spacecraft "Gonets-M"]. *Materialy XXI Mezhdunar. nauch. konf. "Reshetnevskie chteniya"* [Materials XXI Intern. Scientific. Conf. "Reshetnev reading"]. Krasnoyarsk, 2017, Vol. 1, P. 38–40 (In Russ.).

9. Nazarenko A. I., Skrebushevskiy B. S. *Evolutsiya i ustoychivost' sputnikovykh sistem* [Evolution and stability of satellite systems]. Moscow, Mashinostroenie Publ., 1981, 284 p.

10. Zhongolovich I. D. [The satellite's disturbances in the Earth's gravitational field]. *Bulleten' instituta teoreticheskoy astronomii*. 1960, Vol. VII, P. 10, 93, 182.

11. Kaula U. *Sputnikovaya geodeziya* [Satellite geodesy]. Moscow, Mir Publ., 1970, 172 p.

12. El'yasberg P. E. *Vvedenie v teoriyu poleta iskusstvennogo sputnika Zemli* [Introduction to the theory of flight satellite]. Moscow, Librokom Publ., 2011, 544 p.

13. Aksenov E. P. T*eoriya dvizheniya iskusstvennykh sputnikov Zemli* [The theory of the motion of satellites]. Moscow, Nauka Publ., 1977, 367 p.

14. Zharov A. N. [Multifunctional system for personal satellite communication Gonets-D1M: current state and prospects]. *Sputnikovaya svyaz' i veshchanie. Spetsial'nyy vypusk.* 2014, P. 72–78.

15. Valov M. V., Golovkov V. V., Tarleckiy I. S., Esipenko A. A., Zimin I. I. [Modernizing small satellite constellation of multifunctional personal communication system "Gonets-D1M"]. *Materialy XX Mezhdunar. nauch. konf. "Reshetnevskie chteniya"* [Materials XX Intern. Scientific. Conf. "Reshetnev reading"]. Krasnoyarsk, 2016, Vol. 1, P. 618–619.

Библиографические ссылки

1. Балк М. Б. Элементы динамики космического полета. М. : Наука. Глав. ред. физ.-мат. лит., 1965. 338 с.

2. Orbital Mechanics / Edited by V. A. Chobotov ; American Institute of Aeronautics and Astronautics. Third Edition, 2002. Pp. 259–263.

3. Cutting E., Born G. H., Frautnick J. C. Orbit Analysis for SEASAT-A // Journal of the Astronautical Sciences. 1978. Vol. XXVI. Pp. 315–342.

4. Smith J. C. Analysis and Application of Frozen Orbits for the Topex Mission / American Institute of Aeronautics and Astronautics. Paper 86-2069-CP, Aug. 1986.

5. Электронная база данных командования воздушно-космической обороны Северной Америки (NORAD) [Электронный ресурс]. URL: https://www.space-track.org (дата обращения: 19.06.2017).

6. Дубошин Г. Н. Небесная механика. Основные задачи и методы. М. : Наука, 1968. 799 с.

7. Satellite Orbits: Models, Methods and Applications. 1st Ed. Oliver Montenburck, Eberhard Gill. – Springer Science & Business Media, 2000. P. 369.

8. Подолякин В. Н., Шмаков Д. Н., Коловский И. К. Исследование изменения драконического периода обращения космического аппарата «Гонец-М» // Решетневские чтения : материалы XXI Междунар. науч. конф. (08–11 ноября 2017, г. Красноярск). В 2 ч. Ч. 1 / под общ. ред. Ю. Ю. Логинова ; СибГУ им. М. Ф. Решетнева. Красноярск, 2017. С. 38–40.

9. Назаренко А. И., Скребушевский Б. С. Эволюция и устойчивость спутниковых систем. М. : Машиностроение, 1981. 284 с.

10. Жонголович И. Д. Возмущения искусственного спутника в гравитационном поле Земли // Бюллетень института теоретической астрономии. 1960. Т. VII, 10, 93. 182 с.

11. Каула У. Спутниковая геодезия. М. : Мир, 1970. 172 с.

12. Эльясберг П. Е. Введение в теорию полета искусственных спутников Земли. 2-е изд. М. : ЛИБРОКОМ, 2011. 544 с.

13. Аксенов Е. П. Теория движения искусственных спутников Земли. М. : Наука, 1977. 367 с.

14. Жаров А. Н. Многофункциональная система персональной спутниковой связи «Гонец-Д1М»: состояние и перспективы развития // Спутниковая связь и вещание. Спец. выпуск. М., 2014. С. 72–78.

15. Модернизация орбитальной группировки малых космических аппаратов многофункциональной системы персональной спутниковой связи «Гонец-Д1М» / М. В. Валов [и др.] // Решетневские чтения : материалы XX Междунар. науч. конф. (09–12 нояб. 2016, г. Красноярск). В 2 ч. Ч. 1 / под общ. ред. Ю. Ю. Логинова ; Сиб. гос. аэрокосмич. ун-т им. М. Ф. Решетнева. Красноярск, 2016. С. 618–619.

UDC 004.38:62

Siberian Journal of Science and Technology. 2018, Vol. 19, No. 1, P. 82–97

THREE-DIMENTIONAL MODELLING OF EXTERNAL MECHANICAL EFFECTS ON DEVICES AND MACHINERY IN SOLIDWORKS SIMULATION

S. G. Martyushev, A. A. Dement'ev*

Research and Production Center "Polus"
56v, Kirova Sq., Tomsk, 634045, Russian Federation
*E-mail: info@polus-tomsk.ru

The applications of space vehicles in the modern world are extensive enough: satellite communication, broadband and narrowband broadcasting, meteorology, scientific research and others.

For this reason, modern space vehicles use the latest achievements of science and technology. It allows us to create easy, compact space vehicles with a wide functional.

The devices developed in the Research and Production Center "Polus" should meet the requirements of advanced reliability both for regular and for emergency operating modes. One of the scopes of application of such devices is designing of space vehicles.

The main task at designing and manufacturing of devices and their components is reliability maintenance. This is a primary requirement to custom-made products for which repair at major failures is extremely labor-consuming. At the same time, serious demands are made to mass, dimensional characteristics, power consumption, payloads, noise characteristics of separate blocks and devices, and other technical parameters. However, it is necessary to consider that at high requirements to characteristics the process of creation of products should be technological.

There are various techniques to define reliability of technical devices and their components. One of such ways is carrying out the whole complex of tests simulating a full cycle of operation of the device or a mechanism. However, experimental techniques have essential disadvantages, namely: high cost and long duration. Mathematical modelling allows us to reduce expenses on mock-up designing, engineering time, risks, to reveal weak points, to develop recommendations for strengthening the design and to give preliminary conclusions about firmness of the device to loads.

Along with thermal, electrostatic and frequency characteristics, mechanical effects play an important role, i. e. dynamic and static loads. In this paper, the results of modelling of external mechanical effects on the device are presented. Numerical modelling of quasi-static loading and effect on the device of random vibration is conducted and the modal analysis is carried out. Oscillation modes of the first three resonant frequencies of the device, stress, displacements and accelerations diagrams are obtained. Load factors, the maximum values of displacements and accelerations at impact actions are determined.

Keywords: modelling, mechanical analysis, durability, quasi-static loading, vibration, shock load.

Сибирский журнал науки и технологий. 2018. Т. 19, № 1. С. 82–97

ТРЕХМЕРНОЕ МОДЕЛИРОВАНИЕ ВНЕШНИХ МЕХАНИЧЕСКИХ ВОЗДЕЙСТВИЙ НА ПРИБОРЫ И УСТРОЙСТВА В SOLIDWORKS SIMULATION

С. Г. Мартюшев, А. А. Дементьев*

АО «НПЦ «Полюс»
Российская Федерация, 634045, г. Томск, пл. Кирова, 56в
*E-mail: info@polus-tomsk.ru

Области применения космических аппаратов в современном мире достаточно обширны: спутниковая связь, широкополосное и узкополосное вещание, метеорология, научные исследования и пр.

Именно поэтому современные космические аппараты используют все последние достижения науки и техники. Это позволяет создавать легкие, компактные космические аппараты с широким функционалом.

К приборам, разрабатываемым в АО «НПЦ «Полюс», предъявляются требования повышенной надежности как в штатных, так и нештатных режимах работы. Одной из сфер применения подобных приборов является проектирование космических аппаратов.

Главной задачей при проектировании и изготовлении приборов и узлов является обеспечение надежности. Это первостепенное требование к штучным несерийным изделиям, для которых ремонт при серьезных неисправностях чрезвычайно трудоемок. В то же время к ним предъявляются серьезные требования к массовым, габаритным характеристикам, энергопотреблению, полезным нагрузкам, шумовым характеристикам отдельных блоков и приборов, а также прочим техническим параметрам. Однако следует учитывать, что при высоких требованиях к характеристикам процесс создания изделий должен быть технологичен.

Существуют различные методики определения надежности приборов и узлов технических устройств. Одним из таких способов является проведение целого комплекса испытаний, имитирующих полный цикл функционирования прибора или устройства. Однако экспериментальные методики имеют существенные недостатки, а именно, высокую стоимость и большую временную длительность. Математическое моделирование позволяет уменьшить расходы на макетное проектирование, сократить время разработки, уменьшить риски, выявить слабые места, разработать рекомендации по усилению конструкции и дать предварительное заключение о стойкости прибора к нагрузкам.

Наряду с термическими, электростатическими и частотными характеристиками важную роль играют механические воздействия. Динамические и статические нагрузки. Представлены результаты моделирования внешних механических воздействий на прибор. Проведено численное моделирование квазистатического нагружения и воздействия на прибор случайной вибрации, проведен модальный анализ. Получены моды колебаний первых трех резонансных частот прибора, эпюры напряжений, перемещений и ускорений. Определены коэффициенты запаса прочности, максимальные значения перемещений и ускорений при ударных воздействиях.

Ключевые слова: моделирование, механический анализ, прочность, квазистатическое воздействие, вибрация, ударные нагрузки.

Introduction. At present, when developing radioelectronic and electronic equipment, much attention is paid to the creation of three-dimensional models of devices. This allows you to reduce the cost of breadboard design and development time, to identify weak points, to develop recommendations for strengthening the design and to give a preliminary conclusion about the resistance of the device to loads. In this regard, numerical modelling is widely used in the design as an initial stage of complex testing of devices. With the help of specialized software the problems of strength, stability, dynamics, composites mechanics, hydrodynamics and heat transfer are solved [1–13].

The specific features of the devices, being developed in the Research and Production Center "Polus", is that they must be rigid and strong. The load-bearing elements of the structure consist of plates and frames. In conditions of weight limitations, it is necessary to ensure the structural strength of devices and machinery in accordance with the specification.

Thus, the purpose of this work is to analyze the design of the device for resistance to external mechanical effects.

The analysis extends to the automation unit (AB). Mechanical loads are defined according to the specifications. The analysis was carried out by means of the SolidWorks software [14; 15].

The design of the automation unit (AB). According to the dimensional outline the AB has dimensions 340×200×200 mm and weight (6.7 ± 0.2) kg.

The automation unit is structurally composed of four unified bases of the torque control channels (TCC) and a filter located on the upper surface of the TCC, tightened at the corners by pins. The cases of the TCC are made of the alloy MA2-1 State Standard 21990–76 and have a wall thickness of 2 mm and a base of 3 mm. On each of the four bases, PCBs of glass fiber textolite STF-2-35-OS technical specification TU 16-503.161–83 are pressed. The side surfaces of the AB are covered with covers of the alloy MA2-1 State Standard 21990–76 with the thickness of 3 mm. To mount the device on its body on both sides there are six mounting feet.

Finite element model of the device. The modelling process begins with the creation of a geometric model of the AB (fig. 1), performed in accordance with the set of design documentation. In the model there are no elements that lack the effect of strengthening of the structure, but their mass and the mass of radioelectronic devices are taken into account.

The software automatically creates a combined grid on a geometric model (fig. 2). The number of grid nodes is 1 501 193, and the elements – 888 873. The quality of the grid is determined by means of the Jacobian. For the given grid with a minimum (2 mm) and maximum (25 mm) side dimensions of its elements, the Jacobian is 29.4 (fig. 3). Its acceptable value is considered not more than 40.

The following material parameters were taken into account in the analysis (tab. 1): density; Poisson's ratio; modulus of elasticity (Young's modulus); tensile yield strength; strength limit.

The requirements for resistance to external effects. In accordance with the requirements specification the device must remain operational after various mechanical effects. During the modelling quasi-static effects, impact loads specified in the form of a shock spectrum and random and sinusoidal vibrations were used.

Modal Analysis. The eigenfrequencies, forms (modes) of vibrations of the AB model (fig. 4–6) and the resulting coefficient of mass participation are determined by the modal analysis (fig. 7).

Modelling of quasi-static effect and sinusoidal vibration. Border conditions:

– all elements of the model have a global contact with one another;

– the effect of gravity (acceleration of gravity) is taken into account;

– type of material model – linear, elastic, isotropic;

– the device is rigidly fixed over the entire surface of the mounting feet;

– the impact is applied to the base of the model consecutively in each of the three mutually perpendicular directions.

The natural frequencies of the AB model, obtained as a result of the modal analysis, exceed 150 Hz. Therefore, the calculation of sinusoidal vibration can be replaced by calculation for a quasi-static effect, since the stress arising in the elements of the model under the effect of a sinusoidal vibration will correspond to the stress under quasi-static loads.

In the case of quasi-static effect on the AB model, the maximum stress appears in the bases of the TCC (tab. 2).

As a result of the calculation, the values of the maximum stress and displacements under the effect along each of the three mutually perpendicular directions were obtained.

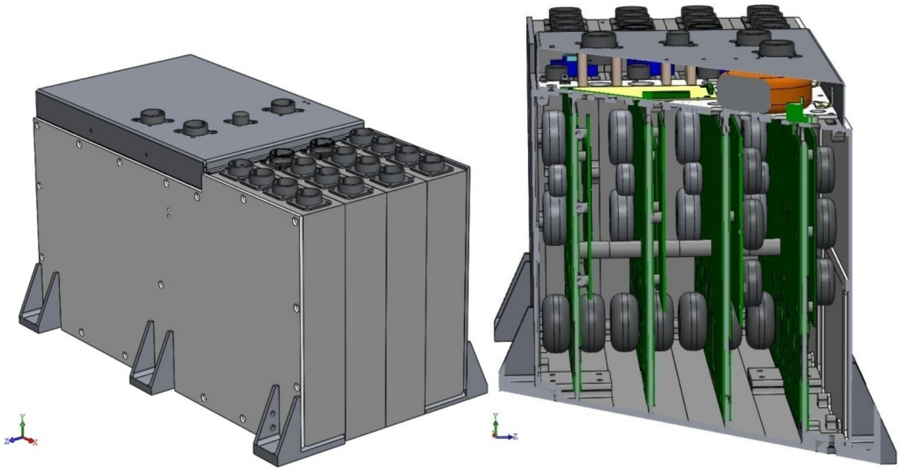

Fig. 1. Geometrical model of automation block (AB)

Рис. 1. Геометрическая модель БА

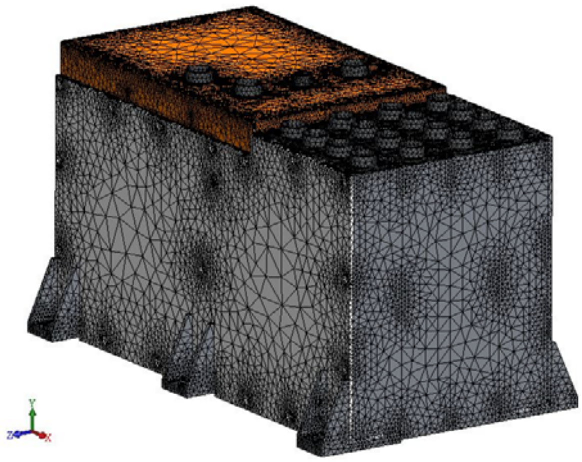

Fig. 2. A grid on geometrical model AB

Рис. 2. Сетка на геометрической модели БА

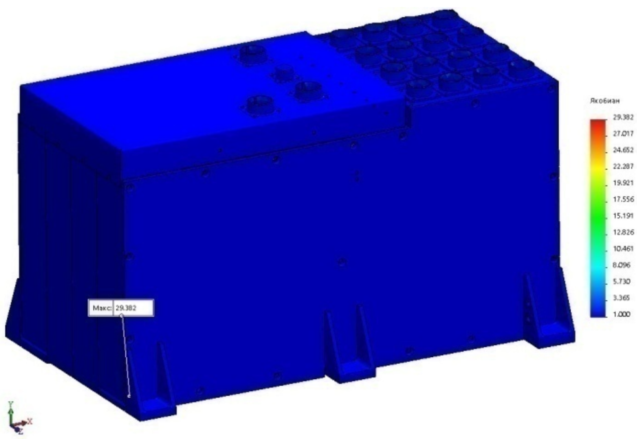

Fig. 3. Jacobian distribution

Рис. 3. Эпюра якобиана

Table 1

Physical-mechanical characteristics of used materials

Material parameter	Parameter value			
	Steel 10 short-time strength, State Standard 1050–88	Magnesium alloy MA2-1, State Standard 21990–76	Aluminum alloy AMg6 2, State Standard 21631–76	Glass textolite, STF-2-35-OS technical specification TU 16-503.161–83
Density kg/m^3	7 856	1 790	2 640	1700
Elastic modulus MPa	186 000	41 160	69 500	21 000
Poisson’s ratio	0.3	0.33	0.33	0.15
Tensile yield strength, MPa (kgf/mm^2)	205 (20.9)	137.3 (14)	147 (15)	–
Ultimate strength, MPa (kgf/mm^2)	333 (34)	245.25 (25)	294 (30)	300 (30.6)

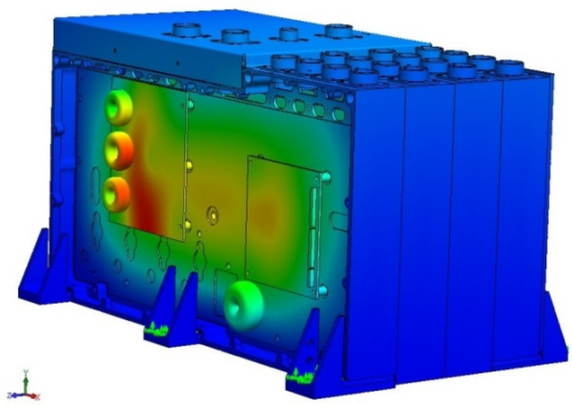

Fig. 4. First form of oscillations of model AB on frequency of 286 Hz

Рис. 4. Первая форма колебаний модели БА на частоте 286 Гц

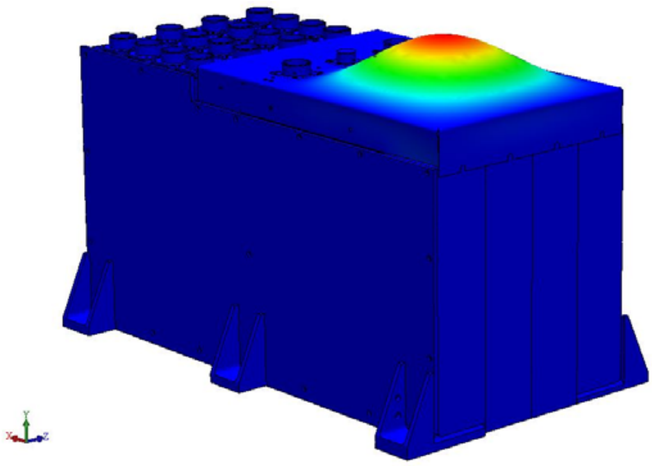

Fig. 5. Second form of oscillations of model AB on frequency of 316 Hz

Рис. 5. Вторая форма колебаний модели БА на частоте 316 Гц

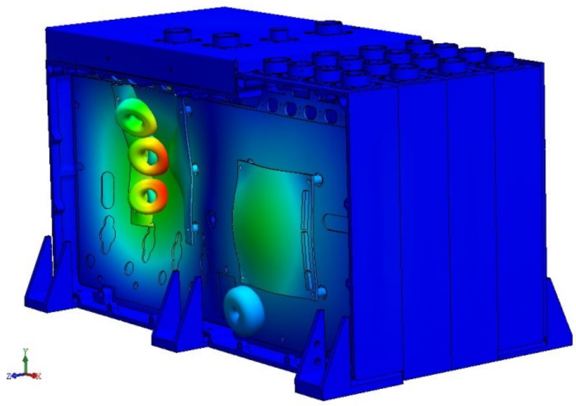

Fig. 6. Third form of oscillations of model AB on frequency of 362 Hz

Рис. 6. Третья форма колебаний модели БА на частоте 362 Гц

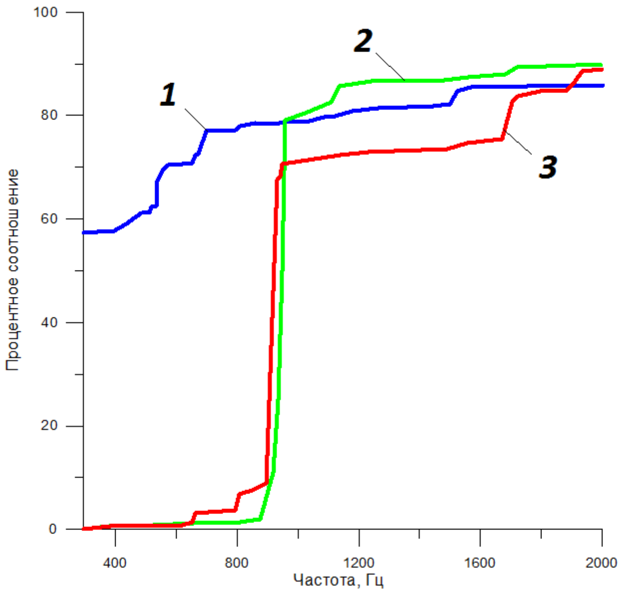

Fig. 7. Result factor of mass participation:
1 – mass participation in a direction of *OZ* axis; *2* – mass participation in a direction of *OY* axis; *3* – mass participation in a direction of *OX* axis

Рис. 7. Результирующий коэффициент массового участия:
1 – массовое участие в направлении оси *OZ*; *2* – массовое участие в направлении оси *OY*; *3* – массовое участие в направлении оси *OX*

Table 2

Values of maximum stress and displacements *OX*, *OY*, *OZ* axes at quasi-static load

Direction of effect	The maximum stress, MPa	The maximum displacement, mm
Along *OX* axis	9.7	0.012
Along *OY* axis	7.3	0.063
Along *OZ* axis	15.9	0.072

The load factor of η elements of the AB model is calculated by the formula

$$\eta = \frac{\sigma_b}{\sigma_{\text{von Mises}}} \geq 1, \tag{1}$$

where σ_b is the yield strength of the material, MPa; $\sigma_{\text{von Mises}}$ is the calculated value of the stress according to Mises, MPa.

For principal stresses σ_1, σ_2, σ_3, the Mises stress is expressed as

$$\sigma_{\text{von Mises}} = \sqrt{\frac{(\sigma_1 - \sigma_2)^2 + (\sigma_2 - \sigma_3)^2 + (\sigma_1 - \sigma_3)^2}{2}}.$$

The minimum load factor in the base of the TCC along the *OZ* axis is $\eta = 8.6$.

Stress and displacement distributions in the AB model under the effect of quasi-static accelerations along three mutually perpendicular axes are obtained (fig. 8–13). The maximum stress along the *OZ* axis occurs at the base of the TCC.

Modelling of the effect of random vibration. Border conditions:

– all elements of the model have a global contact with one another;

– damping in the model is 2 % of the critical;

– type of material model – linear, elastic, isotropic;

– the device is rigidly fixed over the entire surface of the mounting feet;

– the impact is applied to the base of the AB model consecutively in each of the three mutually perpendicular directions.

The maximum stress occurs at the base of the TCC at random vibration in the direction of the OX axis (tab. 3). The values of the maximum stress, accelerations and displacements at the level σ under the effect along each of the three mutually perpendicular directions are obtained.

The damping factor with respect to the critical damping was assumed to be 0.02. The finite element model of the device is presented in Section 2.

The minimum load factor in the base of the TCC along the *OZ* axis at the level 3σ, calculated by the formula (1), is η = 1.39.

Forms and values of accelerations, displacements and stress in the AB model at the effect of random vibration in the direction of the axes in accordance with tab. 3 are shown in fig. 14–22. In some drawings several elements of the design are hidden for the better visualization of maximum accelerations, displacements and stress.

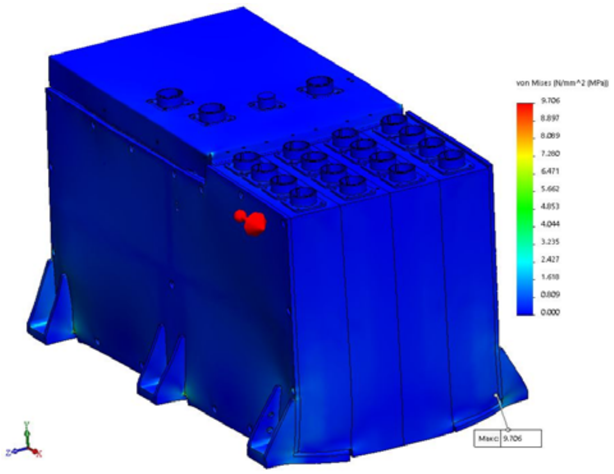

Fig. 8. Distribution of stress in AB model
at quasi-static load along *OX* axis

Рис. 8. Распределение напряжений в модели БА
при квазистатическом воздействии по оси *OX*

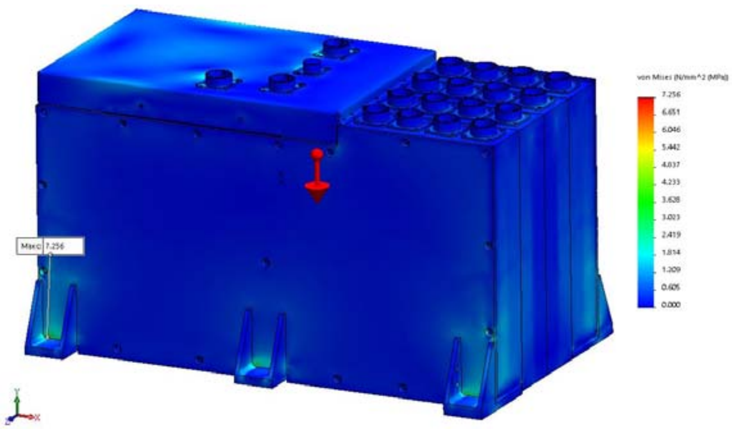

Fig. 9. Distribution of stress in AB model
at quasi-static load along *OY* axis

Рис. 9. Распределение напряжений в модели БА
при квазистатическом воздействии по оси *OY*

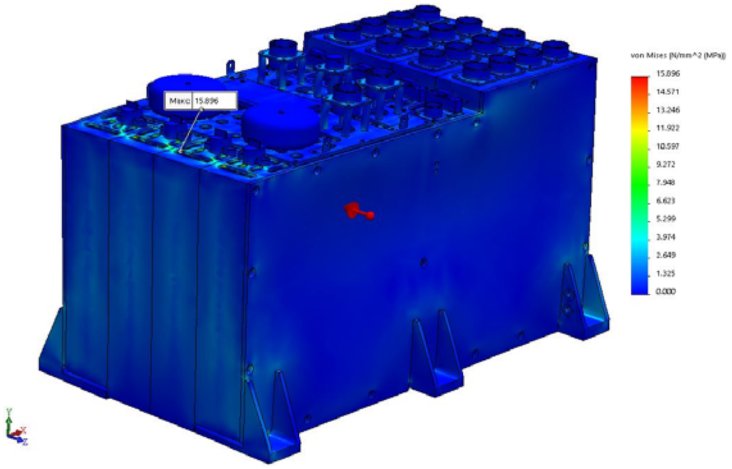

Fig. 10. Distribution of stress in AB model
at quasi-static load along *OZ* axis

Рис. 10. Распределение напряжений в модели БА
при квазистатическом воздействии по оси *OZ*

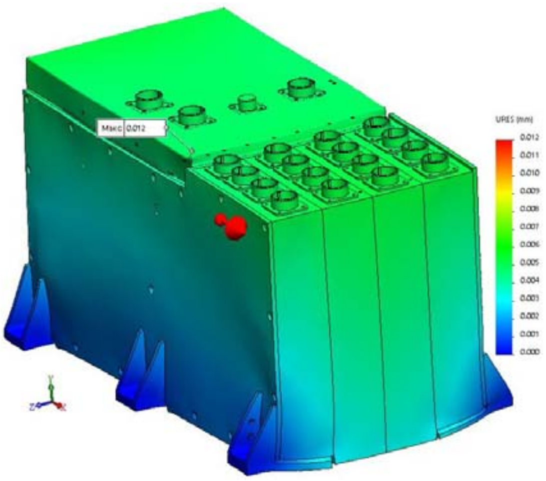

Fig. 11. Distribution of displacement in AB model
at quasi-static load along *OX* axis

Рис. 11. Распределение перемещений в модели БА
при квазистатическом воздействии по оси *OX*

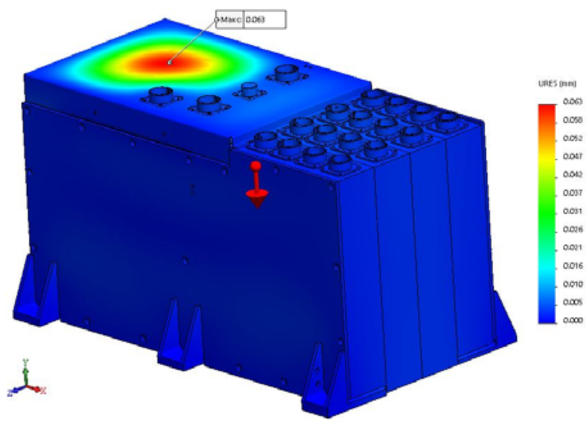

Fig. 12. Distribution of displacement in AB model
at quasi-static load along *OY* axis

Рис. 12. Распределение перемещений в модели БА
при квазистатическом воздействии по оси *OY*

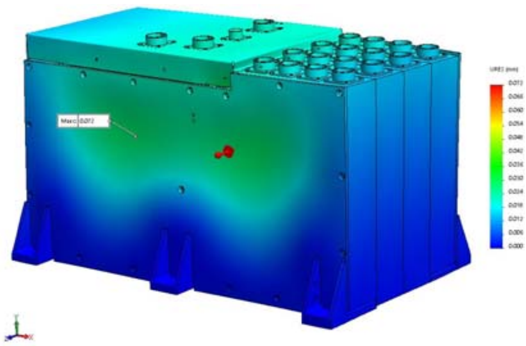

Fig. 13. Distribution of displacement in AB model
at quasi-static load along *OZ* axis

Рис. 13. Распределение перемещений в модели БА
при квазистатическом воздействии по оси *OZ*

Table 3

Values of maximum stress, displacements and accelerations along *OX*, *OY*, *OZ* axes at effect of random vibration

Direction of impact	The maximum stress, MPa	The maximum displacement, mm	The maximum acceleration, *g*
Along *OX* axis	29.8	0.006	10.98
Along *OY* axis	5.66	0.177	72.09
Along *OZ* axis	32.9	0.135	56.05

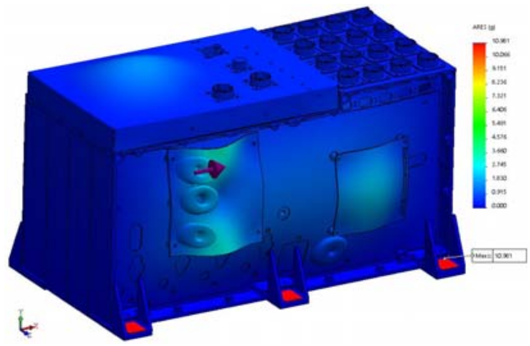

Fig. 14. Distribution of accelerations in AB model
at effect of random vibration along *OX* axis

Рис. 14. Распределение ускорений в модели БА
при воздействии случайной вибрации по оси *OX*

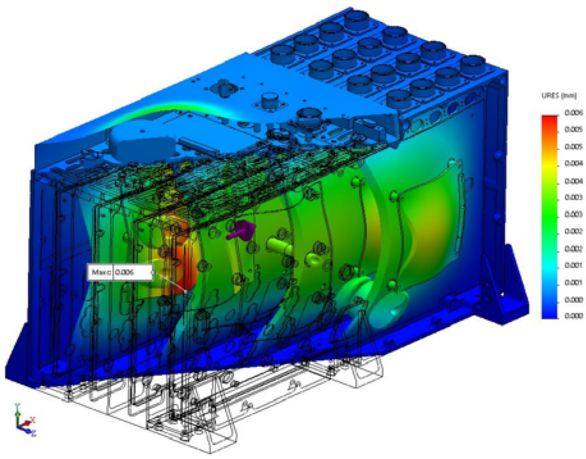

Fig. 15. Distribution of displacements in AB model
at effect of random vibration along *OX* axis

Рис. 15. Распределения перемещений в модели БА
при воздействии случайной вибрации по оси *OX*

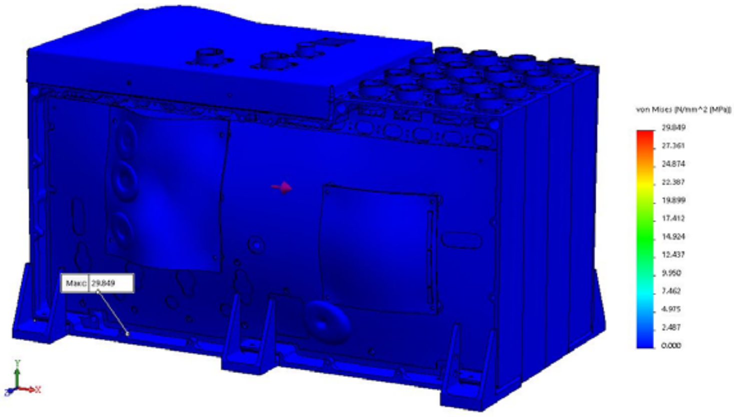

Fig. 16. Distribution of the stress in AB model
at effect of random vibration along *OX* axis

Рис. 16. Распределение напряжений в модели БА
при воздействии случайной вибрации по оси *OX*

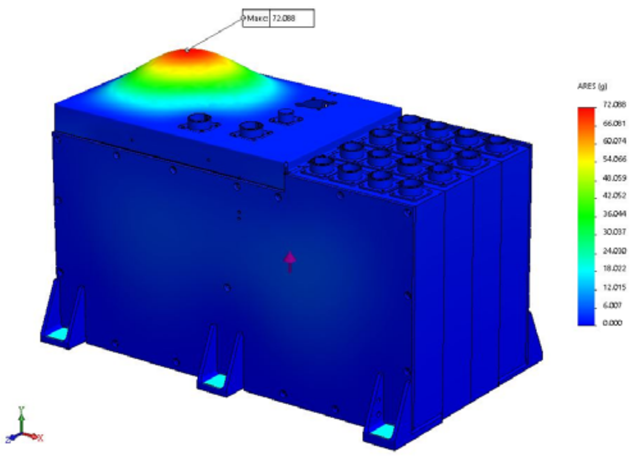

Fig. 17. Distribution of accelerations in AB model
at effect of random vibration along *OY* axis

Рис. 17. Распределение ускорений в модели БА
при воздействии случайной вибрации по оси *OY*

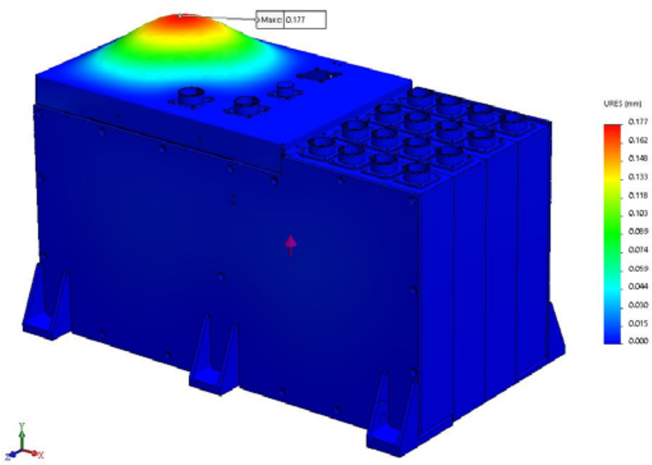

Fig. 18. Distribution of displacements in AB model
at effect of random vibration along *OY* axis

Рис. 18. Распределение перемещений в модели БА
при воздействии случайной вибрации по оси *OY*

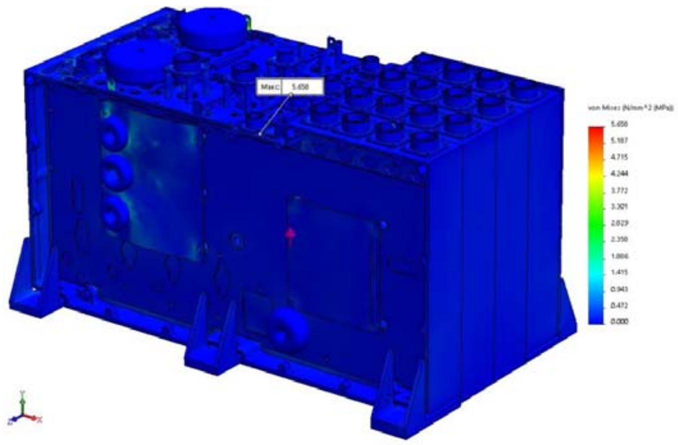

Fig. 19. Distribution of the stress in AB model
at effect of random vibration along *OY* axis

Рис. 19. Распределение напряжений в модели БА
при воздействии случайной вибрации по оси *OY*

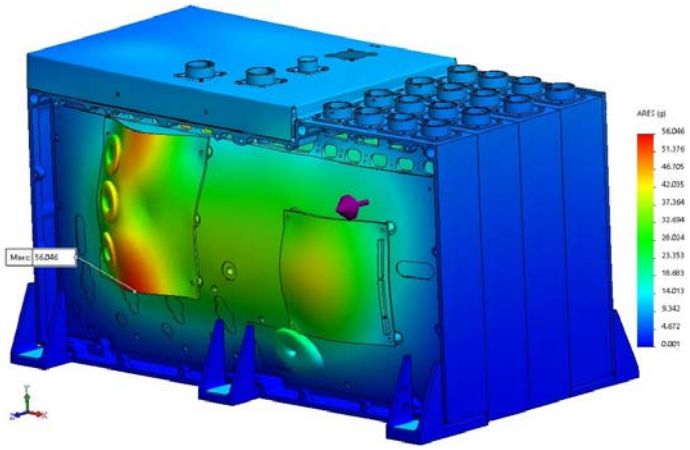

Fig. 20. Distribution of accelerations in AB model
at effect of random vibration along *OZ* axis

Рис. 20. Распределение ускорений в модели БА
при воздействии случайной вибрации по оси *OZ*

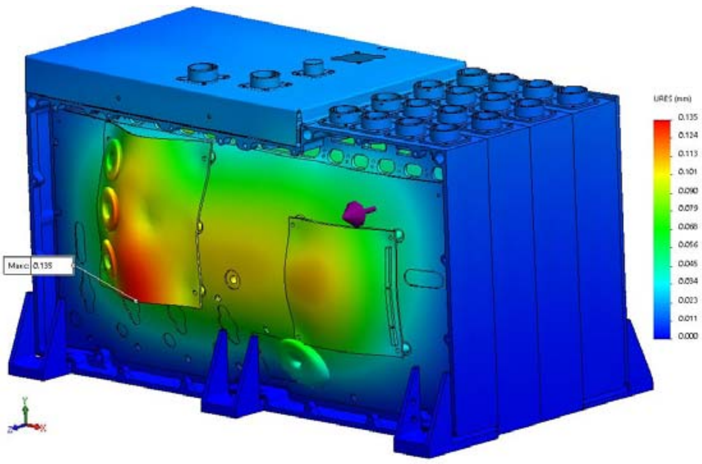

Fig. 21. Distribution of displacements in AB model
at effect of random vibration along *OZ* axis

Рис. 21. Распределение перемещений в модели БА
при воздействии случайной вибрации по оси *OZ*

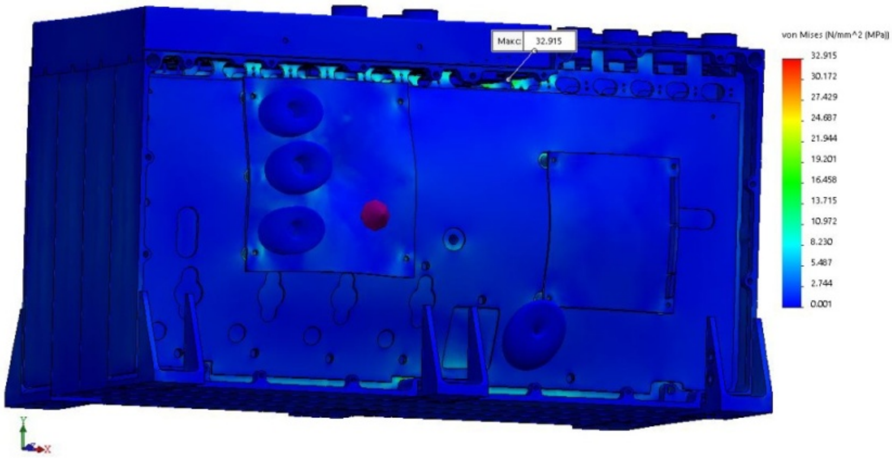

Fig. 22. Distribution of stress in AB model
at effect of random vibration along *OZ* axis

Рис. 22. Распределение напряжений в модели БА
при воздействии случайной вибрации по оси *OZ*

To predict the fatigue strength of the AB at given levels of effect of broadband random vibration, the predicted service life of the device can be determined from the formula

$$T = \frac{T_В}{F_0(\sigma / \sigma_Д)^m}, \qquad (2)$$

where $T_В$ is the number of loading cycles; F_0 is the lower resonance frequency of the structure, Hz; σ is the maximum stress at the effect of broadband random vibration, MPa; $\sigma_Д$ is the fatigue strength endurance of the material, MPa; *m* is the index of the slope of the fatigue curve of the material.

For the bases of the TCC, the following parameters [16] were applied in the calculation: $T_В$ = $1{\cdot}10^7$ s; F_0 = 286.6 Hz; m = 9.55. Steel MA2-1 has the following characteristics: σ = 32.915 MPa; $\sigma_Д$ = 100 MPa.

Substituting the values of the parameters in formula (2), we get the predicted service life of the device $T = 1.4{\cdot}10^9$ s.

Modelling of the shock action. Modelling of the shock action on the AB, given in the form of an amplitude-frequency spectrum according to tab. 4, is carried out separately along each of the three mutually perpendicular axes: *OX*, *OY*, *OZ* (fig. 23–31).

Border conditions:

– all elements of the model have a global contact with one another;

– damping in the model is 2 % of the critical;

– type of material model – linear, elastic, isotropic;

– the device is rigidly fixed over the entire surface of the base;

– the impact in the form of a frequency spectrum is applied to the base of the AB consecutively in each of the three mutually perpendicular directions.

The maximum stress at the effect on the *OZ* axis occurs at the base of the TCC.

The most loaded element of the AB model is the base of the TCC at shock action along the *OZ* axis. The load factor of the side plate is $\eta = 1.25$.

Conclusion. The results of the analysis showed the following:

– the calculated minimum eigenfrequency of the AB model is f_{01} = 286.6 Hz, which meets the requirements of the technical specifications;

– the minimum load factor at quasi-static action and sinusoidal vibration is 8.64 in the direction of the *OZ* axis;

– the minimum load factor at random vibration is 1.39 in the direction of the *OZ* axis;

– the maximum accelerations at random vibration along the *OX*, *OY*, *OZ* axes at the level of 3σ are 32.94g, 216.27g and 168.14g respectively;

– the minimum load factor at shock action along the *OZ* axis is 1.25;

– the maximum displacements at shock action along the *OX*, *OY*, *OZ* axes are 0.213, 0.56 and 0.76 mm respectively;

– the maximum accelerations at shock action along the *OX*, *OY*, *OZ* axes are 158.51g, 247.53g and 297.55g respectively.

The most critical types of loading are impact in the direction of the *OZ* axis and the impact of random vibration in the direction of the *OZ* axis. At the same time, the load factor in the base of the TCC is 1.25 and 1.39 respectively.

Based on the results of the analysis, locations for the installation of vibration-survey converters have been determined to measure the changes in the amplitude-frequency characteristics of the AB before and after the dynamic effects. When carrying out mechanical tests, the vibration-survey converters are installed on the side cover of the TCC, on the side of the base of the TCC located in the middle of the device (fig. 32), and on the upper part of the base of the TCC between the connectors at points *1*, *2* and *3*.

Thus, the analysis has shown that the design of the AB model meets the requirements of the technical specifications for resistance to external mechanical effects.

Table 4

Values of maximum stress, displacements and accelerations along *OX*, *OY*, *OZ* axes at shock action

Direction of impact	The maximum stress, MPa	Safety factor, η	The maximum displacement, mm	The maximum acceleration, *g*
Along *OX* axis	29.222	4.7	0.213	158.512
Along *OY* axis	79.083	1.74	0.555	247.531
Along *OZ* axis	109.84	1.25	0.758	297.549

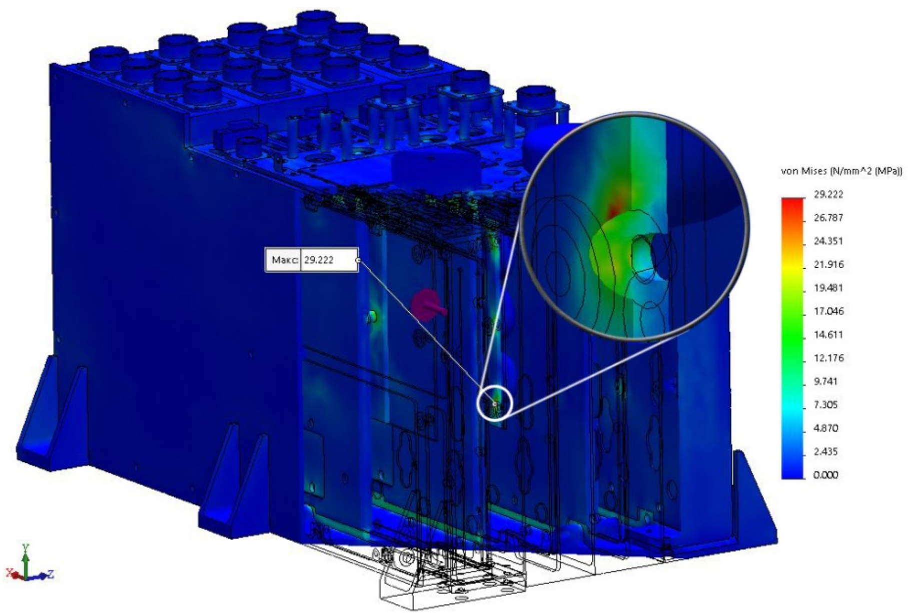

Fig. 23. Distribution of stress in AB model
at shock action along *OX* axis

Рис. 23. Распределение напряжений в модели БА
при ударном воздействии по оси *OX*

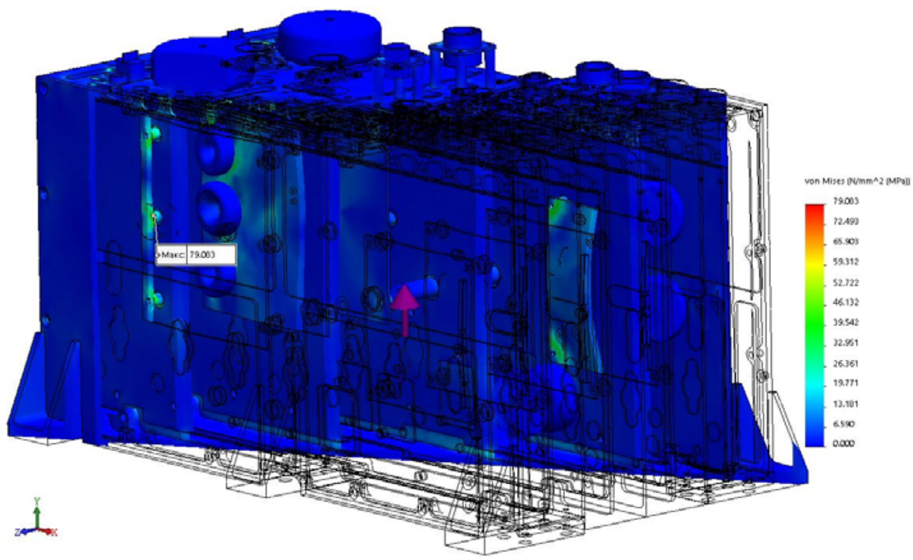

Fig. 24. Distribution of stress in AB model
at shock action along *OY* axis

Рис. 24. Распределение напряжений в модели БА
при ударном воздействии по оси *OY*

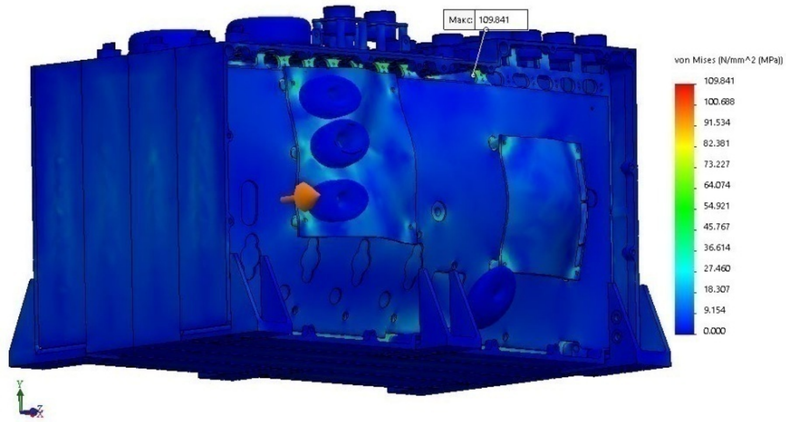

Fig. 25. Distribution of stress in AB model
at shock action along *OZ* axis

Рис. 25. Распределение напряжений в модели БА
при ударном воздействии по оси *OZ*

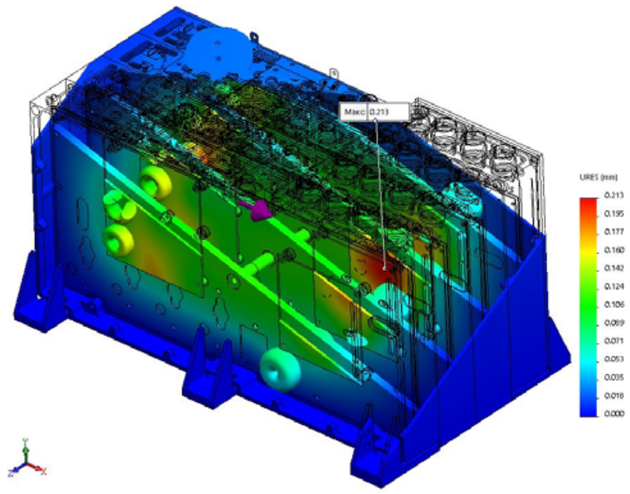

Fig. 26. Distribution of displacements in AB model
at shock action along *OX* axis

Рис. 26. Распределение перемещений в модели БА
при ударном воздействии по оси *OX*

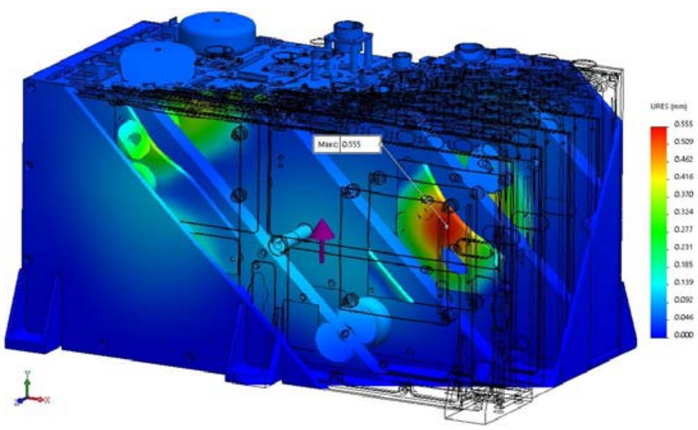

Fig. 27. Distribution of displacements in AB model
at shock action along *OY* axis

Рис. 27. Распределение перемещений в модели БА
при ударном воздействии по оси *OY*

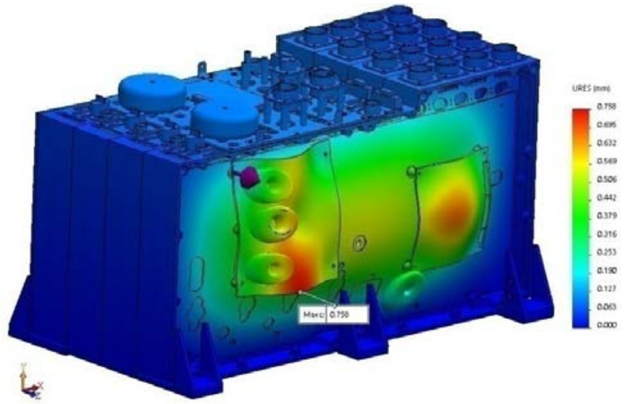

Fig. 28. Distribution of displacements in AB model
at shock action along *OZ* axis

Рис. 28. Распределение перемещений в модели БА
при ударном воздействии по оси *OZ*

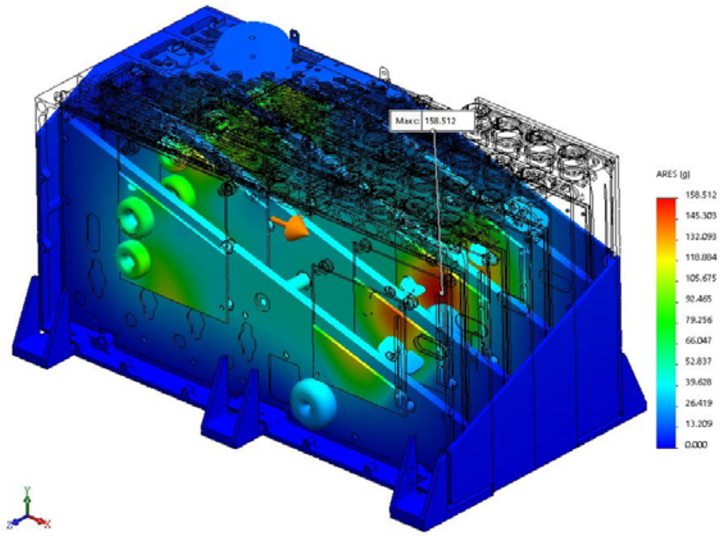

Fig. 29. Distribution of accelerations in AB model
at shock action along *OX* axis

Рис. 29. Распределение ускорений в модели БА
при ударном воздействии по оси *OX*

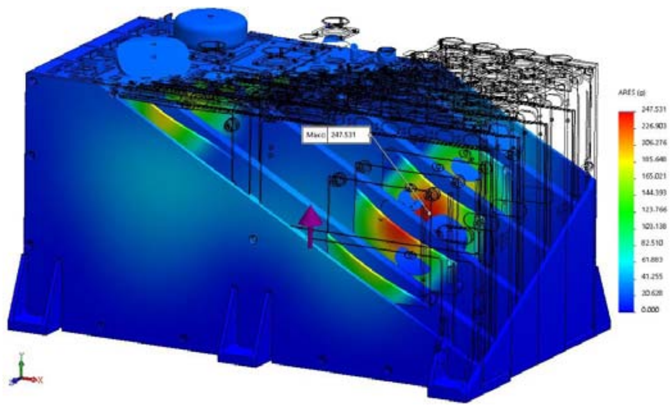

Fig. 30. Distribution of accelerations in AB model
at shock action along *OY* axis

Рис. 30. Распределение ускорений в модели БА
при ударном воздействии по оси *OY*

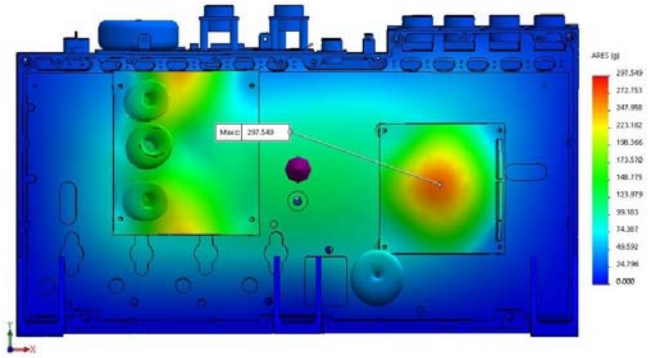

Fig. 31. Distribution of accelerations in AB model
at shock action along *OZ* axis

Рис. 31. Распределение ускорений в модели БА
при ударном воздействии по оси *OZ*

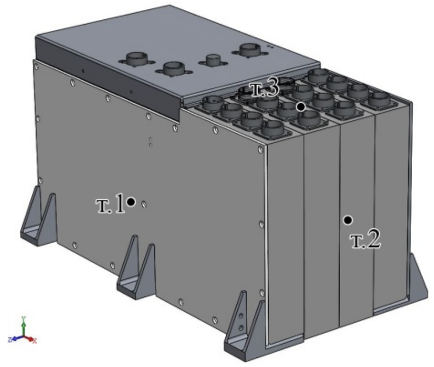

Fig. 32. Installation location
of vibration-survey converters on AB

Рис. 32. Места установки
виброизмерительных преобразователей на БА

References

1. Gómez-López L. M., Miguel V., Martínez A., Coello J., Calatayud A. Simulation and Modeling of Single Point Incremental Forming Processes within a Solidworks Environment. *Procedia Engineering*. 2013, Vol. 63, P. 632–641.

2. Iveta Glodová, Tomáš Lipták, Jozef Bocko. Usage of Finite Element Method for Motion and Thermal Analysis of a Specific Object in SolidWorks Environment. *Procedia Engineering*. 2014, Vol. 96, P. 131–135.

3. Hong-yang Zhang, Tong-chun Li, Zong-kun Li. Modeling in SolidWorks and analysis of temperature and thermal stress during construction of intake tower. *Water Science and Engineering*. 2009, Vol. 2, Iss. 1, P. 95–102.

4. Aniket Shrikant Ambekar, Sivakumar R., Anantharaman N., Vivekenandan M. CFD simulation study of shell and tube heat exchangers with different baffle segment configurations. *Applied Thermal Engineering*. 2016, Vol. 108, P. 999–1007.

5. Liang Yu., Yan Li Jiang, Sen Kai Lu, Peng Liu, Wen Feng Wang. 3D FEM for Sintering of Solar Cell with Boron Back Surface Field Based on Solidwork Simulation. *IERI Procedia*. 2012, Vol. 1, P. 81–86.

6. Bellos E., Korres D., Tzivanidis C., Antonopoulos K. A. Design, simulation and optimization of a compound parabolic collector. *Sustainable Energy Technologies and Assessments*. 2016, Vol. 16, P. 53–63.

7. Evangelos Bellos, Christos Tzivanidis, Ilias Daniil, Kimon A. Antonopoulos. The impact of internal longitudinal fins in parabolic trough collectors operating with gases. *Energy Conversion and Management*. 2017, Vol. 135, P. 35–54.

8. Ján Vavro Jr., Ján Vavro, Petra Kováčiková, Radka Bezdedová. Kinematic and Dynamic Analysis of Planar Mechanisms by Means of the Solid Works Software. *Procedia Engineering*. 2017, Vol. 177, P. 476–481.

9. Xiaohu Yang, Xiangzhao Meng, Zhenni Wang, Liwen Jin, Qunli Zhang, Qiancheng Zhang, Tian Jian Lu. Direct Numerical Simulation on Melting Phase Change Behavior in Open-cell Metal Foam. *Energy Procedia*. 2017, Vol. 105, P. 4254–4259.

10. Song Wei, Liu Yuanzhou, Zhu Ke, Zheng Tuanfeng. Numerical Simulation of Forced External Circulation Standing Column Well Based on CFD. *Procedia Engineering*. 2017, Vol. 205, P. 3178–3185.

11. Ssomad M. A. H. A., Hudzari R. M., Noordin M. N. A., Sapuan S. M., Soran A. J. Finite Element Analysis for Stress Distribution of Hand Tool Harvester. *Procedia Engineering*. 2013, Vol. 68, P. 219–224.

12. I. S. S. Sharifah, A. T. B. S. Tengku Nurul, M. K. Nor Khairusshima. Thermal Modelling and Analysis

of Batik Canting Design. *Procedia Engineering*. 2017, Vol. 184, P. 326–333.

13. Qin Yang, Zhiguo Zhang, Mingyue Liu, Jing Hu. Numerical Simulation of Fluid Flow inside the Valve. *Procedia Engineering*. 2011, Vol. 23, P. 543–550.

14. Alyamovskiy A. A. *Inzhenernye raschety v SolidWorks Simulation* [Engineering calculations in SolidWorks Simulation]. Moscow, DMK Press Publ., 2010, 464 p.

15. Alyamovskiy A. A. *SolidWorks Simulation. Inzhenernyy analiz dlya professionalov: zadachi, metody, rekomendatsii* [SolidWorks Simulation. Engineering analysis for professionals: problems, methods, recommendations]. Moscow, DMK Press Publ., 2015, 562 p.

16. *Fizicheskoe materialovedenie. T. 3. Fiziko-mekhanicheskie svoystva metallov i splavov* [Physical material science. Vol. 3. Physics-mechanical properties of metals and alloys]. Ed. R. U. Kana, P. Khaazena. Moscow, Metallurgia Publ., 1987.

Библиографические ссылки

1. Simulation and Modeling of Single Point Incremental Forming Processes within a Solidworks Environment / L. M. Gómez-López [et al.] // Procedia Engineering. 2013. Vol. 63. P. 632–641.

2. Glodová I., Lipták T., Bocko J. Usage of Finite Element Method for Motion and Thermal Analysis of a Specific Object in SolidWorks Environment // Procedia Engineering. 2014. Vol. 96. P. 131–135.

3. Hong-yang Zhang, Tong-chun Li, Zong-kun Li. Modeling in SolidWorks and analysis of temperature and thermal stress during construction of intake tower // Water Science and Engineering. 2009. Vol. 2. P. 95–102.

4. CFD simulation study of shell and tube heat exchangers with different baffle segment configurations / A. S. Ambekar [et al.] // Applied Thermal Engineering. 2016. Vol. 108, 5 Sep. P. 999–1007.

5. 3D FEM for Sintering of Solar Cell with Boron Back Surface Field Based on Solidwork Simulation / Liang Yu [et al.] // IERI Procedia. 2012. Vol. 1. P. 81–86.

6. Design, simulation and optimization of a compound parabolic collector / E. Bellos [et al.] // Sustainable Energy Technologies and Assessments. 2016. Vol. 16. P. 53–63.

7. The impact of internal longitudinal fins in parabolic trough collectors operating with gases / E. Bellos [et al.] // Energy Conversion and Management. 2017. Vol. 135. P. 35–54.

8. Kinematic and Dynamic Analysis of Planar Mechanisms by Means of the SolidWorks Software / J. Vavro Jr. [et al.] // Procedia Engineering, 2017. Vol. 177. P. 476–481.

9. Direct Numerical Simulation on Melting Phase Change Behavior in Open-cell Metal Foam / Xiaohu Yang [et al.] // Energy Procedia. 2017. Vol. 105. P. 4254–4259.

10. Numerical Simulation of Forced External Circulation Standing Column Well Based on CFD / Song Wei, [et al.] // Procedia Engineering. 2017. Vol. 205. P. 3178–3185.

11. Finite Element Analysis for Stress Distribution of Hand Tool Harvester / M. A. H. A. Ssomad [et al.] // Procedia Engineering. Vol. 68. 2013. P. 219–224.

12. I. S. S. Sharifah, A. T. B. S. Tengku Nurul, M. K. Nor Khairusshima. Thermal Modelling and Analysis of Batik Canting Design // Procedia Engineering. 2017. Vol. 184. P. 326–333.

13. Numerical Simulation of Fluid Flow inside the Valve / Qin Yang [et al.] // Procedia Engineering. 2011. Vol. 23. P. 543–550.

14. Алямовский А. А. Инженерные расчеты в SolidWorks Simulation. М. : ДМК Пресс, 2010. 464 с.

15. Алямовский А. А. SolidWorks Simulation. Инженерный анализ для профессионалов: задачи, методы, рекомендации. М. : ДМК Пресс, 2015. 562 с.

16. Физическое материаловедение. В 3 т. Т. 3. Физико-механические свойства металлов и сплавов : пер. с англ. / под ред. Р. У. Кана и П. Хаазена. М. : Металлургия, 1987.

UDC 519.688

Siberian Journal of Science and Technology. 2018, Vol. 19, No. 1, P. 98–105

DETERMINATION OF TOTAL IONIZATION DOSE BY RAY TRACE ANALYSIS BASED ON A GEODESIC SPHERE

G. N. Sherstennikova*, A. S. Shaura

JSC "IRZ"
19, Bazisnaya Str., Izhevsk, 426034, Russian Federation
*E-mail: vakilova@irz.ru

When designing the spacecraft, it is necessary to take into account the deleterious action of various factors in outer space. The main factor limiting active life of spacecraft is ionization radiation and it is the cause of most failures. Its influence is accompanied by ionization losses of the energy of charged particles in active and passive areas of semiconductors and integrated circuits; that leads to emergence of radiation effects and it is characterized by the value of absorbed dose. At present there are several approaches to forecast the value of total ionization dose (TID): Monte-Carlo methods, methods that take into account only standard shield geometry (sphere, plane) and ray trace analysis (or sector-based analysis).

The paper presents a modification of ray trace analysis that uses a geodesic sphere for sector construction and provides regularly distribution of tracing rays in space unlike classical approach with using a parametrical representation of a sphere. Our approach enables to take into consideration real density of materials and allows using fewer sectors to meet the requirements of the method 154.PM–129 and keeping calculation accuracy. This is especially important for carrying out element-by-element radiation analysis taking into account heterogeneous protection through shielding of calculated point by elements of spacecraft design.

This method is implemented as an extension for SolidWorks CAD. The input data for calculation are the following: 3d-model of equipment component as a part of spacecraft and radiation attenuation tables. The accuracy and the speed of the analysis depends on the number of tracing rays, and it is possible to carry out the calculation for several types of ionizing radiation at the same time.

As an example of using the proposed method and a software module, we carried out radiation analysis of the block of the on-board digital computer for the spacecraft "Sfera"; its active life duration is 10 years on a high-elliptic orbit and 15 years on a geostationary orbit. As a result, we revealed that for the elements of the block minimum and maximum total ionization doses differed substantially. It means that taking into account shielding properties of structural elements of device and blocks makes significant contribution to TID calculation.

Keywords: total ionization dose, ray trace analysis, ionization radiation, SolidWorks, geodesic sphere.

Сибирский журнал науки и технологий. 2018. Т. 19, № 1. С. 98–105

ОПРЕДЕЛЕНИЕ НАКОПЛЕННОЙ ДОЗЫ МЕТОДОМ СЕКТОРИРОВАНИЯ НА ОСНОВЕ ГЕОДЕЗИЧЕСКОЙ СФЕРЫ

Г. Н. Шерстенникова*, А. С. Шаура

АО «Ижевский радиозавод»
Российская Федерация, 426034, г. Ижевск, ул. Базисная, 19
*E-mail: vakilova@irz.ru

При проектировании космических аппаратов (КА) необходимо учитывать повреждающее действие от различных факторов космического пространства. Основным фактором, ограничивающим срок активного существования космических аппаратов, является ионизирующее излучение – причина большинства отказов и сбоев. Его воздействие сопровождается ионизационными потерями энергии заряженных частиц в активных и пассивных областях полупроводников и интегральных схем, что приводит к проявлению радиационных эффектов, и характеризуется величиной поглощенной дозы. В настоящее время существует несколько подходов к прогнозированию величины накопленной дозы: методы Монте-Карло, методы, учитывающие только стандартную геометрию защиты (сфера, плоскость), и лучевой анализ (или секторирование).

Представлена модификация лучевого анализа с построением секторов на основе геодезической сферы, которая в отличие от классического подхода с использованием параметрического представления позволяет получить трассирующие лучи, равномерно распределенные в пространстве. Такой подход дает возможность учитывать реальные плотности материалов, обходиться меньшим количеством секторов для выполнения требований методики 154.ПМ – 129 и сохранения точности расчета, что особенно актуально при проведении *поэлементного радиационного анализа с учетом неоднородной защиты, так как происходит экранирование рассчитываемой точки элементами конструкций КА.*

Данный метод реализован в виде расширения для САПР SolidWorks. В качестве исходных данных для расчета выступает 3D-модель блока в составе КА и заданные в техническом задании таблицы ослабления. Точность и скорость выполнения анализа зависит от количества трассирующих лучей, при этом возможно проведение расчета одновременно для нескольких видов ионизирующего излучения.

В качестве примера использования предложенного метода и программного модуля проведен радиационный анализ блока БЦВК для КА «Сфера» со сроком активного существования 10 лет на высокоэллиптической орбите и 15 лет – на геостационарной. В результате расчета было получено, что для элементов внутри блока минимальная и максимальная накопленные дозы отличаются примерно на порядок, что говорит о том, насколько заметный вклад в расчет может внести учет защитных свойств элементов конструкций аппарата и блоков.

Ключевые слова: накопленная доза, метод секторирования, ионизирующее излучение, SolidWorks, геодезическая сфера.

Introduction. During the performance of their missions, spacecraft are exposed to various destabilizing factors affecting the availability of radio electronic equipment and its element base. Among the many known factors (space vacuum, micrometeorites, null gravity, infrared emission, etc.), the primary item limiting the active life of devices and the application of specific electronic components in on-board equipment is the ionizing radiation of outer space [1]. According to GSFC Space Science Mission Operations Team, 59 % of all space missions were affected by perturbations of “space weather”. Changes in space weather are mainly related to solar activity, which causes fluctuations in the radiation background of the Van Allen belts, resulting in temporary anomalies in the operation of satellites, important electronic components are destroyed, solar cells are being degraded, etc. In January 1994, two Canadian communication satellites (Telesat’s Anik E1, E2) were disabled in a geostationary orbit, similar anomalies occurred in January 1997 with Teslar 401 satellite, and in May 1998 with Equator-S, Polar and Galaxy-IV [2]. According to ESWW conference materials published in 2012–2015 [3], in the periods from 2001–2015, there were more than 10 failures of “Thaicom 5”, “Galaxy 15”, “AMC 14”, “Arabsat 4A”, “Artemis-Ariane 5”, “Inmarsat”, and according to the materials of “Central Research Institute of Mechanical Engineering” only in 2015 there were 30 failures. In this regard, the assessment of radiation resistance of products designed for space is a necessary development stage.

The main sources of ionizing radiation are cosmic rays, divided into solar, galactic (representing charged high-energy particles, born and accelerated beyond the limits of the solar system) and the natural radiation belts of the Earth [4]. Radiation is a stream of primary charged particles – electrons, protons and heavy charged particles, as well as secondary particles – products of nuclear transformations of primary charged particles.

The effect of ionizing radiation on radio electronic equipment is accompanied by ionization losses of particle energy in active and passive regions of semiconductors and integrated circuits; that leads to the manifestation of radiation effects [5]:

– dose effects in gradual degradation of electronic component parameters as a result of accumulation of absorbed dose;

– displacement effects caused by structural damage due to knockout atoms from the lattice point with subsequent degradation of the basic electrophysical characteristics of silicon;

– single effects, caused by the passage of a separate charged particle through the sensitive volume of a semiconductor.

Single radiation effects have a probabilistic nature; dose effects and displacement effects are cumulative, therefore, when creating modern spacecraft designed for the lifetime of 10–15 years with complex configuration, it is required to know the spatial distribution of the absorbed dose in the elements of spacecraft construction, taking into account their mutual screening.

At the present time there are several approaches to forecast the value of total ionization dose (TID): the Monte Carlo methods, which are based on modeling the trajectories of individual particles [6]; methods that take into account only standard shield geometry; and methods that use sectoring or the construction of tracing beams. The Monte Carlo methods allow to provide arbitrary protection and they directly model the material-radiation interaction, but they are the most difficult to implement and resource-intensive to use, although, as a rule, they use known libraries GEANT4 [7] and MCNPX [8]. Modeling only the simplest shield geometry (sphere, plane) implemented in the majority of known programs – CREME96 [9], COSRAD [10], SHIELDOSE [11], OMERE [12], does not allow to carry out element-by-element analysis and complex screening [13]. Therefore, in practice, it is the most reasonable to use the sectoring method (ray trace analysis), since it allows us to take into account the heterogeneity of protective properties of blocks, equipment and constructional elements of spacecraft in various directions, and it is much easier to implement then Monte Carlo methods.

Ray trace analysis. When performing element analysis to determine the value of the accumulated dose in accordance with branch standard 134–1034 [14], the ray trace analysis is used. Its algorithm is stated in 154. PM-129 [15] and consists of the following steps.

Step 1. On the element of block being considered, we select the point M where we need to determine the dose. The space around it is divided into a number of sectors with solid ω_{ij} angles (fig. 1), and in the direction of each ij

sector we construct a tracing l_{ij} ray with the start at the design point M.

Step 2. For each l_{ij} ray we define the l_{ijk} intersections with the elements of spacecraft construction, other blocks and components.

Step 3. Taking into account the density ρ_k of intersected bodies, we determine the effective protection X_{ij} in each ij direction:

$$X_{ij} = \sum_{k=1}^{K} l_{ijk} \cdot \rho_k . \qquad (1)$$

Step 4. After that, using the tables of attenuation, we determine the contribution $D(X_{ij})\cdot\omega_{ij}$ of each sector to the final accumulated dose and carry out summation over all ij directions:

$$D_\Sigma = \frac{1}{2\pi} \sum_{i=1}^{m} \sum_{j=1}^{n} D(X_{ij}) \cdot \omega_{ij} . \qquad (2)$$

The key stages of the algorithm are the construction of tracing rays and the determination of their intersections with the elements of spacecraft construction.

Tracing ray construction. As a rule, to construct sectors and rays, the parametric representation of a sphere is most often used with the help of azimuth and zenith angles (UV – parametrization of the sphere, fig. 1). With this partition, the cells are different in shape and area, and the sectors are not only significantly different in magnitude, but their distribution in space is highly unequal: on the poles of the sphere there are more sectors and they are smaller than in the equatorial region (fig. 2, *a*).

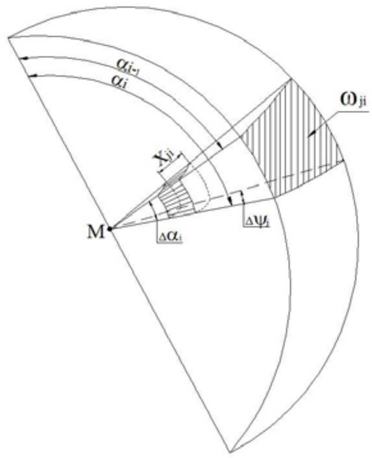

Fig. 1. The scheme of constructing sectors
for UV-parameterization of a sphere [15]

Рис. 1. Схема построения секторов
при UV-параметризации сферы [15]

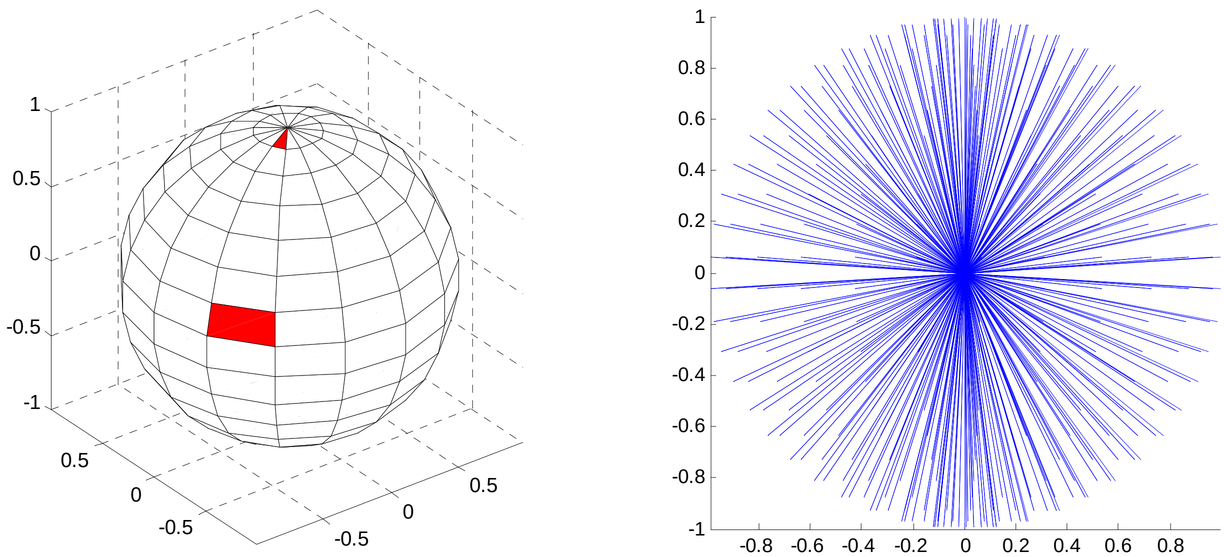

a *b*

Fig. 2. Two-parametrical representation of a sphere: *a* – cells are different in form and area; *b* – unequal distribution of tracing rays

Рис. 2. Двухпараметрическое представление сферы: *а* – различные по форме и площади ячейки;
б – неравномерное распределение трассирующих лучей

Increasing the number of sectors rises the ratio of maximum and minimum area of cells, and for 500–600 sectors the ratio is ten times. As a result, there is unequal distribution of rays, condensation on the poles and rarefied in the region of the equator (fig. 2, *b*). In some cases, this inequality in the distribution of tracing rays in space leads to the dependence of the accumulated dose on the orientation of the divided sphere relative to spacecraft due to the presence of various kinds of holes, connectors, stiffeners, etc. in the models. In this regard, the requirement of the methodology 154.PM-129 [15] of ensuring equal protection within the sector is often ignored, so we refused this partition and turned to constructing sectors based on the geodesic sphere.

Geodesic sphere is a result of sphere triangulation using the method of recursive decomposition of icosahedrons (fig. 3). Its specific feature is that faces differ minimally from regular triangles and they are almost equal in area at the same time [16].

The number of faces and vertices of a geosphere depends on the triangulation order: the higher the degree of triangulation, the greater the number of faces and vertices of the geosphere. With the increase of triangulation order, the grid becomes smoother, and its faces approach the surface of the sphere (fig. 4, *a*). The tracing rays constructed on such a grid are uniformly distributed in space (fig. 4, *b*), and solid angles formed by the sectors are almost similar in size.

This approach allows us to use a smaller number of sectors to meet the requirements of the methodology 154. PM-129 [15] and maintain the accuracy of the calculation.

Definition of intersections. The next important step of the algorithm is to determine the intersections of rays with constructional elements. This is the most time-consuming operation in terms of time and computing costs, so it does not make any sense to look for intersections of each ray with each body for complex 3D-models. However, using the algorithms of computational geometry it is possible to quickly determine whether the ray intersects elementary geometric bodies, such as a sphere and a rectangular parallelepiped [17].

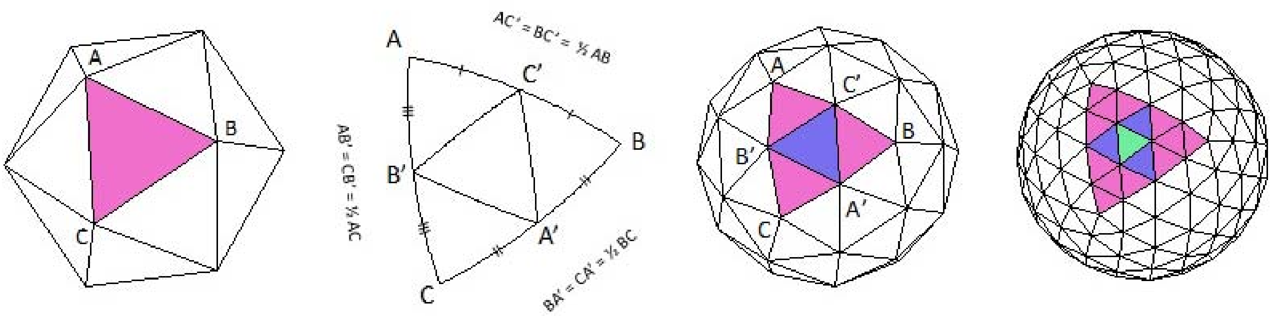

Fig. 3. The principle of geosphere construction by recurrent splitting of regular icosahedrons

Рис. 3. Принцип построения геосферы путем рекуррентного разбиения икосаэдра

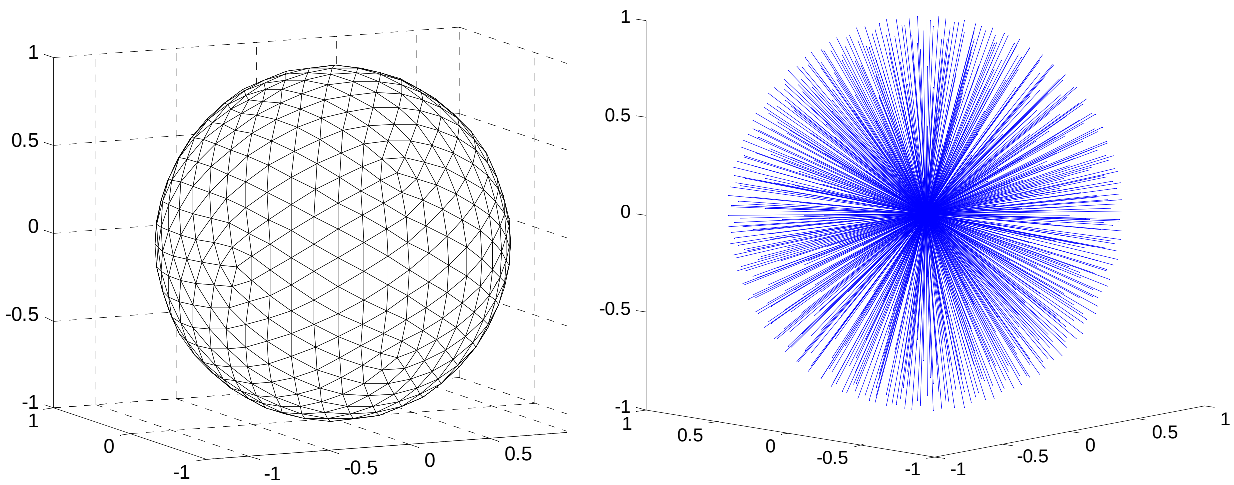

a *b*

Fig. 4. Geosphere application for approximation of spherical surface:
a – geodesic sphere (642 vertices and 1280 faces); *b* – the corresponding distribution of tracing rays

Рис. 4. Применение геосферы для аппроксимации сферической поверхности:
а – геодезическая сфера (642 вершины и 1280 граней); *б* – соответствующее распределение трассирующих лучей

A rectangular parallelepiped with faces parallel to the coordinate planes can be circumscribed around any considered body of spacecraft models. Such a parallelepiped is uniquely determined by any two its vertices (x_-, y_-, z_-) and (x_+, y_+, z_+) adjacent to one of its diagonals. The ray with the start at the point (x_0, y_0, z_0) and the directing vector (l, m, n) is described by a parametric system of equations:

$$\begin{cases} x = x_0 + lt, \\ y = y_0 + mt, \\ z = z_0 + nt. \end{cases} \quad (3)$$

Let's consider the relative position of the ray and each pair of planes parallel to the coordinate and containing opposite faces of the parallelepiped (fig. 5, *a*).

For the pair of planes $x = x_-$ and $x = x_+$ parallel to the plane YZ, the ray given by the system (3), for $l = 0$, is parallel to them and does not intersect the chosen parallelepiped for $x_0 < x_-$ or $x_0 > x_+$. Otherwise, we calculate the relations:

$$t_{1x} = \frac{x_- - x_0}{l} \text{ and } t_{2x} = \frac{x_+ - x_0}{l}.$$

Suppose $t_{1x} < t_{2x}$, subsequently $t_{near} = t_{1x}$, and $t_{far} = t_{2x}$ (fig. 5, *b*). Assuming that m ≠ 0, and considering the second pair of $y = y_-$ and $y = y_+$ planes containing the faces of the parallelepiped, we find the values t_{1y} and t_{2y}:

$$t_{1y} = \frac{y_- - y_0}{m} \text{ and } t_{2y} = \frac{y_+ - y_0}{m}.$$

If $t_{1y} > t_{near}$, then $t_{near} = t_{1y}$, and if $t_{2y} < t_{far}$, then $t_{far} = t_{2y}$. For $t_{near} > t_{far}$ or $t_{far} < 0$, the ray does not pass through the parallelepiped. Assuming that $n \neq 0$, we consider the last pair of planes $z = z_-$ and $z = z_+$ and find t_{1z} and t_{2z}:

$$t_{1z} = \frac{z_- - z_0}{n} \text{ and } t_{2z} = \frac{z_+ - z_0}{n}.$$

If as a result of similar comparisons we get $0 < t_{near} < t_{far}$ or $0 < t_{far}$, in this case the ray intersects the selected parallelepiped, and further it makes sense to look for possible intersections of the ray with curvilinear surfaces of the body inscribed in this parallelepiped to determine the entry and exit points of the ray, segments of its path inside the body.

To determine intersections with curved surfaces, we can use the built-in functions *IModelDoc2*::*RayIntersections* and *IModelDoc2*::*GetRayIntersectionsPoints* from *SolidWorks.Interop.sldworks* in *API SolidWorks* [18].

Having found all the intersections, we need to calculate the effective protection in each direction. Fig. 6 shows an example of tracing rays passing through the elements and the parts of a real block construction. On the selected fragment the beam passes through 4 bodies: a microcircuit, two layers of a board and a block cover.

Knowing the l_{ijk} segments traversed by the ray in the intersected bodies of the model, and the apparent densities ρ_k of these bodies (fig. 6, *b*), we determine the effective protection X_{ij} in the ij direction by the formula (1). Next, we determine the total accumulated dose of ionizing radiation (2).

Software implementation. From the point of view of a design engineer, it is most convenient to calculate accumulated doses of ionizing radiation directly in CAD used for the design, an engineer makes changes in the design and arrangement of individual blocks, calculates and introduces protective screens. We used SolidWorks, therefore we created a calculation module for it that allowed us to use the available CAD capabilities and at the same time solve new tasks effectively. As input data for for the calculation we used 3D-model of the spacecraft block and the tables of attenuation given in the technical enquiry.

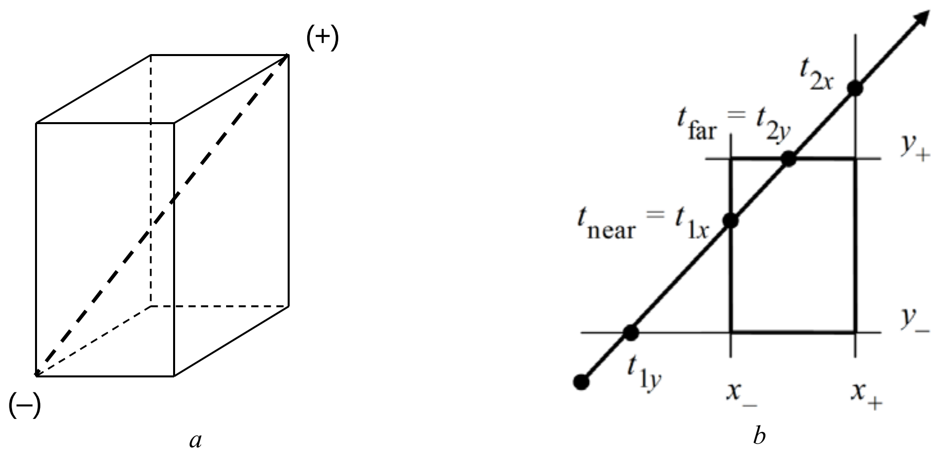

Fig. 5. General concept of definition of the intersection points of a ray and a rectangular parallelepiped [17]: *a* – defining a rectangular parallelepiped by means of two vertices adjacent to one diagonal; *b* – relative position of a ray and each pair of the parallel planes containing opposite faces of parallelepiped

Рис. 5. Общий принцип определения точек пересечений луча и прямоугольного параллелепипеда [17]: *а* – задание параллелепипеда с помощью двух вершин, прилежащих к одной диагонали; *б* – взаимное расположение луча и каждой пары параллельных плоскостей, несущих противоположные грани параллелепипеда

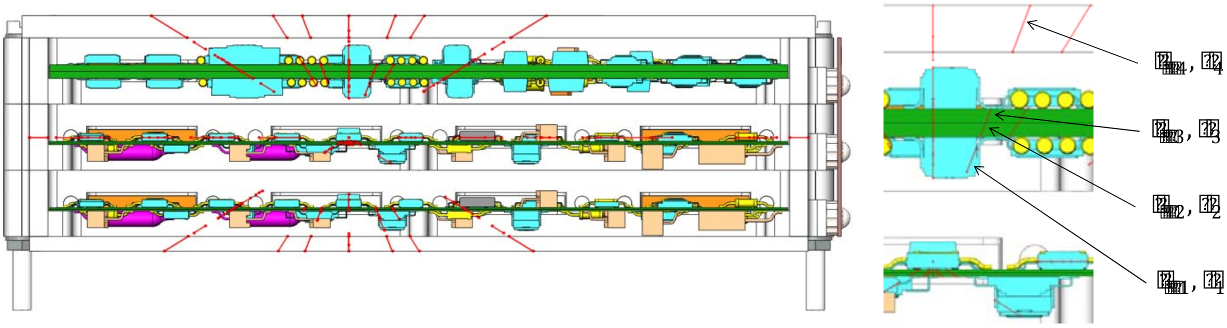

a *b*

Fig. 6. Example of tracing rays passing through constructional elements of the block: *a* – cut-away view of the block and rays; *b* – line segments l_{ijk} passed by the ray in constructional elements and apparent densities of materials ρ_k corresponding to them

Рис. 6. Пример прохождения трассирующих лучей через элементы конструкции блока: *а* – общий вид блока и лучей в разрезе; *б* – отрезки l_{ijk}, проходимые лучом в элементах конструкций, и соответствующие им объемные плотности материалов ρ_k

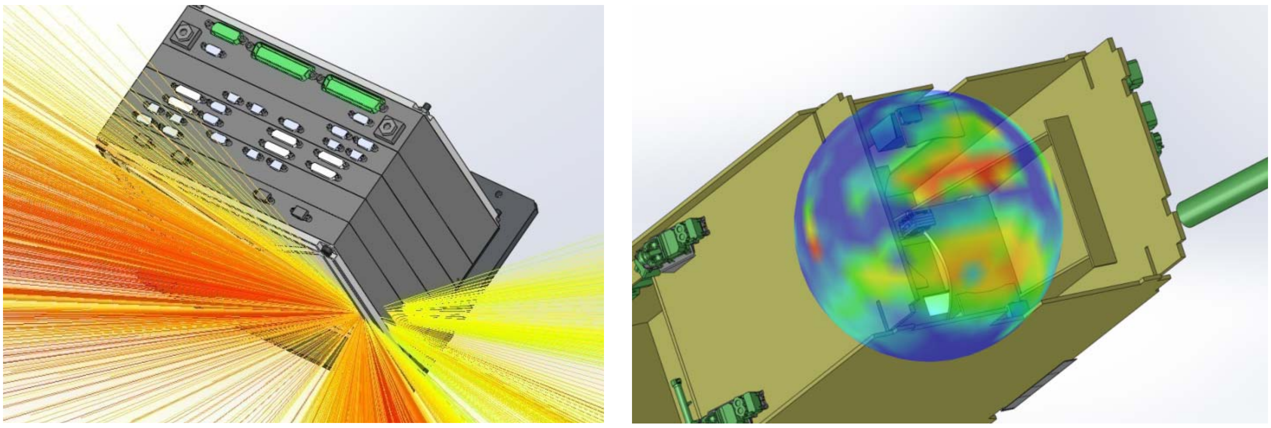

a *b*

Fig. 7. Visual representation of calculation results: *a* – directions making the greatest contribution to a total ionization dose; *b* – general representation of space distribution of effective protection

Рис. 7. Визуальное представление результатов расчета: *а* – направления, вносящие наибольший вклад в накопленную дозу; *б* – общее представление о пространственном распределении эффективной защиты

The calculation can be performed simultaneously for several types of ionizing radiation (protons, electrons, total impact), while the number of tracing rays can be chosen in advance, thus determining the accuracy and the speed of the analysis.

The results can be presented visually in order to simplify the task of identifying the weakest points in the design of protection. Fig. 7, *a* shows the course of the rays, colored in accordance with their contribution to the total dose, by applying the filter to select the most dangerous directions. The projection of effective protection of each sector on the spherical shell circumscribed around the analyzed block is presented in fig. 7, *b*.

Analysis of results. As an example of the use of the proposed method and software module, we carried out a radiation analysis of the on-board digital computer systemblock for “Sfera” spacecraft with active life duration 10 years in a highly elliptical orbit and 15 years in geostationary orbit. We analyzed more than 400 sensing elements, while the 3D-model of the block of the spacecraft included more than 2500 bodies.

Increasing the fineness of splitting and the number of rays straining after greater accuracy significantly influences the time of the analysis, so in this case it is always necessary to look for the compromised solution between the desired accuracy and admissible duration of calculation. The graphs (fig. 8) show that the computation time increases exponentially with increase of the number of rays. At the same time, the accuracy of the calculation increases as well, but, for example, at 10 000 rays the decrease of the maximum deviation of accumulated doses from 7 to 3 % requires 4 times more time.

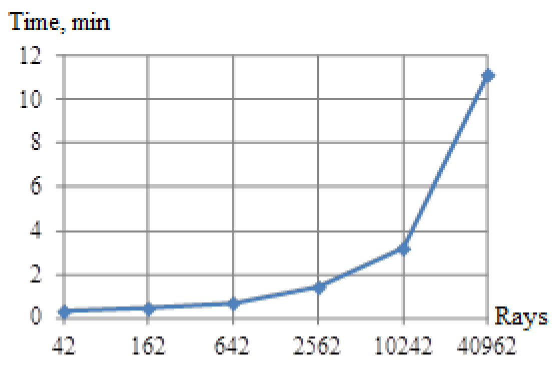

a

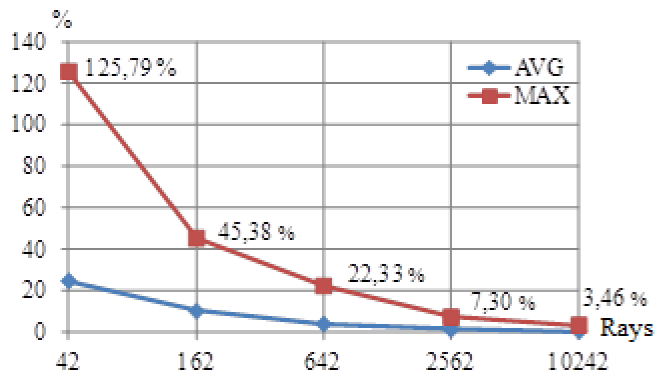

b

Fig. 8. Duration and accuracy of calculation depending on the number of rays: *a* – calculation time for a one point; *b* – average (AVG) and maximum (MAX) value of accumulated dose deviations

Рис. 8. Продолжительность и точность расчета в зависимости от количества лучей: *а* – время расчета одной точки; *б* – средняя (AVG) и максимальная (MAX) величина отклонений накопленных доз

For the elements of the block, the minimum accumulated dose was 5.3 krad, and the maximum one was 50.2 krad; that means that within one product the values of the minimum accumulated dose for specific electronic components may differ significantly, and that taking into account protective properties of the constructional elements of the apparatus and blocks can make a significant contribution to the calculation. This means that element-by-element radiation analysis has significant advantages over the evaluation of the stability of blocks as single and indivisible components of spacecraft.

Conclusion. The approach presented in the work and its software implementation allow performing element-by-element radiation analysis in the development of on-board equipment spacecraft taking into account real geometry of constructions and material density.

Determining the value of accumulated dose at various points of the developed block at the designing stage makes it possible to place less resistant elements into more protected areas, it is especially important for import substitution.

Further project development includes designing the host of functions offering locations and the level of required protection, as well as the addition of the possibility to take into account the emission of point sources (e. g. spacecraft engines).

References

1. Pershenkov V. S., Skorobogatov P. K., Ulimov V. N. *Dozoviye effekty v izdeliyakh sovremennoy mikroelektroniki* [Dose effects in modern microelectronics products]. Moscow, NIYAU MIFI Publ., 2011, 172 p. (In Russ.).

2. Kuznetsov V. D. [Space weather and risks of space activities]. *Kosmicheskaya tekhnika i tekhnologii*. 2014, No. 3 (6), P. 3–13 (In Russ.).

3. European space weather week. Available at: http://www.stce.be/ESWW (accessed 26.10.2017).

4. Kulakov V. M., Ladygin Ye. A., Shakhovtsov V. I. *Deystvie pronikayushchey radiatsii na izdeliya elektronnoy tekhniki* [Effect of nuclear radiation on electronic products]. Moscow, Sov. Radio Publ., 1980, 224 p. (In Russ.).

5. Tapero K. I., Ulimov V. N., Chlenov A. M. *Radiatsionnyye effekty v kremniyevykh integral'nykh skhemakh kosmicheskogo primeneniya* [Radiation effects in silicon integrated circuits for space applications]. Moscow, Binom, Laboratoriya znaniy Publ, 2014, 304 p. (In Russ.).

6. Biyelayev A. F. Fundamentals of the Monte Carlo method for neutral and charged particle transport. The University of Michigan Department of Nuclear Engineering and Radiological Sciences, 2001, P. 338.

7. Brun R., Bruyant F., Carminati F. et al. GEANT: Detector Description and Simulation Tool. Publication Geneva: CERN, 1993, P. 430.

8. X-5 Monte Carlo Team, MCNP-A General Monte Carlo N-Particle Transport Code. Los Alamos National Laboratory, April 2003.

9. Tylka A. J. et al. CREME96: A Revision of the Cosmic Ray Effects on Micro-Electronics Code. *IEEE Trans, on Nuclear Science.* 1997, Vol. 44, No. 6, P. 2150–2160.

10. Integrirovannyy paket programm COSRAD. Available at: http://www.cosrad.sinp.msu.ru (accessed 26.10.2017).

11. Seltzer S. M. SHIELDOSE: A Computer Code for Space-Shielding Radiation Dose Calculations, National Bureau of Standards, NBS Technical Note 1116, U. S. Government Printing Office, Washington D. C., 1980.

12. Varotsou A. OMERE Advanced Manual, TRAD, 2010, P. 48.

13. Anashin V. S., Grigor'yeva S. B., Kozyukova O. S. *Analiz sovremennogo programmnogo obespecheniya dlya otsenki lokal'nykh usloviy funktsionirovaniya SBIS na bortu kosmicheskikh apparatov v chasti ioniziruyuschikh oblucheniy kosmicheskogo prostranstva* [Analysis of modern software for assessing local operating conditions VLSIC on board spacecraft in the part of ionizing radiation of outer space]. MES-2014. IPPM RAN. 2014 (In Russ.).

14. *OST 134-1034–2012. Apparatura, pribory, ustroystva i oborudovaniye kosmicheskikh apparatov. Metody ispytaniy i otsenki stoykosti bortovoy radioelektronnoy*

apparatury kosmicheskikh apparatov dlya obespecheniya elektronnogo i protonnogo izlucheniy kosmicheskogo prostranstva po dozovym effektam [OST 134-1034–2012 Test methods and estimations of firmness of space vehicles onboard radio-electronic equipment for providing space electronic and proton radiations on dose effects, Application Standard]. Moscow, Standartinform Publ., 2012, 43 p. (In Russ.).

15. *Metodika rascheta pogloshchennykh doz ioniziruyushchikh izlucheniy kosmicheskogo prostranstva dlya orbit izdeliy razrabotki OAO "ISS". 154.PM - 129. OAO "ISS".* [Method of calculating the total ionization doses of ionizing radiation from outer space for orbits of JSC "ISS"] 2005 (In Russ.).

16. Wang N. and J.-L. Lee. Geometric properties of the icosahedral-hexagonal grid on the two-sphere. *SIAM J. Sci. Comput.* 2011, No. 33, P. 2536–2559.

17. Nikulin Ye. A. *Komp'yuternaya geometriya i algoritmy mashinnoy grafiki* [Computer geometry and computer graphics algorithms]. SPb., BKHV Peterburg Publ., 2003, 560 p.

18. 2012 SOLIDWORKS API Help – RayIntersections Method (IModelDoc2) Available at: http://help.solidworks.com/2012/English/api/sldworksapi/solidworks.interop.sldworks~solidworks.interop.sldworks.imodeldoc2~rayintersections.html (accessed: 26.10.2017).

Библиографические ссылки

1. Першенков В. С., Скоробогатов П. К., Улимов В. Н. Дозовые эффекты в изделиях современной микроэлектроники : учеб. пособие. М. : НИЯУ МИФИ, 2011. 172 с.

2. Кузнецов В. Д. Космическая погода и риски космической деятельности // Космическая техника и технологии. 2014. № 3 (6). С. 3–13.

3. European space weather week [Электронный ресурс]. URL: http://www.stce.be/ESWW (дата обращения: 26.10.2017).

4. Действие проникающей радиации на изделия электронной техники / В. М. Кулаков [и др.]. М. : Сов. Радио, 1980. 224 с.

5. Таперо К. И., Улимов В. Н., Членов А. М. Радиационные эффекты в кремниевых интегральных схемах космического применения. М. : Бином. Лаборатория знаний, 2014. 304 с.

6. Alex F. Bielajew. Fundamentals of the Monte Carlo method for neutral and charged particle transport / The University of Michigan Department of Nuclear Engineering and Radiological Sciences. 2001. P. 338.

7. GEANT: Detector Description and Simulation Tool / R. Brun [et al.] // Publication Geneva : CERN, 1993. P. 430.

8. X-5 Monte Carlo Team, MCNP-A General Monte Carlo N-Particle Transport Code / Los Alamos National Laboratory. 2003.

9. CREME96: A Revision of the Cosmic Ray Effects on Micro-Electronics Code / Tylka A. J. [et al.] // IEEE Trans, on Nuclear Science. 1997. Vol. 44, No.6. Pp. 2150–2160, Dec.

10. Интегрированный пакет программ COSRAD [Электронный ресурс]. URL: http://www.cosrad.sinp.msu.ru (дата обращения: 26.10.2017).

11. Seltzer S. M. SHIELDOSE: A Computer Code for Space-Shielding Radiation Dose Calculations, National Bureau of Standards. NBS Technical Note 1116. U. S. Government Printing Office, Washington, D. C., 1980.

12. Varotsou A. OMERE Advanced Manual. TRAD, 2010. P. 48.

13. Анализ современного программного обеспечения для оценки локальных условий функционирования СБИС на борту космических аппаратов в части ионизирующих излучений космического пространства / В. С. Анашин [и др.] // МЭС-2014. М. : ИППМ РАН. 2014.

14. ОСТ 134-1034–2012. Аппаратура, приборы, устройства и оборудование космических аппаратов. Методы испытаний и оценки стойкости бортовой радиоэлектронной аппаратуры космических аппаратов к воздействию электронного и протонного излучений космического пространства по дозовым эффектам. М. : Российское космическое агентство, 2012.

15. Методика расчета поглощенных доз ионизирующих излучений космического пространства для орбит изделий разработки ОАО «ИСС». 154.ПМ – 129. ОАО «ИСС», 2005.

16. Wang N., Lee J.-L. Geometric properties of the icosahedral-hexagonal grid on the two-sphere // SIAM J. Sci. Comput. 2011, № 33. P. 2536–2559.

17. Никулин Е. А. Компьютерная геометрия и алгоритмы машинной графики. СПб. : БХВ – Петербург, 2003. 560 с.

18. 2012 SOLIDWORKS API Help – Ray Intersections Method (IModelDoc2) [Электронный ресурс]. URL: http://help.solidworks.com/2012/English/api/sldworksapi/solidworks.interop.sldworks~solidworks.interop.sldworks.imodeldoc2~rayintersections.html (дата обращения: 26.10.2017).

Раздел
Part
3

ТЕХНОЛОГИЧЕСКИЕ ПРОЦЕССЫ И МАТЕРИАЛЫ

TECHNOLOGICAL PROCESSES AND MATERIALS SCIENCE

UDC 621.762

Siberian Journal of Science and Technology. 2018, Vol. 19, No. 1, P. 108–119

STUDY OF CONSOLIDATION FEATURES FOR FRAGMENTALLY NANOSTRUCTURED HARD METAL COMPOSITES

Yu. I. Gordeev[1], V. B. Jasinski[1], N. E. Anistratenko[1], A. S. Binchurov[1], V. N. Vadimov[1, 2*]

[1]Siberian Federal University
79/10, Svobodny Av., Krasnoyarsk, 660041, Russian Federation
[2]JSC "Academician M. F. Reshetnev" Information Satellite Systems"
52, Lenin Str., Zheleznogorsk, Krasnoyarsk region, 662972, Russian Federation
[*]E-mail: vladimir-vadimov@mail.ru

The results of experimental studies combined with modeling and prediction methods for the properties of hard metal composites show that modification with additives of ceramic nanoparticles and composite powders (WC-Co) allows to control microstructure parameters and provides the increase in binding durability and the level of physicomechanical properties of a hard alloy in general. Simultaneous complex application of submicrocrystalline WC carbides coated with Co layer and alloying additives of Al_2O_3 nanoparticles – grain growth inhibitors of the main phase, can be considered as the most perspective direction of nanostructured hard metal with increased hardness, strength and crack resistance production. The coating of carbide particles with a binder layer is an effective starting method that allows to obtain a volumetric billet with maintaining the unique properties of the initial nanopowders and ensures a uniform distribution of the phases (WC, Co, Al_2O_3). Such a multiphase fragmented nanostructured composite is characterized by additional heterogeneity, determined by differences in size and elastic phases properties. By combining the sizes and properties of the phase components in such a heterogeneous composite, it is possible to provide an increase in the fracture energy, i. e., Palmkvist crack resistance up to 16–18 MPa $m^{1/2}$ (due to inhibition on nanoparticles inclusions, stress reliefs and changes in intercrystalline crack trajectory, its length decrease). Based on the proposed stereological models and the experimentally established relationships between composition and microstructure parameters, the required volume concentrations of nanoparticles additives and composite powders (WC–Co) were determined.

Keywords: hard metal composites, nanopowders of ceramic, inhibitors, composite carbides, modeling and microstructure parameters, fracture resistance.

Сибирский журнал науки и технологий. 2018. Т. 19, № 1. С. 108–119

ИЗУЧЕНИЕ ОСОБЕННОСТЕЙ КОНСОЛИДАЦИИ ФРАГМЕНТАРНО НАНОСТРУКТУРИРОВАННЫХ ТВЕРДОСПЛАВНЫХ КОМПОЗИТОВ

Ю. И. Гордеев[1], В. Б. Ясинский[1], Н. Е. Анистратенко[1], А. С. Бинчуров[1], В. Н. Вадимов[1, 2*]

[1]Сибирский федеральный университет
Российская Федерация, 660041, г. Красноярск, просп. Свободный, 79/10
[2]АО «Информационные спутниковые системы» имени академика М. Ф. Решетнёва»
Российская Федерация, 662972, г. Железногорск Красноярского края, ул. Ленина, 52
[*]E-mail: vladimir-vadimov@mail.ru

Результаты экспериментальных исследований в сочетании с методами моделирования и прогнозирования свойств твердосплавных композитов показывают, что модифицирование с помощью добавок керамических наночастиц и композиционных порошков (WC–Co) позволяет управлять параметрами микроструктуры и обеспечивает повышение прочности связующего и уровня физико-механических свойств твердого сплава в целом. Одновременное комплексное применение субмикрокристаллических карбидов WC, покрытых слоем связки Co, и легирующих добавок наночастиц Al_2O_3 – ингибиторов роста зерна основной фазы, можно рассматривать как наиболее перспективное направление производства наноструктурированных твердых сплавов с повышенной твердостью, прочностью и трещиностойкостью. Покрытие карбидных частиц слоем связки является эффективным стартовым методом, позволяющим получать объемные заготовки с сохранением уникальных свойств исходных нанопорошков, и обеспечивает равномерное распределение фаз (WC, Co, Al_2O_3). Такой многофазный фрагментарно наноструктурированный композит характеризуется дополнительной гетерогенностью, определяемой различиями размеров и упругих свойств фаз. Комбинируя размеры и свойства фазовых составляющих в таком гетерогенном композите, можно обеспечить увеличение энергии разрушения, т. е. трещиностойкости, по Палмквисту до 16–18 МПа $м^{1/2}$ (за счет торможения на включениях наночастиц, релаксации напряжений и изменения траектории интеркристаллитной трещины, уменьшения ее длины).

На основе предложенных стереологических моделей и экспериментально установленных взаимосвязей между составом и параметрами микроструктуры были определены требуемые объемные концентрации добавок наночастиц и композитных порошков (WC–Co).

Ключевые слова: твердосплавные композиты, нанопорошки керамики, ингибиторы, композитные карбиды, моделирование и параметры микроструктуры, трещиностойкость.

Introduction. The analysis of accumulated information on scientific research in the field of new structures and hard-alloy composites manufacturing techniques development, production practice and application of various functional purpose products shows that special attention is paid to the use of powder materials components in a composite structure in the nanocrystalline state.

The conventional global trend in the hard-alloy composites structure and properties improving is formation in them a superfine-grained structure with carbide phase sizes less than 300–400 nanometers. The problems of hard alloys quality improvement can be efficiently solved due to their nanostructuring by tungsten carbide nanodimensional powders use. It is well known that when using traditional methods of consolidation for obtaining high density of a sintered composite, high temperature and sintering holding time are necessary and lead to the initial sizes increase and to carbide grains growth [1–4]. Simultaneous use of nano and submicrocrystalline carbides and alloying additives of grain growth inhibitors of the main phase nanoparticles can be considered as the most perspective direction of nanostructured hard alloys with the increased hardness, durability and crack resistance production, which has to increase product endurance under conditions of heavy shock, thermomechanical loading [5] The main inhibitors are chrome carbides, vanadium, niobium, tantalum, titanium. Doping is carried out by various methods, for example, such as chemical, mechanical (high-energy spherical grind), etc. [3]. Forming the complex carbides with the main carbide phase or being dissolved in cobalt, alloying elements influence not only on a microstructure, but also on mechanical and operational characteristics of an alloy [6–8].

A preliminary coating layer binding on carbides, i. e. producing composition powders in various ways, such as dusting, mechanical coating, coprecipitation, consecutive chemical reactions, two-stage processing, etc. can be an efficient processing method as well. The coating of carbide particles with a binding layer is the starting method which allows to get volumetric billet maintaining the unique properties of initial nanopowders [9–11]. Matrix solid phase and covering-binding material are initially homogeneously distributed on the volume of a composite particle, so the properties uniformity of initial powders structure fragments is relayed on all composite volume. Nanodimensional cobalt film presence on carbides powders provides sintering temperature decrease and in combination with high speeds of heating and the existence of inhibiting nanoparticles additives in the structure prevents carbide grains growth [3; 12–15].

Additional modifying by additives of nanoparticles provides the increase in binding durability and the level of physicomechanical properties of a composite in general. Such polyphase fragmentary nanostructured composite is characterized by additional heterogeneity determined by distinctions of the sizes and resilient properties of phases [2]. The range of such nanostructured hard metals possible use will only extend as such modifying changes the surface, chemical and reactionary processes at homogenization and as a result, structural parameters and properties of a composite in general.

Materials and methods. The morphology and microstructure of powders and sintered materials were investigated with the scanning submicroscopy (SEM) of JEOL JSM-7001F use. A particle size distribution of initial and mixed powders were defined by the method of laser diffraction SALD-7101 Shimadzu of the scanning supermicroscope. Samples microstructure was investigated on polished surfaces by means of scanning electron microscopes Hitachi “TM1000” and JEOL JSM-7500FA. The structure and the nature of fracture surfaces were analyzed with the JAMP 9500F microscope use. The X-ray diffraction analysis was carried out on the D8 ADVANCE device. Mechanical propeties determination was performed: Vickers hardness of HV30 with a hardness gage (ABK-A, Akashi) use at 30 kgfs loading; crack resistance K1C dimpling by the Palmkvista method; durability by the three-point bending method on the Shimadzu AG-IS 100 kN; studying of wear-resistance according to the ASTM B611-85 standard.

The nanopowders received by the shock-wave synthesis method or the method of electroexplosion were used as additives for hard alloys modifying. The powders morphology is shown on fig. 1, average particle size in the range from 0.067–of 0.1 microns for Al_2O_3 (*a*, *b*); 0.008 microns for ZrO_2 (Y_2O_3). Composition powders (WC–Co) obtained by complex application of chemical and microwave synthesis methods [10] with 0.2–0.4 microns size (fig. 1, *c*).

Results and discussion. Hard-alloy composites investigated in the work are composite materials, heterogeneous in structure, at least, with one phase showing nanomaterial properties**.** When developing structures, manufacturing techniques and numerical assessment methods of new three-phase hard-alloy composites generation composites formed by a combination of carbides grains (including plated by a binding metal layer), actually binding with the distributed on its volume modifying nanoadditives of oxides, nitrides proceeded from the following assumptions and prerequisites:

– when sintering the prevention of carbide grain growth at the expense of nanoparticles inhibitors additives is provided;

– the distribution of the main phases (a carbide basis, binding, and the nanoparticles distributed on binding volume nanoparticles) is homogeneous, uniform in structure;

– submicronic carbide grains are located at a well predictable distance therefore the package density of a three-phase composite can be regulated (simulated) proceeding from a ratio of micron carbide volume fractions (V_m) and nanodispersible (V_f) fraction and their average sizes (d_m, d_f);

– when modelihg it is necessary to consider differences in a kinetics of mass transfer and reactivity of phase components in a sintering process.

In works [13–15] it was shown that the effectiveness of hard alloys modifying by Al_2O_{3f} nanoparticles essentially depends on sizes, concentration and volume fractions of all composite WC–Co–Al_2O_3(ZrO_2) components.

At the random nature of void filling between carbide grains various structural fragments created by oxide-coated particles which have various degree of contact and internal microporosity can be formed. Conditionally fragments between carbide grains can be presented in the form of three main types of structures – their analytical (model) description compared to the results of the microstructure experiment studies and properties results are given below.

1. The single isolated inclusions of nanoparticles. At small concentration of nanoparticles additives in the local volume of a cobalt layer the fragments presented in fig. 2 are formed.

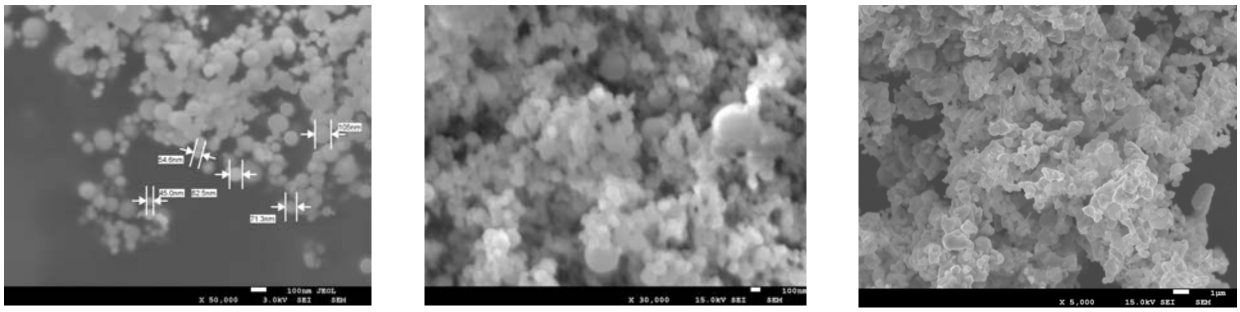

a *b* *c*

Fig. 1. SEM nanopoweder morphology: *a* – aluminum oxide; *b* – circonium oxide; *c* – tungsten carbide composite particles coated with Co-layer (WC–Co)

Рис. 1. SEM-морфология нанопорошков: *а* – оксид алюминия; *б* – оксид циркония; *в* – композитные частицы карбида вольфрама, покрытые слоем кобальта (WC–Co)

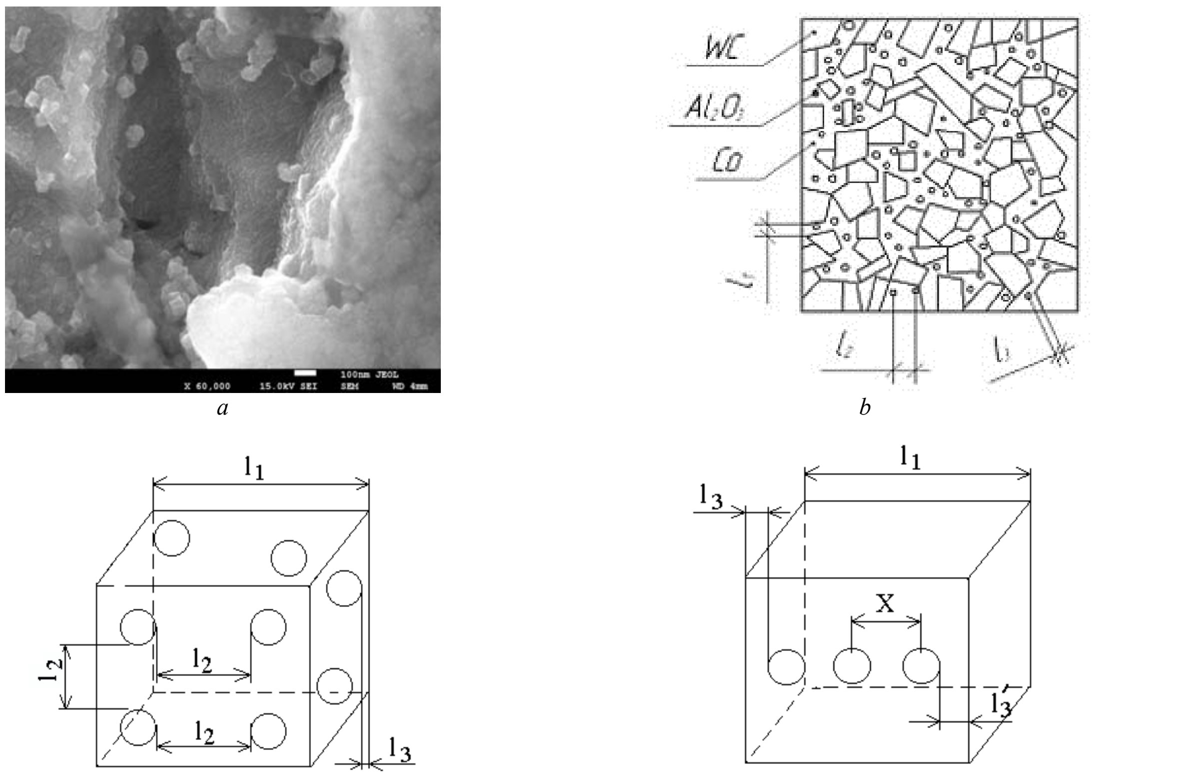

a *b* *c* *d*

Fig. 2. Geometric model of a hard alloy modified by nanoparticles: *a* – structure (fracture) fragment between carbide grains of a hard-alloy composite including Al_2O_3 nanoparticles; *b* – microstructure scheme; *c*, *d* – single volumes of cobalt binding

Рис. 2. Геометрическая модель твердого сплава, модифицированного наночастицами: *а* – фрагмент структуры (излома) между карбидными зернами твердосплавного композита с включениями наночастиц Al_2O_3; *б* – схема микроструктуры; *в*, *г* – единичные объемы кобальтового связующего

Realization of this kind of fragments a WC–Co-nanoparticle composites structures is optimum from the point of view of the known mechanisms of dispersion metals hardening [2; 15]. Injected into a binding layer isolated and statistically uniformly distributed nanoparticles promote decrease of its thickness $\lambda_{эфф} = f(l_1, l_2, n_2)$ (fig. 2, *a–c*), which has to provide an increase of binding durability and, as result, hard-alloy composites in general according to mechanics of phases provisions. The efficient thickness of a cobalt layer choice $\lambda_{эфф}$ was made on the basis of probability approach on the model more detailed described in [13–15] and various optional versions of a crack distribution through binding layers by width of l_1, l_2, l_3, which sizes depend on nanoparticles additives contents and sizes. At the same time it was supposed that the material in unit volume of a cobalt binding (l_1^3) between carbide grains modified by nanoparticles, is dispersiblly strengthened according to the known Orovana mechanisms, i. e. durability of such fragment of the binding material modified by nanoparticlesadditives above, than at basic material cobalt:

$$\sigma'_B = 480 + \frac{1550}{\lambda'}, \text{ а } \lambda' = \lambda_{эфф}. \tag{1}$$

The destruction viscosity (crack resistance) of such fragmentary nanostructured hard-alloy composite can be determined by the formulas offered in works [16; 17] and adapted to the hard-facing alloys modified by nanoparticles:

$$K_{1c} = \left\{ \frac{R \cdot (\lambda + d_m) \cdot \sigma'_B \cdot V_m \cdot E'}{C_1} \right\}^{\frac{1}{2}}, \tag{2}$$

where R – empirical reduction coefficient; d_m – the average size of carbide grain; V_m –volume ratio of carbide fraction; E' – the given elastic modulus; C_1 – contact ability of carbide edges.

The results of calculations for the offered model show satisfactory convergence of calculation data with the experimental [14].

By the experimental methods it was determined that ceramics nanoparticles Al_2O_{3f} in the quantity of 0,05–0,25 % on weight, not only dispersiblly strengthen a cobalt layer (H_μ microhardness, measured by the micronanohardness testing method, increases up to 22.01 GPa), but also provide flexure strength increase (to 25 %) – crack resistance according to Palmkvista (up to 50 %) (fig. 3), decrease in an abraser wear ~ 1.5 times. Minimum values of a wear are observed approximately in the same areas of additives (~ 0.25 % of masses.), which provide durability increase.Tthe offered model calculations results show satisfactory convergence of calculation datas with experimental (fig. 3) [18].

Additional contribution to material wear resistancel increase is brought, apparently, by the increased resilience to an attrition of the aiuminium oxide itself (H_μ Al_2O_3 – 18–20 GPa). Substantially increase in the common level of strength properties is explained by the inhibiting effect of nanoparticles additives, the average size of carbide grain monotonically decreases with increase in their concentration [19]. Material hardness and density values do not differ significantly from basic material and are at the level: but values of a microhardness of binding layer material – cobalt, which was estimated by means of nanomicrohardness gage increase as the known effect of dispersible hardening at the level of structure fragments is implemented (Co – Al_2O_3), slightly different.

2. Agglomerates from nanoparticles. Electronic and microscopic research shows that actual parameters of a hard-alloy composite microstructure differ from the geometrical model presented in item 1. It is quite understandable on the assumption of physical reasons. At increase in nanoparticles concentration in local volumes because of poor uniformity of components interfusing, their contact ability degree increases and there occurs a formation of units with developed internal microporosity. During a unequigranular hard-alloy composites sintering process, the change of interphase energy happens first of all due to nanodisperse phases specific surface area decrease that can be followed by their agglomerating to larger micron formations and possible subsequent coagulation (fig. 4).

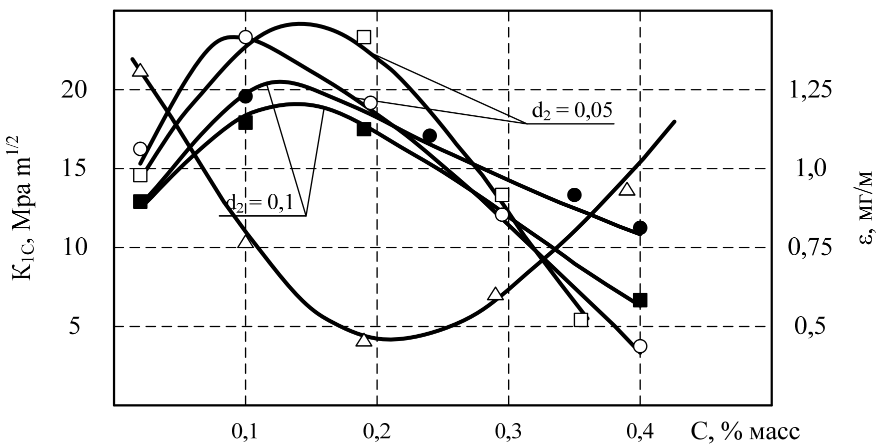

Fig. 3. Nanoparticles size (d_2) vs crack resistance (K_{1C}) of WC–Co – nano Al_2O_3 composite: (• – calculation; □ – experiment) and wear rate

Рис. 3. Влияние размера наночастиц (d_2) на трещиностойкость (K_{1C}) композита WC–Co – нано-Al_2O_3:(• – расчет; □ – эксперимент) и интенсивность износа

However the noted structural metamorphoses are, to some extent, inevitable at traditional widely applicable in hard alloys production mixture-preparation methods.

When reaching critical concentration of some nanoparticles and emergence of pressure between carbide grains at a liquid-phase sintering, manifestation of self-organization effects is revealed – a volume space structural grid formation. Its basic elements are, apparently, contacts between nanoparticles and the nanoparticles in total forming the exact regular space cells with sizes of 100 nanometers in total (fig. 5, *b*). The agglomerates formed by ceramics nanoparticles become nanostructured i. e. pass into a totally new state. Emergence of such space fragments and transitions from free-dispersible to the bound-dispersible (aggregated) systems also a composite properties change. It can be explained on the basis of the well-known physical principles of ultradispersion mediums sintering theory, including nanostructural hard alloys [1–5; 20]. The existence of such fragments is illustrated by the results of a microstructure research (fig. 5). Besides, there can be formed crystal grains of α-phase Al_2O_3 inclusions (fig. 5, *a*), micron sizes, formed at the increased compounds density of a nanophase and as a result of sufficiently high pressures action in the intercarbide space during a sintering process (about 1370 ºC sintering point is enough for nano Al_2O_3 crystallization).

3. Unequigranular heterogeneous structure. The actual microstructure of the hard-alloy composites modified by nanoparticles is heterogeneous, nonuniform on distribution and morphology of the additional oxide-coated phase created from nanoparticles. Formation of various types of structures (item 1, 2) can occurs at the same time on different mechanisms depending on various nanoparticles concentration in local volumes between the main carbide phase grains. During a sintering process various competing homogenization processes are implemented, their transformations also occur. It is confirmed by the results of own microstructure electronic and microscopic research and of other authors data [1–4; 21]. Typical images of fragmentary nanostructured materials from polished surfaces of samples are provided in fig. 5, 6.

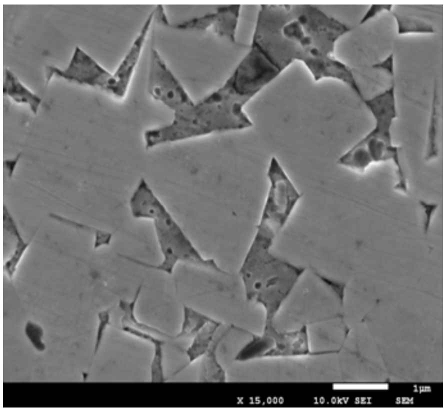

a

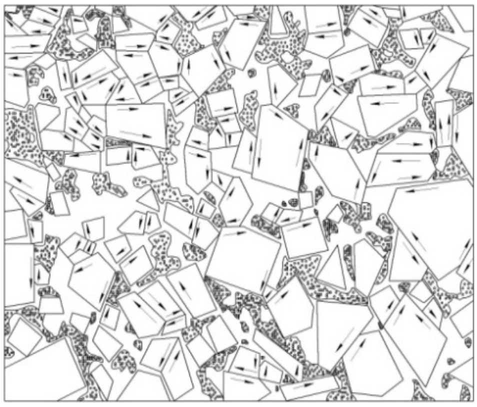

b

Fig. 4. Nanoparticles distribution within hard-alloy composite WC–Co–Al_2O_3 (nano):
a – concept scheme; *b* – microstructure fragment

Рис. 4. Распределение наночастиц в структуре твердосплавного композита WC–Co–Al_2O_3 (нано):
а – принципиальная схема; *б* – фрагмент микроструктуры

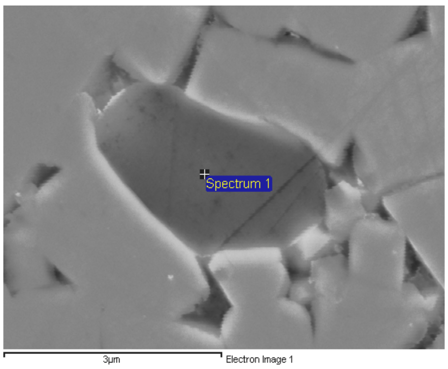

Spectrum	O	Al	W

a

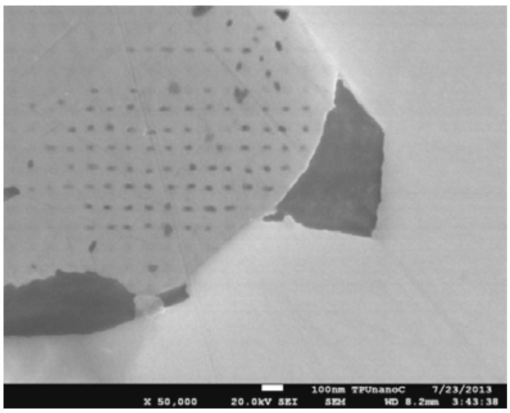

b

Fig. 5. Evolution of agglomerate structures from nanoparticles: *a* – crystallites; *b* – quasi-nanostructured fragment

Рис. 5. Эволюция структуры агломератов из наночастиц: *а* – кристаллиты; *б* – квазинаноструктурированный фрагмент

On the microscopic (micron) level statistically uniformly distributed on material volume basis structural fragments in total (combination) form a new composite of a more complex level. The additional heterogeneity caused by distinctions of resilient phases characteristics describes such polyphase composite. It is revealed in inhomogeneity of a strain-srtess state at a liquid-phase sintering when manufacturing (at phase boundaries, in the course of contraction, consolidation) and at external mechanical impact on the compacted material.

In particular, it is confirmed by material destruction viscosity research data according to the Palmkvista method in combination with a microstructure study. Cracks which are formed in the material as a result of an indentor (a diamond pyramid of Vikkers) introduction, draw attention essentially because they are potential carriers of indirect information on durability, operational material resistance, reflect changes in destruction mechanisms corresponding to various types of structure (fig. 2, 4).

The crack which moves (propagates) mainly on WC interface boundaries – WC, WC–Co slows down (fig. 7, *a*, *b*), relaxes on nanoparticles Al_2O_3, ZrO_2 dispersible inclusions, or on their conglomerates (fig. 7, *c*) distributed on cobalt layers volume.

It is necessary to emphasize in this regard that emergence of discrete cracks approximately corresponds to the area of particles additives up to 0.2 % of masses. Similar changes in destruction mechanisms of the hard-alloy nanostructured composites at cracks propagation are indicated in research results [22; 23].

Thus, combining phase components sizes and properties of in such heterogeneous composite, the energy of destruction increase (increase in trajectory length of an intercrystalline crack) is provided [24]. Despite structure inhomogeneity of an actual three-phase composite and existence of various types of fragments, the common integral level of physicomechanical properties in the field of optimum additives increases research [14; 18].

4. Polydisperse material on the basis of composite powders. Based on the positive experimental results and the discovered features of heterophase hard-alloy composites structure formation, the geometrical model (fig. 2) also explicitly described in works [14], was specified and corrected, taking into account the known and new results of calculated and experimental studies of bimodal and polymodal disperse system package density as well.

The offered specified stereological model is quadruple contacting in threes same size composite matrix particles (WC–Co). Carbide phase particles during modeling are conditionally accepted to be spherical. The centers of these spheres are tops of a tetrahedron which edges are formed by radiuses of R_i (fig. 8).

On the basis of the conducted experimental studies the specified stereological model is offered [25]. During its realization the maximal package density and uniformity of composite phase components relative distributionis are provided. The modifying additives of nanoparticles homogeneously distributed in a binding layer promote its thickness decrease $\lambda_{эфф} = f(l_1, l_2, n_2)$ (fig. 8, *a*–*c*) that according to a geometrical model (p. 2.1) has to provide an increase of binding durability and as a result, a hard-alloy composite in general.

A single volume (V_c) of such structure fragment with a particles bimodal distribution by sizes ($\bar{d}_m$, $\bar{d}_f$) can be defined proceeding from the ratio: $V_c = N_m v_m + v_p$, where N_m – a number of carbide particles; v_m – the average volume of carbide particles. Voidage (v_p) between carbide particles proceeding from the known stereology provisions can be accepted equal to $v_p = 0.20776\ (d_m / 2)^3$.

As a way of pressing density increase it is offered to enter tfa nano phase v_f additional volume equal to the volume of voids, i. e $v_p = N_f v_f$. This condition is actually impracticable as the secondary nanoparticles dense packing forms own voids of v_{pf} (fig. 8, *b*), i. e. N_f has to be reduced to N_f* by the volume of v_{pf} which is offered to equate to the volume ratio of metal binding $v_b = v_{pf} = 0.20776\ (d_f /2)^3$ (the quantity of N_f* particles can be calculated by analogy proceeding from the ratios given above). With this approach to the solution of a composite structure model operation problem its maximal density is provided.

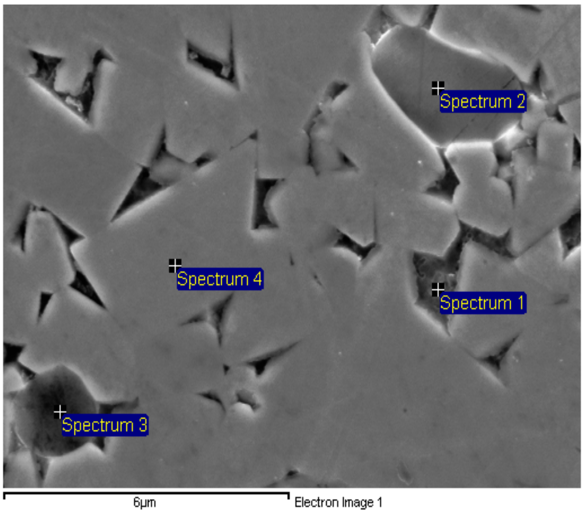

Spectrum	C	O	Al	Co	W
Spectrum 1	13.40	3.65	1.17	74.6	7.25
Spectrum 2	–	58.94	37.08	0.71	3.27
Spectrum 3	–	57.02	31.32	6.16	5.50
Spectrum 4	46.03	–	–	–	53.9

Fig 6. Forming of different structure fragments within heterogeneous hard-alloy composite

Рис. 6. Формирование различных фрагментов структуры гетерогенного твердосплавного композита

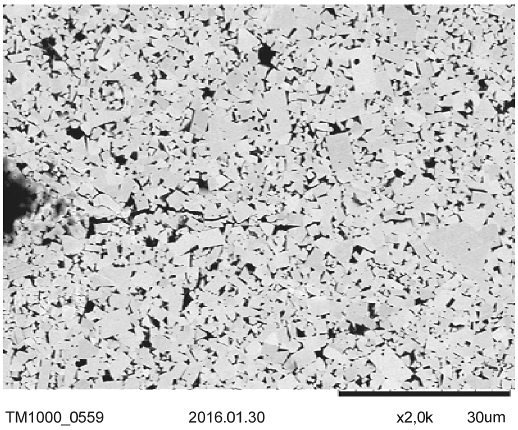

a

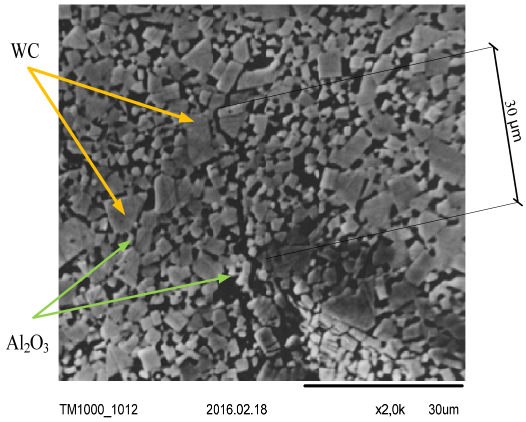

b

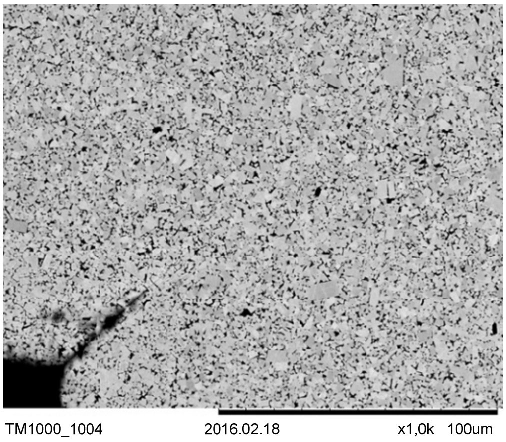

c

Fig. 7. Crack-propagation pattern due to the Vickers Pyramid dint: (*a*, *b*) – crack stopping at nanoparticle inclusions (binder metal on the surface of polished section has been removed by etching); (*c*) stress relaxation in the front of crack propagation (contrasting etching of the section)

Рис. 7. Характер распространения трещин от угла отпечатка пирамидки Виккерса: *а*, *б* – торможение трещины на включениях наночастиц (металл связки с поверхности полированного шлифа удален травлением); *в* – релаксация напряжений во фронте распространения трещины (контрастное травление шлифа)

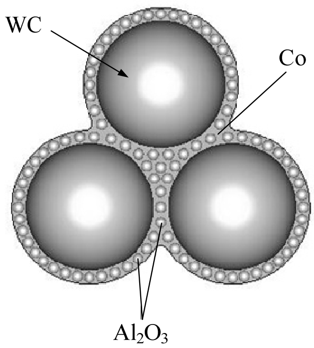

a

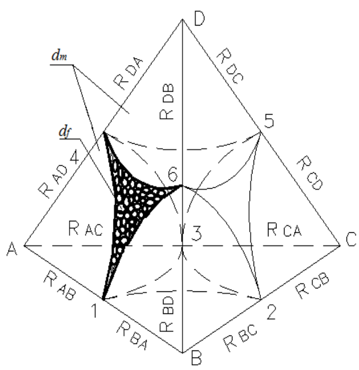

b

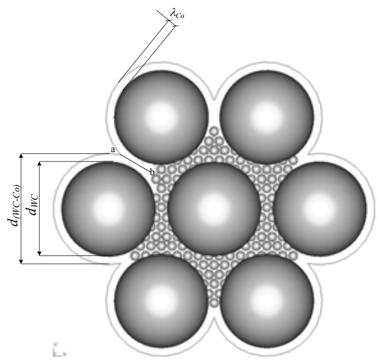

c

Fig. 8. Stereological model of a three-phase composite:
a – packing scheme; *b* – geometric model of the system d_m(WC–Co) – nanoagents of ceramic d_f (Al_2O_{3f}, ZrO_{2f}); *c* – three-phase structure parameters

Рис. 8. Стереологическая модель трехфазного композита:
а − схема упаковки; *б* − геометрическая модель системы d_m(WC–Co) – нанодобавки керамики d_f (Al_2O_{3f} , ZrO_{2f}); *в* – параметры трехфазной структуры

Composite powders use is expedient, proceeding as well from physical reasons as well, because the existence of a thin-layer binding activates the processes of consolidation, mass transfer at the lower sintering point.

The formation condition in a monolayer sintering process (binding – nanoparticles) and at the same time demands obtaining a hard alloy dense structure from composite powders (WC–Co) demands at "sewing together" of different models, considered in the work, realizations of the following ratios:

$$\beta_0 \cdot \sum_{i=1}^{Nm} \left(d_m + d_f \right)^3 = N_m \cdot v_m + N_m \cdot v_\rho - N_f \cdot v_f, \quad (3)$$

$$v_h = 4\pi((R_m + h)^3 - R_m^3)/3R_m^3, \quad (4)$$

where β_0 – the coefficient defining a form of structure; h – layer thickness of a nanoparticles monolayer with d_f size; v_h – layer volume with h thickness.

Meanwhile, the numerical values of parameters of a composition particle and coat layer thickness from metal binding on composite carbides powders can be defined from a simple ratio:

$$\frac{V_h}{V_{cm}} = \frac{\sigma h}{\bar{d}_m}, \quad (5)$$

where V_{cm} – composite particle volume.

On the basis of a new stereological model (fig. 8) estimating calculations of nanoparticles additives necessary to generate pressings with the greatest package density were made. For particle sizes of a composite carbide phase with sizes in the range of d_m (WC) from 0.3 to 0.8 microns and the sizes of ceramic nanoparticles d_f from 0.008 to 0.1 microns used in the experimental part of work the necessary concentration of nanoparticles additives in mixture composition made $V_f = 0.30$ or about 3 % of masses. The results of experimental studies allowed to specify calculated formulas by means of semiempirical coefficients and to define optimum concentration of nanoparticles additives in the range from 1 to 3 % of masses.

The use of composition submicronic powders (WC–Co) received by various methods [9–11] can be the way of implementation of this kind of heterogeneous structures with the maximal package density and at the same time providing high uniformity of the relative composite phase components distribution. In the experimental part of work the composition powders received a traditional chemical deposition on the carbon carrier in combination with microwave influence [10] (fig. 9) are used.

X-ray phase analysis results showed that the made powder hard-alloy mixtures, alloyed by oxides nanoparticles in the number of 1 %, have the average size of tungsten carbide crystal grains about 150 nanometers. Alloying additive content Increase from 1 to 3 % finds a tendency to decrease of nanoparticles coalescence effects of tungsten carbide when processing in the spherical activator and US- activation [26].

In case of composition layer powders (WC–Co) of the submicronic sizes as a basis and additional alloying of inhibitors nanoparticles additives Al_2O_3 use, the structure created as a result of a simple hard alloy sintering consists of almost isolated carbide grains partially blocked at the expense of a cobalt ductile coat (fig. 10, *a*). The intercarbide space is filled with a composition powders coat layer (Co–WC) and additives of oxides nanoparticles (fig. 10, *a*).

Efficiently influence the processes of such hard alloys structurization is also possible due to the use of the alternate methods of consolidation, intensive plastic and a shear deformation at mixtures formation (for example extrusion or rolling), stage-by-stage stepped heating with withstanding temperatures corresponding to the consolidation mechanisms change, the so-called operated sintering, high-speed and low-temperature compression sintering, electrospark plasma sintering, methods of thermomechanical cycling (which are widely applied for steels and alloys) and thermomechanical ultrasound processing. The physical sense of such influence is that in a peculiar material "buildup", structurization processes activation at consolidation, decrease in the average size and carbide grains contact ability. Finally it will allow to reduce a sintering point and to create and keep more fine-grained structure of a hard alloy composite WC–Co–Al_2O_3, WC–Co–ZrO_2. Studying of alloys consolidation features on the basis of submicronic composite powders (WC–Co) with initial sizes of carbide grain about 0.8 microns show that intensive contraction occurs already at a temperature 1320–1350 ºC that is on hard-phase sintering stages. These data are well consistent with the results given in works [1; 3]. In temperatures intervals from 1370–1420 ºC there is a partial grain recrystallization of the phase WC to the sizes of 1.5 microns. However at the same time the submicronic carbide phase of initial composite powders in combination with additives of oxides nanoparticles (fig. 10, *a*) remains in a cobalt layer between these carbide grains. Finally, positive structural changes provide additional increase of a strength properties level. Additional experimental studies conducted in collaboration with National Research Tomsk Polytechnic University (TPU) [26] demonstrate that critical threshold concentration cut-off levels of nanoparticles additives in the nanostructured hard-alloy composites *WC–Co–nano* $Al_2O_3(ZrO_2)$, received by the electrospark plasma sintering method, is 3 % of masses. In total the calculated results (on the model) and the experimental studies (methods of a scanning electron microscopy in combination with the elememt-by-element analysis use and standard methods of physical tests) allowed to realize microstructure parameters with relatively high distribution uniformity of phase components (tungsten carbides grains, a metal binding layer and modifying additives of nanoparticles) on a volume of a hard-alloy composite (fig. 11).

Increase in content of alloying additive to 3 % leads to slowing down of grain growth processes: the average size of coherent scattering area (CSA) for these samples was in the range from 151 to 163 nanometer (fig. 12, *b*). The average size of CSA cobalt bindings according to X-ray analysis does not exceed 22 nanometers [26].

Thus, the received results demonstrate positive influence of nanoparticles additives on properties of reference hard alloys (see the table) that is explained, first of all, by their structural parameters change.

Formation of nanostructural fragments in the volume of a metal cobalt layer provides decrease to the submicronic sizes of its thickness between carbide grains, the effect known in materials science as the effect of dispersible hardening, is implemented.

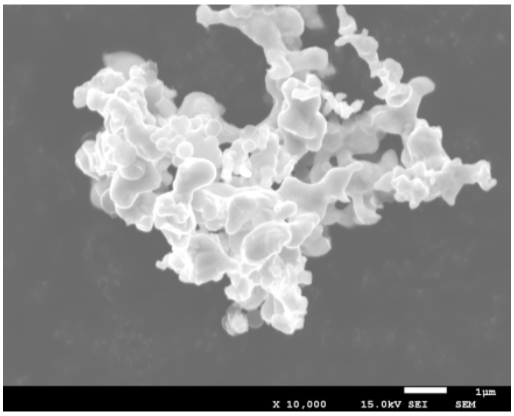

a

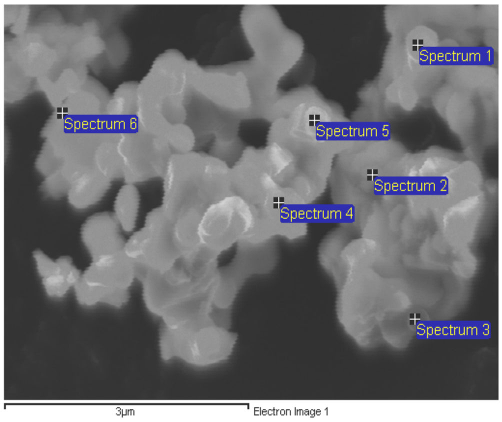

b

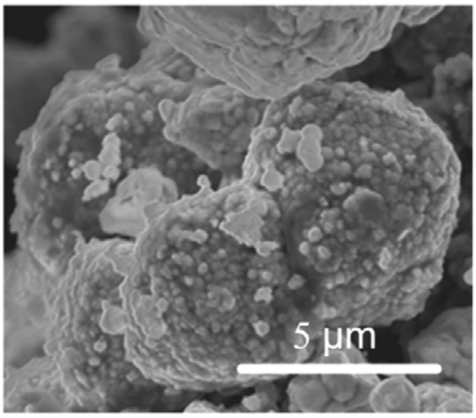

c

All results in atomic %				
Spectrum	C	O	Co	W
Spectrum 1	76.22	3.35	2.09	18.34
Spectrum 2	61.08	3.93	7.11	27.88
Spectrum 3	86.56	1.48	1.35	10.61
Spectrum 4	73.87	3.36	1.61	21.16
Spectrum 5	73.22	2.61	1.83	22.35
Spectrum 6	80.20	3.71	3.19	12.91

Fig. 9. WC–Co composite powders morphology:
a – microwave synthesis composite powders; *b* – results of powders elementary analysis; *c* – powders (WC–Co) produced by chemical method

Рис. 9. Морфология композитных порошков WC–Co:
а – композитные порошки микроволнового синтеза; *б* – результаты их элементного анализа; *в* – порошки (WC–Co), полученные химическим методом

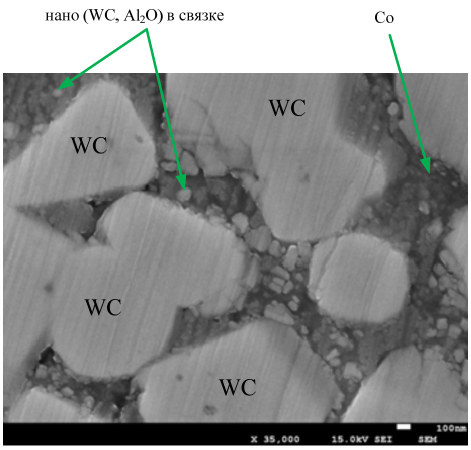

a

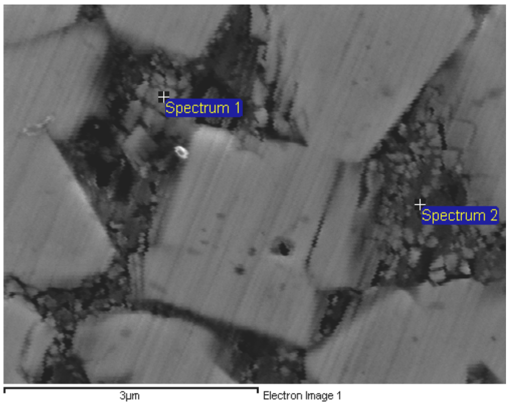

Spectrum	C	O	Co	Al	W
Spectrum 1	24.94	10.44	8.44	1.44	54.74
Spectrum 2	16.89	–	2.56	2.20	78.35

b

Fig. 10. Microstructure of hard alloys obtained from composite powders WC–Co: *a* – SEM; *b* – elementary analysis results

Рис. 10. Микроструктура твердых сплавов полученных из композитных порошков WC–Co: *а* – SEM; *б* – результаты элементного анализа

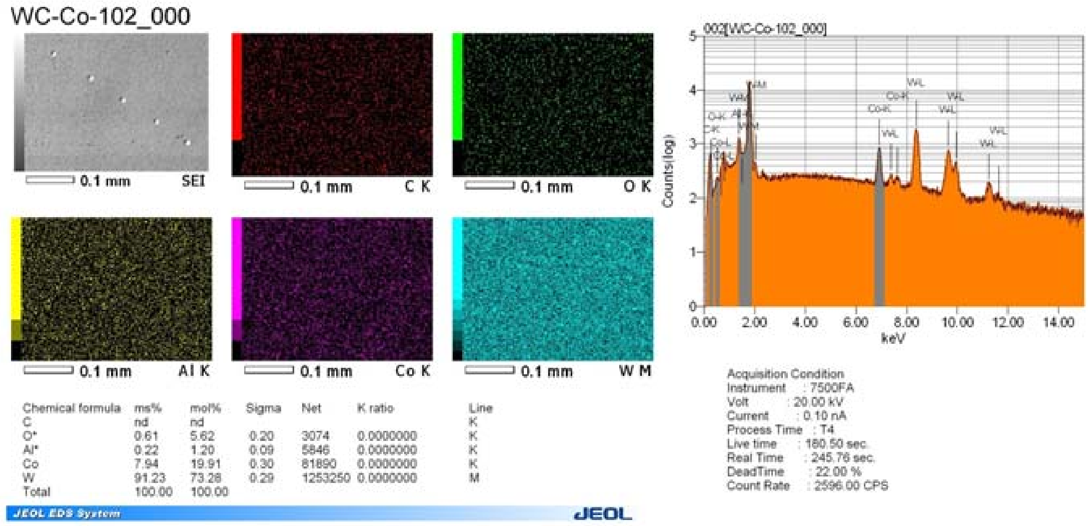

Fig. 11. Electron microscope images: nanostructured hard alloy, EDS map for local deposit of alloying constituent on the surface of hard-alloy composite produced on the basis of micron carbide powders with aluminum oxide

Рис. 11. Электронно-микроскопические изображения наноструктурированного твердого сплава, EDS-карта локального залегания легирующего компонента на поверхности твёрдосплавного композита, изготовленного на основе микронных порошков карбидов с добавками оксида алюминия

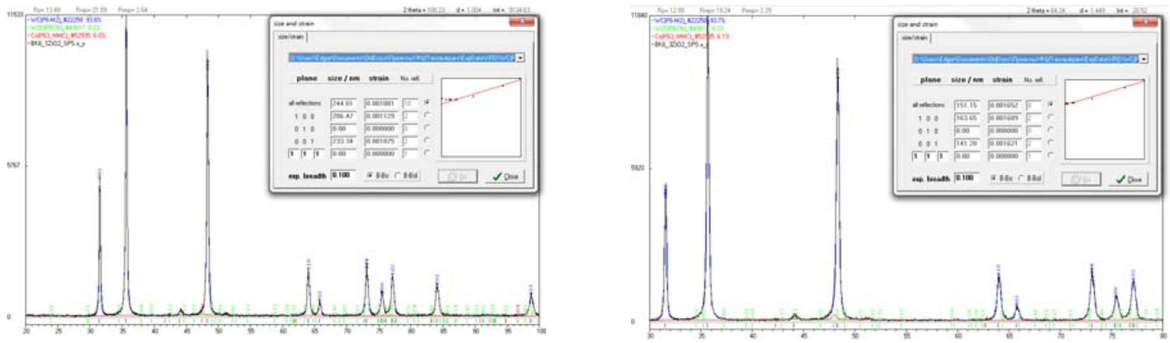

a *b*

Fig. 12. X-ray structure analysis of hard-alloy composites consolidated by electro-impulse plasma sintering method using nanoparticle additives: *a* – 1 %; *b* – 3 %

Рис. 12. Результаты рентгеноструктурного анализа твердосплавных композитов, консолидированных методом ЭИПС с количеством добавок наночастиц: *а* – 1 %; *б* – 3 %

Some strength characteristics of hard-alloy composites

Composition of the material		Physicomechanical characteristics		
		Hardness HV, ГПа	Tensile strength at bending R_{bm}, ГПа	Crack resistance K_{Ic}, МПа · м$^{1/2}$
Microcrystalline, ВК15 + Al_2O_3		12.7	2.54	21.6
Microcrystalline, ВК10КС + Al_2O_3		15.1	2.68	19.3
Quasy-nanocrystalline	ВК6	19.5 ± 0.6	2.03 ± 0.1	9.1 ± 0.6
	ВК6 + 2 % ZrO_2	20.4 ± 0.6	2.17 ± 0.1	9.3± 0.7
	ВК6 + 4 % ZrO_2	22.0 ± 0.6	2.09 ± 0.1	9.7

Conclusion. The conducted complex parametrical research results demonstrate that when modifying hard-alloy composites by nanoparticles the principle of "composition-structure-property", known in materials science, is implemented. In total, the received results of experimental studies in combination with methods of computer modeling and prediction of hard-alloy composites properties, modified by additives of ceramics nanoparticles, provide expansion of opportunities for structure and hard alloys properties operation.

Composite submicronic powders (WC–Co) use in combination with modifying nanoparticles Al_2O_3, ZrO_2 (inhibitors) is an efficient starting method of nanostructured hard-alloy composites quality improvement. The calculated results (on the model) and the experimental studies comparison show satisfactory coincidence of the predicted microstructure parameters and strength properties with the obtained.

References

1. Fang Zak Z., Wang Xu, Taegong Ryu, Kyu Sup Hwang, Sohn H. Y. Synthesis, sintering, and mechanical properties of nanocrystalline cemented tungsten carbide – A review *Int. Journal of Refractory Metals & Hard Materials*. 2009, Vol. 27, P. 288–299.

2. Andrievski R. A., Glezer A. M. Strength of nanostructures. *Physics-Uspekhi.* 2009, Vol. 52, No. 4, P. 315–334.

3. Panov V. S., Zaitsev A. A. Trends of development the technology ultrafine and nanosized tungsten carbide WC–Co – A review *Proceedings of the universities. Powder metallurgy and functional coatings*. 2014, No. 3, P. 38–48.

4. González Oliver C. J. R., Álvarez E. A., García J. L. Kinetics of densification and grain growth in ultrafine WC-Co composites. *Int. Journal of Refractory Metals and Hard Materials*. 2016, Vol. 59, P. 121–131.

5. Rempel’ A. A., Kurlov A. S., Tsvetkov Yu. V. *Tungsten carbide nanopowder for WC–C_o hard alloys, Proceedings of the Fourth All-Union Conference on Nanomaterials.* Moscow, IMET RAN Publ., 2011, P. 71.

6. Sun L., Jia C., R. Lin Cao, Lin C. Effects of Cr_3C_2 additions on the densification, grain growth and properties of ultrafine WC–11Co composites by spark plasma sintering. Sun, *Int. J. Refract. Met. Hard. Mater*. 2008, Vol. 26, P. 357–361.

7. Huang S. G., Liu R. L., Li L. NbC as grain growth inhibitor and carbide in WC–Co hardmetals. *International Journal of Refractory Metals & Hard Materials.* 2008, No. 26, P. 389–395.

8. Cholsong P., Ji L., Zhimeng G. Microstructure and properties of ultrafine WC-10Co composites with chemically doped VC. *Rare metals.* 2011, Vol. 30, No. 2, P. 183–188.

9. Vollath D., Szabo D. V. Coated nanoparticles: A new way to improved nanocomposites. *Journal of Nanoparticle Research.* 1999, Vol1, P. 235–242.

10. Nikolaenko I., Kedin N., Shveikin G. Synthesis of ultrafine powder (W, Ti) C by microwave heating in a stream of argon. *International Journal of Materials Research.* 2014, Vol. 105, No. 12, P. 1232–1235.

11. Essaki K., Rees E. J., Burstein G. T. Synthesis of Nanoparticulate Tungsten Carbide Under Microwave Irradiation. *J. Amer. Ceram. Sos.* 2010, Vol 93, No. 3, P. 692–695.

12. Yamamoto T., Ikuhara Y., Watanabe T. et al. High resolution microscopy study in Cr3C2-doped WC–Co. *Journal of Materials Science.* 2001, Vol. 36, P. 3885–3890.

13. Gordeev Y., BucaemskyA., Seher G., Teremov S. *Powder metallurgy world congress and exhibition*. 1998, Vol. 4, P. 140–146.

14. Gordeev Yu., Abkaryan A., Zeer G. Design and research of cemented carbides and ceramic composites modified by nanoparticles. *Advanced Materials*. 2012, No. 5, P. 76–88.

15. Gordeev Yu., Abkaryan A. [Possibility of increasing the strength of carbide materials and operational stability of the cutting tool through the use of thermomechanical processing] *Stanki i instrument.* 2013, No. 3, P. 30–34.

16. Nakamura M., Gurland J. The fracture toughness of WC–Co twoophase alloys: A preliminary model, *Metall. Trans.* A. 1980, Vol. 11, No. 1, P. 141–146.

17. Godse R., Gurland J. Applicability of the critical strength criterion to WC–Co, *J. Mater. Sci. Eng. A*. 1988, Vol. 106, P. 331–336.

18. Gordeev Yu., Abkaryan A., Zeer G., Lepeshev A. [Effect of alloying additions of ceramic nanoparticles on the structural parameters and properties of hard alloys]. *Vestnik SibGAU*. 2013, No. 3(49), P. 171–181 (In Russ.).

19. Gordeev Y. I., Abkaryan A. K., Binchurov A. S., Jasinski V. B., Vadimov B. H. [Design and investigation of hard metalls composites modyfied by nanoparticles and thermomechanical treatment with a high level of mechanical and operating properties]. *Vestnik SibGAU.* 2014, No. 4 (56), P. 209–218 (In Russ.).

20. Kurlov A. S. Vacuum sintering of WC-8 wt.% Co hardmetals from WC powders with different dispersity. *International Journal of Refractory Metals and Hard Materials.* 2011, No. 29 (2), P. 221–231.

21. Gordeev Y. I., Abkaryan A. K., Binchurov A. S., Jasinski V. B. Design and Investigation of Hard Metal Composites Modified by Nanoparticles. *Advanced Materials Research*. 2014, Vol. 1040, P. 13–18.

22. Dvornik M. I, Mikhaylenko Ye. A. [Modeling the process of crack propagation in submicron and nanostructured hard metals]. *Mechanics of composite materials and structures*. 2014, Vol. 20, No. 1, P. 3–15.

23. Dvilis E. S., Khasanov O. L., Bikbaeva Z. G., Polisadova V. V., Struts V. K., Omarov G. Z., Khasanov A. O. Pattern of the B4C Ceramics Surface Deformation at Local Loading. *Advanced Materials Research*. 2014, Vol. 872, P. 60–64.

24. Pozdnyakov V., Glezer A. [Structural mechanisms of destruction of nanocrystalline materials]. *Solid State Physics*. 2005, Vol. 47, No. 5, P. 793–800.

25. Gordeev Y. I., Abkaryan A. K., Binchurov A. S., Lepeshev A. A., Yasinski V. B. Influence of Additives of Nanoparticles on Structure Formation of Fine-Grained Hardmetals. *Key Engineering Materials*. 2017, Vol. 743, P. 3–8.

26. Gordeev Yu., Abkaryan A., Binchurov A., Jasinski V., Karpov I., Lepeshev A., Hasanov O., Dvilis E. [Development of effective ways to control the structure and properties of carbide composites modified nanoparticles]. *Journal of Siberian Federal University. Series: Techniques and Technologies.* 2014, Vol. 7, No. 3. P. 270–289.

Библиографические ссылки

1. Synthesis, sintering, and mechanical properties of nanocrystalline cemented tungsten carbide – A review / Zak Z. Fang [et al.] // Int. Journal of Refractory Metals & Hard Materials. 2009. Vol. 27. Pp. 288–299.

2. Andrievski R. A., Glezer A. M. Strength of nanostructures // Physics-Uspekhi. 2009. Vol. 52, no. 4. P. 315–334.

3. Panov V. S., Zaitsev A. A Trends of development the technology ultrafine and nanosized tungsten carbide WC–Co – A review // Proceedings of the universities. Powder metallurgy and functional coatings. 2014, no. 3. Pp. 38–48.

4. González OliverGonzález Oliver C. J. R., Álvarez E. A., García J. L. Kinetics of densification and grain growth in ultrafine WC-Co composites // Int. Journal of Refractory Metals and Hard Materials. 2016, № 59. P. 121–131.

5. Rempel' A. A., Kurlov A. S., Tsvetkov Yu. V. Tungsten carbide nanopowder for WC–Co hard alloys // Proceedings of the Fourth All-Union Conference on Nanomaterials. M. : IMET RAN, 2011. P. 71.

6. Effects of Cr_3C_2 additions on the densification, grain growth and properties of ultrafine WC–11Co composites by spark plasma sintering / L. Sun [et al.] // Int. J. Refract. Met. Hard. Mater. 2008. Vol. 26. P. 357–361.

7. NbC as grain growth inhibitor and carbide in WC–Co hardmetals / S. G. Huang [et al.] // International Journal of Refractory Metals & Hard Materials. 2008. № 26. P. 389–395.

8. Cholsong P., Ji L., Zhimeng G. Microstructure and properties of ultrafine WC–10Co composites with chemically doped VC // Rare metals. 2011. T. 30, № 2. P. 183–188.

9. Vollath D., Szabo D. V. Coated nanoparticles: A new way to improved nanocomposites // Journal of Nanoparticle Research. 1999, Vol. 1. P. 235–242.

10. Nikolaenko I., Kedin N., Shveikin G. Synthesis of ultrafine powder (W, Ti) C by microwave heating in a stream of argon // International Journal of Materials Research. 2014. Вып. 105, № 12. P. 1232–1235.

11. Essaki K., Rees E. J., Burstein G. T. Synthesis of Nanoparticulate Tungsten Carbide Under Microwave Irradiation // J. Amer. Ceram. Sos. 2010. T. 93, № 3. C. 692–695.

12. High resolution microscopy study in Cr_3C_2-doped WC–Co / T. Yamamoto [et al.] // Journal of Materials Science. 2001. № 36. P. 3885–3890.

13. Powder metallurgy world congress and exhibition / Y. Gordeev [et al.] 1998. Vol. 4. P. 140–146.

14. Gordeev Yu., Abkaryan A., Zeer G. Design and research of cemented carbides and ceramic composites modified by nanoparticles // Advanced Materials. 2012, № 5. P. 76–88.

15. Гордеев Ю. И., Абкарян А. К. Возможности повышения прочности твердосплавных материалов и эксплуатационной стойкости режущего инструмента путем применения термомеханической обработки // Станки и инструмент. 2013. № 3. С. 30–34.

16. Nakamura M., Gurland J. The fracture toughness of WC–Co twoophase alloys: A preliminary model // Metall. Trans. A. 1980. Vol. 11, № 1. Pp. 141–146.

17. Godse R., Gurland J. Applicability of the critical strength criterion to WC–Co // J. Mater. Sci. Eng. A. 1988, Vol. 106. Pp. 331–336.

18. Гордеев Ю. И. [Влияние добавок легирующих керамических наночастиц на структурные параметры и свойства твердых сплавов] / Ю. И. Гордеев [и др.]. Вестник СибГАУ, 2013. Т. 49, № 3. С. 174–181.

19. Конструирование и исследование наноструктурированных твердосплавных композитов с повышенным уровнем прочностных и эксплуатационных характеристик за счет модифицирования наночастицами и термомеханической обработки / Ю. И. Гордеев [и др.] // Вестник СибГАУ. 2014. № 4 (56). С. 209–218.

20. Kurlov A. S. Vacuum sintering of WC–8 wt. % Co hardmetals from WC powders with different dispersity // International Journal of Refractory Metals and Hard Materials. 2011. № 29 (2). Pp. 221–231.

21. Design and Investigation of Hard Metal Composites Modified by Nanoparticles / Y. I. Gordeev [et al.] // Advanced Materials Research. 2014. Vol. 1040. Pp. 13–18.

22. Дворник М. И., Михайленко Е. А. Моделирование процесса распространения трещины в субмикронных и наноструктурных твердых сплавах // Механика композиционных материалов и конструкций. 2014. Т. 20, № 1. С. 3–15.

23. Pattern of the B4C Ceramics Surface Deformation at Local Loading / E. S. Dvilis [et al.] // Advanced Materials Research. 2014. Vol. 872. P. 60–64.

24. Поздняков В. А., Глезер А. М. Структурные механизмы разрушения нанокристаллических материалов // Физика твердого тела. 2005. Т. 47, № 5. С. 793–800.

25. Influence of Additives of Nanoparticles on Structure Formation of Fine-Grained Hardmetals / Y. I. Gordeev [et al.] // *Key Engineering Materials*. 2017. Vol. 743. Pp. 3–8.

26. Гордеев Ю. И. Разработка эффективных путей управления структурой и свойствами твердосплавных композитов, модифицированных наночастицами / Ю. И. Гордеев [и др.] // Журнал Сибирского федерального университета. Сер.: «Техника и технологии». 2014. Т. 7, № 3. С. 270–289.

UDC 621.22

Siberian Journal of Science and Technology. 2018, Vol. 19, No. 1, P. 120–136

METHODS OF PREPARATION OF THE EXPERIMENT FOR INVESTIGATION OF UNIVERSAL JOINTS ON NEEDLE BEARINGS

S. P. Eresko, T. T. Eresko, E. V. Kukushkin*, V. A. Menovshikov, A. A. Orlov

Reshetnev Siberian State University of Science and Technology
31, Krasnoyarsky Rabochy Av., Krasnoyarsk, 660037, Russian Federation
*E-mail: ironjeck@mail.ru

The main directions of development and improvement of performance data of universal joints needle bearings of transport technological machines are considered. The questions and tasks requiring the solution at the level of forming of new calculation procedures are specified. Modern achievements in researches of endurance failures and low-cyclic fatigue of needle bearings are considered. The main overview of the works performed in this direction is provided. The analysis of modern ideas of fatigue processes of needle bearings is given. The analysis of the current state of question on research of plastic deformation at static contact loading of needle bearings is given. Questions of forecasting of durability of needle bearings of universal joints are considered. The main questions connected with processes of forming of fatigue cracks in materials of needle bearings of universal joints in zones of power contact are considered. On the basis of the analysis of the used sources it was revealed that it is necessary to resolve the issues connected with improvement of performance data of universal joints needle bearings and questions of calculation of bearing capacity of power contact of rolling bearings and technology of receiving qualitative materials. For carrying out tests we used the test facility for universal joints allowing tests without overheat of system of braking due to cooling of working fluid and also improving operating conditions due to ensuring smoothness of regulation of braking torque. For measurement of roughness of surfaces the USB BV-7669M Profilograph profilometer was used. For measurement of hardness of surfaces of thorns of crosspiece of universal joints the HBRV-187,5 hardness gage was used. The technique of carrying out tests includes the following stages: marking of crosspieces of universal joints; measurement of roughness, hardness, geometry of crosspieces of universal joints; stage of tests; repeated measurements of roughness, hardness and geometry of crosspieces of universal joints; cutting of the studied universal joints and production of microsections for metallographic examinatons of active and passive surfaces of thorns of crosspieces of universal joints; processing of results of researches. The given technique of planning of experiments is intended for receiving experimental data of researches of universal joints at different stages of operation that will allow to estimate influences of errors of production on performance data of universal joints and to prove the reasons of formation of face and deep cracks.

Keywords: endurance failures, needle bearings, modern representations of researches, test facility, design of experiments, tests of joints.

Сибирский журнал науки и технологий. 2018. Т. 19, № 1. С. 120–136

МЕТОДИКА ПОДГОТОВКИ ЭКСПЕРИМЕНТА ПО ИССЛЕДОВАНИЮ КАРДАННЫХ ШАРНИРОВ НА ИГОЛЬЧАТЫХ ПОДШИПНИКАХ

С. П. Ереско, Т. Т. Ереско, Е. В. Кукушкин*, В. А. Меновщиков, А. А. Орлов

Сибирский государственный университет науки и технологий имени академика М. Ф. Решетнева
Российская Федерация, 660037, г. Красноярск, просп. им. газ. «Красноярский рабочий», 31
*E-mail: ironjeck@mail.ru

Рассматриваются основные направления развития, улучшения и совершенствования рабочих характеристик карданных передач на игольчатых подшипниках транспортно-технологических машин. Указываются вопросы и задачи, требующие решения на уровне формирования новых методик расчёта. Рассматриваются современные достижения в исследованиях усталостных разрушений и малоцикловая усталость игольчатых подшипников. Приведен основной обзор выполненных работ в данном направлении. Дан анализ современных представлений об усталостных процессах игольчатых подшипников. Дан анализ современного состояния вопроса по исследованию пластического деформирования при статическом контактном нагружении игольчатых подшипников. Рассмотрены вопросы прогнозирования долговечности игольчатых подшипников карданных передач. Рассматриваются основные вопросы, связанные с процессами формирования усталостных трещин в материалах игольчатых подшипников карданных передач в зоне силового контакта. На основе анализа используемых источников было выявлено, что необходимо решить вопросы, связанные с усовершенствованием *рабочих характеристик карданных передач на игольчатых подшипниках, и вопросы расчёта несущей способности силового контакта подшипников качения и технологии получения качественных материалов. Для проведения испытаний использовался стенд для испытаний карданных передач, конструкция которого позволяет испытывать карданные передачи, исключая перегрев системы торможения за счет охлаждения рабочей жидкости, а также улучшить условия эксплуатации за счет обеспечения плавности регулирования тормозного момента. Для измерения шероховатости поверхностей использовался USB профилограф-профилометр БВ-7669М. Для измерения твердости поверхностей шипов крестовины карданного шарнира был использован твердомер HBRV-187,5. Методика проведения испытаний включает в себя следующие этапы: маркировка крестовин карданных шарниров; замер шероховатости, твердости, геометрии крестовин карданных шарниров; стадия испытаний; повторные замеры шероховатости, твердости, геометрии крестовин карданных шарниров; Разрезка исследуемых карданных шарниров и изготовление микрошлифов для металлографических исследований активной и пассивной поверхностей шипов крестовин карданных шарниров; обработка результатов исследований. Приведенная методика планирования экспериментов предназначена для получения экспериментальных данных исследований карданных передач на разных стадиях эксплуатации, которые позволят оценить влияния погрешностей изготовления на рабочие характеристики карданных шарниров и обосновать причины образования поверхностных и глубинных трещин.*

Ключевые слова: усталостные разрушения, игольчатые подшипники, современные представления исследований, испытательный стенд, планирование эксперимента, испытания шарниров.

Introduction. At the present stage of development of science and technology the problem of improvement of quality and competitiveness of universal joints needle bearings of different technological and hoisting-and-transport machines is essential for scientific and technical progress. But still many questions did not receive definite answer [1–15].

Now many researches are conducted and many methods of calculation of parts contact strength, durability and reliability are developed, but they do not offer accurate concepts and explanations of work of identical parts under absolutely identical conditions with different values of durability.

The analysis of the current state of science of wear lets know that without understanding of the process of wear creation of effective methods of fight against this phenomenon is impossible. The analysis of works [16–26] showed that hypothesis or the point of view were not always based on pilot experiments.

Due to the development of the reactive equipment, atomic-power engineering and creation of unique products and engineering designs in the different industries of mechanical engineering, the problem of low-cyclic durability of elements of designs becomes urgent in the 1950s. Due to the different processes of destruction of needle bearings at low and high levels of maximum voltages of cycle, we distinguish two types of fatigue: low-cyclic and multi-cycle. The low-cyclic fatigue is fatigue of material at which the fatigue damage or destruction happens at elasto-plastic deformation. The multi-cycle fatigue is fatigue of material at which the fatigue damage or destruction happens generally at elastic deformation.

Fatigue strength is an ability not to collapse under the influence of alternating loads during preset time of loading. It is supposed that the level of influences is such that the plastic deformations arising at the same time in metal in the course of loading are so small that it is difficult to find them, i. e. generally in the course of loading metal undergoes only elastic deformations. In case of the higher level of influences when plastic deformations become noticeable, and durability is rather small, there is low-cyclic fatigue [27].

At low-cyclic wear joint action of normal and tangent loadings at friction leads to the fact that the maximum tangent voltage arises not on the surface, but under the contact spot at small depth where damages gather and cracks are formed. If the material is fragile, the crack arises on its surface. Low-cyclic wear is observed during plastic deformation of surfaces (without cutting) of softer material by ledges the harder one. In places of such deformation side piles that at the subsequent passes can separate in the form of products of wear too are quite often formed [28].

Main part. Bearing blocks are the most important structural elements of machines and make the main part of frictional units. Failures of machines often happen because of failures of bearing blocks that limit durability of machines. Even at rather high-quality production of parts of bearing blocks, for example, of needle rolling bearing, the characteristic of universal joint can be unsatisfactory, and there may happen a sudden failure. By the failure we do not necessarily mean destruction of the rubbing (working) surfaces, but exit of one of characteristics of bearing blocks out of the allowed limits.

Bearing blocks of agricultural machinery fail generally because of the abrasive wear connected with hit of dirt and dust. The most widespread criterion of failure of the bearing blocks of the general application working in cars, tractors, pumps, reducers, machines, lifting-and-conveying machines is endurance failure. At the same time other characteristics, such as rigidity, level and range of vibration, antitorque moment, durability, etc. also are important for bearing blocks of special application.

The durability of separate parts of bearing blocks confirmed with bench tests does not guarantee sufficient durability of all node. The latter circumstance is connected with the fact that the loadings operating in node and actual temperature can significantly differ from the bench ones. Besides, assembly and mounting change gaps, tightness and form of working surfaces of bearing blocks. The contradiction between quality of bearing blocks and the bearing itself, which is shown in nodes with rolling bearings, is especially distinct [29–32].

At production of bearing blocks features of their work are often not considered. So, for example, universal joints needle bearings in parameters of undulation and roughness of working surfaces of the bearing not always conform to requirements of working conditions. Ball bearings for spindle of the machine have small limiting rapidity, which is caused by the considerable heat release from sliding friction and rolling friction leading to thermal expansion of internal ring and balls and thermal jamming (inadmissible increase of antitorque moment of shaft). The solution demands constructive changes in the bearing, namely decrease in heat release and increase in rapidity. It can be made by production of the bearing with large number of smaller balls. Such bearings developed by V. F. Grigoriev showed rather high rapidity. It is clear that at system approach to design of bearing blocks it is possible to provide required heat release and, as a result, required extreme rapidity of the bearing at design stage in advance.

Researches of plastic deformation of steel surfaces at static contact loading are given in R. G. Shtribek, S. V. Pinegin, A. Palmgren, D. Teybor's works. It was found out that at pure rolling of two cylinders under loading exceeding a certain level their surfaces are displaced rather central part in the direction of rotation as a result of plastic shifts in subsurface layer. U. Hamilton in the work showed that plastic shifts amass with quantity of cycles of loading. In K. Johnson's work it is shown that plastic deformation happens until Hertz tension does not become less than four limits of flowability at simple shift [11; 16; 26].

In the generalizing work by D. V. Orlov and S. V. Pinegina plastic deformation of the steel tempered parts at static loading, the pulsing contact and rolling under loading is investigated. Dependences of sizes of residual plastic deformation of surfaces on the level of tension, sizes and hardness are received. Calculations of tension taking into account plastic formings are carried out. The questions connected with justification of form of sample for carrying out material tests on contact fatigue are studied insufficiently.

The classical mechanics of contact interactions is connected, first of all, with the name of Heinrich Hertz. In 1882 he solved the problem about contact of two elastic bodies with the bent surfaces. This classical result is the cornerstone of mechanics of contact interaction also nowadays. Only a century later K. Johnson and other authors found the similar solution for adhesive contact (JKR – the theory).

Bases of the theory of contact voltages and deformations are developed by H. Hertz, N. M. Belyaev, A. N. Dinnik [11] and gained further development in a number of works of domestic and foreign scientists. Because of complexity of decisions of contact tasks the following assumptions were made: materials of bodies are homogeneous and isotropic; deformation happens in elastic limits and none of bodies receives plastic deformation; tangent loadings are absent in the zone of contact; both surfaces are absolutely smooth; the site of contact is small in comparison with the characteristic sizes of the compressed bodies; the hydrodynamic film between surfaces is absent. But at this stage of development only small part of assumptions takes place during the work of real parts, including contact task of H. Hertz which is the basis of engineering calculations of contact voltages and deformations.

Further progress of mechanics of contact interaction in the middle of the 20th century is connected with F. F. Bowden and D. Teybor. They were the first to show the importance of accounting of surface roughness of the contacted bodies. The roughness leads to the fact that the valid area of contact between the rubbing bodies is much less than seeming area of contact. These conceptions significantly changed the direction of many tribological researches. F. F. Bowden and D. Teybor's works caused emergence of number of theories of mechanics of contact interaction of rough surfaces.

The main works in the field of contact interaction are those of D. Arkhard who came to conclusion that at contact of elastic rough surfaces the area of contact is approximately proportional to normal force. The further important contribution to the theory of contact of rough surfaces was made by D. A. Grinvud and G. P. Villiamson. The main result of these works is the proof that the valid area of contact of rough surfaces in crude approximation is proportional to the normal force while characteristics of separate microcontact (pressure, the amount of micro-contact) poorly depend on loading [31; 32].

The main role belongs to the bearing blocks working in the conditions of rolling under loading and its influence on operability of the hinge. However, despite the numerous researches worked in this direction new topical issues appear continually. The process of violation of kinematics of the bearing and its influence on operability of universal joints in general is not investigated fully. It is connected with damage of bodies and paths of rolling, influence and distribution of resistance to rolling on the areas of the rolling contact. Influence of thermal wear equally promotes change and destruction of paths of rolling and is the first-priority question demanding detailed consideration.

In actual practice during the work of needle bearings slipping of balls happens extremely seldom. Lubricant and other factors determine the size of external tangent loadings [16].

In I. Ya. Shtayerman's work number of space flat tasks was considered. Galin solved problems with friction and coupling of surfaces on contact taking into account the speed of deformation, anisotropy of material, variable on elasticity module depth, and also dynamic character of the phenomena on moving contact. N. I. Glagolev executed the solution of flat contact task taking into account friction forces and received the distribution law of normal and tangent loads with different distribution of sites of coupling and sliding on contact piece for the free and loaded with the moment wheel. The attempt is made to theoretically estimate wear of wheel and rail for case of plane-strain cylinders on empirical formulas of wear.

M. M. Saverin conducted an in-depth study of joint action of normal and tangent loads on tension at contact compression of the cylinder with the plane. In B. I. Kovalsky and M. M. Saverin's works tension at joint action of normal and tangent loads is deeply investigated [11].

Aspects of durability and hypothesis of destruction of materials at contact and cyclic loadings were described by A. Griffitson [4; 21] who explained discrepancy in durability of perfect and real brittle bodies with availability of defects like cracks. E. Orovan, G. I. Taylor and A. D. Polyani developed the theory of dislocations and suggested to connect decrease in durability and plasticity of solid bodies with availability of dislocations [21].

T. Ekobori offered a way of determination of durability and causes of destruction of solid body in which macrostress concentration from defects like dislocation pile-up is considered simultaneously [21]. At repeated and variable loading cracks arise in the most plastically deformed microvolumes of material, borders of grains detain plastic deformation, the fatigue crack develops on body of grain and does not extend on borders of grains, when crossing borders of grains it extends with the slowed-down speed, the cyclic load causes in grains of structure of metal of strip of loosening [22].

The concentrators of tension which are sources of development of contact and fatigue microcracks can be of two types. The first include localized defects such as scratches, grinding scratches, dents, areas of altered microstructure in the form of burns. To the second, we classify local discontinuities in the continuity and homogeneity of the metal in the form of nonmetallic inclusions, inclusions of carbides, pores, shells and other metallurgical defects. Influence of different concentrators of tension on contact fatigue is considered in works [5–8; 22–24]. When rolling under load, depending on the location of the stress concentrators that are most strongly influenced in specific conditions, the primary crack can occur on the surface of the part or under it. In this case, the surface crack will lead to the exfoliation of the metal particle and the resulting pit will be a new stress concentrator, which will cause the emergence of new microcracks, which lead to the separation of metal particles and the increase in the area of the crumpled site. This process is called pitting [16].

In case of development of fatigue crack from subsurface defect, it can be connected to the next microcracks. The trajectory and speed of its development depend on orientation of the microcracks lying close, and also on mechanical properties of the neighboring sites of metal. At the same time under surface several microcracks can develop. With cyclic loading, the crack that is in the most favorable conditions for its growth reaches the surface of the part and then the metal is chipping. And chipping depth from surface stress concentrators is several times greater than from surface defects [24].

In case of the so-called “the pulsing contact” primary fatigue cracks appear on surface of contour of spot of contact and extend deep into material. Extensive experimenttal data about arrangement of the possible centers of destruction at contact cyclic loading is given in work [24].

In P. Tardi and Ya. Stiklovari’s works consider that all microcracks in bearings made of steel ShH15 develop from nonmetallic inclusions in area of coverage of Hertz maximum tangent voltages [7]. N. N. Kachanov [25], also leaning on experimental material, believes that fatigue cracks can arise not only at depth of action of the maximum tangent voltages, but also slightly higher or below it. N. N. Kachanov bases these reasons that emergence of the plastic shifts leading to fatigue cracks depends not only on the theoretical level of tangent tension, but also on the strength of the stress concentrators, the main ones being nonmetallic inclusions.

The idea of structure of solid bodies is revealed in the theory of dislocations [3; 18; 19]. Properties of metals and alloys are connected with emergence, movement and interaction of dislocations. At the heart of all ideas of durability and plasticity of metal materials data on their dislocation structure lie. Availability of dislocations explains sharp distinction between durability of real and reference metal. The dislocation structure in volume of real crystalline solid is implemented on the surface of body in the form of thin system of steps, hollows and ledges.

External mechanical influences define conditions for development of these or those leading processes in surface layers of metal of needle bearings. Under the influence of current changes serviceable condition of surface layer when material has the phase composition, structure and properties other than initial state forms. In the surface layer, that is in working order, there are processes the opportunities of which development depend on initial state of surface layer and operating conditions of needle bearings.

Depending on the nature of the processes happening during frictional unit operating time after the termination of its work in surface layer there are following residual changes: mechanical hardening or loss of strength; phase hardening or loss of strength without change or with change of chemical composition; change of microrelief of friction surfaces of needle bearings and tension of surface layer.

In modern representation the structure of surface layers of metal materials is multilayer [20]. After impact of shock impulse on the surface of material the central area of the place of blow will reflect acts of microjet current of material after passing of wave of deformation. After repeated impact of shock impulses, this zone will look like the hardened liquid with chaotic structure. Interaction of the central shock deformed area with the next objects of material can happen at the expense of rotational mechanisms to possible analogy to processes of current of viscous liquid in the oppressed layer. But at the same time, interaction of the central flow with laminar underlayer can be followed by emergence of whirlwinds. The vortex layer in metals can consist of several couples of vortex cords with counter rotation of cords in each couple. From outside rotational formations will kind of slide on laminar underlayer, representing structure with not equiaxial cells. Band and checkerboard structures are also rotational. The checkerboard structure has static deformation about 50–60 % and is represented by set of rectangular formations of different orientation. The band structure consists of rotational bands arranged in series and capable of moving deep into the material under the action of the stress field. Rotational structures are capable of changing one another according to the mechanism of kinetic phase transformations [20].

To date, these structures can be attributed to any mechanical action, including surface friction, but the finest outer layer will be so-called secondary structure, i. e.

strongly deformed and containing oxygen, sulfur and other elements.

At present, a lot of research has been done in this direction, but the issue of the mechanism of fatigue destruction is at the initial stage of development, which is confirmed by the search for the criterion of fatigue failure and the proposal of new solutions.

The quantitative assessment of contact fatigue is expressed in the number of loading cycles or in hours of operation before the occurrence of fatigue failure of surfaces. Cyclically changing contact stresses cause the formation of cracks and separation of material particles, surface destruction in the form of pits of chipping (pitting), cracks, peeling flaking [16].

The question is acute on the problem of modeling the processes of low cycle fatigue of needle bearings. A large number of phenomena accompanying this process are known, which can not be placed within the framework of any of the proposed theories. These include heat-activated accumulation of damages, wearing in of surfaces during friction, cyclicity of wear, kinetic phase transitions of defect structures, physico-chemical and structural modification of the material of the surface layer, etc.

As in the operation of needle bearing huge pressure on the actual spots of contact develops, formation of particles of wear at fatigue wear of needle bearings happens only after a set of cycles of contact interaction, causing periodic embrittlement and dispersion of surface layers. Each contact in surface layer causes irreversible changes of some diagnostic variable which identification is a necessary step in search of objective criterion of wear resistance of materials.

Studying of needle bearing destruction as the process developing during finite time and depending on loading speed is of great importance. In this case the criteria of classical fracture mechanics based on the theory of continuous environments cannot authentically reflect essence of real physical processes. With extremely high speeds of deformation, flashes of high local temperatures, concentration of high pressures there is not only smooth "shift" of phase point of condition of material in phase space, but also change of the leading mechanism of damageability. Therefore it is important to consider not only accumulation of damages, but also the mechanism which is responsible for specific way of destruction of bonds [33].

Particular interest in the mechanics of needle bearing failure with low-cycle fatigue is a time factor. It involves a wide range of tasks for forecasting the durability of structural materials and managing the life of products. It was noted in [34] that "the establishment of regularities in the evolution of the system requires the introduction of the time factor into the equation of the mechanical state". A lot of work has been devoted to the study of the relationship of time to strength parameters, but most of them are related to the study of the long-term strength of materials in creep, which is due to the applied importance of this problem. Since the rate of time flow in the system depends on the degree of influence of the deflecting factors [33; 34], the question of the zero value of the parameter arises. Is it possible to estimate the zero value of the system time in the same way as for temperature, pressure, entropy or other parameters. With what physical phenomenon the point of reference of time is connected at the analysis of durability of materials. An analysis of this problem shows that the time factor of modern science has not yet been sufficiently studied. The traditional perception of the longevity of the system as a time from the beginning of its loading to the moment of destruction is not physically justified.

Wear of universal joints depends on the physical and chemical and mechanical processes proceeding in contact. The kinematics of the movement of interfaces (sliding, roll, roll with sliding, roll under loading, etc.), structure and composition of surface and near-surface layers of materials, condition of lubricant layer, formation of surface connections, geometrical characteristics of contacting surfaces and their change in time has great influence on the process [16].

Due to the different processes of destruction of needle bearings at low and high levels of maximum voltages of cycle, we will consider questions of low-cyclic fatigue and formation of fatigue cracks in materials of needle bearings of universal joints, occurring at elasto-plastic deformation. It is supposed that the level of influences is such that the plastic deformations arising at the same time in metal in the course of loading are so small that it is difficult to find them, i. e. generally metal in the course of loading undergoes only elastic deformations. In case of the higher level of influences when plastic deformations become noticeable, and durability is rather small, there is low-cyclic fatigue. At low-cyclic wear joint action of normal and tangent loadings at friction leads to the fact that the maximum tangent voltage arises not on surface, and under contact spot at small depth where damages gather and cracks are formed [16; 28].

The endurance failure of surface layer occurs in the needle bearings which are exposed to long loading by variable efforts. Fatigue cracks arise on friction surfaces and extend deep into layer. Being gradually extended, small cracks form grid on certain limited or big sites of surface. Disclosure of cracks happens under the influence of the pulsating pressure of lubricant.

Crack, having reached the basis of antifrictional layer, changes the direction, extending on joint between the basis and layer, afterwards certain sites of surface layer chip. Chipping of large pieces of surface layer is followed by formation of surface "wounds" which are hammered with the wear products operating as abrasive. Flawing increases wear of friction surfaces, sharp edges make the cutting action, and near edges there is chipping of surface of material.

Cyclically changing contact voltages cause the surface destructions in the form of chipping poles called pitting. Formed abscesses ranging in size from a few hundredths of a millimeter to several millimeters increase during the operation of the friction unit, and surface peeling occurs.

In his works, I. V. Kragelsky developed an equation for frictional fatigue and developed a frictional fatigue model that takes into account processes at the level of influence of surface roughness, with relative sliding of rubbing bodies, a disruption occurs as a result of repeated deformation of the abraded material by the rigid micro-irregularities of the counterbody [16].

The process of accumulation of damages in sliding of bodies in a rolling condition under load has a certain staging. At first there is accumulation of elastic lattice distortions and increases density of dislocations. After achievement of critical density of dislocations there are submicroscopic cracks. Together with irreversible distortions of crystal lattice interatomic bonds are broken and separate microvolumes collapse [16; 28; 34].

By Ya. G. Panovko [16] researches it is established that in couples of friction at operation there are forced harmonic oscillations with frequencies up to 100 kHz and above. Sizes of vibratory frequencies are defined by the speed of relative movement and degree of roughness of contacting surfaces. Amplitudes of oscillation depend on physicomechanical properties of the contacting couples in conditions of loading. Forced oscillations are the cause of the appearance and development of fatigue cracks, resulting in destruction. Particular interest in the mechanics of needle bearing failure with low-cycle fatigue is a time factor. It involves a wide range of tasks for forecasting the durability of structural materials and managing the life of products.

Problem definition of research. The carried-out analysis showed that the problem of low-cyclic fatigue of needle bearings is studied insufficiently. All this detains development of the specified methods of calculation of parts that in turn affects rates of improvement of machine components designs, and, therefore, the over-all performance decreases at the expense of untimely exit of the equipment out of operation.

The question of the mechanism of physical aspect of metal fatigue and endurance failure of balls under the influence of temperature and fatigue wear is studied not completely and demands more careful studying as well as research of interrelation of primary endurance failures with dislocation of cyclically repeating or alternating tensions in material of parts.

Among other things, it is necessary to consider the influence of mechanical and thermal methods of surface hardening of parts on their fatigue contact strength with a complex alternation of stresses throughout the entire loading cycle during rolling under load.

Influence of radial, axial, angular fluctuations of balls of needle bearings is not studied sufficiently so far, as well as the issue of range of possible fluctuations of shaft of universal joints is not fully handled.

The problem of heat release and thermal conductivity is not fully addressed in the rolling of parts under load, and there is no system for predicting the temperature regimes of the operation of units and ways to reduce heat generation [1; 16; 17; 35–39].

For calculation of bearing capacity of modern designs and machine components, exposed in use to difficult complex of cyclically changing loadings, it is necessary to know stress and deformation fields in zones of the maximum strength, and also behavior of material during elasto-plastic cyclic deformation [40].

On the basis of this, the conditions for the emergence of limiting states are used – breaking strength, the appearance of unacceptable movement, etc. The most intensively developed direction when creating criteria for low-cycle strength under loading is the concept of equivalent parameters. According to this concept, choosing a corresponding equivalent parameter, a complex stress state leads to an equivalent linear stress state.

To assess the limiting state of materials in the theory of low-cycle fatigue, the criteria of four groups are used: deformation, force, energy and criteria based on the account of material damage. Deformational and energy criteria have become most widespread in the calculation practice [41].

In practice, equivalent parameters are widely used, which are a direct application of the criteria of plastic flow. A bright development of this approach was the work of M. Brown and K. Miller, who proposed two parameters for describing the low cycle fatigue: maximum shear deformation and normal deformation in the plane of maximum shear. At present, there is a significant number of modifications to this approach. Generalizing the work in this direction, apparently, is the work of A. Mackind and K. Neal in which a technique is proposed for constructing the function of destruction and a description on its basis of curves of equal durability. The authors have shown that all the criteria previously proposed in the framework of the equivalent approach are special cases of the destruction function [42].

Deformation criteria are based on the fact that under a rigid loading regime, the quasistatic fracture region is absent on the low-cycle fatigue curves, therefore the limiting state of the material can be estimated by the amplitude (swing) values of the total deformation, its elastic or plastic components. However, if for uniaxial or proportional deformation these criteria are sufficiently effective and simple, then for multiaxial low-cycle loading they do not always give acceptable results. In accordance with energy criteria, the limiting state in the material occurs when the total energy associated with its hardening reaches a critical value. In this regard, the energy approach to the assessment of fatigue damage and the destruction of metals is more general, because it uses as a measure of material damage the specific scattered energy or the specific work of plastic deformation per loading cycle. The latter circumstance is important when considering biaxial or multiaxial fatigue, when cyclic trajectories with the same range of deformations, but with different cycle shapes, correspond to different levels of durability. The practical use of energy criteria with respect to disproportional deformation causes specific requirements for the choice of a theory of plasticity for a more accurate prediction of the elastoplastic hysteresis loops, and it involves some difficulties in calculating the specific work of plastic deformation.

Attempts of overcoming shortcomings of deformation and power approaches led to development of the modified deformation criteria allowing considering both influence of amplitude of deformations, and the additional hardening that is strongly expressed at disproportionate deformations. The present work is devoted to the analysis of recently published experimental results on the behavior of various metallic materials under biaxial low-cycle fatigue and the development of approaches for creating an effective modified deformation criterion on their basis [41].

The problem of low-cyclic fatigue of elements of machines and designs which arose in connection with intensification of operation of products in the conditions of high thermomechanical loading at the quasistationary nature of repeated static power and temperature influences develops in relation to problems of assessment of endurance and durability on the basis of deformation interpretation of criteria of destruction [43].

Problem of low-cyclic fatigue of the bearing elements of designs and machine components with the broad range of temperatures and speeds of loading in relation to low-cyclic fatigue (without taking into account the temperature-time factor) and long cyclic durability (taking into account temperature and time factor), including two main directions: research of kinetics of stress fields and deformations in the zones of the maximum strength defining places of the accelerated accumulation of damages and destruction; studying of properties of materials by number of cycles and deformation time [44].

Proceeding from the aforesaid it is necessary:

1. Carrying out tests of universal joints at different stages of operation (breaking-in, normal operation, failure).

2. Errors of production impact assessment on performance data of universal joints.

3. Justification of the reasons of formation of face and deep cracks.

Description of the equipment. For laboratory tests the stand for tests of universal joints will be used, the design of the stand is presented in fig. 1, 2. The stand consists of the electric motor *1* which output end is connected to the technology transfer *2* connected to the tested universal joint *3*, mounted on the main frame *4*. The output shaft of universal joint *3* is connected to input shaft of the distributing reducer *5* mounted on additional frame *6*. The device of loading is hydraulic and represents hydraulic pump *7* which shaft is attached to output shaft of distributing reducer *5*. The input channel of hydraulic pump *7* is connected to hydraulic tank *8* with working fluid, and its output channel is attached to the input channel of throttle *9* regulating loading. Between the throttle and hydraulic pump the manometer *10* calibrated in terms of braking torque and the safety valve *11* for release of excessive pressure in hydraulic tank *8* are installed. The output channel of throttle is connected to hydraulic tank, via the heat exchanger *12*.

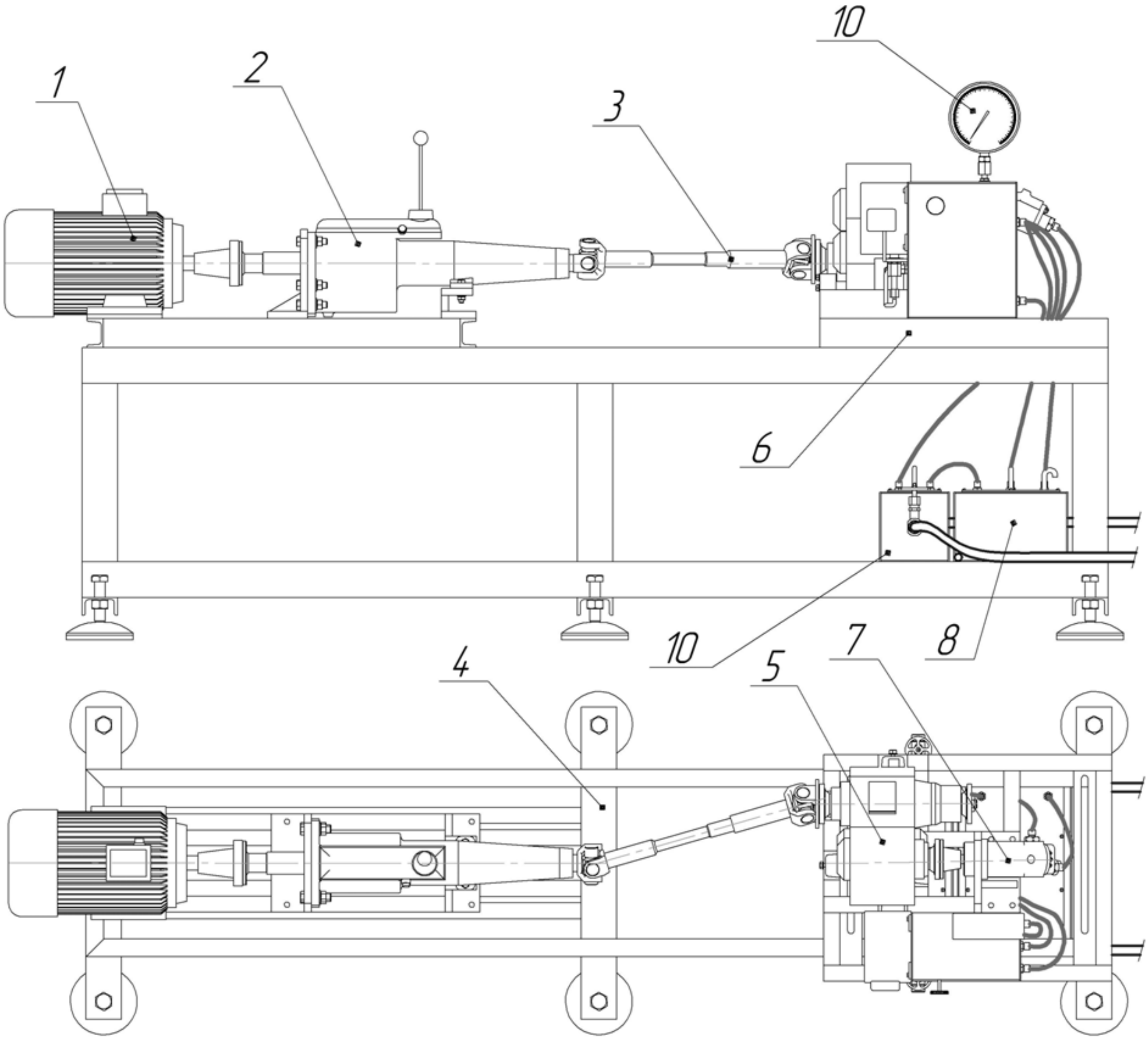

Fig. 1. The stand for research of universal joints

Рис. 1. Стенд для исследования карданных передач

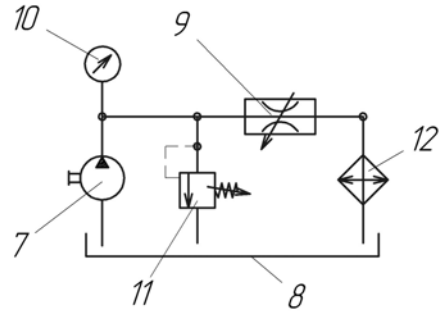

Fig. 2. The hydraulic scheme of the stand
for research of universal joints

Рис. 2. Гидравлическая схема стенда
для исследования карданных передач

The stand works as follows: the torque from the electric motor *1* is transferred to the tested universal joint *3* through technology transfer *2*, hydraulic pump *7* at the same time transfers to the tested universal joint the braking torque created and regulated by throttle *9*, value of braking torque is defined with the help of the manometer *10* calibrated in terms of braking torque. With an excess of operating pressure, the safety valve *11* is activated to prevent a jump in the set pressure of the hydraulic fluid in the hydraulic system that releases excess pressure into the hydraulic tank *8*. The heat exchanger *12* cools the working fluid.

The size of corner of break of universal joint is change by movement of the cross movable frame having the nonius by means of which the corner of break of universal joint for the corresponding length of universal joint is exposed.

The design of the offered stand allows to test universal joints, excepting overheat of system of braking due to cooling of working fluid, and also to improve operating conditions due to ensuring smoothness of regulation of braking torque. The stand offers simplicity of design and system of setup of braking torque by means of adjustable throttle and the manometer of pressure of working fluid calibrated in terms of braking torque [45–52].

For measurement of roughness of surfaces the USB BV-7669M Profilograph profilometer was used. The profilograph profilometer is intended for registration, the analysis of profile and measurement of parameters of roughness, outer and inner surfaces which section represents straight line to the planes of measurement. Before use calibration of the sensor, i. e. setup of sensitivity of measuring channel of the sensor by means of sample of the Ra parameter, adjusting with rated value, which is part of the profilometer was carried out.

For measurement of hardness of surfaces of thorns of crosspiece of universal joints the HBRV-187.5 hardness gage was used. The hardness gage is intended for determination of hardness by Rockwell, Brinell and Vikkers's methods. The hardness gage is widely used at the enterprises of mechanical engineering and metallurgy, laboratories of higher education institutions and research institutes for determination of hardness. The hardness gage consists of frame, the main lever mechanism, the mechanism of loading and unloading, the optical measuring screen, the mechanism of the choice of loading and the mechanism of raising of worktable. The frame is the closed body in which there are all mechanisms, except table, screw rod and part of the main rod. The hardness gage is the optical measuring instrument mainly by Rockwell's method. The device transforms depth of cup to units of hardness and directly displays on the projection screen which is on the front panel of the hardness gage. The surface of the studied sample should be equal, smooth and pure; there should not be traces, pollutants, stratifications, cracks, dredging, etc. on it. The bearing surface of the sample and worktable also should be pure for achievement of the best contact. The surface of the sample should be flat, the radius of curvature should not exceed 15 mm.

The technique of carrying out tests includes the following stages:

1. Marking of crosspieces of universal joints. The arrangement of crosspieces on shafts was recorded on lubricators, which serve to determine the leading and trailing spikes of the joint of the universal joint (fig. 3).

The account of numbers of thorns of crosspiece of universal joints begins with the hinge face where the lubricator is, and proceeds in ascending order clockwise.

2. Measurement of surface roughness, hardness and geometry. Surface roughness; geometrical sizes of universal joints; hardness of universal joints were measured before tests.

The roughness of surfaces was measured according to the scheme in fig. 4 on every thorn of crosspiece No. *1–4* from four points t. *1–4* in a straight line along thorn axis. Ra – arithmetic average deviation of profile and Sm – average step of roughnesses of profile of surface roughness were received as parameters of surface roughness values.

We measure the geometrical sizes of universal joints according to the scheme in fig. 5, these are diameters of thorns of crosspiece of d_i, length between end faces of thorns of crosspiece is of $l13$ and $l24$, diameters of glasses of needle bearings of D_i.

We measure the hardness of universal joints on each thorn of crosspiece (fig. 4) in current t. *1*.

3. Testing stage. According to researches [16] the stage of breaking-in comes to an end in the range from 1 to 5 hours of universal joints operation therefore we will use time intervals from 1 o'clock in each hour, i. e. to

carry out tests on the first universal joints – 1 hour, on the second – 2 hours, etc. After detection of changes (transition to stage of low-cyclic fatigue from stage extra earnings), we will investigate the received interval with more exact step.

4. Repeated measurements of roughness, hardness, geometry according to item 2.

5. Cutting of the studied universal joints and production of microsections for metallographic examinatons of active and passive surfaces of thorns of crosspieces of universal joints according to the scheme (fig. 6)

6. Processing of results of researches by method of the smallest squares, which based on minimization of the sum of squares of deviations of some functions from required variables and assessment of errors of measurements, creation of curve of fatigue (Veller's curve) (fig. 7).

The problem of preliminary experiment consists in check:

1. Operability of test stands [45–47] of author's development and possibility of carrying out tests of universal joints at different stages of operation [53–54] (breaking-in, normal operation, failure); assessment of impact of errors of production on performance data of universal joints for justification of the reasons of formation of face and deep cracks.

2. Sensitivity of systems and elements of the test stand [55].

3. Carrying out preliminary tests for verification of the plan of tests and investigation of significant levels and factors, the accuracy of levels and classes of the test stand, identification of error of measurements.

4. Dependences of the constructive modes and parameters of criterion function, such as torsional moment and braking which are not connected with long-run, resource tests, so-called kinematic sizes.

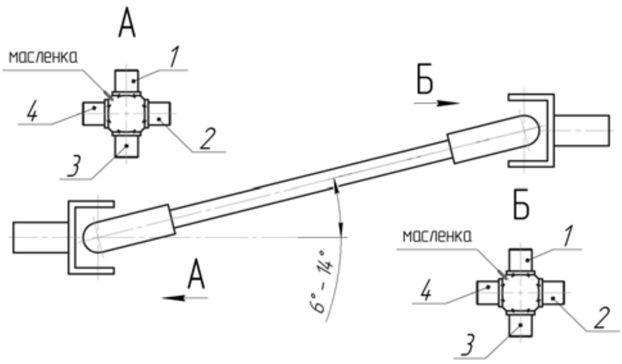

Fig. 3. The scheme of installation of the tested joints of the prop shaft

Рис. 3. Схема установки испытуемых шарниров карданного вала

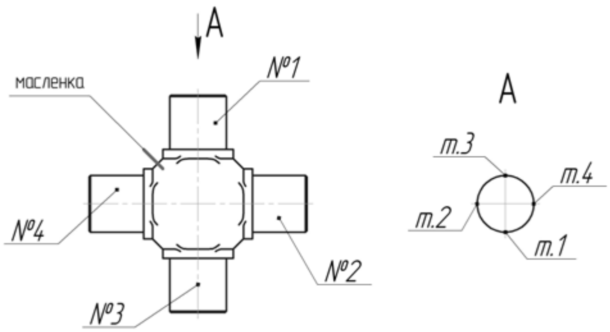

Fig. 4. Scheme for measuring roughness and hardness of surfaces

Рис. 4. Схема измерения шероховатости и твердости поверхностей

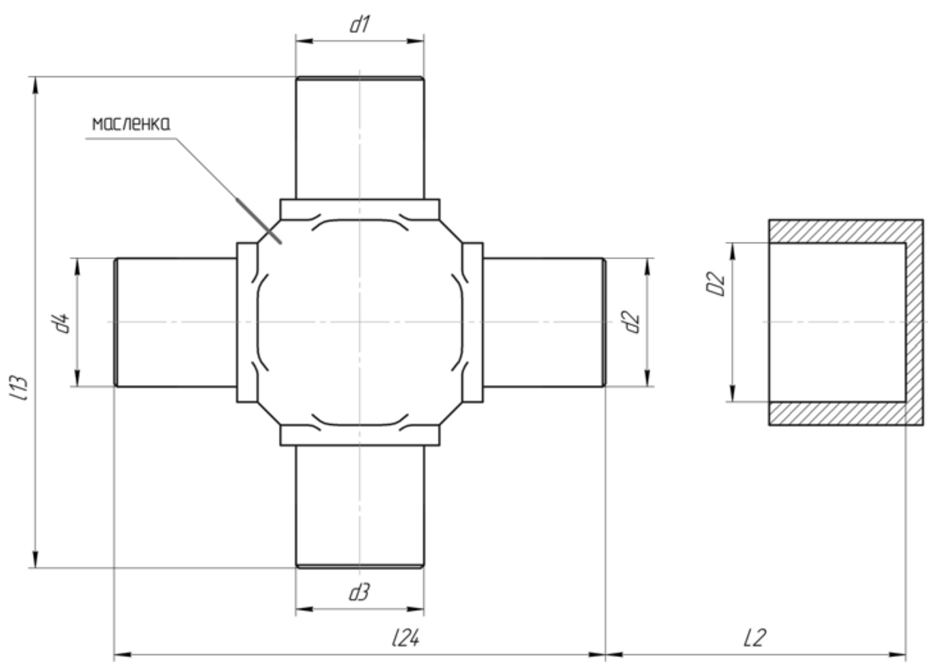

Fig. 5. Scheme of measurement of sizes of universal joints

Рис. 5. Схема измерения размеров карданных шарниров

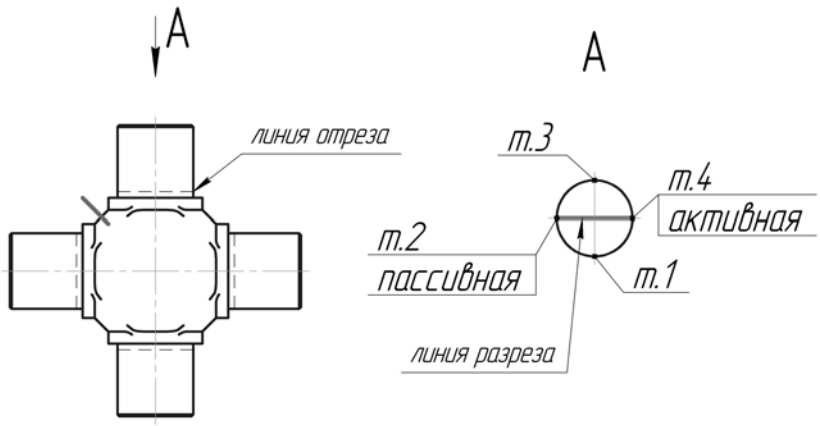

Fig. 6. Scheme of cutting of the studied universal joints for production of microsections

Рис. 6. Схема разрезки исследуемых карданных шарниров для изготовления микрошлифов

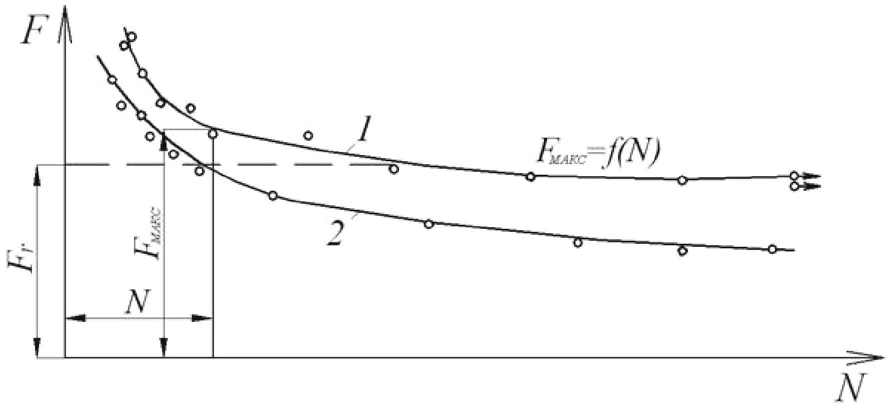

Fig. 7. Fatigue Curve (Veller's curve)

Рис. 7. Кривая усталости (кривая Веллера)

Table 1

Summary data table of hardness of universal joints

Number of the hinge	Hardness, HRC			
	1 thorn	2 thorn	3 thorn	4 thorn
1	56.5	54.5	54.5	56.0
2	58.5	58.5	58.5	58.5
3	53.5	53.5	53.5	53.5
4	55.0	56.0	56.5	56.0
5	59.0	59.0	58.5	59.0
6	60.5	60.5	63.5	61.5

For performance of preliminary experiment, measurements according to technique of carrying out tests were carried out, results of measurements are given in tab. 1–3.

Conclusion. In conclusion we will note that the most essential in all given work, is that the low-cyclic fatigue of needle bearing, process of forming of fatigue cracks in materials of needle bearings of universal joints at low-cyclic fatigue of needle bearings is topical issue and demands additional research in this direction. Many shortcomings of domestic machines, their low resource are connected with underestimation of dynamics during the calculating, design and operation. Physical processes at rolling friction of needle bearing are caused by patterns of interaction of solid bodies, at elastic and plastic deformation of microroughnesses of surfaces, heat transfer, adhesion and hydrodynamics of lubricant. The carried-out analysis showed that the problem of "low-cyclic" fatigue of needle bearings is studied insufficiently, and many shortcomings of domestic machines, their low resource are connected with underestimation of dynamics during the calculating, design and operation. Physical processes at rolling friction of needle bearing are caused by patterns of interaction of solid bodies, at elastic and plastic deformation of microroughnesses of surfaces, heat transfer, adhesion and hydrodynamics of lubricant.

Table 2

Summary table of measurements of roughness measurements on the surfaces of universal joints

Parameter	Thorn № 1				Thorn № 2				Thorn № 3				Thorn № 4			
	т. 1	т. 2	т. 3	т. 4	т. 1	т. 2	т. 3	т. 4	т. 1	т. 2	т. 3	т. 4	т. 1	т. 2	т. 3	т. 4
	Crosspiece 1															
Ra	0.735	0.767	0.621	0.759	0.669	0.745	0.708	0.715	0.614	0.644	0.589	0.623	0.673	0.642	0.595	0.621
Sm	0.085	0.078	0.065	0.075	0.078	0.081	0.078	0.077	0.071	0.071	0.069	0.067	0.071	0.067	0.070	0.066
	Crosspiece 2															
Ra	0.461	0.454	0.454	0.482	0.412	0.372	0.478	0.451	0.393	0.413	0.335	0.401	0.504	0.419	0.454	0.508
Sm	0.057	0.065	0.072	0.059	0.060	0.060	0.063	0.058	0.062	0.075	0.073	0.062	0.062	0.070	0.073	0.070
	Crosspiece 3															
Ra	0.375	0.472	0.397	0.420	0.381	0.423	0.447	0.409	0.384	0.634	0.421	0.394	0.326	0.323	0.390	0.404
Sm	0.058	0.062	0.071	0.063	0.068	0.061	0.060	0.068	0.065	0.053	0.072	0.062	0.056	0.062	0.061	0.061
	Crosspiece 4															
Ra	0.863	0.662	0.759	0.896	0.708	0.659	0.646	0.705	0.759	0.689	0.630	0.644	0.743	0.727	0.887	0.835
Sm	0.077	0.075	0.090	0.078	0.079	0.066	0.066	0.078	0.066	0.081	0.069	0.067	0.066	0.068	0.072	0.075
	Crosspiece 5															
Ra	0.381	0.571	0.599	0.450	0.406	0.410	0.498	0.500	0.458	0.726	0.451	0.451	0.382	0.394	0.484	0.538
Sm	0.067	0.081	0.073	0.081	0.073	0.070	0.067	0.078	0.073	0.074	0.060	0.070	0.071	0.070	0.076	0.090
	Crosspiece 6															
Ra	0.372	0.310	0.408	0.271	0.603	0.518	0.334	0.345	0.414	0.337	0.426	0.461	0.379	0.515	0.310	0.322
Sm	0.080	0.070	0.058	0.059	0.072	0.067	0.064	0.068	0.081	0.068	0.079	0.062	0.064	0.072	0.069	0.066

Table 3

Summary table of measurements of dimensions of universal joints

Diameter of the bearing, mm.				Diameter of the bearing, mm.				The size between end faces of thorns, mm.	
*d*1	*d*2	*d*3	*d*4	*D*1	*D*2	*D*3	*D*4	*l*13	*l*24
Crosspiece 1									
16.29	16.28	16.29	16.29	16.30	16.33	16.34	16.35	79.96	79.95
Crosspiece 2									
16.28	16.28	16.29	16.29	16.36	16.35	16.32	16.33	79.98	79.99
Crosspiece 3									
16.28	16.29	16.29	16.29	16.35	16.34	16.33	16.35	80.01	80.01
Crosspiece 4									
16.29	16.29	16.29	16.29	16.28	16.32	16.35	16.33	79.86	79.95
Crosspiece 5									
16.61	16.61	16.60	16.60	16.67	16.64	16.72	16.63	80.01	80.00
Crosspiece 6									
16.61	16.61	16.60	16.61	16.67	16.70	16.63	16.70	79.99	79.99

On the basis of the analysis [1–26] it was revealed that it is necessary to resolve the issues connected with improvement of performance data of needle bearings universal joints and questions of calculation of bearing capacity of power contact of rolling bearings and technology of receiving qualitative materials. The given technique of planning of experiments is intended for receiving experimental data of research of universal joints at different stages of operation which will allow to estimate influences of errors of production on performance data of universal joints, including author's developments [54–59] and to prove the reasons of formation of face and deep cracks.

As a result of carrying out preliminary experiment dependences of the constructive modes and parameters of criterion function, such as torsional moment and braking which are not connected with long-run, resource tests, so-called kinematic sizes will be received. Operability of test stands [45–47] of author's development and possibility of carrying out tests of universal joints at different stages of operation is checked (breaking-in, normal operation, failure); impact assessment of errors of production on performance data of universal joints for justification of the reasons of formation of face and deep cracks. Sensitivity of systems and elements of the test stand is checked. The plan of tests and technique of tests for determination of significant levels and factors, accuracy of levels and classes of the test stand, identification of error of measurements are checked.

References

1. Kukushkin E. V., Menovshchikov V. A. [Main directions of development, improve and perfect the performance driveline on needle bearings]. *Materialy XVI mezhdunarodnoy nauchnoy konferentsii "Reshetnevskie chteniya"* [Materials XVI Intern. Scientific. Conf "Reshetnev reading"]. Krasnoyarsk, 2012, P. 254–256 (In Russ.).

2. Kukushkin E. V., Menovshchikov V. A., Eresko T. T. [The analysis of modern concepts and approaches in the study of fatigue failures of needle bearings]. *Materialy XVII mezhdunarodnoy nauchnoy konferentsii "Reshetnevskie chteniya"* [Materials XVII Intern. Scientific. Conf "Reshetnev reading"]. Krasnoyarsk, 2013, P. 287–288 (In Russ.).

3. Kotrell A. H. *Teoria dislokacii* [Dislocation theory]. Moscow, Mir Publ., 1969, 95 p.

4. Ekobori T. *Phizika i mekhanika razrushenia i prochnosti tverdikh tel* [Physics and fracture mechanics and strength of solids]. Moscow, Metallurgy Publ., 1971, 264 p.

5. Litma Uidner. [Dissemination of contact fatigue from sources of surface and subsurface origin]. *Teoreticheskie osnovy inzhenernykh raschetov*. 1966, No. 3, P. 94 (In Russ.).

6. Spector A. G., Zelbet B. M., Kiselev S. A. *Struktura i svoistva podshipnikovikh stalei* [The structure and properties of the bearing steel]. Moscow, Metallurgy Publ., 1980, 263 p.

7. Tardy P., Stiklovari Y. [Effect of vacuum treatment on the resistance bearing steel]. *Stal'*. 1977, No. 5, P. 452–455 (In Russ.).

8. Finkel V. M. *Phizicheskie osnovi tormojenia razrushenia* [Physical fundamentals of braking failure]. Moscow, Metallurgy Publ., 1977, 360 p.

9. Kukushkin E. V., Menovshchikov V. A. [Low Cycle Fatigue needle bearing]. *Materialy IX Vserossiyskoy nauchno-prakticheskoy konferentsii "Aktual'nye problemy aviatsii i kosmonavtiki"* [Materials IX Intern. Scientific. Conf "Current issues of aviation and cosmonautics"]. Krasnoyarsk, 2013, P. 154–155 (In Russ.).

10. Eresko T. T., Kukushkin E. V., Menovshchikov V. A. [Current status of the issue on the study of plastic deformation under static loading, the contact needle roller bearings]. *Materialy X Vserossiyskoy s mezhdunarodnym uchastiem nauchno-tekhnicheskoy konferentsii "Mekhaniki XXI veku"* [Materials X Russian international participation scientific conference "Mechanics of XXI century"]. Bratsk, Bratsk State University Publ., 2014, P. 37–40 (In Russ.).

11. Nesterov V. M. *Razrabotka metodov ocenki soprotivlenia kontaktnoi ustalosti kinstrukcionnikh materialoc. Dokt. Diss.* [Development of methods for evaluation of contact fatigue resistance of structural materials. Doct. Diss.]. Moscow, 1984, 238 p.

12. Kukushkin E. V., Menovshchikov V. A., Eresko T. T. [Questions of formation of fatigue cracks in materials needle bearing universal joints]. *Materialy X Vserossiyskoy nauchno-prakticheskoy konferentsii "Aktual'nye problemy aviatsii i kosmonavtiki"* [Materials X Intern. Scientific. Conf "Current issues of aviation and cosmonautics"]. Krasnoyarsk, 2014, P. 148–150 (In Russ.).

13. Gubanova A. V., Kukushkin E. V., Maslova O. E., Menovshchikov V. A. [Influence of mechanical and thermal methods of superficial work-hardening of details on their tireless pin durability of cardan hinges on needle-shaped bearing]. *Materialy XX mezhdunarodnoy nauchnoy konferentsii "Reshetnevskie chteniya"* [Materials X Intern. Scientific. Conf "Reshetnev reading"]. Krasnoyarsk, 2016, P. 403–405. (In Russ.).

14. Eresko A. S., Kukushkin E. V., Oseev D. S., Menovshchikov V. A., Pyataev D. A. [Effects of vibrations on working conditions of cardan joints]. *Materialy XX mezhdunarodnoy nauchnoy konferentsii "Reshetnevskie chteniya"* [Materials X Intern. Scientific. Conf "Reshetnev reading"]. Krasnoyarsk, 2016, P. 405–407 (In Russ.).

15. Eresko T. T., Zhabinskaya. A. N., Kukushkin E. V., Menovshchikov V. A. [Intercommunication of primary tireless destructions with distribution of cyclic repetitive or alternating tensions of cardan hinges]. *Materialy XX mezhdunarodnoy nauchnoy konferentsii "Reshetnevskie chteniya"* [Materials X Intern. Scientific. Conf "Reshetnev reading"]. Krasnoyarsk, 2016, P. 409–411 (In Russ.).

16. Menovshchikov V. A., Eresko S. P. *Issledovanie i sovershenstvovanie igolchatikh podshipnikov kardanikh peredach transportno-tekhnologicheskikh mashin* [Study and improvement of needle bearing universal joint transmission of transport and technological machines]. Krasnoyarsk, KrasGAU Publ., 2006, 283 p.

17. Pinegin S. V. *Kontaktnay prochnost i soprotivlenie kachaniu* [Contact resistance and rolling resistance]. Moscow, Mechanical Engineering Publ., 1969, 243 p.

18. Kostecki B. I. *Trenie, smazka i iznos v mashinakh* [Friction, lubrication and wear in machines]. Kiev, Engineering Publ., 1970, 396 p.

19. Kostecki B. I., Nosovskii I. G. *Iznosostoikost i antifrikcionnost detaley mashin* [Wear resistance and anti-friction machine parts]. Kiev, Engineering Publ., 1965, 208 p.

20. Vladimirov V. I. [Problems of physics and wear]. *FHOM*. 1974, No. 2, P. 23–30 (In Russ.).

21. Ekobori T. *Nauchnie osnovi prochnosti i razrushenia materialov* [Scientific bases of strength and fracture of materials]. Kiev, Naukova Dumka Publ., 1978, 351 p.

22. Troshchenko V. T. *Prochnost metallov pri peremennikh nagruzkakh* [The strength of metals under variable loads]. Kiev, Naukova Dumka Publ., 1978, 173 p.

23. Martin, Borghese, Eberhardt [Microstructural changes of bearing steel subjected to cyclic loading]. *Teoreticheskie osnovy inzhenernykh raschetov*. 1966, No. 3, P. 1–18.

24. Martin, Eberhardt [Determination of the possible destruction of the centers of the contact fatigue conditions rolling]. *Teoreticheskie osnovy inzhenernykh raschetov.* 1967, No. 4, P. 241–253.

25. Kachanov N. N. [The nature and the nature of the destruction of the working surfaces of the bearing parts]. *Trudy instituta (VNIPP).* 1963, No. 3 (35), P. 45–59 (In Russ.).

26. Pinegin S. V., Shevelev I. A., Gudchenko V. M., Sedov V. I., Blokhin Y. N. *Vliyanie vneshnikh faktorov na kontaktnuyu prochnost' pri kachenii* [The influence of external factors on the strength of the rolling contact]. Moscow, Nauka Publ., 1972, P. 19–46.

27. Troshchenko V. T. *Ustalost i neuprugost metallov* [Fatigue and inelasticity metals]. Kiev, Naukova Dumka Publ., 1971, 267 p.

28. Berkovich I. I., Gromakovskiĭ D. G. [Tribology. Physical fundamentals, mechanics and engineering applications]. Samara, Samara. state. tehn. Univ Publ., 2000, 268 p.

29. Johnson K. L. Contact mechanics. Cambridge University Press, 6. Nachdruck der 1. Auflage, 2001.

30. Popov V. L. Kontaktmechanik und Reibung. Ein Lehr- und Anwendungsbuch von der Nanotribologie bis zur numerischen Simulation, Springer-Verlag, 2009, 328 p.

31. Popov V. L. Contact Mechanics and Friction. Physical Principles and Applications, Springer-Verlag, 2010, 362 p.

32. Hyun S., Robbins M. O. Elastic contact between rough surfaces: Effect of roughness at large and small wavelengths. *Trobology International.* 2007, Vol. 40, P. 1413–1422.

33. Ibatullin I. D. *Kinetika ustalostnoy povrejdaemosti i razrushenia poverkhnostnikh sloev*. [Kinetics of fatigue of damage and destruction of the surface layers]. Samara, Samara. state. tehn. University Press Publ., 2008, 387 p.

34. Regel V. R., Sloutsker A. I. [Structural and dynamic heterogeneity – the basis fizikiraz rusheniya solids]. *Sorosovskiy obrazovatel'nyy zhurnal.* 2004, Vol. 8, No. 1, P. 86–92.

35. Prigogine I., Kondepudi D. *Sovremennay termodinamika. Ot teplovikh dvigatelei do dissipativnikh struktur.* [Modern thermodynamics. From Heat Engines to Dissipative Structures]. Moscow, Mir Publ., 2002, 461 p.

36. Lokshina N. G. *Razvitie konstrukcii igolchatikh podshipnikov i ikh primenenie* [Development of designs of needle roller bearings and their application]. Moscow, NIINavtoprom Publ., 1967, 57 p.

37. Johnson K. L. Contact mechanics. Cambridge University Press, Cambridge, 1987, 452 p.

38. Ivanova V. S. *Sovremennoe predstavlenie o prirode ustalostnogo razrushenia i novie napravlenia issledovanii. Ustalost metallov i splavov* [Modern ideas about the nature of fatigue failure, and new areas of research. Fatigue of metals and alloys.]. Moscow, Nauka Publ., 1971.

39. Ivanova V. S., Terentiev V. F. *Priroda ustalosti metallov*. [Nature metal fatigue]. Moscow, Metallurgy Publ., 1975, 455 p.

40. Savyk A. Ya., Ivanov P. A., Kukushkin E. V., Novoselova V. O. Space-rocket machines low-cycle fatigue problems review. Materials 15 International Scientific Conference "Youth. Society. Modern science, technologies & innovations". 2016, P. 32–34.

41. Borodii M. B. [Analysis of experimental data at low-cycle fatigue deformation]. *Problemy prochnosti.* 2000, No. 1, P. 13–21 (In Russ.).

42. Yu Hai Shen. *Malociklovay ustalost materialov pri mnogoosnom deformirovanii. Diss. Kand. Tehn. Nauk* [Low-cycle fatigue of materials under multiaxial deformation. Diss. Cand. Tehn. Sci.]. Kiev, 17 p.

43. Gusenkov A. P., Kotov P. I. *Malociklovay ustalost pri neizometricheskom nagrujenii*. [under non-isothermal low cycle fatigue loading]. Moscow, Mashinostroenie Publ., 1983, P. 232–238.

44. Makhutov N. A, Gadenin M. M., Gokhfel'd D. A. *Uravnenia sostoaniy pri malociklovom nagrujenii* [Equations of state under low-cycle loading]. Moscow, Nauka Publ., 1981, 244 p.

45. Eresko S. P., Eresko T. T., Kukushkin E. V., Menovshchikov V. A. *Stend dlya ispytaniya kardannykh sharnirov* [The test stand driveline]. Patent RF, no. 153924, 2015.

46. Kukushkin E. V., Menovshchikov V. A., Eresko S. P., Eresko T. T. *Stend dlya ispytaniya kardannykh peredach* [The test stand driveline]. Patent RF, no. 149002, 2014.

47. Eresko S. P., Eresko A. S., Eresko T. T., Eresko V. S., Kukushkin E. V., Menovshchikov V. A., Struchkov A. V., Khomenko I. I. *Stend dlya ispytaniya kardannykh peredach* [The test stand driveline]. Patent RF, no. 162876, 2016.

48. Kukushkin E. V., Eresko S. P., Eresko T. T., Menovshchikov V. A., Orlov A. A. [Stand construction for testing the universal joint on needle bearings in wide range of sizes with the angle changing driveline]. *Transport. Transportnye sooruzheniya. Ekologiya*. 2016, No. 2, P. 58–73. Doi: 10.15593/24111678/2016.02.05 (In Russ.).

49. Kukushkin E. V., Menovshchikov V. A., Eresko T. T. [Booth design for testing universal joints with needle bearings]. *Materialy XIX mezhdunarodnoy nauchnoy konferentsii "Reshetnevskie chteniya"* [Materials XV Intern. Scientific. Conf "Reshetnev reading"]. Krasnoyarsk, 2015, P. 337–339 (In Russ.).

50. Eresko A. S., Eresko S. P., Eresko T. T., Kukushkin E. V., Menovshchikov V. A., Orlov A. A. [Calculation of the hydraulic system of brake device

of stand for the test of transmissions of transport-technological machines]. *Transport. Transportnye sooruzheniya. Ekologiya*. 2016, No. 4, P. 60–79. Doi: 10.15593/24111678/2016.04.06 (In Russ.).

51. Eresko S. P., Eresko T. T., Kukushkin E. V., Menovshikov V. A., Khomenko I. I. [Planning of experiment on research of cardan transmissions on the needle-shaped bearing]. *Materialy XII Mezhdunarodnoy nauchno-prakticheskoy konferentsii "Aktual'nye problemy aviatsii i kosmonavtiki"* [Materials XII Intern. Scientific. Conf "Current issues of aviation and cosmonautics"]. Krasnoyarsk, 2016, P. 368–370 (In Russ.).

52. Eresko S. P., Eresko T. T., Kukushkin E. V., Menovshchikov V. A., Khomenko I. I. [Planning of experiment on research of cardan transmissions on the needle-shaped bearing]. *Vestnik SibGAU*. 2016, No. 17, No. 4, P. 1062–1071 (In Russ.).

53. Kukushkin E. V., Menovshchikov V. A., Eresko S. P., Eresko T. T. *Kardannyy sharnir* [Joint]. Patent RF, no. 141878, 2014.

54. Kukushkin E. V., Menovshchikov V. A., Orlov A. A., Eresko S. P., Eresko T. T. *Kardannyy sharnir* [Joint]. Patent RF, no. 146989, 2014.

55. Gadisov R. A., Eresko A. S., Kukushkin E. V. [Automation of measuring of data-outs of elements of hydraulic drive]. *Materialy XII Mezhdunarodnoy nauchno-prakticheskoy konferentsii "Aktual'nye problemy aviatsii i kosmonavtiki"* [Materials XII Intern. Scientific. Conf "Current issues of aviation and cosmonautics"]. Krasnoyarsk, 2016, P. 355–357 (In Russ.).

56. Eresko S. P., Eresko T. T., Kukushkin E. V., Menovshchikov V. A. [Comparative analysis of structures universal joints unequal angular velocity]. *Vestnik SibGAU*. 2015, No. 16, P. 720–728 (In Russ.).

57. Eresko T. T., Kukushkin E. V., Menovshchikov V. A. [The design of the universal joint with replaceable spikes spider]. *Materialy XVIII mezhdunarodnoy nauchnoy konferentsii "Reshetnevskie chteniya"* [Materials XV Intern. Scientific. Conf "Reshetnev reading"]. Krasnoyarsk, 2014, P. 298–300 (In Russ.).

58. Kukushkin E. V., Menovshchikov V. A., Eresko T. T. [New universal joint design]. *Materialy XI Vserossiyskoy nauchno-prakticheskoy konferentsii "Aktual'nye problemy aviatsii i kosmonavtiki"* [Materials XI Intern. Scientific. Conf "Current issues of aviation and cosmonautics"]. Krasnoyarsk, 2015, P. 211–213 (In Russ.).

59. Kukushkin E. V., Eresko T. T., Mednikov D. M. New construction of universal joints. Materials 14-th International Scientific Conference "Youth. Society. Modern science, technologies & innovations". 2015, P. 232–234.

Библиографические ссылки

1. Кукушкин Е. В., Меновщиков В. А. Основные направления развития, улучшения и совершенствования рабочих характеристик карданных передач на игольчатых подшипниках // Решетневские чтения : материалы XVI Междунар. науч. конф. / Сиб. гос. аэрокосмич. ун-т. Красноярск, 2012. С. 254–256.

2. Кукушкин Е. В., Меновщиков В. А., Ереско Т. Т. Анализ современных представлений и подходов при исследовании усталостных разрушений игольчатых подшипников // Решетневские чтения: материалы XVII Междунар. науч. конф. / Сиб. гос. аэрокосмич. ун-т. Красноярск, 2013. С. 287–288.

3. Котрелл А. Х. Теория дислокаций. М. : Мир, 1969. 95 с.

4. Екобори Т. Физика и механика разрушения и прочности твердых тел. М. : Металлургия, 1971. 264 с.

5. Литман Уиднер. Распространение контактной усталости от источников поверхностного и подповерхностного происхождения // Теоретические основы инженерных расчётов. 1966. № 3. С. 94

6. Спектор А. Г., Зельбет Б. М., Киселева С. А. Структура и свойства подшипниковых сталей. М. : Металлургия, 1980. 263 с.

7. Тарди П., Стикловари Я. Влияние вакуумной обработки на стойкость подшипниковой стали // Сталь. 1977. № 5. С. 452–455.

8. Финкель В. М. Физические основы торможения разрушения. М. : Металлургия, 1977. 360 с.

9. Кукушкин Е. В., Меновщиков В. А. Малоцикловая усталость игольчатого подшипника // Актуальные проблемы авиации и космонавтики : материалы IX Всерос. науч.-практ. конф. / Сиб. гос. аэрокосмич. ун-т. Красноярск, 2013. С. 154–155.

10. Ереско Т. Т., Кукушкин Е. В., Меновщиков В. А. Современное состояние вопроса по исследованию пластического деформирования при статическом контактном нагружении игольчатых подшипников // Механики XXI веку : материалы X Всерос. науч.-техн. конф. Братск : БрГУ, 2014. С. 37–40.

11. Нестеров В. М. Разработка методов оценки сопротивления контактной усталости конструкционных материалов. М, 1984. 238 с.

12. Кукушкин Е. В., Меновщиков В. А., Ереско Т. Т. Вопросы формирования усталостных трещин в материалах игольчатых подшипников карданных шарниров // Актуальные проблемы авиации и космонавтики : материалы X Всерос. науч.-практ. конф. / Сиб. гос. аэрокосмич. ун-т. Красноярск, 2014. С. 148–150.

13. Влияние механических и термических способов поверхностного упрочнения деталей на их усталостную контактную прочность карданных шарниров на игольчатых подшипниках / А. В. Губанова [и др.] // Решетневские чтения : материалы XX Междунар. науч. конф. / Сиб. гос. аэрокосмич. ун-т. Красноярск, 2016. С. 403–405.

14. Влияние вибрации на условия работы карданных шарниров / А. С. Ереско [и др.] // Решетневские чтения : материалы XX Междунар. науч. конф. / Сиб. гос. аэрокосмич. ун-т. Красноярск, 2016. С. 405–407.

15. Взаимосвязь первичных усталостных разрушений с дислокацией циклически повторяющихся или чередующихся напряжений карданных шарниров / Т. Т. Ереско [и др.] // Решетневские чтения : материалы XX Междунар. науч. конф. / Сиб. гос. аэрокосмич. ун-т. Красноярск, 2016. С. 409–411.

16. Меновщиков В. А., Ереско С. П. Исследование и совершенствование игольчатых подшипников карданных передач транспортно-технологических машин. Красноярск : Изд-во КрасГАУ, 2006. 283 с.

17. Пинегин С. В. Контактная прочность и сопротивление качению. М. : Машиностроение, 1969. 243 с.

18. Костецкий Б. И. Трение, смазка и износ в машинах. Киев : Техника, 1970. 396 с.

19. Костецкий Б. И., Носовский И. Г. Износостойкость и антифрикционность деталей машин. Киев : Техника, 1965. 208 с.

20. Владимиров В. И. Проблемы физики и изнашивания // ФХОМ. 1974. № 2. С. 23–30.

21. Екобори Т. Научные основы прочности и разрушения материалов. Киев : Наукова думка, 1978. 351 с.

22. Трощенко В. Т. Прочность металлов при переменных нагрузках. Киев : Наукова думка, 1978. 173 с.

23. Мартин, Боргезе, Эберхардт. Микроструктурные изменения в подшипниковой стали, подвергаемой циклическому нагружению // Теоретические основы инженерных расчётов. 1966. № 3. С. 1–18.

24. Мартин, Эберхардт. Определение возможных центров разрушения в условиях контактной усталости при качении // Теоретические основы инженерных расчётов. 1967. № 4. С. 241–253.

25. Качанов Н. Н. О характере и природе разрушения рабочих поверхностей деталей подшипников // Труды института (ВНИПП). 1963. № 3 (35). С. 45–59.

26. Влияние внешних факторов на контактную прочность при качении / С. В. Пинегин [и др.]. М. : Наука, 1972. С. 19–46.

27. Трощенко В. Т. Усталость и неупругость металлов. Киев : Наукова думка, 1971. 267 с.

28. Беркович И. И., Громаковский Д. Г. Трибология. Физические основы, механика и технические приложения : учебник для вузов. Самара : Самар. гос. техн. ун-т, 2000. 268 с.

29. Johnson K. L. Contact mechanics / Cambridge University Press, 6. Nachdruck der 1. 2001.

30. Popov V. L. Kontaktmechanik und Reibung. Ein Lehr- und Anwendungsbuch von der Nanotribologie bis zur numerischen Simulation. Springer-Verlag, 2009. 328 p.

31. Popov V. L. Contact Mechanics and Friction. Physical Principles and Applications. Springer-Verlag, 2010. 362 p.

32. Hyun S., Robbins M. O. Elastic contact between rough surfaces: Effect of roughness at large and small wavelengths // Trobology International. 2007. Vol. 40. P. 1413–1422.

33. Ибатуллин И. Д. Кинетика усталостной повреждаемости и разрушения поверхностных слоев. Самара : Самар. гос. техн. ун-т, 2008. 387 с.

34. Регель В. Р., Слуцкер А. И. Структурно-динамическая гетерогенность – основа физики разрушения твердых тел // Соросовский образовательный журнал. 2004. Т. 8, № 1. С. 86–92.

35. Пригожин И., Кондепуди Д. Современная термодинамика. От тепловых двигателей до диссипативных структур. М. : Мир, 2002. 461 с.

36. Локшина Н. Г. Развитие конструкций игольчатых подшипников и их применение. М. : НИИНавтопром, 1967. 57 с.

37. Johnson K. L. Contact mechanics / Cambridge University Press. Cambridge, 1987. 452 p.

38. Иванова В. С. Современные представления о природе усталостного разрушения и новые направления исследований // Усталость металлов и сплавов. М. : Наука, 1971.

39. Иванова В. С., Терентьев В. Ф. Природа усталости металлов. М. : Металлургия, 1975. 455 с.

40. Space-rocket machines low-cycle fatigue problems review / A. Ya. Savyk [et al.] / A. Ya. Savyk [et al.] // Youth. Society. Modern science, technologies & innovations : Materials 15 Intern. Scientific Conf. Materials 15 Intern. Scientific Conf. 2016. P. 32–34.

41. Бородий М. В. Анализ экспериментальных данных малоцикловой усталости при непропорциональном деформировании // Проблемы прочности. 2000. № 1. С. 13–21.

42. Юй Хай Шень. Малоцикловая усталость материалов при многоосном деформировании : автореф. ... дис. канд. техн. наук. Киев : Изд-во Политехн. ин-та. 17 с.

43. Гусенков А. П., Котов П. И. Малоцикловая усталость при неизотермическом нагружении. М. : Машиностроение, 1983. С. 232–238.

44. Махутов Н. А., Гаденин М. М., Гохфельд Д. А. Уравнения состояния при малоцикловом нагружении. М. : Наука, 1981. 244 с.

45. Пат. 153924 Российская Федерация, МПК^7 G 01 M 13/02 (2006.01). Стенд для испытаний карданных шарниров / Ереско С. П., Ереско Т. Т., Кукушкин Е. В., Меновщиков В. А. № 2014147821/28 ; Заяв. 26.11.2014 ; опубл. 10.08.2015, Бюл. № 22. 2 с.

46. Пат. 149002 Российская Федерация, МПК^7 G 01 M 13/02 (2006.01). Стенд для испытаний карданных передач / Кукушкин Е. В., Меновщиков В. А., Ереско С. П., Ереско Т. Т. № 2014120845 ; заяв. 22.05.2014 ; опубл. 20.12.2014, Бюл. № 35. 1 с.

47. Пат. 162876 Российская Федерация, МПК^7 G 01 M 13/02 (2006.01). Стенд для испытаний карданных передач / Ереско С. П., Ереско А. С., Ереско Т. Т., Ереско В. С., Кукушкин Е. В., Стручков А. В., Хоменко И. И. № 2015157365 ; заяв. 30.12.2015 ; опубл. 27.06.2016, Бюл. № 18. 2 с.

48. Конструкция стенда для проведения испытаний карданных шарниров на игольчатых подшипниках в широком диапазоне размеров с изменением угла излома карданной передачи / Е. В. Кукушкин [и др.] // Транспорт. Транспортные сооружения. Экология. 2016. № 2. С. 58–73. DOI: 10.15593/24111678/2016.02.05.

49. Кукушкин Е. В., Меновщиков В. А., Ереско Т. Т. Конструкция стенда для проведения испытаний карданных шарниров на игольчатых подшипниках // Решетневские чтения : материалы XIX Междунар. науч. конф. ; Сиб. гос. аэрокосмич. ун-т. Красноярск, 2015. С. 337–339.

50. Расчет гидравлической системы тормозного устройства стенда для испытания трансмиссий транспортно-технологических машин / А. С. Ереско [и др.] // Транспорт. Транспортные сооружения. Экология. 2016. № 4. С. 60–79. DOI: 10.15593/24111678/2016.04.06.

51. Планирование эксперимента по исследованию карданных передач на игольчатых подшипниках / С. П. Ереско [и др.] // Актуальные проблемы авиации и космонавтики : материалы XII Междун. науч.-практ. конф. / Сиб. гос. аэрокосмич. ун-т. Красноярск, 2016. С. 368–370.

52. Планирование эксперимента по исследованию карданных передач на игольчатых подшипниках / С. П. Ереско [и др.] // Вестник СибГАУ. 2016. Т. 17, № 4. С. 1062–1071.

53. Пат. 141878 Российская Федерация, МПК^7 F 16 D 3/26. Карданный шарнир / Кукушкин Е. В., Меновщиков В. А., Ереско С. П., Ереско Т. Т. № 2014102339/11 ; заявл. 24.01.2014 ; опубл. 20.06.2014, Бюл. № 17. 2 с.

54. Пат. 146989 Российская Федерация, МПК^7 F 16 D 3/26. Карданный шарнир / Кукушкин Е. В., Меновщиков В. А., Орлов А. А., Ереско С. П., Ереско Т. Т.; № 2014119234/11 ; заявл. 13.05.2001 ; опубл. 27.10.2014, Бюл. № 30. 2 с.

55. Гадисов Р. Э., Ереско А. С., Кукушкин Е. В. Автоматизация измерений выходных параметров элементов гидропривода // Актуальные проблемы авиации и космонавтики: материалы XII Междунар. науч.-практ. конф. / Сиб. гос. аэрокосмич. ун-т. Красноярск, 2016. С. 355–357.

56. Сравнительный анализ конструкций карданных шарниров неравных угловых скоростей / С. П. Ереско [и др.] // Вестник СибГАУ. 2015. Т. 16, № 3. С. 720–728.

57. Ереско Т. Т., Кукушкин Е. В., Меновщиков В. А. Конструкция карданного шарнира со сменными шипами крестовины // Решетневские чтения : материалы XVI Междунар. науч. конф. / Сиб. гос. аэрокосмич. ун-т. Красноярск, 2014. С. 298–300.

58. Кукушкин Е. В., Меновщиков В. А., Ереско Т. Т. Новая конструкция карданного шарнира // Актуальные проблемы авиации и космонавтики : материалы XI Всерос. науч.-практ. конф. / Сиб. гос. аэрокосмич. ун-т. Красноярск, 2015. С. 211–213.

59. Kukushkin E. V., Eresko T. T., Mednikov D. M. New construction of universal joints // Youth. Society. Modern science, technologies & innovations : Materials 14 Intern. Scientific Conf., 2015. P. 232–234.

UDC 621.383

Siberian Journal of Science and Technology. 2018, Vol. 19, No. 1, P. 137–145

INFLUENCE OF THE In/Ga RELATION IN THE GAS PHASE ON THE CHARACTERISTICS OF THE $In_XGa_{1-X}P$ EPITAXIAL LAYERS OF CASCADE SOLAR CELLS

A. A. Naumova[1*], A. A. Lebedev[1, 2], B. V. Zhalnin[1], E. V. Slyshchenko[1, 2], N. T. Vagapova[1]

[1]JSC "Research-production enterprise "Kvant"
16, 3-rd Mytish chinskaya, Moscow, 129626, Russian Federation
[2]The National University of Science and Technology "MISiS"
4, Leninsky Av., Moscow, 119049, Russian Federation
[*]E-mail: otdel_17@npp.kvant.ru

The modern solar arrays for the most spacecrafts consists of solar cells which are formed by the thirty nano- and micro-dimensional epitaxial layers based on AIIIBV materials forming triple junction InGaP / InGaAs / Ge. This article presents the results of a study of experimental samples of thin single-crystal epitaxial $In_xGa_{1-x}P$ layers with different indium and gallium concentrations (x = 38 to 53 %) that were grown on Ge – substrate by MOCVD industrial equipment. The theme of present investigation is the influence of epitaxial growth parameters on the crystal structure characteristics.

The ratio of the components of the third group in the gas phase were calculated from the specified technological parameters. The rocking curves obtained by high-resolution two-crystal X-ray diffractometry were investigated. The lattice parameter and the ratio of indium to gallium in the solid phase were calculated. A high perfection of a single-crystal structure with an insignificant broadening of the X-ray diffraction peaks was observed in the range from 45 to 53 %. It is shown that the broadening of the diffraction peak of the structure can be the criterion of estimation of the quality of the grown structure in addition to the mismatch of diffraction maximum. Also the In / (In + Ga) ratio in the solid phase was calculated using the method of photoluminescence effect measuring. It was shown in comparison of data of x-ray diffraction with photoluminescence method the composition determination by photoluminescence method should be considered only as estimated.

Keywords: solar cell, solar battery, epitaxial layer, gas-phase epitaxy, photoelectric converter, X-ray diffractometry, photoluminescence, AIIIBV, semiconductor structure.

Сибирский журнал науки и технологий. 2018. Т. 19, № 1. С. 137–145

ВЛИЯНИЕ СООТНОШЕНИЯ In / Ga В ГАЗОВОЙ ФАЗЕ НА ХАРАКТЕРИСТИКИ ЭПИТАКСИАЛЬНЫХ СЛОЕВ $In_XGa_{1-X}P$ КАСКАДНЫХ СОЛНЕЧНЫХ ЭЛЕМЕНТОВ

А. А. Наумова[1*], А. А. Лебедев[1, 2], Б. В. Жалнин[1], Е. В. Слыщенко[1, 2], Н. Т. Вагапова[1]

[1]АО «Научно-производственное предприятие «Квант»
Российская Федерация, 129626, г. Москва, ул. 3-я Мытищинская, 16
[2]Национальный исследовательский технологический университет «МИСиС»
Российская Федерация, 119049, г. Москва, Ленинский просп., 4
[*]E-mail: otdel_17@npp.kvant.ru

На сегодняшний день для энергообеспечения подавляющего большинства космических аппаратов используются солнечные батареи, состоящие из солнечных элементов, структура которых образована тремя десятками нано- и микроразмерных эпитаксиальных слоев на основе материалов AIIIBV, формирующих каскады InGaP / InGaAs / Ge. Приведены результаты исследования экспериментальных образцов тонких монокристаллических эпитаксиальных слоев типа $In_xGa_{1-x}P$ с различным содержанием индия и галлия (x = от 38 до 53 %), выращенных методом газофазной эпитаксии из металлоорганических и гидридных соединений в установке промышленного типа на германиевой подложке. Предметом исследования является влияние параметров эпитаксиального роста на характеристики кристаллической структуры.

Расчетным методом получено соотношение компонентов третьей группы в газовой фазе из заданных технологических параметров. Исследованы кривые качания, полученные с помощью высокоразрешающей двухкристальной рентгеновской дифрактометрии, рассчитан параметр решетки и соотношение индия и галлия в твердой фазе. В диапазоне от 45 до 53 % наблюдается высокое совершенство монокристаллической структуры с незначительным уширением дифракционных рентгеновских пиков. Показано, что критерием оценки качества выращенной структуры наряду с рассогласованием дифракционных максимумов может служить уширение дифракционного пика структуры. Также соотношение In / (In + Ga) в твердой фазе получено *посредством метода измерения эффекта фотолюминесценции. При сравнении данных, полученных с помощью рентгеновской дифрактометрии и метода измерения эффекта фотолюминесценции, показано, что определение состава с помощью метода измерения фотолюминесценции следует рассматривать только оценочно.*

Ключевые слова: солнечный элемент, солнечная батарея, эпитаксиальный слой, газофазная эпитаксия, фотоэлектрический преобразователь, рентгеновская дифрактометрия, фотолюминесцения, AIIIBV, полупроводниковая структура.

Introduction. Due to the increased requirements for onboard spacecraft systems, there is a need to create solar array (SA) with high performance and energy characteristics and increased service life (more than 15 years). The SA will convert sunlight directly into electricity with high efficiency, creating almost constant power at low operating costs [1]. The most promising elements for a modern SA for operating as a part of the spacecraft and satellites are cascade solar cells (SC) based on AIIIBV materials.

Modern triple-junction CS is a complex planar device. Generating semiconductor part of such a solar cell, produced by Metalorganic Chemical Vapour Deposition (MOCVD), consists of three dozen nano- and micro-sized functional layers forming triple junction InGaP / InGaAs / Ge. Due to the relatively large surface of the device – about 30 cm^2 [2; 3], in order to achieve high characteristics of the structure, it is particularly important to comply with the requirements for uniformity of properties of all layers of the structure. To create a multi-layer SC, using different materials, a large number of technological operations are necessary, each of which requires careful monitoring of the process parameters and properties of the product, since the deviation from the norm at each stage can affect the properties of the finished structure and the output characteristics of the SC [3]. Intermediate control of properties allows detecting defects at each stage (epitaxial growth of semiconductor structure, post-growth processes: photolithography, metallization, deposition of anti-reflection coating, the formation of overall dimensions, etc. [2]) and reject defective wafers. To identify the causes of possible defects, it is necessary to determine the dependences between the properties of the structure and the technological parameters of the process [3].

One of the main factors for improving the efficiency of SC is the perfection of growth of semiconductor layers, namely: matching the lattice parameters, the minimum concentration of defects in the crystal structure and achieving high homogeneity of the composition on the entire surface of the wafer. The mismatch of lattice parameters is of the first importance, as it is in itself a measure of deformation in the layer [4]. Therefore, for the development of special epitaxial layers with precise matching of the lattice parameter in the process of growth, it is essential to have full data about the ratio in the gas stream of the elements of the third group In / Ga of the periodic system of chemical elements for obtaining a target composition in the structure of the epitaxial layer $In_xGa_{1-x}P$ (the main material not only of modern triple junction solar cell, but other promising photovoltaic devices), i. e. it is necessary to study the dependence of the ratio of the composition in the gas and solid phase.

Experimental Details. For a detailed study of the epitaxial layer of $In_xGa_{1-x}P$ on the subject of the influence of the epitaxial growth parameters on the characteristics of the crystal structure model samples of simplified structure of more than 60 pieces with different content of indium and gallium (x = from 38 to 53 %) doped with silicon and tellurium, on the germanium substrate with a diameter of 100.0 ± 0.4 mm were manufactured. The samples were grown by the MOCVD method on the installation of an industrial type Veeco E450. Schematic images of the structures assigned are shown in fig. 1, as well as the technological parameters for each layer assigned in the calculations, were obtained applying the program for the analysis and comparison of recipes Veeco RCPAnalysis [5; 6].

Method of gas-phase epitaxy of metal-organic and hybrid compounds. The feature of MOCVD method lies in the fact that in the epitaxial reactor creates a high temperature area, which receives a gas mixture containing decomposable compounds [7]. In the reactor, the release and deposition of the substance on the substrate occurs, and gaseous reaction products are carried out by the flow of hydrogen carrier gas. For the preparation of compounds AIIIBV, as the source of III group element is used metal-organic compounds, for example, trimethylgallium (TMGa) and trimethylindium (TMIn) for the synthesis of InGaP. As a source of group V elements such gas as phosphine (PH_3) is used.

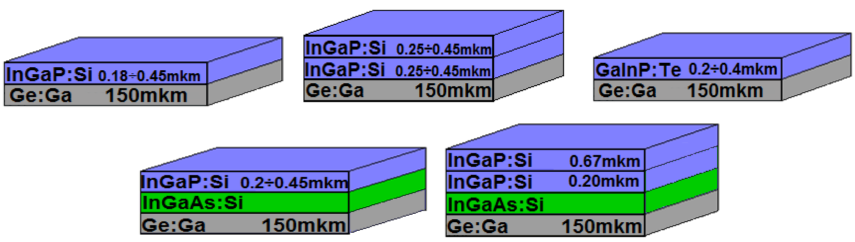

Fig. 1. Schematic representations of the structure of model samples (for epitaxial layers $In_xGa_{1-x}P$ values of thickness are indicated)

Рис. 1. Схематические изображения структуры модельных образцов (для эпитаксиальных слоев $In_xGa_{1-x}P$ указаны значения толщины)

Since the structure of the SC consists of many semiconductor layers, with different chemical composition and different levels of alloying and doping, before the process of creating the entire semiconductor structure in one cycle of epitaxial growth it is necessary to use the software installation epitaxial growth recipe.The recipe is a table in which the technological parameters for each metal-organic and hydride compound at each time of the epitaxial growth process are specified, as well as the temperature in different zones of the growth chamber, etc. [3; 8].

To obtain an epitaxial layer with specified properties, such as the crystal lattice parameter, the band gap width, it is necessary to control the chemical composition of the growing layers, determined by the composition of the gas mixture and the distribution of metal-organic compounds in the reactor.

The composition of the gas mixture is set by such technological parameters as the speed of flow of substances, the pressure in babbler and temperature [9; 10]. The schematic design of the bubbler for dosing liquid volatile alkyl TMGa and bubbler for TMIn into the reactor is shown in fig. 2.

Physico-chemical calculation of the ratio of elements of the third group In / Ga in the gas phase. In order to calculate the flow of the component in the gas phase for each metal-organic compound, it is necessary to use the following formula (1):

$$V^{\text{газ}}_{\text{TMGa,TMIn}} = \frac{S \cdot P_v}{(P_b - P_v) \cdot V}, \quad (1)$$

where S is the flow of substance through the bubbler, cm^3/min; P_b – pressure in the bubbler, Pa; P_v – the partial pressure of metal-organic compounds at a given temperature, Pa; V – the molar volume of ideal gas (under normal conditions), cm^3/mol.

The saturated steam pressure is determined by individual equations, depending on the temperature (T) according to the tabular data [11]. For TMGa according to the expression (2), and for TMIn according to the expression (3):

$$\log_{10} P_{v(\text{TMGa})} = 8.070 - \frac{1703}{T}, \quad (2)$$

$$\log_{10} P_{v(\text{TMIn})} = 10.52 - \frac{3014}{T}. \quad (3)$$

Thus, having considered the equations (1), (2), (3) it can be concluded that the velocity of the molar flow at the outlet of the bubbler can be controlled by changing the velocity of the hydrogen flow, the pressure in the bubbler and the bubbler temperature. The increase in pressure in the bubbler (P_b) reduces the velocity, temperature rise (equivalent to an increase in P_v), as well as the flow of hydrogen – increases the molar velocity. Thus, the given values are technological parameters that can be changed to achieve the required composition of the layer.

Despite the perfection of the MOCVD method in the technology of semiconductor production, the periodic inspection of key parameters of epitaxial structures is required [3], in addition, such a procedure is necessary for the synthesis of new layers. One of the main methods is a method of x-ray diffraction (XRD).

Methods of measurement using high-resolution two-crystal x-ray diffraction. To determine the lattice parameter of separate compounds on the XRD Vector measurements were carried out, which resulted in a rocking curve.

It should be noticed that, the maximum contribution to the intensity, gives the thickest layer of the structure, namely Ge substrate. The presence of broadening and any other stand-alone peaks indicates the presence of layers mismatched from the lattice parameters [12].

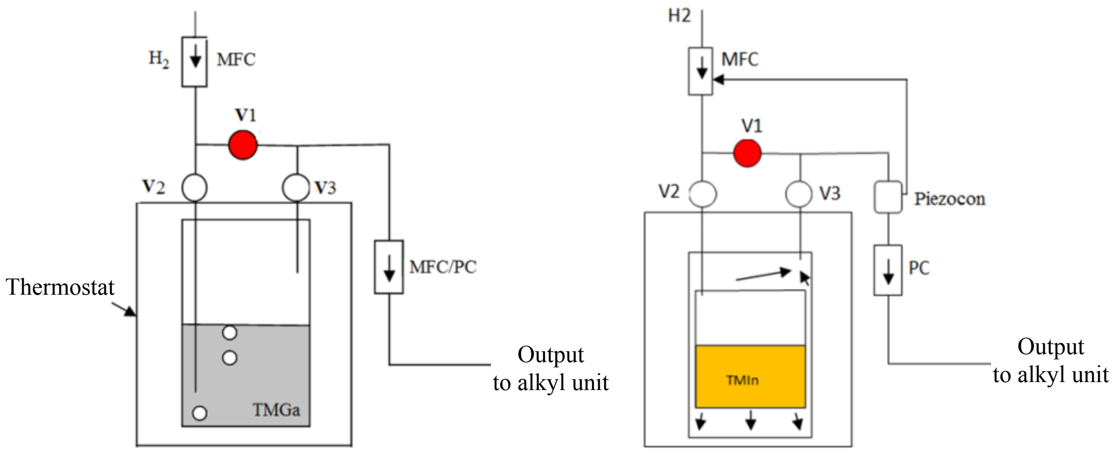

Fig. 2. Construction of bubbler: $V1$, $V2$, $V3$ – pneumatic valves; MFC – device for supplying a given flow of hydrogen; MFC/PC (PC) – pressure controller – device for maintaining the preset pressure in the bubbler; Piezocon – the device that determines the molar concentration of TMIn at the outlet of the bubbler

Рис. 2. Конструкция барботёров: $V1$, $V2$, $V3$ – пневматические клапаны; MFC – прибор подачи заданного потока водорода; MFC/PC (PC) – контроллер давления – прибор поддержания заданного давления в барботёре; Piezocon – прибор, определяющий мольную концентрацию TMIn на выходе из барботёра

A classic example of the rocking curve for the epitaxial layer of InGaP is shown in fig. 3. In structures with different number of misaligned layers, the rocking curves are characterized by the presence of one narrow peak with high intensity and spaced from it by a certain number of angular seconds of the peak with lower intensity. When the peak is located with lower intensity to the left of the main, there is an increase in the lattice parameter relative to the substrate, while the location to the right of the main one is a decrease:

$$a^2 = \frac{d^2}{n} \cdot (H^2 + K^2 + L^2), \tag{4}$$

where a is the lattice parameter, Å; d is the inter-plane distance between the reflecting planes, Å; n is an integer describing the diffraction order of the reflection; H, K, L – the indices of the interference;

$$a_{\mathrm{In}_x\mathrm{Ga}_{1-x}\mathrm{P}} = x \cdot a_{\mathrm{InP}} + (1-x) \cdot a_{\mathrm{GaP}}, \tag{5}$$

where x is the content of In in the solid solution.

The obtained experimental data are well placed on the line based on the table data on the Vegards rule, but there are some deviations near the table value of the Ge lattice parameter. Since in this case it is difficult to separate the peaks of the substrate and the epitaxial layer, there is an error in determining the distance between them. An example of such a rocking curve is shown in fig. 4, *a*.

For samples with a significant deviation of the lattice parameter, the rocking curves are characterized by a large value of the broadening of the peak is about 800 arcseconds (fig. 4, *c*). For the classical rocking curve of the faultless structure, the distance between the peaks of the order of 200–400 arcseconds and the broadening is less than 200 (fig. 4, *b*).

The XRD survey, the data processing of the rocking curves of experimental samples of epitaxial structures, as well as data for calculating the composition of solid solution from the gas phase composition, a diagram of dependence of the lattice parameter (the primary axis) and the broadening of the x-ray peak (secondary axis) the ratio of In / Ga in the epitaxial layer of $\mathrm{In}_x\mathrm{Ga}_{1-x}\mathrm{P}$ was made (fig. 5).

The lattice parameter increases with the increase in the percentage of indium in $\mathrm{In}_x\mathrm{Ga}_{1-x}\mathrm{P}$. Basically, all experimental data are well placed on the straight line, the misalignment of the lattice parameter is 0.1–0.26 %. In the range of 45 to 53 % monocrystalline structure is characterized by high perfection. When the ratio of In and Ga is 1:1 the epitaxial layer is characterized by the best properties with the most similar value of the lattice parameter in accordance with the Ge. The deviation from the composition for these samples ranges from 0.5 to 3 %.

Additionally, studies have been carried out to determine the homogeneity of the solid solution throughout the surface of the sample. Due to the center symmetry of the growth chamber, single rocking curves are measured along the sample radius. The comparison of measurement results shown in fig. 6 indicates a homogeneous growth of the epitaxial structure in composition according to table, which makes it reasonable to survey at the central point with multiple measurements and confirms the reliability of the data obtained.

Thus, according to the results of studies on the high-resolution two-crystal XRD it is possible to conclude about the state of samples of SC, the presence of misaligned layers, defects and the possibility of further work with the resulting epitaxial structures, as well as if necessary to make adjustments to the recipe for epitaxial growth.

Method for measuring the effect of photoluminescence. To determine the composition of the solid solution by using the method of measuring the effect of photoluminescence (PL) at 2000 RPM equipment. This method is easier to implement, the equipment allows to obtain the maps to analyze the uniformity of properties, but the method is indirect and it is necessary to take into account the contribution of other factors (alloying).

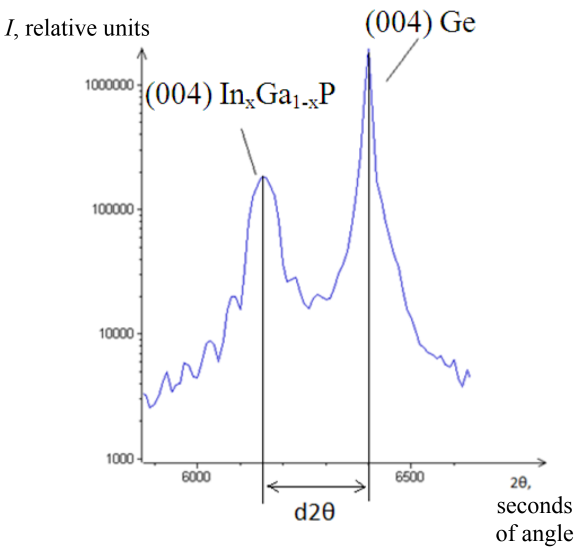

Fig. 3. Experimentally obtained classical rocking curve for an epitaxial layer InGaP

Рис. 3. Экспериментально полученная классическая кривая качания для эпитаксиального слоя InGaP

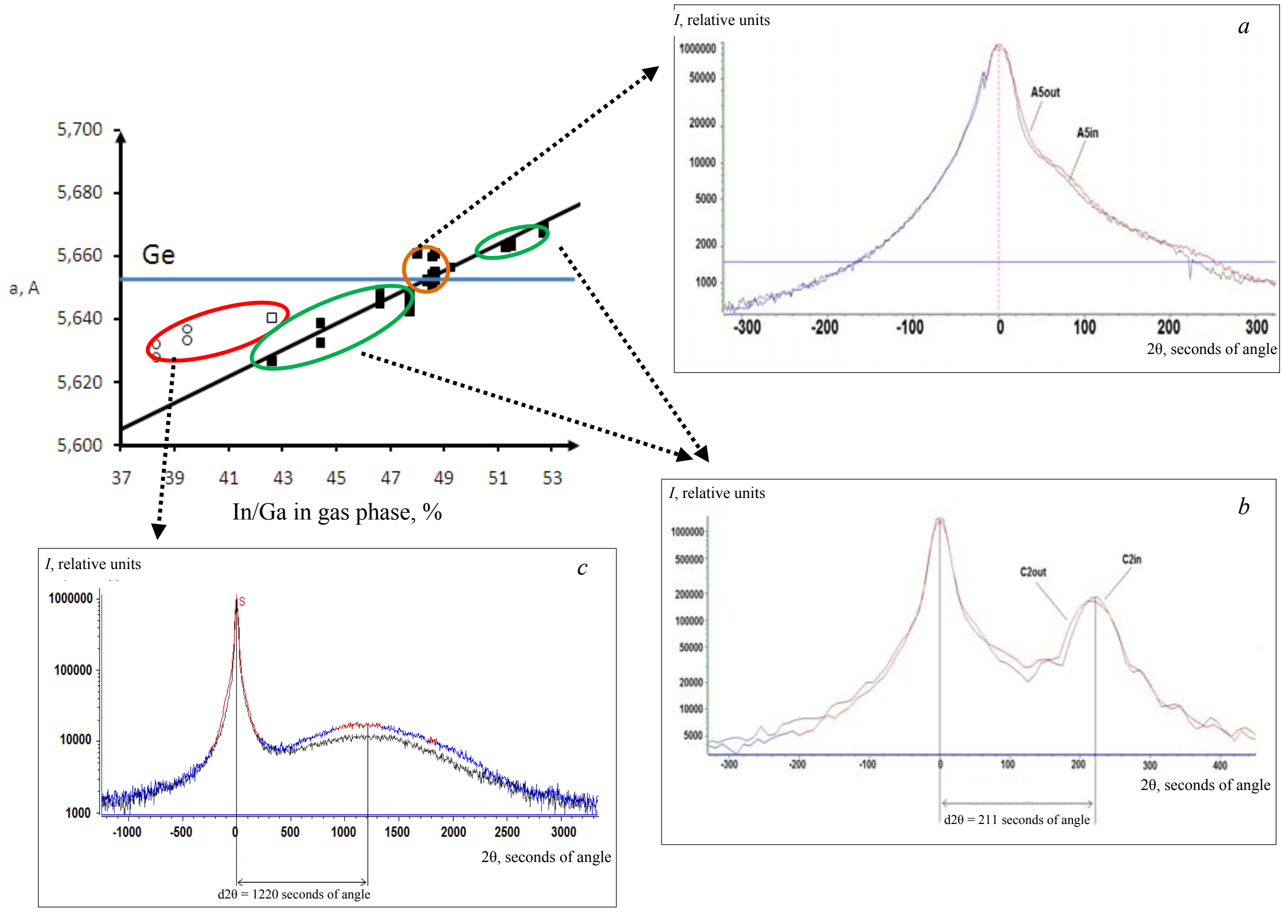

Fig. 4. Rocking curves for a different ratio In / Ga in the solid phase

Рис. 4. Кривые качания для различного соотношения In / Ga в твердой фазе

The results values calculation of the of the lattice parameter and the composition of the solid solution of epitaxial layer $In_xGa_{1-x}P$ for 5 points

№ survey point	*d*2θ, arcsecond	θ, °	*a*, Å	Δ*a*/*a*$_{Ge}$, %	Ga, %	In, %
1	290.4	33.03	5.6518	0.108	51.87	48.13
2	295.8	33.03	5.6517	0.110	51.90	48.10
3	300.3	33.04	5.6516	0.112	51.92	48.08
4	296.1	33.03	5.6517	0.111	51.90	48.10
5	282.3	33.03	5.6519	0.105	51.83	48.17

According to the data illustrated in fig. 7, we can judge about the uniformity in thickness and composition of the epitaxial structure at the stage of growth, because the PL signal depends on the width of the band gap of the material given by the chemical composition.

Spectral maps show the distribution of the integral intensity of PL, wavelength peak, intensity peak and full width at half maximum of the spectrum on the planar epitaxial structure [3; 10]. Spectral maps (fig. 7) stored in a format that allows determining the spectrum data at each point of the epitaxial structure. In particular, the data is processed by the elements of the technology support system [13; 14].

Using the results obtained, it is possible to determine the homogeneity of the studied layer and calculate the value of the band gap width using the formula (6):

$$E_g = \frac{h \cdot c}{\lambda}, \tag{6}$$

where E_g is photon energy, eV; λ is photon wavelength (characteristic wavelength of photoluminescence spectrum), nm; *h* – Planck's constant, eV/sec; *c* – is the speed of light, m/sec.

The obtained results show the uniform distribution of peak spectra of PL (electron-optical properties) over the entire surface of the sample, while the average deviation of the maximum spectra of PL is 2.8 %.

When comparing the data of the ratio of In / Ga in the solid phase measured by the two methods for samples dopped with Si and Te, it is seen that the composition data obtained by PL measurement should be considered as estimated. The results are presented in fig. 8.

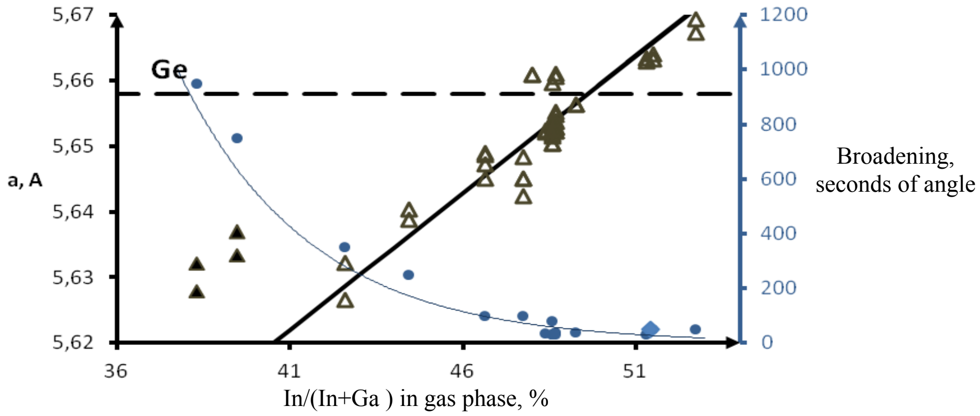

Fig. 5. The graph of the dependence of the lattice parameter and the broadening of the x-ray peak on the ratio In / Ga in the epitaxial layer $In_xGa_{1–x}P$: triangular points – the experimental data of the lattice parameter; points – the broadening of the diffraction peaks of some samples; the dotted line – the value of the lattice parameter Ge; direct line – data constructed according to Vegard's rule

Рис. 5. График зависимости параметра решетки и уширения рентгеновского пика от соотношения In / Ga в эпитаксиальном слое $In_xGa_{1–x}P$: треугольные точки – полученные экспериментальные данные параметра решетки; круглые точки – значения уширения дифракционных пиков некоторых образцов; пунктирная линия – значение параметра решетки Ge; прямая линия – данные, построенные по правилу Вегарда

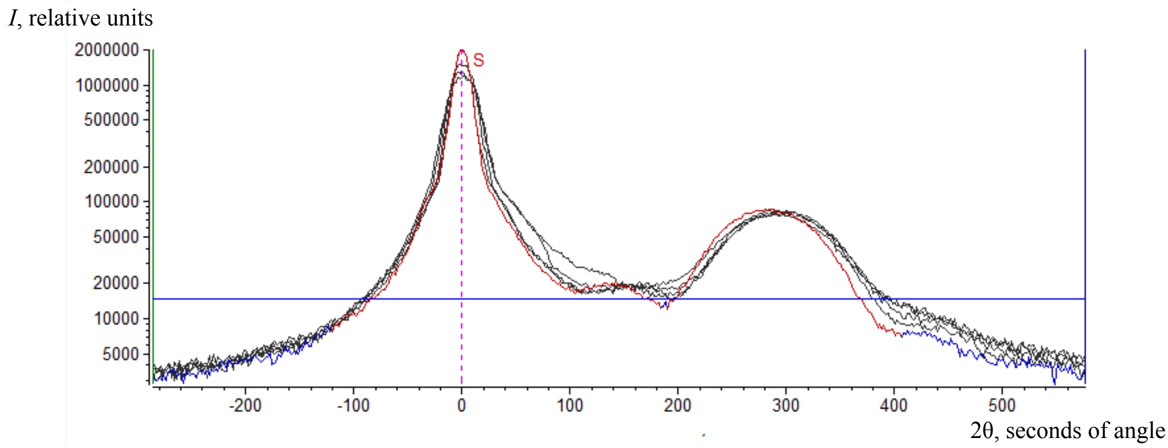

Fig. 6. A set of rocking curves obtained along the radius of the sample

Рис. 6. Набор кривых качания, полученных вдоль радиуса образца

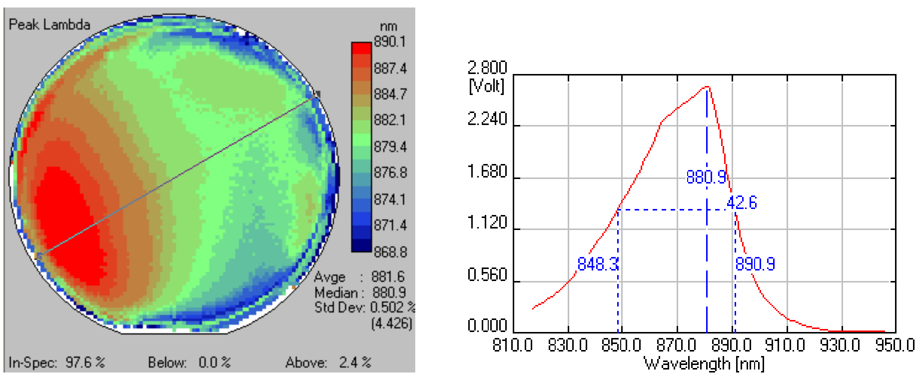

Fig. 7. Spectral map and single photoluminescence spectrum for one sample

Рис. 7. Спектральная карта и единичный спектр ФЛ для одного образца

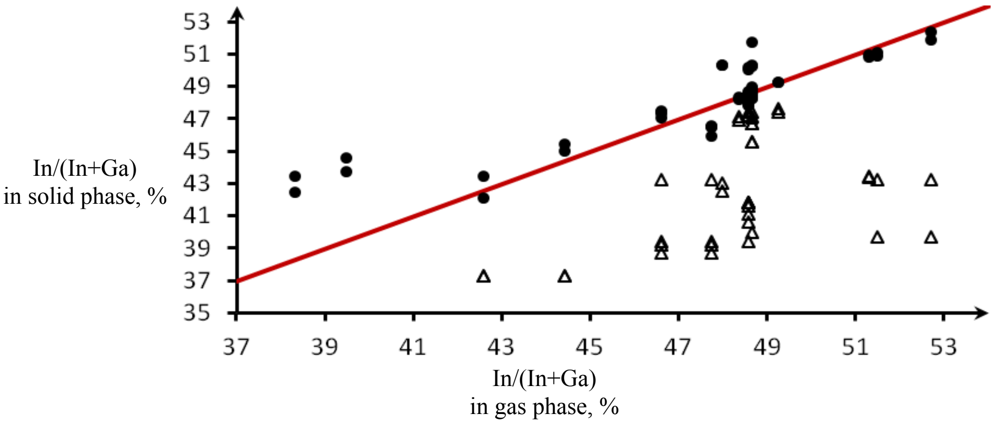

Fig. 8. Graphs of the ratio In / Ga of the epitaxial layer $In_xGa_{1-x}P$ in the solid phase, obtained by means of X-ray diffractometry and photoluminescence from the ratio in the gas phase: round shaded points – the results obtained with the X-ray diffractometry method; triangular unpainted dots – results obtained using the photoluminescence method; a straight line – the line of consistency

Рис. 8. Графики зависимости соотношения In / Ga эпитаксиального слоя $In_xGa_{1-x}P$ в твердой фазе, полученные с помощью методов РД и ФЛ от соотношения в газовой фазе: круглые закрашенные точки – результаты, полученные с помощью метода РД; треугольные незакрашеные точки – результаты, полученные с помощью метода ФЛ, прямая линия – линия соответствия данных

For $x < 0.63$ $Ga_xIn_{x-1}P$ material, the following expression [15] is true to calculate the composition of the epitaxial layer:

$$E_g = 1.34 + 0.69 \cdot x + 0.48 \cdot x^2. \quad (7)$$

Conclusion. The research, the results of which are presented in this article, was completed as a part of the determining of the conditions of a highly homogeneous, defect-free growth of epitaxial layers. The general scheme of such studies was tested mainly on InGaAs layers [16; 17].

In the course of the work, the following important results were obtained:

– the optimal technological parameters of epitaxial growth in the composition of the solid solution $In_xGa_{1-x}P$ are determined;

– it is revealed that for the solid solution $In_xGa_{1-x}P$ in the range from 45 to 53 % there is a high perfection of single crystalline structure, a slight broadening of diffractional x-ray peaks (less than 200 acrsecond);

– it is shown that the criterion for assessing the quality of the grown structure, along with the misalignment of diffraction maximum, can be the broadening of the diffraction peak of the structure.

Additionally, it is shown that:

– the plotted rocking curves along the radius of the sample indicate a high homogeneity of the solid solution over the entire surface of the sample (deviation of the lattice parameters 0.01 %), which makes it reasonable to detect at the central point in multiple measurements and confirms the reliability of the data obtained;

– the composition of the solid solution determined using the method of measuring the effect of photoluminescence, should be considered as evaluative.

The obtained results allow us to move to the next stage of work to determine the optimal technological parameters for the growth of perfect epitaxial layers of $In_xGa_{1-x}P$ on a substrate of Ge in the structure of the modern and perspective high-performance cascade SC for space applications, namely achieving the required electrical characteristics using precision dopping [17; 18]. It is also possible to use the created and tested on the compound $In_xGa_{1-x}P$ algorithm for similar studies of other materials.

Acknowledgements. The authors are grateful to employees of department “Development of perspective phototransducers and technologies” of JSC “NPP “Kvant”.

The software and programs (SWComplexAnalysis, RCPAnalysis) are elements of the technology support system developed under the program “UMNIK”, an agreement with the Innovation Promotion Foundation № 9106GU2015 of 24.12.15.

Благодарности. Авторы выражают благодарность работникам отдела разработки перспективных фотопреобразователей и технологий АО «НПП «Квант».

Использованные в работе программы (SWComplexAnalysis, RCPAnalysis) являются элементами системы сопровождения технологии, разработанной в рамках программы «УМНИК», соглашение с Фондом содействия инновациям № 9106ГУ2015 от 24.12.15 г.

References

1. Alferov Zh. I., Andreev V. M., Rumyantsev V. D. [Trends and prospects for the development of solar photovoltaics]. *Fizika i tekhnika poluprovodnikov*. 2004, Vol. 38, No. 8, P. 6–12 (In Russ.).

2. Zhalnin B. V., Kagan M. B., Semenov V. V. et al. [Development and creation of pilot production of nanostructured cascade solar cells in the A3B5 system].

Avtonomnaya energetika: tekhnicheskiy progress i ekonomika. 2009, No. 26, P. 6–12 (In Russ.).

3. Lebedev A. A., Tsynikin S. A., Lednev A. M. et al. [System for monitoring the parameters of epitaxial growth of semiconductor nanoheterostructures of solar cells for space applications]. *Avtonomnaya energetika: tekhnicheskiy progress i ekonomika*. 2013, No. 31, P. 15–24 (In Russ.).

4. Naumova A. A. [Determination of the lattice parameter of thin single-crystal $In_xGa_{1-x}P$ epitaxial layers on Ge substrate]. *Tezisy doklada 71-e Dni nauki studentov NITU "MISiS" mezhdunarodnye, mezhvuzovskie i institutskie nauchno-tekhnicheskie konferentsii* [Theses of the report 71st Days of Science of Students of NITU "MISiS" international, interuniversity and institute scientific and technical conferences]. Moscow, 2016, P. 440–441 (In Russ.).

5. Tsynikin S. A., Lebedev A. A., Zhalnin B. V. *RCPAnalysisVer 1.0 Programma dlya analiza i sravneniya retseptov Veeco, ikh vizualizatsii v vide grafikov i obrazov, real'nykh geterostruktur, sopostavleniya retseptov s eksperimental'nymi dannymi* [RCPAnalysis Ver 1.0 Program for the analysis and comparison of Veeco recipes, their visualization in the form of graphs and images, real heterostructures, comparison of recipes with experimental data]. Certificate of state registration of the program RF № 2014662698, 13.10.2014.

6. Lebedev A. A., Lednev A. M., Tsynikin S. A. [Construction of a system for tracking the technology of manufacturing solar cells for space applications based on A3B5 compounds]. *Tezisy dokladov XX Nauchno-tekhnicheskoy konferentsii molodykh uchenykh i spetsialistov OAO "RKK "Energiya" im. S. P. Koroleva"* [Abstracts of the XX Scientific and Technical Conference of Young Scientists and Specialists of OJSC "RKK "Energia", S. P. Korolev"], Korolev, 2014, P. 385–386.

7. Andreev V. M., Dolginov L. M., Tret'yakov D. N. *Zhidkostnaya epitaksiya v tekhnologii poluprovodnikovykh priborov* [Liquid epitaxy in semiconductor technology]. Moscow, Sovetskoe radio Publ., 1975, P. 328.

8. Stringfellow G. B. Organometallic Vapor-Phase Epitaxy. *Theory and Practice. Academic Press, second edition*. 1999, P. 240–253.

9. Brieland W. G., Coltrin M. E., Creighton J. R. at al. Organometallic vapor phase epitaxy (OMVPE). *Materials Science and Engineering*. 1999, R24, P. 49.

10. Lebedev A. A., Tsynikin S. A., Lednev A. M. [Program for visualization and evaluation of the inhomogeneity of epitaxial growth of semiconductor nanoheterostructures in the manufacture of solar cells for space applications]. *Sbornik materialov molodezhnoy konferentsii "Novye materialy i tekhnologii v raketno-kosmicheskoy i aviatsionnoy tekhnike"* [Collection of materials of the youth conference "New Materials and Technologies in Rocket-Space and Aviation Engineering"]. Zvezdnyy gorodok, 2013, P. 54–60 (In Russ.).

11. High performance chemicals for advanced semiconductor application. SAFC Hitech Enabling Technology. Available at: www.safchitech.com (accessed 10.11.2015).

12. Bouen D. K., Tanner B. K. *Vysokorazreshayushchaya rentgenovskaya difraktometriya i topografiya* [High-resolution x-ray diffractometry and topography]. St. Petersburg, Nauka Publ., 2002, P. 61–80.

13. Shaskol'skaya M. P. *Kristallografiya* [Crystallography]. Moscow, Vysshaya shkola Publ., 1984, P. 93–106.

14. Tsynikin S. A. SWComplexAnalysis. Certificate of state registration of the program RF № 2013610577, 20.03.2013.

15. Levinshtein M., Rumyantsev S., Shur M. Handbook series semiconductor parameters. IoffeInstitute and Rensselaer Polytechnic Institute. 1999, Vol. 2, P. 37–62.

16. Platonov N. D. [Investigation of growth conditions for highly homogeneous epitaxial single-crystal heterostructures based on $Al_xGa_{1-x}As$, $In_xGa_{1-x}As$, $In_xGa_{1-x}P$, created by the MOSGFE method]. *Tezisy doklada 70-e Dni nauki studentov NITU "MISiS" mezhdunarodnye, mezhvuzovskie i institutskie nauchno-tekhnicheskie konferentsii* [Theses of the report 70st Days of Science of Students of NITU "MISiS" international, interuniversity and institute scientific and technical conferences]. Moscow, 2015, P. 403 (In Russ.).

17. Platonov N.D. [Investigation of the electrical characteristics of layers of epitaxial single-crystal structures based on $In_{0.01}Ga_{0.99}As$, depending on the type and degree of doping] *Tezisy doklada 71-e Dni nauki studentov NITU "MISiS" mezhdunarodnye, mezhvuzovskie i institutskie nauchno-tekhnicheskie konferentsii* [Theses of the report 71st Days of Science of Students of NITU "MISiS" international, interuniversity and institute scientific and technical conferences]. Moscow, 2016, P. 439–440 (In Russ.).

18. Smirnov A. A. [Investigation of experimental structures of the $In_xGa_{1-x}P$ / Ge type in order to adapt the ECP method and optimize the technological parameters of the epitaxial growth of semiconductor structures of solar cells]. *Tezisy doklada 72-e Dni nauki studentov NITU "MISiS" mezhdunarodnye, mezhvuzovskie i institutskie nauchno-tekhnicheskie konferentsii* [Theses of the report 72st Days of Science of Students of NITU "MISiS" international, interuniversity and institute scientific and technical conferences]. Moscow, 2017, P. 426–427 (In Russ.).

Библиографические ссылки

1. Алферов Ж. И., Андреев В. М., Румянцев В. Д. Тенденции и перспективы развития солнечной фотоэнергетики // Физика и техника полупроводников. 2004. Т. 38, № 8. С. 937–948.

2. Разработка и создание опытного производства наноструктурных каскадных ФЭП в системе А3В5 / Б. В. Жалнин [и др.] // Автономная энергетика: технический прогресс и экономика. 2009. № 26. С. 6–12.

3. Система контроля параметров эпитаксиального роста полупроводниковых наногетероструктур солнечных элементов космического назначения / А. А. Лебедев [и др.] // Автономная энергетика: технический прогресс и экономика. 2013. № 31. С. 15–24.

4. Наумова А. А. Определение параметра решетки тонких монокристаллических эпитаксиальных слоев $In_xGa_{1-x}P$ на Ge подложке // 71-е Дни науки студентов НИТУ «МИСиС» : тез. докладов междунар. науч.-техн. конф. М., 2016. С. 440–441.

5. Программа для анализа и сравнения рецептов Veeco, их визуализации в виде графиков и образов, реальных гетероструктур, сопоставления рецептов

с экспериментальными данными : свид. о государственной регистрации программы RCPAnalysis Ver 1.0 / С. А. Цыникин, А. А. Лебедев, Б. В. Жалнин № 2014662698 ; заявл. 13.10.2014 ; регистр. 05.12.2014.

6. Лебедев А. А., Леднев А. М., Цыникин С. А. Построение системы сопровождения технологии изготовления солнечных элементов космического назначения на основе соединений А3В5 // Тезисы докладов XX науч.-техн. конф. молодых ученых и специалистов ОАО «РКК «Энергия» им. С. П. Королёва» (10–14 ноября 2014, г. Королёв). С. 385–386.

7. Андреев В. М., Долгинов Л. М., Третьяков Д. Н. Жидкостная эпитаксия в технологии полупроводниковых приборов. М. : Советское радио, 1975. С. 328.

8. Stringfellow G. B. Organometallic Vapor-Phase Epitaxy. Theory and Practice. Second edition. Academic Press, 1999. P. 240–253.

9. Organometallic vapor phase epitaxy (OMVPE) / W. G. Brieland [et al.] // Materials Science and Engineering. 1999. R24. P. 49.

10. Лебедев А. А., Цыникин С. А., Леднев А. М. Программа визуализации и оценки неоднородности эпитаксиального роста полупроводниковых наногетероструктур при изготовлении солнечных элементов космического назначения // Новые материалы и технологии в ракетно-космической и авиационной технике : сб. материалов молодёжной конф. Звёздный городок. 2013. С. 54–60.

11. High performance chemicals for advanced semiconductor application. SAFC Hitech Enabling Technology [Электронный ресурс]. URL: www.safchitech.com (дата обращения: 10.07.2017).

12. Боуэн Д. К., Таннер Б. К. Высокоразрешающая рентгеновская дифрактометрия и топография. СПб. : Наука, 2002. С. 61–80.

13. Шаскольская М. П. Кристаллография. М. : Высш. шк., 1984. С. 93–106.

14. Свид. о государственной регистрации программы SWComplexAnalysis / Цыникин С. А. № 2013610577 ; заявл. 28.01.2013 ; зарегистр. 20.03.2013.

15. Levinshtein M., Rumyantsev S., Shur M. Handbook series semiconductor parameters // Ioffe Institute and Rensselaer Polytechnic Institute. 1999. Vol. 2. P. 37–62.

16. Платонов Н. Д. Исследование условий роста высокооднородных эпитаксиальных монокристаллических гетероструктур на основе соединений $Al_xGa_{1-x}As$, $In_xGa_{1-x}As$, $In_xGa_{1-x}P$, созданных методом МОСГФЭ // 70-е Дни науки студентов НИТУ «МИСиС» : междунар. науч.-техн. конф. М., 2015. С. 403.

17. Платонов Н. Д. Исследование электрических характеристик слоёв эпитаксиальных монокристаллических структур на основе $In_{0.01}Ga_{0.99}As$, в зависимости от типа и степени легирования // 71-е Дни науки студентов НИТУ «МИСиС» : тез. докладов междунар. науч.-техн. конф. М., 2016. С. 439–440.

18. Смирнов А. А. Исследование экспериментальных структур типа $In_xGa_{1-x}P$ / Ge с целью адаптации метода ЭХП и оптимизации технологических параметров эпитаксиального роста полупроводниковых структур ФЭП // 72-е Дни науки студентов НИТУ «МИСиС» : тез. докладов междунар. науч.-техн. конф. М., 2016. С. 426–427.

UDC 331:658.5

Siberian Journal of Science and Technology. 2018, Vol. 19, No. 1, P. 146–151

INCREASING THE LEVEL OF TECHNOLOGICAL DISCIPLINE BY INTRODUCING THE CODING SYSTEM USING STATISTICAL METHODS IN THE ANALYSIS

I. S. Tikhomirova*, S. M. Ryzhkova

JSC "Academician M. F. Reshetnev" Information Satellite Systems"
52, Lenina Str., Zheleznogorsk, Krasnoyarsk region, 662972, Russian Federation
*E-mail: mis88_88@mail.ru

The paper presents the results of the introduction of a coding system for violations of technological discipline in the organization by making a statistical analysis of violations. Compliance with technological discipline is a necessary condition and basis for ensuring the required quality of manufactured products. Breaking the discipline leads to the production of defective goods, to a decrease in product quality, to deterioration of working conditions, and to accidents and breakdowns of technological equipment. In this paper, we present the procedure for analyzing recurring violations based on the collected data from 12 production departments of one organization. For the implementation of the coding system the authors collected, processed and analyzed data using statistical methods such as a checklist, a histogram, a Pareto chart, a diagram of the causes and results. The use of statistical methods does not require large expenditures and makes it possible to judge the state of the phenomena (objects, processes) with a given degree of accuracy and reliability. An important feature of the application of the presented methodology is the ability to predict and regulate problems at all stages of the product life cycle and, on the basis of this, to develop optimal management decisions. Statistical methods are effective tools for collecting and interpreting data, as well as analyzing quality information.

Coding violations of technological discipline makes it possible to identify recurring violations, develop corrective and preventive actions, both at the level of the production department and at the level of the organization as a whole. The results obtained are of considerable interest and can be used both at enterprises of space industry and at other engineering enterprises.

Keywords: technological discipline, statistical methods, preventive actions, corrective actions.

Сибирский журнал науки и технологий. 2018. Т. 19, № 1. С. 146–151

ПОВЫШЕНИЕ УРОВНЯ ТЕХНОЛОГИЧЕСКОЙ ДИСЦИПЛИНЫ ПУТЕМ ВВЕДЕНИЯ СИСТЕМЫ КОДИРОВАНИЯ С ИСПОЛЬЗОВАНИЕМ СТАТИСТИЧЕСКИХ МЕТОДОВ ПРИ ПРОВЕДЕНИИ АНАЛИЗА

И. С. Тихомирова*, С. М. Рыжкова

АО «Информационные спутниковые системы» имени академика М. Ф. Решетнёва»
Российская Федерация, 662972, г. Железногорск Красноярского края, ул. Ленина, 52
*E-mail: mis88_88@mail.ru

Представлены результаты внедрения системы кодирования нарушений технологической дисциплины в организации путем проведения статистического анализа нарушений. Соблюдение технологической дисциплины является необходимым условием и основой обеспечения требуемого качества изготавливаемой продукции, нарушение ее приводит к выпуску брака, к снижению качества продукции, ухудшению условий труда, авариям и поломкам технологического оборудования. Представлен порядок проведения анализа повторяющихся нарушений на основе собранных данных с 12 производственных подразделений одной организации. Для внедрения системы кодирования нарушений были организованы сбор, обработка и анализ данных с использованием статистических методов, таких как контрольный листок, гистограмма, диаграмма Парето, диаграмма причин и результатов. Применение статистических методов не требует больших затрат и позволяет с заданной степенью точности и достоверностью судить о состоянии исследуемых явлений (объектов, процессов). Важной особенностью применения представленной методологии является возможность прогнозировать и регулировать проблемы на всех этапах жизненного цикла продукции и на основе этого вырабатывать оптимальные управленческие решения. Статистические методы являются эффективными инструментами сбора и интерпретации данных, а также анализа информации о качестве.

Кодирование нарушений технологической дисциплины позволяет выявить повторяющиеся нарушения, разрабатывать корректирующие и предупреждающие действия как на уровне производственного подразделения, так и на уровне организации в целом. Полученные результаты представляют значительный интерес и могут быть использованы как на предприятиях космической отрасли, так и на других предприятиях машиностроения.

Ключевые слова: технологическая дисциплина, статистические методы, предупреждающие действия, корректирующие действия.

Introduction. According to the analysis made by "Roskosmos" State Corporation the existing level of technological discipline at the enterprises of the rocket and space industry in 2015–2016 does not ensure the solution of the tasks assigned to "Roskosmos" State Corporation to reduce the accident rate.

In order to ensure the required level of technological discipline in the creation of spacecraft, the JSC "ISS" named after academician M. F. Reshetnev decided to introduce a coding system for violations of technological discipline.

The purpose of the implementation of the system is the development of preventive actions to prevent recurring violations of technological discipline at the organization level.

Implementation objectives:

– detection of recurring violations in all production units of the organization;

– analysis of recurring violations;

– development of measures to prevent violations and improve the technological processes, both at the level of structural departments and at the level of the organization as a whole.

Introducing the coding system. The first stage of the introducing the system was the detection of all violations of technological discipline through the analysis of acts of external and internal checks on technological discipline, monthly and annual reports on the quality of production departments [1; 2].

The second stage is the identification of recurring violations of technological discipline.

The third stage is the analysis of the objects of control where recurring violations were revealed. On the basis of results of the analysis, the following control objects were identified [1]:

– manufacturing process;

– materials, component parts, electrical goods, semi-finished products, blanks;

– details and assembly units, kits, products;

– performers of the technological process;

– design documentation (hereinafter referred to as "DD") and technological documentation (hereinafter – TD);

– equipment; jigs, fixtures and tools (hereinafter – JFT) for monitoring and testing;

– workplace;

– circulation of products.

The fourth stage is the division of recurring violations among the objects of control.

The fifth stage is the coding of recurring violations. All objects of control are numbered from 1 to 9.

In each object recurring violations are encoded. Tab. 1 shows an example of coding violations at the control object 4 "Performers of the Technological Process".

In each object it was accepted to enter the code – "Others", in case the detected violation does not fit into any code.

The sixth stage is the introduction of the coding system into the organization quality management system by re-publishing the organization standard for control of technological discipline.

After the introduction the system was tested in all production departments. Each inspection of technological discipline is recorded in the journals or in the acts of inspections; in case of a violation a violation code is inserted in a special column [3]. Each production department carries out a monthly analysis of technological discipline (the number of audited control objects according to types of inspections, the number of violations detected, the violation code). All information is transferred to the quality control department of the organization (hereinafter – QCD) for analysis throughout the organization [3–6]. Processing the data on violations of technological discipline is shown in fig. 1.

Once in every six months all production departments make quality analysis with the release of the report which has a section on the analysis of technological discipline. Measures are being developed on the basis of the analysis results to prevent recurring violations [7–9].

Table 1

Coding the violations at control object 4 "Performers of the Technological Process"

Control object	Violations at the control objects	Code of violation
4. Performers of the technological process	Non-compliance between the performer's qualification and the qualification specified in TD	401
	Certification of the performer has not been carried out (JSC included)	402
	There is no mark in the certificate for admission to work	403
	Failure to comply with HSE requirements, fire safety	404
	Non-submission of the first detail (operation) indicated in TP for control	405
	Incorrect registration of the accompanying document (not issued, missing, errors in registration)	406
	Non-closure of previous operations not permitted by the schedule of parallel-sequential operations	407
	Violation of the requirements of TP, TS, DD	408
	Non-compliance with the requirements for technological and special clothing	409
	Work without an antistatic wrist strap	410
	Others	411

The results of the analysis of technological discipline in production departments, the data are transferred to the QCD for analysis at the level of the organization as a whole. According to the results of the quality reports analysis for the first half of 2017 the QCD analyzed the violations of the technological discipline throughout the organization. Fig. 2 presents recurring violations of technological discipline in the organization for the first half of 2017 in the form of a histogram (a special type of a bar graph that allows one to visualize the distribution of statistical data) [10–14].

The results of the analysis for the first half of 2017: the organization checked 6348 objects, revealed 1102 violations (17 %); recurring violations are the following:

– certification of JFT, equipment, control and testing has expired (9 %);

– general comments on DD and TD (8.2 %);

– unsatisfactory state of production culture (8.2 %);

– mistakes made by performers in the design of accompanying documents (8 %);

– non-closure of previous operations (6.6 %);

– general comments on workplaces (4 %).

Pareto chart showing the reasons of technological discipline violations was constructed to study the recurring violations (fig. 3). Pareto Chart is one of the quality management tools that helps to determine priorities in the selection of problems; it helps to identify the problems that have the greatest impact on the process [11–15].

Pareto diagram is a bar graph where each column reflects the relative contribution to the problem of an individual factor, all the columns being arranged in descending order from left to right [14].

It can be seen from the diagram that the greatest impact on the level of technological discipline was made by four violations (they are indicated by a grey background).

Having determined specific problems that require priority solutions with the help of Pareto diagram it is necessary to take the next step, that is, to identify the main causes of the problems, i. e. to carry out their analysis. A diagram of causes and results (also called a fish skeleton) was constructed during the analysis of causes of the problems. This diagram is a quality management tool used to determine causes of the problems [14].

Fig. 4 is a diagram of the causes and results of recurring violations of technological discipline. The figure shows four violations of technological discipline, identified from Pareto chart, which need paying most attention to. These reasons are placed with arrows along the “ridge”. Then using “Brainstorming Method” [14] the QCD group listed the most probable causes of these problems.

According to the diagram it is clear that the main causes of violations of technological discipline are inattention and lack of competence of employees.

The identified reasons allow to develop measures to solve the problems and thus to plan improvements. Measures were taken to prevent recurring violations of technological discipline after the analysis. The activities are presented in tab. 2.

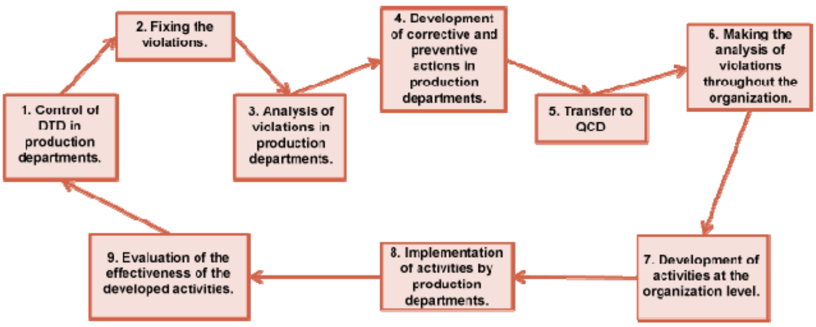

Fig. 1. Processing the data on violations of technological discipline

Рис. 1. Процесс обработки данных по нарушениям технологической дисциплины

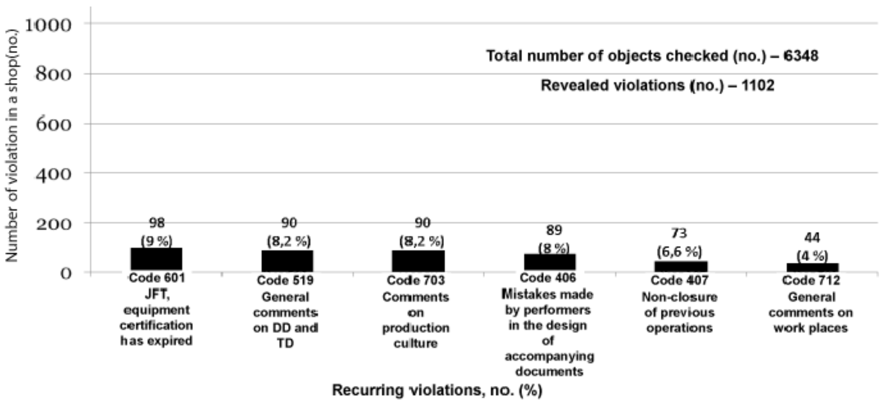

Fig. 2. Recurring violations of technological discipline in the production departments for the first half of 2017

Рис. 2. Повторяющиеся нарушения по технологической дисциплине
по производственным подразделениям за I полугодие 2017 года

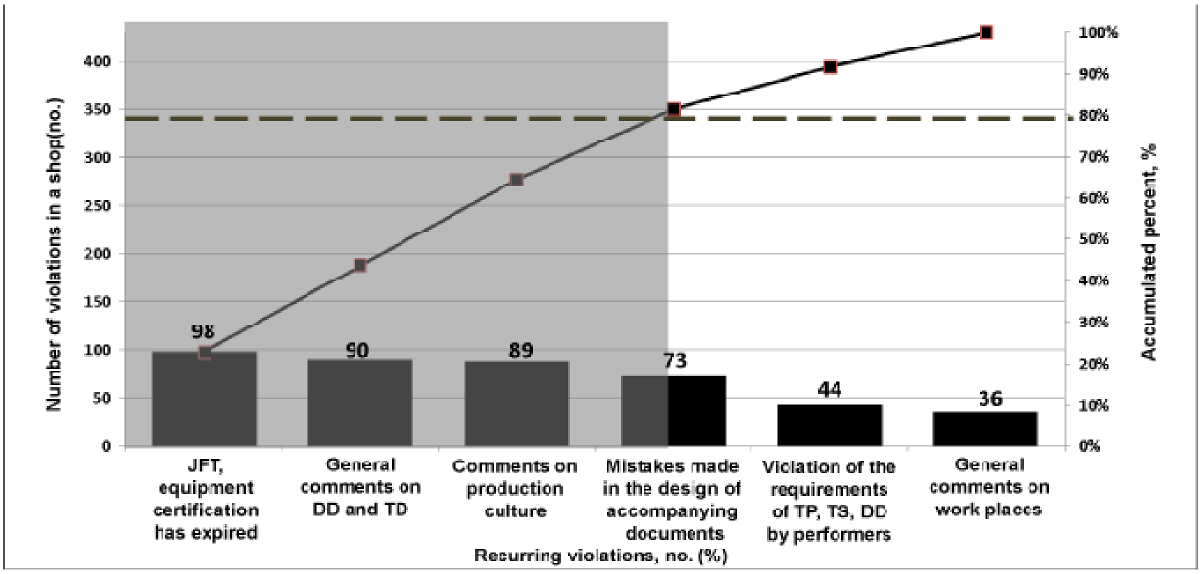

Fig. 3. Pareto diagram of recurring violations in the organization

Рис. 3. Диаграмма Парето повторяющихся нарушений по организации

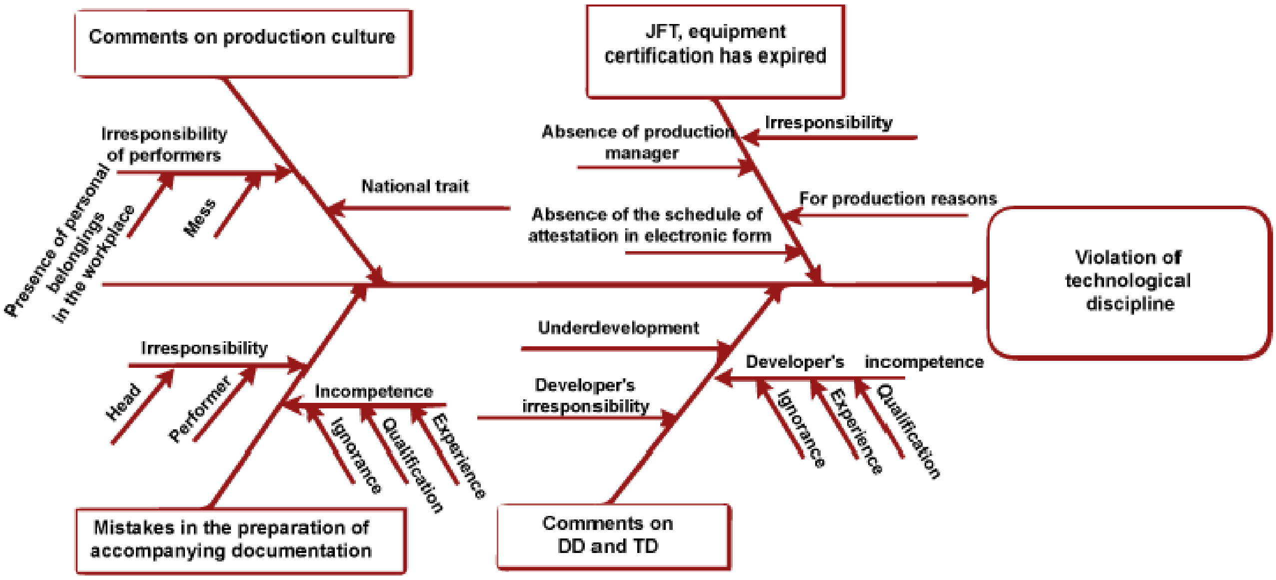

Fig. 4. Diagram of causes and results of recurring violations in the organization

Рис. 4. Диаграмма причин и результатов повторяющихся нарушений по организации

Table 2

Measures to prevent recurring violations of technological discipline

Measures to prevent recurring violations	Responsible for implementation	Supervisor	Deadline
1. Deliver required minimum of technical knowledge to technologists on the timely implementation of changes in AI in technological processes, as well as on additional monitoring of the state of DD and TD when issuing them from the archive	Chief of Technological Bureau	Chief of technical control bureau (hereinafter – TCB)	15.09.2017 г.
2. Deliver required minimum of technical knowledge to technologists to comply with the requirements of standards for the completion of technological passports and maintenance of technical processes	Chief of Technological Bureau	Chief of TCB	15.09.2017 г.
3. To develop the schedule of attestation of JFT and equipment in electronic form	Responsible for preparation of production	Chief of a workshop	12.10.2017 г.

End of table 2

Measures to prevent recurring violations	Responsible for implementation	Supervisor	Deadline
4. Issue an order to assign duties for compliance with the schedule of certification of equipment in the absence of the person responsible for the preparation of production and certification of JFT, equipment (vacation, business trip, sick leave)	Chief of a workshop	Chief of TCB	15.09.2017 г.
5. Deliver required minimum of technical knowledge to performers about the requirements of standards for the preparation of accompanying documentation	Chief of TCB	Chief of a workshop	15.09.2017 г.
6. Work through the entire range of JFT and include the missing positions in the certification schedule	Responsible for preparation of production	Chief of a workshop	10.10.2017 г.
7. During the shop "Hour of quality" to discuss with the chiefs of production sites the problem of the observance of order by the performers at their workplaces and the absence of dusting materials in the clean zones	Chief of TCB	Chief of a workshop	05.09.2017 г.
8. Deliver required minimum of technical knowledge to performers according to the requirements of the standard on culture of production	Head of Production Section	Chief of TCB	05.09.2017 г.

Conclusion. The analysis of data for the first quarter of 2017 after the approbation of the coding system showed an increase in the number of violations detected during internal inspections in departments (in the first half of 2016 the number of violations revealed was 13.8 % of violations from the number of objects, and in the first half of 2017 it was 19.6 %); in its turn, the number of violations revealed by external control (factory commissions, external audits) decreased in comparison with 2016 (from 20 to 17.6 %), which may indicate that the work on the development of corrective and preventive actions ongoing within departments has led to a reduction in the number of comments made by external audits.

One of the further strategic goals for the implementation of the coding system is the creation and implementation of an automated system that includes special software for the efficient analysis of the received data on violations of technological discipline and the timely development of corrective and preventive actions, both at the level of structural departments and at the level of the organization as a whole.

References

1. Methodic recommendations. System of labor quality management. Standing order. Moscow, Official issue, 1988, 153 p.

2. Svitkin M. Z., Matsyta V. D., Rakhin K. N. *Menegment kachestva i obespechenie kachestva produktsii na osnove mejdunarodnyh standartov ISO* [Management and procuring of quality based on international ISO-standarts]. 1999, SPb., VSEGEI Pabl., 403 p.

3. Gludkin O. P., Gorbunov N. M., Gurov A. I., Zorin U. V. *Vseobshee upravlenie kachestvom* [Common quality management]. Moscow, Laboratoriya bazovih znanyi Pabl., 2001, 599 p.

4. Kume Kh. *Statisticheskie metodi povisheniya kachestva* [Statistic methods of quality increasing]. 1990, Moscow, Financy I statistika Pabl., 304 p.

5. Henry R. Neave. The Deming dimension. SPC PRESS (Statistical Process Control). 1990, P. 440.

6. Kedrova S. E. [Quality Instruments. Pt. V. Control lists]. *Metody menedzhmenta kachestva*. 2000, No. 5, P. 23–30 (In Russ.).

7. GOST ISO 9001–2011. *Sistema menegmenta kachestva. Trebovania* [State Standard ISO 9001–2011. Quality management systems – Requirements]. Moscow, Standartinform Publ., 2012.

8. *GOST ISO 9000–2011. Sistema menegmenta kachestva. Osnovnie polozhenya i slovar'* [State Standard ISO 9000–2011. Quality management systems – Fundamentals and vocabulary]. Moscow, Standartinform Publ., 2012.

9. *ISO 19011–2012. Rukovodyashchiye ukazaniya po auditu system menedzhmenta* [State Standard ISO 19011–2012. Guidelines for auditing management systems]. Moscow, Standartinform Publ., 2013.

10. Kedrova S. E. [Quality Instruments. Part. IV. Histograms]. *Metody menedzhmenta kachestva*. 2000, No. 3, P. 28–33.

11. Shotmiller Jr. Statistical management of processes-evolution into a new century. *Quality management methods*. 2005, No. 5, P. 36–43.

12. [Statistical process control]. *Vse o kachestve. Otechestvennye razrabotki*. 2001, Iss. 6, 60 p. (In Russ.).

13. *Statisticheskie metodi upravleniya processami* [Statistical methods of process management]. N. Novgorod, Prioritet Publ., 1997, 170 p.

14. Dranishnikov S. V., Serebryakova L. I., Pervishina E. P., Drozdov A. V. *Statisticheskie metodi v upravlenii kachestvom. Sem prostih instrumentov* [Statistical methods of quality management]. Krasnoyarsk, 2014, 147 p.

15. Razy M. L. *Primenenie diagrammi Pareto na praktike* [Practice application of Pareto diagram]. Available at: http://www.elitarium.ru/diagramma-pareto-princip-80-20-reshenie-mrtod-abc-analiz/.

Библиографические ссылки

1. Взамен ОСТ 92-0200–83. Методические рекомендации. Система управления качеством труда. Основные положения : МДК 92-004–88. Изд. офиц. 85 с.

2. Свиткин М. З., Мацута В. Д., Рахлин К. Н. Менеджмент качества и обеспечение качества продукции на основе международных стандартов ИСО. СПб. : Изд-во Санкт-Петерб. карт. фабрики, 1999. 403 с.

3. Всеобщее управление качеством / О. П. Глудкин [и др.]. М. : Лаборатория базовых знаний, 2001. 599 с.

4. Кумэ Х. Статистические методы повышения качества. М. : Финансы и статистика, 1990. 304 с.

5. Нив Г. Р. Пространство доктора Деминга : пер. с англ. Тольятти : Городской общественный фонд «Развитие через качество», 1998. Т. 1. 336 с.

6. Кедрова С. Э. Инструменты качества. Ч. V. Контрольные листки // Методы менеджмента качества. 2000. № 5. С. 23–30.

7. ГОСТ ISO 9001–2011. Система менеджмента качества. Требования. Изд. офиц. М. : Стандартинформ, 2012.

8. ГОСТ ISO 9000–2011. Система менеджмента качества. Основные положения и словарь. Изд. офиц. М. : Стандартинформ, 2012.

9. ГОСТ Р ИСО 19011–2012. Руководящие указания по аудиту систем менеджмента. М. : Стандартинформ, 2013.

10. Кедрова С. Э. Инструменты качества. Ч. IV. Гистограммы // Методы менеджмента качества. 2000. № 3. С. 28–33.

11. Шоттмиллер Дж. Статистическое управление процессами – эволюция в новое столетие // Методы менеджмента качества. 2005. № 5. С. 36–43.

12. Статистическое управление технологическим процессом // Всё о качестве. Отечественные разработки. М. : НТК «Трек», 2001. Вып. 6. 60 с.

13. Статистические методы управления процессами (SPC). Руководство : пер. с англ. Н. Новгород : АО НИЦ КД : СМЦ «Приоритет», 1997. 170 с.

14. Статистические методы в управлении качеством. Семь простых инструментов : учеб. пособие / С. В. Дранишников [и др.]. Красноярск, 2014. 147 с.

15. Разу М. Л. Применение диаграммы Парето на практике [Электронный ресурс]. URL: http://www.elitarium.ru/diagramma-pareto-princip-80-20-reshenie-mrtod-abc-analiz/.

UDC 539.21:537.86

Siberian Journal of Science and Technology. 2018, Vol. 19, No. 1, P. 152–160

DIELECTRIC PROPERTIES OF SOLID SOLUTIONS OF MANGANESE CHALKOGENIDES SUBSTITUTED BY IONS OF GADOLINIUM

A. M. Kharkov, M. N. Sitnikov, A. N. Masyugin, V. V. Kretinin, U. I. Rybina

Reshetnev Siberian State University of Science and Technology
31, Krasnoyarskiy Rabochiy Av., 660037, Russian Federation
E-mail: khark.anton@mail.ru

The paper describes materials based on solid solutions $Gd_xMn_{1-x}S$ and $Gd_xMn_{1-x}Se$, which in the future can be used in aerospace industry as sensors, detectors, and information writer-readers.

In solid solutions $Gd_xMn_{1-x}A$ (A = S, Se) ($x \le 0.2$), capacitance and tangent of the dielectric loss angle were measured at the frequency of 10 kHz without a magnetic field and in the magnetic field of 8 kOe in the temperature range 100–500 К. The growth of the dielectric permittivity and the maximum of dielectric losses in the low-temperature region were observed. The displacement of the temperature of the maximum of the imaginary part of the permittivity in the direction of high temperatures is found with increasing concentration. For two compositions, a magnetocapacitance effect was observed. The magnetocapacitance effect $\delta\varepsilon_H = (\varepsilon(H,T)-\varepsilon(0,T))/\varepsilon(0,T))$ was determined as a result of investigation of the complex dielectric permittivity.

The synthesis of new chalcogenide compounds in the cationic substitution of manganese by gadolinium in the MnS and MnSe systems will make it possible to clarify the effect of the anion system, as a result of studying its magnetoresistive properties with concentration in the gadolinium ion flux region along the $x \le 0.2$ lattice.

Dielectric losses are described in the Debye model with the freezing of dipole moments and in the model of orbital-charge ordering.

Keywords: solid solutions, electrical capacity, dielectric permittivity, magneto-capacitance effect.

Сибирский журнал науки и технологий. 2018. Т. 19, № 1. С. 152–160

ДИЭЛЕКТРИЧЕСКИЕ СВОЙСТВА ТВЕРДЫХ РАСТВОРОВ ХАЛЬКОГЕНИДОВ МАРГАНЦА, ЗАМЕЩЕННЫХ ИОНАМИ ГАДОЛИНИЯ

А. М. Харьков, М. Н. Ситников, А. Н. Масюгин, В. В. Кретинин, У. И. Рыбина

Сибирский государственный университет науки и технологий имени академика М. Ф. Решетнева
Российская Федерация, 660037, г. Красноярск, просп. им. газ. «Красноярский рабочий», 31
E-mail: khark.anton@mail.ru

Описаны материалы на основе твердых растворов $Gd_xMn_{1-x}S$ и $Gd_xMn_{1-x}Se$, которые в перспективе могут использоваться в аэрокосмической отрасли в качестве сенсоров, датчиков, устройств записи-считывания информации.

В твердых растворах $Gd_xMn_{1-x}A$ (A = S, Se) ($x \le 0{,}2$) проведены измерения емкости и тангенса угла диэлектрических потерь на частоте 10 кГц без магнитного поля и в магнитном поле 8 кЭ в интервале температур 100–500 К. Обнаружен рост диэлектрической проницаемости и максимум диэлектрических потерь в области низких температур. Найдено смещение температуры максимума мнимой части диэлектрической проницаемости в сторону высоких температур с ростом концентрации. Для двух составов обнаружен магнитоемкостный эффект. Магнитоемкостный эффект $\delta\varepsilon_H = (\varepsilon(H,T) - \varepsilon(0,T))/\varepsilon(0,T))$ был определен в результате исследования комплексной диэлектрической проницаемости.

Синтез новых халькогенидных соединений при катионном замещении марганца гадолинием в системах MnS и MnSe позволит выяснить влияние анионной системы в результате исследования его диэлектрических свойств с концентрацией в области протекания ионов гадолиния по решетке $x \le 0{,}2$.

Диэлектрические потери описываются в модели Дебая с замерзанием дипольных моментов и в модели орбитально-зарядового упорядочения.

Ключевые слова: твердые растворы, электроемкость, диэлектрическая проницаемость, магнитоемкостный эффект.

Introduction. Materials in which the interrelation of magnetic and electrical properties manifests itself [1], that is, magnetoelectrics and multiferroics, [2] are of interest both from the fundamental and from the applied point of view. Particular attention is attracted to materials that exhibit magnetoelectric properties at room and higher temperatures in connection with practical applications in microelectronics for recording and storing information. Such studied materials include bismuth ferrite $BiFeO_3$ [3]. The giant magneto-capacitance effect was observed in $LuFe_2O_4$ [4] at room temperature and is explained by the charge fluctuation with different spin in Fe^{2+} and Fe^{3+} ions as a result of removing the degeneracy between two types of charge order by an external magnetic field. The dependence of the orbital magnetic moments on the polar distortions induced by the electric field gives an "ion-orbit" contribution to the magnetoelectric response [5].

At a high level of doping, an orbitally disordered state may arise, which is energetically favorable in comparison with antiferroorbital ordering due to a decrease in the kinetic energy. Analogously to disordered spin systems, when ferromagnetic polarons exist in the paramagnetic region [6], in the high-temperature range, the orbital polarons contribute to the kinetic properties of such systems [7]. The shape of the orbital polarons depends on the configuration of the electronic orbitals. In the presence of an orbital magnetic moment, for example, for electrons in t_{2g}-states, the orbital polarons have a magnetic moment. In this case, the energy of the orbital polaron depends on the direction and magnitude of the external magnetic field. The anisotropy of the electron density distribution in the lattice leads to anisotropy of the dielectric permittivity, which can be controlled by a magnetic field.

In electrically non-uniform systems, the Maxwell–Wagner effect [8] and contact effects can lead to giant values of dielectric permittivity and dielectric relaxation in the absence of dipole relaxation [9]. The Maxwell-Wagner effect can also induce magneto-capacitance in the absence of interaction between the magnetic and electrical subsystems, provided the magnetoresistance exists in the material [10]. Such effects clearly demonstrate that the presence of magneto-capacitance is not sufficient to classify these compounds as multiferroics. On the other hand, the magneto-capacitance without a magnetoelectric coupling can be more practical for technological applications as the existence of a long-range magnetic order is not required.

An electrically non-uniform system with orbital degeneracy is obtained by replacing divalent manganese ions with trivalent gadolinium ions. Thus, the starting compounds of manganese selenide and gadolinium selenide are, respectively, a semiconductor and a degenerate semimetal whose electrical resistance is 10^6–10^9 times different from each other [11]. Gadolinium selenide and manganese selenide have an antiferromagnetic structure of the second ordering type with Neel temperature $T_N = 63$ K [12] and $T_N = 137$ K [13]. The spin-orbit and the Jahn-Teller interaction remove the degeneracy of the t_{2g} electronic states and induce splitting of the electron spin excitation spectrum. As a result, dielectric properties can be controlled by electric and magnetic fields.

The aim of this paper is to establish the role of anions and the effect of cation substitution on the magnetoelectric coupling in orbital-degenerate electronic states in $Gd_xMn_{1-x}A$ solid solutions (A = S, Se).

Experimental results and their discussion. Synthesis of solid solutions $Gd_xMn_{1-x}A$ (A = S, Se) and their certification were described in detail earlier in [14]. The magneto-capacitance effect $\delta\varepsilon_H = (\varepsilon(H,T) - \varepsilon(0, T)) / \varepsilon(0, T))$ is determined by the investigation of the complex dielectric permittivity. The spectral and temperature dependences of dielectric constants can be used to detect the dipole electric moment and to determine its characteristics, even when it is a question of a local dipole moment in small clusters without the presence of long-range order. Dielectric properties also reflect the information about charge transport and charge ordering processes. The response of the dielectric properties to the action of the magnetic field will make it possible to determine the basic mechanisms that determine the behavior of the dielectric and electric transport properties.

The capacitance and tangent of the dielectric loss angle (tg δ) were measured on the AM-3028 component analyzer in the temperature range 90–450 K without a magnetic field and in the magnetic field $H = 8.6$ kOe. The magnetic field was applied parallel to the plates of a flat capacitor. Fig. 1 shows the temperature dependences of the real Re (ε) and imaginary Im (ε) = tg δRe (ε) parts of the dielectric constant of the sample $Gd_{0.04}Mn_{0.96}S$. Heating the sample causes a sharp increase in dielectric losses, the imaginary part of the dielectric constant increases threefold, and the imaginary part increases by 5 % at $T = 102$ K. As the temperature increases, the dielectric constant gradually increases and decreases sharply at $T = 172$ K with a slight increase. The change in the permittivity $Gd_{0.04}Mn_{0.96}S$ within one percent in the magnetic field was not detected. A sharp change in the dielectric permittivity is due to structural distortions of the lattice from the cubic to the rhombohedral structure observed in the non-stoichiometric manganese sulfide at $T = 168$ K.

Fig. 2 shows the temperature dependences of the real Re (ε) and imaginary Im (ε) = tg δRe (ε) parts of the dielectric permittivity of the sample $Gd_{0.05}Mn_{0.95}Se$. In the temperature range 220–330 K, the real part of the dielectric permittivity increases twofold and shifts with increasing frequency towards higher temperatures. The temperature of the maximum of the dielectric losses increases with increasing frequency and is described by a nonlinear function of the logarithm of frequency. The frequency dependence of the complex dielectric permittivity does not correspond to the Debye and Cole-Cole models, which describe the dielectric properties of homogeneous systems with the exponential dependence of the relaxation of the polarization parameter.

The frequency of the dielectric relaxation corresponding to the maximum of Im (ε) has an activation character and is well described by the function $\ln\omega = A\exp(-\Delta E/kT)$ (fig. 2, *b*), where the activation energy $\Delta E = 0.051$ eV and the exponential satisfies the condition $\exp(-\Delta E / kT) << 1$ at $T < 350$ K. Below this temperature, the relaxation frequency and time (τ) can be represented as:

$$\omega = B\exp\left(\exp\left(-\frac{\Delta E}{k_BT}\right)\right) = B\left(1+\exp\left(-\frac{\Delta E}{k_BT}\right)\right); \tau = \frac{\tau_0}{1+\exp\left(-\frac{\Delta E}{k_BT}\right)}. \quad (1)$$

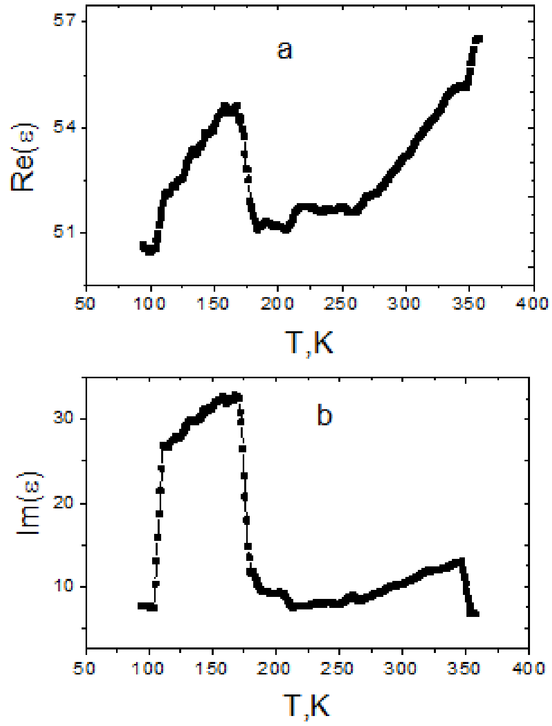

Fig. 1. Real (*a*) and imaginary (*b*) components of the dielectric permittivity for sample $Gd_{0.04}Mn_{0.96}S$ at the frequency of 10 kHz from the temperature

Рис. 1. Реальная (*a*) и мнимая (*b*) компоненты диэлектрической проницаемости для образца $Gd_{0,04}Mn_{0,96}S$ на частоте 10 кГц от температуры

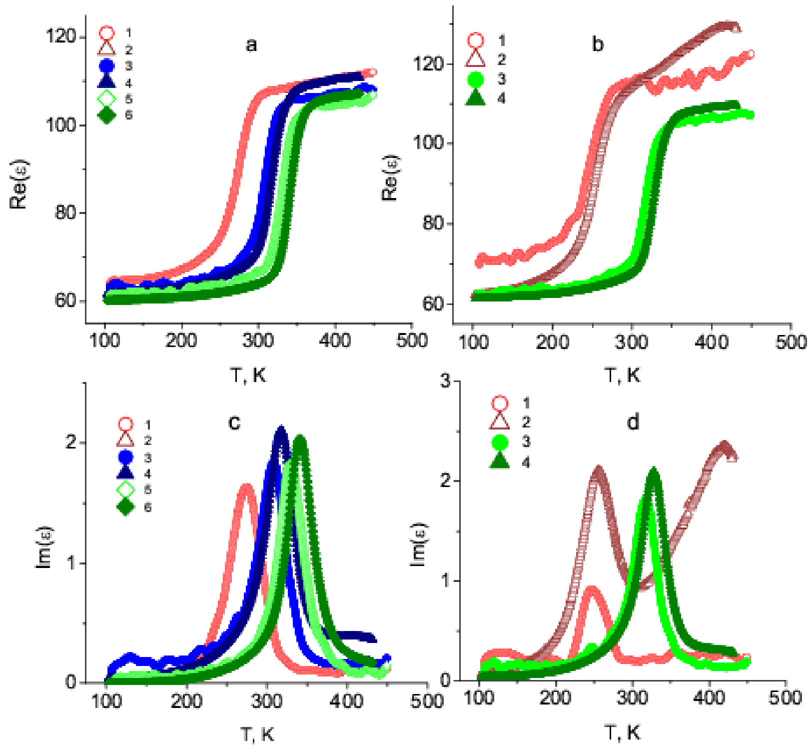

Fig. 2. Real Re (ε) (*a*, *b*) and imaginary Im (ε) (*c*, *d*) (*c*, *d*) components of the dielectric permittivity of the sample $Gd_{0.05}Mn_{0.95}Se$ in the magnetic field $H = 0$ (*1*, *3*, *5*), $H = 8$ kOe (*2*, *4*, *6*) at frequencies ω = 5, 50, 300 kHz (*a*, *c*), ω = 1, 100 kHz (*b*, *d*) from the temperature

Рис. 2. Реальная Re(ε) (*а*, *б*) и мнимая Im(ε) (*в*, *г*) компоненты диэлектрической проницаемости образца $Gd_{0,05}Mn_{0,95}Se$ в магнитном поле $H = 0$ (*1*, *3*, *5*), $H = 8$ кЭ (*2*, *4*, *6*) на частотах ω = 5, 50, 300 кГц (*а*, *в*), ω = 1, 100 кГц (*б*, *г*) от температуры

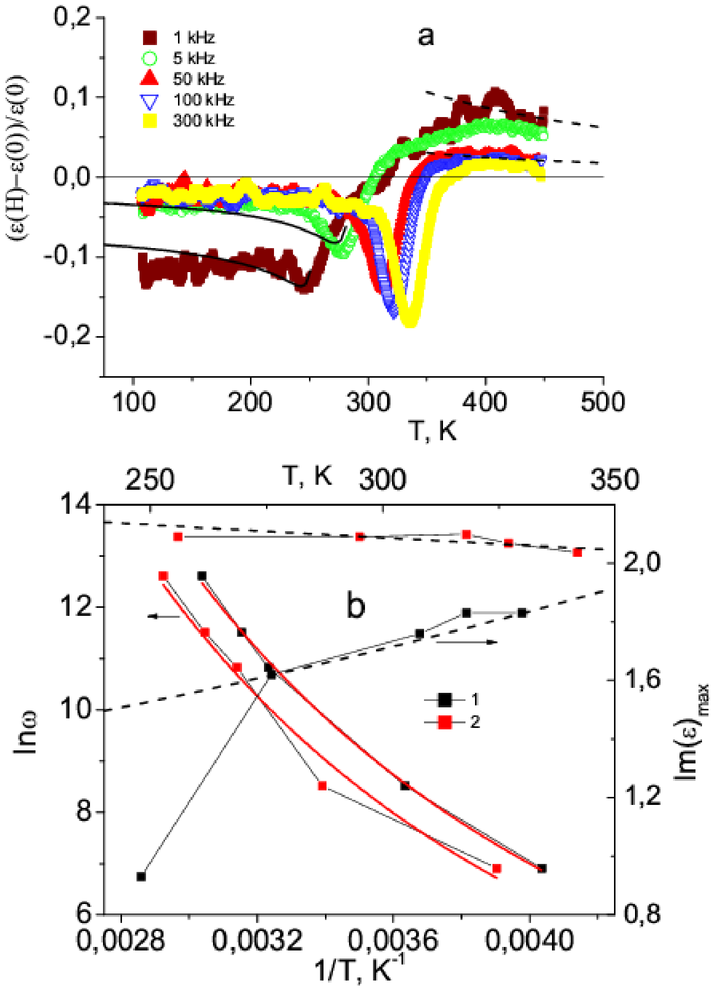

Fig. 3. Magnet capacity δε $Gd_{0.05}Mn_{0.95}Se$ at frequencies ω = 1, 5, 50, 100, 300 kHz in the magnetic field H = 8 kOe for the composition with x = 0.05 of the temperature (*a*); logarithm of the relaxation frequency from the reciprocal temperature without a field (*1*) and in the magnetic field H = 8 kOe (*2*), adjustment function (*1*) (left axis) (*b*). The maximum of Im(ε) as a function of temperature. Adjustment functions $Im(\varepsilon)_{max} = AN_{pe} + BN_{ph}$ (dashed line) (right axis)

Рис. 3. Магнитоемкость δε $Gd_{0,05}Mn_{0,95}Se$ на частотах ω = 1, 5, 50, 100, 300 кГц в магнитном поле H = 8 кЭ для состава с x = 0,05 от температуры (*a*); логарифм частоты релаксации от обратной температуры без поля (*1*) и в магнитном поле H = = 8 кЭ (*2*), подгоночная функция (*1*) (левая ось) (*б*). Максимум Im(ε) от температуры. Подгоночные функции $Im(\varepsilon)_{max} = AN_{pe} + BN_{ph}$ (пунктирная линия) (правая ось)

The activation energy in formula (1) corresponds to the polaron energy (ε_p) relative to the chemical potential (μ), $-\Delta E = \varepsilon_p - \mu < 0$. The relaxation time is proportional to the polaron density $\tau \propto N_p$. If the polaron energy exceeds the chemical potential $\varepsilon_p > \mu$, then this is a polaron of the hole type $N_{ph} = A / (1 + \exp(\Delta E / kT))$. The imaginary component of the dielectric permittivity, due to scattering of polarons by optical phonons, is proportional to $Im(\varepsilon)_{max} \propto (N_{pe} + N_{ph})$. The maxima of the dielectric losses increase with increasing frequency and temperature without a magnetic field and smoothly decrease in the magnetic field (fig. 3, *b*) as a result of the restructuring of the electronic structure in a magnetic field. So in the zero field, the spectral weight of polarons with a hole-type conductivity with the ratio N_{ph} / N_{pe} = 5.5 prevails, and in a magnetic field – the spectral weight of polarons with the electron type N_{pe} / N_{ph} = 2.3, which qualitatively describes the experimental results (fig. 3, *b*).

The temperature at which the dielectric permittivity increases sharply and the maximum of the dielectric losses is observed, shifts to high temperature area in a magnetic field. The activation energy increases by 5 % in a magnetic field of 8 kOe. The magneto-capacity δε = = (ε (H) – ε (0)) / ε (0) for the composition with x = 0.05 is presented in fig. 3, *a*. When heated, the magneto-capacity changes sign and decreases with increasing frequency.

Having divided all the charge carriers into two groups – bound and free charges, we can write the dielectric permittivity of the medium as the sum of the dielectric permittivity of the "lattice" and the contribution of free carriers. Outside the absorption bands, the imaginary part of the permittivity of bound charges (lattices) is usually neglected. The ensemble of carriers was considered as a sum of particles that do not interact with one another. In semiconductors with electron doping, the electrons are delocalized in a certain region and the delocalization radius increases with increasing temperature. We represent the functional dependence in the form of a correlation radius $\xi = A / (1 - T_c / T)$, where T_c is the temperature of charge ordering of electrons in t_{2g} orbitals. Localized electrons induce local ion displacements and lead to local polarization with an effective dipole moment, whose dynamic susceptibility is described in the Debye model.

With decreasing temperature at T_g as a result of the interaction between dipoles through the lattice, local dipoles "freeze". The relaxation time of dipoles is described by the Arrhenius function: $\tau_g = \tau_0 \exp(\Delta E / kT)$, where ΔE is the activation energy. The dielectric susceptibility can be written as:

$$\mathrm{Re}(\chi)/N = \chi_{L0} + \chi_0/(1 + (\omega\tau_g)^2) + B/(1 - T_c/T), \qquad (2)$$
$$\mathrm{Im}(\chi)/N = \chi_0\omega\tau_g/(1 + (\omega\tau_g)^2) + \chi_0\omega\tau_c/(1 + (\omega\tau_c)^2),$$

where χ_{L0} is the temperature-independent contribution to the susceptibility; χ_0 is the static susceptibility of the dipoles; B is the constant; τ_g is the relaxation time of the dipoles at the freezing point; τ_c is the relaxation time of the electric charges upon transition to the orbital charge ordering, $\tau_c = A / \chi^z = A / (1 - T_c / T)^{z\nu}$, where z is the dynamic index, and ν is the index of the correlation radius ($\nu = 1$). The contribution of free charge carriers is neglected, since the value of σ^{Im} of conductivity is several orders of magnitude greater than the conductivity at constant current.

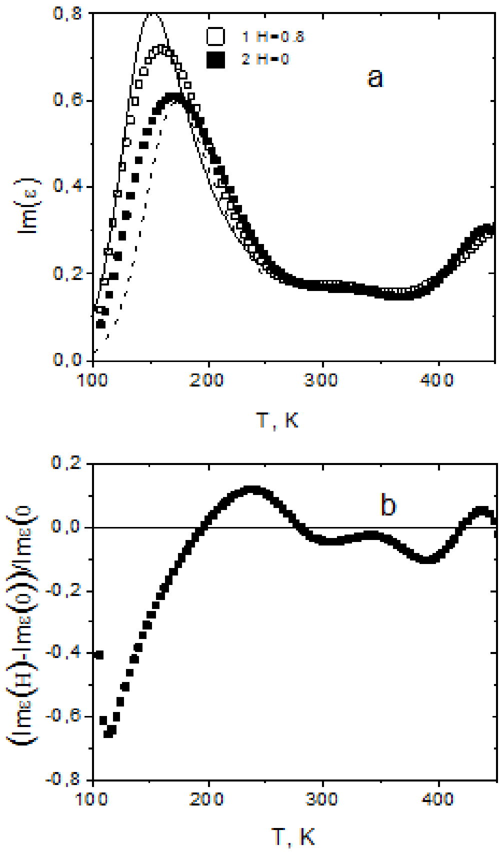

Fig. 4. Imaginary part of the dielectric permittivity (*a*) of a solid solution $Gd_{0.2}Mn_{0.8}S$, measured at a frequency of 10 kHz, without a field (*1*) and in the magnetic field H = 8 kOe (*2*) as a function of temperature. Adjustment function (1b) with activation energy of 900 K (*3*), 1050 (*4*), $z\nu = 2$ (*a*). Relative change of the imaginary part of the dielectric permittivity in a magnetic field from the temperature (*b*)

Рис. 4. Мнимая часть диэлектрической проницаемости (*а*) твердого раствора $Gd_{0,2}Mn_{0,8}S$, измеренной на частоте 10 кГц, без поля (*1*) и в магнитном поле H = 8 кЭ (*2*) от температуры. Подгоночная функция (1b) с энергией активации 900 К (*3*), 1050 (*4*), $zv = 2$ (*а*). Относительное изменение мнимой части диэлектрической проницаемости в магнитном поле от температуры (*б*)

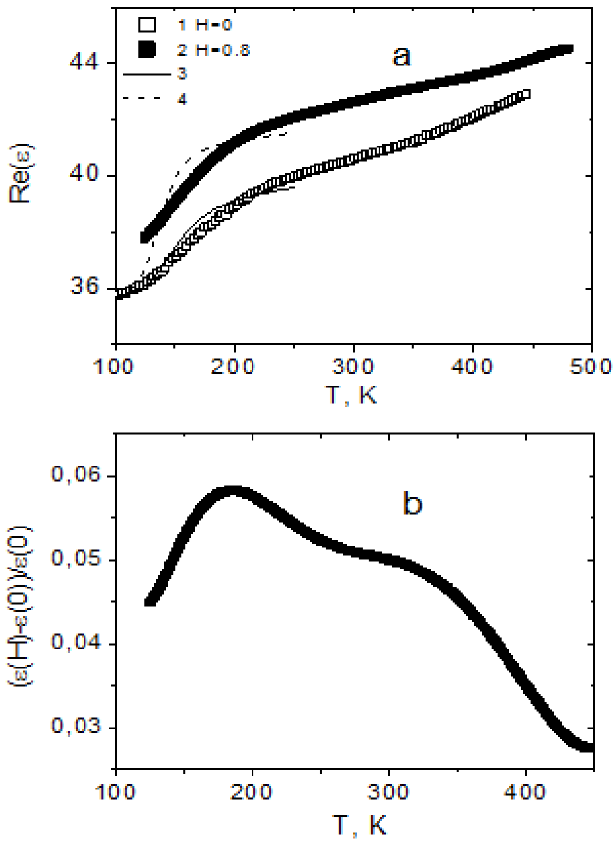

Fig. 5. The real part of the dielectric permittivity (*a*) of a solid solution $Gd_{0.2}Mn_{0.8}S$, measured at the frequency of 10 kHz without a field (*1*) and in the magnetic field H = 8 kOe (*2*) as a function of temperature. Adjustment function (1a) with activation energy of 900 K (*3*), 1050 (*4*), zv = 2 (*a*). The magnetic capacity in a magnetic field is H = 8 kOe of temperature (*b*)

Рис. 5. Реальная часть диэлектрической проницаемости (*а*) твердого раствора $Gd_{0,2}Mn_{0,8}S$, измеренной на частоте 10 кГц без поля (*1*) и в магнитном поле H = 8кЭ (*2*) от температуры. Подгоночная функция (1а) с энергией активации 900 K (*3*), 1050 (*4*), zv = 2 (*а*). Магнитоемкость в магнитном поле H = 8 кЭ температуры (*б*)

When the concentration of gadolinium ions exceeds the concentration of percolation x_c = 0.16, the resistance varies within one order and has a minimum at T = 325 K in the temperature range 100 K < T < 500 K in a solid solution $Gd_xMn_{1-x}S$. In a magnetic field, the resistance also increases and the minimum in the temperature dependence shifts toward high temperatures to T = 380 K. The temperature dependence of the magnetoresistance changes sign from positive to negative at T = 320 K and disappears at the temperature of 475 K. In this solid solution, there are two conduction channels for gadolinium ions and for the interface of Mn–Gd ions. Therefore, the electronic contribution to the susceptibility should be taken into account.

Regardless of the type (electrons or holes), free charge carriers reduce the real part of the dielectric permittivity. This decrease becomes more significant with increasing the concentration and decreasing effective mass of charge carriers. The decrease in the dielectric permittivity by free charge carriers is associated with their inductive contribution to the result of the interaction of the alternating field with matter.

For the composition $Gd_{0.2}Mn_{0.8}S$, the dielectric permittivity is due to localized electrons in the sublattice of manganese ions and conduction electrons in the gadolinene subsystem. Conductivity at constant current varies by a factor of three, and the imaginary part of the dielectric susceptibility changes by an order of magnitude in the temperature interval 100–400 K (fig. 4). The temperature dependence of Im (ε (ω)) has two maxima at T = 170 K and T = 442 K. In the magnetic field H = 8 kOe, the low-temperature peak shifts toward high temperatures to T = 170 K (fig. 4). Dielectric losses decrease in a magnetic field, except for the temperature range 194–279 K and in 417–451 K (fig. 4). The low-temperature maximum in the dielectric permittivity at T = 170 K is described in the localized electron (2) model with the freezing of dipole moments with an activation energy ΔE = 800 K without a magnetic field and in the magnetic field ΔE = 1000 K. The adjustment function describes the experimental data in fig. 4.

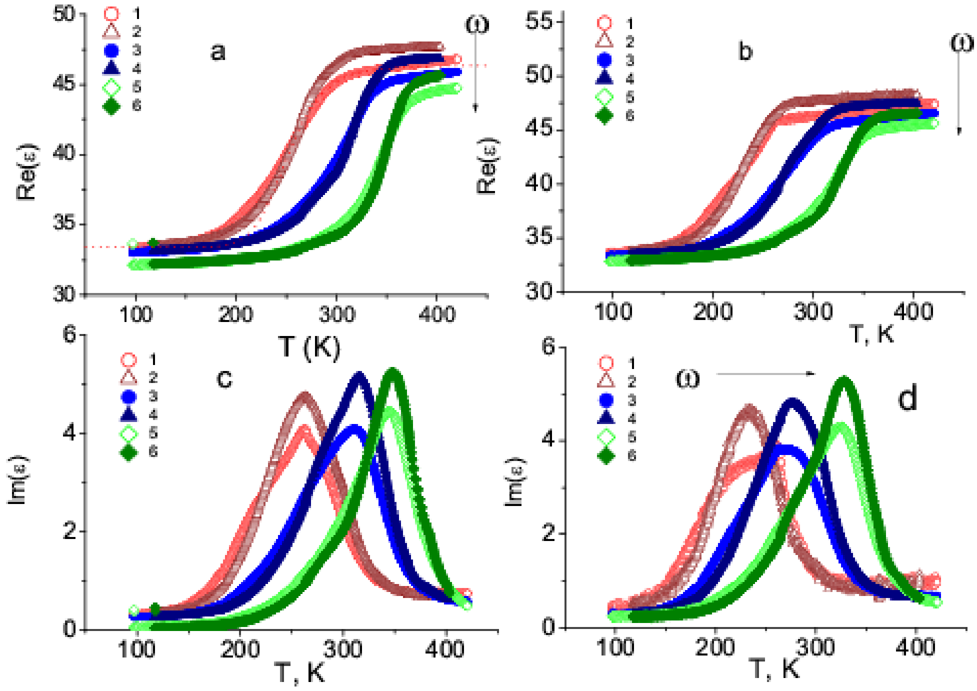

Fig. 6. Real Re (ε) (*a*, *b*) and imaginary Im (ε) (*c*, *d*) parts of the dielectric permittivity of the sample $Gd_{0.2}Mn_{0.8}Se$ without a field (*1*, *3*, *5*) and in the magnetic field H = 8 kOe (*2*, *4*, *6*) at frequencies ω = 5, 50, 300 kHz (*a*, *c*), ω = 1, 10, 100 kHz (*b*, *d*) as a function of temperature

Рис. 6. Реальная Re(ε) (*а*, *б*) и мнимая Im(ε) (*в*, *г*) части диэлектрической проницаемости образца $Gd_{0.2}Mn_{0.8}Se$ без поля (*1*, *3*, *5*) и в магнитном поле H = 8 кЭ (*2*, *4*, *6*) на частотах ω = 5, 50, 300 кГц (*а*, *в*), ω = 1, 10, 100 кГц (*б*, *г*) от температуры

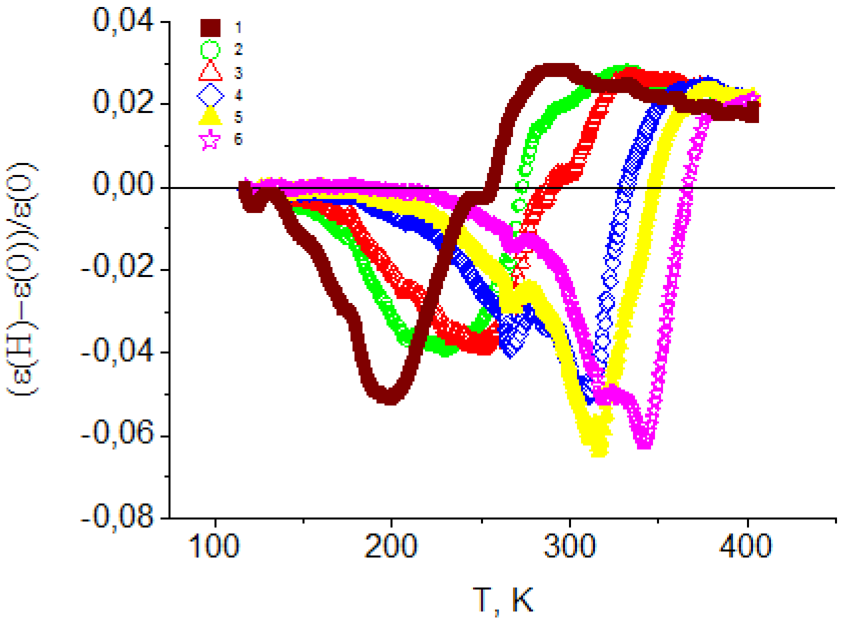

Fig. 7. The magnetic capacity δε $Gd_{0.2}Mn_{0.8}Se$ at the frequencies ω = 1(*1*), 5(*2*), 10(*3*), 50(*4*), 100(*5*), 300 (*6*) kHz in the magnetic field H = 8 kOe for a composition with x = 0.2 of temperature

Рис. 7. Магнитоемкость δε $Gd_{0,2}Mn_{0,8}Se$ на частотах ω = 1(*1*), 5(*2*), 10(*3*), 50(*4*), 100(*5*), 300(*6*) кГц в магнитном поле H = 8 кЭ для состава с x = 0,2 от температуры

This maximum can be associated either with the reorientation of electric dipoles, or with charge transfer between the nonequivalent positions in the crystal lattice of the material, which in a sense is equivalent to the reorientation of electric dipoles. The growth of the magnetoresistance in $Gd_{0.2}Mn_{0.8}S$ [15] in a magnetic field disproves the version associated with charge transfer. The decrease of dielectric losses in a magnetic field is associated with redistribution of the electron density over t_{2g} orbitals, for example, between d_{zx} d_{zy}, which is equivalent to the rotation of an electric dipole. Partial ordering of the dipoles will lead to an increase in polarization. The position of the anomaly in the dielectric permittivity is due to the characteristic relaxation time of the considered subsystem.

The imaginary part of the dielectric permittivity is shown in fig. 5. In the temperature range (130–210) K, a sharp increase in the dielectric permittivity is observed. In the magnetic field H = 8 kOe, Re (ε (ω)) increases and the relative change in permittivity $\delta\varepsilon_H = (\varepsilon (H, T) - \varepsilon (0, T)) / \varepsilon (0, T))$ reaches the maximum of 6 % at T = 184 K. A sharp decrease in permittivity with decreasing temperature is also described in the model of freezing of dipole moments with an activation energy ΔE = 800–1000 K.

As the concentration of gadolinium ions increases, the dispersion of inhomogeneous electronic states and local magnetic fields increases too. The temperature range of the dielectric losses increases for the composition with x = 0.2 (fig. 6), the temperatures of the maxima of the imaginary part of the dielectric permittivity practically do not shift in the magnetic field, and the dielectric loss increases (fig. 6). In a magnetic field, the dielectric permittivity increases more sharply (fig. 6), as a result of which the magneto-capacity changes its sign from a negative value 5–7 % to a positive 4–5 % in the temperature range 140–400 K (fig. 7).

The temperatures of the maxima of dielectric losses increase within one percent in a magnetic field and increase with increasing frequency. The relaxation frequency is described by the exponential dependence (1) with the activation energy ΔE = 0.035 eV. The dielectric losses are due to the scattering of hole type polarons.

Conclusion. For the composition $Gd_{0.04}Mn_{0.96}S$, a sharp abrupt decrease in the dielectric permittivity at low temperatures is found, which is associated with lattice structural distortion. As the concentration of gadolinium ions increases, the low-temperature maximum of the imaginary dielectric permittivity increases too and shifts to high temperatures, just as in a magnetic field. In solid solutions $Gd_xMn_{1-x}Se$, the magneto-capacitance effect was observed at temperatures several times higher than the Neel temperature, with a change in sign with respect to temperature. The logarithm of the relaxation frequency of dielectric losses exponentially increases with heating and depends on the magnetic field.

The decrease in dielectric losses in a magnetic field is caused by the redistribution of localized electrons by t_{2g}, and by the shift in the energy of the electron density maximum relative to the chemical potential, which leads to an increase in the activation energy. These results are well described in the Debye model with the freezing of dipole moments. The increase in the dielectric permittivity above room temperature is caused by an increase in the electron delocalization radius and the disappearance of the orbital-charge ordering. Delocalization of electrons and the transition to the band type conductivity leads to a positive magneto-capacity as a result of Maxwell–Wagner effect.

References

1. Eerenstein W., Mathur N., Scott J. Multiferroic and magnetoelectric materials. *Nature*. 2006, Vol. 442, P. 759–765.

2. Pyatakov A. P., Zvezdin A. K. [Magnetoelectric materials and multiferroics]. *UFN*. 2012, Vol. 182, No. 6, P. 593–620 (In Russ.).

3. Yang J. C., He Q., Suresha S. J., Kuo C. Y., Peng C. Y., Haislmaier R. C., Motyka M. A. Orthorhombic $BiFeO_3$. *Phys. Rev. Lett*. 2012, Vol. 109, P. 247606.

4. Kambe T., Fukada Y., Kano J., Nagata T., Okazaki H., Yokoya T., Wakimoto S., Kakurai K., Ikeda N. Magnetoelectric effect driven by magnetic domain modification in $LuFe_2O_4$. *Phys. Rev. Lett.* 2013, Vol. 110, P. 117602.

5. Scaramucci A., Bousquet E. Linear Magnetoelectric Effect by Orbital Magnetism. *Physical Review Lett.* 2012, Vol. 109, No. 19, P. 654–662.

6. Kagan M. U., Kugel K. I. [Inhomogeneous charge states and phase separation in manganites]. *UFN*. 2001, Vol. 171, P. 577–596 (In Russ.).

7. Kugel K. I., Rakhmanov A. L., Sboychakov A. O., Khomskii D. I. Doped orbitally ordered systems: Another case of phase separation. *Phys. Rev. B,* 2008, Vol. 78, P. 155113.

8. Maxwell J. C. Treatise on Electricity and Magnetism. 3rd ed. Dover, New York, 1991, 335 p.

9. Catalan G. Magnetocapacitance without magnetoelectric coupling. *Appl. Phys. Lett.* 2006, Vol. 88, P. 902–908.

10. Parish M. M., Littlewood P. B. Magnetocapacitance in non-magnetic inhomogeneous media. *Phys. Rev. Lett.* 2008, Vol. 11, P. 99–105.

11. Aplesnin S. S., Bandurina O. N., Ryabinkina L. I., Romanova O. B., Eremin E. V., Gorev M. V., Vorotynov A. M., Balaev D. A., Vasilev A. D., Galyas A. I., Demidenko O. F., Makovetskiy G. I. [The relationship of the magnetic and electrical properties of chalcogenides $MnSe_{1-x}Te_x$]. *Izvestiya RAN. Seriya fizicheskaya*. 2010, Vol. 74, P. 741–743 (In Russ.).

12. Costa M. M. R., de Almeida M. J. M., Nuttall W. J., Stirling W. G., Tang C. C., Forsyth J. B., Cooper M. J. A magnetic x-ray diffraction investigation of gadolinium selenide. *J. Phys.: Condens. Matter*. 1996, Vol. 8, P. 2425.

13. Romanova O. B., Ryabinkina L. I., Sokolov V. V., Pichugin A. Yu., Velikanov D. A., Balaev D. A., Galyas A. I., Demidenko O. F., Makovetskii G. I., Yanushkevich K. I. Magnetic properties and the metal-insulator transition in $Gd_xMn_{1-x}S$ solid solutions. *Solid State Comm*. 2010, Vol. 150, P. 602–604.

14. Aplesnin S. S., Ryabinkina L. I., Romanova O. B., Sokolov V. V., Pichugin A. Yu., Galyas A. I., Demidenko O. F., Makovetskiy G. I., Yanushkevich K. I. [Magnetic and electric properties of the cation-substituted sulfides $Me_xMn_{1-x}S$ (Me = Co, Gd)]. *FTT*. 2009, Vol. 51, P. 661–664 (In Russ.).

15. Aplesnin S. S., Sitnikov M. N. [Magnetotransport effects in the ferromagnetic state in $Gd_xMn_{1-x}S$]. *ZhETF*. 2014, Vol. 100, P. 104–110 (In Russ.).

Библиографические ссылки

1. Eerenstein W., Mathur N., Scott J. Multiferroic and magnetoelectric materials // Nature. 2006. Vol. 442. P. 759–765.

2. Пятаков А. П., Звездин А. К. Магнитоэлектрические материалы и мультиферроики // УФН. 2012. Т. 182, № 6. С. 593–620.

3. Orthorhombic $BiFeO_3$ / J. C. Yang [et al.] // Phys. Rev. Lett. 2012. Vol. 109. P. 247606.

4. Magnetoelectric effect driven by magnetic domain modification in $LuFe_2O_4$ / T. Kambe [et al.] // Phys. Rev. Lett. 2013. Vol. 110. P. 117602.

5. Scaramucci A., Bousquet E. Magnetoelectric Effect by Orbital Magnetism // Phys. Rev. Lett. 2012. Vol. 109. № 19. P. 654–662.

6. Каган М. Ю., Кугель К. И. Неоднородные зарядовые состояния и фазовое расслоение в манганитах // УФН. 2001. Т. 171. С. 577–596.

7. Doped orbitally ordered systems: Another case of phase separation / K. I. Kugel [et al.] // Phys. Rev. B. 2008. Vol. 78. P. 155113.

8. Maxwell J. C. Treatise on Electricity and Magnetism. 3rd ed. Dover, New York, 1991. 335 p.

9. Catalan G. Magnetocapacitance without magnetoelectric coupling // Appl. Phys. Lett. 2006. Vol. 88. P. 902–908.

10. Parish M. M., Littlewood P. B. Magnetocapacitance in non-magnetic inhomogeneous media // Phys. Rev. Lett. 2008. Vol. 11. P. 99–105.

11. Взаимосвязь магнитных и электрических свойств халькогенидов $MnSe_{1-x}Te_x$ / С. С. Аплеснин [и др.] // Известия РАН. Серия физическая. 2010. Т. 74. С. 741–743.

12. A magnetic x-ray diffraction investigation of gadolinium selenide / M. M. R. Costa [et al.] // J. Phys.: Condens. Matter. 1996. Vol. 8. P. 2425.

13. Magnetic properties and the metal-insulator transition in $Gd_xMn_{1-x}S$ solid solutions / O. B. Romanova [et al.] // Solid State Comm. 2010. Vol. 150. P. 602–604.

14. Магнитные и электрические свойства катионзамещенных сульфидов $Me_xMn_{1-x}S$ (Me = Co, Gd) / С. С. Аплеснин [и др.] // ФТТ. 2009. Т. 51. С. 661–664.

15. Аплеснин С. С., Ситников М. Н. Магнитотранспортные эффекты в парамагнитном состоянии в $Gd_xMn_{1-x}S$ // ЖЭТФ. 2014. Т. 100. С. 104–110.

Раздел
Part
4

ЭКОНОМИКА

ECONOMICS AEROSPACE INDUSTRY

УДК 338.6

Сибирский журнал науки и технологий. 2018. Т. 19, № 1. С. 162–172

СОВРЕМЕННЫЕ ПРОБЛЕМЫ СИСТЕМЫ ЦЕНООБРАЗОВАНИЯ ПРИ ФОРМИРОВАНИИ СМЕТНОЙ СТОИМОСТИ НА ТЕРРИТОРИИ РОССИЙСКОЙ ФЕДЕРАЦИИ

Г. А. Власова[1*], Н. В. Князева[1], Т. А. Шиндина[2]

[1]Южно-Уральский государственный университет (национальный исследовательский университет)
Российская Федерация, 454080, г. Челябинск, просп. Ленина, 76
[2]Национальный исследовательский университет «Московский энергетический институт»
Российская Федерация, 111250, г. Москва, ул. Красноказарменная, 14
[*]E-mail: galina-v89@mail.ru

В настоящее время среди наиболее актуальных проблем в системе ценообразования в строительной отрасли является устаревшая база сметных норм и расценок. Как частные инвесторы, так и государство, являющиеся заказчиками строительных работ, заинтересованы в определении достоверной стоимости проекта при подготовке сметной документации. Ведь в условиях экономической нестабильности для строительных компаний и отрасли в целом ключевым моментом развития является снижение себестоимости строительной продукции. Рассмотрены основные проблемы нормирования и определения стоимости основных ресурсов строительства, а также сформулированы задачи реформирования действующей базы сметных нормативов. По результатам проведения хронометражных работ разработаны нормы и расценки на строительные работы по современным технологиям. Доказана необходимость актуализации базы и переход на ресурсный метод сметного ценообразования.

Ключевые слова: инвестиционно-строительный проект, сметная стоимость строительства, сметные нормы и расценки, стоимость ресурсов в строительстве, ресурсный метод определения сметной стоимости, хронометраж строительных процессов.

Siberian Journal of Science and Technology. 2018, Vol. 19, No. 1, P. 162–172

MODERN PROBLEMS OF THE PRICING FORMATION SYSTEM FOR THE FORMATION OF ESTIMATE VALUE IN THE TERRITORY OF THE RUSSIAN FEDERATION

G. A. Vlasova[1*], N. V. Knyazeva[1], T. A. Shindina[2]

[1]South Ural State University (national research university)
76, Lenina Av., Chelyabinsk, 454080, Russian Federation
[3]National Research University “Moscow Power Engineering Institute”
14, Krasnokazarmennaya Str., Moscow, 111250, Russian Federation
[*]E-mail: galina-v89@mail.ru

Currently, among the most pressing problems in the system of pricing in the construction industry is the outdated base of estimates and rates. Both private investors and the state, that are the customers of construction works, are interested in determining the reliable cost of the project when preparing the estimate documentation. After all, in the conditions of economic instability for construction companies and the industry as a whole, the key point of development is the reduction of the cost of construction products. The main problems of rationing and determination of the cost of the basic construction resources are considered in the article, and the tasks of reforming the existing database of estimated standards are formulated. Based on the results of timekeeping, standards and quotations for construction work on modern technologies have been developed. The necessity of actualization of the base and transition to the resource method of the estimated pricing is proved.

Keywords: investment and construction project, estimated cost of construction, estimated norms and prices, cost of resources in construction, resource method for estimating the estimated cost, timing of construction processes.

Введение. Ценообразование на строительную продукцию всегда являлось важным элементом эффективного управления инвестиционным проектом. От того, насколько точно составлена смета, в первую очередь зависит конечный срок реализации проекта и его экономическая эффективность. Так, по разным оценкам, вовремя и в рамках бюджета завершаются только 40–50 % проектов в мире [1]. Известны даже случаи, когда первоначальная смета проекта превышалась более чем в 10–15 раз [2]. Особенно это становится актуальным в условиях экономического кризиса, когда практически все предприятия меняют стиль ценообразования на свою продукцию: если в период подъема цены диктует рынок, то во времена спада топ-менеджмент сталкивается с проблемой более точного определения и возможного снижения нижней границы цены–себестоимости.

Этот принцип полностью применим и к строительному рынку, который, обладая, с одной стороны, некоторой неэластичностью, всегда является точным отражением экономической ситуации в стране. Данную закономерность легко можно проследить при анализе статистических данных. Так, даже при незначительных снижениях значений показателя ВВП в краткосрочном периоде наблюдается падение объемов ввода жилья в эксплуатацию и снижение инвестиционных вложений корпораций (табл. 1).

В ситуации, когда реальные доходы населения падают уже несколько лет и роста платежеспособного спроса на жилье в ближайшее время не ожидается, ключевым моментом развития не только отдельных строительных компаний, но и отрасли в целом становится снижение себестоимости строительной продукции [3].

Данный процесс возможен только при условии постоянного совершенствования системы сметного ценообразования, в том числе актуализации сметных нормативов в строительстве и создания открытой и единой базы сметных расценок на строительную продукцию, включая стоимость на все виды строительных ресурсов (материалы и изделия; машины и механизмы; трудовые ресурсы строительных рабочих).

Следует отметить, что метод сметного нормирования, применяемый в строительной отрасли, имеет свои особенности, так как учитывает особенности строительной продукции, особенности строительного производства и особенности взаимодействия различных участников инвестиционно-строительного комплекса, которые необходимо учитывать в ходе совершенствования действующей системы ценообразования, которая в настоящий момент представляет сочетание методик, методов, сметных норм, цен и расценок.

Сметное нормирование, применяющееся в деятельности инвестиционно-строительного комплекса, является важным инструментом, позволяющим обеспечить эффективность использования денежных средств, что особенно актуально в вопросах, связанных с бюджетным финансированием проектов. В этой связи исследования, направленные на совершенствование действующей системы ценообразования в строительстве, представляются весьма актуальными.

Обзор актуальных проблем системы сметного ценообразования. Многие специалисты в области ценообразования и сметного нормирования в России отмечают, что действующая в настоящий момент сметно-нормативная база далека от идеальной, несмотря на долгую историю и постоянное реформирование, она до сих пор основана на нормах, созданных еще в середине прошлого века, хоть и с некоторыми доработками.

Проведенный нами анализ сложившейся ситуации позволил выделить в сметном деле три существенные проблемы, оказывающие негативное влияние на точность определения стоимости строительства.

1. Нет единой базы стоимости работ. Укрупненная схема системы сметного ценообразования РФ приведена на рис. 1. Основой всех сметных расчетов в строительстве являются элементные сметные нормы – нормы расхода основных видов ресурсов при выполнении конкретных строительных работ. В настоящее время разработаны нормы на общестроительные работы, ремонтно-строительные, монтажные и пусконаладочные работы. И уже на основании утвержденных норм рассчитывается величина единичной расценки (федеральной или территориальной), при этом федеральные расценки применяются для строительных проектов, расположенных на территории Москвы и Московской области, а также проектов, финансируемых за счет федерального бюджета. Стоимость других строительных проектов должна рассчитываться на основании местных территориальных расценок.

При рассмотрении действующей сметно-нормативной базы на федеральном и территориальных уровнях можно увидеть наличие следующих вариантов модификации сметно-нормативной базы 2001 г.: это редакции 2001, 2008 и 2009 гг. К примеру, нормативная база 2008 г. является обязательной только при определении сметной стоимости строительства, осуществляемого по государственному заказу. При строительстве за счёт средств частных инвесторов стоимость может определяться по любым сметным нормативам.

Таблица 1

Динамика основных экономических показателей в РФ

Год	2008	2009	2010	2011	2012	2013	2014	2015	2016	2017
ВВП, млрд руб.	41276	38807	46308	60282	68163	73133	79199	83387	85917	92081
ВВП в физическом объеме, %	105,2	92,2	104,5	104,3	103,7	101,8	100,7	97,5	99,8	101,5
Динамика реальных доходов населения, %	102,4	103,0	105,9	100,5	104,6	104,0	99,3	96,8	94,2	–
Ввод в действие жилья, млн м^2	79,2	72,5	70,3	77,2	82,0	87,1	104,4	106,2	103,4	103,5

Рис. 1. Сметно-нормативная база в Российской Федерации

Fig. 1. Estimated and regulatory base in the Russian Federation

Это приводит к новым проблемам в вопросах формирования стоимости на продукцию строительства и возникновению разногласий между участниками инвестиционно-строительного комплекса [4].

Разнообразие различных сметно-нормативных баз приводит к тому, что стоимость строительства одного и того же объекта, в зависимости от источника финансирования (а заодно и применимой базы расценок), может отличаться в разы, что является крайне нелогичным и, следовательно, не отражает реальную стоимость строительной продукции.

2. Устаревший метод ценообразования. Основной метод, применяемый в сметном ценообразовании в настоящее время, – базисно-индексный. То есть при определении стоимости строительно-монтажных работ (СМР) используются цены базисного года (2000–2001 гг.), которые увеличиваются в соответствии с утвержденными индексами изменения стоимости СМР. По этой причине рассчитанная на основе данной системы стоимость строительно-монтажных работ часто не отражает действительность. На практике используемые технологии заменяют на наиболее близкие, а стоимость материалов принимают по прайсам подрядчика, что, с одной стороны, невозможно проверить, а с другой – практически всегда ведет к удорожанию работ.

Стоит отметить, что в последнее время все же наметился тренд использования ресурсного метода и разработки так называемых открытых расценок, которые только предполагают наличие ряда материалов, но не включают в себя их стоимость. Такие расценки дают возможность сметчикам вносить в расчет именно те ресурсы, которые определены проектом, и по их текущей стоимости, что, конечно, увеличивает точность расчетов. Но относительное количество открытых расценок в базе еще очень мало, чтобы сделать их применение повсеместным.

3. База стоимости строительных работ морально устарела. В базе присутствуют не все современные технологии, и тем более не все строительные материалы и изделия. Это произошло по той причине, что в ходе реформирования вместо работы по формированию нормативов на новые технологии и обновлению старых нормативов, ограничились арифметическим пересчётом норм и расценок.

В результате основная часть расценок, присутствующих в базе, основана на принципах определения сметных затрат на строительство по старой административной схеме [5], на основе устаревших технологических решений по организации работ [6], а также с использованием материалов, которые в настоящее время заменены более технологичными и эффективными. Все это вместе требует кардинального реформирования системы сметного нормирования в строительстве [7].

По причине такого морального устаревания базы норм и расценок у многих строительных компаний появляется необходимость самостоятельной разработки расценок на виды строительных работ, которые они часто применяют: организации, работающие по госзаказу, – федеральные расценки, а остальные – отраслевые и корпоративные. Однако не все компании могут себе позволить каждый раз разрабатывать новые расценки, особенно в период кризиса, поэтому проблема морального устаревания базы практически является нерешаемой без государственного вмешательства.

Основные проблемы сметного ценообразования и возможные пути их решения приведены на рис. 2.

Нельзя не замечать эти существующие проблемы определения стоимости строительства на разных этапах строительного производства для различных участников инвестиционно-строительного комплекса. Приведение сметно-нормативной базы к реалиям сегодняшнего дня (использование новых материалов, технологий и методов строительства) является насущной проблемой всего строительного комплекса.

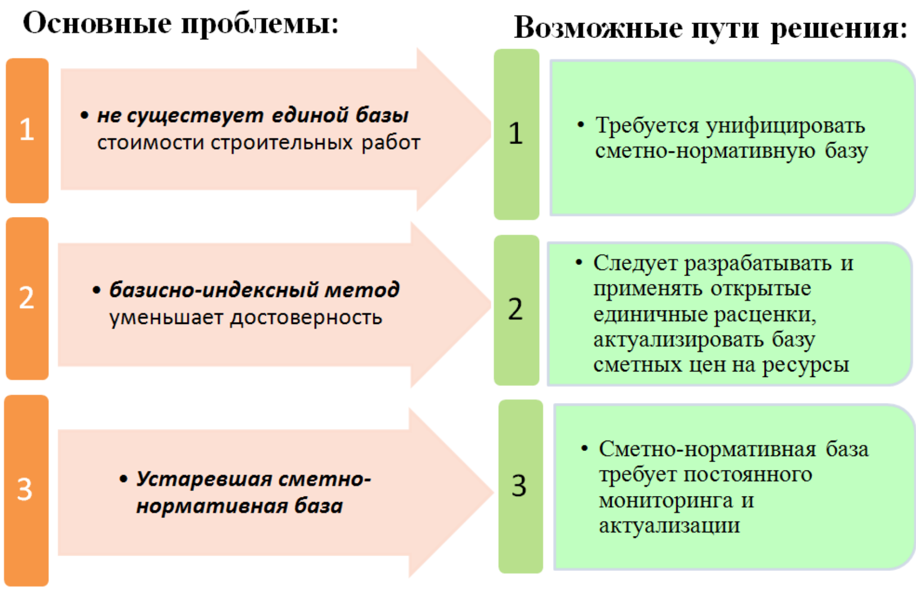

Рис. 2. Основные проблемы системы сметного ценообразования

Fig. 2. The main problems of the budget pricing system

В соответствии с Федеральным законом № 369-ФЗ от 03.07.2016 г. [8] была создана федеральная государственная информационная система ценообразования в строительстве, которая предоставляет возможность доступа к системе сметных норм, расценок и стоимости строительных ресурсов всех участников инвестиционно-строительного процесса в сети Интернет [9]. Однако на сегодняшний момент такая база хоть и включает в себя актуальные цены на строительные ресурсы, остается основанной на нормативах затрат труда и ресурсов, разработанных еще в прошлом веке. Это, несомненно, может свести все положительные моменты реформы на нет.

Поэтому важной составляющей реформы ценообразования является разработка и утверждение нормативов на новые, современные технологии строительных работ, по которым отсутствуют государственные сметные нормы, а также актуализация существующих норм и расценок.

Только имея полную базу стоимости ресурсов и нормативов работ, которая должна обновляться постоянно, можно говорить о переходе к адекватной, современной и точной системе ценообразования.

Опыт разработки сметных норм и расценок на строительные работы. Единственным решением указанных проблем и повышения точности сметного ценообразования является разработка норм и расценок (желательно открытых) на отсутствующие в базе строительные работы, а также актуализация существующих [10].

В рамках данной работы были разработаны сметные нормы и единичные расценки на 4 вида строительных работ – три из них отсутствовали в базе, а четвертый был актуализирован. В качестве примера для описания процесса разработки была взята работа по устройству наливного пола типа «Полиплан 1001».

Методические рекомендации по разработке государственных элементных сметных норм на строительные, специальные строительные и ремонтно-строительные работы определяют единые правила в ходе разработки государственных элементных сметных норм на строительные, специальные строительные и ремонтно-строительные работы.

Основной задачей государственных элементных сметных норм является определение состава и потребности в строительных ресурсах, которые необходимы для реализации строительных, специальных строительных и ремонтно-строительных работ.

Государственные элементные сметные нормы включают в себя современные и рациональные методы, технологию и организацию строительной деятельности. Сметные нормы основываются на применении более производительных машин и на использовании высококачественных строительных материалов, конструкций и изделий, которые впоследствии обеспечат безопасность и будут отвечать потребительским требованиям.

Государственные элементные сметные нормы создаются исходя из условий выполнения строительных, специальных строительных и ремонтно-строительных работ с использованием строительных машин и материальных ресурсов, произведённых на территории страны.

Разработка государственных сметных норм происходит с учётом того, что работы производятся в нормальных условиях, не осложнённых внешними факторами, и при положительной температуре воздуха. Усложняющими факторами принимают стеснённость, загазованность, работу вблизи действующего оборудования, в районах со специфическими условиями (высокогорье и др.), предусмотренными проектом, а также другие более сложные производственные условия.

Государственные элементные сметные нормы включают количественные показатели расхода строительных ресурсов:

– затраты труда рабочих-строителей в человеко-часах (чел. ч);

– время эксплуатации машин и механизмов в машино-часах (маш. ч);

– расход материалов, изделий, конструкций в физических (натуральных) единицах измерения.

Разработка государственных элементных сметных норм – ГЭСН (ГЭСНр) состоит из следующих ключевых этапов:

1) сбор и подготовка исходных данных и нормативной базы;

2) формирование списка рабочих операций и подсчет объемов работ на принятый измеритель технологического процесса;

3) составление калькуляции затрат строительных ресурсов на принятый измеритель технологического процесса;

4) формирование сводок (выборок) строительных ресурсов из калькуляции затрат строительных ресурсов на измеритель элементных сметных норм;

5) составление таблиц ГЭСН (ГЭСНр) по установленной форме с кодированием строительных ресурсов;

6) формирование проекта ГЭСН (ГЭСНр), комплектование обосновывающих материалов, необходимых для представления проекта ГЭСН (ГЭСНр) на утверждение.

Сбор и подготовка исходных данных для разработки государственных элементных сметных норм осуществляется следующим образом:

– уточняются характерные особенности конструкций, сооружений и видов работ, подлежащих нормированию;

– анализируются действующие ГЭСН (ГЭСНр) на предмет наличия (отсутствия) сметных норм на аналогичные виды работ и конструкций;

– определяется необходимый состав исходных данных.

Чёткий перечень исходных данных составляется с учётом специфики работ, особенностей строительных конструкций и технологии производства соответствующих видов работ.

В структуру нормативной базы для разработки государственных элементных сметных норм входят:

– правила и требования по проектированию, организации, производству и приемке работ, установленные действующими нормативными документами по указанным вопросам;

– Единый тарифно-квалификационный справочник работ и профессий рабочих, профессиональные стандарты;

– единые и ведомственные нормы и расценки на строительные, монтажные и ремонтно-строительные работы (далее – ЕНиР, ВНиР) 1987 года выпуска (с последующими дополнениями), утвержденная отраслевая нормативная база по труду (отраслевые нормы времени по видам работ);

– правила разработки норм расхода материалов в строительстве;

– правила разработки и применения нормативов трудноустранимых потерь и отходов материалов в строительстве.

После подготовки исходных данных формируется перечень рабочих операций, которые входят в структуру технологического процесса, с подсчетом объемов работ на измеритель технологического процесса.

В качестве измерителей используются единицы измерения, характерные для определённого вида работ или возводимых конструкций, сложившиеся и принятые в практике строительства и не требующие сложных расчетов при разработке сметной документации.

После формирования списка рабочих операций и объема работ составляется калькуляция затрат строительных ресурсов на измеритель технологического процесса. В калькуляции затрат строительных ресурсов определяются состав и расход следующих ресурсов:

– затраты труда рабочих-строителей, занятых непосредственно на выполнении строительных, специальных строительных и ремонтно-строительных работ, внутрипостроечном транспорте, в чел. ч;

– потребность в машинах и механизмах, используемых непосредственно при выполнении строительных, специальных строительных и ремонтно-строительных работ, а также на внутрипостроечном транспорте, в маш. ч;

– расход материальных ресурсов в принятых натуральных (физических) единицах измерения.

Нормы затрат труда рабочих-строителей при разработке государственных элементных сметных норм определяются на основании действующей нормативной базы по труду (сборники ЕНиР и ВНиР, утвержденная отраслевая нормативная база по труду) и при помощи методов технического нормирования.

Нормы затрат труда, приведенные в сборниках ЕНиР и ВНиР, в утвержденной отраслевой нормативной базе по труду используют только в тех случаях, когда рассчитанная в них методика осуществляемых работ, а также численно-квалификационный состав звена исполнителей являются соответствующими для вида работ, на который создается государственная элементная сметная норма.

Потребность в материальных ресурсах определяется на основании действующих сборников нормативных показателей расхода материалов на основные виды строительных и специальных строительных работ.

При отсутствии соответствующих норм расхода строительных материалов необходимое количество материальных ресурсов для выполнения определённого вида работ (рабочей операции) определяется по имеющимся исходным данным: рабочим чертежам, спецификациям, технологическим картам и т. п. В случае, когда исходных данных недостаточно, нормы расхода материальных ресурсов определяются методами технического нормирования с учетом правил разработки норм расхода материалов в строительстве.

Затраты, возникающие в связи с доставкой материалов от места их приобретения до приобъектного склада (включая выгрузку на приобъектном складе), в состав элементных сметных норм не включаются. Порядок определения указанных затрат устанавливается соответствующими нормативно-методическими документами.

На основании сводок затрат труда рабочих-строителей, потребности в строительных машинах, механизмах и затратах труда машинистов, расхода материальных ресурсов формируется элементная сметная норма.

Элементные сметные нормы на однородные виды строительных, специальных строительных, ремонтно-строительных работ или конструкций, отличающихся отдельными характеристиками, объединяются в таблицы ГЭСН. В таблицы ГЭСН (ГЭСНр) включаются:

– названия и технические характеристики норм;

– список работ, включающий полный перечень всех работ;

– измерители норм;

– средний разряд работы;

– показатели норм по элементам затрат (строительным ресурсам).

Каждому виду элементов затрат присваивается свой определённый код, соответствующий Классификатору строительных ресурсов. Если же такого номера не оказывается на отдельные ресурсы, то вместо него вписывают временное обозначение. Централизованно уполномоченная организация присваивает шифр таблицам государственных элементных сметных норм.

Полное обозначение государственной элементной сметной нормы (шифр) имеет следующую структуру:

XX-XX-XXX-XX,

где 1-й и 2-й знаки – номер сборника; 3-й и 4-й знаки – номер раздела сборника; 5-й, 6-й и 7-й знаки – номер таблицы раздела; 8-й и 9-й знаки – порядковый номер нормы в таблице.

С целью единого порядка разработки и подготовки к использованию и обработки в специализированных программах для составления сметных документаций на строительные, специальные строительные, ремонтно-строительные работы, монтаж оборудования и пусконаладочные работы организациями-разработчиками используются методические указания для определения единого порядка разработки и оформления единичных расценок (ЕР).

Единичные расценки базируются на основе ГЭСН на строительные, специальные строительные, ремонтно-строительные работы, монтаж оборудования и пусконаладочные работы.

Наименование единичных расценок, их шифры, шифры таблиц и единицы расценок должны быть полностью аналогичны обозначениям ГЭСН, созданным в соответствии с методическими рекомендациям по разработке государственных элементных сметных норм.

Оплата труда рабочих при разработке ЕР определяется на основании:

– показателей трудоемкости (затрат труда в чел. ч) соответствующих видов работ, а также среднего разряда работ (для строительных, специальных строительных, ремонтно-строительных работ, ремонтно-строительных работ и монтажа оборудования) и состава исполнителей работ (пусконаладочных работ); вышеприведенные показатели основываются на соответствующих ГЭСН, ГЭСНр, ГЭСНм, ГЭСНп;

– показателей уровня заработной платы рабочих (стоимости 1 чел. ч) по каждому субъекту РФ в уровне цен на установленную дату.

Формула расчета размера средств на оплату труда рабочих ($З^{смр}$) для включения в ЕР:

$$З^{смр} = Т \cdot З_{ср}, \tag{1}$$

где Т – затраты труда рабочих, определяемые по соответствующим ГЭСН, ГЭСНр, ГЭСНм, ГЭСНп (ОЭСН), чел. ч.; $З_{ср}$ – заработная плата рабочего-строителя, соответствующая среднему разряду работ, установленному ГЭСН, ГЭСНр, ГЭСНм, руб/чел. ч.

Для расчета показателя $З_{ср}$ применяется следующая формула, исходя из заработной платы труда рабочего 1-го разряда и соответствующего тарифного коэффициента:

$$З_{ср} = З_1 \cdot К_{Т}^{смр}, \tag{2}$$

где $З_1$ – показатель оплаты труда рабочего-строителя 1-го разряда, руб./чел. ч; $К_{Т}^{смр}$ – тарифный коэффициент среднего разряда работ.

Размер средств на оплату труда пусконаладочного персонала ($З^{пнр}$) для включения в единичную расценку рассчитывается по формуле

$$З^{пнр} = \sum \left(Т_i \cdot З_i \right), \tag{3}$$

где $Т_i$ – затраты труда каждой категории пусконаладочного персонала, определяемые по соответствующим ГЭСНп, чел. ч; $З_i$ – показатель оплаты труда каждой соответствующей категории пусконаладочного персонала, руб./чел. ч.

Показатель $З_i$ рассчитывается, исходя из оплаты труда рабочего-строителя 1-го разряда и соответствующего тарифного коэффициента, по формуле

$$З_i = З_1 \cdot К_{Т}^{пнр}, \tag{4}$$

где $К_{Т}^{пнр}$ – тарифный коэффициент соответствующей категории пусконаладочного персонала.

Порядок определения в единичных расценках стоимости эксплуатации машин и механизмов на строительные, специальные строительные, ремонтно-строительные работы и монтаж оборудования осуществляется на основании:

– показателей затрат на эксплуатацию соответствующих машин и механизмов, определяемых по ГЭСН, маш. ч, на установленный измеритель расценки;

– сметных цен на эксплуатацию машин и механизмов для соответствующего субъекта РФ, разработанных в уровне цен на установленную дату, руб./маш. ч.

При расчете стоимости эксплуатации машин ($С_{эм}$) используется формула

$$С_{эм} = \sum \left(Э_i \cdot Ц_{эмi} \right), \tag{5}$$

где $Э_i$ – затраты на эксплуатацию каждой машины, принимаемые по соответствующей элементной сметной норме, маш. ч; $Ц_{эмi}$ – сметная цена на эксплуатацию каждой машины, руб./маш. ч. При этом, в том числе приводится показатель оплаты труда машинистов, руб./маш. ч.

Порядок определения в единичных расценках стоимости материальных ресурсов определяется на основании следующих данных:

– расхода материалов, изделий, конструкций на производство строительных, специальных строительных, ремонтно-строительных работ и монтаж оборудования, определяемого по соответствующим ГЭСН на установленный измеритель сметной нормы;

– сметных цен на материальные ресурсы для соответствующих административно-территориальных регионов страны в уровне цен на установленную дату.

Формула для стоимости материальных ресурсов ($С_{мат}$) имеет вид:

$$С_{мат} = \sum \left(М_i \cdot Ц_i \right), \qquad (6)$$

где $М_i$ – расход каждого вида материалов, изделий, конструкций, включаемых в единичную расценку, в натуральных единицах измерения; $Ц_i$ – сметная цена каждого вида материальных ресурсов, включаемых в ЕР, руб. на соответствующую единицу измерения материального ресурса.

Если норма расхода ресурсов уточняется в проектных решениях, то стоимость этих материальных ресурсов в единичной расценке на строительные, специальные строительные, ремонтно-строительные работы не учитывается. Наименования таких материальных ресурсов (без указания типа, марки, класса и т. д.) вносятся в таблицу единичной расценки ниже стоимостных показателей с указанием норм их расхода на принятый измеритель ЕР.

В случае, когда норма расхода материальных ресурсов зависит от проекта и в соответствующей таблице государственных элементов сметных норм на строительные, специальные строительные, а также ремонтно-строительные работы, то на месте их расхода указывается литера «П», при составлении ЕР наименования таких материальных ресурсов приводятся ниже стоимостных показателей, а на месте расхода аналогично устанавливается литера «П».

При составлении единичных расценок на монтаж оборудования принимаются в расчет затраты на материальные ресурсы, перечень и расход которых указан в ГЭСНм на соответствующие виды работ, в том числе:

– основные, остающиеся в деле (подкладочные и прокладочные материалы, болты, гайки, электроды и др.);

– вспомогательные, не остающиеся в деле, для изготовления и устройства приспособлений, необходимых для производства монтажных работ (бревна, брусья, доски и т. п.), с учетом их оборачиваемости, а также вспомогательные материальные ресурсы, не остающиеся в деле, используемые для индивидуального испытания смонтированного оборудования, сушки и других целей (электроэнергия, газ, пар, вода, воздух, топливо).

При разработке единичных расценок на монтаж оборудования потребность во вспомогательных ненормируемых материальных ресурсах, используемых при производстве монтажных работ (обтирочные материалы – ветошь, концы, бумага и др.; промывочные материалы – керосин, бензин; смазочные материалы – машинное масло, солидол, тавот и т. п.), определяется в размере 2 % от оплаты труда рабочих и включается в стоимость материалов в составе прямых затрат единичной расценки.

В состав расценки при разработке ЕР на монтаж оборудования не включается стоимость материальных ресурсов, расход которых обусловлен проектной документацией. Перечень указанных материальных ресурсов принимается в соответствии с общими положениями или приложениями к соответствующим сборникам ГЭСНм.

Также стоит обратить внимание, что в единичную расценку на монтаж оборудования не включается стоимость материалов и изделий, расходуемых непосредственно в процессе монтажа, но, согласно установленному порядку, относимых к механизмам.

Разработанные единичные расценки по соответствующим видам работ сводятся в таблицы, которые составляются по специальным формам, приведенным в Приказе Минстроя России от 08.02.2017 г. № 75/пр.

Таблицам единичных расценок присваивается шифр, состоящий из таких элементов, как номер сборника, номер раздела в составе сборника и порядковый номер таблицы. Также рекомендуется при присвоении номера таблиц оставлять резерв номеров для выпуска дополнений к действующим единичным расценкам.

Код единичной расценки состоит из девятизначного числа, со знаками, расположенными в следующей последовательности:

ХХ-ХХ-ХХХ-ХХ,

где 1-й, 2-й знаки относятся к номеру сборника; 3-й, 4-й знаки – номер раздела (отдела) указанного сборника; 5-й, 6-й, 7-й знаки – номер таблицы из указанного раздела; 8-й, 9-й знаки – порядковый номер ЕР в указанной таблице.

Сборник единичных расценок состоит из технической части, таблицы сметных норм и приложения.

Техническая часть сборников единичных расценок состоит из следующих разделов:

1) общие положения;
2) исчисление объемов работ.

Для каждого разработанного проекта ЕР оформляются следующие обосновывающие документы:

– проекты таблицы единичных расценок, по форме соответствующие приведенным методическим рекомендациям;

– пояснительная записка, включающая в себя основания необходимости разработки единичной расценки, где указывается вид разрабатываемой единичной расценки (для последующего ее включения в номенклатуру действующих единичных расценок), а также уровень цен, в котором разработана единичная расценка; представляются реквизиты организации-заказчика и организации-разработчика проектов, наименование и адрес заявителя; включается другая информация, имеющая, по мнению заявителя, отношение к разработке данной единичной расценки;

– таблица расчета единичной расценки;

– показатели часовой оплаты труда, сметные цены на эксплуатацию машин и механизмов, а также сметные цены на материалы, изделия и конструкции, используемые при разработке соответствующих таблиц единичных расценок.

Проект таблицы ЕР и обосновывающие документы к данному проекту согласовываются уполномоченными представителями разработчика единичных расценок и организации-заказчика. Согласованные документы и пояснительная записка к проекту таблицы сброшюровываются, прошиваются, заверяются печатью и подписью руководителя (уполномоченного заместителя руководителя) заявителя и направляются на утверждение в уполномоченный исполнительный орган государственной власти в установленном порядке.

В рамках данной статьи авторами была разработана единичная расценка на новый вид строительных работ, которая в настоящее время отсутствует в базе: устройство наливного пола типа «Полиплан 1001», на примере государственного бюджетного учреждения здравоохранения «Челябинский областной клинический онкологический диспансер» по ул. Блюхера, 42, г. Челябинск.

Методика разработки единичных расценок и сметных норм, описанная выше, определена приказом Минстроя РФ № 75/пр «Об утверждении методических рекомендаций по разработке единичных расценок на строительные, специальные строительные, ремонтно-строительные работы, монтаж оборудования и пусконаладочные работы» [11], а также приказом Минстроя РФ № 76/пр «Об утверждении методических рекомендаций по разработке государственных элементных сметных норм на строительные, специальные строительные и ремонтно-строительные работы» [12]. В соответствии с данной методикой разработка единичной расценки состоит из следующих этапов: утверждение технологической карты, хронометраж строительных работ и камеральные расчеты.

Следует отметить, что в настоящее время выбранная нами технология отсутствует в базе территориальных единичных расценок, технологическая карта процесса была составлена нами самостоятельно на основе рекомендаций производителя строительных материалов, используемых в данном виде работ.

Для обоснования затрат труда строительных рабочих при разработке сметных норм и расценок был произведен хронометраж, включающий в себя как минимум по 3 наблюдения. В результате авторами были проведены хронометражные наблюдения на 4 захватках, общей площадью наружных стен 125,6 м^2.

Проанализировав данные хронометража, был сформирован перечень рабочих операций, входящих в структуру технологического процесса, с подсчетом объемов работ на измеритель технологического процесса. Далее на основании полученной информации составляется калькуляция затрат строительных ресурсов на измеритель технологического процесса. В калькуляции затрат строительных ресурсов включаются следующие показатели:

– затраты труда рабочих-строителей, занятых непосредственно на выполнении строительных, специальных строительных и ремонтно-строительных работ, внутрипостроечном транспорте, в чел. ч;

– потребность в машинах и механизмах, используемых непосредственно при выполнении строительных, специальных строительных и ремонтно-строительных работ, а также на внутрипостроечном транспорте, в маш. ч;

– расход материальных ресурсов в принятых натуральных (физических) единицах измерения.

На основании указанной выше информации формируется элементная сметная норма по устройству наливного пола, представленная в табл. 2, в которой отражены затраты труда рабочих строителей, потребность в строительных машинах, механизмах и затратах труда машинистов, расход материальных ресурсов. Состав работ включает в себя шлифование основания, обеспыливание поверхности, грунтование швов, затирку швов, приготовление раствора для грунтования, грунтование основания, приготовление смеси «Полиплан 1001», заливку наливного пола, устранение излишков воздуха с поверхности пола, лакирование поверхности.

Разработка государственных элементных сметных норм производится на основе принципа усреднения с определением нормативного количества строительных ресурсов, необходимого и достаточного для выполнения соответствующего вида работ.

На основании разработанных государственных элементных сметных норм была выведена единичная расценка по устройству наливного пола типа «Полиплан 1001», которая приведена в табл. 3, составляющейся по форме, приведённой в методических рекомендациях по разработке единичных расценок.

Таблица 2

Элементная сметная норма по устройству наливного пола типа «Полиплан 1001», измеритель – 100 м^2

№ п/п	Код затрат	Наименование элементов затрат	Ед. измер.	Показатели норм
1	1	Затраты труда рабочих	чел. ч	4,34
1.1.	1-1050	Средний разряд работы		4,8
2	3	МАШИНЫ И МЕХАНИЗМЫ		
2.1.	330301	Машина шлифовальная электрическая	маш. ч	1,53
2.2.	330302	Машина шлифовальная угловая	маш. ч	1,21
2.3.	331305	Пылесос промышленный	маш. ч	1,11
2.4.	331451	Перфоратор электрический	маш. ч	0,49
3		МАТЕРИАЛЫ		
3.1	101-8076	Герметик полиуретановый «Эмфимастика PU-25», однокомпонентный	кг	0,98
3.2	101-2786	Грунтовка полимерная типа «BOLIX O»	кг	11,783

Окончание табл. 2

№ п/п	Код затрат	Наименование элементов затрат	Ед. измер.	Показатели норм
3.3	101-5870	Грунтовка полиуретановая «Праймер 1101»	кг	43,767
3.4	101-5869	Покрытие полиуретановое монолитное «Полиплан 1001» (2,3 кг/1 м^2 при толщине слоя 1,5 мм)	кг	230,000
3.5	113-0659	Финиш-лак 105	кг	20,000

Таблица 3

Единичная расценка по устройству наливного пола типа «Полиплан 1001»

Номера расценок	Наименование и характеристика строительных работ и конструкций	Ед. измерения	Прямые затраты, руб.	В том числе, руб.				Затраты труда	
				оплата труда рабочих	эксплуатация машин		материалы	рабочих-строителей, чел. ч	машинистов, чел. ч
(Коды неучтенных материалов)	Наименование и характеристика неучтенных расценками материалов				всего	в том числе оплата труда	расход неучтенных материалов		
1	2	3	4	5	6	7	8	9	10
ХХ-ХХ-ХХХ	Устройство наливного пола типа «Полиплан 1001»	100 м^2	18536,51	229,59	14,02	–	18292,90	16,82	–

В ходе разработки элементной сметной нормы и расценки оказалось, что затраты труда отличаются в меньшую сторону более чем в два раза от самой ближайшей аналогичной нормы (ГЭСН 11-01-052-01) [13], при этом технология устройства пола и используемые материалы отличаются от учтенных в базе. Подобные результаты были получены и при анализе остальных полученных расценок [14]. Это можно объяснить еще и тем, что совершенствование используемой в строительных работах техники обеспечивает не только рост производительности труда и его облегчение, но и снижение затрат труда на единицу продукции при использовании новых машин и механизмов.

Полученные результаты исследования доказывают необходимость постоянного мониторинга действующей сметно-нормативной базы [15] с целью исключения устаревших и не находящих применения в современных условиях и добавления новых норм и расценок. Кроме того, более целесообразно проектировать расценку открытой, оставляя сметчику свободу выбора материалов разных товарных марок и параметров.

Заключение. Сметное нормирование в строительстве является одним из ключевых элементов системы взаимоотношений участников инвестиционного строительного комплекса. В то же время это очень многогранный процесс, который постоянно и активно меняется вслед за развитием строительных технологий и изменениями в законодательстве государства. Сметная стоимость является исходной точкой любого инвестиционного проекта, независимо от его цели и вида финансирования, на ее основании производятся расчеты эффективности проекта и принимается решение о его реализации. Именно на основании сметной стоимости определяются договорные цены на строительные работы, оплачиваются расходы на сырье и материалы, расходы на оборудование и заработная плата рабочих. И, наконец, сметная стоимость строительства лежит в основе балансовой стоимости основных фондов предприятия в виде построенных зданий и сооружений. Поэтому повышение точности расчетов при определении стоимости строительства является весьма актуальной задачей как для строительных компаний, так и для инициатора проекта (заказчика) при любом уровне финансирования.

Анализ состояния системы сметного нормирования в РФ показал, наряду со всеми положительными изменениями, наличие трех основных проблем:

– основной метод, применяемый в сметном ценообразовании в настоящее время – базисно-индексный, который сам по себе уменьшает достоверность расчета за счет обобщенных индексов изменения стоимости;

– не существует единой базы стоимости строительных работ – каждый подрядчик может использовать одну из множества баз сметных нормативов как федерального, так и территориального или отраслевого уровня;

– в существующей базе присутствуют не все современные технологии, и тем более не все строительные материалы и изделия – база требует постоянного мониторинга и актуализации.

В результате проведения хронометражных работ и разработки на их основании сметных норм и расценок оказалось, что во всех четырех случаях стоимость каждого из ресурсов, необходимых в соответствующей работе, значительно отличается от самой близкой имеющейся нормы. И если несовпадение в стоимости материалов является логичным и может быть решено переходом только на открытые расценки, то отличия в трудозатратах делают большинство существующих расценок полностью неактуальными.

Таким образом, необходимым этапом реформы системы ценообразования является разработка и утверждение нормативов на новые, современные технологии строительных работ, по которым отсутствуют государственные сметные нормы, а также актуализация существующих норм и расценок и постоянный мониторинг базы. Только имея полную базу стоимости ресурсов и нормативов работ, которая должна обновляться постоянно, можно говорить о переходе к адекватной, современной и точной системе ценообразования.

Благодарности. Статья выполнена при поддержке Правительства РФ (Постановление № 211 от 16.03.2013 г.), соглашение № 02.A03.21.0011.

Acknowledgments. The work was supported by the Government of the Russian Federation, Act № 211 dated 16.03.2013, contract № 02.A03.21.0011.

Библиографические ссылки

1. Pulse of the ProfessionTM In-Depth Report: The Essential Role of Communications / Project Management Institute, Inc. The Essential Role of Communications, 2013.

2. Voropayev V. I., Gelrud Y. D. Gelrud. Mathematical Modeling of Project Management Problems for Regulators // PM World Journal. 2013. Vol. II, iss. XII.

3. Федеральная служба государственной статистики РФ [Электронный ресурс] : офиц. сайт. URL: http://www.gks.ru (дата обращения: 01.03.2018).

4. Князева Н. В., Овчинникова М. С. Актуальные проблемы системы сметного ценообразования в России // Наука ЮУрГУ : материалы 69-й науч. конф. Южно-Уральский государственный университет, 2017. С. 205–212.

5. Горячкин П. В. О состоянии вопросов ценообразования и сметного нормирования в строительстве // Градостроительство. 2010. № 6. С. 50–58.

6. Сомов М. Ю. Проблемные вопросы сметного нормирования в строительстве // Актуальные вопросы экономических наук. 2016. № 48. С. 101–107.

7. Калинина О. Н. Совершенствование сметно-нормативной базы с помощью применения функционально-стоимостного анализа // Вестник Южно-Российского государственного технического университета (Новочеркасского политехнического института). Сер. «Социально-экономические науки». 2015. № 6. С. 94–101.

8. О внесении изменений в Градостроительный кодекс Российской Федерации и статьи 11 и 14 Федерального закона «Об инвестиционной деятельности в Российской Федерации, осуществляемой в форме капитальных вложений» : федер. закон № 369-ФЗ от 03.07.2016 г. : принят Государственной Думой РФ 22 июня 2016 г.

9. Федеральная государственная информационная система ценообразования в строительстве [Электронный ресурс] : офиц. сайт. URL: https://fgiscs.minstroyrf.ru/

10. Князева Н. В. Управление прибыльностью предприятия на основе анализа стоимости объектов капитального строительства // Региональная конкурентоспособность и образование в контексте глобальных вызовов : сб. ст. участников Междунар. науч.-практ. конф. IV Уральского вернисажа науки и бизнеса. 2017. С. 154–159.

11. Методические рекомендации по разработке единичных расценок на строительные, специальные строительные, ремонтно-строительные работы, монтаж оборудования и пусконаладочные работы : утв. Приказом Министерства строительства и жилищно-коммунального хозяйства Российской Федерации от 8 февраля 2017 г. № 75/пр.

12. Методические рекомендации по разработке государственных элементных сметных норм на строительные, специальные строительные и ремонтно-строительные работы : утв. Приказом Министерства строительства и жилищно-коммунального хозяйства Российской Федерации от 8 февраля 2017 г. № 76/пр.

13. Государственные элементные сметные нормы на строительные и специальные строительные работы : утв. приказом Минстроя РФ № 1038/пр. от 30.12.2016 г. // Сб. 11. Полы.

14. Аполозова Е. А., Хохулина К. В., Князева Н. В. Актуальные проблемы системы сметного ценообразования в России // Управление инвестициями и инновациями. 2017. № 2. С. 16–22.

15. Экономика строительства : учебник / под общ. ред. И. С. Степанова. 3-е изд., доп. и перераб. М. : Юрайт-Издат, 2007. 620 с.

References

1. Pulse of the ProfessionTM In-Depth Report: The Essential Role of Communications. Project Management Institute, Inc. The Essential Role of Communications, May 2013.

2. Voropayev V. I, Gelrud Y. D. Mathematical Modeling of Project Management Problems for Regulators. PM World Journal. (ISSN 2330-4480). Vol. II, Issue XII – December. 2013.

3. *Federal'naya sluzhba gosudarstvennoy statistiki RF. Ofitsial'nyy sayt* [Federal Service of State Statistics of the Russian Federation. Official site]. Available at: http://www.gks.ru (accessed 01.03.2018).

4. Knyazeva N. V., Ovchinnikova M. S. [The latest problems of the system of estimated pricing in Russia]. *Nauka YuUrGU materialy 69-y nauchnoy konferentsii* [Science of SUSU materials of the 69th scientific conference]. Yuzhno-Ural'skiy gosudarstvennyy universitet, 2017, P. 205–212 (In Russ.).

5. Goryachkin P. V. [On the state of questions of pricing and budgetary rationing in construction]. *Gradostroitel'stvo*. 2010, No. 6, P. 50–58 (In Russ.).

6. Somov M. Yu. [Problematic issues of budgetary rationing in construction]. *Aktual'nye voprosy ekonomicheskikh nauk.* 2016, No. 48, P. 101–107 (In Russ.).

7. Kalinina O. N. [Perfection of the estimate-normative base by means of application of functional-cost analysis]. *Vestnik Yuzhno-Rossiyskogo gosudarstvennogo tekhnicheskogo universiteta (Novocherkasskogo politekhnicheskogo instituta). Seriya: Sotsial'no-ekonomicheskie nauki.* 2015, No. 6, P. 94–101 (In Russ.).

8. Federal Law No. 369-FZ of July 3, 2016 "On Amendments to the Town-Planning Code of the Russian

Federation and Articles 11 and 14 of the Federal Law" On Investment Activities in the Russian Federation in the Form of Capital Investments". Adopted by the State Duma of the Russian Federation on June 22, 2016.

9. *Federal'naya gosudarstvennaya informatsionnaya sistema tsenoobrazovaniya v stroitel'stve. Ofitsial'nyy sayt* [Federal state information system of pricing in construction. Official website]. Available at: https://fgiscs.minstroyrf.ru/.

10. Knyazeva N. V. [Enterprise profitability management based on the analysis of the value of capital construction objects]. *Sbornik statey uchastnikov Mezhdunarodnoy nauchno-prakticheskoy konferentsii IV Ural'skogo vernisazha nauki i biznesa "Regional'naya konkurentosposobnost' i obrazovanie v kontekste global'nykh vyzovov"* [Collected papers of the participants of the International Scientific and Practical Conference of the IV Urals Vernisage of Science and Business "Regional Competitiveness and Education in the Context of Global Challenges"]. 2017, P. 154–159.

11. Methodical recommendations for the development of single quotations for construction, special construction, repair and construction work, installation of equipment and commissioning. Approved by the Order of the Ministry of Construction and Housing and Communal Services of the Russian Federation of February 8, 2017 No. 75 / pr.

12. Methodical recommendations for the development of state elemental estimates for construction, special construction and repair and construction work. Approved by the Order of the Ministry of Construction and Housing and Communal Services of the Russian Federation of February 8, 2017 No. 76 / pr.

13. State elemental estimates for construction and special construction work. Approved by Order of the Ministry of Construction of the Russian Federation No. 1038 / pr. from 30.12.2016. Collection 11. Floors.

14. Apolozova E. A., Khokhulina K. V., Knyazeva N. V. [The latest problems of the system of budget pricing in Russia]. *Upravlenie investitsiyami i innovatsiyami.* 2017, No. 2, P. 16–22 (In Russ.).

15. Stepanov I. S. *Ekonomika stroitel'stva* [Economics of construction]. Ed. I. S. Stepanova. Moscow, Yurayt-Izdat Publ., 2007, 620 p.

UDC 339.976.2

Siberian Journal of Science and Technology. 2018, Vol. 19, No. 1, P. 173–181

ECONOMIC METHODS OF SPECTRUM/ORBIT MANAGEMENT FOR SATELLITE NETWORKS

V. V. Makarov[1], V. V. Nozdrin[2*]

[1]The Bonch-Bruevich Saint Petersburg State University of Telecommunications
22/1, Bol'shevikov Av., Sankt-Petersburg, 193232, Russian Federation
[2]International Telecommunication Union
CH-1211, Place des Nations, Geneva, Switzerland
[2]E-mail: vadim.nozdrin@itu.int

Satellite systems continue to play an important role in developing of telecommunication and broadcasting services market by offering an effective technical solution for the transmission and dissemination of various types of information to mobile and fixed subscriber receivers. This trend is raising demand for the spectrum-orbit resource (SOR) which provides the operation of any radio-electronic system and this leads to a shortage of this valuable resource. The international administrative management system, based on technical and normative principles and procedures set in the Radio Regulations, which successfully coped with its tasks of SOR distribution under conditions when several satellite nations have an insignificant number of satellites in the geostationary orbit, under conditions of current loading, shows its inefficiency. The procedure of obtaining authorization to use the resource involves considerable expenditure of time and material resources raising transaction costs on development of satellite projects and increasing financial risks, which makes investment in satellite projects less attractive. In this regard there is a question of the necessity of stimulating rational use of SOR methods introduction.

We are considering the possibility of introducing economic methods into the international SOR management system as an additional tool to encourage the rational use of the resource. An analysis of the existing approaches of contemporary economic theory has identified some basic options for applying economic methods to the SOR management system. For the planned frequency bands, distributed for satellite services, the introduction of national assignments rent system is offered. For unplanned frequency bands, the introduction of payments for the SOR use is being considered. On the basis of electromagnetic compatibility of satellite communication systems assessment analysis, the methods to determine payments for SOR based on assessments of a satellite system aggressivity in terms of creating interference and of its sensitivity to interference from other systems are offered.

Keywords: satellite communication; orbit capacity; transactional costs; economic methods of spectrum management; spectrum pricing.

Сибирский журнал науки и технологий. 2018. Т. 19, № 1. С. 173–181

ЭКОНОМИЧЕСКИЕ МЕТОДЫ УПРАВЛЕНИЯ ИСПОЛЬЗОВАНИЕМ ОРБИТАЛЬНО-ЧАСТОТНОГО РЕСУРСА СПУТНИКОВЫМИ СИСТЕМАМИ

В. В. Макаров[1], В. В. Ноздрин[2*]

[1]Санкт-Петербургский государственный университет телекоммуникаций им. проф. М. А. Бонч-Бруевича
Российская Федерация, 193232, г. Санкт-Петербург, просп. Большевиков, 22, корп. 1
[2]Международный союз электросвязи
Швейцария, Женева, Площадь Наций, CH-1211
[2]E-mail: vadim.nozdrin@itu.int

Спутниковые системы продолжают играть важную роль в развитии рынка услуг связи и вещания, предоставляя эффективное техническое решение для передачи различного рода информации на мобильные и фиксированные абонентские приемники. Такая тенденция повышает спрос на использование орбитально-частотного ресурса (ОЧР), обеспечивающего работу любого космического аппарата, что ведет к феномену нехватки этого ценного ресурса. Международная административная система управления, основанная на технических и нормативных принципах и процедурах, изложенных в Регламенте радиосвязи, успешно справлявшаяся со своими задачами по распределению ОЧР в условиях существования нескольких спутниковых держав с незначительным количеством спутников на геостационарной орбите, в условиях текущей загрузки демонстрирует свою неэффективность. Процедура получения разрешения на использование ресурса требует больших временных и материальных затрат, что повышает транзакционные издержки на развитие спутниковых проектов и риски, что, в свою очередь, снижает привлекательность инвестирования в спутниковые проекты. В этой связи встает вопрос о необходимости внедрения методов, стимулирующих рациональное использование ОЧР.

[*] ***The opinions expressed herein are those of the author and do not reflect an ITU official position.***

Рассматривается возможность внедрения в международную систему управления ОЧР экономических методов в качестве дополнительного инструмента, стимулирующего оптимизацию использования ресурса. Проведенный анализ существующих подходов современной экономической теории позволил определить основные варианты применения экономических методов к системе управления ОЧР. Для плановых полос частот, распределенных для спутниковых служб, предлагается введение системы аренды национальных присвоений. Для неплановых полос частот рассматривается введение платы за использование РЧС. На основе анализа оценки электромагнитной совместимости систем спутниковой связи предложена методика определения платы за РЧС, основанная на оценке агрессивности спутниковой системы с точки зрения создания помехи и ее чувствительности по отношению к помехам от других систем.

Ключевые слова: спутниковая связь, емкость орбиты, транзакционные затраты, экономические методы управления использованием РЧС, ценообразование радиочастотного спектра.

Introduction

Satellite systems in the 21st century allow to provide efficient decisions on delivering modern communication services and broadcasting, successfully creating the competition to terrestrial telecommunication systems or even dominating in a number of markets. The latest achievements in the field of satellite technologies development, in particular increase in a total spacecraft (SC) capacity up to 1 Tbit/s, introduction of all-electric satellites, increase in the maximal efficient loading of launch vehicles and a possibility of their reuse, decrease in time of satellites production lead to the considerable decrease in specific cost of satellite capacity, stimulating strengthening of satellite technologies competitiveness. The prospects of satellite operators development to a large extent depend on availability of the spectrum-orbit resource (SOR) protected from harmful interference. In this regard under conditions of the geostationary orbit (GSO) current loading, the questions of SOR international management system improvement necessity are more often brought up [1; 2].

The measures directed to increase in effectiveness of SOR use which are being considered at the moment, in particular, by the relevant Study Groups of the Radiocommunication Sector of the International Telecommunication Union (ITU) are administrative or technical. Nevertheless, some research and existing experience show that economic methods are one of the potent instruments to improve efficiency of natural resource use [3; 4]. In this article the definition and criteria of SOR use efficiency are discussed, the assessment of SOR use influence on economic indicators of satellite communication project is carried out, the main shortcomings of the developed control system of SOR use are presented and offers on application of economic methods of SOR management for the purpose of increase in economic effect of its operation are made.

The efficiency of the spectrum-orbit resource use by satellite communication systems

It is possible to recognize the combined channel capacity created by the satellites located on a particular GSO arc as efficiency of SOR use, that it is possible to write in the generalized form as [5]:

$$E = C / \Delta\theta \, \Delta f, \qquad (1)$$

where E – effectiveness of OFR use; C – system total capacity, Mbit/s; $\Delta\theta$ – angular width of a GSO arc; Δf – frequency bandwidth occupied by satellites.

As technical solutions directed to efficiency increase, application of homogeneous systems, minimally admissible angular spacing in an orbit, a polarization isolation, increase in accuracy of keeping the satellite in the given position, optimum admissible interference level were considered. Nevertheless, the analysis of satellite communication projects components leads to the interesting conclusion – possibilities of OFR use are defined not only by technical, but also by economic criteria.

Let us explain the foresaid. We will consider the typical project of a satellite system. The main components of capital costs are expenses on satellite designing and production, its launch, including insurance, creation of a necessary ground segment. The satellite cost is determined by the requirements to technical parameters, defined by the required services in the specified service area with wanted quality. Nevertheless, with grow of SOR utilisation, more and more influence on system parameters is exerted by the need to provide electromagnetic compatibility (EMC). In particular, it demands the increase in receivers protection from interference, increase of diameter of the Earth station (ES) antenna, optimization of radio signals processing methods, the adaptive transceivers use recustomizing working parameters depending on a specific electromagnetic situation. It leads to the considerable rising of equipment costs and, in general, to the increase in the required capital investments. Another negative result of incompatibility leading to larger economic losses is the impossibility of all satellite system capacity use in connection with harmful interference. In addition, there is a growing influence of one more component on economic efficiency of satellite communication systems projects – expenses on registration of the corresponding assigning frequences of an orbital position in ITU. Whether this problem is objective or it is related to inefficiency of the applied methods of management? To answer this question it is necessary to consider the existing international control system of use of SOR.

International management system of the orbital-frequency resource use

According to the Radio Regulations (RR) [6] all frequency bands used for satellite communication systems are divided into two types – planned and unplanned. The management of SOR use in them is based on different technical principles and regulation procedures, but they have to pursue one objective – provide the access to SOR to the greatest possible quantity of systems on the condition of harmful interference lack. The choice of the procedure is defined in RR by the frequency band in use and the type of radio service.

The criticism of planned approaches is that they are practically not used per se. The main plans drawback for the majority countries of the world is the restriction of a service area by the national territory. It deprives satellite communication of its main advantage – an opportunity to provide services in larger areas and leads to the fact that realization of satellite systems within national allocations will be economically unprofitable for the majority of countries of the world.

As a result it turns out that plans are interesting only to a limited number of national administrations. Application of additional to plans modification procedures allows them to get advantages at the expense of others which do not use it and, for the reasons stated above, most likely, will never use. In practice modification in most cases leads to deterioration in conditions or impossibility of national allocations use in the Plans.

The main objectives of various procedures explained in RR concerning unplanned frequency bands application are effective SOR use and the greatest possible satisfaction of the real requirements of administrations for their use. Consideration of applications in this case is based on the principle "first came – first served".

The existing approach was being developed in the conditions of satellite communication birth. In the process of a resource loading and increase in demand for satellite communication services the so-called problem of "paper" satellites started to appear. Administrations of some countries tried to occupy a resource for the purpose of access complication to it by others and reservation for the future particular and indefinite requirements. In this regard some international measures directed to the solution of the existing problems have been taken.

First of all, temporary restrictions of all procedures completion date were set, now it is 7 years since the date of application for SOR registration in ITU, and confirmation obligation of system input was assumed. In addition, practically for all satellite networks to which the procedure of coordination is applied, administrations have to submit the request of a specified form confirming the reality of the plans for network development to ITU. In particular, it has to contain the data on a satellite manufacturer and launcher, the reference to the contract and also the information on launch time and place. Also the payment for satellite applications processing, based on recovery of ITU costs on this activity was introduced.

The adopted decisions have yielded some positive results, the number of "paper satellites" decreased, but they have not disappeared. Administrations still have no effective incentives to abandon unused positions, emissions and frequencies. Moreover, there are apparent prerequisites to creation of technical obstacles for competitors access to the spectrum and the orbit that is directed to market protection or, what is even worse, to the subsequent registered position speculation that recently happens even more often. In practice it results in the following:

– in the Master International Frequency Register (MIFR) of ITU there are applications which underwent all required procedures to a decision making to combat paper satellites, but they were either never really used or the actual operation of the corresponding satellites already ended;

– the data entered in applications for SOR in ITU defines the worst situation for compatibility, usually indicating the maximal and minimal modes which are not put into practice;

– often bilateral negotiations on coordination conduct to particular concessions on restriction or change of the stated network parameters. In most cases the corresponding applications do not reflect these agreements, they still contain initially stated and obviously not used modes;

– some administrations provide information on launch confirmation to the Bureau and, according to the administrative procedure due diligence, it does not correspond to reality.

Such practice does not make MIFR to reflect an actual reality of SOR use and unreasonably increases the number of networks with which an applicant has to be coordinated.

Current situation conducts to the fact that the international spectrum management system in itself imposes the considerable additional costs for satellite projects, reducing their investment attractiveness, and, thus, limiting possibilities of SOR use. Its inefficiency causes the growth in necessary initial investments, reduces net profit and increases the project discount rate. Let us explain this conclusion.

As later an operator of satellite communication addresses for a necessary resource, as higher its costs of carrying out calculations, the EMC analysis for the purpose of an optimum position choice, working parameters, used frequency bands and coordination are. A number of researches have considered this phenomenon of satellite projects growing expenses which in economic terminology was named "latecomer's expenses" [7]. By different estimates "latecomer's expenses" for the satellite project make about 5–10 million US dollars and they are growing in the process of SOR loading It is also necessary to note that ITU regisration on average demands more than 5 years, that is often longer than a production cycle itself, from the moment of contract signing to SC launch to an orbit.

In addition, the increase in actual and paper orbit loading leads to the fact that, starting the project, the operator does not know conditions of getting access to a resource use, what depends on agreements with the concerned administrations. The answer to a question whether it will be possible to provide the intended services in the certain area on particular diameter antennas with the guaranteed quality is very uncertain. Indeterminacy is a serious obstacle to any investment project implementation, it involves risk and credit rate increase. Thus, the successful future of satellite communication is closely related to the international regulation procedures which create serious obstacles on the way of modern satellite projects development now. In these conditions taking actions directed to efficiency of SOR use increase is required.

General provisions of the modern economics of social welfare

The main task of economics of social welfare is rational economy management, rational activity, that is optimum resources distribution for achievement of goals [8–10]. The inefficiency arising when using sharing resources, with free access, has been the problem under study in economy for a long period. The lack of proper mechanism of access to a resource regulation at increase in demand leads to inefficiency of distribution and use, exhaustion, overfilling or pollution.

The choice of economic methods is first of all caused by the choice of the ownership form. So far there are three approaches which allow to solve a problem of the "tragedy of the commons", in particular:

– centralized administrative-command management;

– private property;

– collective property.

According to the single Soviet Nobel prize winner in Economics L.V. Kantorovich research results, in the conditions of state property for the resource use, the optimality of its use can be reached due to introduction of the differentiated rent determined by the state planning authority [11]. Besides a differential payment the state, in case if it is possible, can establish particular quotas for a resource use and maintain justice, that is rules of a resource use at the expense of heavy fines.

Under certain conditions market economy and private property also lead to effective use of restricted resources. So, according to the principle of "the invisible hand" particular solutions of separate institutes in the conditions of perfect economy (that is the competition without monopolies) are socially optimum [12], leading to the growth of social welfare. Distribution of resources in a situation of competitive equilibrium is economically efficient. Deepening of this principle has led to the development of the first theorem on economy of social welfare, according to which it is considered that "if the market where all participants of trade act is competitive, then all mutually beneficial commercial transactions will be concluded sooner or later, and the equilibrium distribution of resources arising as a result will be economically efficient" [13]. It is considered that a cumulative effect of it for the society is maximum if it is impossible to redistribute it so that at least it is better for someone and it is worse to nobody. Such distribution of resources is known as "Pareto optimality criteria". However the unambiguous adherence to this criteria, when making a decision, considerably limits the choice of optimization options because there is always someone to whom it is worse at any decision, therefore in some cases practical use of this criteria is difficult.

The optimality of competitive economy according to Pareto depends on various prerequisites. They become apparent in the course of market failure consideration, it is when the perfect competition does not lead to economic optimum. Direct influence of the negative externalities is the main reason of a market failure. Besides, market failure in some cases is bound to non-performance in most cases of the main condition of economy of welfare theorems – competition optimality, for example, in connection with the existence, due to various technological, economic reasons, of companies having the dominating positions in this or that market which received their positions at the initial resource distribution. In this case there are many possible optimal situations according to Pareto, the choice of one of them demands participation in the process of the regulator authority helping the market to cope with fiasco causing unefficient resources use. Therefore, less strict "Pareto potential optimality criteria" is more achievable [14]. This criterion establishes that redistribution of resources leads to the social welfare gains in general, and, therefore, has to be carried out if those who get better after the redistribution can completely compensate for losses of those to who get worse, and at the same time to benefit more from a resource use than before redistribution. It should be noted that besides the competitive environment existence, a condition of market criteria realization is the possibility of legible determination of the property rights to the used resource with a possibility of their sale.

Later economic research showed that the collective property in some cases can cope with a problem of unefficient resource use [15]. The main conclusion is that under certain conditions collective management of a resource of the physical or legal entities pursuing personal benefit can result in the greatest economic effect. To these to conditions, in particular, belong:

– clear definition of resource boundaries and each owner's shares with the right to withdraw them from collective use;

– the rules of distribution limiting place, time, technology and/or quantity of a resource;

– possibility of each owner participation in definition of instructions for a resource use;

– control of implementation of the established rules from owners;

– sanctions against violators of the adopted rules;

– definition of procedures for conflicts solutions both in collective community and between community and the authorities;

– absence of external intervention, in particular the state institutes, in a decision-making process concerning collective property.

Practically all developed countries of the world in a varying degree apply economic methods in a management system of a radio-frequency spectrum use applied by the terrestrial radio communication systems and broadcasting [16; 17]. Let us consider whether their use to OFR used by satellite networks is possible.

Application of economic methods of the orbital-frequency resource use management options

Planned frequency bands. From the economic point of view SOR management in planned frequency bands is administrative, administrations divided a resource among themselves on the basis of the particular technical and regulatory principles, after their realization the national operator can acquire the right to use SOR from the administration by the agreed basic principles – providing equal access to this natural resource for all countries. According to the economic theory, if a management system is not changed, then the introduction of a differential fee has to stimulate effective SOR use. Nevertheless, introduction of a payment for national assignments in the Plans will not achieve this result and will not be supported by administrations. The principles of effectiveness were already initially underlain in the basis of the Plans, the most admissible channel capacity in a particular frequency band was defined and the choice of technical parameters and orbital positions was based on providing EMC on the condition of national territory covering. The unified technical parameters that are all homogeneous systems were applied to planning, what provides optimal SOR loading.

For increase in effectiveness of planned bands use it is possible to consider two possible methods:

1. Cancellation of plans. Plans as it was considered above, do not work and create considerable administrative difficulties, partially bureaucratic, not related to the technical condition of RFS or orbit loadings, as in some cases coordination has to be carried out with paper systems, which are retained by a number of administrations proceeding from positions of uncertain future use and sometimes from purely political ambitions.

2. Replanning for the purpose of creation of conditions for the market of the rights to use SOR. Procedures of planned frequency bands use create very good basis for the secondary market of the rights to use SOR development. One of market mechanisms operating conditions is legible determination of property rights. Concerning the property rights to use SOR, they were formulated as follows [18]:

– definition of the used frequency bands;

– maximal power or spectral mask;

– a service area and the maximal power outside a service area.

The analysis of the existing satellite plans shows that all these conditions are already consolidated by the international legislation, only legal permission to a possibility of sale or rent is necessary. Nevertheless the mechanism does not work and it is explained by the same drawback mentioned earlier – restriction of a service area of the planned assignment with a national covering. The problem can be solved due to replanning on the basis of a regional covering. The optional version of replanning is presented in fig. 1. Orbital positions can be defined on GSO uniformly, proceeding from practical reasons it is possible to establish, over 3 degrees. At the same time the administrations which received a resource in one point must have the right to use an arc in ±1.5º from the nominal position. Realization of a particular technical mask has to providethe lack of interference for networks in the neighboring clusters.

The plan can be used as follows:

1. Administration can keep a possibility of the position planned use in case of future needs. Capacity of national assignment will decrease, due to the service area expansion, but at the same time the national system of any administration can be commercially viable having a potential of a service area choice up to regional. At the same time two main planned advantages – equal access of all administrations to an orbit and a possibility of national satellite system realization without the need for carrying out coordination remain.

2. Neighbors in a cluster in one orbital position can combine their capacity, jointly realizing more broadband systems on the basis of mutual arrangement.

3. In case of plans for the development of characteristic system absence, the administration will have a possibility of the rights rent to administrations which need an additional resource, on a temporary basis at the mutual agreement and on condition of technical restrictions of the plan realization (a position A7’). The ITU Radiocommunication Bureau can undertake a task of information collection from administrations which are ready to lease the rights to SOR use to make it publicly available. The present possibility establishes conditions for the secondary market of the rights to RFS use creation.

4. Bases for more effective use of an arc in a cluster are created. If new operators (for example, positions of A7 and A8) are able to provide compatibility with satellites in a nominal position and to satisfy conditions of systems protection in the neighboring clusters on the basis of technical masks realisation or arrangements with administrations in the neighboring clusters, they can have an opportunity to use other orbital positions in a cluster, different from the nominal. Even in case if the administration already has its national system, it will be interested in carrying out the research directed to combination of two or several systems within the national assignment to gain additional benefits from a resource use.

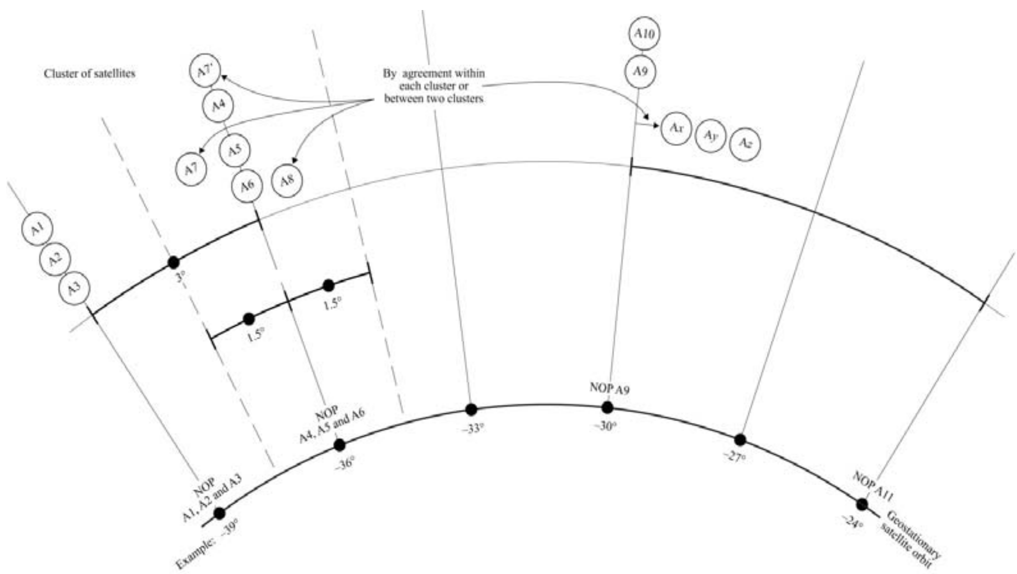

Fig. 1. Option of Satellite planned bands

Рис. 1. Вариант плана для спутниковых служб

The offered approach allows to keep advantages of the plan and to eliminate its defects. Administrations will be interested in achievement of the arrangement with operators striving to use their planned resource. It will force them to publish actual parameters of their systems in case they exist, or not to preserve the national assignment in case of uncertain future use. It will be stimulated with an opportunity to get actual material compensation. Even if there is the need, carrying out coordination will be executed between a very restricted number of negotiators, at the same time each of them will be interested in the positive agreement. The registration of new assignments by the Bureau of a radio communication can be carried out on the basis of the notification of the administration owning the right to use the corresponding national allocation. All these procedures in a complex will promote realization of economic conditions of restricted resource use effectiveness according to a potential criterion according on Pareto.

The main problem when compiling a plan, as it is offered above, is that it has to be created for SOR which it is not occupied with existing systems yet. One of the simplest probable options of introduction is the use of new frequencies distributions for satellite services in higher and not loaded yet frequency bands for planning. Another more composite opportunity is replanning of the existing plans with the term of realization of 15 years that will allow to finish operation to all satellites which already use the discussed frequency band. In addition, a new plan has to contain regulatory provisions describing actions of administrations concluding renting transactions of their frequency assignments.

Unplanned frequency bands. Unlike the planned, the unplanned frequency bands are not suitable for introduction of the market approach as it is quite difficult to define the property rights. Each frequency filing is developed for the specific project, that it must have the parameters corresponding to the requirement specification for the particular satellite. In practice there have already been several transactions when the position notified by one administration has already been used for the SC belonging to another administration. It leads to the fact that the notified parameters considerably differ from actually used, complicating protection of the used assignments as the filing was developed for another satellite. Also it is necessary to consider thatunplanned frequency bands are really very loaded and the change of SOR management procedure can create considerable difficulties for a large number of operators.

One of the most optimal ways to improve EMC of satellite systems among themselves is the ban on expansion of the stated service areas and satellite antenna strengthening diagrams, which often happens in practice. Modern RR text contains only appeals to cover zones restriction without legible definitions and restrictions. As a result there are such applications where a service area – the territory of a small country, but an aiming point of SC – on the equator, and a contour of the antenna gain countur (AGC) – global. Let us illustrate on the example how the notified service area influences a number of networks which have to be involved in coordination process. Calculations results of requirements for coordination on the basis of the criterion of noise temperature $\Delta T/T$ of actually notified system using Ku-range on the line down are given in table At the reduction of a service area with the global (fig. 2), that is the minimal angle of arrival is equal 0º (a contour of an external ellipse) to a service area with the minimal angle of arrival 40º (a contour of an internal ellipse) requirements for coordination decrease in total by 7 %.

Impact of service area reduction to number of coordination concerned networks

Minimum arrival angle	0º	10º	25º	30º	40º
A number of coordination concerned networks	260	258	253	248	231

One more approach to increase SOR use efficiency is the achievement of the greatest possible uniformity of satellite systems. Such two satellite systems which meet the condition are homogeneous:

$$\theta_{1\text{-}2} = \theta_{2\text{-}1}, \qquad (2)$$

That is the minimal necessary spacing $\theta_{1\text{-}2}$ between satellites 1 and 2 from the point of view of interference from system 2 on system 1 is equal to a spacing angle $\theta_{2\text{-}1}$, necessary for preservation on the given interference level from system 1 to system 2. Proceeding from these conditions, the homogeneous systems provide equality of the required angular spacing on the relation to each other that allows to avoid creation of an excess margin on the protective relation in the direction of one of these systems, less sensitive to interference and to realize a minimal spacing angle between considering SC. Ratios between power parameters of two homogeneous systems show that conditions of uniformity can be satisfied for systems with different parameters, for example, with different sizes of service areas, AGC of ES and etc.

Fig. 2. Illustration of satellite service area decreasing

Рис. 2. Иллюстрация уменьшения зоны обслуживания спутника

Based on above mentioned it is possible to come to conclusion that the payment for SOR use has to be proportional to the size of an occupied resource that will force the operator not to occupy (and not to declare) an excessive resource. Let us consider a problem of increase in SOR use efficiency from the technical point of view. It is defined that the technical factors influencing efficiency of GSO use and providing conditions EMC of satellite communication systems and broadcastings are in particular [19]:

– the improved space selectivity of AN antennas;

– the improved space selectivity of the SC onboard antennas;

– increase in accuracy of SC keeping in a calculated position of GSO;

– application of different polarizations – simultaneous work of a SC on two orthogonal (circular or the linear) polarizations;

– application of efficient methods of signals transfer and reception, low-sensitive to interference;

– development of new, more high-frequency ranges.

The angular spacing on GSO between the adjacent SC working in the common frequency ranges in the modern networks usually does not exceed 2º–3°, in certain cases it is possible to reduce it to 1° and even to 0° (at not combined cover zones). At coordination of satellite networks and calculation of interference of the ES modern antennas with the improved space selectivity in the direction other than a principal axis, it is recommended to define by reference antenna diagram (AD) as described in [20]. In case the operator of satellite network assumes to use simpler ES, it is necessary to apply the AD from [21]. For ES used in old satellite systems, the AD mathematical description is presented in [22].

Now in practice in overwhelming number of notified n antennas is defined on the basis of [20]. It should be noted that the choice of AD providing higher selectivity can slightly facilitate achievement of agreement for coordination. The carried-out calculations of the required angular spacing on criterion C/I between two randomly chosen systems with identical parameters showed that when using ES with AD presented in [20], the required angular spacing is 3.8 degrees, in [21] – 4.95 degrees and in [22] – 5.6 degrees.

Similarly the increase in space selectivity of the SC onboard antennas on GSO promotes decrease of interference between geostationary satellite systems if their service areas are not overlapped. For this purpose the notified AGC has to repeat the necessary service area as accurately as possible and to degrade quickly beyond its limits.

Accuracy of SC keeping is normalized in RR as $\delta \leq \pm 0.1º$. Such tolerance of SC does not lead to noticeable degradation of a GSO channel capacity when using standard angles of spacing between SCs. Requirements of high accuracy of keeping are still limited by resource opportunities of position correction system of the satellite on GSO therefore when considering effectiveness increase factors of SOR they can be not viewed.

The effect of mutual interference decrease between satellite networks can be reached by using of different polyarizations. It leads to the significant increase in a channel capacity.

The analysis of EMC when sharing SOR satellite systems and technical means of increase in efficiency of GSO use, leads to the conclusion that as an reference parameter defining satellite system aggression from the point of view of creation of interference and requirements for protection it is possible to consider C/N value, the required relation of a signal to thermal noise of a communication link in the lack of interference. The less the required C/N at the invariability of other parameters of satellite systems, the larger SOR efficiency can be reached. The calculations of the required angular spacing on C/I criterion between two randomly chosen systems with identical parameters showed that the decrease in C/N by 0.2 dB leads to the decrease in the required spacing arc by 0.1 degrees. Technically it is possible to reach it due to the choice of optimal signal scrambling and application low-sensitive to interference signals. Besides stimulation of signal interference immunity, the regulator's task is to stimulate the operator to provide data on C/N value close to actual that will give the possibility to clear away the database of the frequency assignments and to simplify coordination.

As discussed above, in the conditions of administrative centralized management by a restricted resource an important role in creation of incentives for SOR efficiency use can play the introduction of a differential fee. A following formula to stimulate SOR efficiency use could be considered:

$$\text{Fee}_{\text{down(up)}} = \sum_{i=1}^{n} \big(C/N_{\max} \cdot \Delta F \cdot K_{sa} \cdot K_{gc} \times$$
$$\times K_{gd} \cdot K_{pl} \cdot K_{es} \cdot C_s)_i, \qquad (3)$$

where $\text{Fee}_{\text{down(up)}}$ – payment for SOR use for one beam, up or down directions; $C/N_{\max}$ – the maximal value of the relation of a signal to the noise for this beam, dB, respectively for the transmitting or receiving beam. The C/N value can be the generalized indicator which is best reflecting assessment of satellite system interference potential and sensibility. The higher the stated C/N, the more is SOR which the system occupies. Besides that this value use will stimulate the operator to introduce more interference-resistant operating modes, it is more important that they will have the economic reasons to make available the data on SOR loading closer to those which are used in practice; ΔF – the frequency bandwidth occupied by one beam, down or up, the Hz; K_{sa} – the coefficient considering the size of service area $K_{sa} = S_{sa}/S_e$, where S_{sa} – the stated service area; S_e – Earth surface area seen from the satellite; K_{gc} – the coefficient considering the AGC SC, $K_{gc} = S_{-3}/S_{sa}$ representing the relation AGC SC of the main beam (–3 dB) S_{-3} to notified service area size S_{sa}; K_{gd} – the coefficient considering contours of power degradation, $K_{gd} = S_{-3}/S_{-20}$ representing the relation of AGC SC size on the contour (-3 dB) to the size of AGC SC on contour (–20 dB) S_{-20}; K_{pl} – the coefficient considering polarization use can be accepted $K_{pl} = 1$ if both types of polarization are used and $K_{pl} = 0.5$ if only one type; K_{es} – the coefficient considering the AD of ES type. On the basis of the explained above reasons and calculations, it is possible to accept $K_{es} = 1$ at application of AD defined in [20], $K_{es} = 1.3$ in [21] and $K_{es} = 1.5$ in [22]; C_g – the monetary value determining the cost of a spectrum resource measure unit, US$ · K/dB · Hz. Determination of this value demands the statistical data analysis related to activities of satellite networks operators for receiving necessary SOR. Introduction of SOR fee does not considerably raise operators expenses, it is necessary to carry out an operators economic benefit assessment in case of the SRS-all database clearing. At the same time it is necessary to consider not only cut in time expenditure and the material resources in carrying out coordination, but potential decrease in risk of investment that was discussed above due to possession of more precise information about SOR use as well. This value has to be different for different ranges, reflecting their current loading and stimulating use of higher, less loaded frequency ranges. The corresponding studying has to be carried out within the research commissions of ITU-R in an attentive dialogue with satellite networks operators. All other required payments for SOR payment definition are obligatory for representation in applications at coordination and registration of satellite networks and are available for all comers registered in SRS-all.

The procedures of unplanned bands description shows that protection of the notified resource starts not from the moment of the actual start of satellite system operation, but from the date of receipt of corresponding coordination request by ITU Radiocommunication Bureau. This date defines date of protection of notified SOR from following applicants. Thus, the payment has to be charged annually for all applications which are registered in SRS-all.

Conclusion

1. The existing international management system of SOR in the conditions of increase in demand for its use does not provide its use efficiency. Implementation of international registration requirements demands considerable resources, raising cost of projects on the development satellite communication and broadcasting networks and, respectively, the risk of investment in their development. All this exerts negative impact on the development of the telecommunication services market and their availability and quality.

2. The management of SOR for satellite communication networks use is based on two procedures: planned and unplanned. The carried-out analysis shows that both of them are not efficient, in most cases without providing realization of the principles which were underlain in their basis.

3. The planned approach is intended to provide equal access to all countries to SOR. The problem of planned distribution of SOR first of all is that national allocations have restrictions of the national territory cover zone. It leads to the fact that for many countries implementation of the satellite project within the resource assigned according to the plan has no economic benefit. The current use of plans is carried out through additional procedures allowing service area expansion by conducting coordination with affected administrations. On the one hand, the systems registered according to such procedure gradually absorb a resource of planned assignments that leads to the fact that their practical use becomes impossible. On the other hand, the administrations trying to receive a resource, which in most cases is not used and it will never be used according to the plan, spend time, financial and human resources, providing paper protection of phantom national assignments and obtaining consent from administrations which own them.

4. The main problems of unplanned frequency bands are paper satellites and paper parameters brought by administrations for protection in the international satellite networks frequency assignments database of MIFR for their subsequent international legal protection. Operators and the administrations which received the registered resource earlier have no incentives to refuse really not used positions, frequency bands and operating modes. On the other hand, due to administrative procedures they have very good potential to considerably complicate competitors life, limiting them in obtaining necessary SOR without any actual technical reason.

5. It is possible to achieve the increase in planned bands efficiency due to replanning, creating conditions for of the market relations development. The planning principles in which in particular the main existing drawback is excluded are offered, the covering of national assignment has to be regional. Terms providing a possibility of trading of rights to use SOR between administrations are offered. At the same time two main advantages of the plan remain – a possibility of providing equal access to SOR and lack of coordination when performing technical restrictions of planned assignment.

6. As the economic method directed to efficient use of SOR it is offered to introduce an annual differential payment for its use for all applications introduced in MIRF. On the basis of the analysis of increase in effectiveness technical methods the formula is developed for such payment definition and recommendations for its components determination are formulated. Technical parameters of satellite networks accounting in the formula will allow to stimulate operators to introduce more efficient in relation to RFS use technologies, and to declare closer parameters to actually used for registration. It will simplify in turn negotiations on coordination and to facilitate access of new satellite systems to invisible but very valuable natural resource.

References

1. Kantor L. Ya. [International registration of satellite communication system as reflection of current international relations]. *Electrosviaz.* 2014, No. 1, P. 12–17 (In Russ.).

2. Kantor L. Ya. [Definition of spectrum/orbit resource, occupied by geostationary satellite communication suystems]. *Electrosviaz*. 2011, No. 10, P. 5–94 (In Russ.).

3. Nozdrin V. V. [Efficient spectrum management: world pactice]. *Electrosviaz.* 2011, No. 10, P. 10–13 (In Russ.).

4. Makarov V. V, Starodubov D. O. [Study of regulatory and economic approaches to spectrum management]. *Trudy mezdunarodnogo simpoziuma Aktual'nye voprosy economiky, menegementa I finansov v sovremennych ysloviiach* [Proc Intl. Sceince. Symp. "Economy, management and finance in modern environment"]. St. Petersburg, 2016, P. 22–25 (In Russ.).

5. Kantor L. Ya., Timofeev V. V. *Sputnikovaia sviaz' i problema geostacionarnoiy orbity.* [Satellite communication and problem of geostationary orbit]. Moscow, Radio i sviaz' Publ., 1988, 167 p.

6. Radio Regulations, Geneva. 2016, P. 465 (In Russ.).

7. Levin H. J. Global claim-staking and latecomer cost in the orbit spectrum resource. Telecommunications Policy. June 1990, P. 450–464.

8. Campbell, Donald. Resource allocation mechanism. Cambridge University Press. 1987, P. 183.

9. Stevenson G. Common property economics. A general theory and land use application. Cambridge University Press, 176 p.

10. Conrad J. Resource Economics. Cambridge University Press. 2010, 285 p.

11. Kantorovich L. V. *Economicheskii raschet nailuchego ispol'zovania resursov* [Economic assessment of resourse best use]. Moscow, Academy of Science Publ., 1960, 134 p. (In Russ.).

12. Walras L. Eleménts d'Economie Politique Pure. Homewood, Irwin, 1954, 38 p.

13. Adhikari B. Literature review on the economics of common property resources. York, 2001, 86 p.

14. Bator F. The Simple analytics of welfare maximization. *American Economic Review.* 1957, Vol. 47, P. 264–286.

15. Ostrom E. The Evolution of Institutions for Collective Action. Cambridge University Press. 1990. 280 p.

16. Makarov V. V., Caturova R. G., Mazurova M. M. et al. *Menegement in telekommunicaciach* [Management in telecommunication]. St. Petersburg, 2011, P. 105–114.

17. Makarov V. V, Starodubov D. O. [Spectrum price as an essential condition for introduction of new services and telecommunication and broadcasting technologies]. *Trudy mezdunarodnogo simpoziuma Aktual'nye voprosy economiky, menegementa I finansov v sovremennych ysloviiach* [Proc Intl. Sceince. Symp. "Economy, management and finance in modern environment"]. St. Petersburg, 2016, P. 52–54 (In Russ.).

18. European Commission Radio Spectrum Policy Group. The RSPG opinion on secondary trading of rights to use radio spectrum. 1 January 2004, 13 p.

19. Kantor L. Ya., Nozdrin V. V. et al. *Electromaggnitnaia sovmestimost'system sputnikovoi svizy*. [Electromagnetic compatibility of satellite communication systems]. Moscow, NIIR Publ., 2009, P. 279.

20. Recommendation ITU-R S.580-5, 12 p.

21. Recommendation ITU-R S.465-5, 14 p.

22. Radio Regulation. Vol. 2, Annex 8. Geneva, 2016, P. 238–239.

Библиографические ссылки

1. Кантор Л. Я. Проблемы международной регистрации систем спутниковой связи как зеркало современных международных отношений // Электросвязь. 2014. № 1. С. 12–17.

2. Кантор Л. Я. Об определении орбитально-частотного ресурса, занятого геостационарной системой спутниковой связи // Электросвязь. 2011. № 10. С. 5–9.

3. Ноздрин В. В. Эффективное управление использованием радиочастотного спектра: мировая практика // Электросвязь. 2011. № 10. С. 10–13.

4. Макаров В. В., Стародубов Д. О. Анализ организационно-экономических подходов к регулированию использования радиочастотного ресурса // Актуальные вопросы экономики, менеджмента и финансов в современных условиях : сб. науч. тр. по итогам междунар. науч.-практич. конф. 2016. С. 22–25.

5. Кантор Л. Я., Тимофеев В. В. Спутниковая связь и проблема геостационарной орбиты. М. : Радио и связь, 1988. 167 с.

6. Radio Regulations. Geneva, 2016. Vol. 1. 430 с.

7. Levin H. J. Global claim-staking and latecomer cost in the orbit spectrum resource. Telecommunications Policy. 1990. С. 450–463.

8. Campbell D. Resource allocation mechanism. Cambridge University Press, 1987. 183 с.

9. Stevenson G. Common property economics. A general theory and land use application. Cambridge University Press, 176 с.

10. Conrad J. Resource Economics. Cambridge University Press, 2010. 285 с.

11. Канторович Л. В. Экономический расчет наилучшего использования ресурсов. М. : Изд-во Академии наук СССР, 1960. 134 с.

12. Walras L. Eleménts d'Economie Politique Pure. Homewood, Irwin, 1954. 38 с.

13. Adhikari B. Literature review on the economics of common property resources. York, 2001, 86 с.

14. Bator F. The Simple analytics of welfare maximization // American Economic Review. 1957. Vol. 47. С. 264–286.

15. Ostrom E. The Evolution of Institutions for Collective Action. Cambridge University Press, 1990. 280 с.

16. Менеджмент в телекоммуникациях / В. В. Макаров [и др.]. СПб., 2011. С. 105–114.

17. Макаров В. В., Стародубов Д. О. Плата за спектр как необходимое условие внедрения новых услуг и технологий связи и телевизионного вещания // Вопросы и проблемы экономики и менеджмента в современном мире : сб. науч. тр. по итогам междунар. науч.-практич. конф. 2016. С. 52–54.

18. European Commission Radio Spectrum Policy Group. The RSPG opinion on secondary trading of rights to use radio spectrum. 2004. 13 с.

19. Электромагнитная совместимость систем спутниковой связи / Л. Я. Кантор [и др.]. М. : НИИР, 2009. 279 с.

20. Recommendation ITU-R S.580-5. 5 с.

21. Recommendation ITU-R S.465-5. 8 с.

22. Radio Regulation. Geneva, 2016. Vol. 2, Annex 8. С. 238–239.

УДК 332.14

Сибирский журнал науки и технологий. 2018. Т. 19, № 1. С. 182–187

СОВЕРШЕНСТВОВАНИЕ ЛОГИСТИЧЕСКОЙ СИСТЕМЫ ПРОИЗВОДСТВЕННОГО ПРЕДПРИЯТИЯ

Н. А. Орлова[1*], Т. А. Шиндина[2]

[1]Южно-Уральский государственный университет (национальный исследовательский университет)
Российская Федерация, 454080, г. Челябинск, просп. Ленина, 76
[2]Национальный исследовательский университет «Московский энергетический институт»
Российская Федерация, 111250, г. Москва, ул. Красноказарменная, 14
[*]E-mail: orlova.nina.a@mail.ru

На сегодняшний день проблемы логистики остаются актуальными, успешное функционирование любой организации, ее конкурентоспособность напрямую зависят от грамотного построения логистической системы предприятия. В России и за рубежом существуют различные институты, цель которых – применение научного потенциала логистики на практике.

Рассматриваются возможности совершенствования логистической системы промышленных предприятий, основываясь на мировом опыте и учитывая рейтинги стран по индексу развития логистики.

Приведен пример совершенствования предприятия, имеющего в своем составе отделы снабжения, складского хранения, транспортные отделы. Положительными эффектами от использования информационной системы в качестве основы управления логистическими потоками внутри предприятия рассматриваются регламентация процесса приемки, получения и хранения МТЦ, стандартизация процесса передачи информации между подразделениями, получение актуальной информации в короткий срок, определение границ ответственности участников процесса, повышение уровня автоматизации процессов приемки, размещения и хранения МТЦ, сокращение влияния человеческого фактора, сокращение временных потерь, сокращение бумажного документооборота.

Ключевые слова: логистика, логистическая система, информационные системы в логистике, логистика на производственном предприятии.

Siberian Journal of Science and Technology. 2018, Vol. 19, No. 1, P. 182–187

IMPROVEMENT OF THE LOGISTIC SYSTEM OF A MANUFACTURING COMPANY

N. A. Orlova[1*], T. A. Shindina[2]

[1]South Ural State University (national research university)
76, Lenin Av., Chelyabinsk, 454080, Russian Federation
[2]National Research University “Moscow Power Engineering Institute”
14, Krasnokazarmennaya Str., Moscow, 111250, Russian Federation
[*]E-mail: orlova.nina.a@mail.ru

Nowadays logistics problems remain relevant. A successful operation of any organization and its competitiveness directly depend on the competent construction of a logistics system of an enterprise. In Russia and abroad there are various institutions whose purpose is to apply the scientific potential of logistics in practice.

The article considers the possibilities of improving the logistics system of industrial enterprises, based on the world experience and taking into account the countries’ ratings on the index of logistics development.

The article gives an example of improvement for the enterprise that has in its composition supply departments, warehouse storage, and transport departments. The positive effects of the use of the information system as the basis for the management of logistical flows within the enterprise are considered: the regulation of the ITC acceptance, receipt and storage process, the standardization of information transfer between units, the receipt of up-to-date information in a short time, the definition of the boundaries of the process participants' responsibility, placement and storage of ITC, reduction of human factor influence, reduction of time losses , reduction of paperwork.

Keywords: logistics, logistic system, information systems in logistics, logistics and production companies.

Введение. На сегодняшний день проблемы логистики остаются актуальными, успешное функционирование любой организации, ее конкурентоспособность напрямую зависят от грамотного построения логистической системы предприятия. В России и за рубежом существуют различные институты, цель которых – применение научного потенциала логистики на практике. Например, в США работает Американское общество транспорта и логистики, в Великобритании – Институт логистики и управления дистрибуцией, в Испании – Центр логистики и многие другие, все они входят в Европейскую логистическую ассоциацию. Кроме того, вопросы логистики широко освещаются в таких изданиях, как Production and Inventory Management, Inbound Logistics, Distribution, International Journal of Logistics Management и многих других. Основную идею современной логистики выразил Martin Ashford, Deloitte & Touche. American Shipper: «Одной из основных характеристик новой нарождающейся экономики будет полностью ориентированное на конкретного потребителя производство “по заказу”. Спрос потребителей на товар “по заказу” привел уже к практике поставок “точно вовремя”. Логистика гарантирует, что Вы получите нужный продукт в нужном месте в нужное время по “правильной” цене».

Логистика объединяет снабжение, хранение, производство, сбыт в один процесс. При этом функции логистики на предприятии включают в себя анализ потребности в материальных ресурсах для обеспечения нужд производства, прогнозирование спроса на продукцию, сбор данных о потребности рынка. Логистика на предприятии также должна рассматривать вопросы оперативного планирования, что подразумевает сокращение запасов при должном уровне производственной и сбытовой эффективности предприятия [1; 2; 4].

Актуальность и степень проработанности проблемы. С целью изучения способов совершенствования логистической системы производственного предприятия изучим мировой опыт в этом вопросе с помощью рейтинга Logistics Performance Index, определяющего индекс развития транспортно-логистического комплекса страны на основе развития национальной таможенной системы международных перевозок, нормативно-правового регулирования логистической деятельности, уровня оказания логистических услуг, эффективности таможенного оформления, возможности отслеживания и контроля грузов. Рейтинг стран по 5-балльной шкале публикуется на сайте Всемирного банка. Рейтинг рассчитывается каждые два года и насчитывает около ста шестидесяти стран. Топ 10 стан по индексу эффективности логистики в 2014–2016 годах занимают преимущественно Европейские страны. Первое место занимает Германия, рейтинг которой составляет 4,23 балла, Люксембург – 2 место, с баллом 4,22 [3]. Для Европейских стран характерна развитость транспортно-логистической инфраструктуры, инновации в информационную систему и технологические схемы логистики. Инновации информационной системы логистики включают в себя формирование баз данных и коммуникационных систем логистики, позволяющих управлять материальными потоками, систем контроля и дистанционного мониторинга качества выполнения операций на разных звеньях логистической системы [5]. Современные европейские предприятия делают упор на удовлетворение растущих потребностей потребителя и предотвращение дополнительных расходов, с этим связанных, за счет оптимального размещения складских помещений, рационализации транспортных маршрутов (выбор наиболее оптимальных путей доставки), применения информационных технологий, оптимальной величины партий продукции, совершенствования систем складирования, погрузочно-разгрузочных операций. Кроме того, современные предприятия предлагают ряд сервисных услуг логистического характера, таких как дополнительная складская обработка, тарировка, консолидация. Китай, занимающий 27 место в рейтинге LPI с баллом 3,66, имеет лидирующие позиции в Азиатско-Тихоокеанском регионе. На сегодняшний день там сформировались четыре центра логистики: логистическое кольцо вокруг Пекина, Шанхай, Гуанчжоу и Шеньчжэнь, Тайванский пролив. Процесс развития логистических возможностей Китая связан с приобретением опыта иностранных логистических компаний, действующих на территории страны, а также за счет внедрения передовых информационных технологий, повышения уровня автоматизации и информатизации логистики, применения инновационных технологий. Опыт стран Западной Европы и Азиатского региона показывает, что развитие логистической сферы основывается на существующем уровне производительных сил в стране, уровне развития рыночных отношений, традициях стран, политической, экономической обстановке, уровне технологического развития [3].

Россия же находится на 99 месте, с индексом 2,37 балла. Эксперты связывают это с нестабильным экономическим, политическим положением, экономическим кризисом, санкциями против Российской Федерации, кроме того, проблемой для России остается низкая эффективность процесса таможенного оформления. Кроме того, Россия имеет низкий рейтинг по срокам поставок товаров. Однако в настоящее время наметилась положительная тенденция в сфере повышения эффективности логистических систем. Активно развиваются межрегиональные транспортные компании, происходит модернизация логистики ФГУП Почта России, ведется строительство платных автомобильных дорог, строятся порты-хабы, крупные логистические комплексы по предоставлению логистических услуг. Таким образом, формированию логистической системы в России может способствовать применение международного опыта внедрения логистических моделей с учетом собственных реалий. По сообщению совместного комитета по логистике Торгово-промышленной палаты России компании активно внедряют информационные технологии в бизнес, в том числе в логистическую сферу, что позволило сократить затраты на перевозки [5–7]. Однако эксперты отмечают, что использование информационных технологий, т. е. программного обеспечения, возможно только тогда, когда оно адаптировано к конкретной организации и доработано ее специалистами.

Методология исследования. Нами проводилось исследование логистической системы производственного предприятия, которое пользуется ERP-системой «Альфа» – интегрированной системой управления, координирующей работу ресурсами предприятия, логистикой и цепями поставок, управление производством.

В ходе составления карты потока материальных ценностей методом применения мозгового штурма были выявлены следующие проблемы, способствующие накоплению материально-технических ценностей на складах отдела складского хранения предприятия:

1. Отсутствует стандарт передачи информации между подразделениями о приходе и приемке товарно-материальных ценностей, информация либо не доходит до конечного потребителя, либо является неактуальной. В процессе передачи информации не используются или используются в небольшой степени информационные системы, программы предприятия. В большом объеме присутствует бумажный документооборот.

2. Отсутствует централизованное управление логистикой предприятия, каждый отдел работает обособленно, выполняя свои конкретные цели. Нет координации процесса перемещения грузов по всей цепочке поставок.

Результаты работы. В ходе проведения исследования была разработана схема приемки (рис. 1), размещения и хранения материально-технических ценностей (МТЦ), которая поможет отделу складского хранения, подразделению (далее – Экспедиция) и управлению закупок решить вышеизложенные проблемы. На схеме показано, что информационная система, получив указание от управления закупок о прибытии грузов, предоставляет информацию в Экспедицию, отдел складского хранения, управление автомобильного транспорта и подразделения-заказчики об ожидаемом времени прибытия груза. Экспедиция нанимает машину в управлении автотранспорта (УАТ), может заранее спрогнозировать объемы поставки, количество грузов, определить потребности в транспорте, тем самым экономя время на погрузочно-разгрузочные операции и избегая складирования грузов. Экспедиция сообщает посредством информационной системы о количестве груза, срочности, дает информацию на склады, какой склад и какой груз ждет. Склады сообщают подразделениям, группа приемки сообщает в управление закупок о получении грузов, вопросы и проблемы решаются без потери времени. Груз выдается в подразделения, исходя из заранее сформированной в системе заявки, транспорт под груз заказан в УАТ. Таким образом, происходит экономия времени приемки товаров и получения конечным пользователем.

На рис. 2 представлена модель процесса управления закупками. Модель построена на основе процессного подхода («вход–сырье», «выход – продукт промышленного назначения»), что позволяет координировать процесс управления закупками.

Новизна данной модели состоит в том, что был доработан и выделен блок в структуре, который обеспечивается аутсорсингом – привлечением консультантов на специализированные проекты.

Подсистема оперативного управления закупками получает от стратегического управления (этап 1) первоначальные и откорректированные планы приобретения и использования внешних ресурсов и критерии формирования производственного заказа (потоки «Заявки», «Предварительные графики»).

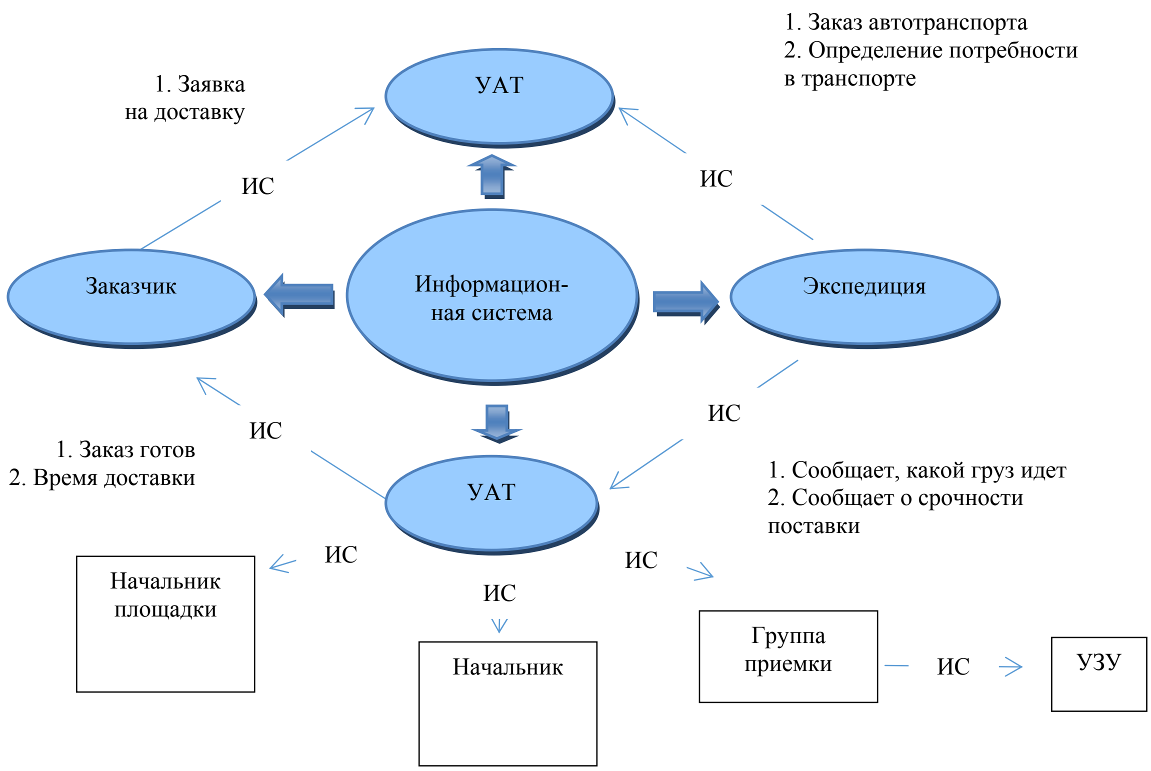

Рис. 1. Приемка, размещение и хранение МТЦ, координируемые информационной системой: УАТ – управление транспортом; ИС – информационная система; УЗУ – управление закупок

Fig. 1. Acceptance, distribution and ITC storage, coordinated by the informational system

В свою очередь, подсистема оперативного управления (этап 2) с определенной периодичностью направляет в подсистему стратегического управления отчетные данные о состоянии ресурсов и выпуске продукции, которые используются для осуществления стратегического контроля и стратегического регулирования закупок в логистической системе.

Данная модель укрупненно состоит из двух этапов. На первом этапе (рис. 3) выявляется потребность в материалах и комплектующих согласно плану выпуска продукции. На данном этапе анализируется внешняя информация от поставщиков, определяются предварительные графики потребности в закупке необходимых материалов и комплектующих с учетом существующих нормативов, осуществляется пролонгация договора с поставщиками в результате проведения мониторинга выполнения условий договоров по срокам, ценам, количеству, качеству и другим параметрам поставок и необходимого для них сервиса, а также ведется поиск новых поставщиков, если в этом есть необходимость.

Вся поступающая рыночная информация (прогнозы цен на ресурсы, величина инфляции, спрос на продукцию промышленного на значения и т. д.) обрабатывается в планово-экономическом отделе, где и разрабатывается впоследствии алгоритм формирования оптимальной производственной программы, проводятся соответствующие экономические расчеты для выявления общих затрат на осуществление всех операций.

В соответствии с утвержденным планом поставок на втором этапе (рис. 4) решаются вопросы складирования, транспортировки материалов и комплектующих внутри предприятия (в производственные цеха, вспомогательные подразделения предприятия) на основании документов, регламентирующих эти сферы деятельности, а также определяются временные интервалы их поступления на склад и частота поставок.

Заключение. Координация действий и взаимосвязь между всеми подразделениями предприятия, установление деловых отношений с поставщиками и потребителями обеспечивают введение предприятия в единую макрологистическую систему, а также экономический, производственный и организационный эффекты.

Положительными эффектами от использования информационной системы в качестве основы управления логистическими потоками внутри предприятия можно назвать регламентацию процесса приемки, получения и хранения МТЦ, стандартизацию процесса передачи информации между подразделениями, получение актуальной информации в короткий срок, определение границ ответственности участников процесса, повышение уровня автоматизации процессов приемки, размещения и хранения МТЦ, сокращение влияния человеческого фактора, сокращение временных потерь, сокращение бумажного документооборота. В процессе мозгового штурма также была предложена идея выделения отдельного подразделения логистики предприятия, так как увеличиваются объемы перевозок как по стране, так и за рубежом, присутствует необходимость четкой координации движения материальных ценностей как на предприятии, так и от поставщиков.

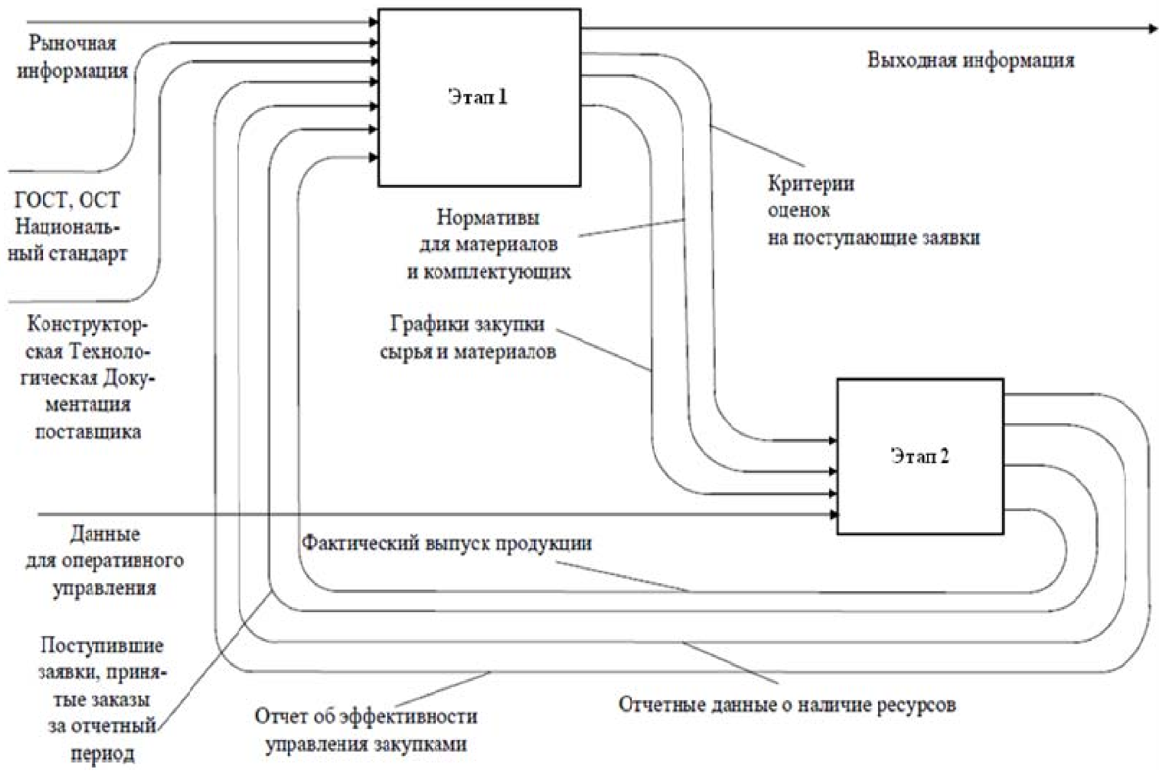

Рис. 2. Модель процесса управления закупками

Fig. 2. Model of the process of purchasing management

Рис. 3. Первый этап модели процесса управления закупками

Fig. 3. The 1st stage of the model of the process of purchasing management

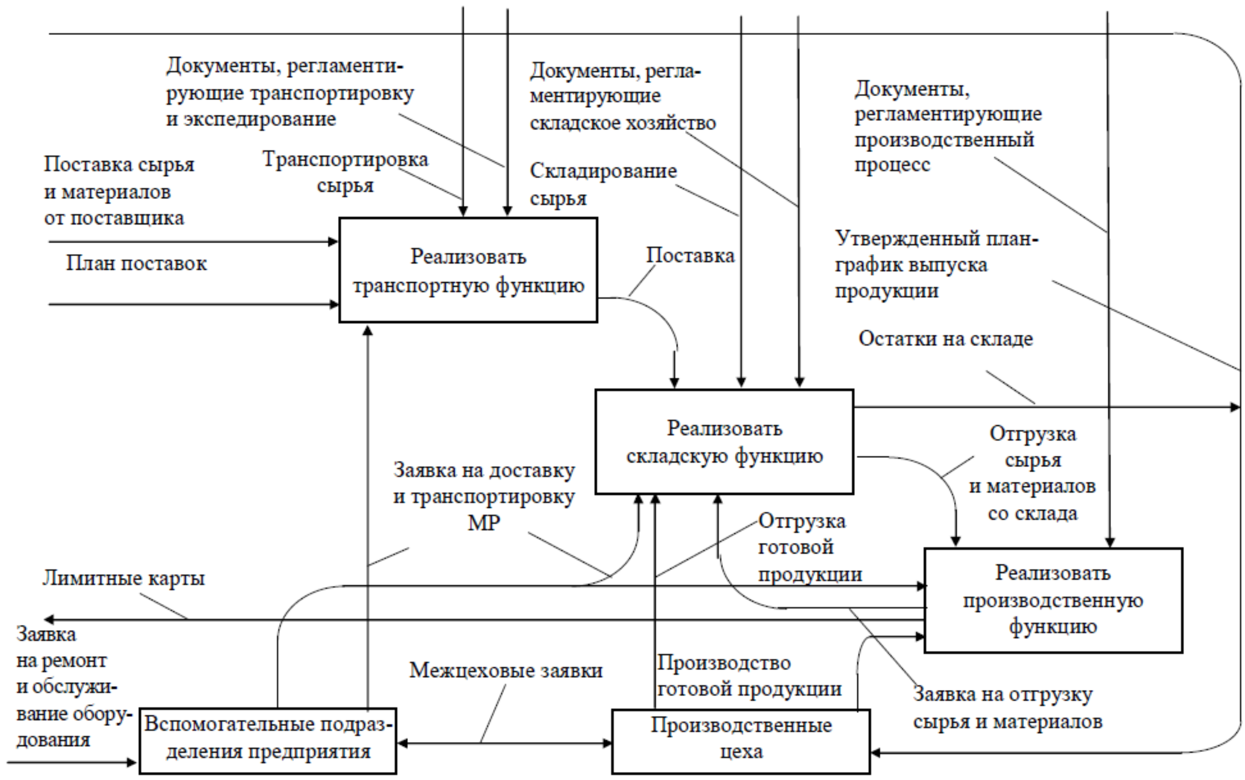

Рис. 4. Второй этап модели процесса управления закупками

Fig. 4. The 2nd stage of the model of the process of purchasing management

Библиографические ссылки

1. Рыкалина О. В. Теория и методология современной логистики : монография. М. : Инфра-М, 2018.
2. Чернова Д. В. Стратегическая логистика сетевой экономики : монография. М. : Креативная экономика, 2005. 144 с.
3. Международный глобальный рейтинг [Электронный ресурс]. URL: https://lpi.worldbank.org/international/global.
4. Старкова Н. О., Сафонова М. В. Тенденции развития логистических услуг на современном мировом рынке // Политематический сетевой электронный научный журнал Кубанского государственного аграрного университета. Краснодар, 2013. С. 480–490.
5. Старков И. С., Старкова Н. О. Моделирование процесса управления изменениями в информационной системе предприятия // Вестник Ростовского государственного университета (РИНХ). Ростов н/Д., 2008. С. 153–157.
6. Рзун И. Г., Успенский А. В., Старкова Н. О. Исследование зарубежного опыта формирования логистических систем // Научный журнал Кубанского университета. Краснодар, 2014. С. 2–12.
7. Степанов Е. А., Шиндина Т. А. Специфика таможенно-логистических механизмов в системе внешней торговли России // Вестник Красноярского государственного педагогического университета им. В. П. Астафьева. 2014. № 4. С. 12–17.

References

1. Rykalina O. V. *Teoriya i metodologiya sovremennoy logistiki* [Theory and methodology of modern logistics]. Moscow, Infra-M Publ., 2018.
2. Chernova D. V. *Strategicheskaya logistika setevoy ekonomiki* [Strategic logistics of the network economy]. Moscow, Kreativnaya ekonomika Publ., 2005, 144 p.
3. *Mezhdunarodnyy global'nyy reyting* [International global rating]. Available at:https://lpi.worldbank.org/international/global (accessed: 12.02.2018).
4. Starkova N. O., Safonova M. V. [Trends in the development of logistics services in the modern world market]. *Politematicheskiy setevoy elektronnyy nauchnyy zhurnal Kubanskogo gosudarstvennogo agrarnogo universiteta.* 2013. P. 480–490 (In Russ.).
5. Starkov I. S, Starkova N. O. [Modeling the process of change management in the enterprise information system]. *Vestnik Rostovskogo Gosudarstvennogo Universiteta (RINKh)*. 2008. P. 153–157 (In Russ.).
6. Rzun I. G., Uspensky A. V., Starkova N. O. [Investigation of foreign experience in the formation of logistics systems]. *Nauchnyy zhurnal Kubanskogo universiteta.* 2014. P. 2–12 (In Russ.).
7. Stepanov E. A., Shindina T. A. [Specificity of customs-logistical mechanisms in the system of foreign trade of Russia]. *Vestnik Krasnoyarskogo gosudarstvennogo pedagogicheskogo universiteta im. V. P. Astaf'eva.* 2014, Vol. 4, P. 12–17 (In Russ.).

СВЕДЕНИЯ ОБ АВТОРАХ

Анистратенко Николай Евгеньевич – аспирант кафедры конструкторско-технологического обеспечения машиностроительного производства, Политехнический институт, Сибирский федеральный университет.

Баляков Дмитрий Федорович – инженер второй категории отдела анализа конструкции космических аппаратов по прочности и динамике, АО «Информационные спутниковые системы» имени академика М. Ф. Решетнева»; аспирант, Сибирский государственный университет науки и технологий имени академика М. Ф. Решетнева. E-mail: d-bolyakov@iss-reshetnev.ru.

Бикеев Егор Вячеславович – инженер-конструктор 2 категории, АО «Информационные спутниковые системы» имени академика М. Ф. Решетнева». E-mail: bikeev@iss-reshetnev.ru.

Бинчуров Александр Сергеевич – аспирант кафедры конструкторско-технологического обеспечения машиностроительного производства, Политехнический институт, Сибирский федеральный университет.

Бирюков Василий Иванович – профессор, доктор технических наук, Московский авиационный институт (национальный исследовательский университет). E-mail: aviatex@mail.ru.

Вагапова Наргиза Тухтамышевна – кандидат химических наук, ведущий научный сотрудник, АО «Научно-производственное предприятие «Квант». E-mail: otd_17@npp.kvant.

Вадимов Владимир Николаевич – инженер-конструктор 2 категории, АО «Информационные спутниковые системы» имени академика М. Ф. Решетнева». E-mail: Vladimir-vadimov@mail.ru.

Васильев Евгений Николаевич – кандидат физико-математических наук, старший научный сотрудник, Красноярский научный центр СО РАН; Институт вычислительного моделирования СО РАН. E-mail: ven@icm.krasn.ru.

Власова Галина Александровна – старший преподаватель кафедры экономики и управления на предприятиях строительства и землеустройства, Высшая школа экономики и управления, Южно-Уральский государственный университет (национальный исследовательский университет). E-mail: galina-v89@mail.ru.

Газизов Тальгат Рашитович – доктор технических наук, профессор кафедры телевидения и управления, Томский государственный университет систем управления и радиоэлектроники. E-mail: talgat@tu.tusur.ru.

Генали Марина Александровна – старший научный сотрудник, АО «Научно-производственное предприятие «Квант». E-mail: marinagenali@gmail.com.

Гордеев Юрий Иванович – кандидат технических наук, доцент кафедры конструкторско-технологического обеспечения машиностроительного производства, Политехнический институт, Сибирский федеральный университет. E-mail: tms-mtf@rambler.ru.

Гришанов Александр Николаевич – соискатель кафедры прочности летательных аппаратов, Новосибирский государственный технический университет. E-mail: a_grishanov@ngs.ru.

Дементьев Александр Александрович – кандидат физико-математических наук, инженер-конструктор II категории, АО «Научно-производственный центр «Полюс». E-mail: daa024@mail.ru.

Ереско Сергей Павлович – доктор технических наук, член-корреспондент Академии наук Высшей школы РФ; профессор, Институт машиноведения и мехатроники, кафедра основ конструирования машин, Сибирский государственный университет науки и технологий имени академика М. Ф. Решетнева. E-mail: ereskosp@mail.sibsau.ru.

Ереско Татьяна Трофимовна – доктор технических наук, доцент, Институт машиноведения и мехатроники, заведующий кафедрой основ конструирования машин, Сибирский государственный университет науки и технологий имени академика М. Ф. Решетнева. E-mail: ereskott@mail.ru.

Жалнин Борис Викторович – кандидат физико-математических наук, начальник отдела; АО «Научно-производственное предприятие «Квант». E-mail: otdel_17@kvant.ru.

Заболоцкий Александр Михайлович – доктор технических наук, профессор кафедры телевидения и управления, Томский государственный университет систем управления и радиоэлектроники. E-mail: zabolotsky_am@mail.ru.

Кадлец Иржи – инженер, кандидат технических наук, начальник отдела обработки сигналов, Институт теории информации и автоматизации. Академия наук Чешской Республики. E-mail: kadlec@utia.cas.cz.

Калабегашвили Георгий Ильич – инженер-конструктор 3 категории, АО «Информационные спутниковые системы» имени академика М. Ф. Решетнева». E-mail: oakheart@iss-reshetnev.ru.

Князева Нина Владимировна – старший преподаватель кафедры экономики и управления на предприятиях строительства и землеустройства, Высшая школа экономики и управления, Южно-Уральский государственный университет (национальный исследовательский университет). E-mail: nv_knyazeva@mail.ru.

Когоут Лукаш – инженер, научный сотрудник, Институт теории информации и автоматизации. Академия наук Чешской Республики. E-mail: kohoutl@utia.cas.cz.

Коловский Игорь Константинович – инженер 2 категории, АО «Информационные спутниковые системы» имени академика М. Ф. Решетнева». E-mail: kolovigor@mail.ru.

Кретинин Василий Васильевич – аспирант, Сибирский государственный университет науки и технологий имени М. Ф. Решетнева. E-mail: kret_vas@mail.ru.

Кукушкин Евгений Владимирович – ассистент кафедры основ конструирования машин, Институт машиноведения и мехатроники, Сибирский государственный университет науки и технологий имени академика М. Ф. Решетнева. E-mail: ironjeck@mail.ru.

Кургузов Алексей Вячеславович – аспирант кафедры ракетных двигателей, Московский авиационный институт (национальный исследовательский университет). E-mail:mandigit@yandex.ru

Лебедев Андрей Александрович – старший научный сотрудник, АО «Научно-производственное предприятие «Квант»; инженер второй категории кафедры физической химии, Национальный исследовательский технологический университет «МИСиС». E-mail: otd_17@npp.kvant.

Лихонина Раиса Николаевна – инженер, аспирант, Институт теории информации и автоматизации. Академия наук Чешской Республики. E-mail: likhonina@utia.cas.cz.

Макаров Владимир Васильевич – доктор экономических наук, профессор, заслуженный деятель науки РФ, заведующий кафедры экономики и менеджмента инфокоммуникаций, Санкт-Петербургский государственный университет телекоммуникаций имени профессора М. А. Бонч-Бруевича.

Мартюшев Семен Григорьевич – кандидат физико-математических наук, ведущий инженер-конструктор, АО «Научно-производственный центр «Полюс».

Масюгин Альберт Николаевич – аспирант, Сибирский государственный университет науки и технологий имени академика М. Ф. Решетнева. E-mail: albert.masyugin@mail.ru.

Матвеев Александр Данилович – кандидат физико-математических наук, доцент, старший научный сотрудник, Институт вычислительного моделирования СО РАН. E-mail: mtv@icm.krasn.ru

Матыленко Михаил Геннадьевич – заместитель начальника отдела, АО «Информационные спутниковые системы» имени академика М. Ф. Решетнева». E-mail: mathylenko@iss-reshetnev.ru.

Медведев Александр Васильевич – доктор технических наук, профессор кафедры системного анализа и исследования операций, Сибирский государственный университет науки и технологий имени академика М. Ф. Решетнева. E-mail: saor_medvedev@sibsau.ru.

Меновщиков Владимир Александрович – доктор технических наук, профессор, профессор кафедры основ конструирования машин, Институт машиноведения и мехатроники, Сибирский государственный университет науки и технологий имени академика М. Ф. Решетнёва. E-mail: menovchikovva@mail.sibsau.ru.

Назаров Владимир Павлович – кандидат технических наук, профессор, заведующий кафедрой двигателей летательных аппаратов, Сибирский государственный университет науки и технологий имени академика М. Ф. Решетнева. E-mail: nazarov@sibsau.ru.

Наумова Анастасия Александровна – научный сотрудник, АО «Научно-производственное предприятие «Квант». E-mail: otdel_17@kvant.ru.

Ноздрин Вадим Викторович – кандидат экономических наук, советник исследовательских комиссий, Бюро радиосвязи, Международный союз электросвязи. E-mail: vadim.nozdrin@itu.int.

Орлова Нина Александровна – кандидат экономических наук, доцент кафедры экономики и управления на предприятиях строительства и землеустройства, Высшая школа экономики и управления, Южно-Уральский государственный университет (национальный исследовательский университет). E-mail: orlova.nina.a@mail.ru.

Подолякин Владимир Никифорович – кандидат технических наук, ведущий инженер, АО «Информационные спутниковые системы» имени академика М. Ф. Решетнева».

Рыбина Ульяна Ильинишна – студент, Сибирский государственный университет науки и технологий имени академика М. Ф. Решетнева.

Рыжкова Светлана Михайловна – начальник бюро отдела технического контроля, АО «Информационные спутниковые системы» имени академика М. Ф. Решетнева». E-mail: OTK5@iss-reshetnev.ru.

Ситников Максим Николаевич – кандидат физико-математических наук, доцент кафедры физики, Сибирский государственный университет науки и технологий имени академика М. Ф. Решетнева. E-mail: kineru@mail.ru.

Слыщенко Евгений Виталиевич – заместитель начальника отдела, АО «Научно-производственное предприятие «Квант»; инженер первой категории кафедры наноструктурных преобразователей энергии, Национальный исследовательский технологический университет «МИСиС». E-mail: otdel_17@kvant.ru.

Тихомирова Ирина Сергеевна – инженер по качеству 2 категории, АО «Информационные спутниковые системы» имени академика М. Ф. Решетнева». E-mail: mis88_88@mail.ru.

Хажибеков Роман Русланович – магистрант кафедры телевидения и управления, Томский государственный университет систем управления и радиоэлектроники, инженер, научно-исследовательская лаборатория «Безопасность и электромагнитная совместимость радиоэлектронных средств». E-mail: r300994@mail.ru.

Харьков Антон Михайлович – кандидат физико-математических наук, доцент кафедры физики, Сибирский государственный университет науки и технологий имени академика М. Ф. Решетнева. E-mail: khark.anton@mail.ru.

Шаров Сергей Константинович – кандидат химических наук, главный технолог, АО «Научно-производственное предприятие «Квант». E-mail: otdel_17@kvant.ru.

Шаура Александр Сергеевич – кандидат технических наук, инженер-программист 2 категории, ООО «ИРЗ». E-mail: shauraa@mail.ru.

Шерстенникова Гульнара Нуршаеховна – инженер-конструтор 2 категории, ООО «ИРЗ». E-mail: vakilova@irz.ru.

Шиндина Татьяна Александровна – доктор экономических наук, доцент, профессор кафедры экономики предприятий электроэнергетики, директор Института дистанционного и дополнительного образования, Национальный исследовательский университет «Московский энергетический институт». E-mail: shindina@74.ru.

Шмаков Дмитрий Николаевич – ведущий инженер, АО «Информационные спутниковые системы» имени академика М. Ф. Решетнева».

Ярещенко Дарья Игоревна – старший преподаватель кафедры интеллектуальных систем управления, Институт космических и информационных технологий, Сибирский федеральный университет. E-mail: YareshenkoDI@yandex.ru.

Ясинский Виталий Брониславович – кандидат технических наук, доцент кафедры конструкторско-технологического обеспечения машиностроительного производства, Политехнический институт, Сибирский федеральный университет. E-mail: VYasinskiy@sfu-kras.ru.

INFORMATION ABOUT THE AUTHORS

Anistratenko Nikolay Evgenievich – postgraduate student, Department of Design-engineering ensuring machine-building production, Polytechnic Institute of Siberian Federal University.

Balyakov Dmitry Fedorovich – the 2nd category engineer, Department of Space craft construction on strength and dynamic analyses, JSC “Academician M. F. Reshetnev “Information Satellite Systems”; postgraduate student, Reshetnev Siberian State University of Science and Technologies. E-mail: d-bolyakov@iss-reshetnev.ru.

Bikeev Egor Vyacheslavovich – the 2nd category design engineer, JSC “Academician M. F. Reshetnev “Information Satellite Systems”. E-mail: bikeev@iss-reshetnev.ru.

Binchurov Aleksandr Sergeevich – postgraduate student, Department of Design-engineering ensuring machine-building production, Polytechnic Institute of Siberian Federal University. E-mail: mexanixs@mail.ru.

Birukov Vasiliy Ivanovich – professor, Dr. Sc., Moscow Aviation Institute (National Research University). E-mail: aviatex@mail.ru.

Dement’ev Aleksandr Aleksandrovich – Cand. Sc., the 2nd category engineer, JSC “Scientific and Industrial centre “Polyus”. E-mail: daa024@mail.ru.

Eresko Sergey Pavlovich – Dr. Sc., corresponding member of Academy of Science of Higher Education Institutions of the Russian Federation, professor, Institute of Mechanical Science and Mechatronics, Department of Principle of machine construction, Reshetnev Siberian State University of Science and Technology**.** E-mail: ereskosp@mail.sibsau.ru.

Eresko Tatyana Trofimovna – Dr. Sc., Docent, Institute of Mechanical Science and Mechatronics, head of Department of Principle of machine construction, Reshetnev Siberian State University of Science and Technology. E-mail: ereskott@mail.ru.

Gazizov Talgat Rashitovich – Dr. Sc., professor of Department of Television and Control, Tomsk State University of Control Systems and Radioelectronics. E-mail: talgat@tu.tusur.ru.

Genali Marina Aleksandrovna – senior research scientist, JSC “Research and Production Enterprise “Kvant”. E-mail: marinagenali@gmail.com.

Gordeev Yuri Ivanovic – Cand. Sc., Docent, Department of Design-engineering ensuring machine-building production, Polytechnic Institute of Siberian Federal University. E-mail: tms-mtf@rambler.ru.

Grishanov Alexandr Nikolaevich – competitor, Department of Aircrafts strength, Novosibirsk State Technical University. E-mail: a_grishanov@ngs.ru**.**

Jasinski Vitaly Bronislavovich – Cand. Sc., Docent, Department of Design-engineering ensuring machine-building production, Polytechnic Institute of Siberian Federal University. E-mail: VYasinskiy@sfu-kras.ru.

Kadlec Jiří – engineer, Cand. Sc., head of the signal processing department, the Czech Academy of Sciences, Institute of Information Theory and Automation. E-mail: kadlec@utia.cas.cz.

Kalabegashvili Georgi Ilyich – the 3d category design engineer, JSC “Academician M. F. Reshetnev “Information Satellite Systems”. E-mail: oakheart@iss-reshetnev.ru.

Kharkov Anton Mikhailovich – Cand. Sc., Docent, Department of Physics, Reshetnev Siberian State University of Science and Technology. E-mail: khark.anton@mail.ru.

Khazhibekov Roman Ruslanovich – Master’s Degree student, Department of Television and Control, Tomsk State University of Control Systems and Radioelectronics; engineer of the research laboratory “Safety and Electromagnetic Compatibility of Radioelectronic Facilities”. E-mail: r300994@mail.ru.

Knyazeva Nina Vladimirovna – senior teacher of Department of Economics and Management at the enterprises of construction and land management, Higher School of Economics and Management, South Ural State University (National Research University). E-mail: nv_knyazeva@mail.ru.

Kohout Lukáš – engineer, scientific researcher, the Czech Academy of Sciences, Institute of Information Theory and Automation. E-mail: kohoutl@utia.cas.cz.

Kolovsky Igor Konstantinovich – the 2nd category engineer, JSC “Academician M. F. Reshetnev “Information Satellite Systems”. E-mail: kolovigor@mail.ru.

Kretinin Vasilii Vasilievich – postgraduate student, Reshetnev Siberian State University of Science and Technology. E-mail: kret_vas@mail.ru.

Kukushkin Evgeny Vladimirovich – assistant of Department of Principle of machine construction, Institute of Mechanical Science and Mechatronics, Reshetnev Siberian State University of Science and Technology. E-mail: ironjeck@mail.ru.

Kurguzov Alexey Vyacheslavovich – postgraduate student of the Department of Missile Engines, Moscow Aviation Institute (National Research University).E-mail: mandigit@yandex.ru

Lebedev Andrey Alexandrovich – senior research scientist, JSC “Research and Production Enterprise “Kvant”; the 2nd category engineer, Department of Physical Chemistry, National Research Technological University “MISIS”. E-mail: otdel_17@kvant.ru.

Likhonina Raissa Nikolaevna – engineer, postgraduate student, the Czech Academy of Sciences, Institute of Information Theory and Automation. E-mail: likhonina@utia.cas.cz.

Makarov Vladimir Vasilevich – Dr. Sc., professor, honored scientist of Russia, head of Department of Economics and Managements in Communication**,** The Bonch-Bruevich Saint-Petersburg State University of Telecommunications.

Martyushev Semen Grigor'evich – Cand. Sc., leading design engineer, JSC "Scientific and Industrial centre "Polyus".

Masyugin Albert Nikolaevich – postgraduate student, Reshetnev Siberian State University of Science and Technology. E-mail: albert.masyugin@mail.ru.

Mathylenko Mikhail Gennadyevich – deputy head of department, JSC "Academician M. F. Reshetnev "Information Satellite Systems". E-mail: mathylenko@iss-reshetnev.ru.

Matveev Aleksandr Danilovich – Cand. Sc., Docent, senior researcher, Institute of Computational Modelling SB RAS. E-mail: mtv@icm.krasn.ru.

Medvedev Alexander Vasilievich – Dr. Sc., professor of Department of System Analysis and Operations Research, Reshetnev Siberian State University of Science and Technology. E-mail: saor_medvedev@sibsau.ru.

Menovschikov Vladimir Alexandrovich – Dr. Sc., professor of Department of Principle of machine construction, Institute of Mechanical Science and Mechatronics, Reshetnev Siberian State University of Science and Technology. E-mail: menovchikovva@mail.sibsau.ru.

Naumova Anastasia Alexandrovna – researcher, JSC "Research and Production Enterprise "Kvant". E-mail: otdel_17@kvant.ru.

Nazarov Vladimir Pavlovich – Cand. Sc., professor, head of Department of Aircraft Engines, Reshetnev Siberian State University of Science and Technology. E-mail: nazarov@sibsau.ru.

Nozdrin Vadim Viktorovich – Cand. Sc., study group counselor, Radiocommunication Bureau, International Telecommunication Union. E-mail: vadim.nozdrin@itu.int.

Orlov Aleksandr Aleksandrovich – postgraduate student, Department of Fundamentals of machine design, Institute of Mechanical Engineering and Mechatronics, Reshetnev Siberian State University of Science and Technology. E-mail: ironjeck@mail.ru.

Orlova Nina Aleksandrovna – Cand. Sc., Docent, Department of Economics and Management at the enterprises of construction and land management, Higher School of Economics and Management, South Ural State University (National Research University). E-mail: orlova.nina.a@mail.ru.

Podolyakin Vladimir Nikiforovich – Cand. Sc., leading engineer, JSC "Academician M. F. Reshetnev "Information Satellite Systems".

Rybina Ulyana Ilinishna – student, Reshetnev Siberian State University of Science and Technology.

Ryzhkova Svetlana Mikhailovna – head of Quality control department, JSC "Academician M. F. Reshetnev "Information Satellite Systems". E-mail: OTK5@iss-reshetnev.ru.

Sharov Sergey Konstantinovich – Cand. Sc., senior principal manufacturing engineer, JSC "Research and Production Enterprise "Kvant". E-mail: otd_17@npp.kvant.

Shaura Aleksandr Sergeevich – Cand. Sc., the 2nd category software engineer, JSC "IRZ". E-mail: shauraa@mail.ru.

Sherstennikova Gulnara Nurshaehovna – the 2nd category design engineer, JSC "IRZ". E-mail: vakilova@irz.ru.

Shindina Tatyana Aleksandrovna – Dr. Sc., Docent, professor of Economics Department of Electric Power Industry, director of the Institute of Distance and Additional Education, National Research University "Moscow Power Engineering Institute". E-mail: shindina@74.ru.

Shmakov Dmitri Nikolaevich – leading engineer, JSC "Academician M. F. Reshetnev "Information Satellite Systems".

Sitnikov Maxim Nikolaevich – Cand. Sc., Docent, Department of Physics, Reshetnev Siberian State University of Science and Technology. E-mail: kineru@mail.ru.

Slyshchenko Evgeny Vitalievich – vice-head of the department, JSC "Research and Production Enterprise "Kvant"; the 1st category engineer of Department of Nanostructured energy converters, National Research Technological University "MISIS". E-mail: otdel_17@kvant.ru.

Tikhomirova Irina Sergeevna – the 2nd category quality engineer, JSC "Academician M. F. Reshetnev "Information Satellite Systems". E-mail: mis88_88@mail.ru.

Vadimov Vladimir Nikolaevich – the 2nd category design engineer, JSC "Academician M. F. Reshetnev "Information Satellite Systems". E-mail: Vladimir-vadimov@mail.ru.

Vagapova Nargiza Tukhtamyshevna – Cand. Sc., leading researcher, JSC "Research and Production Enterprise "Kvant". E-mail: otdel_17@kvant.ru.

Vasil'ev Evgenii Nikolaevich – Cand. Sc., senior researcher, Federal research center "Krasnoyarsk Science Centre SB RAS", Institute of Computational Modelling SB RAS. E-mail: ven@icm.krasn.ru.

Vlasova Galina Alexandrovna – senior teacher of Department of Economics and Management at the enterprises of construction and land management, Higher School of Economics and Management, South Ural State University (National Research University). E-mail: galina-v89@mail.ru.

Yareshchenko Darya Igorevna – senior teacher, Department of Intelligent Control Systems, Institute of Space and Information Technologies, Siberian Federal University. E-mail: YareshenkoDI@yandex.ru.

Zabolotsky Alexander Mikhailovich – Dr. Sc., professor, Department of Television and Control, Tomsk State University of Control Systems and Radioelectronics. E-mail: zabolotsky_am@mail.ru.

Zhalnin Boris Viktorovich – Cand. Sc., head of department, JSC "Research and Production Enterprise "Kvant". E-mail: otdel_17@kvant.ru.